

**STUDIES ON THE MODULATION OF RADIATION INJURY
BY BILIRUBIN AND NAPHTHOQUINONES**

By

Mohd. Nazir Khan

Enrollment No.-LIFE0120074004

BHABHA ATOMIC RESEARCH CENTRE, MUMBAI

A thesis submitted to the

Board of Studies in Life Sciences

In partial fulfillment of requirements

For the degree of

DOCTOR OF PHILOSOPHY

of

HOMI BHABHA NATIONAL INSTITUTE



May, 2012

Homi Bhabha National Institute

Recommendations of the Viva Voce Board

As members of the Viva Voce Board, we certify that we have read the dissertation prepared by **Mohd. Nazir Khan** entitled “**Studies on the Modulation of Radiation Injury by Bilirubin and Naphthoquinones**” and recommend that it may be accepted as fulfilling the dissertation requirement for the Degree of Doctor of Philosophy.

Chairman - Dr. K. B. Sainis **Date:**

Guide/ Convenor - Dr. T. B. Poduval **Date:**

Member 1 - Dr. M. Seshadri **Date:**

Member 2 - Dr. S. V. Chiplunkar **Date:**

Final approval and acceptance of this dissertation is contingent upon the candidate's submission of the final copies of the dissertation to HBNI.

I hereby certify that I have read this dissertation prepared under my direction and recommend that it may be accepted as fulfilling the dissertation requirement.

Date:

Place:

Guide's Signature

STATEMENT BY AUTHOR

This dissertation has been submitted in partial fulfillment of requirements for an advanced degree at Homi Bhabha National Institute (HBNI) and is deposited in the library to be made available to borrowers under rules of the HBNI.

Brief quotations from this dissertation are allowable without any special permission, provided that accurate acknowledgement of source is made. Requests for permission for extended quotation from or reproduction of this manuscript in whole or in part may be granted by the competent authority of HBNI when in his or her judgment the proposed use of the material is in the interests of the scholarship. In all other instances, however, permission must be obtained from the author.

(Mohd. Nazir Khan)

DECLARATION

I, hereby declare that the investigation presented in the thesis has been carried out by me. The work is original and has not been submitted earlier as a whole or in part for a degree/ diploma at this or any other Institution / University.

(Mohd. Nazir Khan)

Dedicated

to my

loving parents

Acknowledgements

I thank Almighty ALLAH for bestowing upon me the strength and good health all throughout these years that gave me endurance to move on. With His blessings, I came across all those who helped me in this endeavour and it's a priceless opportunity for me to thank each and everyone who contributed during my PhD work.

I take my great pride and privilege to say undoubtedly, that as a true guide, it has been well expressed by my esteem guide, Dr. T. B. Poduval, Head, Immunology & Hyperthermia section, Radiation Biology & Health Sciences Division for peerless guidance, expert planning, untiring and bountiful help and support which inspired me to complete my heart felt desired thesis work. His compassionate nature, friendliness, down to earth attitude and practical approach towards life are worth the admiration. Though there have been many ups and downs in my research, his constant faith and confidence in me motivated me to work with renewed zest. Thanks Sir for calming me down at times and for being an oasis of constant encouragement and support. His constant supervision and persistent encouragement created an atmosphere conducive to the academic pursuit. It's with his blessing that the work is in its present form.

I am greatly indebted to Dr. K.B. Sainis, Director, Biomedical Group, B.A.R.C. for giving me the opportunity to work in this Department, for providing the necessary facilities and for their encouragement and support. I am extremely thankful to Dr. M. Seshadri, and Dr. T.P.A. Devasagayam, Former Head, Radiation Biology & Health Science Division, B.A.R.C. for providing the facilities at the institute during the tenure of my research.

I feel great pleasure to express my esteem and profound sense of gratitude to Dr. S. Santosh Kumar, who has been very encouraging and supportive throughout my tenure. He has introduced me to the exciting world of naphthoquinones. His vision versatility, indefatigable stamina and prompt nature are the qualities which have inspired me the time to join his group. I thank him for giving me the chance to work in his group and providing all the necessary facilities.

Words alone are inadequate to convey my deep sense of gratitude to Dr. Deepak Sharma for everything..... He is the one who had suggested me to join this lab when I was wandering in the corridor of Mod Lab in search of guide. Thank you Sir, I shall always be indebted to your decisive suggestion at right time. Being a naïve person in this field, I owe a lot to him for teaching me the knits and grits of the subject. He has introduced me with flowcytometry, the backbone of my thesis work. His deep understanding of the subject and immense knowledge in the field of immunology has inspired me a lot.

I extend my special thanks to Mr. Rahul Checker who teaches me the very first experiment of plasmid protection assay and irradiation of samples right on the first day of joining the lab. I duly acknowledge him for his constructive criticism which helped me do better.

I wish to express my deep sense of gratitude to the members of my doctoral committee chairman, Dr. K.B. Sainis and members Dr. S. V. Chiplunkar, Head, Immunology, ACTREC and Dr. M. Seshadri, for their questions and suggestions, which have improved my research work.

With the depth of my heart I express my earnest gratitude to Shweta, with whom I started this journey, her sisterly affection and helping me whenever I faced problems. Thanks you Shweta for being with me during executions of experiments especially the in vivo, consisting of huge number of groups and also for taking care of so many things that helped me give more time to my experiments. I express my sincere thanks to wonderful friend and brother, Chandan for his utmost help. It was a great pleasure to remember the days spent with you Chandan in the lab especially during Jurkat paper. I am grateful for the understanding and affection you extended towards me. The moments we enjoyed together will be cherished through out my life. I sincerely thank Nutan for her help in microscopy. Her mere presence in the lab provides moral supports. I am thankful to Shareena for her support and enthusiasm. I extend my thanks to Manjutha Subaiah and Smina T Padmanabhan for their affectionate support.

Special thanks to Dr. H. N. Bhilwade for teaching me Comet Assay. I would thank Thakur Sir, Sudha Mam, Patro Sir, Maurya Sir, Manish Sir and Jay Kumar Sir for sharing their hard earned experiences that made my work go smoother. Each one has been a constant source of inspiration. My sincere thanks to Jay Kumar Sir for teaching me Real time PCR and Graph Pad InStat software. Manish Sir deserves special thanks for his help in bacterial experiments. I express my sincere thanks to Dr. Amit Kunwar for helping me deal with the failures I came across. I extend my wholehearted thanks to Mr. Raghavendra Patwardhan, Dr. Maikoh Thoh and Lokesh Gambhir for their help and cooperation. Many thanks to project trainees Aarti Mohan, Neetu Thomas, Mustafa, Bincy Bhaskar, Heena Shabnam, S. G. Christy and Sonam Mishra for their help and support.

With due regards I remember my seniors in the lab. I feel highly obliged and have immense pleasure in expressing my heart felt thanks to Ms. Rashmi Raghu who teaches me each and every technique related to tissue culture work, dissolution of bilirubin during my initial period of work. I acknowledge my sincere and heart felt thanks to Strayo and Jyoti. My special thanks to Jyoti for her teaching handling, grouping and identification of mice. I feel privileged to remember you people throughout my career.

I owe my thanks to all my batchmates specially C. Vijay, Arpana, Mrityunjay, Kirti, Nidhi, Debes, Pankaj, Rohit, Sunil, Naveen and Siba for their affectionate support. My special thanks to Arpana for help and support during training period. C. Vijay needs special note of appreciation for his constant help during search of guide and execution of bacterial experiments. I am especially thankful to Mrityunjay Tyagi for always being available for the scientific discussions I had with him. I am thankful to Arvind and Anuvab for their good wishes.

I express my sincere thanks to Mr. Prayag and Ms. Jisha for their patience in acquiring N number of flowcytometry samples. Help provided by Mr. Manjoor Ali and Ms. Vashumati in confocal microscopy is duly acknowledged. My thanks are due to Mr. K. S. Munankar, Mr. Deepak Kathole, Mr. Narendra Sidnalkar, Mr. Pascal Gonsalves and Ms. Punita for their timely help and technical support during my experiments in the lab and animal house. Many thanks to animal house staff especially Dhakate Ji for timely providing the animals for conducting the experiments. I extend my thanks to the staff of RB&HSD and group office for their kind co-operation in every way.

Words fail to express the amount of love, care, selfless help and affection showered by my sister Sham. I thank to Ansul for his utmost support, compassion and making my stay at BARC, memorable.

My heartfelt appreciation goes to Chabbi Naaj who was always by my side during the ups and downs. Due to her support and reassurance I was never alone with my problems. Her help during the tough times of my research will be indelible from my mind. Telephonic conversation with her had been my biggest stress buster and source of inspiration. Her discussions induced new gush of energy in me whenever I felt low and perturbed. Without her support and understanding I could have never reached my goal.

Life is just not professional; it has its root under the roof of loved ones. I am overwhelmed when it comes to express my gratitude towards my family members. I thank my parents, brother and sister for their supreme moral support and boundless love they have showered upon me. My special thanks to my Abba who instilled in me the undying spirit to fight and never give up. I thank my mother for her blessings.

I pay my reverence to those experimental animals who sacrificed their lives in making my endeavour successful. May ALLAH grant them eternal peace!

Financial assistance provided by DAE is duly acknowledged.

Finally, to err is human!! All those whose mention might have slipped from my mind, deserve my sincere gratitude for their direct or indirect help in this pursuit.

Mohd. Nazir Khan

CONTENTS

	Page No.
<i>SYNOPSIS</i>	I-XII
<i>LIST OF SCHEMES</i>	XIII
<i>LIST OF TABLES</i>	XIV
<i>LIST OF FIGURES</i>	XV-XVI
<i>LIST OF ABBREVIATIONS</i>	XVII-XVIII
 <u>CHAPTER 1: INTRODUCTION AND REVIEW OF LITERATURE</u>	 1-36
1.1 CELLULAR REDOX HOMEOSTASIS	2-3
1.2 ALTERATION OF CELLULAR REDOX AS A NOVEL STRATEGY TO MODULATE RADIATION INJURY (HYPOTHESIS OF THESIS WORK)	4-7
1.3 IONIZING RADIATION AND ITS BIOLOGICAL EFFECTS	8-12
1.3.1 Ionizing radiation and its interaction with matter	8-10
1.3.2 Biological effects of ionizing radiation	10-12
1.4 NEED FOR MODULATION OF RADIATION INJURY	12-16
1.4.1 Radioprotectors	12-15
1.4.2 Radiopotentiators	15-16
1.5 1, 4 NAPHTHOQUINONE (NQ)	16-25
1.5.1 Chemical synthesis of NQ and its derivatives	18-19
1.5.2 Clinical significance of NQ	19-22
1.5.3 Prooxidant effects of NQ	22-23
1.5.4 Biological effects of NQ	24-25
1.6 UNCONJUGATED BILIRUBIN (UCB)	25-36
1.6.1 Chemical structure and formation of bilirubin	26-28
1.6.2 Metabolism of bilirubin	29-31
1.6.3 Biological properties of bilirubin	31-36
1.6.3.1 Cytotoxic effects of bilirubin	32-34
1.6.3.2 Cytoprotective effects of bilirubin	34-36
1.7 AIMS OF THE PRESENT STUDIES	36
 <u>CHAPTER 2: RADIOMODIFYING EFFECTS OF 1, 4 NAPHTHOQUINONE</u>	 37-112
2.1 INTRODUCTION	38-42
2.2 MATERIALS AND METHODS	43-69
2.2.1 Reagents and Chemicals	43

2.2.2 Animal maintenance	44
2.2.3 Cell line and culture	44-45
2.2.4 Treatment with NQ	45
2.2.5 Irradiation schedule	45-46
2.2.6 Preparation of splenic lymphocytes and Bone marrow cell suspension	46-47
2.2.7 Estimation of apoptosis by PI staining	47
2.2.8 Estimation of apoptosis using DNA ladder assay	47-48
2.2.9 Determination of cell size and volume by Flow Cytometry	48-49
2.2.10 Estimation of cell death by Live and Dead assay	49-50
2.2.11 Determination of nuclear blebbing	50
2.2.12 Colony Forming Cell (CFC) Assay	50-51
2.2.13 Clonogenic Cell Survival Assay	51
2.2.14 Purification of CD4+T cells, CD19+B cells	52-53
2.2.15 Human lymphocyte isolation	53
2.2.16 Estimation of caspase activity	53-54
2.2.17 Measurement of change in MMP ($\Delta\psi_m$)	54-55
2.2.18 Measurement of intracellular calcium levels	55
2.2.19 Prooxidant measurements	55-57
2.2.20 Measurement of intracellular GSH levels	57-58
2.2.21 HPLC Separation of Products of Reaction of NQ with NAC	58
2.2.22 Mass Spectrometry (MS) analysis	58
2.2.23 Estimation of nuclear Nrf2 levels by confocal microscopy	58-59
2.2.24 Antibody staining	59-60
2.2.25 Protein tyrosine phosphatase assay	60-61
2.2.26 Transfection of lymphocytes with Nrf2 shRNA plasmid	61
2.2.27 Estimation of mRNA expression by semi-quantitative Reverse Transcription-PCR	61-62
2.2.28 Estimation of mRNA expression by quantitative Real Time PCR	62-64
2.2.29 Administration of NQ to mice and <i>in vivo</i> radioprotection studies	64
2.2.30 Measurement of hematological profile and plasma NO	64-65
2.2.31 Measurement of radioprotective cytokines (IL-1 β and IL-6) in plasma by ELISA	65-66
2.2.32 Measurement of functional response of lymphocytes	66-67
2.2.33 Histopathological studies	67
2.2.34 Endogenous spleen colony formation assay	67-68
2.2.35 <i>In vivo</i> radioprotection studies using apoptotic parameters	68
2.2.36 Survival studies	68-69
2.2.37 Statistical analysis	69
2.3 RESULTS	70-103
2.3.1 NQ protected lymphocytes against radiation induced cell death	70-71
2.3.2 Other prooxidants also protected lymphocytes against radiation induced cell death	72
2.3.3 NQ inhibited radiation induced death in lymphocytes	73-74
2.3.4 NQ restored the radiation induced loss of proliferative potential of hematopoietic stem cells present in spleen	74-75

2.3.5 NQ inhibited radiation induced apoptosis in lymphocyte when added post irradiation	75
2.3.6 NQ protected CD4+T cells and CD19+B cells against radiation induced death	76
2.3.7 NQ protected human PBMNCs and human intestinal epithelial cells (Int407) against radiation induced death	77-78
2.3.8 NQ inhibited radiation induced early events of apoptosis in lymphocytes	78-79
2.3.9 NQ upregulated antiapoptotic proteins in lymphocytes	79-80
2.3.10 NQ perturbed intracellular redox balance by increasing basal ROS levels and depleting cellular GSH levels	80-83
2.3.11 NQ mediated radioprotection was abrogated by thiol-containing antioxidants	83-86
2.3.12 NQ offered radioprotection via activation of Nrf2 in lymphocytes	86-88
2.3.13 NQ upregulated Nrf2 dependent HO-1 expression	88-89
2.3.14 NQ induced phosphorylation of ERK in lymphocytes	89-90
2.3.15 NQ increased intracellular calcium levels	91-92
2.3.16 NQ administration to mice protected against WBI induced immune and myelosuppression	92-96
2.3.17 NQ administration to mice inhibited WBI induced apoptosis in Lymphocytes	96-98
2.3.18 NQ administration to mice elevated radioprotective cytokines	98-99
2.3.19 NQ administration to mice prevented WBI induced loss of functional response of lymphocytes and bone marrow	99-101
2.3.20 NQ administration to mice prevented WBI induced mortality	102-103
2.3.21 NQ did not protect tumor cells	103
2.4 DISCUSSION	104-112
<u>CHAPTER 3: IMMUNOTOXIC AND RADIOMIMETIC EFFECTS OF BILIRUBIN</u>	113-167
3.1 INTRODUCTION	114-118
3.2 MATERIALS AND METHODS	119-129
3.2.1 Reagents and Chemicals	119
3.2.2 Animal maintenance	120
3.2.3 Preparation and treatment schedule of UCB	120-121
3.2.4 Bone marrow and spleen cell suspensions	121
3.2.5 Human lymphocyte isolation	121
3.2.6 Estimation of cell death	121
3.2.7 Estimation of cell death by CFSE staining	121-122
3.2.8 AnnexinV-FITC/PI staining	122-123
3.2.9 Caspase-3, 8 colorimetric assay	123
3.2.10 Measurement of change in MMP and intracellular calcium levels	123
3.2.11 Estimation of DNA strand breaks by alkaline single-cell gel electrophoresis (Comet assay)	123-124
3.2.12 Measurements of RBC hemolysis	124

3.2.13 RNA isolation and quantification	124
3.2.14 Antibody staining	125
3.2.15 Western blot analysis	125-126
3.2.16 Protein tyrosine kinase assay	126
3.2.17 Measurements of ROS levels	126
3.2.18 Measurements of intracellular GSH levels	126-127
3.2.17 ³ H thymidine incorporation assay	127-128
3.2.18 CyQUANT-NF cell proliferation assay	128
3.2.19 Measurement of cytokines	128
3.2.20 Administration of UCB to mice	128-129
3.2.21 Statistical analysis	129
3.3 RESULTS	130-157
3.3.1 UCB exhibited immunotoxic and radiomimetic effects in lymphocytes by inducing cell death and DNA strand breaks	130-132
3.3.2 UCB induced immunotoxic effects in activated lymphocytes	132-133
3.3.3 UCB induced immunotoxic effects in various immune cells	134-135
3.3.4 Purified UCB induced immunotoxic effects in lymphocytes and human PBMNCs	136
3.3.5 UCB exhibited immunosuppressive effects in lymphocytes and macrophages	136-138
3.3.6 UCB exhibited immunotoxic and radiomimetic effects by inducing both apoptotic and necrotic death in splenic lymphocytes	138-140
3.3.7 UCB induced both extrinsic and intrinsic apoptotic pathways in lymphocytes	140-143
3.3.8 UCB induces apoptosis in lymphocytes by activating p38MAPK	143-145
3.3.9 UCB depleted cellular GSH levels in lymphocytes	146-148
3.3.10 Glutathione appeared a key molecule in the prevention of cell death induced by UCB	148-150
3.3.11 UCB induced p38MAPK activation was mediated by depletion of GSH levels	150-151
3.3.12 UCB caused immunotoxicity and immunosuppression <i>in vivo</i>	151-153
3.3.13 UCB induced immunotoxicity is mediated by activation of p38MAPK <i>in vivo</i>	153-155
3.3.14 UCB administration caused oxidative stress <i>in vivo</i>	156-157
3.4 DISCUSSION	158-167
<u>CHAPTER 4: RADIOMODIFYING EFFECTS OF BILIRUBIN</u>	168-205
4.1 INTRODUCTION	169-172
4.2 MATERIALS AND METHODS	173-178
4.2.1 Reagents and Chemicals	173
4.2.2 Animal maintenance	173
4.2.3 Preparation and treatment schedule of UCB	173

4.2.4 Irradiation schedule	174
4.2.5 Bone marrow and spleen cell suspensions	174
4.2.6 Human lymphocyte isolation	174
4.2.7 Estimation of apoptosis	174
4.2.8 Estimation of apoptosis using TUNEL assay	174
4.2.9 Measurement of change in MMP and intracellular calcium levels	174
4.2.10 Estimation of DNA strand breaks by alkaline single-cell gel electrophoresis (Comet assay)	174
4.2.11 Measurements of RBC hemolysis	174
4.2.12 Administration of UCB to mice	175
4.2.13 Antibody staining	175
4.2.14 ³ H thymidine incorporation assay	175
4.2.15 Measurement of cytokines	175
4.2.16 Phagocytic activity of peritoneal exudate cells	175-176
4.2.17 Studies on mouse model of bacterial infection	176-177
4.2.18 Quantification of bacterial load in peritoneal cavity	177
4.2.19 Measurement of serum nitric oxide and cytokines	177-178
4.2.20 Statistical analysis	178
4.3 RESULTS	179-195
4.3.1 UCB potentiated radiation induced apoptosis in lymphocytes	179-181
4.3.2 UCB potentiated radiation induced DNA strand breaks in lymphocytes	181
4.3.3 UCB potentiated radiation induced loss of MMP and calcium release in lymphocytes	181-182
4.3.4 UCB potentiated radiation induced apoptosis of various immune Cells	182-184
4.3.5 UCB pretreatment of mice potentiated WBI induced Immunosuppression	184-185
4.3.6 UCB pretreatment of mice potentiated WBI induced loss of splenocyte subsets	186
4.3.7 UCB pretreatment of mice potentiated WBI induced loss of hematological parameters	186-187
4.3.8 UCB pretreatment of mice potentiated WBI induced apoptosis in various immune cells	188
4.3.9 UCB pretreatment of mice decreased WBI induced loss of functional response of lymphocytes	188-189
4.3.10 UCB pretreatment of mice decreased WBI induced loss of functional response of PECs	189-191
4.3.11 UCB pretreated mice were more susceptible to WBI induced Infection	191-193
4.3.12 UCB pretreatment of mice potentiated WBI induced p38MPAK activation in PECs	193-195
4.4 DISCUSSION	196-205

<u>CHAPTER 5: SUMMARY AND CONCLUSIONS</u>	206-220
5.1 SUMMARY	207-216
5.2 CONCLUSIONS	217-219
5.3 FUTURE PROSPECTS	220
<u>CHAPTER 6: BIBLIOGRAPHY</u>	221-233
<u>ANNEXURE</u>	234-235
<u>LIST OF PUBLICATIONS</u>	236-238
<u>REPRINTS OF PUBLISHED PAPERS</u>	

**STUDIES ON THE MODULATION OF RADIATION INJURY
BY BILIRUBIN AND NAPHTHOQUINONES**

A SYNOPSIS

By

Mohd. Nazir Khan

HBNI, Research Fellow

BHABHA ATOMIC RESEARCH CENTRE, MUMBAI

February, 2012

PREAMBLE

Life forms evolved and developed on earth in a radiation field that was much stronger than existing today. Presently, exposure to ionizing radiation majorly occurs either through therapy and diagnosis or through occupational and environmental exposures. In addition to these, astronauts during spaceflight were exposed to protons and high-energy particles¹. The sustained interest in biological effects of ionizing radiations seems to be chiefly an aftermath of atomic explosions at Hiroshima and Nagasaki, Chernobyl and Tokai-Mura nuclear accidents.

Ionizing radiation exerts its cytotoxic effect on cells and tissues, primarily through indirect effect by radiolysis of water, the major constituent of a cell². Cells of the immune system are extremely sensitive to ionizing radiation^{1,2}. Ionizing radiation is capable of suppressing the immune system. Immunosuppression can make the host vulnerable to infections by opportunistic pathogens, which is followed by a complex physiological response, and is clinically manifested as acute radiation-induced systemic inflammatory response syndrome (AR-SIRS). This syndrome then further leads to sepsis, shock, multiple organ dysfunction and death³⁻⁵.

Since use of ionizing radiation in various aspects of human life is increasing, there is a great need to understand the mechanisms of radiation induced injury to living cells and also to modify the effects of ionizing radiation. Agents that modify the effects of radiation are called radio-modifiers. These can be either radiosensitizers or radioprotectors. The molecule which amplify the harmful effects of radiation to living cells is called radiosensitizer, whereas chemicals which ameliorate radiation induced deleterious effects are known as radioprotectors. Development of radiation modifier enhances the safer use of ionizing radiation for human welfare. Developing such radiation modifiers which modify the host response following radiation injury is a challenge to life scientists and has been a key research area of radiation biologists and radiation chemists.

With this aim, in the present investigation, bilirubin an endogenous degradation product of heme and 1,4 naphthoquinone the parent molecule of many clinically approved drugs, have been evaluated for their radiomodifying activity. Radiomimetic

and immunotoxic effects of bilirubin were explored. This dissertation describes the details and results of these investigations.

AIMS OF THE PRESENT STUDIES:

- To investigate the use of 1,4-naphthoquinone for modification of radiation injury in lymphocytes under *in vitro* and in murine model.
- To evaluate the molecular mechanism of action of 1,4-naphthoquinone in mitigating radiation injury.
- To study the use of unconjugated bilirubin as immunotoxic and radiomimetic drug both *in vitro* and *in vivo* and to delineate the signaling pathways leading to damage and potential molecular targets.
- To investigate the radiomodifying effects of unconjugated bilirubin.

ORGANISATION OF THE THESIS: The work embodied in this thesis is divided into six chapters: (1) Introduction and Review of literature, (2) Radiomodifying effects of 1,4 naphthoquinone, (3) Immunotoxic and radiomimetic effects of bilirubin, (4) Radiomodifying effects of bilirubin, , (5) Summary and conclusions, (6) Bibliography.

CHAPTER 1: INTRODUCTION AND REVIEW OF LITERATURE: As a background to the topics of research investigations contained in the thesis, the introductory chapter reviews the literature pertaining to the current status of our knowledge in radiation injury. This chapter describes novel strategy to modify the deleterious effects of ionizing radiation. The chapter also reviews the brief outline of the radiomodifiers that have been tested by different investigators and also relevant research information in the context of modulating biological and the physiological responses.

The pathophysiological consequences resulting from exposure of individuals to ionizing radiation make them susceptible to opportunistic infections. An inflammatory response is a classical feature of radiation exposure and appears to be a key event in the development of radiation injury⁶. The progression of inflammatory signaling pathways is an outcome of perturbation of intracellular redox homeostasis of host. Maintenance of redox homeostasis is essential to cellular function and survival⁷. Therefore, maintaining

homeostatic equilibrium of cell is central to modify the host response to radiation. In this background, search for molecule which can maintain the homeostatic equilibrium of a cell is a better approach to develop new radiomodifier. Alteration in redox homeostasis can elicit a variety of cellular responses ranging from protective to injurious depending on levels of oxidative stress. Mild oxidative stressor induces the expression of a battery of phase II enzymes under regulation of Nrf2⁸, which could detoxify ROS and electrophilic chemicals induced by subsequent radiation exposure to cells. Whereas, severe oxidative stressor depletes cellular GSH and perturbs mitochondrial membrane potential⁷, which could further deteriorate the host condition after subsequent radiation exposure. Therefore, mild oxidative stressor could be used as radioprotector and severe oxidative stressor could behave as radiosensitizer. For the present thesis work 1,4 naphthoquinone and bilirubin were selected as radiomodifiers.

1, 4-naphthoquinone, the parent molecule of many clinically approved anticancer, anti-infective and anti-parasital drugs like anthracycline, mitomycin, daunorubicin, doxorubicin, diospyrin, and malarone has been studied as a model molecule for biologically important quinones⁹⁻¹³. Quinones, like phyloquinone (vitamin K1) and menadione (vitamin K3) take part in the blood clotting process and ubiquinone (coenzyme Q10), acts as an electron carrier in mitochondrial electron transport chain. In general, the biological activity of a quinone has been attributed to its ability to undergo reversible oxidation-reduction reactions, as well as to its electrophilic nature leading to arylation of cellular nucleophiles such as thiols in cysteine residues of proteins and glutathione¹⁴. The prooxidant property of naphthoquinones is responsible for initiation of tissue damage selectively in tumor cells¹⁵. Considering the ability of low levels of ROS to initiate an adaptive response against further oxidative challenge we hypothesized that 1,4 naphthoquinone might protect against radiation induced damage via activation of Nrf2-ARE pathway.

Bilirubin is a linear tetrapyrrole formed during endogenous degradation of heme in the reticuloendothelial cells mainly in the spleen¹⁶. Although physiological levels of unconjugated bilirubin (UCB) act as an antioxidant, increasing evidences have demonstrated at high concentrations it may be an active participant in the disease process¹⁷. Several studies suggest that UCB possesses multiple biological activities,

including potential immunomodulatory, anti-inflammatory, antimutagenic, antioxidant and anticancer properties¹⁸⁻²¹. UCB decreases immune responses and increased rate of infection have been documented in hyperbilirubinemic patients as happens in case of radiation exposure²². The decreased immune response has been attributed to the immunological anergy induced by UCB. UCB is known to interact with plasma membrane of immune cells causing the perturbation of redox balance of cells²³. Considering the ability to induce profound changes in the redox status of cell, we hypothesize that physiologically relevant concentrations of UCB might cause immunotoxicity like exposure to ionizing radiation in resting cells thus mimicking the radiation effect and sensitizes the effect of radiation in these cells.

CHAPTER 2: RADIOMODIFYING EFFECTS OF 1,4 NAPHTHOQUINONE: In this chapter, studies on use of 1,4 naphthoquinone for ameliorating the harmful effects of radiation in normal lymphocytes is summarized. This chapter also describes the molecular mechanism of action of 1,4-naphthoquinone in mitigating radiation injury.

Exposure to radiation is thought to affect host immune surveillance to a great extent, because their cellular constituents are derived from hematopoietic stem cells which are very sensitive to radiation. In the present study we have chosen murine splenic lymphocytes as a model for assessment of radiation damage because lymphocytes are known to be sensitive to radiation. A radiation dose of 4Gy was selected as it causes both immunosuppression and myelosuppression and further this dose is also used during radiotherapy⁶.

Presence of NQ (0.05-1 μ M) during radiation exposure to lymphocytes inhibited radiation induced apoptosis in a concentration dependent manner, as shown by propidium iodide staining. Radioprotection by NQ was further confirmed by decrease in cell size, DNA-fragmentation and nuclear-blebbing. Further, NQ inhibited early and late events associated with apoptosis for example loss of mitochondrial membrane potential, calcium release in cytoplasm and activation of caspases. Presence of NQ abrogated radiation induced decrease in antiapoptotic proteins Bcl-2 and Bcl-xl in lymphocytes. Interestingly, NQ offered protection to lymphocytes even when added to cells post-irradiation. NQ increased intracellular ROS levels and decreased GSH levels. Radioprotective effect of

NQ was sensitive to presence of thiol containing antioxidant N-acetyl cysteine. Whereas, non-thiol antioxidant MnTBAP failed to abrogate the radioprotective efficacy of NQ suggesting that depletion of thiol levels by NQ may be playing a role in the observed radioprotection. Further, HPLC separation and MS analysis revealed that NQ reacted with NAC and formed an adduct. Exposure of lymphocytes to NQ activated Nrf2 and increased the expression of cytoprotective gene hemeoxygenase-1. NQ increased ERK phosphorylation which is upstream to Nrf2 and this ERK activation was through increased intracellular calcium levels.

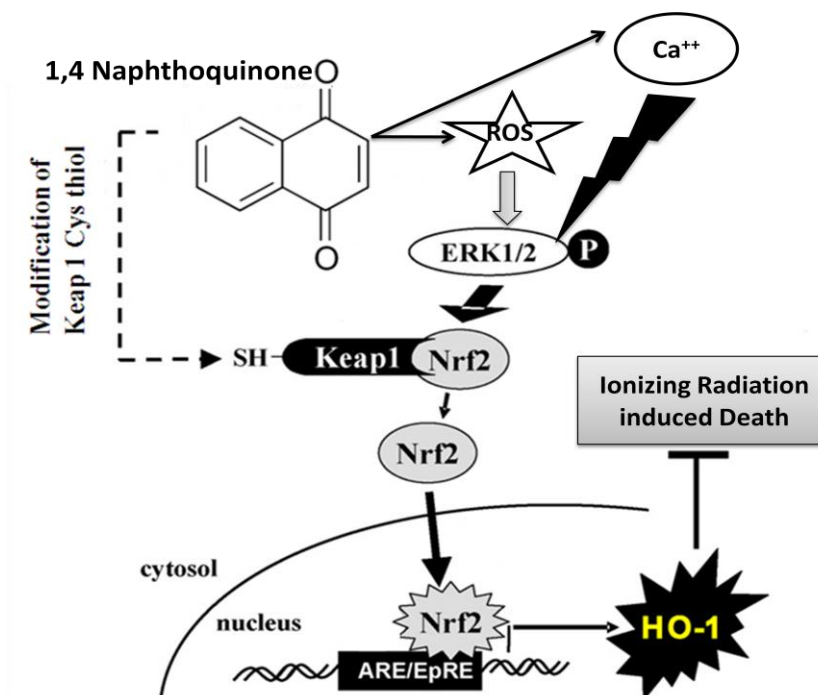


Figure1: Radioprotective effect of 1,4 naphthoquinone

Administration of NQ (2mg/kgbw) to mice offered protection against whole body irradiation (WBI)-induced apoptosis in splenic lymphocytes and loss of viability of spleen and bonemarrow cells. It restored WBI mediated changes in hematological parameters and functional responses of lymphocytes in terms of cell proliferation and cytokine secretion in response to T cell mitogen. NQ administration to mice elevated the plasma levels of radioprotective cytokine IL-1 β and IL-6. Importantly, NQ rescued mice against WBI-induced mortality and prevented WBI induced loss of body weight. An

increase in the LD50/30 from 6.67 Gy for vehicle injection to 7.86 Gy in NQ treated group was observed, which corresponds to a dose modification factor (DMF) 1.18. These results demonstrated that a prooxidant like NQ can protect against radiation-induced apoptosis by activation of multiple prosurvival mechanisms including activation of calcium-ERK1/2-Nrf2 pathway (Figure1).

CHAPTER 3: IMMUNOTOXIC AND RADIOMIMETIC EFFECTS OF BILIRUBIN: This chapter summarizes the studies related to the immunotoxic and radiomimetic effects of unconjugated bilirubin in splenic lymphocytes under *in vitro* and in murine model. This chapter projects potential molecular targets and signaling pathways involved in the immunotoxic effect of unconjugated bilirubin.

A radiomimetic drug is one that imitates the biological effects of radiation like induction of DNA double strand breaks, cytotoxicity, perturbation of cell cycle, induction of apoptotic bodies etc. Bleomycin, alkylating agents and chemicals such as nitrogen mustards are known to be radiomimetic drugs²⁴. We have investigated the radiomimetic and immunotoxic effects of UCB and detailed molecular mechanism of action.

Results showed that exposure of UCB ($\geq 25\mu\text{M}$) was cytotoxic to the immune cells. It induced cell death in a concentration dependent manner in total spleen cells and also in purified splenic T cells, B cells, macrophages, and human peripheral blood mononuclear cells (PBMCs). Treatment of splenocytes with bilirubin inhibited the proliferation of B cells in response to lipopolysaccharide and also inhibited the cytokine production from splenic macrophages. UCB induced cell death was mediated by induction of necrosis and apoptosis in splenocytes as revealed by annexin-V/PI staining. UCB activated both the extrinsic and intrinsic pathways of apoptosis as reflected by changes in CD95 levels, caspase-8 activity (extrinsic apoptosis), Bax levels, mitochondrial membrane potential, cytoplasmic Ca^{+2} (intrinsic apoptosis), caspase-3 activity and DNA fragmentation. Treatment of splenocytes with UCB depleted the cellular GSH level and activated p38MAPK. Further, N-Acetyl Cysteine (NAC), a known GSH precursor and p38MAPK inhibitor (SB203580) attenuated the UCB-induced apoptosis.

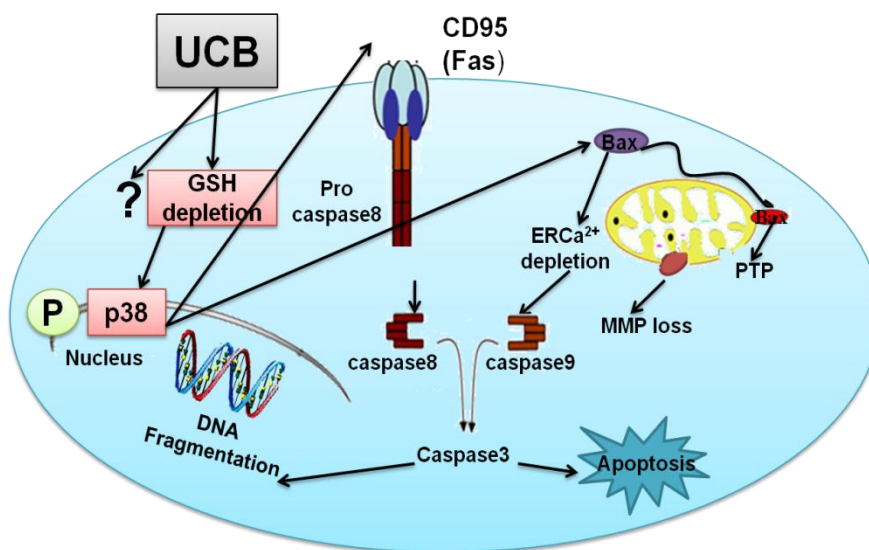


Figure 2: Immunotoxic effect of unconjugated bilirubin

In vivo administration of UCB (25-50mg/kbw) induced atrophy of spleen, depletion of bone marrow cells, leucopenia, decreased lymphocyte count and decreased response to T and B-cell mitogens. UCB administration to mice led to induction of oxidative stress and cell death in splenocytes. Further, administration of UCB to mice caused phosphorylation of p38MAPK in splenocytes. These parameters were attenuated by the administration of NAC and p38MAPK inhibitor. In summary, we conclude that clinically relevant concentrations of UCB induced both apoptosis and necrosis in immune cells by depleting cellular GSH and activating p38MAPK (Figure 2). Our results for the first time demonstrated that bilirubin exhibits immunotoxic effect in murine splenocytes both *in vitro* and *in vivo*.

CHAPTER 4: RADIOMODIFYING EFFECTS OF BILIRUBIN: This chapter details the studies on use of unconjugated bilirubin in modifying radiation response of host under *in vitro* and *in vivo* conditions. Molecular mechanism of radiomodifying effects of UCB has been summarized in this chapter.

Radiomodifying effect of unconjugated bilirubin was studied in murine immune cells in presence of radiation dose of 2Gy. We chose clinically relevant concentrations of UCB between 1-50 μ M for the *in vitro* and 25-50 mg/kbw for *in vivo* studies¹⁸. These

concentrations and doses have been used previously for the study of apoptotic, anti-inflammatory, antimutagenic, antioxidant and anticancer properties of UCB^{18,19,25}. We used molar ratios of UCB to BSA less than 0.7, to make the studies physiologically more relevant. Exposure of lymphocytes with UCB (>25 μ M) induced apoptosis and further augmented radiation induced apoptosis, as evinced by propidium iodide staining, TUNEL assay and DNA fragmentation assay. It also augmented radiation induced DNA strand breaks in lymphocytes.

Administration of UCB to mice increased WBI induced apoptosis in splenic lymphocytes and peritoneal macrophages and also decreased WBI induced loss of viability of splenocytes, macrophages, bonemarrow cells and various hematological parameters. It decreased WBI induced loss of functional responses of lymphocytes (in terms of cell proliferation and cytokine secretion in response to T cell mitogen) and macrophages (in terms of bacterial phagocytosis). Further, increased p38MAPK activation was seen in peritoneal macrophages of UCB administered mice exposed to WBI.

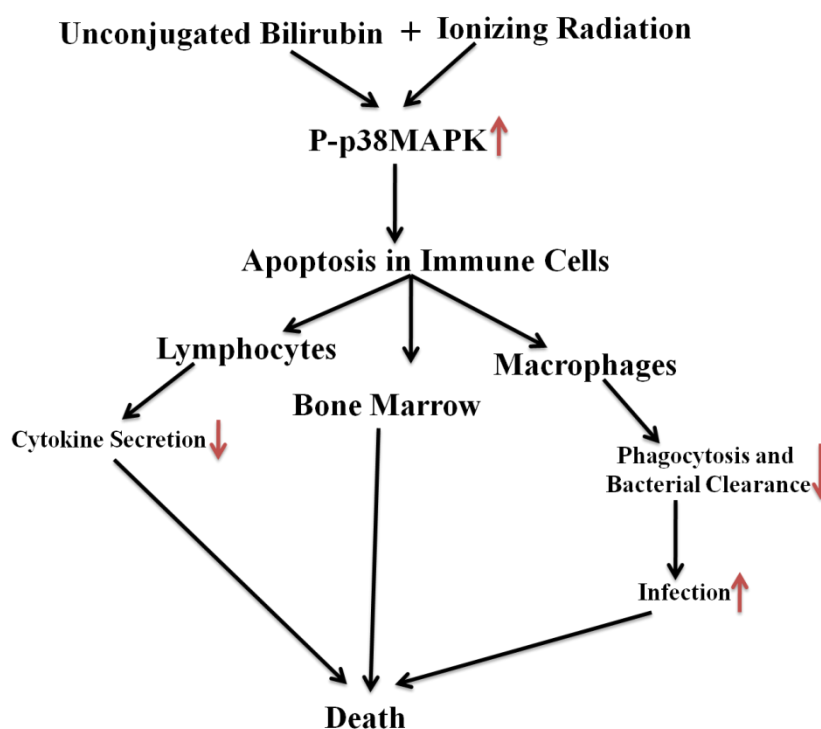


Figure 3: Schematic representation of radiomodifying effect of unconjugated bilirubin

Administration of UCB to mice exposed to WBI decreased the survival rate as compared to only WBI exposed mice. Further, increased mortality was found in bacteria injected mice which were previously administered with UCB and exposed to radiation. The decreased survival of UCB administered mice in presence of WBI is due to increased infection as evinced by increased bacterial load found in the peritoneum of these mice. In summary, we conclude that mice administered with clinically relevant dose of UCB and exposed to WBI showed increased apoptosis in peritoneal macrophages by enhancing p38MAPK activation and thereby decreasing bacterial clearance leading to increased infection resulting into decreased survival of mice (Figure 3).

CHAPTER 5: SUMMARY AND CONCLUSIONS: This chapter discusses the implications of the studies described in chapters 2, 3 and 4. In the present study, we have employed a pro-oxidant as a novel approach for obtaining radioprotection, which is different from use of conventional antioxidant phytochemicals. Our results demonstrate that 1, 4 naphthoquinone may have good potential as a new class of quinonoid radiation protector.

Clinically relevant UCB concentration at relevant UCB to BSA molar ratio mimics the effect of radiation in inducing immunotoxicity, immunosuppression and DNA strand breaks in the murine cells. Our results demonstrate the ability of UCB to cause immunotoxicity besides neurotoxicity, which form the basis of increased infections during hyperbilirubinemia. Exposures of lymphocytes to radiation in presence of bilirubin worsened the radiation effects in terms of induction of apoptosis and DNA strand breaks. Hyperbilirubinemic conditions during radiation exposure in the mice increases susceptibility to infection leading to enhanced death.

The major conclusions drawn from this study are:

1. NQ is a novel radioprotector which protect against radiation-induced apoptosis by activation of multiple prosurvival mechanisms including activation of calcium-ERK1/2-Nrf2-HO-1 pathway.
2. NQ administration rescued mice against WBI-induced mortality and its DMF was found to be 1.18.

3. UCB at clinically relevant concentrations and UCB to albumin molar ratio induced immunotoxic effects in murine splenic lymphocytes by activating p38MAPK signaling pathway.
4. Immunotoxic effects of UCB and decreased phagocytosis in the macrophages isolated from UCB administered mice provided molecular basis of increased infection rate during hyperbilirubinemia.
5. Radiomodifying effects of UCB included increased DNA strand breaks, increased apoptosis, increased injury to hematopoietic system, increased infection and decreased survival rate of mice.

CHAPTER 6: BIBLIOGRAPHY:

1. Weiss, J.F.; Landauer M.R. *Int. J. Radiat. Biol* **2009**, 85, 539–573.
2. Tak, J.K. ; Park, J.W. *Free Radic Biol Med* **2010**, 48, 399-410.
3. Boothman, D.A.; Reichrath, J. *Brit. J. Radiology Suppl.* **2005**, 27,157-160.
4. Lorimore, S.A.; Coates, P.J.; Scobie, G.E.; Milne, G.; Wright, E.G. *Oncogene* **2001**, 48, 7085-7095.
5. Hallahan, D.E.; Kuchibhotla, J.; Wyble, C.; Sialyl, L. *Radiat. Res.* **1997**,147, 41-47.
6. Shukla, J.; Chatterjee, S.; Thakur, V. S.; Premachandran, S.; Checker, R.; Poduval, T. B. *Radiat Res* **2009**, 171,180-187.
7. Li, N.; Nel, A. E. *Antioxid Redox Signal* **2006**, 8, 88-98.
8. Kim, J. W.; Li, M. H.; Jang, J. H.; Na, H. K.; Song, N. Y.; Lee, C.; Johnson, J. A.; Surh, Y. J. *Biochem Pharmacol* **2008**,76,1577-1589.
9. Rowley, D. A.; Halliwell, B. *Biochim Biophys Acta* **1983**,761, 86-93.
10. Yamashita, Y.; Kawada, S.; Fujii, N.; Nakano, H. *Biochemistry* **1991**, 30, 5838-5845.
11. Checker, R.; Sharma, D.; Sandur, S. K.; Khanam, S.; Poduval, T. B. *Int Immunopharmacol* **2009**, 9,949-958.
12. Kim, B. H.; Yoo, J.; Park, S. H.; Jung, J. K.; Cho, H.; Chung, Y. *Arch Pharm Res* **2006**, 29,123-130.
13. Looareesuwan, S.; Chulay, J. D.; Canfield, C. J.; Hutchinson, D. B. *Am J Trop Med Hyg***1999**, 60, 533-541.
14. Wang, X.; Thomas, B.; Sachdeva, R.; Arterburn, L.; Frye, L.; Hatcher, P. G.; Cornwell, D. G.; Ma, J. *Proc Natl Acad Sci U S A* **2006**, 103,3604-3609.
15. Kayashima, T.; Mori, M.; Yoshida, H.; Mizushina, Y.; Matsubara, K. *Cancer Lett* **2009**, 278,34-40.
16. Ostrow, J.D.; Pascolo, L.; Brites, D.; Tiribelli, C. *Trends Mol. Med.* **2004**, 10, 65-70.
17. Kapitulnik, J. *Mol. Pharmacol.* **2004**, 66, 773-779.
18. Liu, Y.; Li, P.;Lu, J.; Xiong, W.; Oger, J.; Tetzlaff, W.; Cynader, M. *J. Immunol.* **2008**, 181, 1887-1897.

19. Bulmer, A.C.; Ried, K.; Blanchfield, J.T.; Wagner, K.H. *Mutat. Res.* **2008**, 658, 28-41.
20. Stocker, R.; Yamamoto, Y.; Mcdonagh, A.F.; Glazer, A. N.; Ames B. N. *Science* **1987**, 235, 1043-1046.
21. Keshavan, P.; Schwemberger, S.J.; Smith, D.L.; Babcock, G.F.; Zucker, S.D. *Int. J. Cancer* **2004**, 112, 433-445.
22. Field, E.; Horst, H.M.; Rubinfeld, I.S.; Copeland, C.F.; Waheed, U.; Jordan J. *Am. J. Surg.* **2008**, 195, 304-307.
23. Vetvicka, V.; Sima, P.; Miler, I.; Bilej, M. *Folia Microbiol. (Praha)* **1991**, 36, 112-119.
24. Elson, L. A. *Radiation and Radiomimetic Chemicals* (Butterworth, London). **1963**.
25. Rao, P.; Suzuki, R.; Mizobuchi, S; Yamaguchi, T.; Sasaguri, S. *Biochem. Biophys. Res. Commun.* **2006**, 342, 1279-1283.

LIST OF SCHEMES

Scheme No.	Page No.
1.1: Balance between oxidant detoxification and generation maintain redox homeostasis	2
1.2: Model of cellular redox homeostasis by balance between pro-oxidants and antioxidants	3
1.3: Hypothesis of radiomodulation (Radioprotection/Radiopotentialiation) by alteration of cellular redox homeostasis	6
1.4: Different types of oxidative DNA damage induced by radiation	9
1.5: Radiation induced different types of syndrome	11
1.6: Structure of 1, 4 naphthoquinone (NQ)	17
1.7: Biosynthesis of naphthoquinone	20
1.8: Redox cycling and thiol arylation of 1,4 NQ	23
1.9: Chemical structure of the naturally occurring unconjugated bilirubin IX- α 4Z,15 Z	26
1.10: Synthesis of bilirubin	27
1.11: Structural isomer of bilirubin formed during phototherapy	28
1.12: Metabolism of bilirubin	30
1.13: Biological effects of bilirubin	32
1.14: Cytotoxic and cytoprotective effects of bilirubin	33
2.1: Hierarchical oxidative stress model and cellular responses	38
2.2: Low levels of ROS offer cytoprotection by adaptive response	41
2.3: Pluripotent hematopoietic stem cells (HSCs) and hematopoiesis	51
2.4: Proposed model of radioprotective effect of NQ	112
3.1: UCB induces immunotoxic effects by unknown mechanisms	116
3.2: Proposed model of radiomimetic and immunotoxic effects of UCB	165
4.1: Hypothesis of radiopotentiating effects of UCB	171
4.2: Schematic representation of radiopotentiating effects of UCB	204
5.1: Role of oxidative stress in the modulation of radiation response of cell	208
5.2: NQ induced activation of prosurvival pathways for radioprotection	211
5.3: Molecular pathways involved in immunotoxic effects of UCB	213
5.4: Pathways involved in UCB induced immunosuppression and infection	214
5.5: Pathways involved in UCB induced radiopotentialiation leading to increased infection and death	216

LIST OF TABLES

Table No.	Page No.
1.1: Physico-chemical properties of NQ	17
1.2: Structural formulas, systematic and trivial names and physical properties of the certain 1,4-naphthoquinones	18
1.3: Physico-chemical properties of bilirubin	26
2.1: Sequence of Primer used for mRNA expression of β -actin and HO-1	62
2.2: Sequence of Primer used for real time PCR analysis	63-64
2.3: NQ restored the radiation induced loss of proliferative potential of hematopoietic stem cells present in spleen	75
2.4: NQ administration to mice prevented WBI induced loss of splenocytes subsets	95
2.5: NQ administration to mice prevented WBI induced loss of hematological parameters	96
2.6: NQ administration to mice prevented WBI induced loss of proliferative potential of HSCs of bone marrow	101
3.1: Molar Ratio of UCB to BSA used in the study	120
4.1: UCB administration to mice potentiated WBI induced loss of splenocytes subsets	186
4.2: UCB administration to mice potentiated WBI induced loss of hematological parameters	187
4.3: UCB pretreated mice were more susceptible to WBI induced infection	193

LIST OF FIGURES

Figure No.	Page No.
2.1: NQ protected lymphocytes against radiation induced death	70
2.2: NQ protected lymphocytes against radiation induced death	71
2.3: Prooxidants protected lymphocytes against radiation induced death	72
2.4: NQ inhibited radiation induced death in lymphocytes	73-74
2.5: NQ restored the radiation induced loss of proliferative potential of hematopoietic stem cells present in spleen	74-75
2.6: NQ inhibited radiation induced apoptosis in lymphocyte when added post irradiation	75
2.7: NQ protected CD4+T cells and CD19+B cells against radiation induced death	76
2.8: NQ protected human PBMNCs and human intestinal epithelial cells (Int407) against radiation induced death	77-78
2.9: NQ inhibited radiation induced early events of apoptosis in lymphocytes	79
2.10: NQ upregulated antiapoptotic proteins (Bcl-2 and Bcl-xl) in lymphocytes	80
2.11: NQ perturbed intracellular redox balance by increasing basal ROS levels and depleting cellular GSH levels	82-83
2.12: NQ mediated radioprotection was abrogated by thiol antioxidants	84-86
2.13: NQ activated Nrf2 in lymphocytes	87-88
2.14: NQ upregulated Nrf2 dependent HO-1 expression in lymphocytes	88-89
2.15: NQ induced phosphorylation of ERK in lymphocytes	90
2.16: NQ increased intracellular calcium levels	92
2.17: <i>In vivo</i> radioprotection by NQ	93-94
2.18: NQ administration to mice inhibited WBI induced apoptosis in lymphocytes	97-98
2.19: NQ administration to mice elevated radioprotective cytokines	99
2.20: NQ administration to mice prevented WBI induced loss of functional response of lymphocytes and bone marrow	100-101
2.21: NQ administration to mice prevented WBI induced mortality	102-103
2.22: NQ did not protect tumor cells against radiation induced death	103
3.1: UCB induced immunotoxic and radiomimetic effects in lymphocytes	130
3.2: UCB induced immunotoxic effects in lymphocytes	131
3.3: UCB induced DNA strand breaks and decreased total RNA content in lymphocytes	132
3.4: UCB induced immunotoxic effects in activated lymphocytes	133
3.5: UCB induced immunotoxic effects in various immune cells	134
3.6: UCB induced immunotoxicity in lymphocytes from both mice	135
3.7: UCB from different sources induced immunotoxicity in lymphocytes	135
3.8: Purified UCB induced immunotoxic effects in lymphocytes and human PBMNCs	136
3.9: UCB exhibited immunosuppressive effects in lymphocytes and Macrophages	137-138

3.10: UCB exhibited immunotoxic effects by inducing both necrotic and apoptotic death	139-140
3.11: UCB induced both extrinsic and intrinsic apoptotic pathways	141-143
3.12: UCB induced apoptosis in lymphocytes by activating p38MAPK	144-145
3.13: UCB depleted cellular GSH levels in lymphocytes	147
3.14: UCB treatment to lymphocytes decreased the basal ROS level	148
3.15: Glutathione appeared a key molecule in the prevention of UCB induced cell death	149-150
3.16: UCB induced p38MAPK activation is mediated by depletion of GSH levels	151
3.17: UCB caused immunotoxicity and immunosuppression <i>in vivo</i>	152-153
3.18: UCB induced immunotoxicity was mediated by activation of p38MAPK <i>in vivo</i>	154-155
3.19: UCB administration caused oxidative stress <i>in vivo</i>	156-157
4.1: UCB potentiated radiation induced apoptosis in lymphocytes	179
4.2: UCB potentiated radiation induced cell death in lymphocytes	180-181
4.3: UCB potentiated radiation induced DNA strand breaks in lymphocytes	181
4.4: UCB potentiated radiation induced loss of MMP and calcium release in lymphocytes	182
4.5: UCB potentiated radiation induced apoptosis of various immune cells	183-184
4.6: UCB pretreatment of mice potentiated WBI induced immunosuppression	185
4.7: UCB pretreatment of mice potentiated WBI induced apoptosis in various immune cells	188
4.8: UCB pretreatment of mice decreased WBI induced loss of functional response of lymphocytes	189
4.9: UCB pretreatment of mice decreased WBI induced loss of functional response of PECs	190-191
4.10: UCB pretreated mice were more susceptible to WBI induced infection	192-193
4.11: UCB pretreatment of mice potentiated WBI induced p38MPAK activation in PECs	194-195

LIST OF ABBREVIATIONS

μl	Microleter
μM	Micromolar
ARE	Antioxidant Response Element
ARS	Acute Radiation Syndrome
ASK-1	Apoptosis Signal Regulated Kinase-1
ATRA	all-trans Retinoic Acid
B _f	Free Bilirubin
BMS	Bone Marrow Syndrome
BSA	Bovine Serum Albumin
B _T	Total Bilirubin
CFSE	Carboxy Fluorescein Diacetate Succinimidyl Ester
Con A	Concanavalin A
DEM	Diethylmaleate
DHE	Dihydroethidium
DHR-123	Dihydrorhodamine-123
DMSO	Dimethyl Sulfoxide
DTNB	Dithiobis 2-nitrobenzoic acid
ERK	Extracellular Signal Regulated Kinase
EtBr	Ethidium Bromide
FDA	Fluorescein Diacetate
GSH	Reduced Glutathione
GSSG	Oxidized Glutathione
GST	Glutathione-S-transferase
Gy	Gray
H ₂ DCF-DA	Dichlorodihydrofluorescein-Diacetate
H ₂ O ₂	Hydrogen Peroxide
HO-1	Hemeoxygenase-1
HPCs	Hematopoietic Progenitor Cells
HSCs	Hematopoietic Stem Cells
I.P.	Intraperitoneally
IFN-γ	Interferon- γ
IL-2, 4, 6, 1	Interleukin-2, 4, 6, 1
JC-1	5,5',6,6'-tetrachloro-1,1',3,3'- tetraethylbenzimidazolylcarbocyanine Iodide
Kbw	Kilogram Body Weight
LPS	Lipopolysachharide
MAP2K	Mitogen Activated protein Kinase Kinase
MAP3K	Mitogen Activated protein Kinase Kinase Kinase
MAPK	Mitogen Activated protein Kinase
MCB	Monochlorobimane
MEK1	Mitogen Activated Extracellular Signal Regulated Kinase1
MEKK1	Mitogen Activated Extracellular Signal Regulated Kinase Kinase1
mM	Milimolar
MMP	Mitochondrial membrane potential

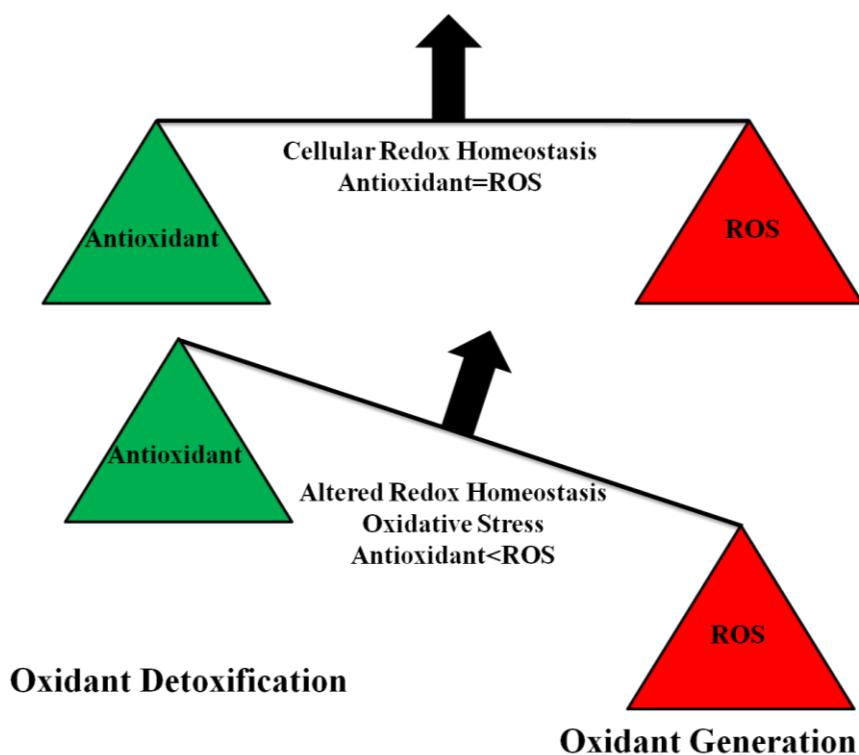
MnTBAP	Mn (III) tetrakis(4-benzoic acid) porphyrin
NAC	N-Acetyl Cysteine
NaOH	Sodium Hydroxide
NO	Nitric Oxide
NQ	1, 4 Naphthoquinone
NQO1	NADPH-quinoneoxidoreductase1
Nrf2	Nuclear Factor -E2 related Factor 2
PECs	Peritoneal Exudate Cells
PI	Propidium Iodide
PS	Phosphatidylserine
PTP	Permeability Transition Pore
ROS	Reactive Oxygen Species
SAPK	Stress Activated Protein Kinase
SB203580	4-[4-(4-fluorophenyl)-2-(4-methylsulfinylphenyl)-1H-imidazol-5-yl]pyridine
SIRS	Systemic Inflammatory Response Syndrome
SnPP	Tin-protoporphyrin
SOD	Superoxide Dismutase
t-BHQ	t-Butyl Hydroquinone
TNF- α	Tumor Necrosis Factor- α
UCB	Unconjugated Bilirubin
UV	Ultraviolet
WBI	Whole Body Irradiation
γ -GCS	γ -Glutamate Cysteine Ligase regulatory subunit

CHAPTER 1

INTRODUCTION AND REVIEW OF LITERATURE

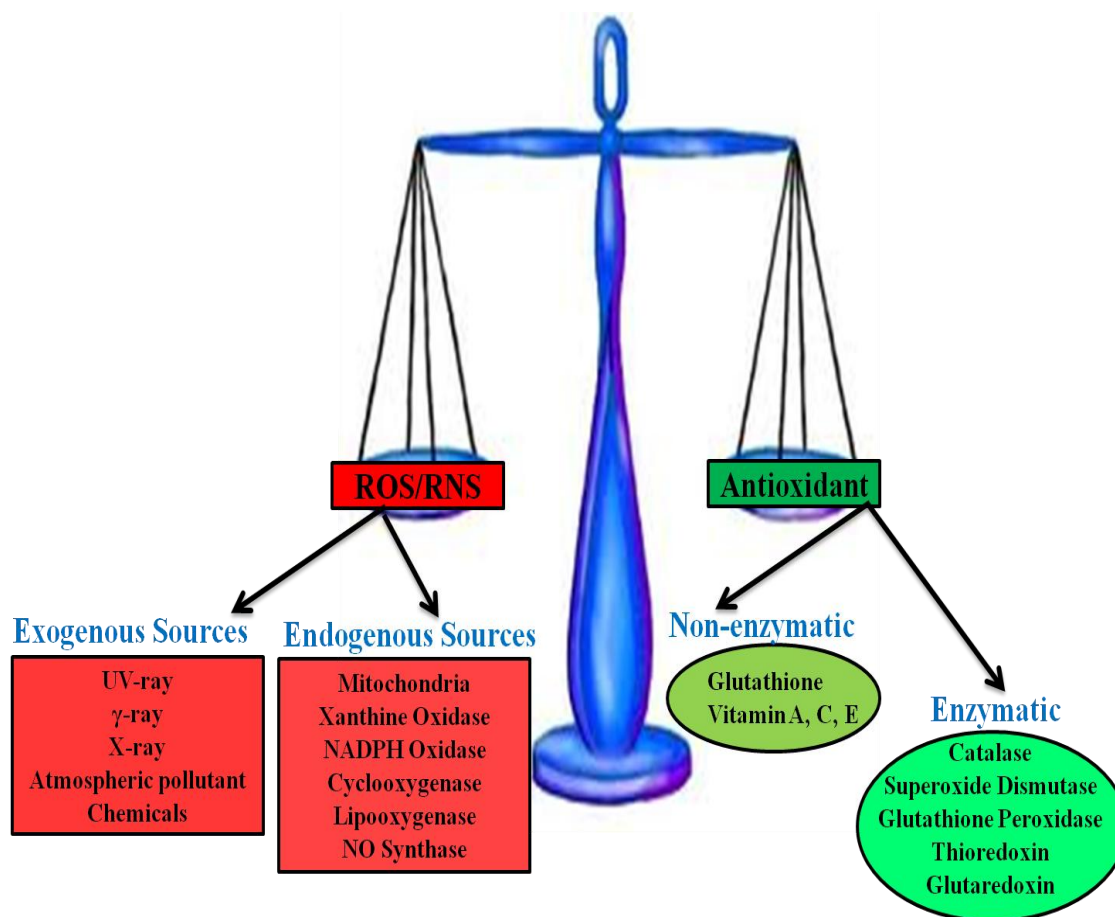
1.1 CELLULAR REDOX HOMEOSTASIS

Redox cellular homeostasis is a delicate balance between the rate and magnitude of oxidant generation and the rate of oxidant detoxification¹. Maintenance of redox homeostasis is essential to cellular function and survival and ensures that the cells respond properly to endogenous and exogenous stimuli². The delicate balance between ROS (reactive oxygen species) generation and elimination is maintained by many complex mechanisms, and a dysfunction of any of these mechanisms could lead to alterations in cellular redox status which can promote cell death or cell survival, depending on the magnitude of the stimuli and extent of oxidative stress³. Oxidative stress is the pathogenic outcome resulting from an imbalanced ratio between ROS production and ROS elimination by cell's antioxidant capacity¹ (Scheme 1.1).



Scheme 1.1: Balance between oxidant detoxification and generation maintain redox homeostasis

A low level of ROS is normally produced in cells during respiratory chain chemical reactions in mitochondria via reduction of oxygen into H_2O , which is the main source of intracellular ROS, the cellular ROS level may be increased during various biological processes including inflammatory reactions⁴. Exposure to oxidative chemicals and external stresses including heavy metals, ultraviolet, ionizing irradiation, drugs and microbial infections may also induce an abnormal increase in ROS levels. Cells are equipped with enzymatic and non-enzymatic antioxidant systems to eliminate ROS and maintain redox homeostasis³ (Scheme 1.2).



Scheme 1.2: Model of cellular redox homeostasis by balance between pro-oxidants and antioxidants

1.2 ALTERATION OF CELLULAR REDOX AS A NOVEL STRATEGY TO MODULATE RADIATION INJURY (HYPOTHESIS OF THESIS WORK):

Although ROS were traditionally been considered as destructive molecules, growing evidence shows that ROS-inducible stress evokes many intracellular events, such as proliferation, gene activation, cell-cycle arrest, and apoptosis⁵. This dual function of ROS, as signaling or damaging molecules, depends mainly on differences in their concentrations, pulse duration and subcellular localization⁶. High amount of ROS function as toxin and induce cell death, whereas low levels behave as second-messenger and known to induce pro-survival pathways by activating redox-sensitive transcription factors like NF-E2–related factor 2 (Nrf2)².

Being highly reactive in nature ROS, when produced at high rate can interact in a nonspecific way with a wide range of macromolecules, including proteins, carbohydrates, lipids, and DNA, thus leading to the alteration and impairment of function of all cellular components leading to apoptosis⁷. There are two major pathways through which apoptosis are induced; one involves death receptors and is exemplified by Fas-mediated caspase-8 activation, and another is the stress or mitochondria-mediated caspase-9 activation pathway. Both pathways converge on caspase-3 activation, resulting in nuclear degradation and cellular morphological change. Oxidative stress induces cytochrome-c release from mitochondria and activation of caspases, p53, and kinases, including apoptosis signal-regulating kinase 1 (ASK1), c-Jun N-terminal kinase, and p38 mitogen-activated protein kinase⁸.

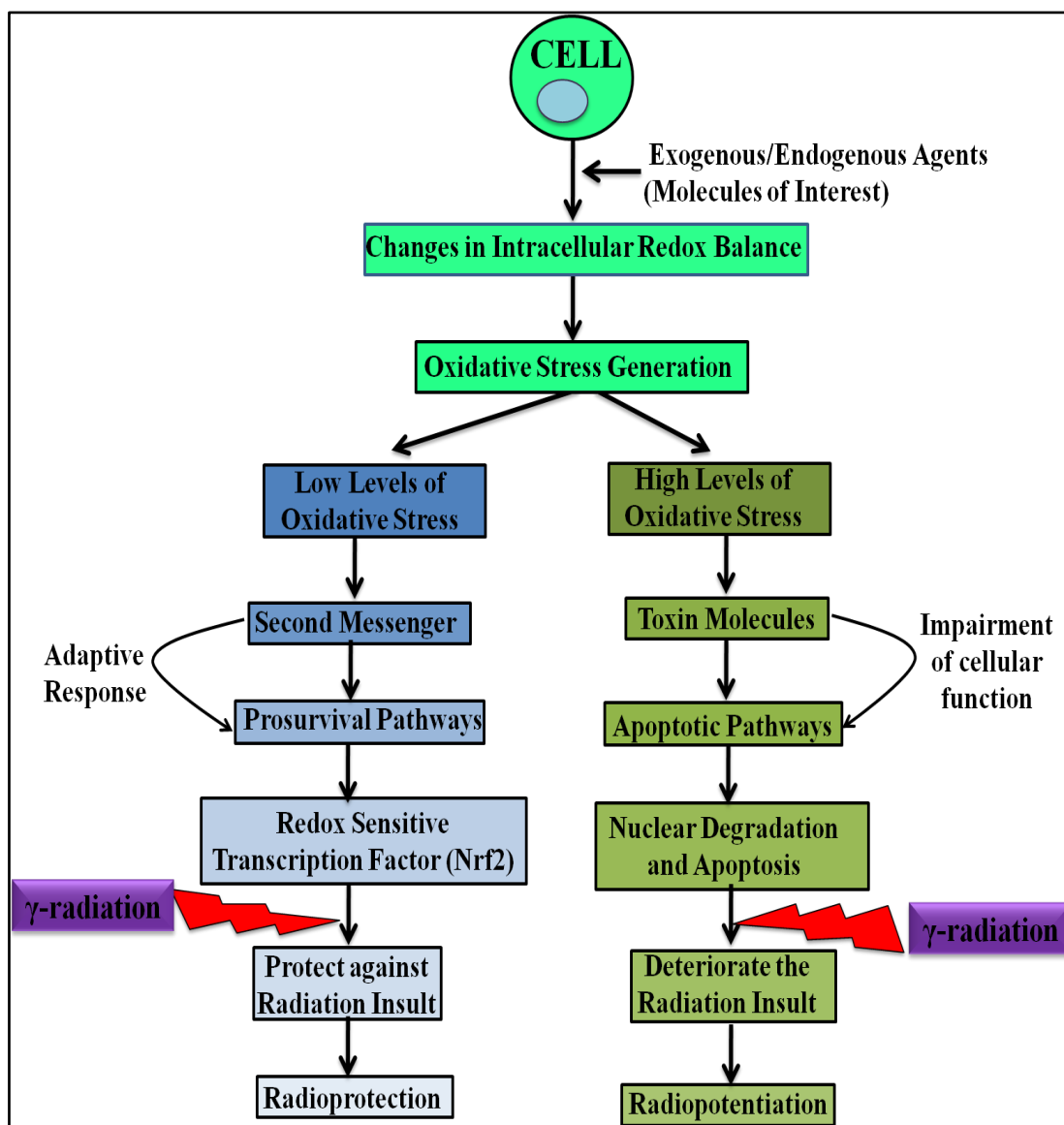
ROS, when generated at low rate serves to maintain the cellular homeostasis and can activate several redox-sensitive prosurvival signaling pathways and function as second messengers in the transduction of several extracellular signals¹. A complex

intracellular redox buffering network has developed to adapt and protect cells against the dangerous effects of oxidative stress, an adaptive response serving to counteract redox perturbations¹.

Modulation of gene expression is a common end point exerted by cells to defend themselves against ROS insults. Transcription factors could be considered immediate response genes that respond to a wide variety of environmental agents inducing oxidative stress⁹. One of the redox sensitive factors is Nrf2 which control the fate of cells through transcriptional upregulation of antioxidant response element (ARE)-bearing genes, including those encoding for endogenous antioxidants, phase II detoxifying enzymes, and transporters¹⁰. Expression of the Nrf2-dependent proteins is critical to maintain cellular redox homeostasis through elimination of toxicants/carcinogens. Hemeoxygenase-1 (HO-1) is one such protein responsible for the degradation of prooxidant heme into ferrous iron, carbon monoxide, and biliverdin, which is converted into bilirubin; its end-products have antioxidant activities that are able to defend cells from oxidative stress¹¹.

In the present thesis, we exploited the above two different modes of cellular redox alteration (low levels and high levels of ROS generation) as a novel strategy in the modulation of radiation injury. We hypothesized that alterations in cellular redox homeostasis can modulate the response of cell to exposure of ionizing radiation. Alteration in cellular homeostasis by exogenous sources can perturbed the intracellular redox balance which could either enhance cell survival or promote cell death upon subsequent radiation exposure, depending on extent of redox perturbation and oxidative stress generation. Oxidative stress generated by initial exposure of cells with exogenous sources either stimulate prosurvival pathways or proapoptotic pathways depending on magnitude of ROS generation and redox perturbation. The final decision, whether the

cells will survive or die due to radiation exposure, is the overall outcome of the integration of signals from redox-sensitive factors and other regulatory mechanisms (Scheme 1.3).



Scheme 1.3: Hypothesis of radiomodulation (Radioprotection/Radiopotential) by alteration of cellular redox homeostasis

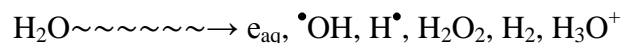
In the present thesis work, by employing either an exogenous agent or an endogenous agent (molecules of interest) we have modulated the redox status of cells. The doses were carefully selected so as to produce either a low oxidative stress or a high oxidative stress generation both *in vitro* and *in vivo* conditions. We hypothesized that the generation of oxidative stress by exposure of mammalian system to the above molecules of interest will modulate the radiation response of cells in two ways-either protect or potentiate the radiation injury. The exogenous agent used in the present thesis, is 1, 4 naphthoquinone (NQ) and endogenous agent used to modulate the redox status of cells are unconjugated bilirubin (UCB). NQ is a model molecule for biologically important quinones and has ability to generate ROS levels by both redox-cycling and thiol arylation¹². We have used optimum concentration of NQ (0.05-1 μ M) so that it can induce low levels of oxidative stress which could protect cells against subsequent radiation challenge via activation of adaptive response pathways like Nrf2 activation. Unconjugated bilirubin (UCB), the major form of bilirubin (about 96%) in the normal plasma, is an active participant in various diseases process at higher concentrations¹³. UCB at clinically relevant concentrations (50-100 μ M) has been shown to induce oxidative stress and activate apoptotic signaling in various cells including murine hepatoma Hepa 1c1c7¹⁴, human adenocarcinoma¹⁵, colon cancer¹⁶, cultured bovine brain endothelial cells¹⁷ and developing rat brain neuron¹⁸. Therefore in the present study, clinically relevant concentrations of UCB between 10-100 μ M has been chosen, so that it can induce high levels of oxidative stress and could further deteriorate the host condition upon subsequent radiation challenge and lead to radiopotentialiation. Hence, NQ would behave as radioprotector by protecting against insult, whereas UCB would behave as radiopotentialiator by potentiating the radiation injury.

1.3 IONIZING RADIATION AND ITS BIOLOGICAL EFFECTS

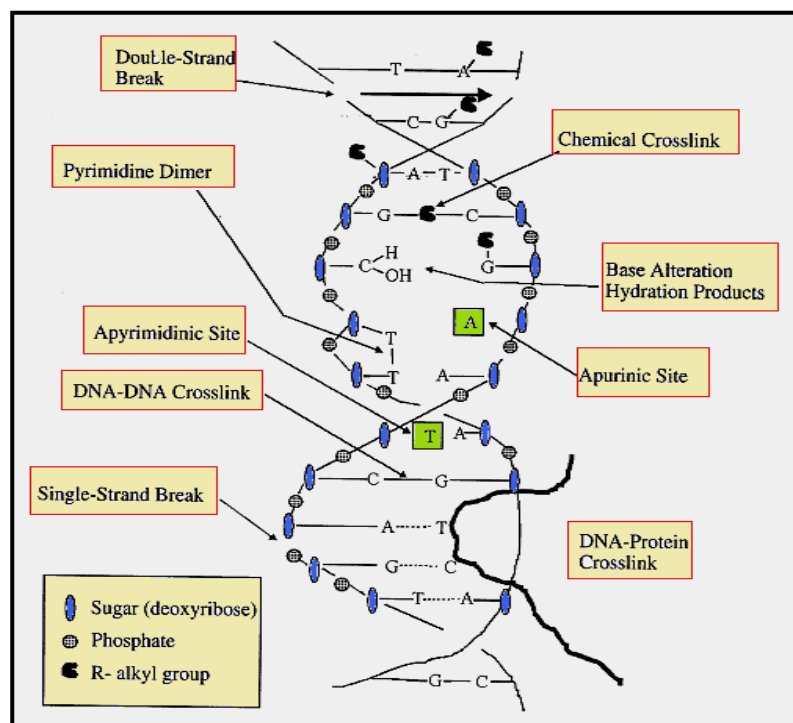
1.3.1 Ionizing radiation and its interaction with matter:

Short wave length electromagnetic radiations (X-rays, γ -rays) and particle radiations (fast electrons, α - particles, protons, deuterons, neutrons, etc) are high-energy radiations (KeV to MeV range) and have ability to ionize the medium through which they pass and hence they are called as ionizing radiation¹⁹. Since the discovery of X-rays by Roentgen in 1895 and radioactivity by Bacquerel in 1896, ionizing radiation has been used increasingly in medicine both for diagnosis and treatment²⁰. Currently ionizing radiation is being used in a large number of therapeutic, industrial and other applications apart from for generation of nuclear power and developing new varieties of high-yielding crops and enhancing storage-period of food materials. Although use of radiation is increasing in our day to day life, it has been considered an enigma to the general public and the use of radiation for therapeutic and other uses has always been associated with some skepticism. The deleterious effects of radiation on human health became evident after study of the health related abnormalities in Japanese atom bomb survivors of 1945. Since then understanding the mechanisms of radiation induced injury to living cells has been a key research area of radiation biologists and radiation chemists²¹. Today it is well established that radiation exposure initiates injury at cellular level. The deleterious effects of ionizing radiation are known to be mediated both through the direct and indirect effects. Direct effect of radiation can be due to absorption of energy directly by DNA, leading to ionization of both the nitrogenous bases and sugar to generate single and tandem DNA damage¹⁹. Indirect effect of ionizing radiation is mediated through ROS and account for approximately 75% of the damage to cells^{19,22}. When ionizing radiation interacts with living cell, water being a major (70%) constituent of the cell, undergoes

radiolysis producing highly reactive free radical species, viz. hydrogen radicals, hydroxyl radicals, hydroperoxyl radicals and superoxide radicals. In addition to this, other molecular species like hydronium ions (H_3O^+) and hydrogen peroxide are also produced²³⁻²⁶.



The relative yields of these species vary with the linear energy transfer (LET) of the radiation. Among the various radical species, hydroxyl radicals have been considered to be primarily responsible for most of the radiation induced cellular damage^{24,25}. Ionizing radiation targets primarily DNA and produces an array of lesions that include single and double strand breaks, base alterations, loss of purines/pyrimidines (apurinic/apyrimidinic sites), damage to the deoxyribose sugar, DNA-protein cross-linkage and damage to the DNA repair system^{27,28} (Scheme 1.4).



Scheme 1.4: Different types of oxidative DNA damage induced by radiation

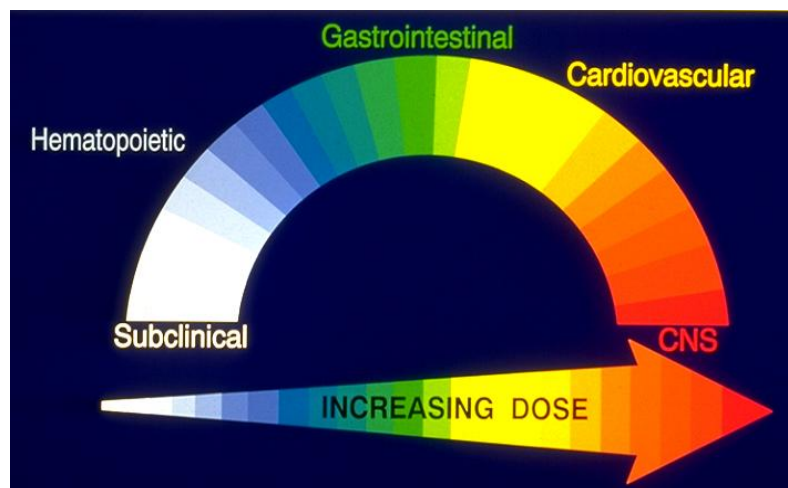
The reactivity of $\cdot\text{OH}$ is in order of pyrimidines > purines > deoxyribose. There are several products of oxidation; the prominent one being thymine glycol. Unlike $\cdot\text{OH}$, the reaction of $^1\text{O}_2$ with DNA is highly specific. Among the bases it reacts only with guanosines and hence $^1\text{O}_2$ induced strand breaks occur specifically at guanine residues. The products of $^1\text{O}_2$ induced DNA damage include 8-hydroxyguanosine (8-OHdG) and cyanuric acid²⁹.

1.3.2 Biological effects of ionizing radiation:

Cellular damage is considered to be the origin of tissue and organ damage leading to acute radiation syndrome and mortality. Not all living cells are equally sensitive to radiation. Those cells which are actively reproducing are more sensitive. This is because dividing cells require correct DNA information in order for the daughter cells to survive. Different cell systems have different sensitivities for example; organs like brain, bone, muscle, thyroid, pituitary, adrenal, and liver are radioresistant, whereas others like the lymphoid organs, reproductive organs, bone marrow, and intestinal crypts are radiosensitive²⁴. Biological effects of radiation are of two types-deterministic and stochastic effects. **Deterministic effects** are those effects which are produced by high levels of radiation exposure and are clinically visible, whereas the effects of low levels of radiation are more difficult to determine because the deterministic effects do not occur at these levels. These effects include some forms of cancer and genetic effects. These effects are called as **stochastic effects**.

Depending on the type and dose of radiation exposure, all these events occur within hours to weeks and sometimes even months after the radiation exposure. Acute doses can cause a pattern of clearly identifiable symptoms (syndromes). These conditions are referred to in general as acute radiation syndrome. Radiation sickness symptoms are

apparent following acute doses ($\geq 1\text{Gy}$). High doses tend to kill cells, while low doses tend to damage or change them. The initial signs and symptoms of the acute radiation syndrome are nausea, vomiting, fatigue, and loss of appetite. As the dose increases above 1.5Gy , one of the three radiation syndromes begins to manifest itself, depending upon the level of the dose.



Scheme 1.5: Radiation induced different types of syndrome

These syndromes are: **Hematopoietic (Bone marrow) syndrome** ($2\text{-}6\text{Gy}$) is characterized by damage to cells that divide at the most rapid pace (such as bone marrow, the spleen and lymphatic tissue). The death of exposed individual takes a relatively longer time (i.e., within 30 days) due to the loss of bone marrow cells and symptoms include internal bleeding, fatigue, bacterial infections, and fever. **Gastrointestinal tract syndrome** ($8\text{-}15\text{Gy}$) is characterized by damage to cells that divide less rapidly (such as the linings of the stomach and intestines). The death of the individual occurs between 3 to 10 days due to failure of the gastrointestinal tract. Symptoms include nausea, vomiting, diarrhea, dehydration, electrolytic imbalance, loss of digestion ability, bleeding ulcers, and the symptoms of blood-forming organ syndrome^{26,30}. **Central nervous system syndrome (CNS)** ($>25\text{Gy}$) is characterized by damage to cells that do not reproduce such

as nerve cells. The death occurs within minutes or up to 48h and symptoms includes loss of coordination, confusion, coma, convulsions, shock, and the symptoms of the blood forming organ and gastrointestinal tract syndromes^{26,30}.

1.4 NEED FOR MODULATION OF RADIATION INJURY

There is an increased use of ionizing radiation in various aspects of human life especially in areas pertaining to radiotherapy of cancer, food preservation, agriculture, industry and power generation. Since use of ionizing radiation in various aspects of human life is seemingly increasing, there is a great need to understand the mechanisms of radiation injury and also to modify the effects of ionizing radiation. Agents that modify the effects of radiation are called radiomodifiers. These can be either radioprotectors or radiopotentiators. The agents which intensify the harmful effects of radiation are called radiopotentiators, whereas agents which ameliorate deleterious effects of radiation are known as radioprotectors. Development of radiation modifier enhances the safer and controlled use of ionizing radiation for human welfare. Developing such radiation modifiers which modify the host response following radiation injury is a challenge to life scientists and has been a key research area of radiation biologists and radiation chemists.

1.4.1 Radioprotectors:

A radioprotector is a chemical compound capable of minimizing the damaging effects of ionizing radiation to normal cells. The potential application of radioprotective chemicals in the event of planned exposures or radiation accidents/incidents has been investigated from the beginning of the nuclear era³¹. Radioprotectors might be useful adjuncts in radiotherapy if they can increase the tolerance of normal tissues while not affecting, or even increasing, sensitivity of tumors. An ideal radioprotector should be

inexpensive, have no toxic implications, and can be orally administered, with rapid absorption and a reasonably good dose modifying factor (DMF)³². In animal studies, DMFs are typically determined by irradiating mice with and without administered agents at a range of radiation doses and then comparing the endpoint of interest³³. The first *in vivo* studies on the protective effects of a sulphur containing amino acid against ionizing radiation were conducted by Patt & co-workers³⁴. They reported that cysteine, a sulfur-containing amino acid, could protect rats from a lethal dose of X-rays. Subsequently Bacq et al. (1951) reported that cysteamine, the decarboxylated form of cysteine, could also protect rats against lethal doses of X-rays³⁵.

In the last one decade, several synthetic sulfhydryl compounds have also been screened for their radioprotective ability³⁶. However, the most effective radioprotective drug developed till date, and the only agent approved by the FDA for use in the protection of normal tissues in patients treated with radiation is amifostine (S-2-[3-aminopropylamino] ethylphosphorothioic acid)^{37,38}. It is a complex aminothiols, which is reported to exhibit multiple biochemical properties like free radical scavenging activity, high affinity for DNA and the structural similarity with cellular polyamine³⁹. Although, amifostine is a clinically approved radioprotector, it exhibits considerable toxicity at radioprotective doses, warranting the search for new effective and non-toxic radioprotectors⁴⁰. Therefore, extensive research on modulation of radiation-induced changes by competent agents using *in vitro* and *in vivo* models is required.

Several novel approaches are on to locate a potent radioprotector. These include mimics of antioxidant enzymes, nitroxides, melatonin, growth factors, immunomodulators, gene therapy, hyperthermia apart from natural products.

Radioprotective agents can be classified as: (i) chemical radioprotectors, (ii) adaptogens, and (iii) absorbents. The first group constitutes mainly sulfhydryl compounds and other antioxidants³³. **Adaptogens** act as stimulators of radioresistance. These are natural protectors that offer chemical protection under low levels of ionizing radiations. They are generally extracted from the plants/animals and have least toxicity. They can influence the regulatory system of exposed organisms, mobilize the endogenous background of radioresistance, immunity, and intensify the overall nonspecific resistance of an organism. **Absorbents** protect organisms from internal radiation and chemicals. Post-irradiation radioprotectors are important when an accidental exposure occurs during operation of equipments with radiation source or intentional exposures during war and such unnatural calamities. The radioprotectors can elicit their action by various mechanisms such as: (1) Suppressing the formation of free radicals, (2) Detoxifying the radiation induced reactive species, (3) Inducing the cellular antioxidant defense machinery such as SOD (superoxide dismutase), GSH (glutathione), Catalase, GPx (glutathione peroxidase), and Prostaglandins etc (4) Enhancing the DNA repair by triggering one or more cellular DNA repair pathways, (5) Delaying cell division and inducing hypoxia in the tissues,⁴¹ (6) Synchronizing cells in S phase of cell cycle to enhance the repair of damage, (7) Stimulation of immune system by various immunostimulatory cytokines like GM-CSF, CSF, G-CSF, and IL-1, 3, 6 and (8) Activator of cellular signal transduction pathways like NF-KappaB activator such as CBLB 502⁴².

In the present study we have used a novel strategy to search for radioprotector, “activation of prosurvival pathways by alteration of redox status of cells with the use of

prooxidants". The strategy of activating prosurvival pathways by use of prooxidants to attain radioprotection has certain advantage over the use antioxidants as radioprotector. For an antioxidant to serve as radioprotector it has to be present in each and every cells of exposed individual, among cells each and every organelle and further antioxidant has to be present throughout the cells in a sufficient enough concentration to nullify the toxic effects of ROS induced by radiation. Achieving such high concentration of antioxidant throughout the system suffice to detoxify free radicals is practically not possible. Further, the efficacy of antioxidant to neutralize free radicals is known to depend not only on its local concentration at the site of radical generation but also on its reaction rate constant with the free radicals. Because of these limitations antioxidants property alone could not completely protect against radiation insult. However, activation of prosurvival pathways by use of prooxidants prior to radiation exposure, prime the cells to counterbalance the radiation insult.

1.4.2 Radiopotentiators:

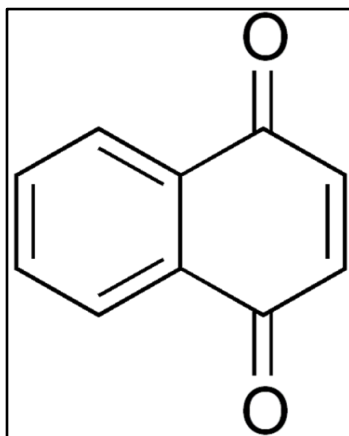
The agents which amplify the harmful effects of radiation and further deteriorate the host conditions are called radiopotentiators. For safe use of ionizing radiation in human welfare, research on radiopotentiators also finds same importance as radioprotectors occupy. Radiopotentiating agents intensify the radiation effects either by inducing the similar apoptotic signaling events as radiation does, or might activate other deleterious and damaging signaling pathways. The final outcome of host conditions depends upon integration of signaling events induced by radiation and radiopotentiators. Radiopotentiator worsen the effects of radiation due to summation of intensity of apoptotic stimuli. Radiopotentiating agents and ionizing radiation might have common

denominators for deteriorating the host conditions and might share common stimulus of apoptotic induction such as activation of MAPK, induction of ROS, depletion of cellular GSH, mitochondrial dysfunction and activation of caspases. Therefore, extensive research on radiopotentiators is critical for proper understanding of modulation of radiation injury. If one knows the agents or conditions which can amplify the deleterious effects of radiation, careful monitoring for presence of such conditions/agents may avoid the excessive damage. Moreover, radiation exposure during course of radiotherapy may be planned in such a way which minimizes the presence of any plausible radiopotentiators.

The work in this thesis deals with studies on 1,4 naphthoquinone and unconjugated bilirubin, therefore a brief introduction about these compounds is given in the subsequent sections.

1.5 1, 4 NAPHTHOQUINONE (NQ)

1, 4 naphthoquinone (NQ), is a bifunctional para-quinone which has been studied as a model of quinone compounds. NQ is also known as 1,4-naphthalenedione, alpha-naphthoquinone, p-naphthoquinone, 1,4-naphthylquinone, 1,4-dihydro-1,4-diketo naphthalene. 1, 4-Naphthoquinone is one of simplest quinone studied. It can be viewed as derivatives of naphthalene through the replacement of two hydrogen atoms by two ketone groups, hence it is also known as 1, 4-naphthalenedione. The structure of 1, 4 naphthoquinone is shown in scheme 1.6.



Scheme 1.6: Structure of 1, 4 naphthoquinone (NQ)

Naphthoquinone is a class of natural phenols based on the C₆-C₄ skeleton, sometimes referred to as a naphthyl functionality. It forms the central chemical structure of many natural compounds, most notably the K vitamins. The physicochemical properties of NQ are listed in table 1.1.

1,4 Naphthoquinone	PROPERTIES
Molecular Formula	C ₁₀ H ₆ O ₂
Molecular Weight	158.15
Appearance	yellow to brown powder
Solubility	Water, DMSO
Melting Point	125-128°C
Density	1.422
Odor	Pungent odor
Photosensitivity	Yes

Table 1.1: Physico-chemical properties of NQ

1.5.1 Chemical synthesis of NQ and its derivatives:

Chemical structure of monomeric naphthoquinones is based on bicyclic system—naphthalene skeleton substitute in position C1 and C4 (1, 4-naphthoquinones) or C1 and C2 (1, 2- naphthoquinones). Dimeric and trimeric naphthoquinones are also known. Most of them are colored compounds. Their colors usually vary between yellow, orange and brown. Almost all naphthoquinones are soluble in alcohol, acetone, chloroform, benzene, DMSO and acetic acid. The simplest, and in the nature the most widespread naphthoquinones, are juglone, lawsone, plumbagin and lapachol. One of the common nucleus of these quinones is 1, 4-naphthoquinone, which share structural homology in wide range of quinoid compounds. Some of the common quinones which have 1, 4 NQ as main nucleus are listed in table 1.2.

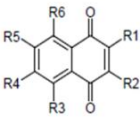
	Substituent	Systematic (Trivial) Name	Molecular Weight	Melting Point [°C]
	-	1,4-naphthoquinone	158.15	119 – 122
	R3 = -OH	5-hydroxy-1,4-naphthoquinone (juglone)	174.14	155
	R1 = -OH	2-hydroxy-1,4-naphthoquinone (lawsone)	174.15	192 – 195
	R1 = -CH ₃ , R3 = -OH	5-hydroxy-2-methy-1,4-naphthoquinone (plumbagin)	188.18	78 – 79
	R1 = -CH ₃	2-methyl-1,4-naphthoquinone (menadion)	172.18	105 – 107
	R3, R6 = -OH	5,8-dihydroxy-1,4-naphthoquinone (naphthazalin)	190.16	237
	R1, R3, R5 = -OH	2,5,7-trihydroxy-1,4-naphthoquinone (flaviolin)	206.17	164 – 168.5
	R1 = - CHOHCH ₂ CH=C(CH ₃) ₂ R3, R6 = -OH	5,8-dihydroxy-2-(1-hydroxy-4-methyl-pent-3-enyl)-1,4-naphthoquinone (shikonin)	288.30	Not available
	R1 = -OH R2 = -CH ₂ CH=C(CH ₃) ₂	2-hydroxy-3-(3-methyl-but-2-enyl)-1,4-naphthoquinone (lapachol)	242.27	141 – 143

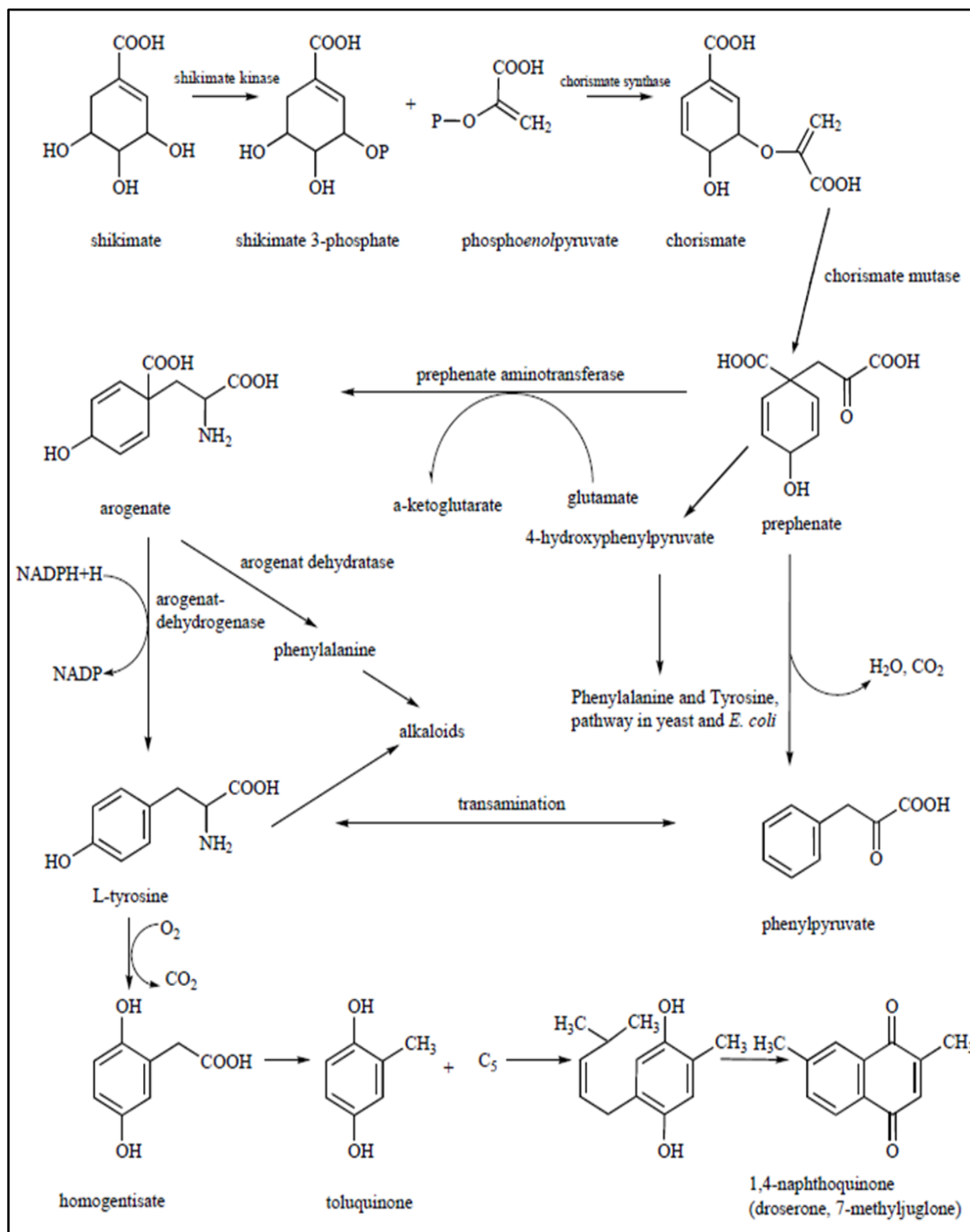
Table 1.2: Structural formulas, systematic and trivial names and physical properties of the certain 1,4-naphthoquinones(Adapted from Babula P et al 2009)

Naphthoquinones are one of the groups of secondary metabolites widespread in nature. The most important higher plant families containing naphthoquinones are Avicenniaceae, Bignoniaceae, Boraginaceae, Droseraceae, Ebenaceae, Juglandaceae, Nepenthaceae and Plumbaginaceae. In plants, they commonly occur in the reduced and glycosidic forms. They are biosynthesized via a variety of pathways including acetate and malonate pathway (plumbagin), shikimate/succinyl CoA combined pathway (lawsone) and shikimate/mevalonate pathway (alkannin). For example Droserone or juglone are biosynthesized via shikimate pathway. Molecule of shikimic acid condense molecule of α -ketoglutaric acid and forms naphthoquinones of droserone or juglone type. The second biosynthetic pathway includes synthesis of shikimic acid through aromatic amino-acid L-tyrosine. Plumbagin and 7-methyljuglone are two important products of this pathway (Scheme 1.7).

1.5.2 Clinical significance of NQ:

NQ is parent molecule of many clinically approved anticancer, anti-infective, anti-parasital drugs. There are many clinically important agents containing a quinone nucleus with excellent anticancer activity (e.g. anthracycline, mitoxantrones, mitomycin, diaziquone, saintopin daunorubicin and doxorubicin). Quinone comprises the second largest class of anti-tumor agents currently in use. Quinones are ubiquitous in nature and probably found in almost all respiring animals and plants, and have important role to maintain their biological functions⁴³.

Quinones, including ubiquinone (coenzyme Q10), acts as electron carrier in mitochondrial electron transport chain besides taking part in the blood clot action as phyloquinone (vitamin K1), which is naphthoquinone derivative⁴⁴.



Scheme1.7: Biosynthesis of naphthoquinone (Adapted from Babula P et al 2009)

Recently, pyrroloquinoline quinone (PQQ), which is a redox cofactor of bacterial dehydrogenases, was reported as a vitamin for mice. Moreover, in the process of

photosynthesis cycle in plant and bacteria, it is well known that plastoquinone has an essential role⁴⁴. In addition to these biological roles, quinones have wide variety of industrial usage, as herbicide, bleaching reagent, and cosmetic. It is reported that quinones serves as a potent inhibitor of some biological functions such as nitric oxide synthase activity and progesterone secretion. Most of the clinically important quinones belong to the groups of DNA intercalating and/or alkylating agents, and/or topoisomerase inhibitors^{45,46}.

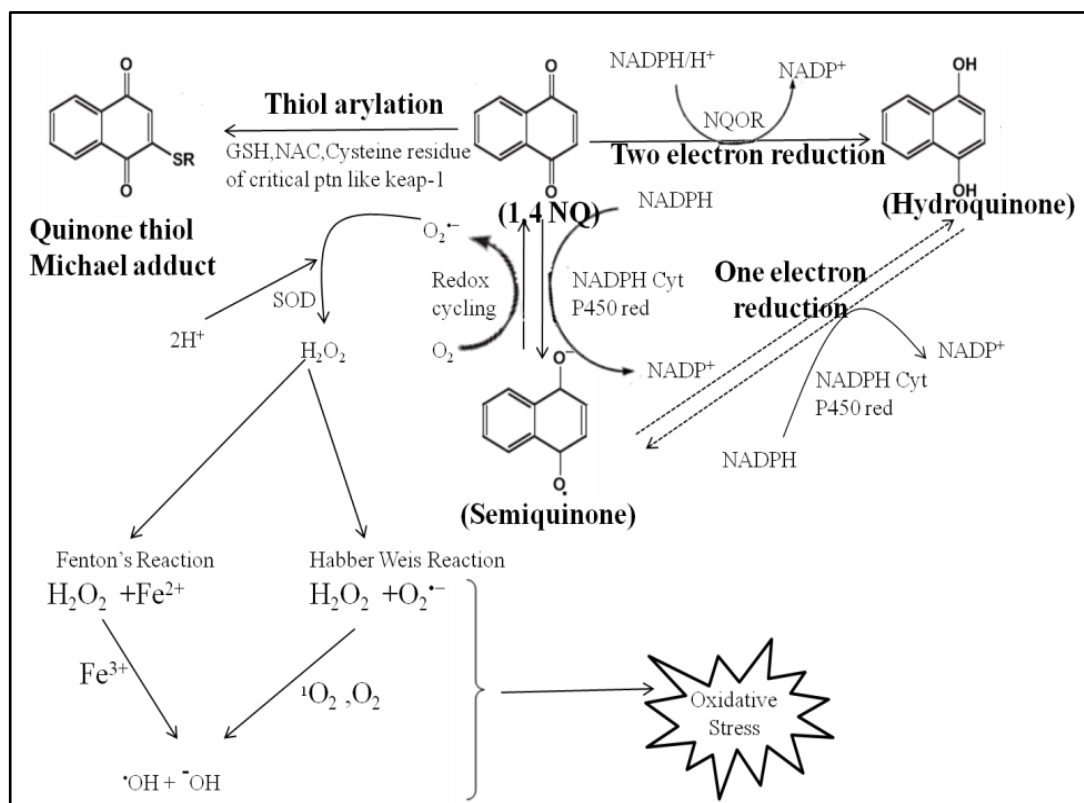
There are many clinically approved drugs which are chemically derivatives of naphthoquinone either in monomeric, dimeric or trimeric form. Monomeric naphthoquinones, are oxygen-derivatives of naphthalene, substituted in position C1 and C4 (1,4-naphthoquinones) or C1 and C2 (1,2- naphthoquinones). **Atovaquone**, a hydroxy derivatives of 1,4 NQ, showed clinical promise for the treatment of malaria and the AIDS-associated diseases, *Pneumocystis carinii* pneumonia and toxoplasmosis⁴⁷. **Mepron** (GlaxoSmithKline) suspension, a formulation of micro-fine particles of atovaquone is currently used as effective antiprotozoal agent against *Pneumocystis carinii*, and *Plasmodium species* by inhibiting dihydroorotate dehydrogenase, a critical enzyme in the requisite pyrimidine biosynthesis, by irreversibly binding to the mitochondrial cytochrome b, c1 complex and as a consequence locking electron transport chain⁴⁷. **Malarone** (Glaxo Wellcome, Inc., Research Triangle Park, NC), a fixed-dose combination of atovaquone and proguanil hydrochloride is effective against strains that are resistant to a variety of other antimalarial drugs, and has a favorable safety profile⁴⁸. **Nanaomycin**, an antibiotics produced by a strain of *Streptomyces* is another hydroxy derivative of 1,4 NQ and involved in heme dependent radical generation and inhibiting

coupling of oxidative phosphorylation⁴⁹. It shows inhibitory effect on proteins, nucleic acids and cell wall peptidoglycans in Gram-positive bacteria. **Diospyrin** a, bisnaphthoquinone which is dimer of hydroxyl derivative of 1,4 NQ act as an antitumor compound capable of inhibiting the growth of *Leishmania donovani* promastigotes by inhibiting type I DNA topoisomerase. It also induces stabilization of the “cleavable complex” mediated by topoisomerase⁵⁰.

1.5.3 Prooxidant effects of NQ:

Quinone undergoes metabolism via redox cycling and form semiquinone radicals either by one electron reduction in the presence of NADPH–cytochrome P450 reductase and NADH–cytochrome b reductase or by DT-diaphorase (quinone reductase) catalyzed two electron reduction followed by a subsequent one electron oxidation. During one electron transfer NADPH act as electron donor and transfer its two high potential electrons in presence of reductase forming semi-quinone radical intermediate which reduces molecular oxygen, producing superoxide anion($O_2^{\bullet-}$), and leads to redox-cycling reactions and continues until system become anaerobic. The resultant superoxide either dismutate spontaneously or reacts with superoxide dismutase (SOD) to form hydrogen peroxide (H_2O_2)^{51,52}. H_2O_2 then participates in Fenton reactions, generating hydroxyl radicals^{52,53}. Apart from these, $O_2^{\bullet-}$ and H_2O_2 can participate in Habber Weis reaction and react together in a process catalyzed by certain metal ions, to form even more deleterious oxygen species such as the hydroxyl radical ($\bullet OH$) and singlet oxygen (1O_2). In contrast, two-electron reduction by NAD(P)H quinone oxidoreductase1 (NQO1) can compete for the quinones with the one-electron reductases and produce hydroquinones or quinols which protects the cell from the formation of reactive intermediates⁵¹. Although the

hydroquinones are generally more stable than their semiquinones with respect to reactions with O_2 , they can undergo autoxidation to yield H_2O_2 ⁵³. Although all quinones are redox-cycling agents that generate ROS, partially substituted quinones also function as arylating agents, reacting with cellular nucleophiles such as thiols on cysteine residues of proteins, glutathione (GSH), and detoxifying reagents such as N-acetylcysteine (NAC). These covalently linked quinone-thiol adduct called Michael adducts also retain the ability to function as redox-cycling agents¹². 1, 4 naphthoquinone, one such bifunctional para-quinone studied in biomedical research is the capable of both redox-cycling and thiol arylation (Scheme1.8).



Scheme1.8: Redox cycling and thiol arylation reaction of 1,4 NQ

1.5.4 Biological effects of NQ:

Quinones are ubiquitous in nature, both as natural products and as pollutants including in diesel exhaust and in foods. They are also generated in the body as a result of xenobiotic metabolism via the cytochrome P450 system. NQ, one of the simplest quinones, has been studied as a model of quinone compounds. The most of biological activities of NQ is due to their ability to accept one and/or two electrons to form radical anion or dianion species. The redox cycling of NQ has therefore, been widely implicated as a mechanism for their cytotoxicity. In general, quinone toxicity has been attributed to the ability to undergo reversible oxidation-reduction reactions, as well as to its electrophilic nature leading to the formation of free radicals^{54,55}. Because of their ability to generate reactive oxygen species (ROS) and induce oxidative stress, quinones possess broad antitumor activities. Antitumor activity of quinones largely depends on their prooxidant property. Quinone occupies second largest family of antitumor drug. To our knowledge, all quinone containing anticancer drugs like adriamycin, mitomycin, diaziquone, daunorubicin and doxorubicin etc. undergo redox cycling at different rate and produces ROS which is responsible for initiation of tissue damage selectively in tumor cells and this seems to be a promising approach for targeting cancer cells^{51,52}.

Kayashima T. et al (2009) using human colon cancer cell (HCT116) showed that NQ strongly inhibited both growth and angiogenesis of these cells by inhibiting HUVEC (human umbilical vein endothelial cell) functions⁵⁶. Further NQ has been shown to induce death in B16F1 melanoma tumor cells via induction of oxidative stress and genotoxicity⁵⁷. Viola Klaus et al (2010) had showed that oxidative stress induced by NQ also induced cytotoxicity in HaCaT human keratinocytes⁵⁸. Cytotoxic and oxidative action

of NQ was paralleled by stimulation of various stress signaling including phosphorylation of the epidermal growth factor receptor (EGFR) and the related ErbB2 receptor tyrosine kinase which are known to be involved in ROS generation. Further, E.C. Cerqueira et al (2011) using molecular modeling tools showed that NQ scaffold had potential to inhibit monoamine oxidase (MAO), therefore may have therapeutic values in stroke, neurodegenerative diseases and aging process⁵⁹.

Moreover, 1,4-naphthoquinone has been evaluated as a corrosion inhibitor in 0.5 M NaCl solutions. This effect is a result of its adsorption on the metal surface and blocking the corrosion process⁶⁰.

1.6 UNCONJUGATED BILIRUBIN (UCB)

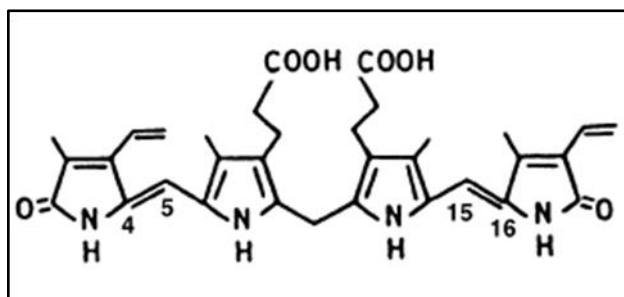
Bilirubin is a linear tetrapyrrole formed during endogenous degradation of heme in the reticuloendothelial cells mainly in the spleen⁶¹. Heme is released from a series of hemeproteins obtained from non-erythroid and erythroid sources mainly hemoglobin. Heme-oxygenase cleaves heme into carbon monoxide & biliverdin and free iron is released in this process. Biliverdin is subsequently reduced into bilirubin by biliverdin reductase⁶². Bilirubin is a highly lipophilic molecule despite containing hydrophilic carboxyl groups, because the latter are unavailable for interaction with water as a result of intramolecular hydrogen bonding to the pyrrole nitrogen atoms. Being an insoluble molecule, it must be glucuronidated by UDP-glucuronosyl transferase in the liver before biliary excretion. The physico-chemical properties of bilirubin are listed in table 1.3.

BILIRUBIN	PROPERTIES
Molecular Formula	$C_{33}H_{36}N_4O_6$
Molecular Weight	584.7
Appearance	Reddish-brown solid
Solubility	Chloroform or Alkaline Solutions
Isomer (Mixture of 3 isomeric forms)	The α -isomer is unconjugated, the β -isomer is monoconjugated, the γ -isomer is bisconjugated.
Molar Extinction Coefficient (454 nm, $CHCl_3$)	59,100-62,300 $M^{-1} cm^{-1}$
Absorption Maxima	440nm
Photosensitivity	Yes

Table1.3: Physico-chemical properties of bilirubin

1.6.1 Chemical structure and formation of bilirubin:

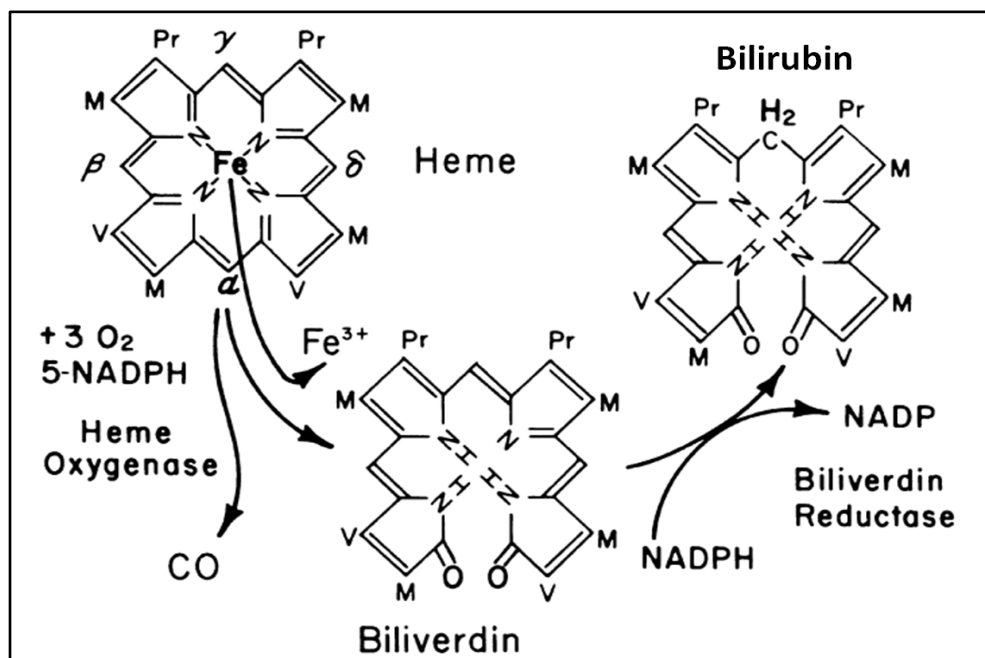
The UCB IX- α 4Z, 15Z molecule, the major compound in mammals, has a peculiar stereo-chemical structure (Scheme1.9). Indeed, all hydrophilic groups are involved in strong hydrogen bonds, and this turns the molecule into a closed molecule with a ridge-tile conformation⁶³.



Scheme1.9: Chemical structure of the naturally occurring unconjugated bilirubin IX- α 4Z,15 Z
(Adapted from Johan Fevery et al 2008)

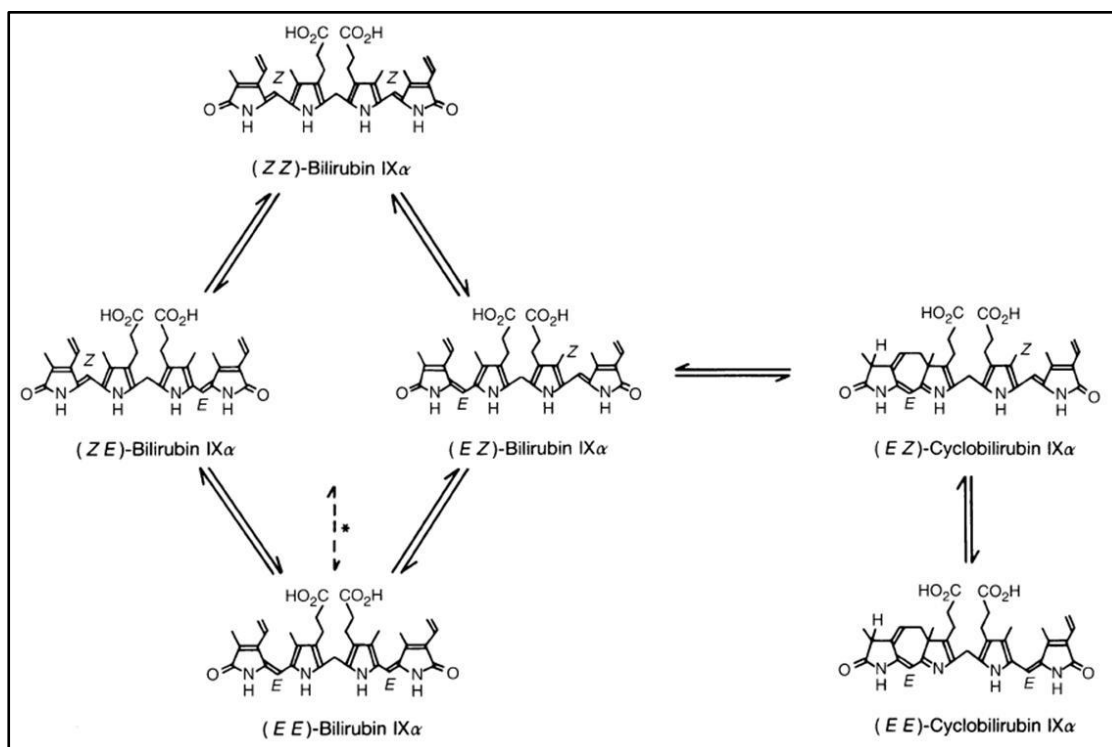
These hydrogen bonds render UCB hydrophobic and they also shield the central -CH₂, which thus becomes inaccessible for the diazo-reagent. Depending on the pH of the plasma, bile or urine, UCB can be present as uncharged diacid, as a monoanion or as a dianion⁶⁴. The uncharged diacid is by far the dominant species at low and physiological pH (>80%) but the ionized fractions become more important in an alkaline milieu, because the pK'a values have been determined to be 8.12 and 8.44, respectively, for the first and for the second anion⁶⁴.

Bilirubin is formed from heme by opening of the heme ring at the carbon bridge. This cleavage is catalyzed by the enzyme heme-oxygenase, and results in liberation of iron, and in the formation of carbon monoxide and biliverdin IX- α (Scheme1.10). The latter is reduced by a cytosolic enzyme biliverdin reductase to bilirubin IX- α . The heme-oxygenase can temporarily be inhibited by mesoporphyrins, and this suppression results in a decreased UCB production as was shown in neonates⁶⁵.



Scheme1.10: Synthesis of bilirubin (Adapted from Johan Fevery et al 2008)

Cleavage at non- α sites is possible; it is probably non-enzymic and occurs only to a minor extent. This results in the formation of other isomers; some can be detected in body fluids, although always in small amounts or under special conditions. The IX- β isomer is present in neonatal urine and in meconium⁶⁶, whereas the IX- β and IX- γ isomers have been detected in Gunn rat bile⁶⁷. Because intramolecular hydrogen bonds cannot be formed in these isomers, they are more hydrophilic, and appear in urine or bile as an unconjugated pigment. Till now, IX- δ has not been demonstrated in mammals. Phototherapy, used in the treatment of neonatal jaundice or in Crigler–Najjar disease, leads to the formation of another group of more hydrophilic derivatives of the natural UCB IX α , such as the 4E,15Z and the 4Z,15E and 4E,15E photoisomers, which can be excreted in bile without conjugation⁶⁴ (Scheme 1.11).



Scheme 1.11: Structural isomer of bilirubin formed during phototherapy
(Adapted from Johan Fevery et al 2008)

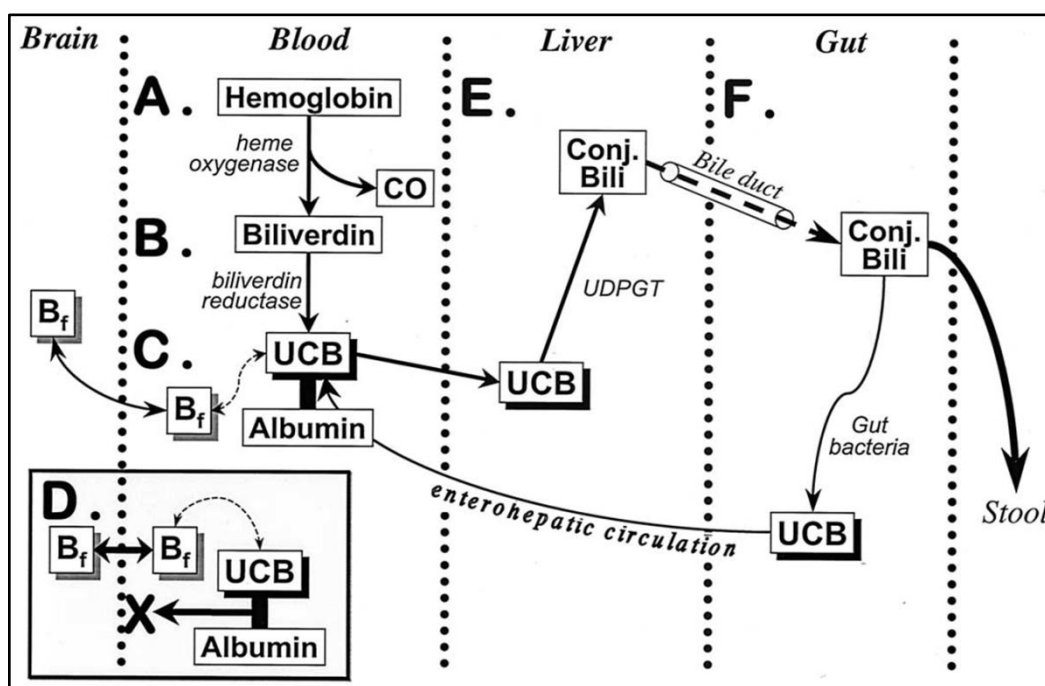
1.6.2 Metabolism of bilirubin:

Bilirubin derives from heme present in hemoglobin and is released during breakdown of senescent erythrocytes (Scheme 1.12, A-C). Approximately 20% of the daily production is derived from heme proteins such as the cytochrome P450 isoenzymes, myoglobin, etc⁶⁸. It is formed in the monocytic macrophages of the spleen and bone marrow and in hepatic Kupffer cells, and is released in plasma. Per 24h 3.8 mg/kg or approximately 250–300mg bilirubin is formed in a normal adult⁶⁹. More is formed in the neonate.

Unconjugated bilirubin (UCB) is nonpolar and insoluble in water, and is bound to serum albumin; thus little unconjugated bilirubin exists in the form of unbound or “free” unconjugated bilirubin (B_f), but it is B_f that freely enters brain, interstitial fluid, and cerebrospinal fluid, and is responsible for neurotoxicity. B_f moves easily through the blood–brain barrier (Scheme 1.12, D) but albumin-bound bilirubin does not enter the brain except when the blood brain barrier is disrupted. Because UCB is extremely poorly soluble in water, it is present in plasma strongly bound to albumin (Scheme 1.12. C). The dissociation constant for the first albumin-binding site is $K_d=7 \times 10^7 M^{-1}$ ⁷⁰. Recent studies by Ostrow and collaborators, and reviewed in Ostrow et al., determined the aqueous solubility of UCB IX- α ZZ to be 70nM in the non-ionized diacid form, which is by far the most prominent species present in blood at physiological pH⁶⁴. The mono-anion is present at approximately 17% and the dianion is minimal⁶⁴.

Entry into the hepatocyte of liver appears to be partly passive⁷¹ and partly mediated by organic anion transporter proteins⁷². In the hepatocytic cytosol, UCB is mostly bound to glutathione-S-transferase A (ligandin), and a small part is bound to the fatty acid-binding protein⁶⁴. Bilirubin is conjugated in hepatocytic microsomes in an ester

linkage with sugar moieties donated by uridine diphosphate (UDP) sugars. The conjugation is catalyzed by UDP glucuronyltransferase (UDP-GT), an enzyme encoded for by the UGT1A1 gene⁷³(Scheme 1.12, E). Both ligandin and UDP-GT appear to be tightly regulated by the nuclear constitutive androstane receptor (CAR)⁷⁴. In humans, conjugation occurs mainly with glucuronic acid, but glucose and xylose conjugates are also present in normal bile. One or two sugar moieties are coupled to the –COOH of the propionic acid side chain(s) of UCB in an ester linkage, resulting in monoconjugated (BMG, bilirubin monoglucoronide) or diconjugated bilirubin (BDG, bilirubin diglucoronide) respectively. The esterification disrupts the intramolecular hydrogen bonds, thereby opening the molecule and rendering the conjugated bilirubin (CB) more water-soluble or amphipathic, allowing excretion in the bile (Scheme 1.12, F).



Scheme 1.12: Metabolism of bilirubin (Adapted from S.M. Shapiro et al 2003)

The bilirubin conjugates formed in the hepatocytes are excreted in bile against a concentration gradient and mediated by the canalicular membrane transporter multidrug resistance-related protein 2 (MRP2) also termed ABC-C2, belonging to the adenosine triphosphate (ATP)-binding cassette family⁷⁵. The conjugates are incorporated into mixed micelles (with bile acids, phospholipids and cholesterol) and pass with the bile into the intestine, where reductive breakdown into urobilinogens occurs by intestinal or bacterial enzymes. A minor part undergoes deconjugation mainly by bacterial enzymes, and the ensuing UCB can undergo intestinal re-absorption, in contrast to CB.

1.6.3 Biological properties of bilirubin:

Bilirubin is insoluble and must be glucuronidated before being excreted in the bile, whereas biliverdin is a water-soluble, nontoxic, easily excretable product and is also a powerful antioxidant, and then what is the reason behind reduction of biliverdin into unexcretable and potentially cytotoxic bilirubin in the mammals? Nature has given anything just; it must have definite biological roles.

Earlier bilirubin was simply considered as a cytotoxic waste product that needs to be excreted from the body, however during the last few decades, the beneficial properties of bilirubin, mainly as an antioxidant, have been identified that begin to elucidate its physiological role⁷⁶. Most current studies on the physiological functions of bilirubin focus on its antioxidant effects. However, increasing evidence suggests that bilirubin possesses multiple biological activities. Some of the important biological effects of bilirubin are summarized in Scheme 1.13



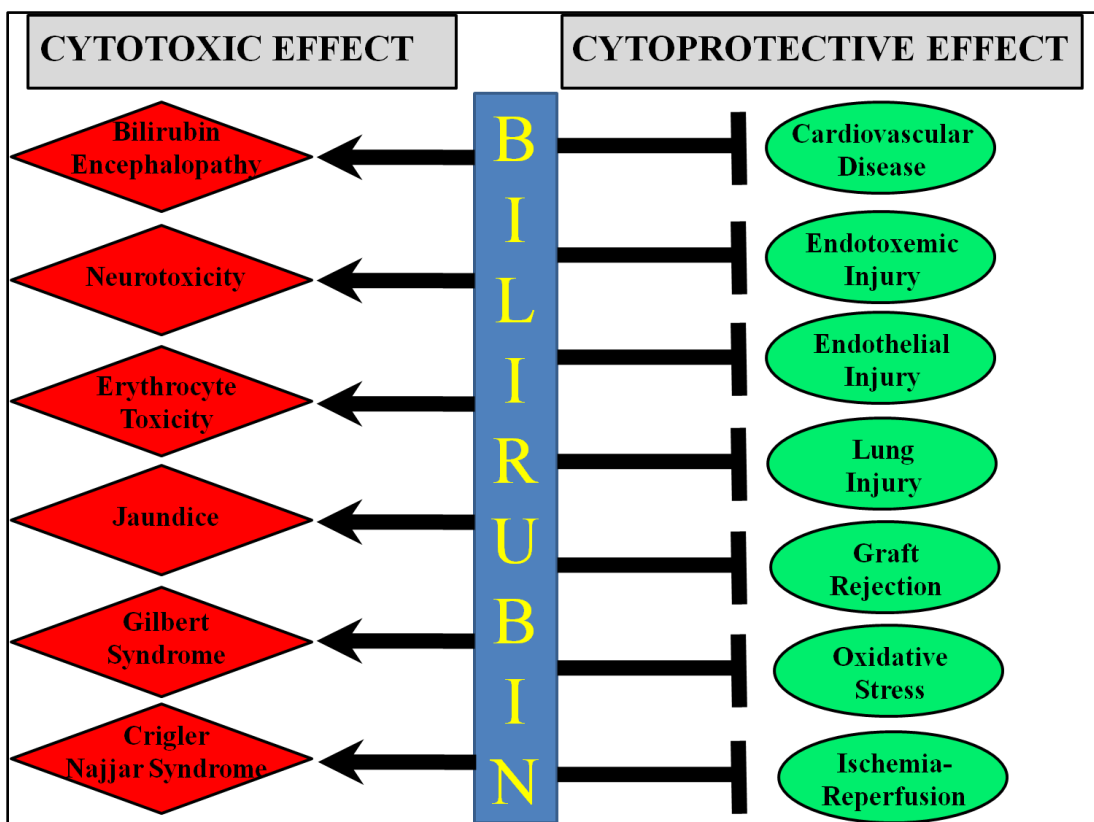
Scheme 1.13: Biological effects of bilirubin

Among its diverse biological effects, bilirubin possesses both cytotoxic to cytoprotective activity¹³. The cytotoxic and cytoprotective effects of bilirubin under both physiological and pathological conditions are briefly summarized in scheme 1.14.

1.6.3.1 Cytotoxic effects of bilirubin:

Plasma UCB levels are usually elevated in normal infants during the first two weeks of postnatal life ($< 200\mu\text{M}$) because of the marked and sudden breakdown of fetal erythrocytes at birth, coupled with a transient inability of the newborn to form bilirubin glucuronides in the liver and excrete them in the bile. Once the UGT1 enzyme and the biliary excretory system reach maturity, at about 1 month of age, plasma UCB levels decrease and reach the adult levels of $\sim 20\mu\text{M}$. When the plasma levels of UCB are excessively elevated and surpass the capacity of albumin for high-affinity binding of

UCB, the unbound (free) fraction of the pigment increases. This fraction may also be elevated in the plasma of newborns with “physiologic jaundice”.



Scheme 1.14: Cytotoxic and cytoprotective effects of bilirubin

Free UCB can easily enter the cells by passive diffusion and cause toxicity. The most vulnerable site is the central nervous system. UCB binds to discrete brain areas, such as the basal ganglia (kernicterus), and produces a wide array of neurological deficits collectively known as bilirubin encephalopathy. These include irreversible abnormalities in motor, sensory (auditory and ocular), and cognitive functions⁷⁷.

Early studies established that mitochondria might be a major target for UCB neurotoxicity, as demonstrated by impairment in mitochondrial function leading to the uncoupling of oxidative phosphorylation¹³. Additional effects of UCB in neural tissues

and neuronal cell lines include inhibition of DNA and protein synthesis, changes in carbohydrate metabolism, and modulation of neurotransmitter synthesis and release. Several studies had demonstrated that UCB exposure to neuronal cells induces oxidative stress via induction of ROS and depletion of cellular GSH, showing potential of UCB as a prooxidant^{78,79}. UCB toxicity was dependent on its concentration and on the UCB/albumin molar ratio. It is interesting that the toxic effects of UCB were directly related to the cells' age in culture. Lin et al. (2003) investigated the effect of UCB on the activation of p38MAP kinase, a member of the MAP kinase superfamily of proteins that function as critical mediators of signal transduction from the cell surface to the nucleus⁸⁰.

UCB is also toxic for non-neural cells. Blood erythrocytes are the immediate target for binding of free (unbound) UCB. Alterations of membrane dynamic properties of erythrocytes were accompanied by the release of phospholipids and cholesterol⁸¹. The loss of inner-located phospholipids induced the externalization of phosphatidylserine⁸².

1.6.3.2 Cytoprotective effects of bilirubin:

The pioneering studies of Stocker et al. introduced the concept that UCB, which was until then regarded as a toxic waste product of heme catabolism, has a beneficial role at low, "physiological" plasma concentrations by acting as a potent antioxidant that scavenges peroxy radicals as efficiently as α -tocopherol^{76,83}. Moreover, when bound to human albumin and at concentrations encountered in normal human plasma, UCB prevents *in vitro* the oxidation of albumin bound fatty acids as well as of the protein itself. One mole of albumin-bound UCB can scavenge two moles of peroxy radicals while being itself oxidized to its nontoxic metabolic precursor biliverdin. Additional studies have shown that UCB, when bound to bovine serum albumin, is oxidized by

hydroxyl, hydroperoxyl, and superoxide anion radicals (in decreasing order of oxidation rates). UCB protects albumin from $\cdot\text{OH}$ -induced oxidative damage and strongly inhibits the $\cdot\text{OH}$ -mediated formation of protein carbonyls⁸⁴. UCB is also an antioxidant *in vivo*, as shown by the reduced oxidative injury to serum proteins and lipids in the first days of life in hyperbilirubinemic neonatal Gunn rats exposed to hyperoxia⁸⁵.

UCB has broad cytoprotective activity. UCB inhibits oxidation of low density lipoprotein (LDL) lipids by interacting with LDL's α -tocopherol⁸⁶. This effect, which is exhibited by both unconjugated and conjugated bilirubin may reduce the risk of atherogenesis⁸⁷. In this context, an inverse relationship was found between serum UCB levels and severity of atherosclerosis in men, in a meta-analysis of 11 published studies⁸⁸. Moreover, a low prevalence of ischemic heart disease was found in patients with Gilbert syndrome⁸⁹. In addition, UCB administration has been shown to prevent acetaminophen-induced glutathione depletion in liver cells¹³. Further, hyperbilirubinemia has been shown to have a protective role in hepatobiliary disease. Both unconjugated and conjugated bilirubin inhibited bile acid-induced apoptosis in rat hepatocytes and suppressed the generation of ROS by these cells⁹⁰.

Both UCB and biliverdin display immunoprotective effects on murine liver and cardiac grafts. A short-term (5 minutes) rinse with micromolar concentrations of UCB, during ex vivo organ reperfusion or preceding *in vivo* transplantation, attenuated biliary dysfunction and cell injury of rat livers harvested as grafts¹³. UCB, by virtue of its antioxidant properties, prevented both short- and long-term experimental autoimmune encephalomyelitis, the rat model for human multiple sclerosis, and suppressed ongoing clinical manifestations of the disease when given after its onset⁹¹. UCB has been shown

to confer cardiovascular, hepatic, neural, and immunoprotection, by virtue of its potent free radical scavenging capacity. Moreover, it is becoming clear that low plasma concentrations of UCB are associated with a low incidence of cardiovascular disorders in humans (e.g., atherosclerosis and ischemic heart disease).

Thus, UCB should be considered as a metabolic “double edged sword”. The final outcome of its cellular effects—toxicity or protection—will depend on: 1) UCB plasma/tissue concentration and extent of binding to plasma albumin; 2) target cell/ tissue involved; 3) type of insult; 4) cellular redox state; and 5) developmental stage.

1.7 AIMS OF THE PRESENT STUDIES:

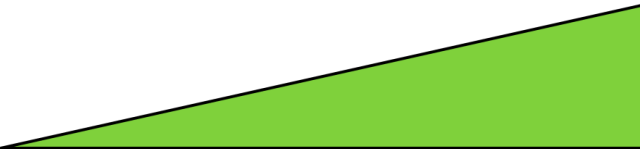
- To investigate the use of 1,4-naphthoquinone for modification of radiation injury in lymphocytes under *in vitro* and in murine model.
- To evaluate the molecular mechanism of action of 1,4-naphthoquinone in mitigating radiation injury.
- To study the use of unconjugated bilirubin as immunotoxic and radiomimetic drug both *in vitro* and *in vivo* and to delineate the signaling pathways leading to damage and potential molecular targets.
- To investigate the radiopotentiating effects of unconjugated bilirubin.

CHAPTER 2

RADIOMODIFYING EFFECTS OF 1, 4 NAPHTHOQUINONE

2.1 INTRODUCTION

Cellular redox homeostasis is the first line of defense against diverse stimuli and is crucial for various biological processes. Under physiologic conditions, cells maintain redox balance through generation and elimination of ROS³. ROS were traditionally thought as destructive molecules that play a crucial role in a variety of pathologic conditions including cancer, neurodegenerative diseases, and aging, but recently, they have been shown also to act as second messengers in varying intracellular signaling pathways that regulate cellular processes such as proliferation, differentiation, and apoptosis⁶. This dual function of ROS, as signaling molecules or toxins, could result from the differences in their concentrations, pulse duration, and subcellular localization⁶. High amount of ROS function as toxin and induce cell death, whereas low levels are behave as second-messenger and known to induce pro-survival pathways by activating redox-sensitive transcription factors like Nuclear Factor-E2-related factor 2 (Nrf2)² (Scheme 2.1).



OXIDATIVE STRESS	Mild	Severe
ROS LEVELS	Low	High
CONSEQUENCES	Activation of antioxidant defense	Cytotoxicity
SIGNALING PATHWAYS	Antioxidant response Element	Caspase
TRANSCRIPTION FACTOR	Nrf2	Mitochondrial PT Pore
CELLULAR RESPONSE	Antioxidant Phase II enzyme	Apoptosis, Necrosis

Scheme 2.1: Hierarchical oxidative stress model and cellular responses: Two tiers of oxidative stress are defined by the levels of ROS. Mild oxidative stress activates antioxidant and phase II enzymes via ARE/Nrf2 signaling pathway. Severe oxidative stress perturbs mitochondrial PT pore, and leads to cell death. (PT=Permeability Transition)

Nrf2 is major redox sensitive transcription factor which is activated by generation of mild oxidative stress and function as master redox switch in turning on the cellular signaling involved in the induction of cytoprotective genes⁹². Nrf2 activation induces the expression of a battery of phase II enzymes like HO-1, NQO1 (NADPH-quinoneoxidoreductase1), GST (glutathione-S-transferase), γ -GCS (γ -glutamate cysteine ligase regulatory subunit), SOD (superoxide dismutase), and GPx (glutathione peroxidase) that detoxify ROS and electrophilic chemicals induced by higher oxidative stress². The activation of these cytoprotective enzymes is the most sensitive cellular response to severe oxidative stressor and used as an attempt to fortify the antioxidant arsenal as the first line of defense⁹². A recent study by Gillian Groeger et al (2009) demonstrated that hydrogen peroxide (H_2O_2) at low concentrations function as cell-survival signaling molecule⁹³. There are several reports in the literature demonstrating protection by prooxidants in neuronal cell lines against oxidative insults⁹⁴⁻⁹⁶. Based on these reports the present study was undertaken to investigate the radioprotective ability of a well known prooxidants, 1, 4-naphthoquinone (NQ) in the lymphocytes. Further, to establish the concept of radioprotection by prooxidants, we have employed several other known prooxidants like H_2O_2 , diethylmaleate (DEM), a known GSH depletor, and t-butyl hydroquinone (t-BHQ) examined their radioprotective ability in lymphocytes. Detailed mechanistic studies on radioprotection by prooxidants were carried out using NQ.

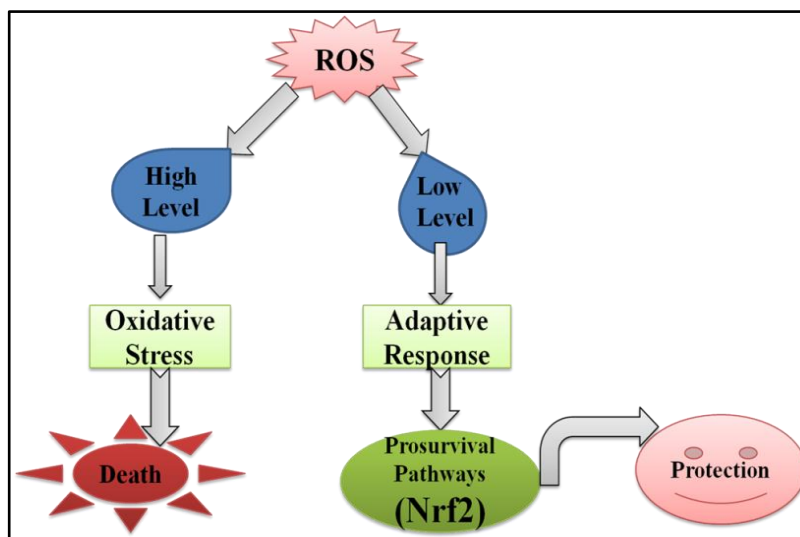
1, 4-naphthoquinone, the parent molecule of many clinically approved anticancer, anti-infective and anti-parasital drugs like anthracycline, mitomycin, daunorubicin, doxorubicin, diospyrin, and malarone has been studied as a model molecule for biologically important quinones^{45,46,48,97,98}. Quinones, like phyloquinone (vitamin K1) and menadione (vitamin K3) take part in the blood clotting process and ubiquinone

(coenzyme Q10), acts as an electron carrier in mitochondrial electron transport chain. In general, the biological activity of a quinone has been attributed to its ability to undergo reversible oxidation-reduction reactions, as well as to its electrophilic nature leading to arylation of cellular nucleophiles such as thiols in cysteine residues of proteins and GSH¹². NQ is a bifunctional para-quinone and capable of both redox-cycling and thiol arylation. The prooxidant property of naphthoquinones is responsible for initiation of tissue damage selectively in tumor cells^{56,99}.

Acute radiation injury is associated with severe damage to immune system¹⁰⁰. In lymphoid organs like spleen and thymus, ionizing radiation induces massive apoptosis. The deleterious effects of ionizing radiation are known to be mediated through both the direct deposition of energy to critical biological molecules¹⁹, and indirectly through the generation of highly reactive free radicals¹⁰¹. Indirect effect of ionizing radiation mediated through free radicals mainly ROS, is known to account for approximately 75% of the damage to cells^{19,22}. Because ROS are major contributor of radiation toxicity, antioxidants that are capable of scavenging free radicals are good candidates to protect against radiation damage¹⁰²⁻¹⁰⁵. Conventional radioprotectors like amifostine, N-acetyl cysteine and other antioxidants are free radical scavengers^{102-104,106}. However, none of the molecules have reached for human consumption as a prophylactic agents or therapeutic agents. Therefore, there is a pressing need to develop safe and effective radiation countermeasure agents to prevent or mitigate the harmful consequences of radiation exposure.

Recent studies suggest that exposure of cells to prooxidants, which are key inducer of redox sensitive transcription factor (Nrf2), results in activation of cytoprotective genes encoding phase-2 detoxifying and antioxidant defense enzymes like

HO-1, MnSOD, GPx etc^{107,108}. Activation of Nrf2/ARE pathway by natural compounds has been implicated in the prevention of cancer, ischemia and inflammatory diseases^{109,110}. Kim et al, reported that activation of Nrf2/ARE pathway led to protection against H₂O₂ induced cell death in rat PC12 cells¹¹¹. Sulfur amino acid deprivation and t-BHQ, a representative prooxidant, induce glutathione-S-transferase A2 primarily through binding of Nrf2 to the antioxidant response element in the promoter region¹¹². Using genetically-modified gain and loss of function mutant of Nrf2, it has been established that constitutive activation of Nrf2 confers radio resistance in non-small-cell lung cancer cells¹¹³. Considering the ability of low levels of ROS to initiate an adaptive response against further oxidative challenge we hypothesized that prooxidants might protect against radiation induced damage via activation of Nrf2-ARE pathway (Scheme 2.2).



Scheme 2.2: Low levels of ROS offer cytoprotection by adaptive response : High levels of ROS induces cell death by inducing oxidative stress, where as low levels of ROS activate prosurvival pathways like Nrf2 by inducing adaptive response and protect cells against subsequent exposure to higher insult.

In the present study, we used a mouse model of radiation injury to study the radioprotective effects of pro-oxidants. This model can help in identifying the complex

patterns of host response that occur in the radiation exposed organism and in developing protocols for the prophylaxis, mitigation and treatment of radiation injuries¹¹⁴. The *in vitro* studies to ameliorate radiation induced apoptosis focused mainly on lymphocytes because it highly sensitive to radiation and function as the key players of adaptive immune response.

2.2 MATERIALS AND METHODS

2.2.1 Reagents and Chemicals:

NQ, RPMI-1640 medium, Iscove's Modified Dulbecco's Media (IMDM), Sodium bicarbonate, Penicillin-streptomycin solution, N,N'-methylene-bis-acrylamide, ethylenediamine-tetra-acetic acid (EDTA), Ethidium bromide (EtBr), Sodium azide, N-Acetyl cysteine (NAC), Propidium iodide (PI), Triton X-100, Sodium citrate, Sodium chloride, Sodium dihydrophosphate, Disodium hydrophosphate, Crystal violet, Tween-20, Agarose, Bovine serum albumin (BSA), 2,7 Dichlorodihydrofluorescein-diacetate (H₂DCF-DA), Dihydrorhodamine-123 (DHR-123), Maleic acid diethyl ester (DEM), Dimethyl sulfoxide (DMSO), Fura-2AM, JC-1, Thapsigargin, BAPTA-AM, all-Trans retinoic acid (ATRA), Sulfanilamide, Naphthyl-ethylene-diamine-hydrochloride (NEDD), TRI reagent for RNA isolation, Enhanced avian first strand synthesis kit, protein tyrosine phosphatase assay kit, Glutathione assay kit and Alexa532 labeled anti-rabbit secondary antibody were purchased from Sigma Chemical Co (USA). Tin protoporphyrin (SnPP) was purchased from Tocris UK. Fetal calf serum (FCS) was obtained from GIBCO BRL. Mn (III) tetrakis(4-benzoic acid) porphyrin (MnTBAP), ERK inhibitor and Concanavalin A (Con A) were purchased from Calbiochem (USA). Easysep Mouse CD4⁺ and CD19⁺ cell sorting kits were purchased from Stem Cell technology (USA). Homogenous caspase assay kit and LightCycler®480 DNA SYBR Green I Master kit were obtained from Roche Applied science (Germany). LIVE/DEAD® fixable dead cell stain kit and lipofectamine were obtained from Invitrogen, Molecular Probes. Mouse methylcellulose complete media was obtained from R&D System, Inc. ELISA sets for detection of cytokines (IL-2, IL-4, IL-6, IFN- γ ,

TNF- α and IL-1 β), Monoclonal antibodies against p-ERK, CD3, CD4, CD14 and Bax labeled with PE and Monoclonal antibodies against CD19 and CD8 labeled with FITC were obtained from BD Biosciences (USA). Antibody against PCNA was obtained from Cell Signaling Technologies (USA). Nrf2 shRNA plasmid was obtained from Santacruz Biotech (USA). Antibody against Nrf2 and PE-labeled anti-HO-1 were purchased from Abcam (USA). Oligonucleotide primers for PCR were purchased from MWG Biotech Pvt. Ltd. The composition of solutions and buffers is given in the Annexure.

2.2.2 Animal maintenance:

Six to eight week old inbred BALB/c male mice, weighing approximately 20-25g, reared in the animal house of Bhabha Atomic Research Centre were used. They were housed in plastic cages at constant temperature (23°C) with a 12/12 h light/dark cycle and were given mouse chow and water *ad libitum*. The guidelines issued by the Institutional Animal Ethics Committee of Bhabha Atomic Research Centre, Government of India, regarding the maintenance and dissections of small animals were strictly followed.

Among several commonly used inbred mouse strains, BALB/c has been found to be sensitive to exposure of ionizing radiation¹¹⁵. MHC haplotype antigens of BALB/c mice are H-2K^d, H-2D^d, H-2L^d, IA^d, and I-E^d. Due to natural genetic variation in nonhomologous end joining (NHEJ) repair pathway which is primary mode of DSB repair in mammalian cells, BALB/c mice were found to be more susceptible to radiation damage¹¹⁶. Therefore, BALB/c mice were used in the present study to examine effects of radiation exposure and its amelioration by administration of NQ.

2.2.3 Cell line and culture:

Int407, a human embryonic intestinal epithelial cell line and MCF-7, a human breast cancer cell line, were purchased from National Centre for Cell Sciences (NCCS),

Pune, India. These cell lines were grown in RPMI-1640 medium supplemented with 10% FCS.

2.2.4 Treatment with NQ:

A 100mM solution of NQ was prepared in DMSO, stored as small aliquots at -20°C , and then diluted as needed in cell culture medium. In all *in vitro* experiments, cells were treated with NQ for 2h in RPMI medium without FCS and were irradiated 4Gy without washing the cells. DMSO (0.1%) was used as vehicle control *in vitro*. Cells were then supplemented with 10% FCS and cultured at 37°C in a 95% air/5% CO_2 atmosphere in CO_2 incubator.

For *in vivo* studies, NQ was dissolved in DMSO and final concentration was adjusted to 0.2mg/ml with 1X-PBS. The solution (2mg per kg body weight or 2mg/kbw) was injected intraperitoneally (i.p.) to mice using 26.5 gauge size needle. The mice in control or radiation group were treated with an equal volume of vehicle. Mice were exposed to 4Gy whole body γ -radiation 0.5h after NQ administration.

2.2.5 Irradiation schedule:

Whole body irradiation (WBI) and *in vitro* irradiation were carried out using Gamma Cell 220 irradiator (AECL, Canada). BALB/c mice were placed in ventilated perspex boxes and exposed to 4Gy whole body γ -radiation at a dose of 2.93 Gy/min. For *in vitro* experiments lymphocytes were resuspended in RPMI-1640 medium without FCS in 24 well plates and exposed to 4Gy radiation. Nrf2 shRNA plasmid transfected cells were irradiated at a dose rate of 1.98Gy/min in a blood irradiator (BRIT, Mumbai).

A radiation dose of 4Gy was selected as it causes both immunosuppression & myelosuppression and leads to important clinical sequel (e.g. infection)¹¹⁴. Further this dose is also used during radiotherapy. Doses of 4Gy or greater are associated with the

development of a hematological syndrome that is often fatal without aggressive medical intervention requiring a bone marrow transplant. The dose of radiation 4Gy, which is used in our study, sits at the threshold of conservative management vs. aggressive management¹¹⁷.

2.2.6 Preparation of splenic lymphocytes and bone marrow cell suspension:

Since spleen is large, radiosensitive and highly organized secondary lymphoid organ which contains both multipotential stem cells and variety of committed progenitor cells that are involved in fighting the systemic infection, our studies mainly focused on effect of radiation on spleen functions. Spleens were aseptically removed and placed in sterile dishes containing RPMI-1640 medium. Single cell suspensions were prepared by gently teasing the spleen on a sterile nylon mesh placed in the dish. Cell suspension was carefully transferred to 15ml sterile tubes and centrifuged at 3000rpm for 5minutes. RBCs were lysed by brief hypotonic shock using ice cold water (5ml, 10 sec) followed by ice cold 2x PBS (5 ml). The RBC membranes were allowed to pellet by centrifuging the tubes at 1000rpm for 30seconds and lymphocytes were carefully decanted into a fresh tube. Lymphocytes were further centrifuged at 3000rpm for 5minutes and the cell pellet was resuspended in RPMI-1640 medium.

Since bone marrow is the main source of hematopoietic stem cells (HSCs) and hematopoietic progenitor cells (HPCs) which are critical component of radiation induced hematopoietic syndrome, we have also studied effect of radiation on bone marrow suppression. For bone marrow isolation, both femur bones of mice were aseptically removed with help of scissor and cell suspensions were prepared by flushing with 1ml cold RPMI-1640 through the marrow of the femur using 1ml syringe. Cells from both femurs of each mouse were centrifuged and suspended in a known volume of medium.

The viability of lymphocytes and bone marrows were estimated by trypan blue dye exclusion methods.

2.2.7 Estimation of apoptosis by PI staining:

Apoptosis can be measured based on reduced DNA content of the cells. This is a consequence of progressive loss of DNA from the cells, due to activation of endonucleases and subsequent leakage of low molecular weight DNA products prior to measurement^{118,119}. The decrease of cellular DNA is apparent in flow cytometer, independent of the type of fluorochrome (PI, Hoechst, 7-aminoactinomycin). This method is quick, simple to perform and reliable and is applicable to all cell types. PI is a DNA intercalating dye that binds to DNA in a stoichiometric manner. Cells containing more DNA take up more PI than the cells containing less amount of DNA. Thus the relative fluorescence of apoptotic cells is lower than that of cells in G0/G1 phase of cell cycle.

Lymphocytes (1×10^6) were incubated with or without NQ (0.05-1 μ M) for 2h prior to irradiation (4Gy) and cultured for 24h at 37°C. These cells were washed with 10mM PBS and incubated with 1ml of staining solution containing 0.5 μ g/ml PI, 0.1% sodium citrate and 0.1% Triton X-100 overnight at 4°C. A total of 20,000 cells were acquired in Partec PAS III flowcytometer and percent apoptotic cells were determined by analyzing sub G1 population (less than 2n DNA content) using FloMax® software.

2.2.8 Estimation of apoptosis using DNA ladder assay:

During apoptosis activation of Ca^{2+} and Mg^{2+} dependent endonuclease causes breakdown of nuclear DNA between the nucleosome resulting into DNA fragments of 180 to 200 base pairs¹²⁰. These DNA fragments reflect endonucleolytic cleavage of interphase chromosomes at nuclease sensitive sites that reside in chromatin fibers as a

result of their folding into loop and rosette structure. The formation of DNA ladder is considered as hallmark biochemical indicator of apoptosis and was performed by using agarose gel electrophoresis as reported earlier¹⁰³. In brief, lymphocytes (1×10^6 cells) pretreated with or without NQ ($1 \mu\text{M}$) for 2h were exposed to radiation (4Gy) and cultured for 24h at 37°C . The cells were washed with PBS and the pellet was suspended in $25 \mu\text{l}$ lysis buffer (50mM Tris HCl, pH 8.0, 10mM EDTA, 0.5% N-lauroyl sarcosine, 0.5mg/ml proteinase K) and incubated at 50°C for 1h. RNase ($5 \mu\text{l}$) was added to the lysate and further incubated for 1h at 50°C . The DNA sample ($10 \mu\text{l}$) was mixed with $2 \mu\text{l}$ gel loading buffer, and electrophoresed in 1.8% agarose gel in TBE buffer (pH8.0) containing EtBr. The bands were visualized and photographed under UV light using Geldoc (Syngene, UK).

2.2.9 Determination of cell size and volume by Flow Cytometry:

A fundamental characteristic of apoptosis is the loss of cell size and volume resulting into shrinkage of cell. Cells which have a decrease in cell volume have a reduced ability to scatter light in the forward direction (low FSC). Furthermore, these apoptotic cells also showed a slight increase in their ability to scatter light at a 90° angle (high SSC), indicating a concurrent increase in cellular density because cytoplasm become dense and organelles are more tightly packed when cells get shrunk. Cell size and changes in the light scattering properties of the cells were determined by flow cytometry as described previously¹²¹.

Lymphocytes (1×10^6 cells) pretreated with or without NQ ($1 \mu\text{M}$) for 2h were exposed to radiation (4Gy) and cultured for 24h at 37°C . For each sample, 20,000 cells were examined by exciting the cells with a 488nm argon laser and determining their position on a forward scatter versus side scatter dot plot. Light scattered in the forward

direction is roughly proportional to cell size, while light scattered at a 90° angle (side scatter) is proportional to cell density. Therefore, as a cell shrinks or loses cell volume, a decrease in the amount of forward scattered light is observed, along with a slight change in side scattered light. A gate based on the properties of the control cells was set on each forward scatter versus side scatter dot plot to separate the normal and apoptotic populations of cells, and remained constant throughout the analysis. The percent of apoptotic cells was determined by statistical analysis of the dot plots using Flowmax® software.

2.2.10 Estimation of cell death by Live and Dead assay:

To measure radiation-induced cell death, LIVE/DEAD® fixable dead cell stain kit (Invitrogen, Molecular Probes) was used and cell death was measured by increase in the fluorescence of dye covalently bound to cellular protein (polyamine) using a flowcytometer. For viable cells, because the dyes cannot penetrate the cell membrane, only cell surface proteins are available to react with the dye, resulting in relatively dim staining. For dead cells, however, the reactive dye can permeate damaged membranes and stain the interior of the cell as well as the cell surface. This results in more intense staining. This is more effective method to detect dead cells than nucleic acid binding dyes like PI, because PI leach out of dead cells with washing.

Lymphocytes (1×10^6) were incubated with or without NQ (1 μ M) for 2h prior to irradiation (4Gy) and cultured for 24h at 37°C. The cells were washed with PBS and the pellets was resuspended in 1ml 1X PBS containing 1 μ l reconstituted fluorescent reactive dye, mix well and incubate at room temperature for 0.5h. The cells were washed twice with 1mL of PBS containing 1% BSA, and resuspended in 1mL of PBS. A total of

20,000 cells were acquired in Partec PAS III flowcytometer and percent dead cells were determined by analyzing high FL-1 using FloMax® software.

2.2.11 Determination of nuclear blebbing:

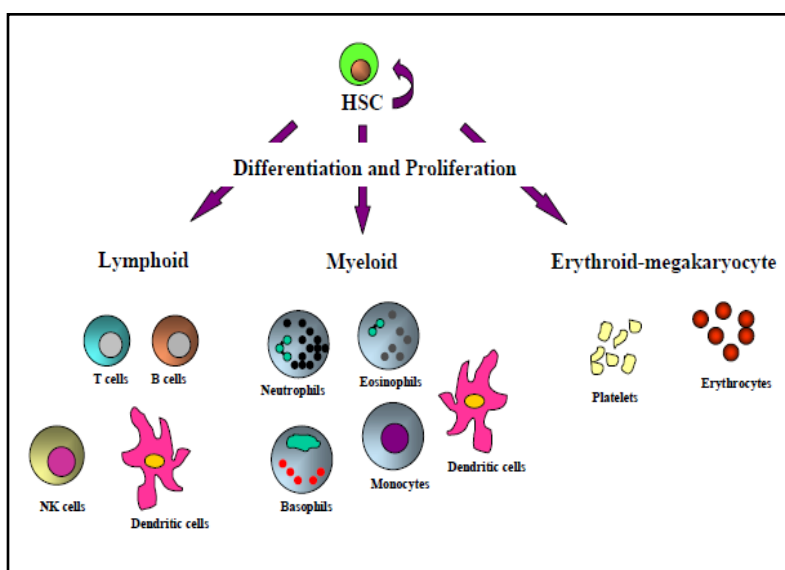
One of the earliest events in apoptosis is shrinkage of the cells which terminate into extensive plasma membrane blebbing followed by karyorrhexis and finally by budding process these cells get fragmented into apoptotic bodies¹²⁰. During budding process chromatin condenses with a uniform and smooth appearance against nuclear membrane culminating into nuclear condensation and fragmentation. This change in nuclear morphology called nuclear blebbing was assessed by confocal laser microscopy using Hoeschst-33258 as nuclear stain. Lymphocytes (1×10^6) were incubated with or without NQ ($1 \mu\text{M}$) for 2h prior to irradiation (4Gy) and cultured for 24h at 37°C. Cells were centrifuged on coverslips, fixed with paraformaldehyde (4%) and were stained with Hoechst dye. Nuclear condensation and fragmentation were counted in 10 randomly selected fields using a LSM510 confocal microscope (Carl Zeiss, Jena GmbH, Germany) with a Krypton-Argon laser, coupled to an Orthoplan Zeiss photomicroscope using a 488nm laser line and a 530nm band pass filter. Approximately 300 nuclei were examined for each sample and results were expressed as percent apoptosis evaluated by dividing the number of apoptotic nuclei by total number of nuclei counted.

2.2.12 Colony Forming Cell (CFC) Assay:

To measure proliferating capacity of hematopoietic stem cells present in the spleen, an *in vitro* CFC assay was performed using mouse methyl cellulose complete media. HSCs exhibit remarkable self-renewal capacity and responsible for the life-long maintenance of the hematopoietic system by the process called hematopoiesis. During hematopoiesis HSCs proliferate and differentiate into 3 different lineage-lymphoid,

myeloid and erythroid-megakaryocyte. It also maintains a small pool of HSCs with the self-renewal capacity that is capable of carrying on hematopoiesis (Scheme2.3).

Multi-potential progenitors (e.g. CFU-GEMM i.e. Colony forming unit-granulocyte, erythroid, macrophage, megakaryocyte) and lineage-committed progenitors (e.g. CFU-E i.e. CFU-erythroid, CFU-GM i.e. CFU-granulocyte macrophage), representing various stages along the differentiation pathway with various differentiation and proliferation potentials, can be identified by this *in vitro* CFC assays.



Scheme 2.3: Pluripotent hematopoietic stem cells (HSC) and hematopoiesis

Splenic lymphocytes (0.2×10^6 cells) suspended in IMDM in microcentrifuge tube were incubated with or without NQ ($1 \mu\text{M}$) for 2h and then exposed to radiation (4Gy). Lymphocytes were supplemented with 2% FCS and incubated with mouse methylcellulose medium (1.3% final concentration) in 6-well plate in triplicate. Keep 3mL of sterile water in a remaining 3 wells of 6-well plate, which serves to maintain the humidity necessary for colony development. Incubate the cells for 11 days at 37°C and 5% CO_2 without disturbing the plate during the incubation period to prevent shifting of the colonies.

2.2.13 Clonogenic Cell Survival Assay:

Clonogenic assay or colony formation assay is an *in vitro* cell survival assay based on the ability of a single cell to grow into a colony. The colony is defined to consist of at least 50 cells. The assay essentially tests every cell in the population for its ability to undergo unlimited division. Clonogenic assay is the method of choice to determine cell reproductive death after treatment with ionizing radiation.

Human embryonic intestinal epithelial cell line (Int407) was seeded at cell density of 1000 cells in 100mm culture dishes and incubated for 24h at 37°C for adherence. Cells were washed with RPMI and treated with or without NQ (1µM) for 2h and then irradiated at 4 or 6 Gy. Cells were allowed to grow for 14 days at 37°C and 5% CO₂ to form colonies. Cells were washed with PBS and resuspended in 4ml PBS containing 4% formaldehyde for 0.5h. Then PBS was removed and colonies were stained with 4ml crystal violet (0.4 g/L) for 0.5h. Unbound crystal violet were removed by immersing the dishes in the sink filled with water, air dried the culture dish and visible blue colonies were counted by naked eye, plating efficiency (PE) and surviving fraction (SF) were recorded as described earlier¹²². PE is the ratio of the number of colonies to the number of cells seeded.

$$PE = (\text{No. of colonies formed} / \text{No of cells seeded}) \times 100\%$$

The number of colonies that arise after treatment of cells, expressed in terms of PE, is called the surviving fraction (SF).

$$SF = (\text{No. of colonies formed after treatment} / \text{No. of cells seeded}) \times PE$$

2.2.14 Purification of CD4+T cells, CD19+B cells:

Separation of cells based on the differential expression of cell surface antigens is an important technique that has facilitated the study of specific subpopulations of

lymphocytes^{123,124}. In the present studies, magnetic sorting was used to purify CD4+T cells, CD19+B cells from total splenic lymphocytes using anti CD4 antibody, anti CD19 antibody coated magnetic nano-particles in a magnetic cell sorter. Cells were resuspended in RPMI and magnetic bead conjugated anti CD4 or anti CD19 antibody was added to cells and incubated for 0.5h. Total volume of cells was made to 2.5ml by addition of ice-cold RPMI medium and cells were placed in a magnet. Magnetically labeled cells were allowed to adhere to the tube for 6-8minutes and unbound cells were carefully decanted into a fresh tube. The residual cells were removed from the magnet and washed two times to further remove the negative cells.

2.2.15 Human lymphocyte isolation:

Informed, signed consent was taken from all the registered healthy volunteers before undertaking these studies. The guidelines issued by the Medical Ethics Committee of Bhabha Atomic Research Centre, Government of India, were strictly followed during these studies. Peripheral venous blood (10ml) was collected from the cubital vein of healthy volunteers under all aseptic precautions and transferred immediately into heparinized vacutainer tubes. The blood was diluted 1:1 with sterile RPMI medium and gently layered on to 10ml Histopaque 1077 in a 50ml centrifuge tube. The tubes were centrifuged at 2500rpm for 20minutes and peripheral blood mononuclear cells (PBMNCs) were collected from buffy coat. The PBMNCs were washed three times with RPMI and viable cells were counted using trypan blue dye exclusion.

2.2.16 Estimation of caspase activity:

Caspases are cysteine-aspartic proteases that play essential roles in apoptosis and have proteolytic activity and are able to cleave proteins at aspartic acid residues. Once caspases are initially activated, there seems to be an irreversible commitment towards cell

death. To date, ten major caspases have been identified and broadly categorized into initiators (caspase-2, 8, 9, 10), effectors or executioners (caspase-3, 6, 7) and inflammatory caspases (caspase-1, 4, 5)^{125,126}. Once caspases are activated, the execution phase of apoptosis is triggered.

Determination of enzymatic activity of different caspases was performed by using homogenous caspase assay kit which specifically detects caspases 2, 3 and 7, caspases 6, 8, 9 and 10 to a lesser extent. Lymphocytes (0.5×10^6) were incubated with or without NQ ($1 \mu\text{M}$) for 2h prior to irradiation (4Gy) and cultured for 24h at 37°C . Cells were washed with PBS and resuspended in $300 \mu\text{l}$ RPMI and further incubated with $300 \mu\text{l}$ substrate working solution freshly prepared at 37°C for 1.5h and plated in 96-well black plate ($200 \mu\text{l}$ per well) in triplicates. Substrate working solution contains lysis buffer and DEVD-Rhodamine110, the fluorimetric substrate of caspases. Lysis buffer lysed the cells and released the activated caspase which cleave the substrate and Rhodamine-110 is released. Fluorescence of the released Rhodamine is measured by using spectrofluorimeter with an excitation filter 490 nm and emission filter 530nm.

2.2.17 Measurement of change in mitochondrial membrane potential ($\Delta\psi\text{m}$):

Mitochondrial membrane potential (MMP) was assessed using the mitochondrial-specific fluorescent probe JC-1 by spectrofluorimetric method. JC-1 has dual emission depending on the state of the MMP. JC-1 forms aggregates in cells with a high red fluorescence indicating a normal MMP. Loss of the MMP results in a reduction in red fluorescence with a concurrent gain in green fluorescence as the dye shifts from an aggregate to monomeric state. Ratio of red to green fluorescence was used as indicator of loss of MMP.

Lymphocytes (1×10^6) were incubated with or without NQ ($1 \mu\text{M}$) for 2h prior to irradiation (4Gy) and cultured for 6h at 37°C . Cells were washed and resuspended in 1ml 1X-PBS and JC-1($5 \mu\text{M}$) was added to cells, mix well and incubated at 37°C for 0.5h and finally plated in 96-well black plate ($200 \mu\text{l}$ per well) in quadruplicates. Fluorescence of JC-1 was recorded by using spectrofluorimeter at 488nm excitation and 535nm emission for monomeric state and 560nm excitation with 610nm emission for aggregate state. Ratio of red to green fluorescence for control group was taken as 100%.

2.2.18 Measurement of intracellular calcium levels:

Fura2-acetoxymethyl ester (AM) was used to measure the intracellular Ca^{2+} levels. During incubation for 30-40 minutes, cells will take up the Fura2-AM. Intracellular esterases cleave intracellular Fura2-AM into the active Fura2. Fura2 fluorescence changes when it is bound to Ca^{2+} . The excitation peak for Fura2 shifts from 369nm for the calcium-free chelator to about 335nm for the calcium-saturated form. Addition of Ca^{2+} increases the fluorescence of Fura2 when excited at 335nm and decreases the fluorescence from excitation at 369nm. Monitoring the increasing signal generated by 335nm excitation or decreasing signal generated by 369nm excitation will indicate the extent of cleavage of the Fura2-AM and subsequent binding of Ca^{2+} ion.

Lymphocytes (1×10^6) treated with and without NQ ($1 \mu\text{M}$) were exposed to various 4Gy of γ radiation and were incubated for 6h at 37°C . They were further incubated with $2 \mu\text{M}$ of Fura2-AM for 0.5h and analyzed in a spectrofluorimeter (BMG Labtech Optima) at 335nm excitation and 500nm emission.

2.2.19 Prooxidant measurements:

Exposure of ionizing radiation to lymphocytes induced oxidative stress by generation of various free radicals-hydrogen peroxide, superoxide, singlet oxygen etc

which are collectively called as ROS. Although oxidative stress can be quantified indirectly by measuring the product of oxidative damage, such as lipid peroxides, protein carbonyl content and DNA adducts, a more direct and sensitive method to quantify oxidative stress is DCF assay which measures the oxidation of DCFH substrate. To detect intracellular ROS, oxidation-sensitive probe H₂DCF-DA was used. Dye can readily cross cell membranes and is hydrolyzed by intracellular esterases to nonfluorescent DCFH. In presence of hydrogen peroxide or other reactive oxygen species as well as heme protein catalysts, such as cytochrome c or peroxidase, DCFH is oxidized to highly fluorescent DCF.

To measure the effect of NQ on intracellular ROS level, lymphocytes (1×10^6) were preloaded with DCFH-DA (20 μ M) for 0.5h at 37°C and then cell were treated with NQ (1 μ M) for indicated time. To measure the effect of NQ on radiation induced ROS level, lymphocytes (1×10^6) were treated with NQ (1 μ M) for 2h and loaded with H₂DCF-DA (20 μ M) for 0.5h at 37°C. The cells were further exposed to radiation (4Gy) and immediately plated in 96-well black plate (200 μ l per well) in quadruplicates and increase in fluorescence resulting from oxidation of DCFH₂ to DCF was measured using a spectrofluorimeter (BMG Labtech Optima) using 485nm excitation and 535nm emission. To rule out the possibility of oxidation of DCFH to DCF by NQ, we have used oxidation insensitive analogue fluorescein diacetate (FDA), 0.5h prior to NQ addition. To ascertain the contribution of H₂O₂ to NQ mediated increase in ROS, lymphocytes were treated with PEG-catalase (50units/ml) for 2h prior to addition of NQ (1 μ M).

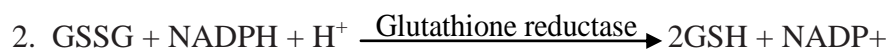
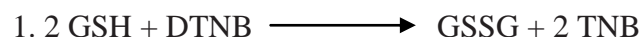
Since mitochondrial complex I is a potent source of ROS which can produce superoxide (as well as hydrogen peroxide), during forward and reverse electron transfer, mitochondrial ROS level were measured by using DHR-123, a mitochondria specific

redox sensitive probes. Lymphocytes (1×10^6) were loaded with DHR123 (5 μ M) for 0.5h prior to NQ addition and increase in fluorescence resulting from oxidation of DHR123 to rhodamine123 was measured using a spectrofluorimeter (BMG Labtech Optima) using 488nm excitation and 543nm emission.

2.2.20 Measurement of intracellular GSH levels:

Reduced glutathione (GSH), a tripeptide (γ -glutamylcysteinylglycine), is the major free thiol in most living cells and serve as key antioxidant and involved in many biological processes such as detoxification of xenobiotics, removal of hydroperoxides, and maintenance of the oxidation state of protein sulfhydryls. Glutathione is present inside cells mainly in the reduced form (90–95% of the total glutathione). Oxidation of glutathione leads to the formation of glutathione disulfide (GSSG). Intracellular GSH status appears to be a sensitive indicator of the overall health of a cell.

GSH was measured by colorimetric assay using glutathione assay kit (Sigma) as per manufacturer's protocol. The biological sample is first deproteinized and then assayed for glutathione. The measurement of GSH uses a kinetic assay in which catalytic amounts (nmoles) of GSH cause a continuous reduction of 5, 5'-dithiobis (2-nitrobenzoic acid) (DTNB) to TNB and the GSSG formed is recycled by glutathione reductase and NADPH. The GSSG present will also react to give a positive value in this reaction.



The combined reaction:



To measure intracellular GSH, lymphocytes (1×10^8) were incubated with DEM (100 μ M) or NQ (1 μ M) for indicated time at 37 $^\circ$ C. DEM was used as a positive control

for GSH depletion. Cells were centrifuged at 14.5krpm to get pellet, resuspended in 3 volume of 5% SSA solution, freeze-thaw the solution using liquid nitrogen and leave for 5minutes at 4°C. Centrifuge the extract at 14,500rpm for 10minutes and supernatant were collected and used for glutathione estimation. To 10µl sample, add 150µl of the working mixture and incubate for 5minute at room temperature and then add 50µl of the diluted NADPH solution and absorbance was recorded at 412nm using spectrophotometer. GSH in the sample was quantified using standard curve.

2.2.21 HPLC Separation of Products of Reaction of NQ with NAC:

A solution of NQ (1mM) dissolved in acetonitrile was added to NAC (10mM). The mixture was incubated for 3h at 37°C in the dark. The samples were then subjected to reverse-phase HPLC analysis using Waters HPLC equipment and 2487 dual wavelength absorbance detector set at 390nm. Analyses were performed with a Nova Pak C18 column (3.9x150mm) at ambient temperature with a mobile phase of acetonitrile (100%) at a flow rate of 1ml/min.

2.2.22 Mass Spectrometry (MS) analysis:

To characterize the products of reaction of NQ with NAC, MS analysis was carried out. MS was performed using a triple quadrupole mass (QqQ) spectrometer with ESI source (Varian, Inc., USA). The ESI source operated in positive ionization mode.

2.2.23 Estimation of nuclear Nrf2 levels by confocal microscopy:

Lymphocytes (2×10^6) were treated with NQ (1µM) for different time intervals from 0 to 12h in micro centrifuge tube. The cells were transferred to 12-well plates which contain round glass coverslips. Plate was centrifuged to pellet down cells onto coverslips. The cells were fixed in 4% paraformaldehyde (500µl) for 10minutes at 4°C. Excess paraformaldehyde was aspirated and the cells were permeablized with 1X PBS

containing 0.02% Tween-20 twice and then blocked with 5% BSA at 37°C for 0.5h. Anti-Nrf2 antibody was added at a dilution of 1:100 in 1% BSA and incubated overnight at 4°C. Cells were then washed with 1X PBS five times before incubating in the dark with Alexa-532 labeled secondary antibody at dilution of 1:200 in 1%BSA for 2h. The secondary antibody solution then was aspirated, and the cells washed twice in PBS. Cells were then incubated in the dark with Hoechst solution for 10minutes at room temperature for nuclear staining. Excess Hoechst were washed with PBS twice, and coverslips were mounted on glass slides with DABCO, an antifade solution. Slides were examined using a LSM510 scanning module (Carl Zeiss Microscopy, Jena GmbH, Germany) with a Krypton–Argon and Helium-Neon laser, coupled to an Orthoplan Zeiss photomicroscope using a 488 and 540nm laser line and a 510 and 633 band pass filter. Overlay images were recorded by superimposing simultaneous images from each channel.

2.2.24 Antibody staining:

Lymphocytes (3×10^6) treated with or without NQ ($1 \mu\text{M}$) were exposed to various 4Gy of γ -radiation and were incubated for 24h at 37°C and processed for intracellular staining with PE labeled anti-Bcl2 or anti-Bcl-xl. In another set of experiments, lymphocytes (3×10^6) were incubated for indicated time intervals in presence or absence of NQ ($1 \mu\text{M}$) and were stained with PE-labeled anti-HO-1 or anti-phosphoERK-1 antibodies according to the method described earlier¹²⁷. Cultured cells were fixed with 4% paraformaldehyde for 10minutes at room temperature and excess of paraformaldehyde were removed by washing once with wash buffer (PBS containing 1% BSA). Cells were permeabilized with PBST (PBS containing 0.02% Tween-20) thrice for 5minutes each, followed by 2 washes with wash buffer and then stained with indicated

PE labeled antibody (1 μ g) for 1h at 4°C. The cells were washed twice and resuspended in 1ml PBS and acquired in flowcytometer and analyzed by using FloMax® software.

For surface staining, splenocytes (1×10^6) obtained from treated animals were stained with PE-conjugated antibodies to CD3 or CD4, or CD14 or FITC-conjugated antibodies to CD8 or CD19 as described earlier¹²⁸. Total spleen cells (1×10^6) were used for direct immunofluorescence staining. Cells were resuspended in 50 μ l buffer (PBS containing 10% FCS and 0.1% sodium azide) and incubated on ice for 10minutes for blocking Fc receptors. The cells were further incubated with 1 μ g of FITC or PE conjugated antibody in buffer for 30minutes on ice in dark, washed three times with the buffer and resuspended in 1ml PBS. The number of CD3+T cells, CD4+T helper cells, CD8+T cytotoxic cells, CD19+B cells and CD14+macrophages in spleen of treated mice was determined by flow cytometry. The total cell yield was calculated by multiplying the proportion of each cell subset by the total number of live cells obtained per spleen.

2.2.25 Protein tyrosine phosphatase assay:

Protein phosphorylation and dephosphorylation are central mechanisms that mediate signal transduction events involved in a wide range of cellular processes like cell-cycle progression, transcriptional regulation, cell growth, differentiation and apoptosis. The protein phosphatases can be divided into two main groups: protein tyrosine phosphatases and protein serine/threonine phosphatases which remove phosphate from proteins/peptides containing phosphotyrosine) or phosphoserine/phosphothreonine, respectively.

Estimation of protein tyrosine phosphatase activity is based on the determination of free phosphate, generated in the dephosphorylation reaction of the PTP (phosphotyrosine peptide) substrate, using Malachite Green/Ammonium Molybdate

reagent. The color is quantitated by spectrophotometry at 620nm and reflects the total amount of free, inorganic phosphate in the sample and thus the relative amount of tyrosine phosphatase activity in the sample.

Lymphocytes were incubated with NQ (1 μ M) for 2h, whole cell lysates were prepared and protein was estimated and phosphatase activity was estimated by colorimetric method using non radioactive protein tyrosine phosphatase assay kit (Sigma) according to manufacturer's protocol.

2.2.26 Transfection of lymphocytes with Nrf2 shRNA plasmid:

Lymphocytes (1.5X10⁶) were plated in 24-well plate in triplicates in antibiotic free RPMI medium. 2 μ g Nrf2 shRNA plasmid or equivalent amount of scrambled plasmid were transfected using lipofectamine transfection reagent. After 6h of transfection, cells were cultured in complete medium for next 18h and then washed once with RPMI and exposed to 2Gy. Cells were then cultured for 24h at 37°C and cell death was estimated by PI staining, live and dead assay and DNA fragmentation assay as described previously.

2.2.27 Estimation of mRNA expression by semi-quantitative Reverse Transcription-PCR:

Lymphocytes (5x10⁶) were treated with or without NQ (1 μ M) for 24h at 37°C and total RNA was extracted and eluted in 30 μ l RNase free water using PerfectPure™ RNA Purification kit (5 Prime). Equal amount of RNA in each group was reverse transcribed to cDNA using two step RT-PCR kit kit (Invitrogen). Equal amount (1 μ l) of cDNA in each group was used for specific amplification of β -actin and HO-1 genes using gene specific primers. The gene specific primers were designed using PRIMER3 software (<http://workbench-sdsc.edu>) and sequences are listed below (Table 2.1). The PCR

conditions were: 94°C 5 minute initial denaturation followed by thirty five cycles of 94°C 45 seconds, 55°C 45 seconds, 72°C 45 seconds and final extension was carried out at 72°C for 10 minutes. Equal amount of each PCR product (10µl) was run on 2% agarose gel containing EtBr in TBE buffer at 60V. The bands in the gel were visualized under UV lamp and relative intensities were quantified using Geldoc software (Syngene).

S.N.	Gene	Primer Sequence (5'→3')
1.	β-actin	Forward Primer: 5'-CATCACTATTGGCAACGAGC-3' Reverse Primer: 5'-GGACTGTTACTGAGCTGCGT-3'
2.	HO-1	Forward Primer: 5'-AACAAGCAGAACCCAGTC-3' Reverse Primer: 5'-TGTCATCTCCAGAGTGTTC-3'

Table 2.1: Sequence of Primer used for mRNA expression of β-actin and HO-1

2.2.28 Estimation of mRNA expression by quantitative Real Time PCR:

Real time PCR is combined with reverse transcription to quantify messenger RNA in cells. Real time PCR enables both detection and quantification of one or more specific sequences in a DNA sample. The quantity can be either an absolute number of copies or a relative amount when normalized to DNA input or additional normalizing genes. Its key feature is that the amplified DNA is detected as the reaction progresses in real time. This is a new approach compared to standard PCR, where the product of the reaction is detected at its end. For detection of products fluorescent dye like SYBR Green I is used which intercalate with double-stranded DNA. An increase in DNA product during PCR therefore leads to an increase in fluorescence intensity and is measured at each cycle, thus allowing DNA concentrations to be quantified.

Lymphocytes (20×10^6) were treated with or without NQ ($1 \mu\text{M}$) for indicated time at 37°C and total RNA was isolated from the samples using Trizol reagent (Sigma) following the manufacturer's instructions and was dissolved in $30 \mu\text{l}$ deionised DEPC-treated water. From this RNA $2 \mu\text{g}$ was converted to cDNA by reverse transcription (cDNA synthesis kit, Sigma) following the manufacturer's instruction. qPCR was carried out using the Rotor Gene 3000 (Corbett Research) machine. The PCR was setup by mixing 10x SYBR green PCR mix (sigma) with $5 \mu\text{l}$ cDNA, 10 picomoles each of forward and reverse gene specific primers, and PCR-grade water in $20 \mu\text{l}$ reaction system. The gene specific primers were obtained from Primer bank and sequences are listed below (Table 2.2). The above reaction mixtures were amplified in the following steps: step 1- denaturation at 95°C for 5 minute; step 2-denaturation at 95°C for 15 seconds ; step 3- annealing at 56°C for 15 seconds; step 4-extension at 72°C for 20 seconds ; step 5- melting curve analysis. Steps from 2 to 4 were repeated for 40 cycles. The specificity of respective amplicons was confirmed from the melting curve analysis. The amplification of each gene was carried out in triplicates for each group. The threshold cycle (the cycle at which the amplification enters into exponential phase) values (Ct value) obtained from above runs were used for calculating the expression levels of genes by REST-384 version 2 software¹²⁹. The expressions of genes were normalized against that of a housekeeping gene, β -actin, and plotted as relative change in the expression with respect to control.

S.N.	Gene	Primer Sequence (5'→3')
1.	Nrf2	Forward Primer: 5'- CTTTAGTCAGCGACAGAAGGAC-3' Reverse Primer: 5'- AGGCATCTTGTTTGGGAATGTG -3'
2.	Map3k1 (MEKK1)	Forward Primer: 5'- AGCACGAGTGGTTGGAGAG -3' Reverse Primer: 5'- CTGGGGATTCCGGCTTCAC-3'

3.	Map2k1 (MEK1)	Forward Primer: 5'- AACGGTGGAGTGGTCTTCAAG-3' Reverse Primer: 5'- CGGATTGCGGGTTTGATCTC-3'
----	------------------	---

Table 2.2: Sequence of Primer used for real time PCR analysis

2.2.29 Administration of NQ to mice and *in vivo* radioprotection studies:

BALB/c mice (5 animals per group) were administered with NQ (0.25-2mg/kbw) and 0.5h after NQ injection these mice were exposed to the 4Gy WBI. Appropriate vehicle was for control or radiation group. These mice were sacrificed on day 5 after WBI and spleen and bone marrow were harvested. Spleen weights were recorded and spleen index was calculated [Spleen index = (spleen weight/body weight) x100] as described previously¹¹⁴. Viability of spleen cells and bone marrow cells were enumerated by trypan blue dye exclusion method. Enumeration of different subpopulations in spleen cells was done by direct immunofluorescence staining as described in section 2.2.24.

2.2.30 Measurement of hematological profile and plasma nitric oxide (NO):

To study the hematological profile, mice (10 animals per group) were administered with NQ (2mg/kbw) or vehicle and were exposed to WBI (4Gy) after 0.5h. Blood was collected from treated mice on day 5 after WBI by retro-orbital puncture and complete blood count was performed using autoanalyzer for assessment of various hematological parameters.

Blood was microcentrifuged at 15000rpm for 15minutes 4°C and supernatant were collected which serve as plasma and used for measurements of NO using Griess reagent as described earlier¹¹⁴. Plasma (100µl) was incubated with 100µl of Griess reagent (1% sulfanilamide, 0.1% NEDD, 2.5% phosphoric acid in distilled water). The absorbance was measured at 550nm using an ELISA plate reader (Bio-Tek Instruments,

USA). Amount of NO in each sample was calculated from a standard curve generated with known dilutions of sodium nitrite.

2.2.31 Measurement of radioprotective cytokines (IL-1 β and IL-6) in plasma by ELISA:

Effect of NQ administration on induction of radioprotective cytokines (IL-1 β and IL-6) was studied by sandwich ELISA. Mice were administered with NQ (2mg/kbw) or vehicle. Blood was collected from treated mice on day 5 after injection and plasma were removed by centrifugation at 15000rpm for 15minutes 4°C and used for estimation of cytokine using cytokine ELISA sets.

Capture antibody for each cytokine was dissolved in bicarbonate buffer and used for coating the wells in a 96 well microtitre plate (1:250 dilution, 100 μ l/well). The plates were sealed with parafilm to avoid evaporation and incubated at 4°C overnight. Unbound antibody was aspirated and wells were washed three times with wash buffer (PBS with 0.05% Tween 20). Wells were blocked with blocking buffer (PBS with 10% FCS) for 1h at room temperature and washed three times with wash buffer (PBS with 0.05% Tween 20). The plasma (100 μ l) was added to three wells in each group. To another set of wells, 100 μ l serial dilutions of cytokine standards IL-1 β (0-500ng/ml) and IL-6 (0-500ng/ml) were added in three replicates and plates were incubated at room temperature for two hours. The wells were aspirated and washed four times to remove any unbound cytokines. Streptavidin conjugated detection antibody and biotin conjugated Horse Radish Peroxidase (HRP) enzyme were dissolved and mixed in blocking buffer in 1:1 ratio and 100 μ l of freshly prepared mixture was added to each well. Plates were incubated at room temperature for 1h. The wells were aspirated and washed five times to remove any unbound antibody. 100 μ l tetramethyl benzidine (TMB) substrate was added

to each well and incubated at room temperature for 15 minutes. Stop solution (1N HCl, 50µl) was added to inhibit further reaction and absorbance was taken at 550nm using an ELISA reader. Standard curves were generated and amount of cytokine in each well was estimated from the standard curve of respective cytokines.

2.2.32 Measurement of functional response of lymphocytes:

Mice (5 animals per group) were administered with NQ (2mg/kbw) or vehicle and were exposed to WBI (4Gy) after 0.5h. These mice were sacrificed on day 5 after WBI and splenic lymphocytes were harvested. Lymphocytes (1×10^6 /ml) obtained from treated animals were cultured in the presence or absence of Con A (10µg/mL) for 24h at 37°C in 2ml complete medium for estimation cytokine. For cell cycle analysis lymphocytes (1×10^6) from treated animals were cultured in presence or absence of Con A (10µg/mL) at 37°C in 1ml complete medium in a 5% CO₂ atmosphere for 72h.

Concentrations of IL-2, IL-4, IL-6 and IFN-γ were evaluated in culture supernatants harvested 24h after Con A addition by using cytokine ELISA sets as described in section 2.2.31. The supernatants obtained from unstimulated and Con A stimulated spleen cells obtained from vehicle administered mouse were used as negative and positive control respectively.

The percentage of cells in different phases of cell cycle (G1, S/G2+M) was estimated from DNA content of individual cells stained with PI and analyzed in a flowcytometer. Cells in G0/G1 phase of cell cycle have 2nDNA. The cells in G2 and M phases of cell cycle contain 4nDNA that is double of that in cells in G0/G1 phase. The cells in S phase show DNA higher than 2n and less than 4n.

The cells were harvested at 72h after stimulation with Con A and washed with 10mM PBS and stained with PI solution. Undivided cells were in G1 phase of cell cycle

(2n DNA content). The sub-G1 population represented the apoptotic cells. The cells containing more than 2n DNA represented S/G2+M phase of cells.

2.2. 33 Histopathological studies:

Mice (5 animals per group) were administered with NQ (2mg/kbw) or vehicle and were exposed to WBI (4Gy) after 0.5h. These mice were sacrificed on day 5 after WBI and spleen and femur bone were collected and fixed in 10% neutral buffered formalin.

Spleen were dehydrated by passing through a graded series of alcohol and embedded in to paraffin blocks. Fixed femur bone were decalcified for 3h and routinely processed with progressive dehydration of tissues in ethanol, clearing in xylene, paraffin vacuum infiltration, and embedded in to paraffin blocks. The sections of 5µm thickness were cut using a rotary microtome (AO 820, USA). The sections of tissues were stained in eosin and Harris haematoxylin and examined using upright trinocular microscope attached to CCD camera.

2.2.34 Endogenous spleen colony formation assay:

Endogenous spleen colony formation assay is used to study the proliferative capacity of HSCs present in the bone marrow. This assay is based on the fact that partially ablated and residual endogenous HSCs in the mice exposed to sublethal dose of ionizing radiation, have ability to proliferate, differentiate and form the colonies within hematopoietic organs like spleen. These macroscopic colonies arise in the spleens of irradiated animals 10-12 days post irradiation. These endogenous spleen colonies appeared as discrete, round or oval and embedded in the red mass of spleen and represent the rapidly proliferating hematopoietic stem cells¹³⁰.

It is reported that mice exposed to lower than two third of LD_{50/30} radiation dose give colonies too numerous to count¹³¹, therefore in the present study radiation dose

greater than two third of LD_{50/30} were used. From the survival study LD_{50/30} for Balb/c mice used in our experimental study was found to be 6.67Gy, and dose equivalent to two third of LD_{50/30} is 4.45Gy. Hence, in the present study we used radiation dose 6Gy that are greater than 4.45Gy. Mice (7 animals per group) were administered with NQ (2mg/kbw) or vehicle and were exposed to WBI (6Gy) after 0.5h. These mice were sacrificed on day 9 after WBI and spleen were collected and fixed in 10% neutral buffered formalin and the spleen colonies formed by proliferation of surviving endogenous hematopoietic cells on surface of spleen were counted with the naked eye¹³⁰.

To confirm that nodules appeared on surface of spleen were rapidly proliferating cells; immune-fluorescence staining was carried out in the splenocytes isolated from nodules bearing spleen. Since PCNA (Proliferating nuclear cell antigen) is considered as marker for cell proliferation, therefore antibody staining was performed with anti-PCNA antibody by the method described in section 2.2.24.

2.2.35 In vivo radioprotection studies using apoptotic parameters:

Mice (5 animals per group) were administered with NQ (2mg/kbw) or vehicle 0.5h prior to WBI (4Gy) and immediately sacrificed and spleen was harvested and single cell suspension of lymphocytes was prepared. Lymphocytes (1×10^6) were cultured for 24h at 37°C. The cells were processed for PI-staining, DNA-fragmentation, nuclear-blebbing, homogenous caspase activity, Bax-staining and change in MMP as described earlier section used for *in vitro* experiments.

2.2.36 Survival studies:

Mice (20 animals per group) were administered NQ (2mg/kbw) or vehicle and were given WBI (7Gy) after 0.5h. To estimate dose modification factor (DMF), radiation doses between 6 to 8.5 Gy were used. Groups of 10 animals each were pretreated with a

single i.p. injection of NQ (2mg/kgbw) and after 0.5h irradiated with 6, 6.5, 7, 7.5, 8, 8.5 Gy. The animals were monitored daily for 30 days after irradiation, and mortality and their body weight were recorded. The average percentage mortality was converted into probit value as reported earlier¹⁰⁵ and DMF was calculated by taking the ratio of radiation LD50/30 in presence and absence of NQ.

2.237 Statistical analysis:

Data are presented as mean \pm SEM. The statistical significance of the differences in respect of all parameters studied between untreated and irradiated groups in presence or absence of NQ was assessed by one way ANOVA with Microcal Origin 7.5 software followed by post-hoc analysis using Scheffe's test. Values of $p < 0.05$ were considered statistically significant.

2.3 RESULTS

2.3.1 NQ protected lymphocytes against radiation induced cell death:

Since lymphocytes, the key players of adaptive immune response are highly sensitive to radiation, we examined the effects of NQ pretreatment on radiation induced apoptosis in splenic lymphocytes. Fig.2.1A shows flow cytometric histograms of PI stained cells exposed to radiation in presence or absence of NQ. NQ (1 μ M) reduced basal cell death in lymphocytes suggesting that it is not toxic to cells at this concentration (Fig. 2.1A). Exposure of cells to radiation induced apoptosis and NQ pretreatment significantly inhibited the radiation induced apoptosis in a concentration dependent manner (Fig. 2.1 B).

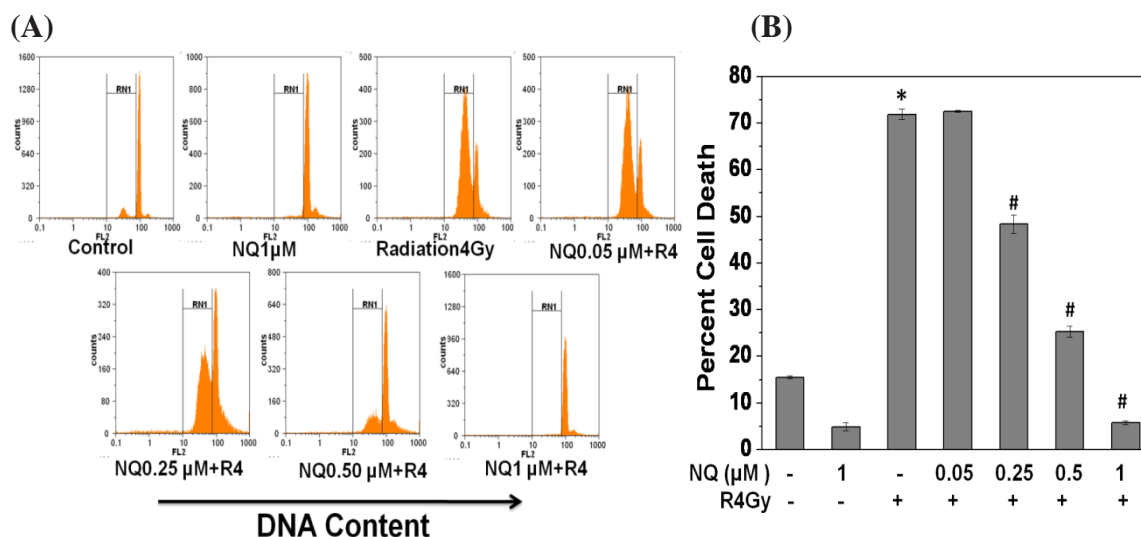


Fig. 2.1: NQ protected lymphocytes against radiation induced death: Murine splenic lymphocytes were incubated with NQ (0.05-1 μ M) for 2h at 37°C, exposed to 4Gy gamma irradiation and further cultured for 24h. The cell death was estimated by PI staining. Twenty thousand cells in each group were acquired using a Partec PASIII flowcytometer and percent death were analyzed by using Flowmax® software. Sub G1 region (RN1) represents percentage of cells undergoing apoptosis. Representative flow cytometric histograms (A) and corresponding bar diagram (B) showing NQ mediated amelioration of radiation induced apoptosis. The data is the representative of two such independent experiments having similar results. Each bar shows the mean \pm SEM from three replicates. * $p < 0.05$, as compared to vehicle treated control and # $p < 0.05$, as compared to irradiated group.

The observed radioprotection by NQ was further confirmed by various techniques like live and dead assay (Fig. 2.2A), DNA-fragmentation (Fig. 2.2B), changes in cell size (Fig. 2.2C), nuclear-blebbing, (Fig. 2.2D) and caspase activity (Fig. 2.2E).

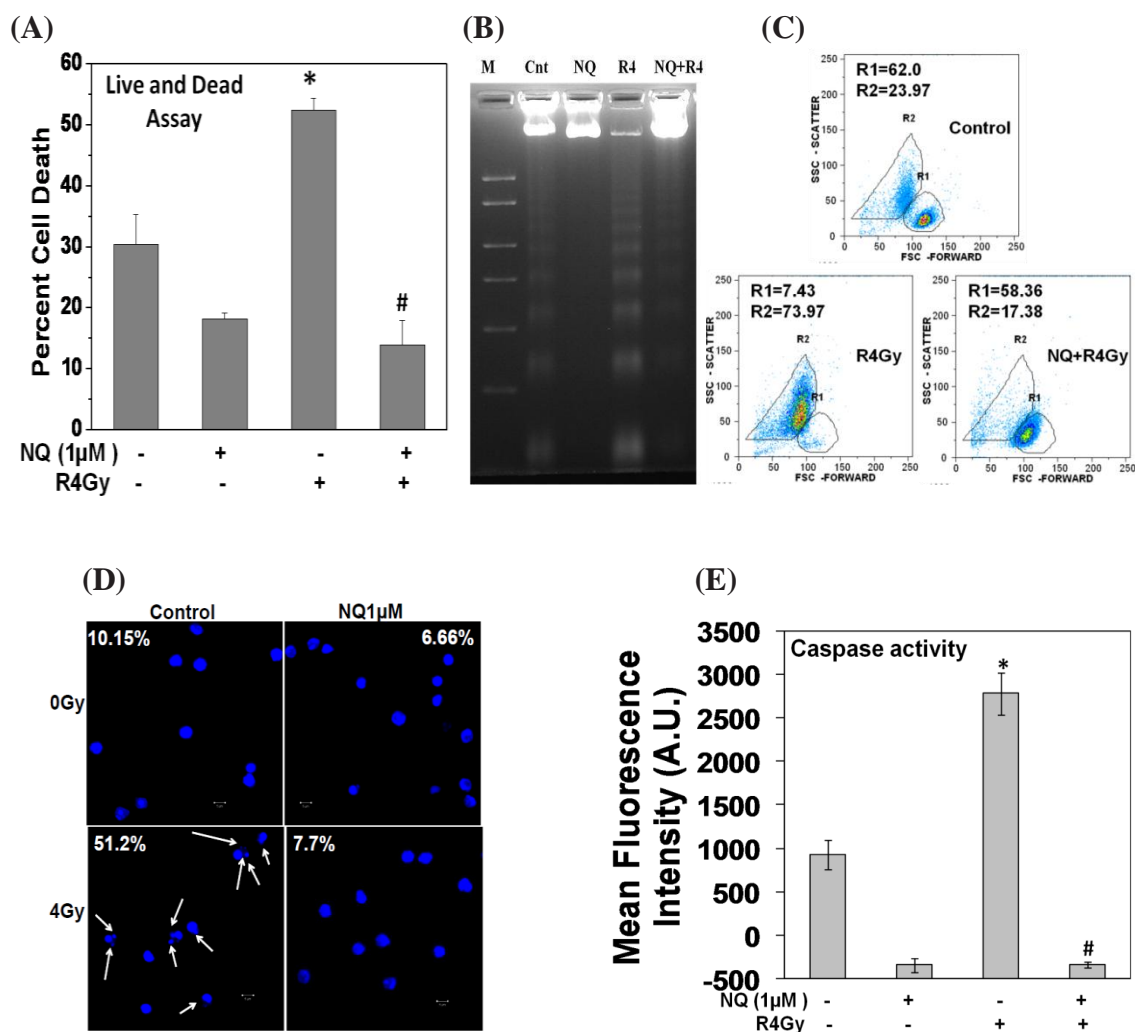


Fig. 2.2: NQ protected lymphocytes against radiation induced death: Murine splenic lymphocytes were incubated with NQ (1μM) for 2h at 37°C, exposed to 4Gy gamma irradiation and further cultured for 24h. The cell death was estimated by (A) live and dead assay, (B) DNA-fragmentation assay, (C) change in forward and side scatter was used to assess the size and density of cells. Cells undergoing apoptosis showed low FSC and increase in cell density. (D) nuclear-blebbing. White arrows indicate the presence of nuclear blebb, and (E) homogenous caspase (2, 3, 6, 7, 9 and 10) activity as described in material method section. The data is the representative of two such independent experiments having similar results. Each bar shows the mean±SEM from three replicates. *p<0.05, as compared to vehicle treated control and #p<0.05, as compared to irradiated group.

2.3.2 Other prooxidants also protected lymphocytes against radiation induced cell death:

To establish the concept of radioprotection by prooxidants, we have employed several other known prooxidants like H_2O_2 , DEM, a known GSH depletory and t-BHQ. The result showed that transient exposure of lymphocytes with H_2O_2 , t-BHQ offered complete protection against radiation induced apoptosis (Fig. 2.3A-C). Similarly DEM, a known GSH depletor¹³² treatment to lymphocytes also gives protection against radiation induced apoptosis (Fig. 2.3D).

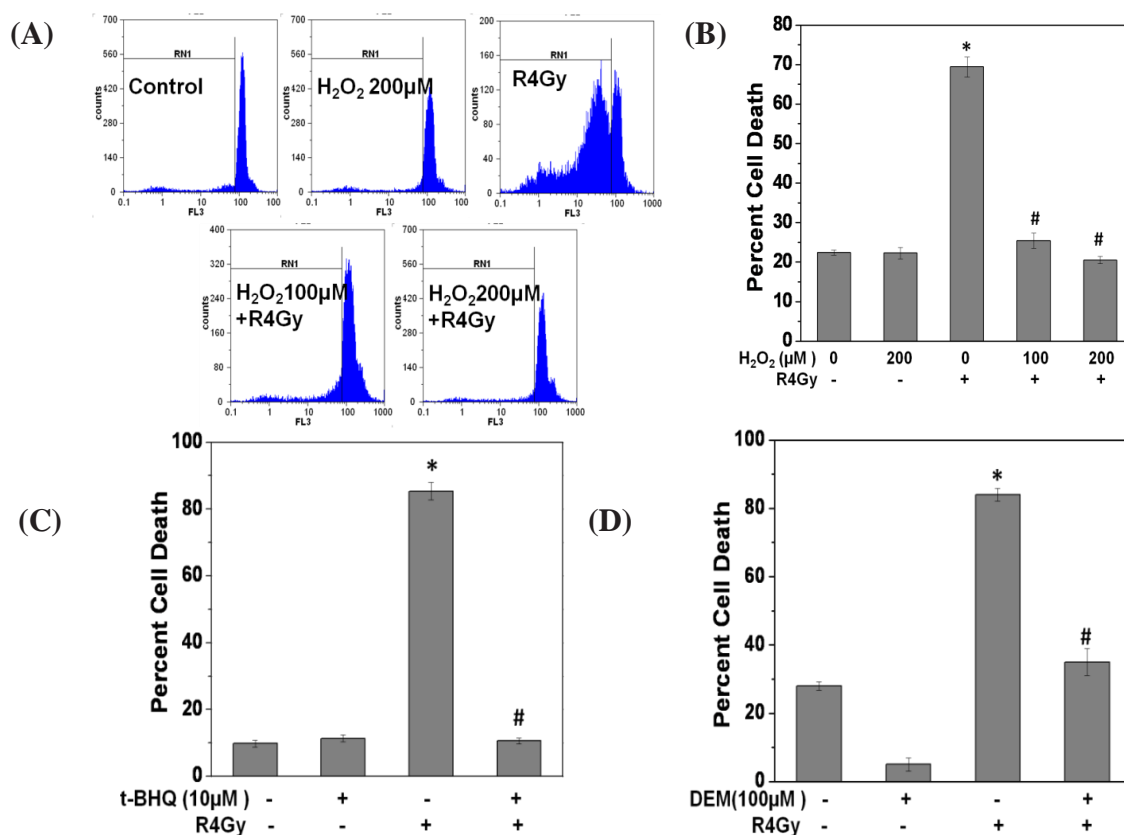


Fig. 2.3: Prooxidants protected lymphocytes against radiation induced death: Lymphocytes were incubated with H_2O_2 (100-200 μ M) for 5 minutes or t-BHQ (100 μ M) or DEM (100 μ M) for 2h at 37°C. The cells incubated with H_2O_2 or t-BHQ, were washed with RPMI to eliminate their potential toxicity. These cells were exposed to 4Gy gamma irradiation and further cultured for 24h, and cell death was measured by PI staining. Representative flowcytometric histogram (A) of H_2O_2 treated cells and stained with PI and Bar diagram (B-D) showing amelioration of radiation induced apoptosis by treatment with (B) H_2O_2 , (C) t-BHQ and (D) DEM. The data is the representative of two such independent experiments having similar results. Each bar shows the mean \pm SEM from three replicates and two such independent experiments were carried out. *p<0.05, as compared to vehicle treated control and #p<0.05, as compared to irradiated group.

2.3.3 NQ inhibited radiation induced death in lymphocytes:

Since pretreatment of lymphocytes with NQ protected against radiation induced apoptosis, therefore to understand whether NQ is required to be present throughout to exhibit radioprotection, cells were washed 2h after NQ addition and exposed to radiation. NQ offered complete protection against radiation induced cell death despite washing the cells (Fig. 2.4A, B). Incubation of cells with NQ (1 μ M) for different time intervals (0 to 4h) before exposing them to radiation revealed 100% protection against radiation induced cell death at all the time points used in our study (Fig. 2.4C). Further radiation dose response study shows that NQ (1 μ M) mitigated radiation induced cell death even up to a dose of 25Gy (Fig. 2.4D). Dose of radiation more than 8Gy showed significant decline in percent apoptosis suggesting that necrosis may be predominant at higher doses of radiation over apoptosis (Fig. 2.4D). These results were in agreement with earlier report from our laboratory¹³³.

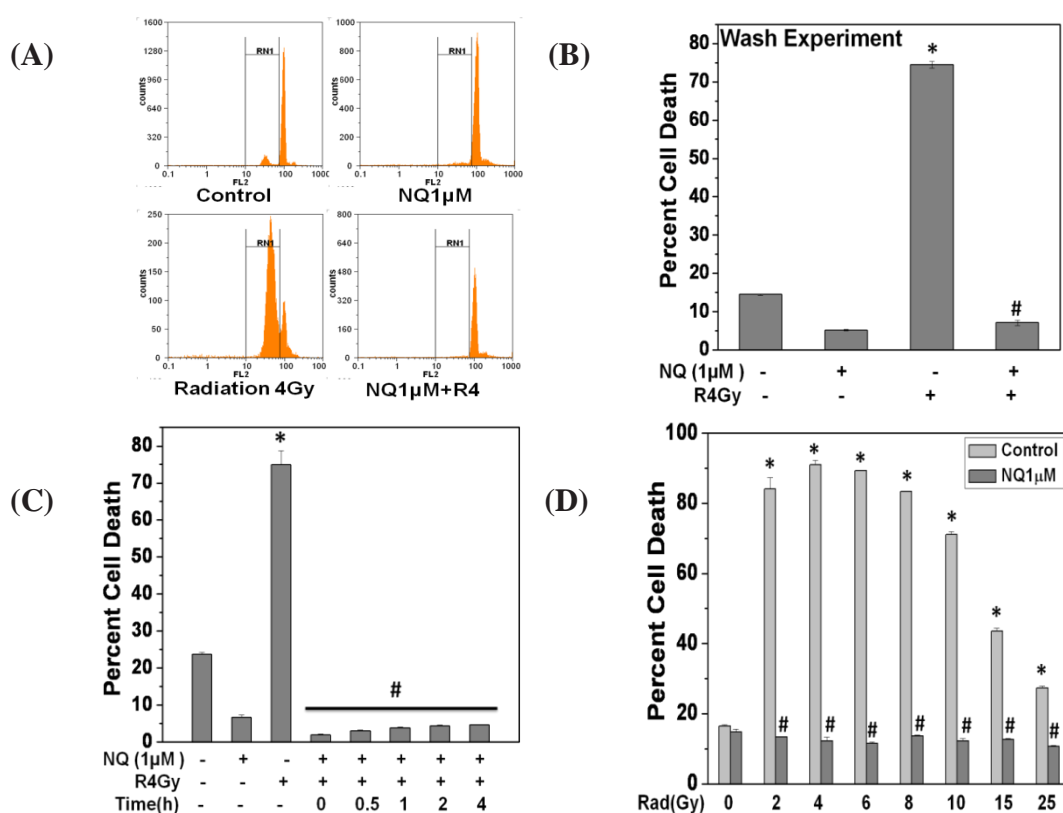
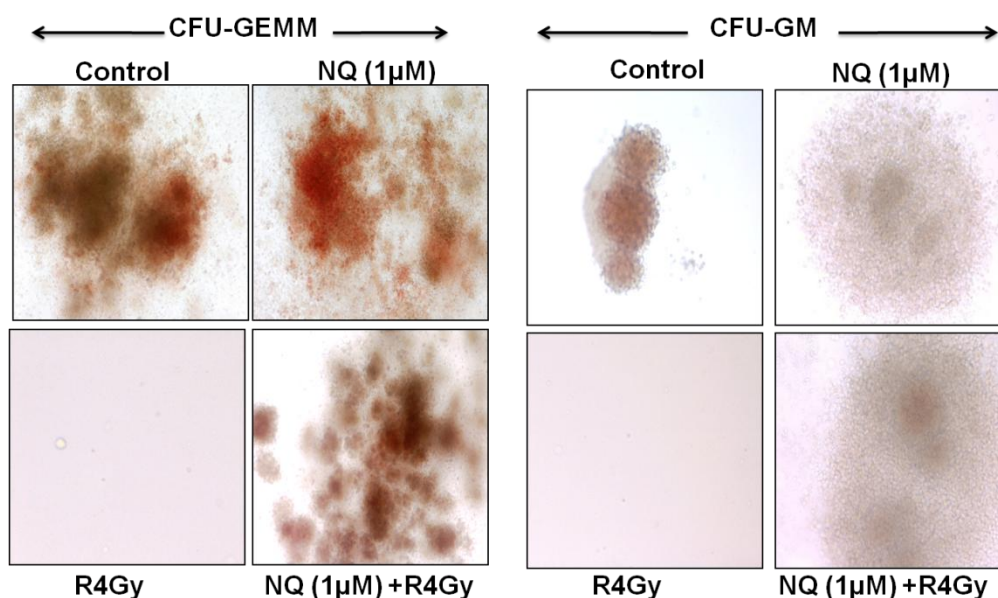


Fig. 2.4: NQ inhibited radiation induced death in lymphocytes: (A, B) Radioprotective effect of NQ is not reversible. Lymphocytes were incubated with NQ (1 μ M) for 2h at 37°C and washed twice with RPMI and then irradiated with 4Gy and cultured for 24h. Cell death was estimated by PI staining. Representative flowcytometric histograms (A) and corresponding bar diagram (B) are shown. (C) Cells were treated with NQ for different time intervals (0 to 4h) before exposing them to radiation and percentage cell death was measured by PI staining. (D) Estimation of cell death in response to different doses of radiation (2-25Gy) in presence or absence of NQ by PI staining. The data is the representative of two such independent experiments having similar results. Each bar shows the mean \pm SEM from three replicates. *p<0.05, as compared to vehicle treated control and #p<0.05, as compared to irradiated group.

2.3.4 NQ restored the radiation induced loss of proliferative potential of hematopoietic stem cells present in spleen:

The stem cell content in the spleen is about 0.01% of total nucleated cells¹³⁴ which has the potential to proliferate and differentiate into heterogeneous populations of different hematopoietic progenitors. Since, stem cells are highly sensitive to radiation, experiment was designed to see whether NQ can protect the proliferating ability of HSCs of spleen and results of CFC assay showed that NQ treatment prior to radiation prevented the radiation induced loss of proliferative capacity of HSCs present in the spleen and restored the ability to proliferate and differentiate into multiple progenitors (e.g. CFU-GEMM) and lineage committed progenitors of erythroid (BFU-E, CFU-E), granulocyte (CFU-G) and monocyte-macrophage (CFU-M) cells (Table 2.3 Fig. 2.5).



Hematopoietic Progenitor cell content of Splenocytes							
	Progenitor cell contents per 0.2×10^6 splenocytes plated (Mean \pm S.E.M.)						
Treatments	CFU-E	BFU-E	CFU-G	CFU-M	CFU-GM	CFU-GEMM	Total Colonies
Control	52 \pm 4.1	27 \pm 2.7	17 \pm 2.0	10.5 \pm 4.5	21 \pm 2.3	1.5 \pm 0.5	129 \pm 11.6
NQ(1 μ M)	28 \pm 3.0	26 \pm 1.0	19 \pm 3.0	3.5 \pm 2.5	24 \pm 8.0	8.5 \pm 0.5	109 \pm 12.3
R4Gy	1.5 \pm 0.5*	4 \pm 1.0*	2 \pm 1.0*	1.5 \pm 0.5*	0 \pm 0.0	0 \pm 0.0	9 \pm 1.1*
NQ1+R4Gy	24 \pm 1.0#	43 \pm 9.5#	4.5 \pm 0.5#	8.5 \pm 3.5#	35 \pm 9.0	17.5 \pm 0.5	132.5 \pm 13.7#

Fig. 2.5 and Table 2.3 NQ restored the radiation induced loss of proliferative potential of hematopoietic stem cells present in spleen: Splenocytes were treated with NQ (1 μ M) for 2h before exposing them to radiation of 4Gy and cultured in methyl cellulose complete medium for 11days as described in material method section. Colonies were enumerated under inverted microscope using scoring grid and representative image of CFU-GEMM and CFU-GM are shown in figure 2.5. *p<0.05, as compared to vehicle treated control and #p<0.05, as compared to irradiated group.

2.3.5 NQ inhibited radiation induced apoptosis in lymphocyte when added post irradiation:

Since NQ pretreatment to lymphocytes offered radioprotection, experiments were designed to whether NQ has therapeutic potential. It was also found that NQ protected significantly against radiation induced cell death even when added after irradiation. Complete protection was observed by addition of NQ upto 2h after irradiation. However, percent protection decreased with increasing time interval (Fig. 2.6).

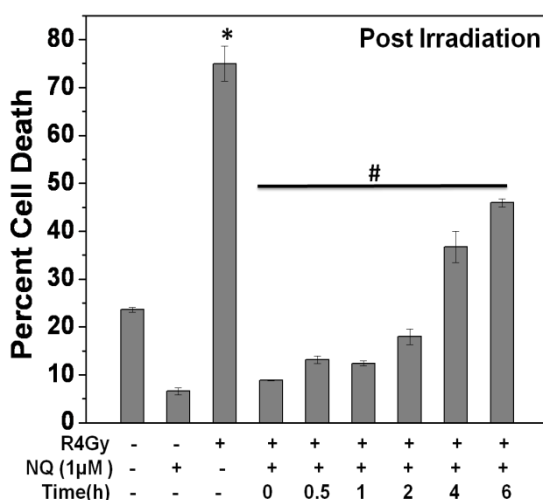


Fig. 2.6: NQ inhibited radiation induced apoptosis in lymphocyte when added post irradiation: NQ (1 μ M) was added to lymphocytes at different time intervals (0-6h) after irradiation (4Gy) and cultured for 24h at 37°C and cell death was measured by PI staining. The data is the representative of two such independent experiments having similar results. Each bar shows the mean \pm SEM from three replicates. *p<0.05, as compared to vehicle treated control and #p<0.05, as compared to irradiated group.

2.3.6 NQ protected CD4+T cells and CD19+B cells against radiation induced death:

Protecting CD4+T cells against radiation induced cell death may aid in effective anti-tumor immune responses following radiotherapy. Purified CD4+T cells or CD19+B cells were exposed to radiation in presence or absence of NQ. NQ (1 μ M) completely protected radiation induced death in CD4+T cells as estimated by increase in preG1 population and DNA fragmentation (Fig. 2.7A-C). Radioprotective effect of NQ was not limited to only CD4+ T cells, it also protected CD19+B cells to the same extent at 1 μ M concentration (Fig. 2.7D).

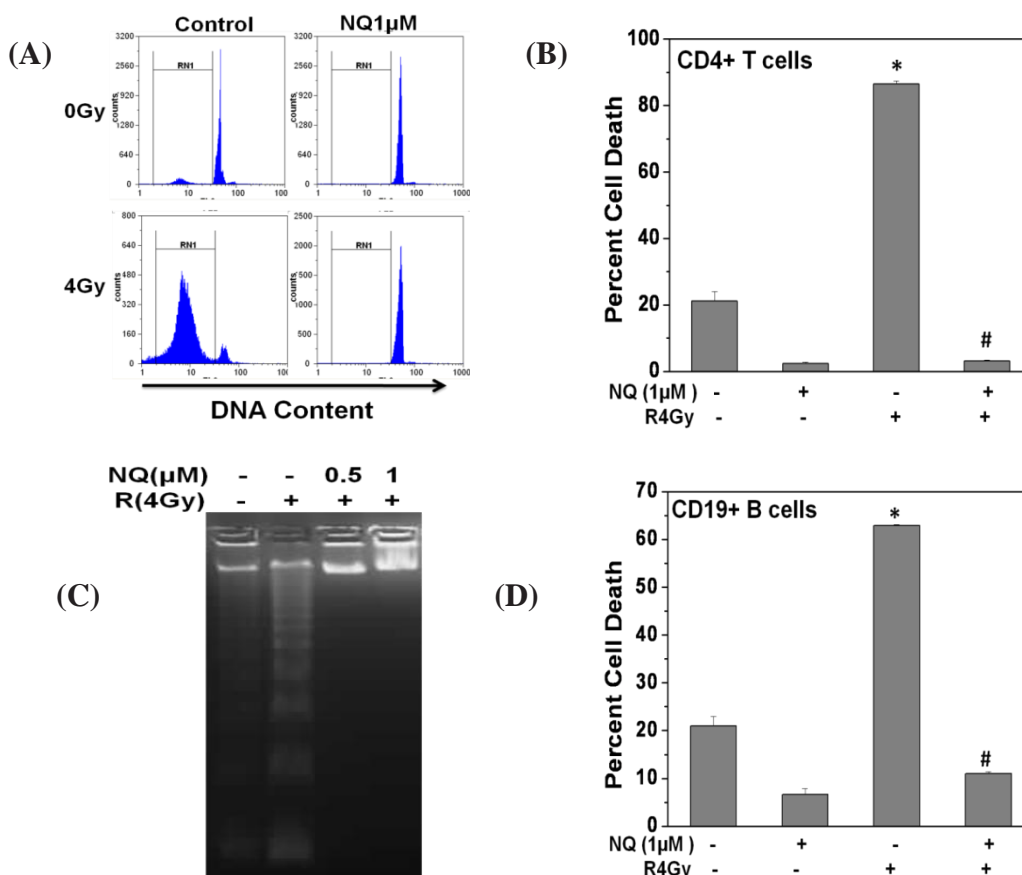
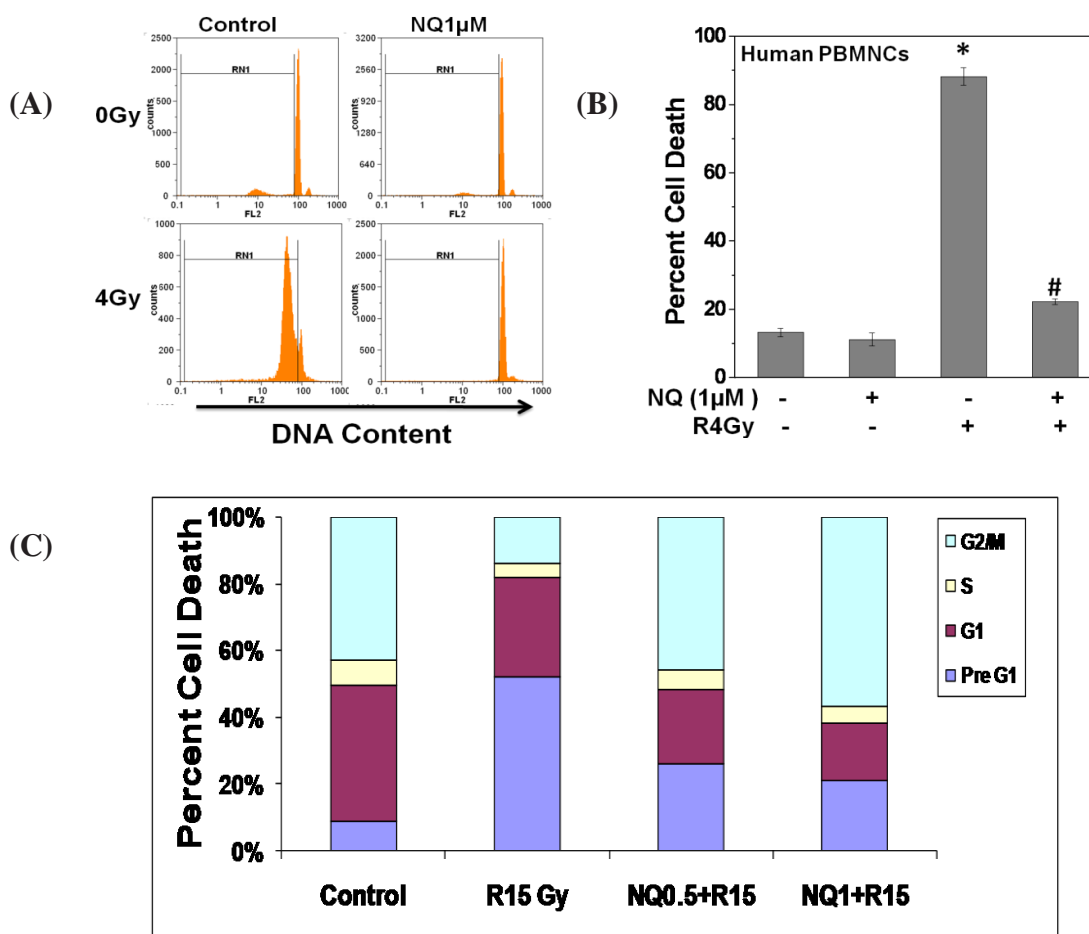


Fig. 2.7: NQ protected CD4+T cells and CD19+B cells against radiation induced death: Purified CD4+ T cells or CD19+ B cells (1×10^6 each) were incubated with NQ (1 μ M) for 2h at 37 $^\circ$, exposed to 4Gy radiation and cultured for 24h. Cell death was estimated by DNA fragmentation assay in CD4+T cells (B) and PI staining in both CD4+ T cells and CD19+ B cells (A, C, D). Representative flowcytometric histograms of CD4+ T cells (A) and corresponding bar diagram (C) are shown. The data is the representative of two such independent experiments having similar results. Each bar shows the mean \pm SEM from three replicates. *p<0.05, as compared to vehicle treated control and #p<0.05, as compared to irradiated group.

2.3.7 NQ protected human PBMNCs and human intestinal epithelial cells (Int407) against radiation induced death:

To ascertain the radioprotective effects of NQ were of general importance for multiple cell types, similar experiment were performed in human PBMNCs and normal human intestinal epithelial cell line (Int407). The results PI staining showed NQ pretreatment completely protected radiation induced death in PBMNCs (Fig. 2.8A, B). Similarly, PI staining in Int407 revealed that radiation (15Gy) induced increase in pre-G1 (death) population and decrease in G2/M (proliferating) population were reversed by pretreatment of NQ (Fig. 2.8C, D). Further, clonogenic assay performed on Int407 revealed that NQ abrogated radiation (4, 6 Gy) induced loss of colony forming ability of these cells (Fig. 2.8E).



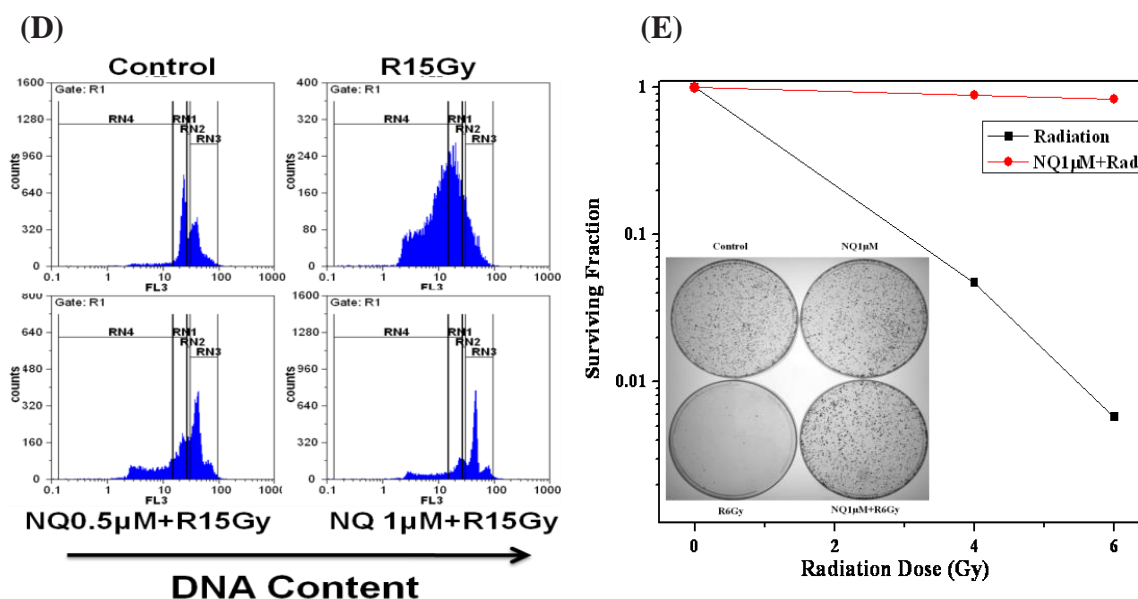


Fig. 2.8: NQ protected human PBMNCs and human intestinal epithelial cells (Int407) against radiation induced death: (A, B) Human PBMNCs (1×10^6) were incubated with NQ ($1 \mu\text{M}$) for 2h at 37° , exposed to 4Gy radiation, cultured for 24h and cell death was estimated by PI staining. (C, D) Int407 (0.4×10^6) cells were allowed to adhere on surface of 6-well plate overnight, washed with RPMI and incubated with NQ ($1 \mu\text{M}$) for 2h at 37° , exposed to 15Gy radiation, cultured for 48h and death was estimated by PI staining. Representative flowcytometric histograms (A, D) and corresponding bar diagram (B, C) showing inhibition of radiation of cell death by pretreatment of lymphocyte with NQ. (E) Int407 (1000 cells) were seeded in 100mm culture dishes and incubated for 24h at 37°C for adherence, washed with RPMI and incubated with NQ ($1 \mu\text{M}$) for 2h, exposed to 4,6Gy radiation and cultured for 14 days. Visible colonies were enumerated after staining with crystal violet. The data is the representative of two such independent experiments having similar results. Each bar shows the mean \pm SEM from three replicates. * $p < 0.05$, as compared to vehicle treated control and # $p < 0.05$, as compared to irradiated group.

2.3.8 NQ inhibited radiation induced early events of apoptosis in lymphocytes:

Since, NQ showed radioprotective effects in lymphocytes by inhibiting radiation induced apoptosis, experiments were carried out to see whether NQ pretreatment could inhibit radiation induced early events of apoptosis. Alteration in intracellular Ca^{2+} homeostasis and mitochondrial membrane integrity leading to loss of MMP are early events of apoptosis. Results showed that treatment of lymphocytes with NQ ($1 \mu\text{M}$) completely inhibited radiation induced loss of MMP and release of calcium into cytoplasm (Fig. 2.9A, B). Taken together these results suggest that NQ showed

radioprotective effects in lymphocytes by inhibiting radiation induced activation of early events of intrinsic apoptotic pathways.

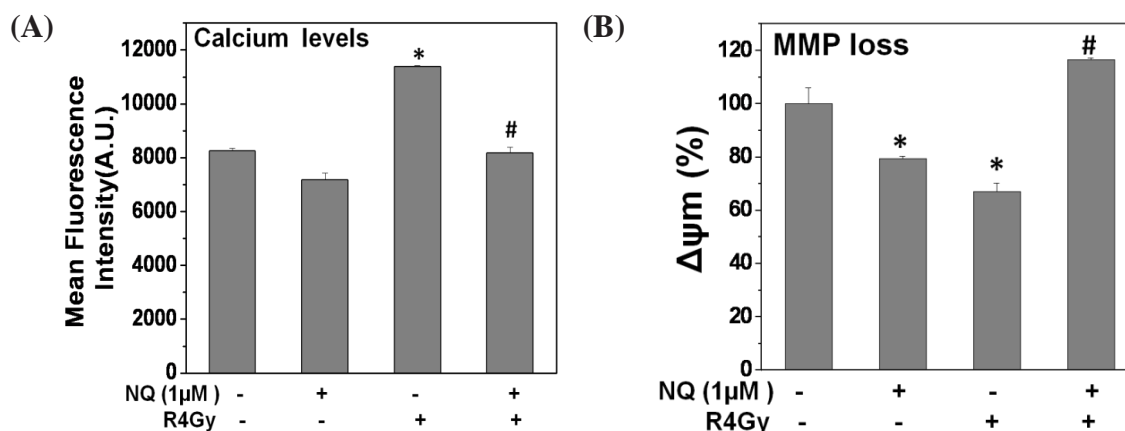


Fig. 2.9: NQ inhibited radiation induced early events of apoptosis in lymphocytes: Splenic lymphocytes (1×10^6) incubated with NQ (1μM, 2h) were exposed to radiation (4Gy) and further culture for 6h and cells were stained with (A) Fura 2-AM (2μM) for measurement of cytoplasmic calcium or (B) JC-1 (5μM) for measurement of MMP. The data is the representative of two such independent experiments having similar results. Each bar represents mean \pm S.E.M. from four replicates. * $p < 0.05$, as compared to vehicle treated control and # $p < 0.05$, as compared to irradiated group.

2.3.9 NQ upregulated antiapoptotic proteins (Bcl-2 and Bcl-xl) in lymphocytes:

Since, apoptosis is negatively controlled by up regulation of several antiapoptotic proteins like Bcl-2, Bcl-xl, experiments were carried out to see the effect of NQ treatment to lymphocytes on upregulation of these antiapoptotic proteins. Flow cytometric analysis of lymphocytes stained with anti-Bcl-2 and anti-Bcl-xl antibodies showed a marginal decrease in levels of these antiapoptotic proteins upon exposure of cells to radiation (Fig. 2.10A-D). Incubation of lymphocytes with NQ alone significantly increased the levels of these antiapoptotic proteins. Further, cells that were treated with NQ prior to exposure to radiation showed significant increase in Bcl-2 and Bcl-xl as compared to untreated group (Fig. 2.10A-D).

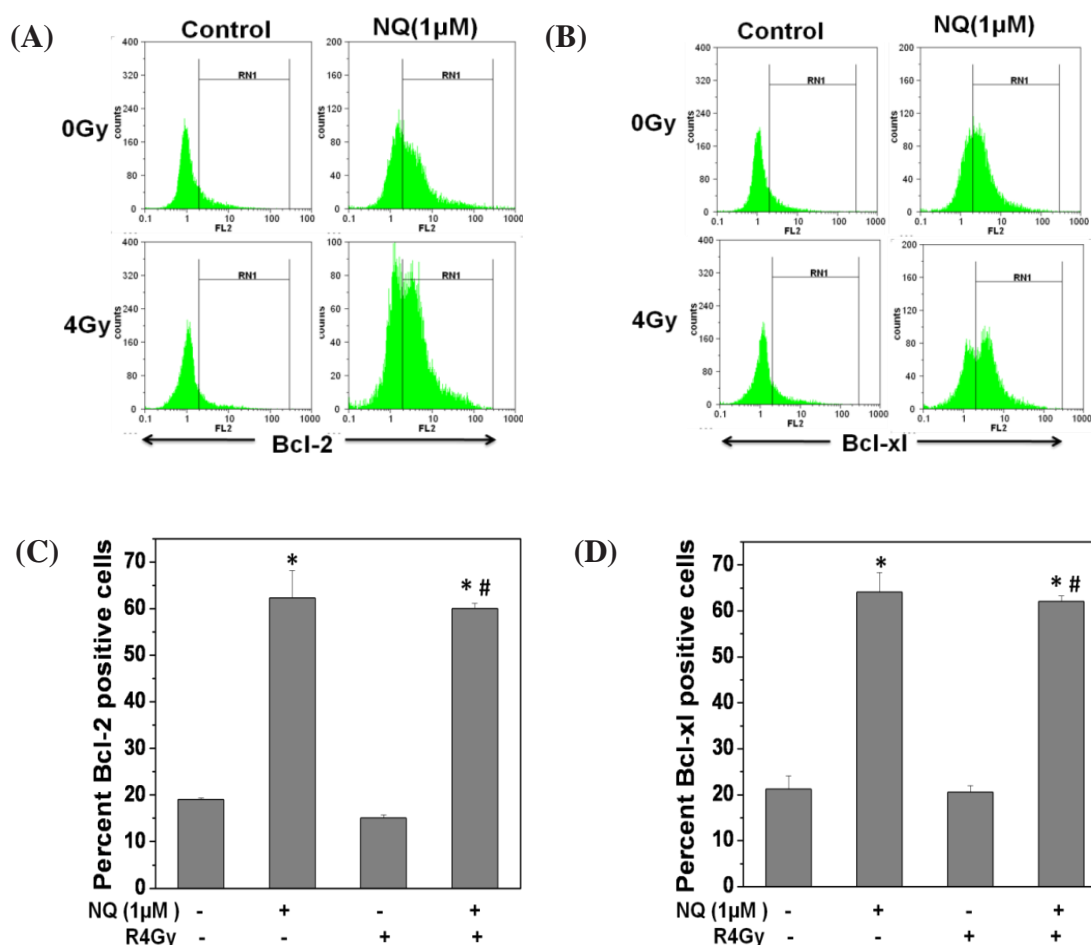


Fig. 2.10: NQ upregulated antiapoptotic proteins (Bcl-2 and Bcl-xl) in lymphocytes: Lymphocytes (3×10^6) were treated with NQ (1μM) for 2h prior to irradiation (4Gy) and cultured for 24h. Cells were stained with PE-labeled anti-Bcl-2 or anti-Bcl-xl antibodies and acquired on a Partec PAS III flow cytometer and percent labeled cells were estimated using Flowmax® software. Representative flowcytometric histograms (A, B) and corresponding bar diagram (C, D) showing upregulation of Bcl-2(A, C) or Bcl-xl (B, D) by treatment of lymphocytes with NQ. The data is the representative of two such independent experiments having similar results. Each bar represents mean±S.E.M. from three replicates. *p<0.05, as compared to vehicle treated control and #p<0.05, as compared to irradiated group.

2.3.10 NQ perturbed intracellular redox balance by increasing basal ROS levels and depleting cellular GSH levels:

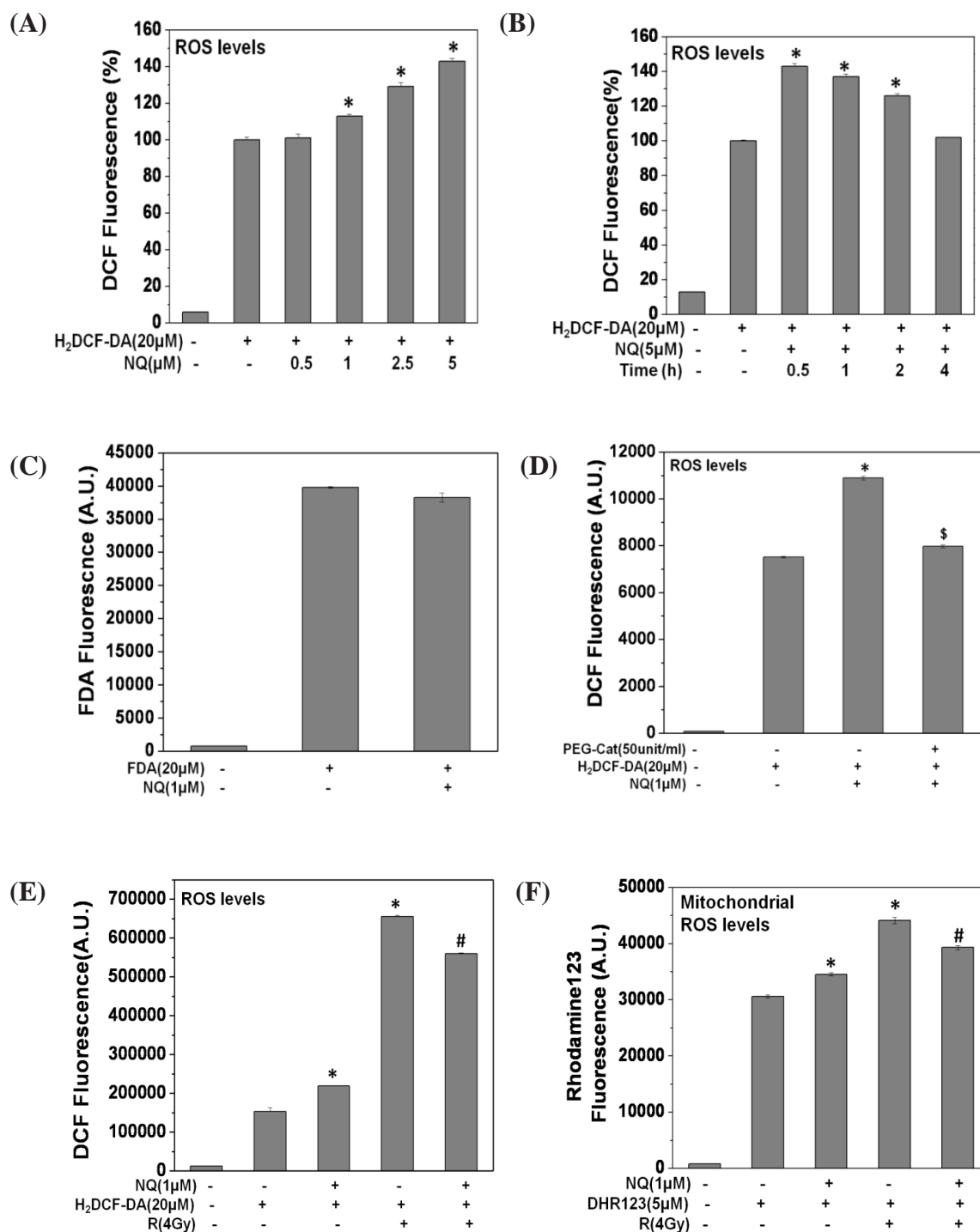
Most of the radioprotectors from natural sources have been shown to act by scavenging of radiation derived free radicals^{101,135,136}. Hence we measured the effect of NQ administration on basal and radiation derived ROS levels, surprisingly NQ elevated

basal ROS levels in splenic lymphocytes in a concentration dependent manner as measured using H₂DCF-DA (Fig. 2.11A). Further, time kinetics study showed that NQ initially increased basal ROS levels within 30minutes of its addition to lymphocytes, followed by a slow decline and reached the control levels within 4h of NQ addition (Fig. 2.11B). The increase in fluorescence intensity of DCF observed in our experiments due to oxidation of H₂DCF by ROS produced by NQ, could also be due to direct oxidation of H₂DCF by NQ itself. To rule out this possibility, we used oxidation insensitive analogue of H₂DCF-DA, fluorescein diacetate (FDA) to monitor the changes in uptake, ester cleavage, or efflux. Results showed that NQ did not increase the fluorescence of oxidation insensitive dye fluorescein diacetate suggesting that increased fluorescence intensity seen with H₂DCF-DA could be attributed to its oxidation by ROS that are generated by NQ (Fig. 2.11C). To further confirmed and identify the nature of ROS induced by NQ, PEG-catalase was used prior addition of NQ and it was observed that NQ mediated increase in fluorescence was significantly suppressed in presence of PEG-catalase which suggest that NQ treatment to lymphocytes induces ROS, major part of which is hydrogen peroxide (Fig. 2.11D).

Further, effect of NQ on radiation induced ROS levels was also determined and results showed that NQ exhibited marginal scavenging (14.67%) of radiation derived ROS (Fig. 2.11E). NQ (1μM) also increased mitochondrial ROS levels and marginally scavenged radiation derived mitochondrial ROS as measured by oxidation of dihydrorhodamine123 ((Fig. 2.11F).

Since cellular redox homeostasis is regulated by balance between intracellular ROS and GSH levels, we have measured effects of NQ treatment to lymphocytes on cellular GSH levels. It was found that NQ depleted intracellular GSH levels significantly

in lymphocytes 2h after treatment in a concentration dependent manner (Fig. 2.11G, H). DEM was used as positive control for GSH depletion.



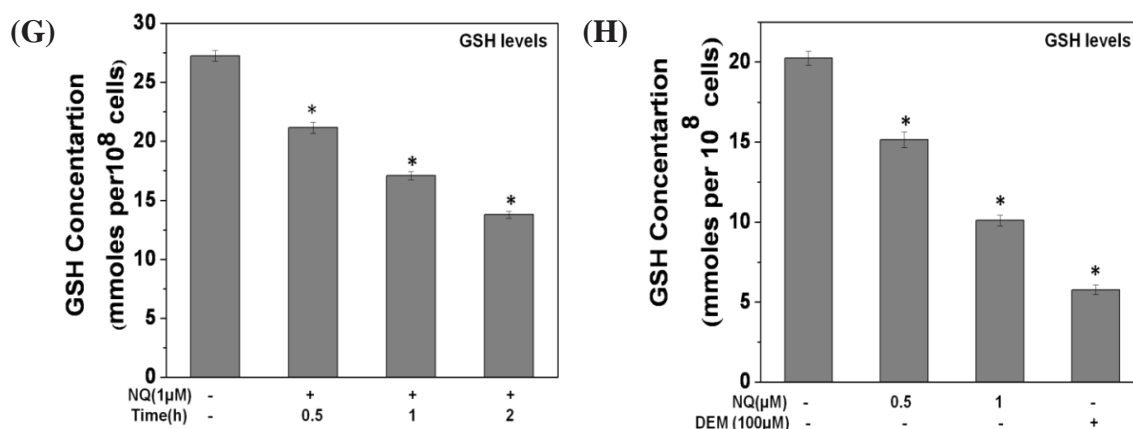


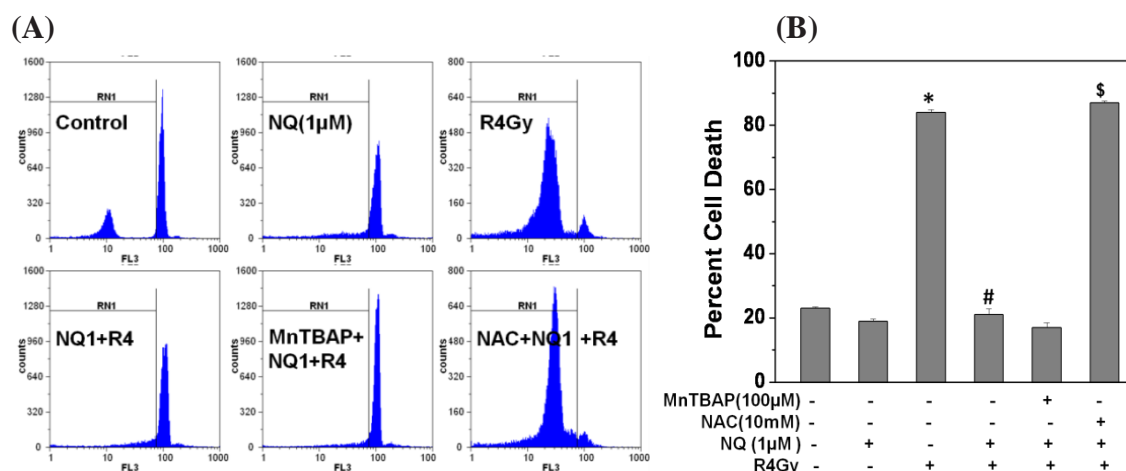
Fig. 2.11: NQ perturbed intracellular redox balance by increasing basal ROS levels and depleting cellular GSH levels: (A, B) NQ increased basal ROS levels in lymphocytes. H₂DCF-DA (20μM) stained lymphocytes (1x10⁶) were treated with NQ (1μM) for (A) 0.5h or (B) indicated time at 37°C and fluorescence emission was measured at 535nm, at excitation wavelength of 485nm. (C) NQ did not increase ROS levels in lymphocytes after incubation with oxidation insensitive analogue FDA. FDA (20μM) stained lymphocytes were treated with NQ (1μM) for 0.5h at 37°C and fluorescence emission was measured at 535nm, at excitation wavelength of 485nm. (D) NQ induced ROS is mainly hydrogen peroxide. Lymphocytes (1x10⁶) were pretreated with PEG-catalase (50unit/ml) for 1h and then stained with H₂DCF-DA (20μM) for 30 minutes and then treated with NQ for 0.5h at 37°C and fluorescence emission was measured at 535nm. (E, F) NQ scavenged radiation induced (E) intracellular and (F) mitochondrial ROS marginally. Lymphocytes (1x10⁶) were treated with NQ for 0.5h, stained with (E) DCFH₂-DA (20μM) or (F) DHR123 (5μM) and irradiated with 4Gy and fluorescence emission was measured at (E) 535nm, at excitation wavelength of 485nm or (F) 543nm, at excitation wavelength of 485nm using spectrofluorimeter. (G, H) NQ depleted intracellular GSH. Lymphocytes (100x10⁶) were treated with NQ (1μM) for (G) indicated time or (H) 2h and GSH level was measured by using glutathione assay kit as described in material and method section. DEM (100μM) treatment to lymphocytes was given for 1h. The data is the representative of four such independent experiments having similar results. Each bar represents mean±S.E.M. from four replicates. *p<0.05, as compared to either DCF or DHR control or vehicle treated control, #p<0.05, as compared to irradiated group and \$p<0.05, as compared to NQ treated control.

2.3.11 NQ mediated radioprotection was abrogated by thiol-containing antioxidants:

To understand the involvement of NQ mediated changes in ROS and GSH levels in the observed radioprotection, thiol and non-thiol antioxidants were used in combination with NQ. Fig. 2.12A, B showed that MnTBAP (non-thiol antioxidant) failed to abrogate the radioprotective efficacy of NQ but NAC (thiol antioxidant) completely inhibited the action of NQ. However when NAC was added to cells 2h after NQ

treatment, it failed to abrogate the radioprotective effect of NQ (Fig. 2.12C). Both NAC and MnTBAP by themselves did not protect against radiation induced cell death at the concentrations used (Fig. 2.12D). This suggested that depletion of thiol levels by NQ may be playing a role in the observed radioprotection.

Since the radioprotective effect of NQ was sensitive to presence of thiol antioxidants, experiments were carried out to determine whether NQ physically interacted with thiol group. NQ was incubated with NAC and subjected to HPLC separation. Retention time of pure NQ on C18 column was 3.2min (Fig. 2.12E, black line). This peak height was attenuated when NQ was preincubated with NAC (blue line). These results indicated that NQ indeed reacts with NAC. To characterize the products, MS analysis was carried out. Molecular mass analysis revealed that the major peak corresponded to NQ–NAC adduct ($M=323.1$) (Fig. 2.12F). In addition to NQ–NAC complex, another peak corresponding to m/z 162 was observed which could be that of unreacted NAC.



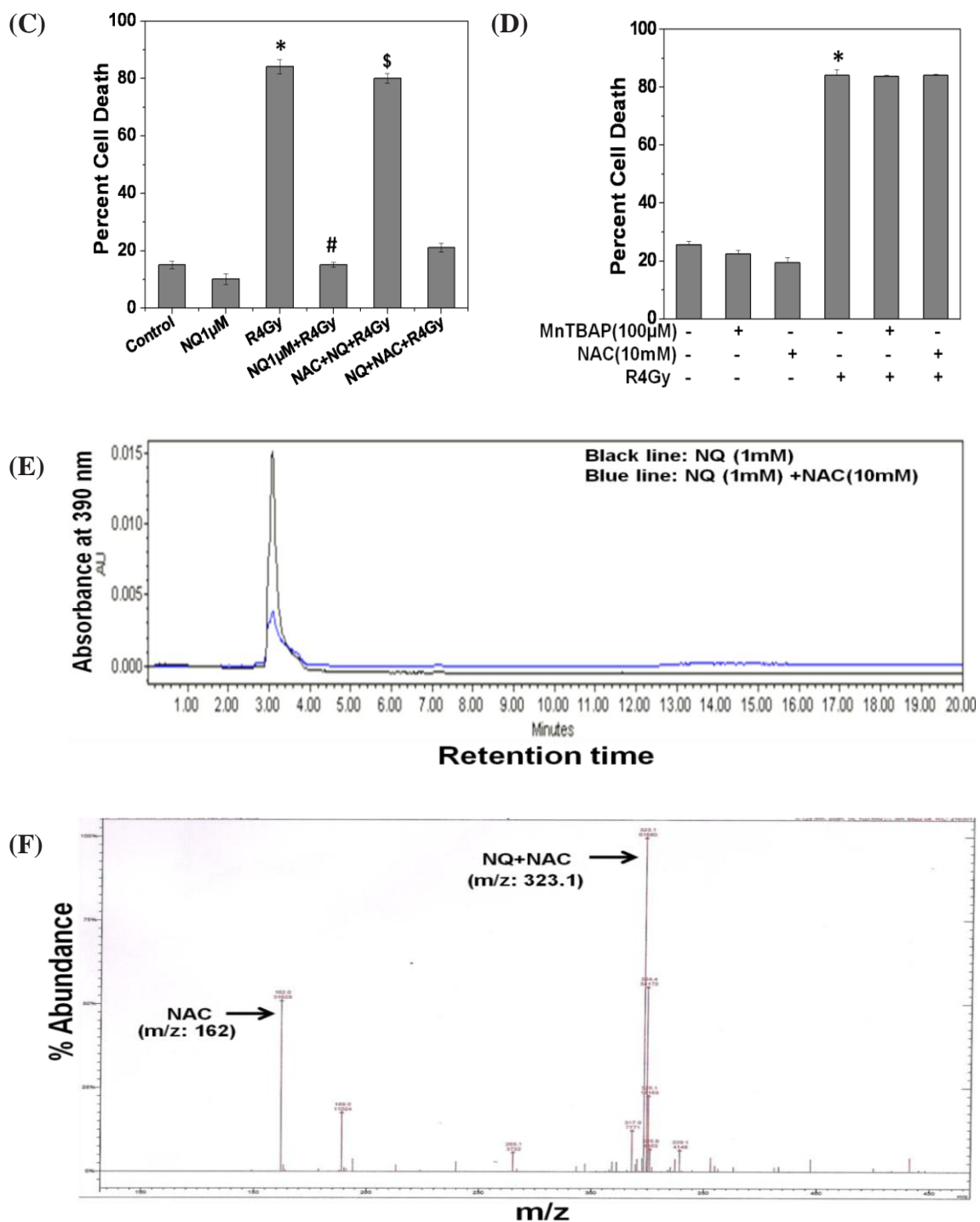


Fig. 2.12: NQ mediated radioprotection was abrogated by thiol-containing antioxidants: (A, B) Lymphocytes (1×10^6) were incubated with NAC (10mM) or MnTBAP (100 μ M) for 1h followed by treatment with NQ (1 μ M) for 2h. Cells were irradiated at 4Gy, cultured for 24h and cell death was estimated by PI staining. Representative flowcytometric histograms (A) and corresponding bar diagram (B) are shown. Radioprotective effects of NQ could not be abrogated by NAC when added 2h after NQ treatment to lymphocytes. (D) MnTBAP or NAC did not protect lymphocytes against radiation induced cell death. (E) HPLC separation of products of reaction of NQ (1mM) with NAC (10mM). NQ was mixed with NAC for 3h in acetonitrile and 50 μ l of the sample was subjected to HPLC. Black line indicates NQ alone and blue line indicates reaction product(s). (F) Identification of products of reaction of NQ with NAC by

mass spectrometry. The samples were subjected to MS analysis using ESI ion trap detector. Major peak at m/z 323.1 corresponded to NQ-NAC adduct and other at m/z 162 may correspond to unreacted NAC. The data is the representative of two such independent experiments having similar results. Each bar represents the mean \pm SEM from three replicates. ^{*} $p<0.05$, as compared to vehicle treated control, [#] $p<0.05$, as compared to irradiated group and ^{\$} $p<0.05$, as compared to irradiated group in presence of NQ.

2.3.12 NQ offered radioprotection via activation of Nrf2 in lymphocytes:

Since scavenging of radiation derived ROS by NQ was a minor contributor to the observed radioprotection, it may be acting through activation of adaptive response pathways. One of them could be activation of a redox sensitive transcription factors like Nrf2. Hence, experiment was carried out to see the activation of Nrf2 by treatment of lymphocytes with NQ. The results of confocal microscopy showed the direct activation of Nrf2 by addition of NQ to lymphocytes (Fig. 2.13A). Significant accumulation of Nrf2 in the nucleus was seen after 4h of addition of NQ to lymphocytes. NQ mediated Nrf2 activation in the lymphocytes was confirmed by real time PCR at RNA level (Fig. 2.13B). ATRA, an inhibitor of Nrf2, completely inhibited radioprotection offered by NQ (Fig. 2.13C, D). ATRA by themselves did not protect against radiation induced cell death at the concentrations used (Fig. 2.13D). These results suggested that NQ offered radioprotection via activation of Nrf2. To further substantiate the role of Nrf2 in radioprotection, Nrf2 knockdown cells were exposed to radiation and radiosensitivity was monitored by different techniques. Results showed that cells transfected with shRNA Nrf2 plasmid were more sensitive to radiation than lymphocytes transfected with control shRNA as estimated by PI staining, DNA fragmentation assay, live and dead cell assay, (Fig. 2.13E-G). The results suggested that Nrf2 activation play a role in radioprotection.

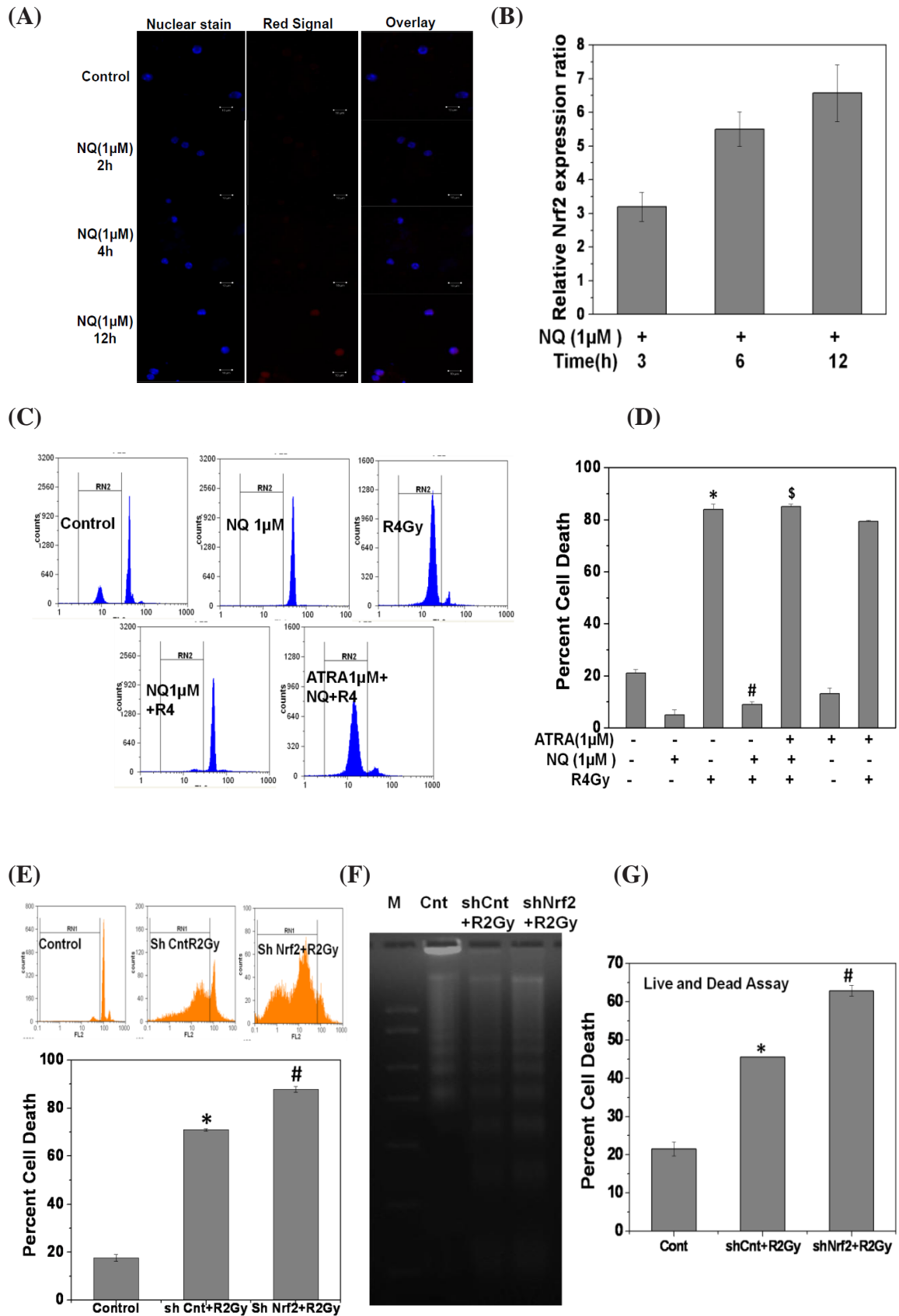
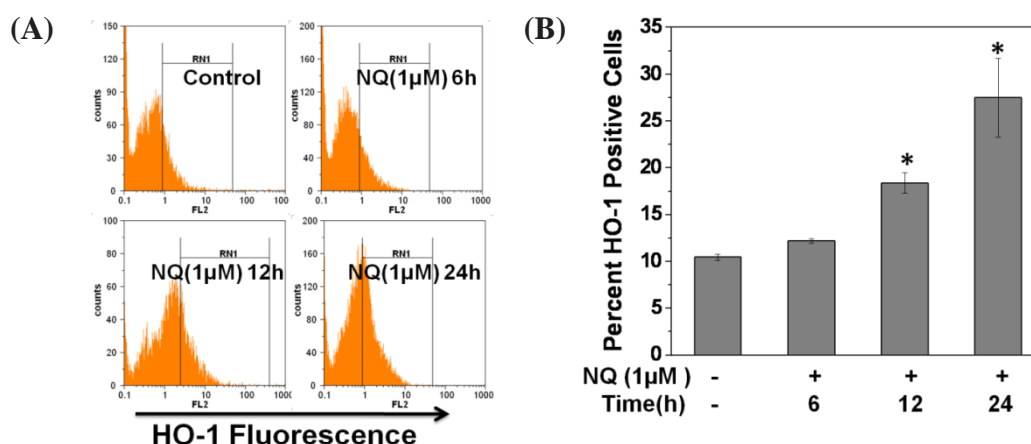


Fig. 2.13: NQ activated Nrf2 in lymphocytes: (A, B) Activation of Nrf2 by NQ. Lymphocytes were treated with NQ for indicated time points and then harvested. (A), Cells were fixed, permeabilized and stained with anti-Nrf2 (Red). Nuclei were stained with Hoechst (blue). Nuclear translocation of Nrf2 from cytoplasm was analyzed by confocal laser microscopy. (B) RNA was isolated, reverse transcribed and quantitative real time RT-PCR analysis was performed for Nrf2. The relative expression ratio with respect to β -actin was calculated and plotted as mean \pm SEM. (C, D) ATRA, an Nrf2 inhibitor abrogated the radioprotective action of NQ. NQ (1 μ M) was added to ATRA (1 μ M) pretreated (6h) lymphocytes and cells were exposed to 4Gy γ -irradiation. Cell death was measured by PI staining. Representative flowcytometric histograms (C) and corresponding bar diagram (D) are shown. (E-G) Nrf2 knock-down lymphocytes were sensitive to radiation. Lymphocytes were transfected with control shRNA or Nrf2 shRNA plasmid for 24h, and then irradiated at 2Gy. Further, cells were cultured for 24h and cell death was assessed by (G) PI staining, (H) DNA fragmentation assay and (F) live and dead assay. The data is the representative of two such independent experiments having similar results. Each bar represents the mean \pm SEM from three replicates. * p <0.05, as compared to vehicle treated control, # p <0.05, as compared to irradiated group and § p <0.05, as compared to irradiated group in presence of NQ.

2.3.13 NQ upregulated Nrf2 dependent HO-1 expression in lymphocytes:

Nrf2 is known to exert its cytoprotective action via activation of several phase II detoxifying enzymes. Hence experiment was carried out to see whether NQ treatment to lymphocytes activated Nrf2 dependent gene like HO-1. It was found that expression of Nrf2 dependent cytoprotective gene, HO-1 was upregulated by NQ in a dose and time dependent manner (Fig. 2.14A-C). NQ induced upregulation of HO-1 was further confirmed by RT-PCR (Fig. 2.14D). As a corollary to this observation, addition of an inhibitor of HO-1 (SnPP) to lymphocytes suppressed radioprotection offered by NQ (Fig. 2.14E). Taken together these results suggested that NQ protected lymphocytes against radiation induced death by activating Nrf2 and its dependent cytoprotective gene HO-1.



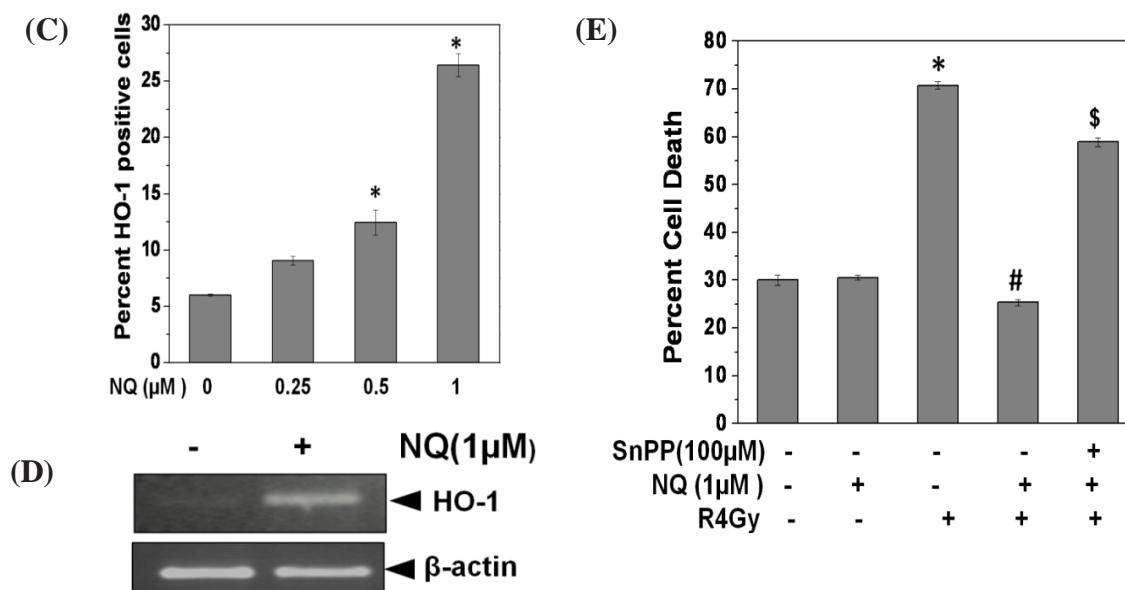


Fig. 2.14: NQ upregulated Nrf2 dependent HO-1 expression in lymphocytes: (A-D) NQ upregulated the expression of cytoprotective gene HO-1. (A-C) NQ activates HO-1 expression in a time and dose dependent manner. Cells were treated with NQ (1μM) for indicated concentrations and stained with PE-labeled anti-HO-1. Representative flowcytometric histograms (A) and Bar graph (B, C) showing the upregulation HO-1. (D) Total RNA isolated from NQ (1μM, 24h) treated lymphocytes was reverse transcribed. RT-PCR analysis of HO-1 genes was carried out. PCR products were resolved on 2% agarose gels containing EtBr. β-actin gene expression was used as an internal control. (E) SnPP an inhibitor of HO-1 abrogated the radioprotective action of NQ. NQ was added to SnPP(100μM) pretreated (1h) lymphocytes, irradiated at 4Gy and cultured for 24h. Cell death was estimated by PI staining. The data is the representative of two such independent experiments having similar results. Each bar represents the mean±SEM from three replicates. *p<0.05, as compared to vehicle treated control, #p<0.05, as compared to irradiated group and \$p<0.05, as compared to irradiated group in presence of NQ.

2.3.14 NQ induced phosphorylation of ERK in lymphocytes:

Since Nrf2 is reported to be activated by ERK^{137,138}, we examined whether NQ induces phosphorylation of ERK in lymphocytes. It was observed that addition of NQ to lymphocytes increased phosphorylation of ERK1/2(or p44/42MAPK or MAPK3/MAPK1) significantly in a time dependent manner (Fig. 2.15A, B). Pharmacological inhibitor of ERK (ERKi) completely abolished NQ mediated radioprotection (Fig. 2.15C). To further elucidate the mechanisms underlying ERK activation by NQ, we then investigated whether NQ had effects on upstream kinases. Real time PCR analysis showed that NQ treatment to lymphocytes activated both MEK1 (or MAP2K1) and

MEKK1 (or MAP3K1) in a time dependent manner (Fig. 2.15D). Additionally, result also showed that NQ induced phosphorylation of ERK was accompanied by inhibition of activity of cellular phosphatases (Fig. 2.15E).

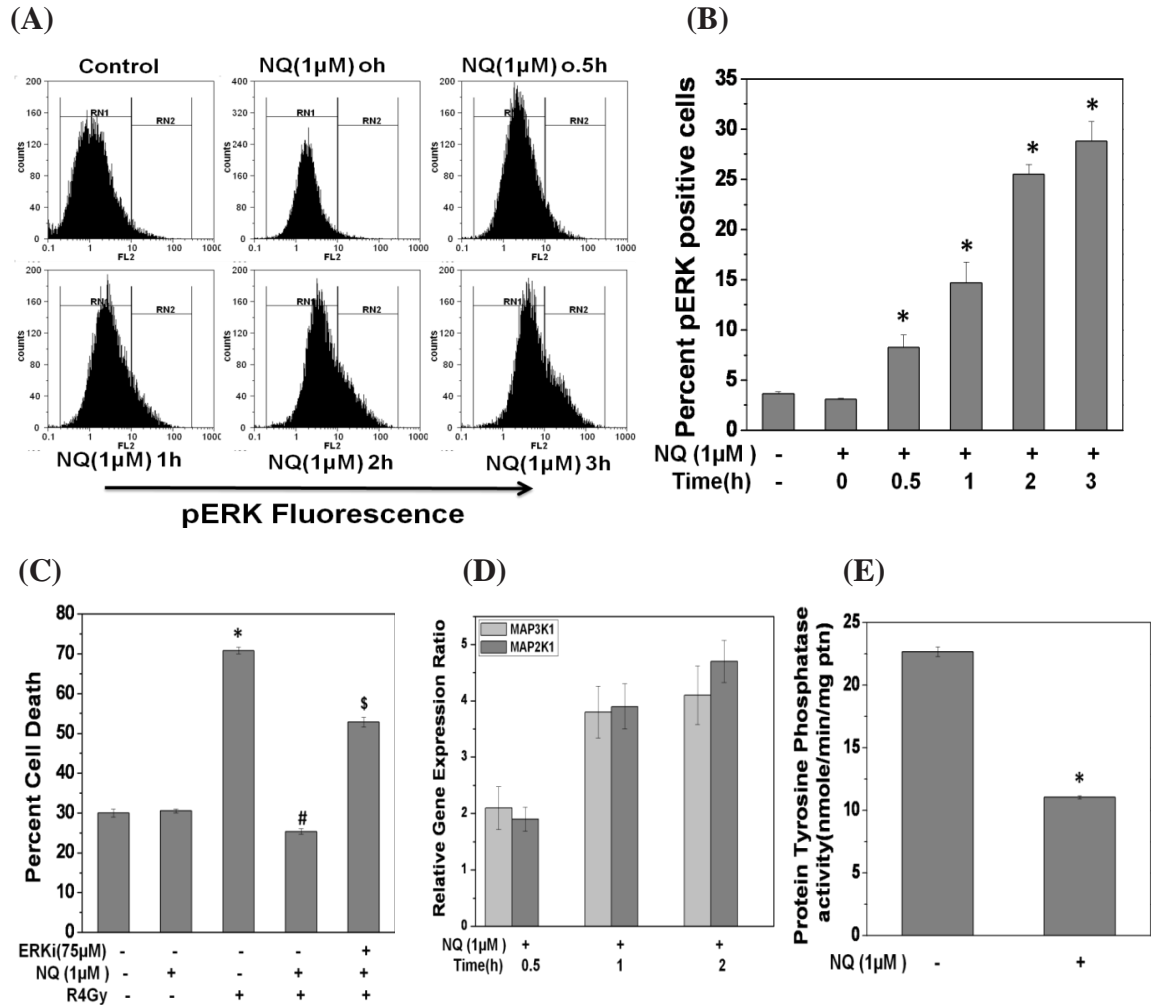


Fig. 2.15: NQ induced phosphorylation of ERK in lymphocytes: (A, B) Cells were treated with NQ (1µM) for indicated time points and stained with PE-labeled anti-pERK. Representative flowcytometric histograms (A) and corresponding bar graph (B) showing the activation of ERK. (C) ERK inhibitor abrogated the radioprotective action of NQ. Lymphocytes were treated with ERK inhibitor (75µM, 1h) prior to addition of NQ (1µM), irradiated at 4Gy and cultured for 24h. Cell death was estimated by PI staining. (D) NQ increased expression of upstream kinases (MEK1, MEKK1). Total RNA isolated from NQ (1µM) treated lymphocytes was reverse transcribed and quantitative real time RT-PCR analysis was performed for MEK1, MEKK1. (E) NQ suppressed protein tyrosine phosphatase activity. Whole cell lysates of NQ (1µM) treated (2h) lymphocytes (5×10^6) were prepared and phosphatase activity was measured as per the manufacturer's protocol. The data is the representative of two such independent experiments having similar results. Each bar represents the mean \pm SEM from three replicates. *p < 0.05, as compared to vehicle treated control, #p < 0.05, as compared to irradiated group and \$p < 0.05, as compared to irradiated group in presence of NQ.

2.3.15 NQ increased intracellular calcium levels:

Earlier report by Schmidt et al. has shown that calcium activates Raf/MEK/ERK pathway¹³⁸. Therefore experiment was carried out to examine whether NQ induced activation of ERK through increases cytoplasmic Ca^{2+} levels. It was observed that treatment with NQ resulted in immediate elevation of intracellular Ca^{2+} , which peaked at 3min, followed by a slow decline (Fig. 2.16A). Cytoplasmic Ca^{2+} is particularly maintained by the out flux of Ca^{2+} from ER membrane-localized IP3-gated channel and influx through the plasma membrane Ca^{2+} ATPase¹³⁹. To confirm the NQ induced release of Ca^{2+} , nifedipine (plasma membrane Ca^{2+} channel blocker), Bapta-AM (intracellular Ca^{2+} specific chelator) and EGTA (extracellular Ca^{2+} chelator) was used in combination with NQ. Apart from these we also used thapsigargin, a specific mobilizer of the ER- Ca^{2+} store as a positive control for Ca^{2+} release. Results showed that both calcium chelator (EGTA and BAPTA-AM), and nifedipine significantly reduced NQ induced release of cytoplasmic calcium (Fig. 2.16B). Further, thapsigargin induced significant release of cytoplasmic calcium (Fig. 2.16B). Further, to substantiate the role of calcium in radioprotection elicited by NQ, lymphocytes were incubated with BAPTA-AM or EGTA or nifedipine, prior to addition of NQ. The cells were then exposed to radiation and cultured for 24h. BAPTA-AM, EGTA and nifedipine significantly abrogated NQ mediated radioprotection (Fig. 2.16C). Thapsigargin which elevated cytosolic calcium concentration similar to NQ, also offered significant protection against radiation-induced cell death (Fig. 2.16C). Further, incubation of lymphocytes with BAPTA-AM prior to treatment with NQ resulted in abrogation of phosphorylation of ERK indicating that NQ offered radioprotection in lymphocytes via Ca^{2+} -ERK-Nrf2 pathway (Fig. 2.16D).

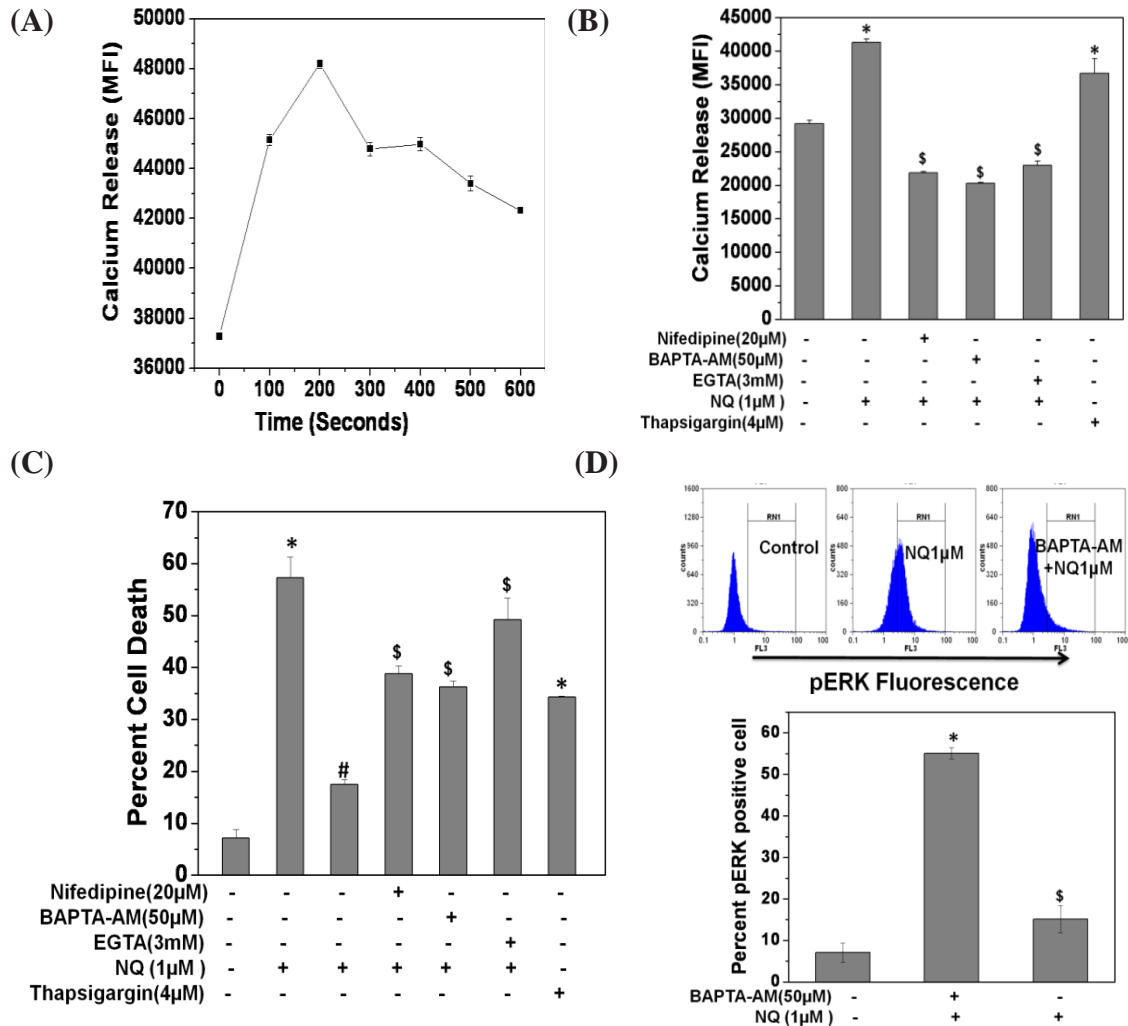


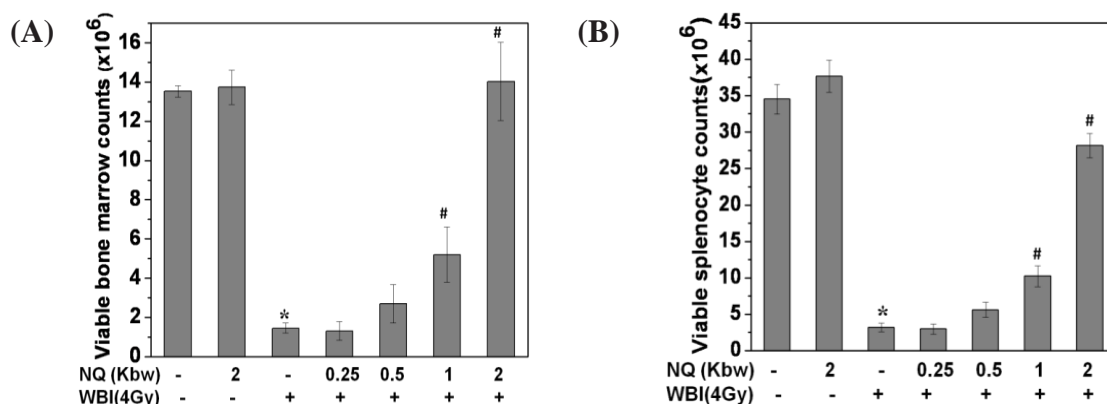
Fig. 2.16: NQ increased intracellular calcium levels: (A) NQ increased intracellular calcium levels: Fura-2AM (2μM) was added 0.5h before NQ (1μM) addition. The data represent intracellular changes of calcium levels with time. (B) Chelators of calcium reduced calcium release by NQ. Thapsigargin, a calcium mobilizer increased cytoplasmic calcium levels. (C) Chelators of calcium inhibited radioprotective action of NQ. Cells were cultured for 24h and cell death was estimated by PI staining. Thapsigargin, a calcium mobilizer offered significant radioprotection to lymphocytes. (D) BAPTA-AM abrogated NQ mediated ERK phosphorylation. Lymphocytes were incubated with BAPTA-AM (50μM) for 0.5h followed by treatment of NQ (1μM) for 3h and then processed for intracellular staining with PE-labeled anti-pERK antibody. The data is the representative of two such independent experiments having similar results. Each bar represents the mean±SEM from three replicates. *p<0.05, as compared to vehicle treated control, #p<0.05, as compared to irradiated group and \$p<0.05, as compared to NQ group or irradiated group in presence of NQ.

2.3.16 NQ administration to mice protected against WBI induced immune and myelosuppression:

In order to evaluate the relevance of *in vitro* results, we examined the ability of NQ administration to ameliorate the WBI-induced immunosuppression and

myelosuppression. Administration of NQ (0.25-2mg/kbw) to mice 0.5h prior to WBI exposure significantly protected against WBI induced loss of bone marrow viability in a dose dependent manner as observed on day 5 postirradiation (Fig. 2.17A). Complete protection against WBI loss of bone marrow viability was observed at NQ dose of 2mg/kbw (Fig. 2.17A). NQ (2mg/ kbw) administration alone, to mice did not induce any loss of bone marrow viability suggesting that this dose is safe for mice (Fig. 2.17A). Similarly, NQ administration also protected the WBI induced loss of splenocytes viability in a dose dependent manner and maximum protection was observed at NQ dose of 2mg/ kbw (Fig. 2.17B). Hence, further studies were performed using NQ dose of 2mg/kbw. Further, WBI induced loss of spleen weight and spleen index was significantly protected by prior administration of NQ (Fig. 2.17C-E).

To determine the ability of NQ to protect hematopoietic tissue (spleen and bone marrow) in irradiated mice, we histologically examined femur bone marrow and spleen on day 5 postirradiation. The results of H&E staining showed that NQ administration prior to WBI exposure protected against WBI-induced bone marrow aplasia, splenic atrophy and splenic hypoplasia (Fig. 2.17F, G). Results of histopathological studies of spleen further suggested that NQ pretreatment to mice inhibited WBI induced hemosiderin deposition (Fig. 2.17H).



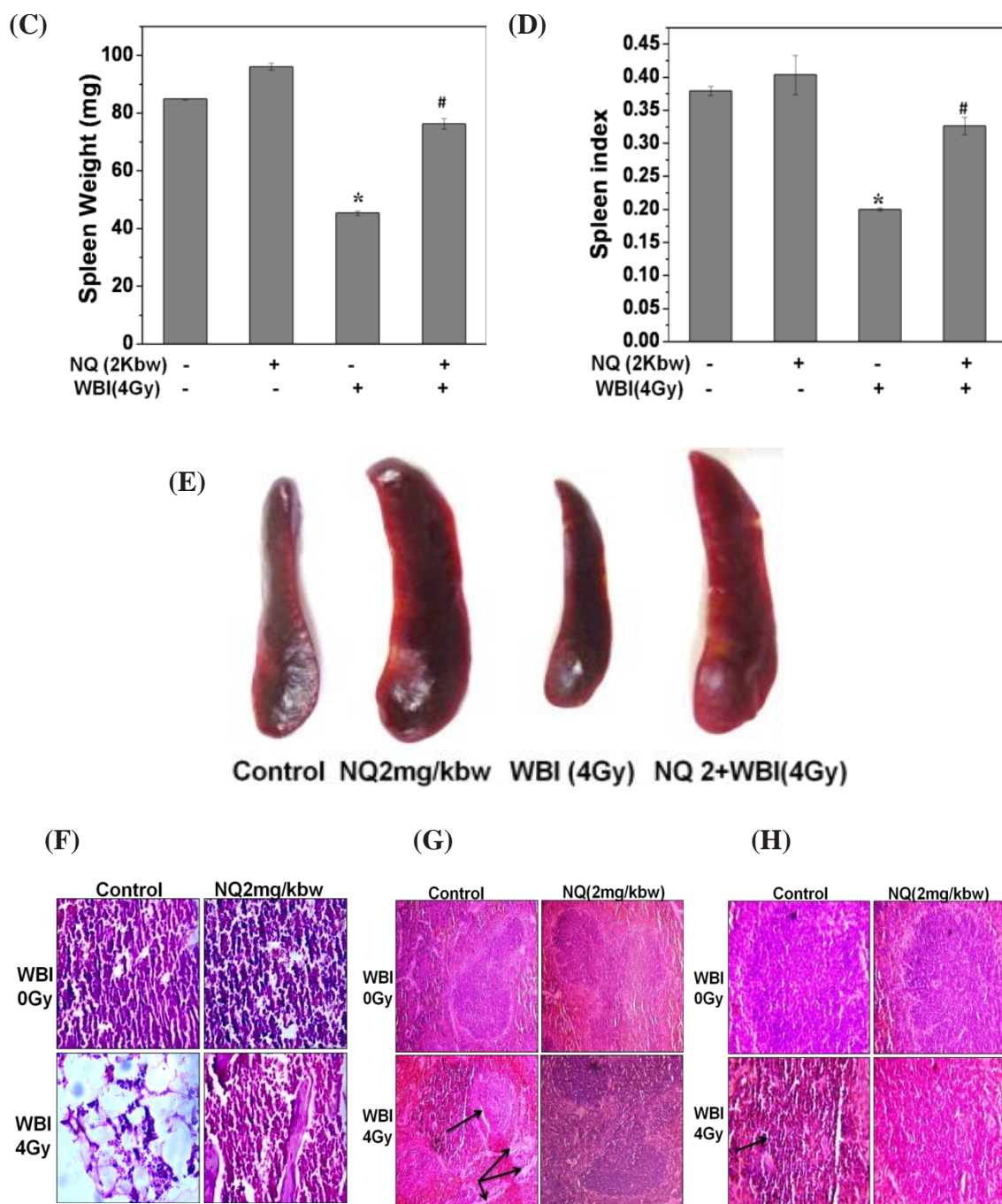


Fig. 2.17: *In vivo* radioprotection by NQ: Mice were administered with NQ (0.25-2mg/kbw) and after 0.5h these mice were exposed to WBI (4Gy) and sacrificed on day5. Viability of (A) splenocyte and (B) bone marrow was assessed by trypan blue dye exclusion method. (C) Spleen weight and (D) spleen index were recorded. (F-H) Isolated femur bone (F) and spleen (G, H) were fixed in 10% neutral buffered formalin, sections of 5 μ m thickness were cut using a rotary microtome, processed for H&E staining and examined using upright trinocular microscope attached to CCD camera. The data is derived from one of the three such independent experiments having similar results. In each experiment, data from five mice per group were assessed and each bar represents mean \pm S.E.M. * $p < 0.05$, as compared to vehicle treated control, # $p < 0.05$, as compared to irradiated group.

Since WBI induced splenic atrophy was inhibited by NQ, we specifically monitored its effect on various phenotypes of spleen cells. NQ restored the counts of different lymphocyte subsets like CD3+T cells, CD4+T helper cells, CD8+T cytotoxic cells, CD19+ B cells and also CD14+macrophages (Table 2.4). Hematological studies showed that NQ treatment protected the mice against WBI induced leucopenia, lymphopenia, neutropenia, thrombocythemia and erythropenia (Table 2.5). Result showed that although relative percentage of neutrophil was increased in mice exposed to radiation as compared to non-irradiated control, the absolute neutrophil counts were decreased suggesting that neutropenia occurred in irradiated mice and NQ administration prevented WBI induced neutropenia (Table 2.5). Further, NQ administration also protected the mice from WBI-induced decrease in hemoglobin level, packed cell volume and mean corpuscular volume (Table 2.5).

Lymphocyte Subsets	No. X10 ⁻⁶ per spleen			
	Control	NQ2mg/kbw	WBI (4Gy)	NQ2+WBI 4Gy
Lymphocytes	37.5±0.09	40.45±0.21	4.2±0.02 *	20.18±0.36 #
CD3+ T Cells	14.71±1.49	17.82±0.33	2.34±0.11 *	10.20±0.91#
CD4+ T Cells	10.37±0.31	13.82±0.26	2.20±0.01 *	6.56±0.56 #
CD8+ T Cells	1.60±0.09	2.34±0.19	0.104±.006 *	1.08±0.60 #
CD19+ B Cells	11.60±0.84	13.23±0.26	0.53±0.07 *	5.50±0.46 #
CD14+ Macrophages	1.74±0.20	1.60±0.16	0.32±0.03 *	0.96±0.11#

Table 2.4: NQ administration to mice prevented WBI induced loss of splenocytes subsets: Mice were administered with NQ (2mg/kbw) or vehicle 0.5h prior to WBI (4Gy) exposure and sacrificed on 5 day postirradiation. The number of CD3+T cells, CD4+ helper T cells, CD8+ cytotoxic T cells, CD19+B cells and CD14+ macrophages in spleen of treated mice was determined by flow cytometry as described in material and methods section. The total cell yield was calculated by multiplying the proportion of each cell subset by the total number of live cells obtained per spleen. The data is derived from one of the two such independent experiments having similar results. In each experiment, data from four mice per group were assessed and each bar represents mean±S.E.M. *p<0.05, as compared to vehicle treated control and #p<0.05, as compared to irradiated group.

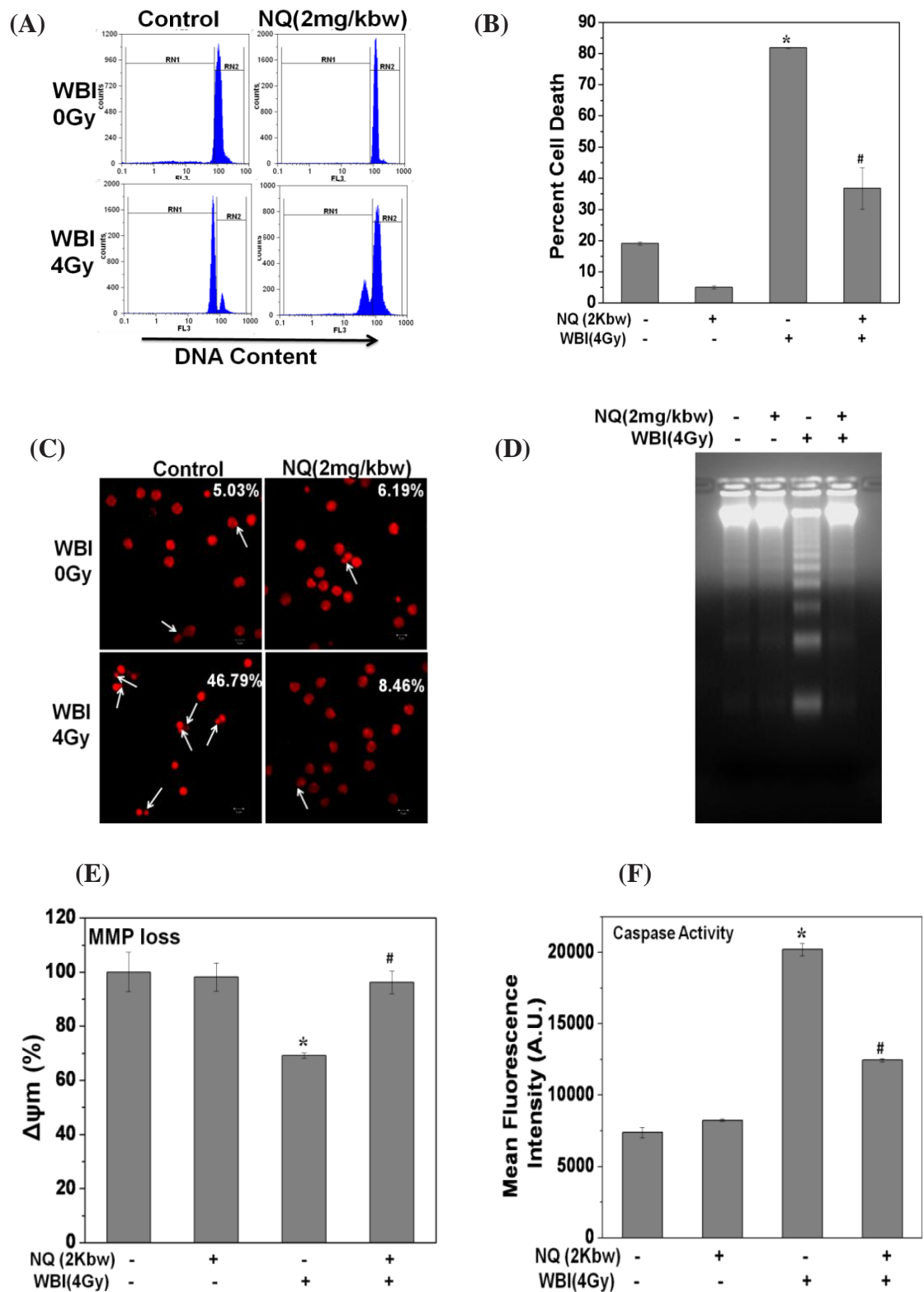
Hematolglcal Parameters	Control	NQ2mg/kbw	WBI(4Gy)	NQ2+ WBI(4Gy)
WBC(X10 ⁴ /ml)	1.05±0.07	1.02±0.1	0.28±0.1 *	0.83±.02 #
Plaelet Counts(X10 ⁶ /ml)	3.34±0.3	3.64±0.2	4.9±0.10 *	2.99±0.2 #
Neutrophils(%)	46.2±1.2	43.8±1.6	59.6±0.9 *	43.4±2.8 #
Lymphocytes(%)	54.8±1.6	54.8±1.6	36.4±0.9 *	55.5±2.9 #
Packed Cell volume(%)	41.44±0.5	41.36±0.3	32.72±0.4 *	40.52±0.5 #
Mean corpuscular volume	73.66 ±1.7	75.55±0.6	57.2±1.3 *	71.52±0.9 #
Hb(g/dl)	15.7±0.2	15.4±0.1	13.28±0.5 *	15.4±0.1 #
RBC(X10 ⁶ /ml)	6.14 ±0.2	5.88±0.2	4.76±0.3 *	6.63±0.3 #

Table 2.5: NQ administration to mice prevented WBI induced loss of hematological parameters: Mice were administered with NQ (2mg/kbw) or vehicle 0.5h prior to WBI (2Gy) exposure and blood from these treated mice was collected in heparinised tube by retro orbital puncture and complete blood count was taken using auto-analyzer. The data is derived from one of the two such independent experiments having similar results. In each experiment, data from seven mice per group were assessed and each bar represents mean±S.E.M. *p<0.05, as compared to vehicle treated control and #p<0.05, as compared to irradiated group.

2.3.17 NQ administration to mice inhibited WBI induced apoptosis in lymphocytes:

Since WBI-induced decrease in viable cell counts of splenocytes is mediated by induction of apoptosis, experiment was setup to see the effect of NQ administration on induction of WBI induced apoptosis. Administration of NQ to mice 0.5h prior to WBI, protected against WBI induced apoptosis (pre-G1 cells), nuclear-blebbing and DNA-fragmentation (Fig.2.18A-D). It was also observed that NQ ameliorated both early (loss of MMP) and late events (caspase activation and Bax expression) associated with radiation induced apoptosis (Fig. 2.18E-H). Since NO is important mediator of radiation injury and involved in radiation induced apoptosis¹¹⁴, we examined the effects of NQ administration on WBI induced NO production in the plasma. It was found that NQ

administration to mice completely inhibited the WBI induced increase in plasma NO levels (Fig. 2.18 I).



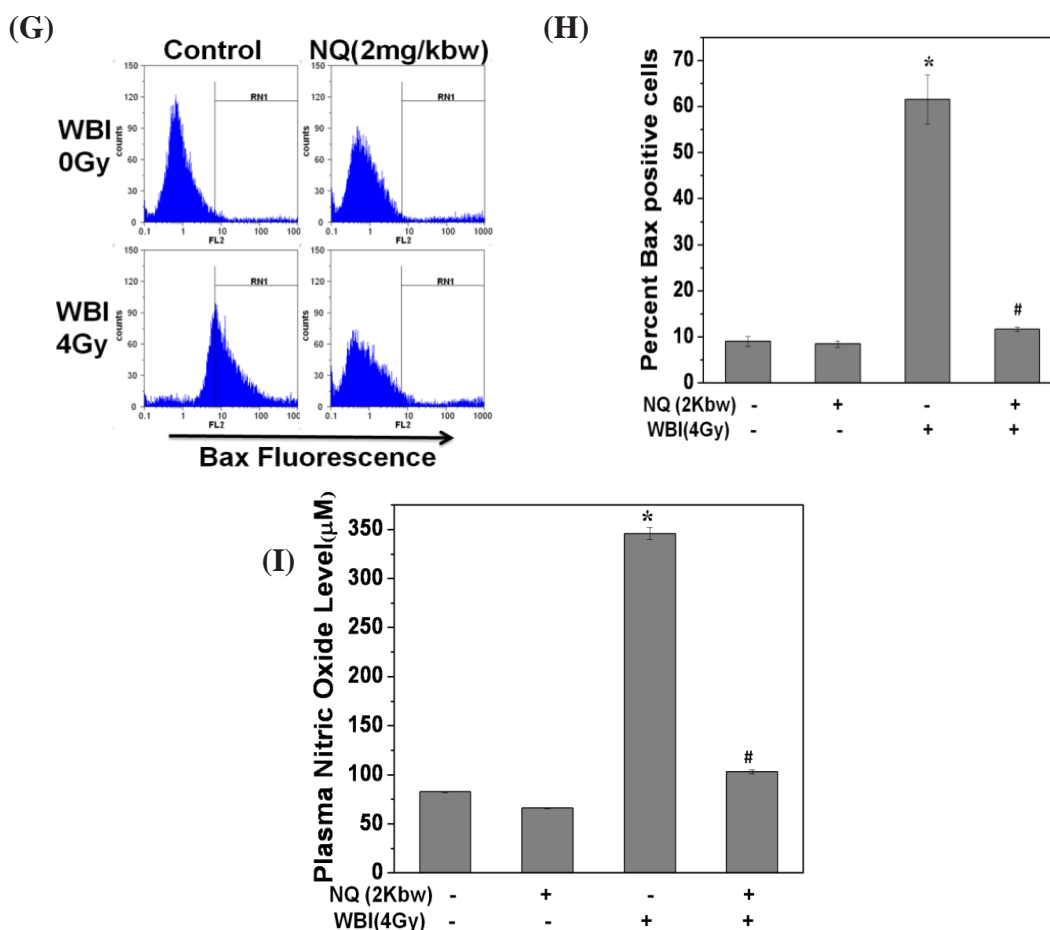


Fig. 2.18: NQ administration to mice inhibited WBI induced apoptosis in lymphocytes: Mice were administered with NQ (2mg/kbw) and after 0.5h these were exposed to WBI (4Gy) and sacrificed immediately. Splenic lymphocytes from different groups were cultured for 24h and various apoptotic parameters were assessed by (A, B) PI staining, (C) nuclear-blebbing, (D) DNA-fragmentation, (E) MMP loss, (F) homogenous caspase (2, 3, 6, 7, 9 and 10) activity (G,H) Bax activation as described in material method section. (I) NQ administration to mice inhibited WBI induced increase in NO in blood plasma. Blood was collected in heparinised tube and plasma was separated by centrifugation and used for measurement of NO by Griess method. The data is derived from one of the two such independent experiments having similar results. In each experiment, data from three mice per group were assessed and each bar represents mean±S.E.M. *p<0.05, as compared to vehicle treated control and #p<0.05, as compared to irradiated group.

2.3.18 NQ administration to mice elevated radioprotective cytokines:

To understand the *in vivo* radioprotective action of NQ, the plasma levels of IL-1 β and IL-6 were estimated. Administration of these cytokines to mice has been reported to stimulate bone marrow stem cells and offer radioprotection. The plasma levels of IL-1 β and IL-6 were significantly elevated with NQ administration to mice (Fig. 2.19).

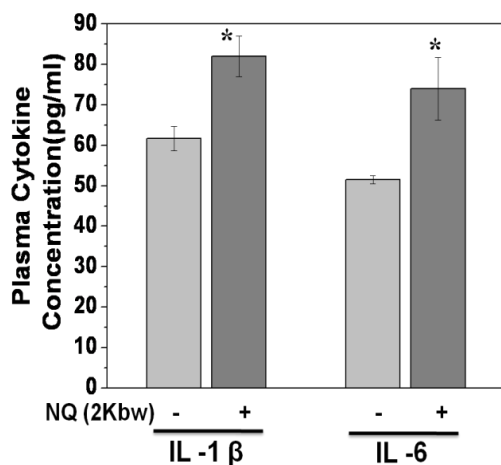


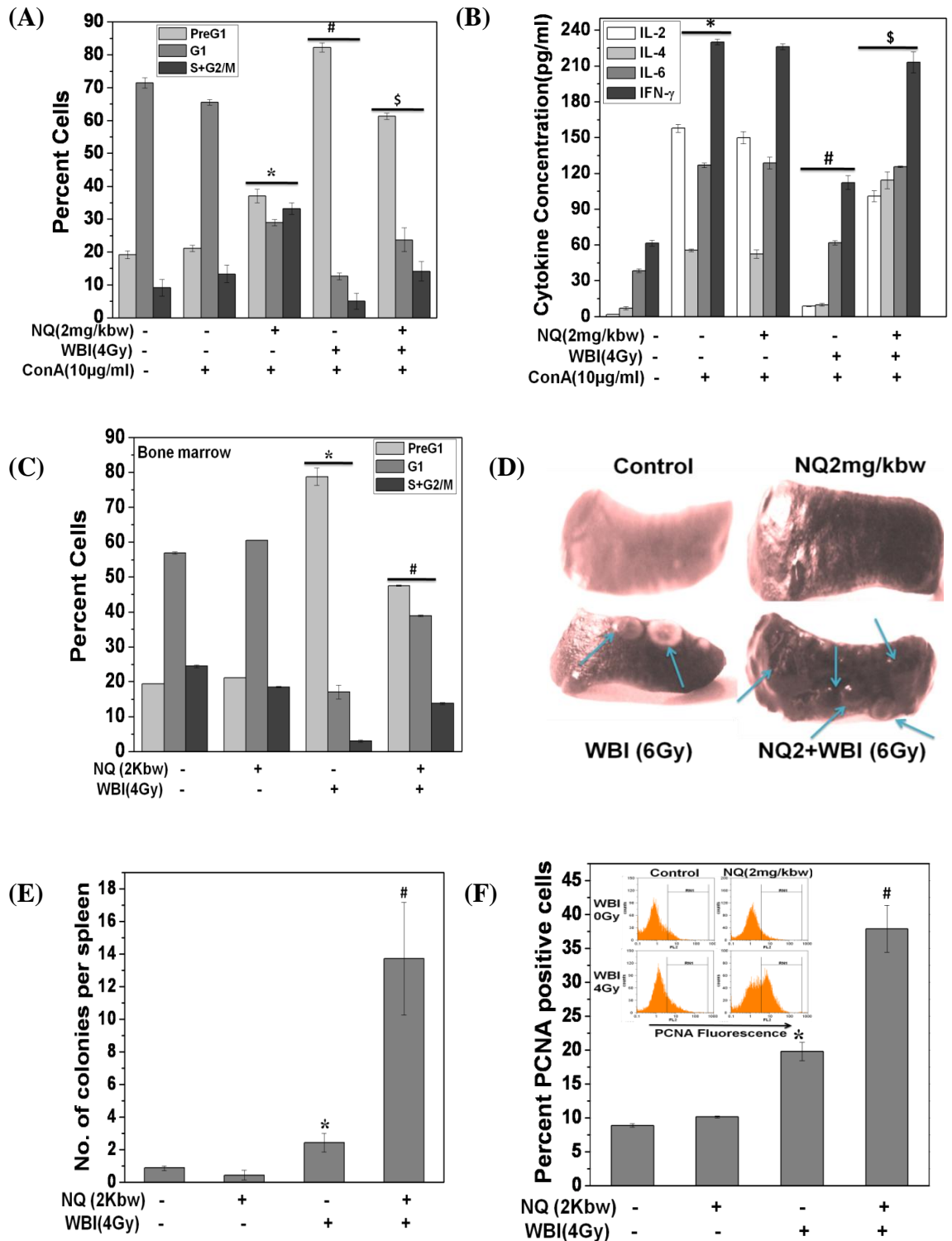
Fig. 2.19: NQ administration to mice elevated radioprotective cytokines: Mice administered with NQ (2mg/kbw) were sacrificed on day 5. Blood was collected in heparinised tube and plasma was separated by centrifugation and used for measurement of cytokines (IL-1 β and IL-6) by ELISA method. The data is derived from one of the two such independent experiments having similar results. In each experiment, data from five mice per group were assessed and each bar represents mean \pm S.E.M. * p <0.05, as compared to vehicle treated control.

2.3.19 NQ administration to mice prevented WBI induced loss of functional response of lymphocytes and bone marrow:

Since NQ rescued WBI mediated loss of viable counts of lymphocytes and bone marrows, experiments were setup to evaluate the functional response of the remnant bone marrows and lymphocytes. It was found that residual T cells from NQ+WBI group responded significantly better than vehicle+WBI group to Con A as measured in terms of cell proliferation (Fig. 2.20A) and production of cytokines like IL-2, IL-4, IL-6 and IFN- γ (Fig. 2.20B). Similarly bone marrow cells from NQ+WBI group showed significantly better proliferation than that of vehicle+WBI group (Fig. 2.20C).

Since NQ administration to mice inhibited WBI induced loss of proliferative potential of bone marrow cells, experiment was carried out to examine the proliferative ability of stem cells present in the bone marrow using endogenous spleen colony formation assay. The colony forming units (CFUs) appeared as nodules on the surface of spleen and embedded in the red mass of spleen. The CFUs number was significantly higher in NQ+WBI group as compared to vehicle+WBI group (Fig. 2.20D, E). These CFUs represent rapidly proliferating cells as evinced by increased expression of PCNA in the nodules appeared on spleen surface (Fig. 2.20 F, G). Further proliferative ability of stem

cells present in the bone marrow was confirmed by *in vitro* CFC assay. It was found that NQ prevented WBI induced loss of ability of stem cells to differentiate into various progenitor cells (Fig. 2.20H, Table 2.6).



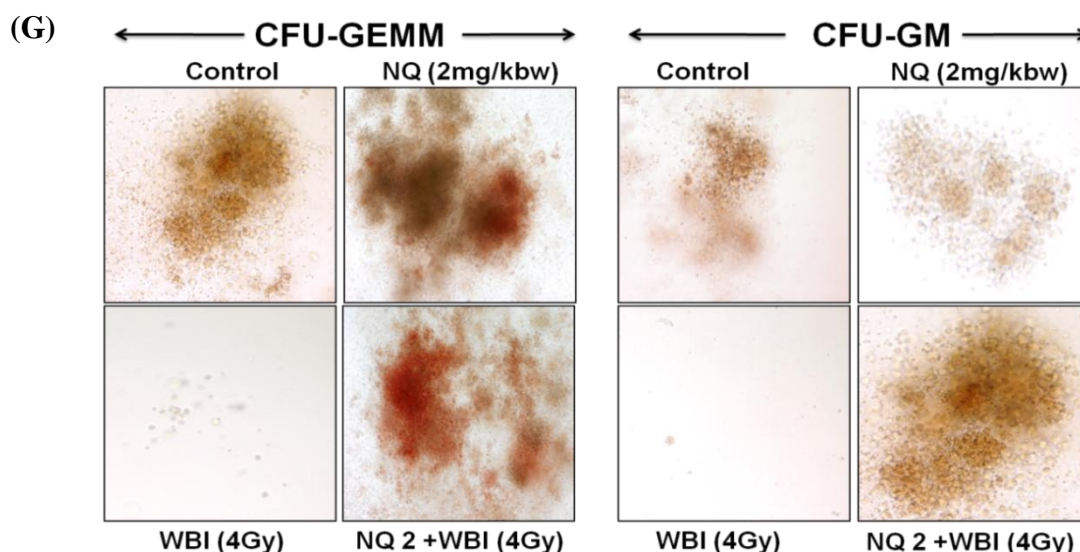


Fig. 2.20: NQ administration to mice prevented WBI induced loss of functional response of lymphocytes and bone marrow: (A, B) NQ administration to mice inhibited WBI induced suppression of Con A induced cell proliferation and cytokine production. Mice were administered with NQ (2mg/kbw) 0.5h prior to WBI (4Gy) exposure and sacrificed on day 5. Lymphocytes were cultured in presence of Con A for (A) 72h or (B) 24h. (A) Cell proliferation was measured by PI staining and (B) different cytokine levels were measured in the supernatant by ELISA. (C) Bone marrow were isolated and cultured for 48h and proliferation was measured by PI staining. (D-F) NQ treatment of mice offered improvement of hematopoietic ability as demonstrated by number of macroscopic colonies appeared on spleen (measured as CFUs) (D, E) as monitored on day 9 after irradiation at 6Gy. A total of 7 mice were used per group for measurement of CFUs. (F) Proliferative potential of CFUs were monitored by immunostaining with PCNA. (G) Proliferative potential of HSCs present in bone marrow of treated mice were assessed by *in vitro* CFC assay. The data is derived from one of the two such independent experiments having similar results. In each experiment, data from five mice per group were assessed and each bar represents mean \pm S.E.M. * p <0.05, as compared to vehicle treated control, # p <0.05, as compared to irradiated group and \$ p <0.05, as compared to irradiated group in presence of NQ.

Hematopoietic Progenitor cell content of Bone Marrow							
	Progenitor cell content per 0.1X10 ⁶ Bone marrow plated (Mean \pm S.E.M.)						
Treatments	CFU-E	BFU-E	CFU-G	CFU-M	CFU-GM	CFU-GEMM	Total Colonies
Control	47.6 \pm 3.2	38.6 \pm 1.8	5.6 \pm 1.2	0.66 \pm 0.3	21.6 \pm 1.7	3 \pm 1	117.7 \pm 14.3
NQ 2mg/kbw	26 \pm 1.5	18.3 \pm 1.7	8.3 \pm 0.8	9.3 \pm 1.4	24.6 \pm 2.3	4 \pm 1	90.5 \pm 10.1
WBI (4Gy)	1 \pm 0.5*	0.3 \pm 0.3*	0.60 \pm 0.3	0.67 \pm 0.3	1.33 \pm 0.6*	0.67 \pm 0.3*	4.57 \pm 0.9 *
NQ2+WBI4Gy	25.3 \pm 0.8#	52 \pm 1.5 #	1.33 \pm 0.3	1 \pm 0.5	10 \pm 0.5 #	4.16 \pm 2.1#	93.79 \pm 11.4 #

Table.2.6: NQ administration to mice prevented WBI induced loss of proliferative potential of HSCs of bone marrow: Mice were administered with NQ (2mg/kbw) 0.5h prior to WBI (4Gy) exposure and sacrificed immediately. Bone marrows were isolated and cultured in methyl cellulose complete medium for 11days. Colonies were enumerated under inverted microscope using scoring grid. The data is derived from one of the two such independent experiments having similar results. In each experiment, data from five mice per group were assessed and each bar represents mean \pm S.E.M. * p <0.05, as compared to vehicle treated control and # p <0.05, as compared to irradiated group.

2.3.20 NQ administration to mice prevented WBI induced mortality:

The protection of hematopoietic tissues like bone marrow and spleen by NQ pretreatment of mice should reflect in the survival of mice exposed to lethal dose of ionizing radiation. Therefore, experiment was setup to see effect of NQ administration on survival of lethally irradiated mice. It was found that NQ administration 0.5h prior to 7Gy WBI was able to significantly prevent radiation induced mortality and weight loss (Fig. 2.21A, B). Further to compare the radioprotective potential of NQ with that of other known radioprotectors, dose modification factor (DMF) was assessed. To determine the DMF of NQ, mortality was recorded up to 30 days after graded doses of radiation (6 to 8.5Gy). An increase in the LD50/30 from 6.67Gy for vehicle injection to 7.86Gy in NQ treated group was observed, DRF was calculated to be 1.18 (Fig. 2.21C).

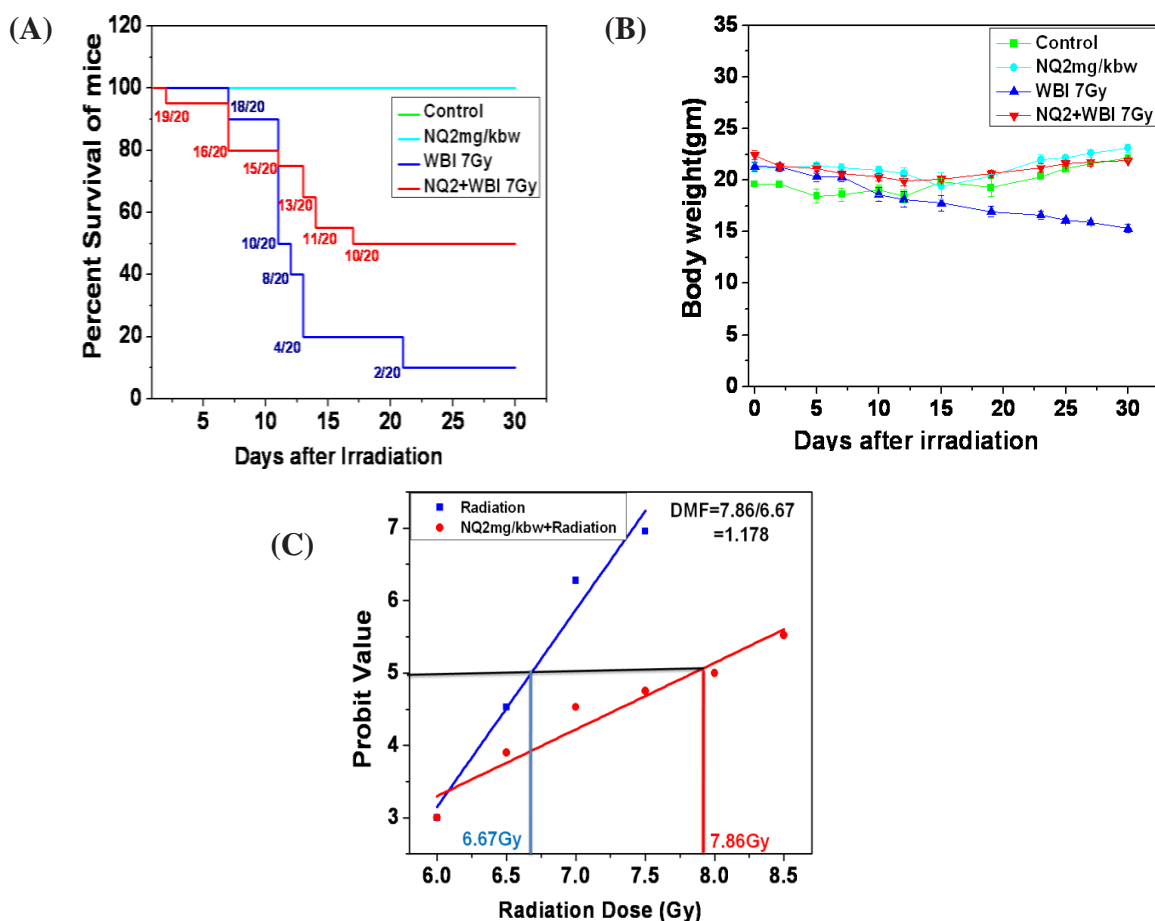


Fig. 2.21: NQ administration to mice prevented WBI induced mortality: Mice were administered with NQ (2mg/kbw) and after 0.5h were exposed to either (A, B) 7Gy WBI or (C) 6.5 to 8.5Gy, survival and body weight of mice were monitored for 30 days. (A) NQ treatment significantly improved 30 day survival rate of mice exposed to lethal dose of ionizing radiation (7Gy). (B) NQ treatment provides protection against WBI (7Gy) induced loss of body weight of mice. (C) NQ administration to mice exposing to different dose of radiation gives a DMF of 1.178. The data is derived from one of the two such independent experiments having similar results. A total of 20 mice were taken per group for monitoring the survival and 10 mice for determining DMF. Log rank test was used to compare mortality of WBI exposed mice administered with or without NQ.

2.3.21 NQ did not protect tumor cells:

To evaluate the effect of NQ on tumor cells, a cell line of human origin MCF-7 was used. It was observed that NQ did not offer any protection to the tumor cells against toxic effect of radiation. However, NQ induced significant cell death in tumor cells. Combination of radiation with NQ further augmented cell death in MCF-7 cells (Fig. 2.22A, B).

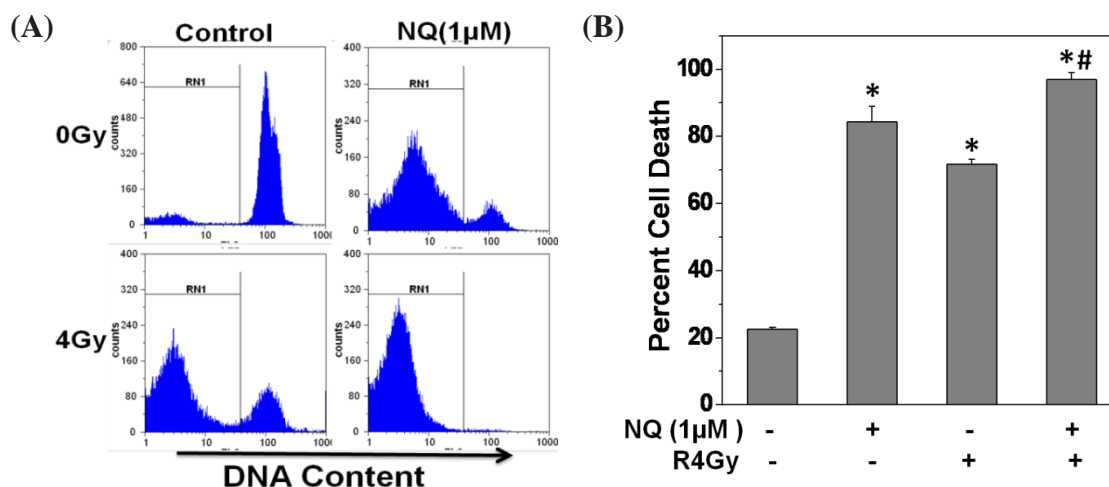


Fig. 2.2: NQ did not protect tumor cells against radiation induced death: MCF-7 cells (0.5×10^6) treated with NQ (1µM) for 2h followed by irradiation at 4Gy. Cells were cultured for 48h at 37°C and cell death was estimated by PI staining. Representative flowcytometric histograms (A) and the corresponding bar diagram (B) showing NQ mediated augmentation of radiation induced death. The data is derived from one of the two such independent experiments having similar results. Each data point shows the mean ± SEM from three replicates. *p<0.05, as compared to vehicle treated control and #p<0.05, as compared to irradiated group.

2.4 DISCUSSION

The present studies were undertaken to test the hypothesis that prooxidants would protect murine splenic lymphocytes against toxic effects of radiation by initiating an adaptive response through activation of Nrf2/ARE pathway. NQ a well-known prooxidant⁵⁶, at optimum concentration offered complete protection to lymphocytes against radiation induced cell death (Fig. 2.1). Our hypothesis was further supported by findings of radioprotective ability of other prooxidants like H₂O₂, DEM and t-BHQ (Fig. 2.3). To the best of our knowledge, this is the first report showing radioprotection by any compound at such low concentrations of 250nM. Interestingly, when NQ was added to cells after irradiation at different time intervals, it offered significant protection to cells (Fig.2.6). Colony forming cell assay in splenocytes and normal human cells (Int407) demonstrated that NQ was able to prevent the loss of proliferative capacity of cells exposed to radiation (Table 2.3, Fig 2.8). These results clearly demonstrated the potent radioprotective potential of NQ *in vitro*.

Molecular mechanism of NQ mediated radioprotection was examined by studying the changes in cellular redox. Addition of NQ to lymphocytes generated significant levels of ROS and failed to completely scavenge radiation derived free radicals suggesting that NQ did not act by antioxidant action (Fig.2.11A-E). Conventional radioprotectors are known to act by various mechanisms like detoxifying radiation induced ROS, elevating endogenous defense molecules like SOD, catalase, GPX, GSH, enhancing the DNA repair, and delaying cell division to allow the repair¹⁴⁰. Several antioxidants and also plant extracts containing antioxidants have been evaluated *in vitro* and *in vivo* models^{33,101,135,136,141,142}. Amifostine that is currently used as an adjuvant in radiotherapy

has been proposed to act as a radioprotector by scavenging radiation derived free radicals¹⁴³. Activators of pro-survival transcription factor NF- κ B or its dependent gene products like cytokines are also shown to offer resistance against radiation-induced toxicity^{42,144}. Administration of glutathione to mice inhibited radiation induced cytogenetic damage¹⁴⁵. Radioprotective effects of thiol compounds include free radical scavenging, hydrogen atom donation, repair of free radicals in target molecules, mixed disulphide formation, and target stabilization by binding to DNA. Conversely, depletion of cellular thiols would lead to increased sensitivity of cells to radiation induced damage¹⁴⁶.

NQ appeared to act as radioprotector by altering cellular redox status. NQ significantly depleted GSH levels and NAC, a thiol containing antioxidant could abrogate NQ mediated radioprotection suggesting that NQ may be directly reacting with thiol groups (Fig. 2.12A). HPLC and MS analysis demonstrated the direct reaction and adduct formation between NQ and NAC (Fig. 2.12E, F). Our findings, for the first time, prove that a thiol depleting prooxidant can exhibit radioprotection in normal lymphocytes. DEM, a known GSH depletor also offered complete protection against radiation induced cell death which further supports our hypothesis (Fig.2.3D). This cellular GSH depleting and ROS producing naphthoquinone initially impinges mild oxidative stress to the cells which activates an adaptive response pathway via activation of redox sensitive transcription factor that can protect cells against toxic effect of subsequent exposure to radiation and other oxidative stressors.

One of the redox sensitive transcription factors Nrf2 is bound to Keap1 which has two critical cysteine residues and modulation of these residues has been shown to activate Nrf2^{92,147}. NQ activated Nrf2 as its nuclear translocation and DNA binding ability was

observed 4h after incubation of lymphocytes with NQ (Fig. 2.13A). ATRA an inhibitor of Nrf2 completely abrogated NQ mediated radioprotection in lymphocytes indicating the involvement of Nrf2 (Fig. 2.13C, D). To further substantiate the involvement of Nrf2, Nrf2 knock-down lymphocytes were found to be more sensitive to radiation than lymphocytes transfected with control shRNA plasmid (Fig. 2.13E-G). These results are in agreement with earlier report by Zhang et al., which showed that constitutive activation of Nrf2 in tumor cells led to radiation resistance^{110,148}. Our studies highlighted the role of Nrf2 in radioprotection of normal lymphocytes. NQ activated Nrf2 dependent gene HO-1. SnPP, an inhibitor of HO-1, abrogated NQ mediated radioprotection (Fig. 2.14E) to about 75% suggesting that along with HO-1 other Nrf2 dependent cytoprotective proteins like MnSOD, NQO1, catalase may be responsible for the observed radioprotection.

NQ may be activating Nrf2 directly through modulation of critical cysteine residues present on Keap1 or through activation of ERK which is upstream to Nrf2. There are several reports implicating ERK in activation of Nrf2¹⁴⁹. We observed that treatment with NQ indeed resulted in phosphorylation of ERK in lymphocytes and a pharmacological inhibitor of ERK suppressed NQ mediated radioprotection (Fig. 2.15A-C). Several previous studies had demonstrated that ERK2 (or p42MAPK or MAPK1) is activated by upstream kinase MEK1¹⁵⁰. MEK1 (or MKK1 or MAP2K1 or MAP Kinase Kinase-1) is a dual specificity protein kinase which in turn activated by upstream kinase MEKK1 (or MAP3K1 or MAP kinase kinase kinase-1). Raf-1 (or c-Raf) is a MAP kinase kinase kinase (MAP3K) that functions downstream of the Ras subfamily of membrane associated GTPases to which it binds directly. Once activated, Raf-1 can phosphorylate to

activate the dual specificity protein kinases MEK1 and MEK2. Our results showed that NQ treatment to lymphocytes activated both MEK1 and MEKK1 (Fig.2.15D).

The activation of MAP kinase pathways may occur through feedback inhibitory mechanisms that involve dephosphorylation by serine/threonine phosphatases, tyrosine phosphatases and through the phosphorylation of upstream kinases. Our results demonstrated that NQ induced ERK activation is mediated by both downregulation of phosphatase and activation of upstream kinase (Fig.2.15D, E). Our results provides experimental support to hypothesis of Klaus V. et al (2010) who had earlier postulated that NQ induced EGFR, ErbB2 and ERK phosphorylation might be mediated through inhibition of phosphatase activity⁵⁸.

Earlier reports by Schmidt, et al (2000) demonstrated that cytoplasmic calcium mediated the activation ERK via Raf/MEK/ERK pathway in keratinocytes¹⁵⁰. NQ mediated increase in phosphorylation of ERK may be occurring through elevation of calcium levels¹⁵⁰ and/or by decreased phosphatase activity. NQ increased intracellular calcium levels within seconds of addition to lymphocytes and also decreased protein tyrosine phosphatase activity (Fig. 2.16A, 2.15E). These results are in corroboration with a recent report by Kim et al., demonstrated that bisdemethoxycurcumin increased intracellular calcium levels leading to activation of ERK¹⁵¹. Another cysteine containing protein target of NQ could be caspases, especially, post-irradiation. Our results, thus, indicate that NQ may activate multiple mechanisms in upregulating prosurvival molecules.

There are several phytochemicals that exhibit radioprotection *in vitro* but fail to translate their activity in *in vivo* models. Hence, it is very important to investigate whether NQ offers similar protective ability in mice. In addition to protecting

lymphocytes *in vitro*, NQ offered *in vivo* radioprotection to lymphocytes and bone marrow cells when administered to mice. Importantly, loss of bone marrow and spleen viability as a result of exposure to WBI was significantly restored in presence of NQ (Fig. 2.17A, B). Further, number of lymphocyte subsets was scored by staining cells with labeled anti-CD3, anti-CD4, anti-CD8, anti-CD19 and anti-CD14 antibodies. There was significant recovery in these subsets obtained from NQ administered mice followed by WBI as compared to only WBI mice (Table 2.6). In addition to protecting lymphocytes *in vitro*, NQ offered *in vivo* radioprotection to lymphocytes evaluated in terms of inhibition of increase in pre-G1 population, nuclear-blebbing, DNA- fragmentation, Bax levels, MMP loss and activation of caspases (Fig. 2.18). These results gain significance in the light of increased demand for syndrome specific radioprotectors. Our results clearly indicated that NQ treatment to mice before irradiation offered radioprotection to hematopoietic cells. Histopathological studies further strengthen our conclusion of hematopoietic protection (Fig. 2.17 F-H).

Hematoxyline and eosine staining of spleen and bone marrow showed that WBI induced splenic atrophy, hypoplasia and bone marrow aplasia was significantly inhibited by NQ pretreatment of mice (Fig. 2.17 F-H). Bone marrow aplasia occurred due to WBI induced loss of bone marrow cellularity and hematopoietic depletion. Splenic atrophy refers to wasting of spleen and was due to reduction in spleen size as a result of depletion splenic cellularity. If splenic atrophy continues it results into hypoplasia which is characterized by lack of splenic tissue. Since spleen play major role in the mechanical filtration of RBCs, atrophy of spleen induced by WBI exposure to mice results in modest increase in circulating RBCs. The destruction of RBCs results into release of iron and its overload lead to deposition of hemosiderin in splenic tissue by the process called

hemosiderosis. Hemosiderin is blackish-brown colored pigment and composed of iron-storage complex of ferritin. Hemosiderin is most commonly found in splenic macrophages and is especially abundant in situations following hemorrhage, suggesting that its formation may be related to phagocytosis of red blood cells and hemoglobin. Our results clearly indicated that NQ pretreatment of mice protected against WBI induced hemosiderin deposition in the spleen (Fig. 2.17H).

The peripheral blood count is considered to be a biologically meaningful parameter to demonstrate the effect of radiation on normal tissue because radiation induced mortality is mainly due to infection as a result of impairment of hematopoietic functions. NQ administration to mice inhibited WBI induced leucopenia (decreased WBC counts), lymphopenia (decreased lymphocyte counts), neutropenia (decreased neutrophil counts) and erythropenia (decreased RBC counts) (Table. 2.5). Further, NQ pretreatment to mice also protected WBI induced decrease in hemoglobin levels, packed cell volume and mean corpuscular volume (Table. 2.5). Mice exposed to WBI showed thrombocythemia (increased platelet counts) 5 days after WBI (Table. 2.5). Exposure of mice to radiation initially decreases platelet counts and as a result of granulocyte reconstitution, mice started recovering from radiation insult and often overshoot the control value within 1-2 week before normalizing¹⁵². Increased platelet counts observed in WBI group of our study may be the result of this overshoot phenomenon.

Exposure of mice to radiation elevated the plasma levels of NO (Fig. 2.18I). This was in agreement with our recent study¹¹⁷. NO is a potent inhibitor of lymphocyte proliferation and has been reported to increase the radiation induced damage through inhibition of activity of DNA repair enzymes¹¹⁷. Administration of NQ resulted in complete abrogation of WBI mediated increase in plasma NO levels (Fig. 2.18I). Further,

NQ augmented the plasma levels of radioprotective IL-1 β and IL-6 (Fig. 2.19). IL-1 β induces neutrophilia by mobilizing polymorphonuclear cells from bone marrow and promote the formation of microthrombi by stimulating increased level of fibrinogen in circulation and thus induces hypoxic condition which protect cell from radiation damage¹⁴⁴. The increased IL-6 level is known to accelerate hematopoietic regeneration, splenic CFUs and accelerated recovery of peripheral WBC and RBC¹⁵².

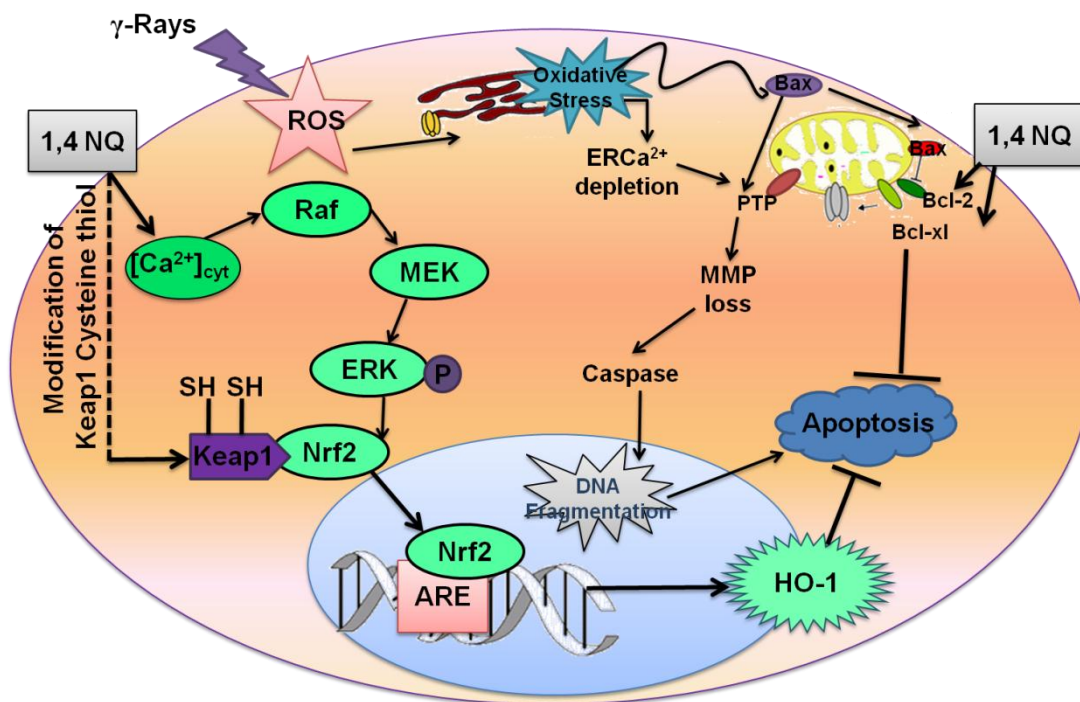
Lymphocytes obtained from WBI treated mice showed significantly decreased proliferation and decreased levels of IL-2, IL-4, IL-6 and IFN- γ in response to a mitogen, Con A as compared to control (Fig. 2.20A, B). However, a significant increase in proliferation and cytokine secretion was observed in lymphocytes taken from NQ administered mice followed by WBI. Our PI staining results demonstrated that NQ pretreatment of mice also protected WBI induced decreased proliferation of bone marrow cells (Fig. 2.20C). Further, NQ administration was found to be very effective in stimulating the regeneration of hematopoietic stem cells as evidenced by the increase in the endogenous spleen colonies. The endogenous hematopoietic spleen colony formation is a considered as good indication of stem cell viability and/or the stimulation, proliferation and survival of cells in animals recovering from exposure to radiation¹⁵³. The possibility that may account for elevated number of endogenous spleen colonies in NQ treated mice subjected to WBI include: 1). Presence of more number of CFUs at the time of irradiation, 2). Increased trapping of CFUs in the spleen of treated mice, and 3) increased radioresistance of CFUs. The exact mechanisms by which NQ stimulate the regeneration of hematopoietic cells are presently not known and needs further investigation.

Survival of mice after exposure to lethal doses of radiation depends on survival of a critical number of HSCs and the ability of these HSCs to repopulate the depleted hematopoietic compartment¹³¹. Therefore, protection conferred to radiosensitive cells like lymphocytes and bone marrow by administration of NQ should be manifested as an improvement in the survival of irradiated animals. NQ pretreatment clearly enhanced the survival of mice exposed to a lethal whole-body irradiation dose of 7Gy by 50% and prevented the loss of weight (Fig. 2.21A, B). The DMF of NQ was 1.18 (Fig. 2.21C) as against 1.33 for amifostine which is a well known radioprotector¹⁵⁴. In general, DMFs of lower than 1.4 for 30 day survival has been reported for naturally occurring radioprotectors like the ocimum flavonoids, polysaccharides and cytokines¹³¹. Hence, NQ may fall into this category of radioprotectors.

An ideal radioprotector should protect normal cells but not tumor cells. Interestingly, NQ did not offer any protection to human breast cancer cell line, MCF-7 but enhanced radiation-induced cell death. It also induced death in MCF-7 cells even in the absence of radiation (Fig. 2.22). Zheng et al (2008), has shown the importance of protecting tumor specific CD4+T cells during radiotherapy through engagement of TLR9¹⁵⁵. In the present study, we have shown that NQ exhibited complete protection against radiation induced cell death in CD4+T cells and CD19+B cells (Fig. 2.7).

In conclusion, NQ offered radioprotection to lymphocytes due to activation of multiple prosurvival mechanisms including upregulation of Ca^{+2} /ERK/Nrf2/HO-1 pathway. The proposed model of NQ mediated radioprotection has been summarized in Scheme 2.4. Further, our results indicate a possible radiation hematopoietic syndrome specific radioprotective role for NQ. To the best of our knowledge, this is the first report

showing a prooxidant and a GSH depletor offering radioprotection at such low concentrations.



Scheme 2.4: Proposed model of radioprotective effects of NQ: NQ upregulated the expression of cytoprotective enzyme HO-1 by activating redox sensitive transcription factor Nrf2 via activation of Ca^{2+} /Raf/MEK/ERK pathway and inhibited radiation induced apoptosis. NQ might also activated Nrf2 by destabilizing Nrf2-Keap1 interaction by binding with cysteine residue of Keap1. NQ also activated antiapoptotic protein Bcl-2 and Bcl-xl which is known to inhibit apoptosis.

CHAPTER 3

*IMMUNOTOXIC AND
RADIOMIMETIC
EFFECTS OF
BILIRUBIN*

3.1 INTRODUCTION

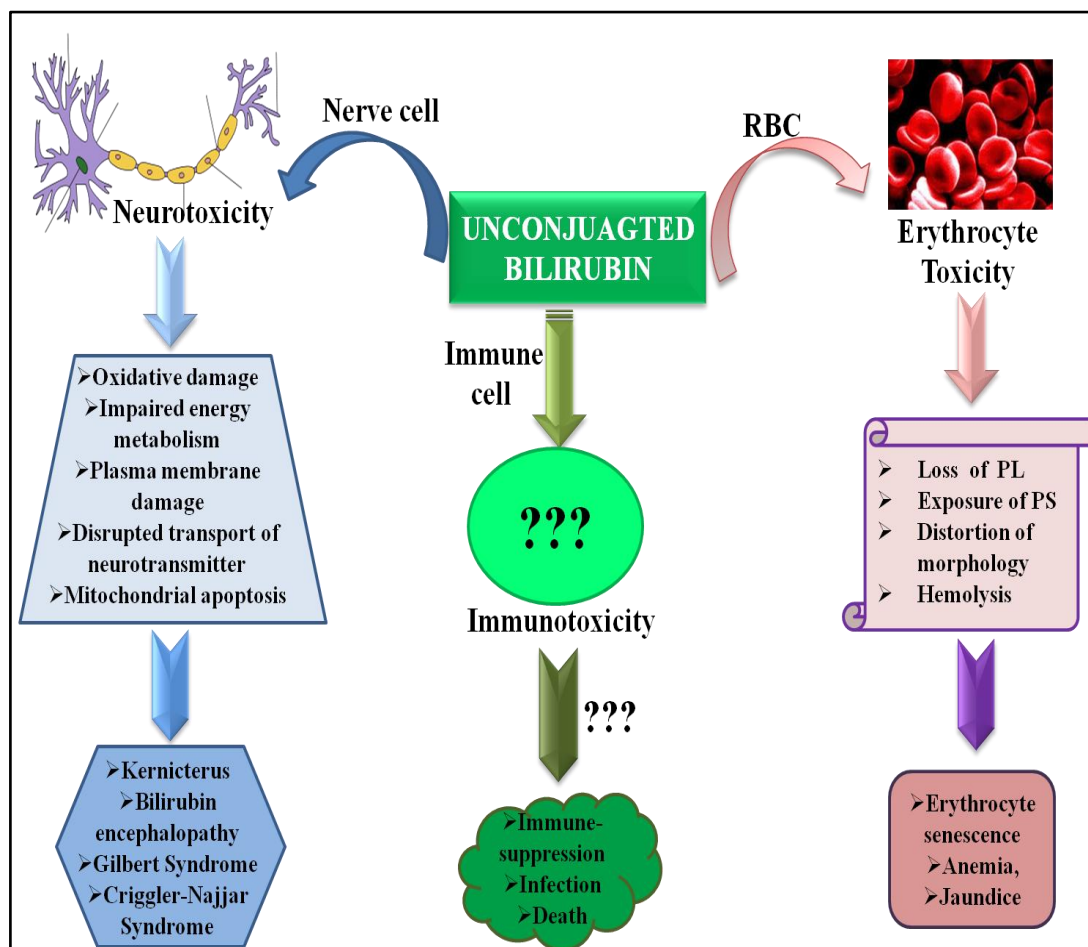
Bilirubin is a linear tetrapyrrole that is formed during endogenous degradation of heme. Heme is metabolized by hemeoxygenase to form carbon monoxide, biliverdin, and free iron. Biliverdin is subsequently transformed to bilirubin by biliverdin reductase¹³. Bilirubin is a highly lipophilic molecule and must be glucuronidated by UDP-glucuronosyl transferase into bilirubin glucuronides which are generally called as conjugated bilirubin⁶⁸. However, about 96% of the bilirubin in normal plasma is unconjugated (UCB) and is extremely poorly soluble in water. It is present in plasma strongly bound to albumin and albumin binding keeps UCB in solution. Several studies during the last few decades have demonstrated the physiological role of UCB mainly as an antioxidant^{76,83,86,156-158}. Its antioxidant potential is attributed mainly to the scavenging of peroxy radicals. The proposed mechanisms by which bilirubin deactivates peroxy radicals include: (i) hydrogen atom transfer from the methylene at position C-10 to peroxy radicals, (ii) peroxy radical addition to the pyrroles, and (iii) single electron transfer¹⁵⁹.

Although physiological levels of UCB act as an antioxidant, increasing evidences have demonstrated, at high concentrations it may be an active participant in the disease process^{13,62}. *In vitro* and *in vivo* studies in humans and rodents have demonstrated that elevated UCB is neurotoxic^{13,18,61,160-162}. Although neuronal cells are considered the main target for UCB toxicity, circulating cells are also affected by increased UCB levels. UCB has been shown to perturb the normal distribution of membrane phospholipids of human erythrocytes by translocating the inner leaflet aminophospholipids (phosphatidyl serine, PS) to the outer leaflet of the membrane leading to distortion of morphology and

induction of hemolysis^{81,82,163}. The earlier studies involving UCB toxicity suggest that it is a potentially toxic molecule to erythrocytes, cultured neurons, neuroblastoma cells, hepatoma cells, colon cancer cells and fibroblast cells^{13,16,18,61,160,164,165}. The ability of UCB to damage mitochondria and induce apoptosis in various cell lines has been demonstrated^{16-18,61,80,161,166-168}. *In vitro* studies have demonstrated the multiple toxic effects of UCB on cell response, membrane integrity, respiration and transport functions⁶¹.

Several studies suggest that UCB possesses multiple biological activities, including potential immunomodulatory and anti-inflammatory properties¹⁶⁹⁻¹⁷¹. UCB decreases immune responses¹⁷¹⁻¹⁷⁷ and increased rates of infection have been documented in hyperbilirubinemic patients¹⁷⁸⁻¹⁸⁰. The roles of bilirubin on the suppression of immune function were first observed more than three decades ago. In 1970 Nejedla observed that hyperbilirubinemia exerted a suppressive effect on antibody formation in newborn infants¹⁸¹. Sima et al (1980) were the first to attribute the immunosuppressive effect of bilirubin demonstrating direct effect on lymphocyte and granulocyte *in vitro* as well as *in vivo*¹⁷⁶. Vetvicka et al (1991) showed that bilirubin was capable of regulating immune functions due to its high lipophilic nature and its direct interaction with cell membranes¹⁸². Additionally, Haga et al (1996) demonstrated that bilirubin inhibit cytotoxic T lymphocyte activity *in vitro* and impairs PHA induced T cell proliferation by decreased IL-2 production in human lymphocytes¹⁷³. The decreased immune response has been attributed to the immunological anergy induced by UCB. However, in contrast to its well established neurotoxic, and erythrocyte toxic action, the immunosuppressive and immunotoxic effects of UCB have not been widely explored (Scheme 3.1). The probable

molecular mechanisms by which UCB induces immunosuppression in the host have also not been investigated and may involve proliferative arrest in lymphocytes or, alternatively, induction of necrosis and apoptosis in mature immune cells.



Scheme 3.1: UCB induces immunotoxic effects by unknown mechanisms: UCB is known to induce erythrocyte toxicity and neurotoxicity by activating multiple pathways leading to bilirubin encephalopathy, kernicterus and jaundice. Although UCB possesses immunotoxic effects, signaling pathways and sequence of events involved in UCB induced immunotoxicity are not known. Molecular mechanism involving UCB induced immunosuppression and infection is poorly understood. (PL; Phospholipid, PS; Phosphatidylserine)

Direct interaction of very high concentration of UCB with plasma membrane of immune cells, at ≥ 3 UCB to albumin molar ratios has been demonstrated¹⁷². The cytotoxicity of UCB at clinically relevant concentrations and molar ratios of UCB to albumin has not been evaluated using cells of the immune system. In contrast to the great

interest in elucidating the molecular mechanisms of UCB induced neurotoxicity, fewer studies addressed the possibility of UCB also being toxic for non-neural cells^{15,81,82,183-185}. Characterizing the potential immunotoxicity of UCB is critical for understanding the potential risk of elevated UCB in hyperbilirubinemic patients.

Since UCB has been shown to suppress the immune response and induces toxicity in the cells of immune system¹⁸⁶, we hypothesize that UCB may imitate the biological effects of radiation and possesses radiomimetic effects, in addition to its other established biological effects. A radiomimetic drug is one that mimics the biological effects of radiation like induction of DNA strand breaks, cytotoxicity, perturbation of cell cycle, induction of apoptotic bodies etc. Bleomycin, alkylating agents and chemicals such as nitrogen mustards are known to be radiomimetic drugs^{187,188}. Survey of literature indicates that the toxicity of UCB depends on the free UCB present (B_f), concentration of UCB used, cell type studied, the source of UCB/impurities present in the commercial preparations and the end point selected for the studies¹³. However, data pertaining to the mechanisms underlying the potential radiomimetic and immunotoxic effects of UCB are lacking.

Considering the importance of immunotoxicity data of UCB in human health, we carried out exhaustive studies to delineate the cellular and molecular mechanism by which pathologically relevant concentration of UCB can cause immunotoxicity in murine splenic resting immune cells like T cells, B cells, macrophages and human PBMCs. Since in humans the normal plasma level of UCB is around 20 μ M and levels as high as 170 μ M in neonates are still considered physiological, we chose clinically relevant concentrations of UCB between 10-100 μ M for the present studies¹⁷⁰. These

concentrations have been used previously for the study of several biological properties of UCB including apoptotic, anti-inflammatory, anti-mutagenic, antioxidant and anticancer^{15,169,171,189}. Since toxicity of UCB is determined by the plasma B_f that is not bound to plasma proteins and lipoproteins^{164,180,190}, we used molar ratios of UCB to BSA less than 0.7, to make the studies physiologically more relevant. The effect of *in vivo* administration of UCB on the host immune competence was also studied. Purified UCB and UCB sourced from different manufacturers were also used, to see the toxicity if any, contributed by the impurities present in the commercial preparations.

3.2 MATERIALS AND METHODS

3.2.1 Reagents and Chemicals:

UCB, Lipopolysaccharide (LPS), 5-Sulfosalicylic acid (SSA), Dithiobis 2-nitrobenzoic acid (DTNB), NADPH, Glutathione reductase (GR), Glutathione (GSH), Oxidized GSH, (GSSG), Triethanolamine, 2-Vinylpyridine, Monochlorobimane (MCB), Dihydroethidium (DHE), Methylene blue, Ethylene glycol-bis (2- aminoethylether)-N,N,N',N'-tetra-acetic acid (EGTA), HEPES, Trizma base, Glycine, Glycerol, Dithiothreitol (DTT), 2-Mercaptoethanol (2-ME), Phenylmethanesulfonyl fluoride (PMSF), Leupeptin, Aprotinin, Benzamidine, Igepal (NP40), Sodium dodecyl sulphate (SDS), N,N,N',N'-Tetramethylethylenediamine (TEMED), Caspase-3,8 colorimetric assay kit, AnnexinV-FITC/PI staining assay kit and, Protein tyrosine kinase assay kit were purchased from Sigma Chemical Co (USA). Carboxy fluorescein diacetate succinimidyl ester (CFSE) was procured from Molecular Probes, The Netherlands. CyQUANT-NF cell proliferation assay kit was purchased from Molecular Probes, Invitrogen. Caspase 3, 8, 9 inhibitor, SB203580 and UCB were purchased from calbiochem (USA). Fluorescein diacetate (FDA) was purchased from MP Biochemicals. Antibodies to mouse anti-phospho-p38, anti-p38 for Western blotting were purchased from Cell Signaling Technologies (USA). Horseradish peroxidase (HRP) enzyme conjugated secondary antibody and enhanced chemiluminiscence Western blotting kit were obtained from Roche Applied science (Germany). All other chemicals used were described in chapter 2, section 2.2.1

3.2.2 Animal maintenance:

As described in chapter 2, section 2.2.2

3.2.3 Preparation and treatment schedule of UCB:

All preparations of UCB and experiments involving *in vitro* as well as *in vivo* were performed with minimal light to prevent its photo degradation. To ensure its chemical integrity, UCB stock solution was prepared just before the experiment as described previously⁹⁰ Briefly, stock solution of 900 μ M UCB was prepared by dissolving 1.05mg of UCB in 2ml of 0.1N NaOH. After complete dissolution, 4ml of BSA (450 μ M) was added to UCB stock to get a final concentration of 300 μ M of UCB and BSA. The culture medium contained 10% FCS, which corresponds to a BSA concentration of approximately 45 μ M, was considered for calculating the molar ratios of UCB to BSA¹⁶. The bilirubin/albumin molar ratios in the different UCB concentrations were shown in Table 3.1.

Table 3.1: Molar Ratio of UCB to BSA used in the study

UCB concentration	BSA concentration	Molar Ratio of UCB/BSA
10 μ M	55 μ M	0.18
25 μ M	70 μ M	0.36
50 μ M	95 μ M	0.53
100 μ M	145 μ M	0.69

For *in vivo* studies, UCB was dissolved in 0.1N NaOH solution and final concentration was adjusted to 2.5-5 mg/ml with 5% BSA. The solution was (25-50mg/kbw) injected i.p. to mice.

Experiments involving purified UCB were performed after further purifying the commercial preparation according to the method of McDonagh and Assisi et al to eliminate potential lipid contaminants¹⁹¹. Briefly, 40mg of UCB was dissolved in 50ml of chloroform and heated upto boiling and then it was kept until it comes to room temperature. The solution (which contains some undissolved solid) was washed with 0.1M NaHCO₃ (3x30ml), dried over anhydrous Na₂SO₄ (2gm) and filtered. About one third of the volume of chloroform was removed by distillation and methanol was added by parts in small volume to the boiling solution until a faint turbidity appeared. The solution was cooled to room temperature and precipitate was filtered after 2h. The crystalline precipitate was washed with chloroform-methanol mixture (1:1) and dried at room temperature and used as purified bilirubin.

3.2.4 Bone marrow and spleen cell suspensions:

As described in chapter 2, section 2.26.

3.2.5 Human lymphocyte isolation:

As described in chapter 2, section 2.2.15

3.2.6 Estimation of cell death:

As described in chapter 2, section 2.2.7

3.2.7 Estimation of cell death by CFSE staining:

CFSE consists of a fluorescein molecule containing 2 acetate moieties and a succinimidyl ester functional group. In this form, it is membrane permeant and non-fluorescent. After diffusion into the intracellular environment, endogenous esterases remove the acetate groups, rendering the molecule highly fluorescent and nonpermeant to

the cell membrane. In addition, the succinimidyl ester reacts with free amine groups of intracellular proteins, forming dye protein adducts that are unable to exit from the cell. These long term conjugates allow stable labeling of cells with CFSE¹⁹². The cell death in CFSE labeled cells results in leaching of fluorescence with a concurrent decrease in cell size and can be monitored by decreased CFSE fluorescence along with decrease in FSC using flowcytometry.

Splenic lymphocytes were stained with CFSE (20 μ M, 5minutes) and washed three times using ice cold RPMI medium containing 10% FCS. Lymphocytes (1x10⁶) were treated with UCB (10-100 μ M) and cultured for 24 h at 37 °C in a 95% air/5% CO₂ atmosphere. The cell death was measured by dye dilution with concurrent decrease in cell size using Partec PAS III flowcytometer. Percent dead cells that showed a decrease in CFSE fluorescence intensity (low FL1) and low FSC were calculated using FloMax® software and were expressed as percent dead cells.

3.2.8 AnnexinV-FITC/PI staining:

The annexins are a group of homologous proteins which bind phospholipids in the presence of calcium. Annexin V-FITC is a fluorescent probe which binds to phosphatidylserine (PS) in the presence of calcium. At the onset of apoptosis, PS which is normally found on the internal part of the plasma membrane, becomes translocated to the external portion of the membrane. The PS becomes available to bind to the annexin V-FITC conjugate in the presence of calcium. The procedure consists of the binding of annexin V-FITC to PS in the membrane of cells, which are beginning the apoptotic process, and the binding of PI to the cellular DNA in cells where the cell membrane has been totally compromised.

Lymphocytes (1×10^6) were incubated with UCB (25-100 μ M) for 24h at 37°C in RPMI-1640 medium supplemented with 10% FCS in 5% CO₂ atmosphere. The cells were washed twice with PBS and resuspended in 1x binding buffer containing 5 μ l of annexin V- FITC conjugate and 10 μ l of PI solution and incubated at room temperature for 10 minutes in dark. A total of 20,000 cells were acquired in Partec PAS III flowcytometer and analyzed using FloMax® software.

3.2.9 Caspase-3, 8 colorimetric assay:

To measure the activation of caspase-3, 8 in the cell treated with or without UCB (100 μ M, 24h), colorimetric assay kit (Sigma) was used as per manufacturer's protocol. The assays were performed in 96-well plate, which measured the cleavage product p-nitro aniline released from the C-terminal peptide bond at 405nm.

To study the effect of caspase inhibitor on UCB induced cell death, lymphocytes were pretreated with inhibitor of caspase-8 (Caspase8i, 30 μ M), caspase-9 (Caspase9i, 30 μ M) caspase-3 (Caspase3i, 20 μ M) for 1h, followed by treatment with UCB (100 μ M) for 24h at 37°C and cell death was estimated by PI staining.

3.2.10 Measurement of change in MMP and intracellular calcium levels:

As described in chapter 2, section 2.2.17 and 2.2.18.

3.2.11 Estimation of DNA strand breaks by alkaline single-cell gel electrophoresis (Comet assay):

Splenic lymphocytes (0.1×10^6 cells/ml) were cultured for 4h in presence or absence of UCB and two microscopy slides from each group were prepared and processed for comet assay¹⁹³. The fully frosted microscope slides were layered with 1ml of 0.8% low melting agarose dissolved in saline containing cell suspension at 38°C and the slides were placed at 4°C for 10minutes for solidification. After solidification, the

slides were immersed in ice chilled lysis buffer containing 2.5M NaCl, 100mM EDTA, 10 mM Tris-HCl, pH 10.0 and 1% DMSO and 1% Triton X-100 for 1h at 4°C. The slides were then removed from the lysis buffer and equilibrated in alkaline solution for 20 minutes, followed by electrophoresis for 0.5h at 25V, 399mA. After electrophoresis, the slides were neutralized and stained by 5X SYBR Green-II dye. The images were captured using a Carl Zeiss Axioplan fluorescence microscope (Germany). Fifty images per slide were analyzed for percentage DNA content in the tail, tail length, tail moment, and olive tail moment using CASP software.

3.2.12 Measurements of RBC hemolysis:

Blood was collected from healthy mice by retro orbital puncture and immediately diluted to 50 times with isotonic PBS and incubated with or without UCB (50μM) for 4h at 37°C and RBCs hemolysis was monitored to examine the integrity of RBC membrane as described previously¹⁹⁴.

The RBC suspension (200μl) treated as above was transferred to ELISA plates in quadruplicate and centrifuged in a plate centrifuge at 3000rpm for 10minutes at room temperature. The supernatants (100 μl) were transferred to ELISA modules and the OD was measured at 405nm in an ELISA reader (Universal Microplate reader, Bio-Tek Instruments). A blank was also run that contained RBCs in isotonic NaCl solution (0.9 g/dl). The OD of the supernatant from the ELISA plate well, which contained RBC suspension in 0.09% NaCl was considered as 100% hemolysis and used to convert the remaining OD values to percentage hemolysis.

3.2.13 RNA isolation and quantification:

As described in chapter 2, section 2.2.27.

3.2.14 Antibody staining:

As described in chapter 2, section 2.2.24.

3.2.15 Western blot analysis:

To determine the levels of phospho-p38, cytoplasmic extracts were prepared from UCB (100 μ M) treated splenic lymphocytes as described previously¹⁹⁵. Cells were washed with ice-cold PBS and suspended in 0.1ml lysis buffer (10mM HEPES, pH 7.9, 10mM KCl, 0.1mM EDTA, 0.1mM EGTA, 1mM dithiothreitol, 0.5mM PMSF, 2mg/ml leupeptin, 2mg/ml aprotinin, and 0.5mg/ml benzamidine). These cells were allowed to swell in ice for 15minutes, after which 25 μ l of 10% NP40 was added and tubes were vortexed once for 60seconds, incubated on ice for 5minutes and again vortexed three times for 25seconds each with intermittent incubation on ice for 5minute each. The supernatants were collected by centrifuging the cells at 8,000 rpm for 6minute at 4°C and used as cytosolic fraction. The protein content was determined using Bradford reagent (BioRad Protein assay kit). Equal amount of protein (50 μ g) from each sample was resolved on 10% SDS PAGE at 120volts. The proteins were electro-transferred onto nitrocellulose membranes. Membrane was blocked with 5% fat free milk in PBST for 0.5h. Further, membranes were probed with primary antibodies for phospho-p38 overnight at 4°C in 1% fat free milk. Membranes were washed three times with PBST to remove non-specific binding (mild shaking, 15minutes) with PBST buffer. HRP-conjugated mouse Immunoglobulin secondary antibody was freshly prepared in 1% fat free milk and used for staining (2hr). Non-specific binding was removed by washing three times (mild shaking, 15minutes) with PBST buffer. Specific bands were visualized on X-ray films upon addition of substrate provided in Enhanced Chemiluminiscence Kit

(Roche, Germany)¹⁹⁶. The membranes were stripped and reprobed with anti-p38 antibody for loading control.

3.2.16 Protein tyrosine kinase assay:

Protein tyrosine phosphorylation is a central mechanism that mediates signal transduction events involved in a wide range of cellular processes like cell cycle progression, transcriptional regulation, cell transformation, proliferation, differentiation, and apoptosis.

The determination of protein tyrosine kinase (PTK) activity is based on an ELISA assay using a PTK-specific random polymer substrate poly-Glu-Tyr (PGT) coated multiwell plate. PGT can be phosphorylated by a wide range of PTKs. The phosphorylation reaction is initiated by the addition of a protein tyrosine kinase present in the cell extracts prepared from UCB (100 μ M, 3h) treated lymphocytes. The color is quantitated by spectrophotometry at 492nm using ELISA reader and reflects the relative amount of tyrosine kinase activity in the sample.

3.2.17 Measurements of ROS levels:

As described in chapter 2, section 2.2.19

3.2.18 Measurements of intracellular GSH levels:

MCB dye was used to measure intracellular GSH¹³². Splenocytes (1x10⁶) were incubated with or without UCB (100 μ M) for indicated time at 37°C and MCB (40 μ M, 0.5h at 37°C) was loaded into the cell suspension. Fluorescence emission from cellular sulfhydryl-reacted monochlorobimane was measured using a spectrofluorimeter (BMG Labtech Optima), flowcytometer and confocal microscope. DEM was used as positive

control for GSH depletion¹⁰⁰. MCB is also known to react with small-molecular-weight thiols other than GSH but GSH forms the major monochlorobimane reactive thiol¹³².

Cellular GSH exists predominantly in the reduced form, but small amounts of the oxidized disulfide form GSSG can also be detected. The GSH/GSSG ratio often is taken as an indicator of cellular redox status. GSH and GSSG levels were also determined by an enzymatic recycling procedure using Tietze method⁷⁸. The sulfhydryl group of the molecule reacts with DTNB producing a yellow colored 5-thio-2-nitrobenzoic acid (TNB), and the disulfide is reduced by NADPH in the presence of glutathione reductase. GSSG was determined by derivatization of GSH by reaction with 2-vinylpyridine for 1h at 4°C. Supernatants were assayed in 100mM sodium phosphate buffer, containing 0.62mM EDTA, 1.7mM NADPH and 20.2mM DTNB. The rate of TNB formation was monitored following addition of 1.2U of glutathione reductase, at 420nm. Glutathione concentrations were calculated using appropriate standards.

3.2.17 ³H thymidine incorporation assay:

Tritiated thymidine incorporation assay was used to monitor the proliferation of cells. The thymidine is incorporated into dividing cells and the level of this incorporation, measured using a liquid scintillation counter, is proportional to the amount of cell proliferation¹¹⁴.

Splenic lymphocytes (1×10^6 /ml) suspended in RPMI-1640 medium containing 10% FCS were treated with UCB (10-100 μ M, 4h) and stimulated with the B-cell mitogen LPS (50 μ g/ml) for 48h at 37 °C in 95% air/5% CO₂ atmosphere in a 96-well plate. For *ex vivo* assay of proliferation, lymphocytes isolated from vehicle or UCB treated mice (25, 50mg/kgbw, 24h) were stimulated with LPS or ConA for 48h or 72h respectively. Cells

were pulsed with ^3H thymidine (0.5 μCi /well, specific activity 6500mCi/mM, Board of Radiation & Isotope Technology, Department of Atomic Energy, Mumbai, India) and further cultured for next 16h. Cells were harvested on glass fiber filters using a Multimash-2000 harvester (Dynatech Laboratories Inc.). The incorporated radioactivity was counted in a liquid scintillation counter (LKB) and was expressed as counts per minute (CPM).

3.2.18 CyQUANT-NF cell proliferation assay:

The CyQuant assay kit employs a DNA binding dye in combination with a plasma membrane permeabilization reagent to facilitate the interaction of dye with nuclear DNA. Lymphocytes (1×10^6) were treated with UCB (10-100 μM , 4h) and then stimulated with LPS (50 $\mu\text{g/ml}$) for 48h at 37°C. Proliferation was estimated by the changes in the total DNA content using CyQUANT-NF cell proliferation assay according to manufacturer's protocol. Fluorescence signals were recorded using a plate reader (Fluostar Optima, BMG Labtech) with excitation at 485nm and emission at 530nm and expressed as mean fluorescence intensity (MFI).

3.2.19 Measurement of cytokines:

As described in chapter 2, section 2.2.31.

3.2.20 Administration of UCB to mice:

Mice (5 animals per group) were administered with UCB (25, 50 mg/kgbw) i.p. and sacrificed 24h after injection. The viability and spleen index were estimated as described chapter 2, section 2.2.29. Hematological parameters were assessed in the blood obtained from retro-orbital puncture of treated mice 24h after UCB administration.

Estimation of cell death in lymphocytes obtained from UCB treated mice was performed by esterase activity assay. Splenic lymphocytes (1×10^6) isolated 24h after UCB (25mg/kbw) injection, were cultured for 24h at 37°C in complete medium. The cells were stained with FDA (20μM) for 0.5h at 37°C. Fluorescence intensity of FDA stained cells was measured at an excitation wavelength of 485nm and emission wavelength of 533nm. Decrease in fluorescence intensity was taken as decrease in the viability of cell.

Experiments involving p38MAPK activation and GSH estimation, mice were sacrificed at 1, 2 and 3h following UCB administration. SB203580 (p38MAPK inhibitor) was dissolved in DMSO and administered i.p. at a dose of 5mg/kbw, 2h prior to challenge with UCB. In experiments to determine the effect of altered GSH levels, mice were treated with NAC (100mg/kbw) dissolved in PBS solution 0.5h prior to UCB administration¹⁹⁷.

3.2.21 Statistical analysis:

Data were presented as mean±SEM. Data from all the experiments were analyzed using one-way ANOVA followed by post hoc analyses using the Scheffe test. Significance was set at $p < 0.05$.

3.3 RESULTS

3.3.1 UCB exhibited immunotoxic and radiomimetic effects in lymphocytes by inducing cell death and DNA strand breaks:

To study the immunotoxic and radiomimetic effects of UCB, murine splenic lymphocytes were cultured in the presence or absence of UCB (10-100 μ M) for 24h and cell death was estimated by PI staining. The results shown in Fig. 3.1A, B clearly indicated that UCB concentration $\geq 25\mu$ M induced cell death in naïve splenic lymphocytes in a concentration dependent manner.

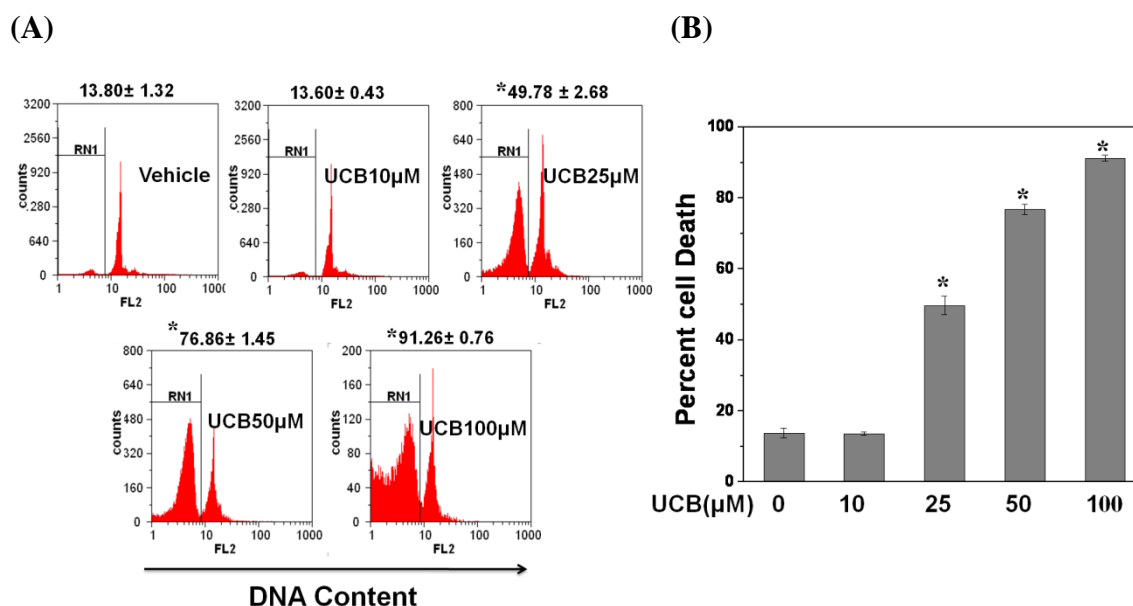


Fig. 3.1: UCB induced immunotoxic and radiomimetic effects in lymphocytes: Splenic lymphocytes (1×10^6) were treated with UCB (10-100 μ M) for 24h at 37°C and cell death was estimated by PI using Partec PAS III flowcytometer and percent apoptotic cells were determined by analyzing sub G1 population (less than 2n DNA content) using Flowmax® software. Representative flowcytometric histograms (A) and corresponding bars graph (B) showing UCB induced death in lymphocytes. The data is the representative of two such independent experiments having similar results. Each bar represents mean \pm S.E.M. from three replicates. * $p < 0.05$, as compared to vehicle group.

The immunotoxic effect of UCB was further confirmed by CFSE dye dilution along with monitoring the cell size. Results demonstrated that CFSE labeled cells treated

with UCB (10-100 μ M) showed significant dye dilution along with concurrent decrease in cell size as evinced by low FSC (Fig. 3.2). The decrease in CFSE fluorescence in UCB treated lymphocytes was not due to proliferation of cells but was due to induction of cell death in treated lymphocytes as evinced by concurrent decrease in cell size (Low FSC).

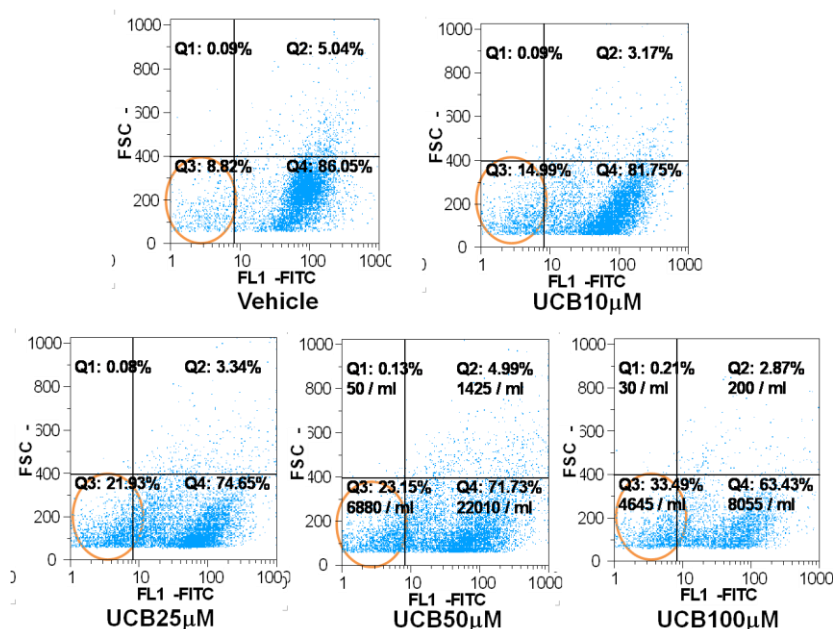


Fig. 3.2: UCB induced immunotoxic effects in lymphocytes: CFSE labeled lymphocytes were treated with UCB (10 μ M-100 μ M) and cultured for 24h at 37°C. Percent dead cells were calculated from decrease in mean fluorescence intensity of CFSE (FL1) along with decreased FSC (Q3 Panel). The data is the representative of two such independent experiments having similar results.

Since DNA is the major target of radiation, therefore to study the radiomimetic effects of UCB in lymphocytes we examined the ability of UCB to induce DNA damage. The results of comet assay showed that treatment of lymphocytes with UCB (10-100 μ M, 4h) induced DNA strand breaks in a concentration dependent manner (Fig. 3.3A, B). Further, UCB treatment to lymphocytes decreased the total RNA content in a concentration dependent manner (Fig. 3.3C). The results suggested that treatment of lymphocytes with UCB (\geq 25 μ M) exhibited radiomimetic effects by inducing cell death, DNA strand breaks and decreasing the total RNA content.

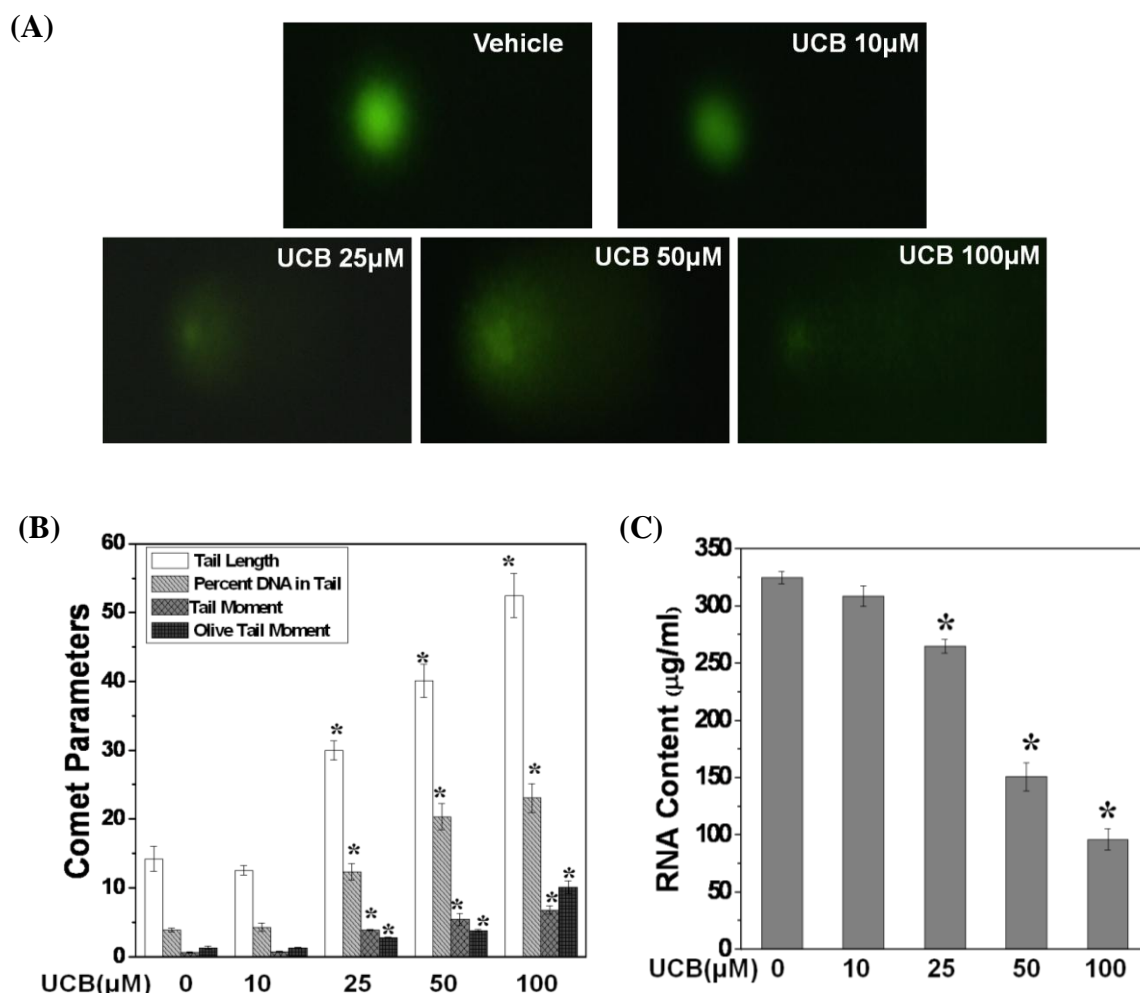


Fig. 3.3: UCB induced DNA strand breaks and decreased total RNA content in lymphocytes: Splenic lymphocytes (0.1×10^6) were treated with UCB (10-100 µM) for 4h at 37°C and DNA strand breaks were estimated by alkali comet assay. (A) Representative images of comet assay and (B) bar graph showing UCB induced DNA damage in lymphocytes. (C) Total RNA contents in lymphocytes (5×10^6) treated with UCB (10-100 µM, 24h) were isolated and quantified using spectrophotometer. The data is the representative of two such independent experiments having similar results. Each value represents mean \pm S.E.M. from 50 cells * $p < 0.05$, as compared to vehicle group.

3.3.2 UCB induced immunotoxic effects in activated lymphocytes:

Since, in disease-free young and young-adult mice majority of the splenic lymphocytes are naïve, experiments were carried out to see the immunotoxic effects of UCB in activated lymphocytes. LPS is a B-cell mitogen and was used to stimulate and activate the purified CD19+B cells pretreated with or without UCB (25-100 µM) and

immunotoxic effects were studied by examining by cell cycle analysis using PI staining. Results showed that UCB treatment arrested the cell population at pre G1 phase of the cell cycle and reduced the LPS induced increase in S+G2/M population. These results demonstrate that UCB is immunotoxic not only in naïve cells but also in LPS activated cells.

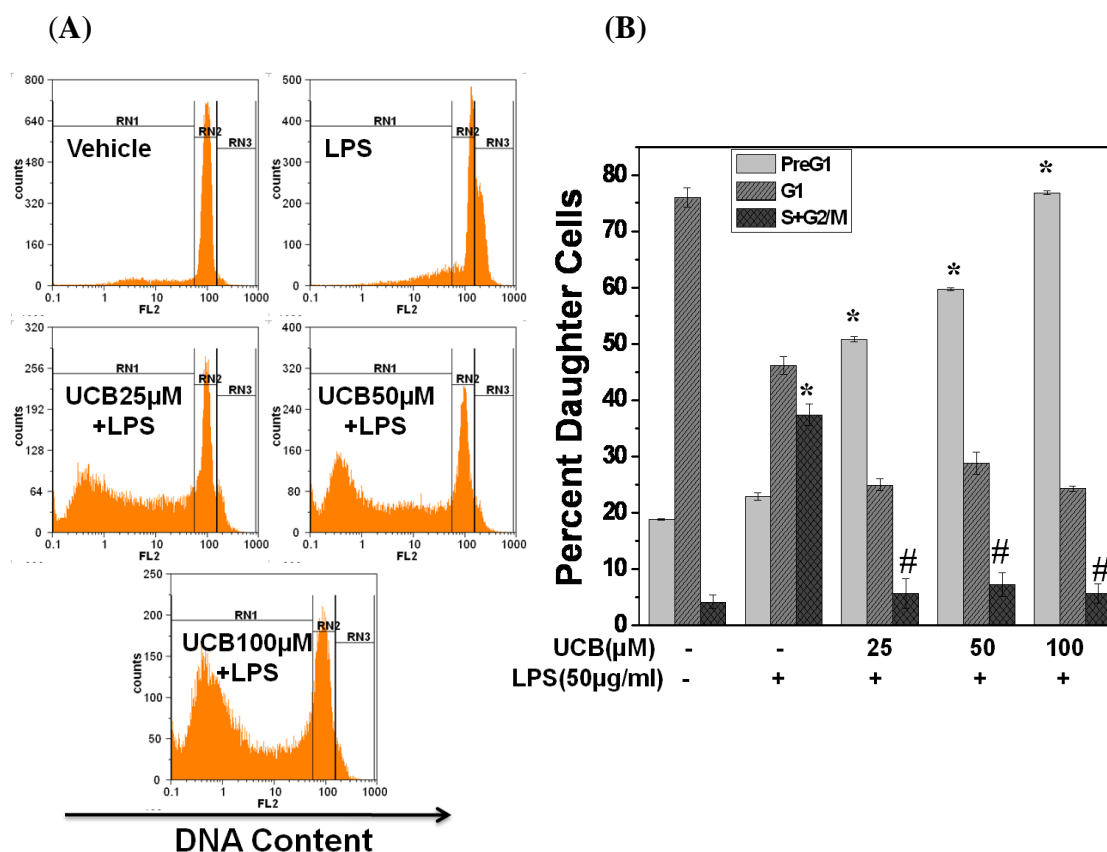


Fig. 3.4: UCB induced immunotoxic effects in activated lymphocytes: Purified CD19+B cells (1×10^6) were pre-treated with UCB (25-100 μ M) for 4h before stimulation with LPS (50 μ g/ml) for 48h at 37°C and cell cycle analysis was performed by PI staining. **(A)** Representative flowcytometric histograms of PI labeled cells and **(B)** corresponding bar graph representing UCB induced inhibition of cell cycle progression. RN1, RN2 and RN3 in flowcytometric histograms stand for Region 1 (hypodiploid/apoptotic cells), Region 2 (cells in G0/G1 phases of cell cycle) and Region 3 (Cells in S/G2/M phases of cell cycle) respectively. The light gray bars represent percentage of cells containing less than 2n DNA (sub-G1/apoptotic cells), gray bars show cells containing 2n DNA (in G1 phase) and the dark gray bars indicate the cells containing more than 2n DNA (in S+G2/M phase). The data is the representative of two such independent experiments having similar results. Each bar represents mean \pm S.E.M. from three replicates. * $p < 0.05$, as compared to vehicle group and # $p < 0.05$, as compared to LPS control group.

3.3.3 UCB induced immunotoxic effects in various immune cells:

To address the issue of differential sensitivity if any of the immune cells present in the spleen, we isolated CD4+T cells, CD19+B cells and macrophages from spleen and tested the sensitivity of these purified cells to UCB. Results showed that UCB induced similar immunotoxicity in all the cell population studied (Fig. 3.5). Considering these results, further experiments were performed using unfractionated splenic lymphocytes as the source of immune cells, because the whole population mimics the *in vivo* situation more closely compared to the use of enriched cell population. Further to establish the clinical relevance of this data, immunotoxicity of UCB was studied in human PBMNCs and it was also found to be equally susceptible to UCB induced cell death (Fig. 3.5).

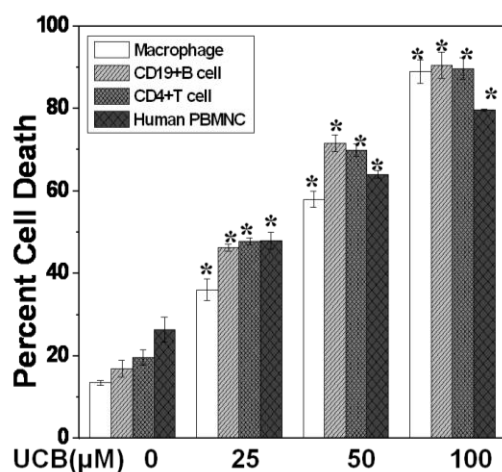


Fig. 3.5 : UCB induced immunotoxic effects in various immune cells: Purified mouse splenic CD4+T cells or CD19+B cells or macrophages, or human PBMNCs (1×10^6 each) were treated with UCB (25-100 μM) and cultured for 24h at 37°C and cell death was estimated by PI staining. The data is the representative of two such independent experiments having similar results. Each bar represents mean ± S.E.M. from three replicates. *p<0.05, as compared to vehicle group.

Further, to see the effects of UCB on immune cells from the mice with different genetic background, experiments were designed to see the immunotoxicity of UCB in splenic lymphocytes from Swiss mice. The Swiss inbred mice bear an intra H-2 recombination between H-2^d and H-2^b haplotypes. The MHC haplotype antigens of Swiss mice are (H-2K^d, H-2D^b, I-A^b, I-E^b)¹⁹⁸. H-2 genotypes of BALB/c mice are H-2K^d, H-2D^d, I-A^d, and I-E^d. The results of PI staining of UCB treated lymphocytes isolated from

Balb/c or Swiss mice showed that UCB induced similar immunotoxicity in both the mice (Fig. 3.6).

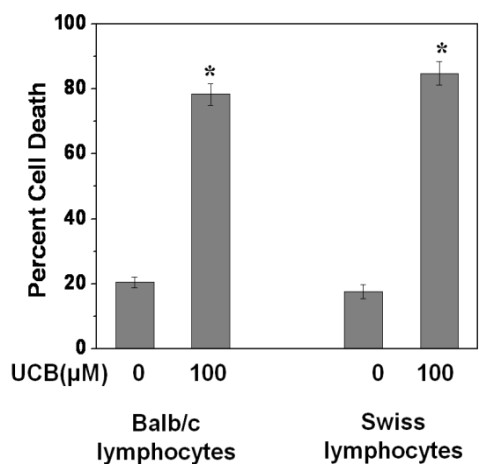


Fig. 3.6: UCB induced immunotoxicity in lymphocytes from both mice: The cell death in lymphocytes isolated from Balb/c or Swiss mice treated with UCB (100μM, 24h) were estimated by PI staining. The data is the representative of two such independent experiments having similar results *p<0.05, as compared to vehicle group.

To rule out the possibility of variation in chemical integrity of UCB, similar experiments was performed using UCB sourced from other manufacturer (Calbiochem) and result showed that UCB from both the commercial preparation (Sigma, Calbiochem) was toxic to splenic lymphocytes (Fig. 3.7). Considering above, further experiments were performed using UCB obtained from Sigma Chemicals Co (USA) in Balb/c splenic lymphocytes.

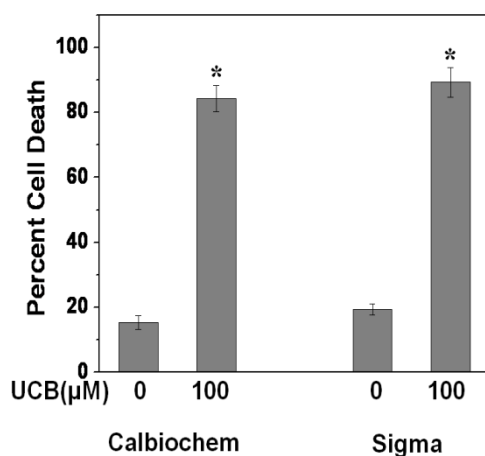


Fig. 3.7: UCB from different sources induced immunotoxicity in lymphocytes: The cell death in lymphocytes treated with UCB (100μM, 24h) from Calbiochem or Sigma was estimated by PI staining. The data is the representative of two such independent experiments having similar results. *p<0.05, as compared to vehicle group.

3.3.4 Purified UCB induced immunotoxic effects in lymphocytes and human PBMNCs:

To eliminate the possible effect of surface-active contaminants usually present in the commercial UCB preparations¹⁹¹, similar experiments were conducted using purified UCB. Commercial UCB was purified by the method of McDonagh and Assisi (1972)¹⁹¹. Purified UCB was found to be equally toxic to splenocytes and human PBMNCs (Fig. 3.8). The results indicated that toxicity was due to UCB and not due to the possible contaminants present in the preparation.

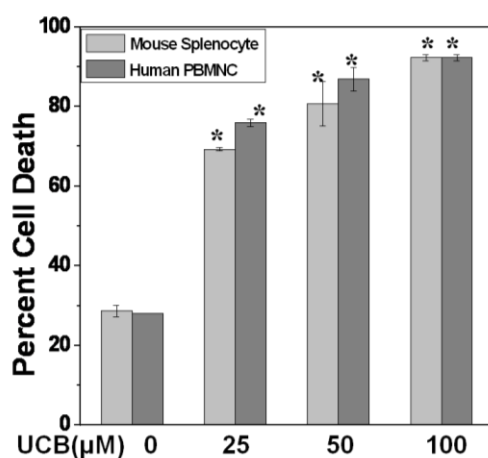
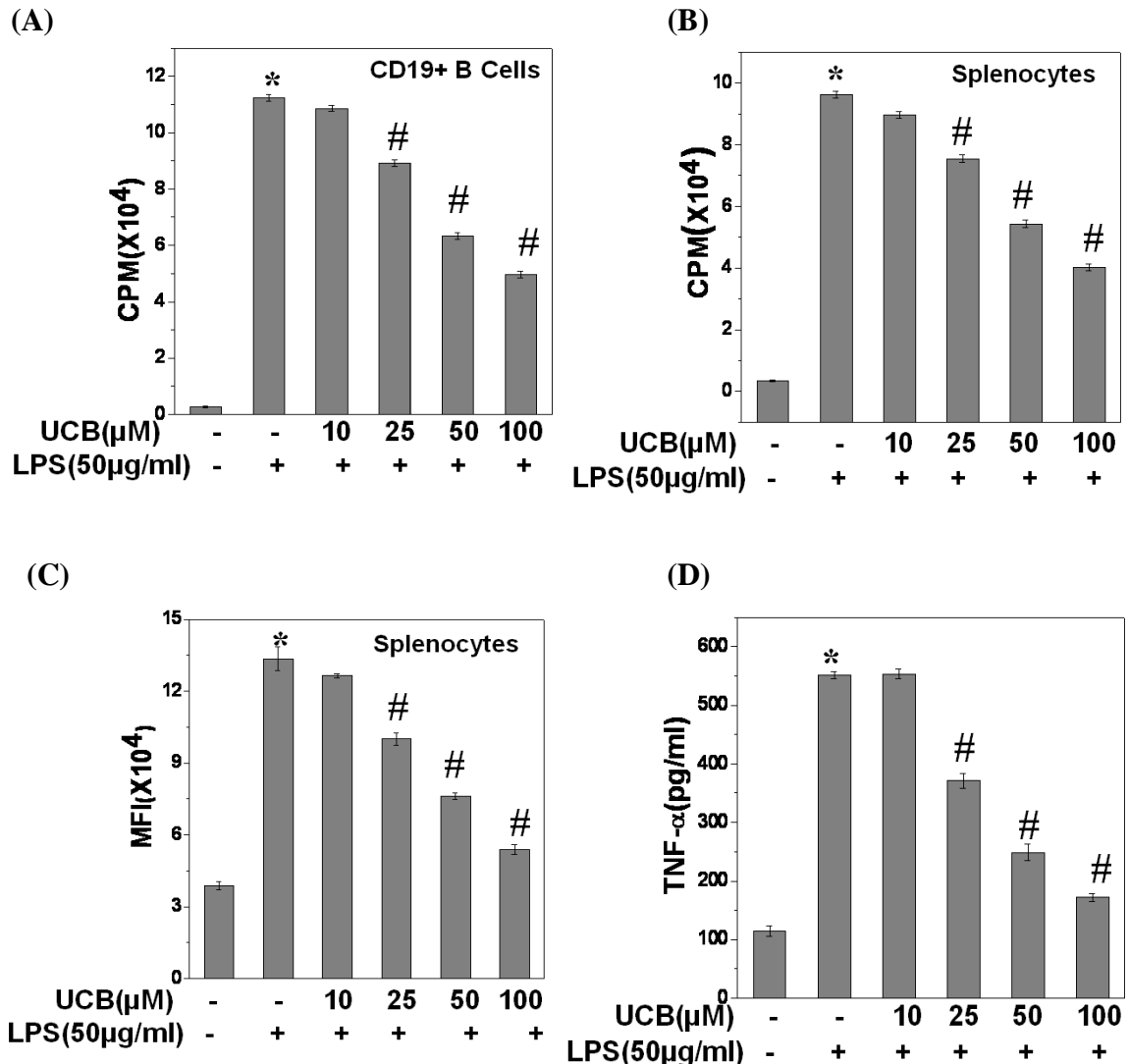


Fig. 3.8: Purified UCB induced immunotoxic effects in lymphocytes and human PBMNCs: Lymphocytes or human PBMNCs (1×10^6 each) were treated with purified UCB (25-100 μM) and cultured for 24h at 37°C and cell death was estimated by PI staining. The data is the representative of two such independent experiments having similar results. Each bar represents mean \pm S.E.M. from three replicates. * $p < 0.05$, as compared to vehicle group.

3.3.5 UCB exhibited immunosuppressive effects in lymphocytes and macrophages:

Since, UCB induced immunotoxic effects in LPS activated B cells, experiments were carried out to see the effects of UCB on the proliferative responses of CD 19+ B cells in response to LPS stimulation. Results showed that UCB pre-treatment inhibited LPS induced proliferation of B cells in a concentration dependent manner (Fig. 3.8A). Similar experiments were performed in unfractionated splenocytes using ^3H thymidine incorporation and CyQuant-NF cell proliferation assay and it was found that LPS induced proliferation of splenocytes were inhibited by UCB (Fig. 3.8B, C).

Since proliferation of B cells is triggered by activation of cytokine cascades, studies were performed to assess the effects of UCB on cytokine release from macrophages in response to LPS stimulation. UCB inhibited LPS induced cytokine release (IL-1 β , IL-6 and TNF- α) from splenic adherent macrophages in a concentration dependent manner starting from 25 μ M (Fig. 3.8D-F). The results clearly indicated that UCB at clinically relevant concentration of 25 μ M significantly compromised the immune function of B cells and macrophages. Taken together these results demonstrated that the immunosuppressive effects of UCB were mediated by induction of cell death.



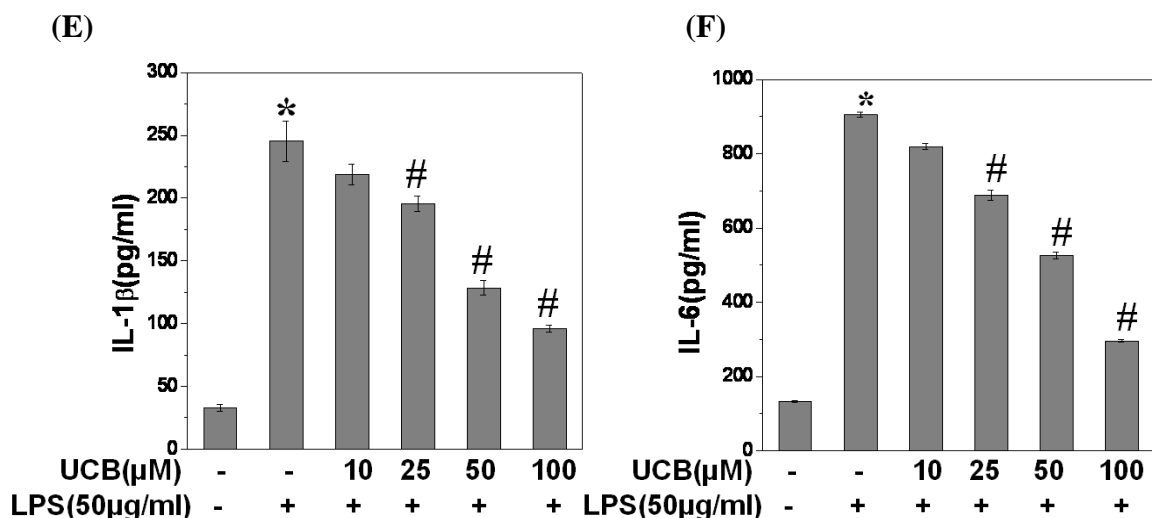
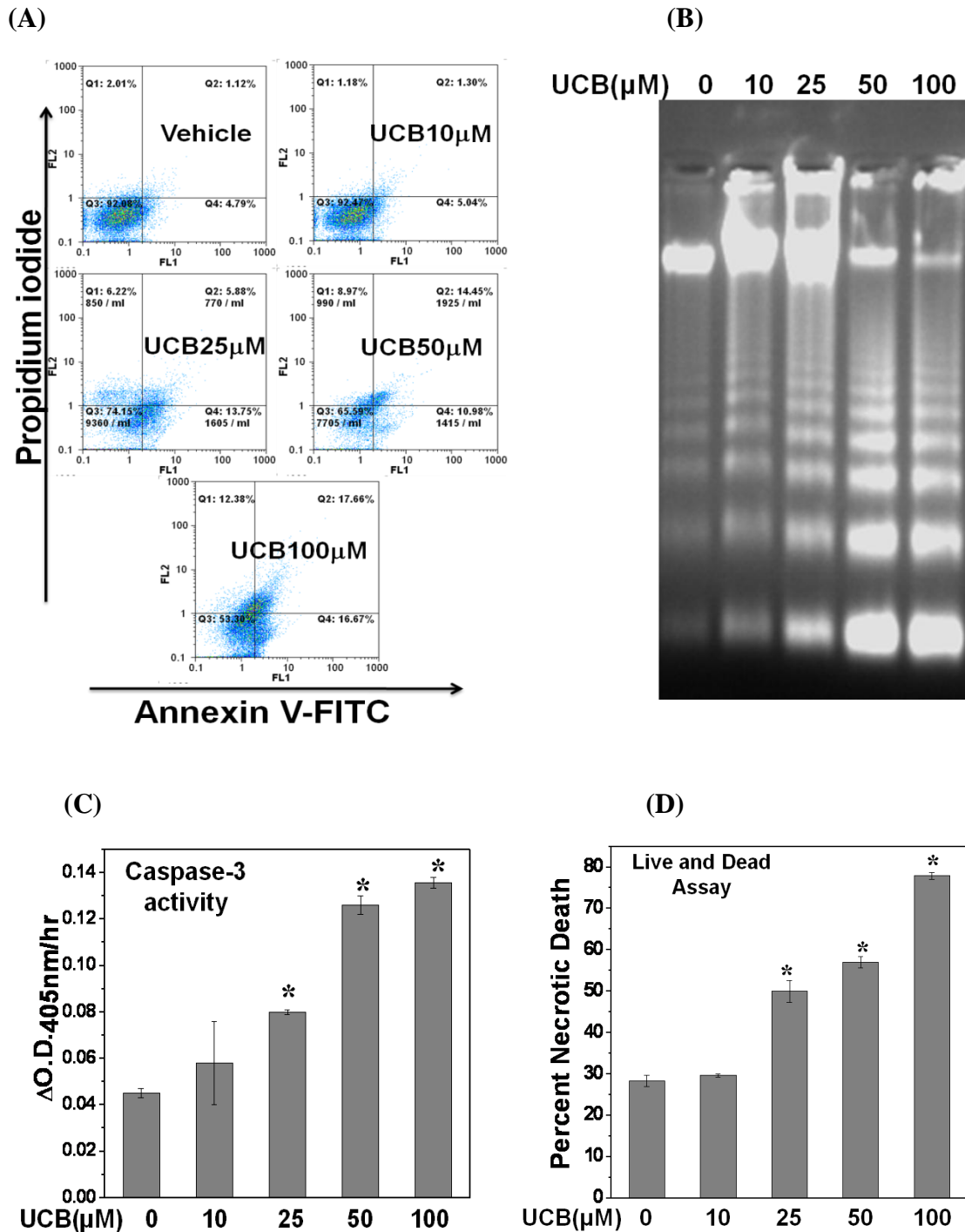


Fig. 3.8: UCB exhibited immunosuppressive effects in lymphocytes and macrophages: (A-C) UCB inhibited LPS induced immune cell proliferation as assessed by (A, B) ^3H thymidine incorporation assay and (C) CyQUANT NF cell proliferation assay. CD19+ B cells (Fig.1A) or splenocytes (Fig.1B, C) (1×10^6 each) were treated with UCB (10-100 μ M, 4h) and stimulated with LPS (50 μ g/ml) for 48h at 37°C and cell proliferation was monitored. (D-F) UCB inhibited LPS induced production of TNF- α , IL1- β and IL-6 from splenic adherent macrophage. Splenocytes (5×10^6) were allowed to adhere in 24-well plate for 4h at 37°C. The adherent macrophages were incubated with UCB (10-100 μ M) for 4h and then stimulated with LPS (50 μ g/ml) for 6h. The levels of TNF- α , IL1- β and IL-6 in the culture supernatants were estimated by ELISA. The data is the representative of three such independent experiments having similar results. Each bar represents mean \pm S.E.M. from three replicates. * $p < 0.05$, as compared to vehicle group and # $p < 0.05$, as compared to LPS group.

3.3.6 UCB exhibited immunotoxic and radiomimetic effects by inducing both apoptotic and necrotic death in splenic lymphocytes:

Since, UCB exhibited immunotoxic and radiomimetic effects in lymphocytes by inducing cell death, annexinV/PI staining in UCB treated lymphocytes was performed to vivisect the mode of UCB induced cell death. The results showed that treatment of lymphocytes with UCB ($\geq 25\mu\text{M}$) induced both apoptosis and necrosis (Fig. 3.9A). UCB induced apoptotic death was confirmed by DNA fragmentation and caspase-3 activation assay (Fig. 3.9B, C). Results of live and dead assay, trypan blue dye exclusion test and methylene blue staining confirmed that UCB at a concentration of $\geq 25\mu\text{M}$ led to a significant increase in necrotic death in lymphocytes (Fig. 3.9D, E). UCB induced

hemolysis in RBCs, further confirmed the ability of UCB to cause plasma membrane damage (Fig. 3.9F). These results clearly demonstrated that UCB treatment induced immunotoxicity and imitated the effects of radiation by inducing both apoptosis and necrosis in lymphocytes.



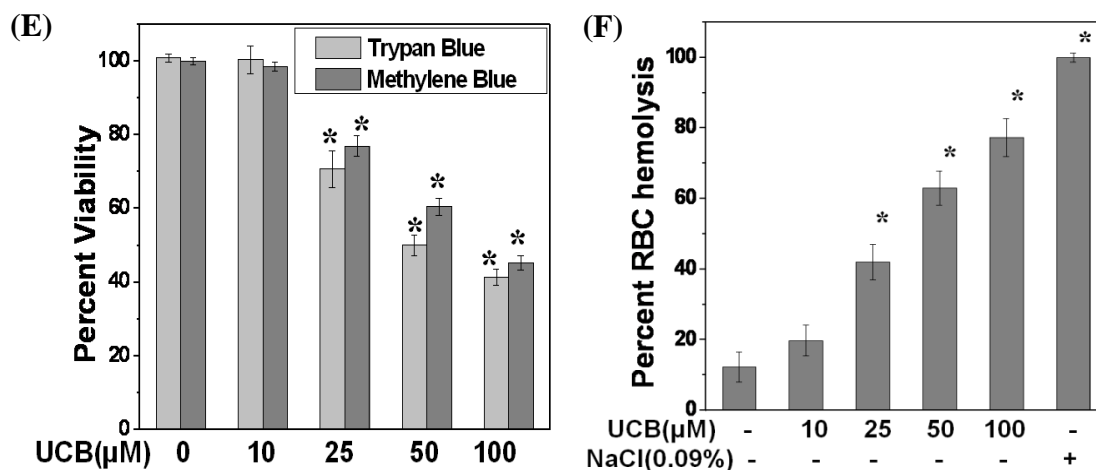
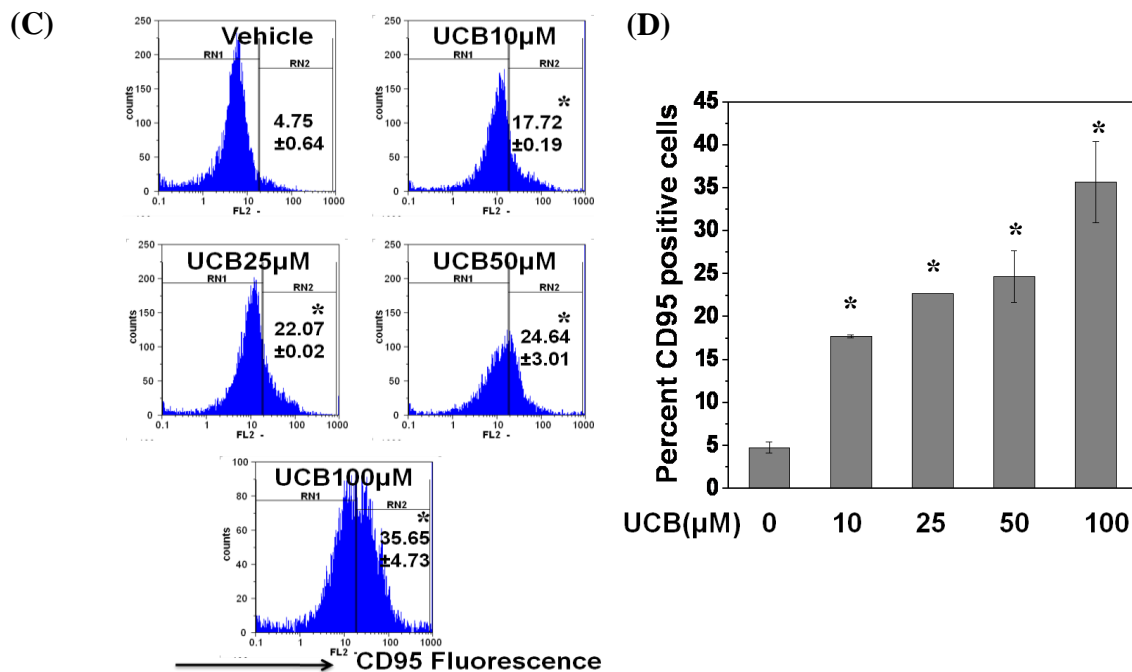
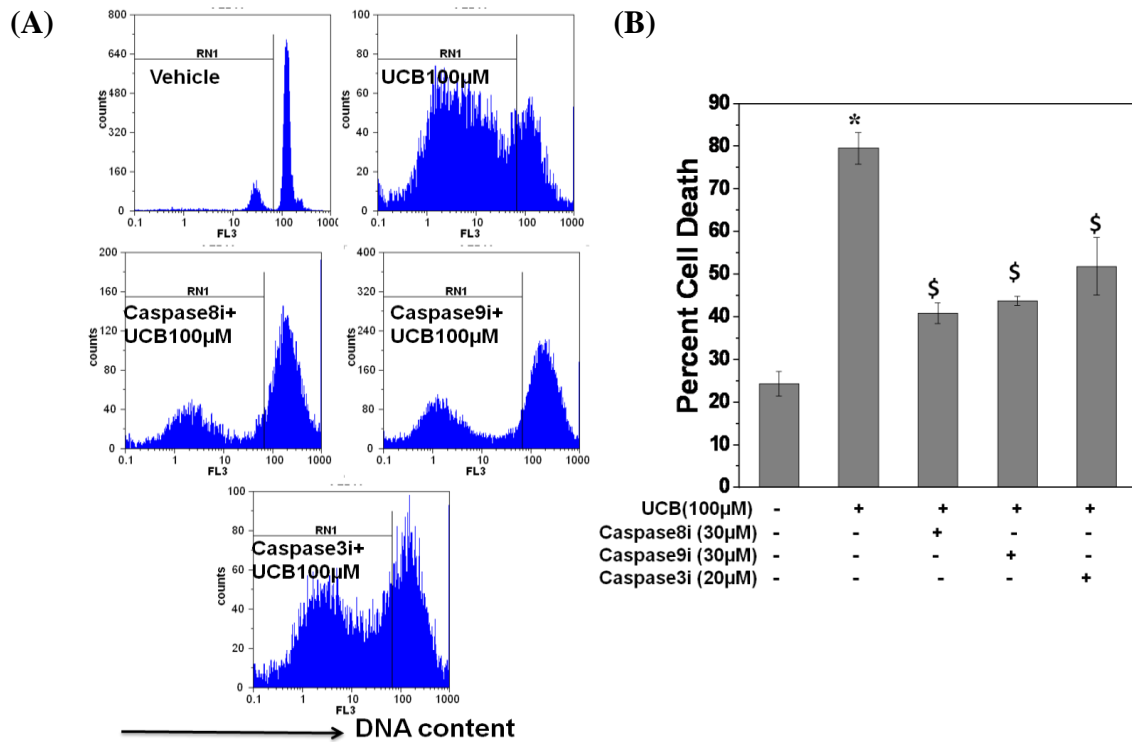


Fig. 3.9: UCB exhibited immunotoxic effects by inducing both necrotic and apoptotic death: Lymphocytes (1×10^6) were treated with UCB (10-100 μM) for 24h at 37°C and cell death was estimated by (A) AnnexinV/PI staining, (B) DNA fragmentation assay and (C) caspase-3 activation (D) Live and dead assay and (E) trypan blue and methylene blue counting. (F) UCB induced membrane damage in erythrocytes assessed by hemolysis of RBCs. 100% hemolysis is represented by hemoglobin release in 0.09% NaCl. The data is the representative of two such independent experiments having similar results. Each bar represents mean \pm S.E.M. * $p < 0.05$, as compared to vehicle group.

3.3.7 UCB induced both extrinsic and intrinsic apoptotic pathways in lymphocytes:

Since caspase-8 and caspase-9 are involved in the extrinsic and intrinsic apoptotic pathways respectively, and caspase-3 is common to both the pathways, the inhibitors of these enzymes were used to find out the mode of apoptotic death. The results showed that these inhibitors attenuated the UCB induced apoptosis in lymphocytes, suggesting the involvement of both the apoptotic pathways in UCB induced cell death (Fig. 3.10A, B). The upregulation of CD95 (Fas) expression and the increase in caspase-8 activity by UCB treatment to lymphocytes in a concentration dependent manner, suggested the contribution of extrinsic apoptotic pathway (Fig. 3.10C-E). The exposure of lymphocytes to UCB, activated Bax, increased cytoplasmic calcium and induced loss of MMP in a concentration dependent manner, indicating the involvement of intrinsic apoptotic pathway as well (Fig. 3.10D-F). Taken together these results suggested that UCB induced

apoptosis in lymphocytes was mediated by activation of both extrinsic and intrinsic the apoptotic pathways and thus mimicked the effects of radiation in activation of apoptotic pathways in lymphocytes.



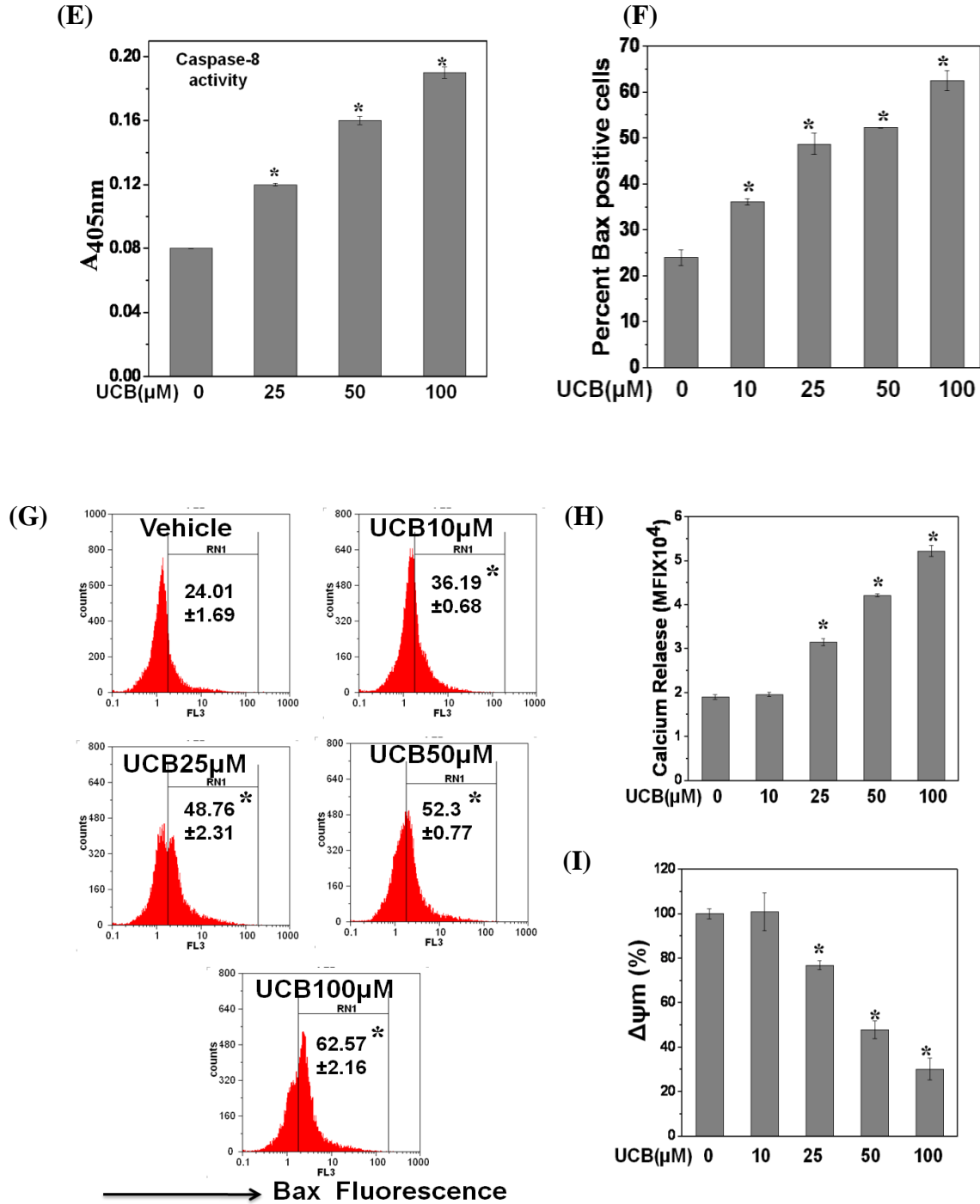


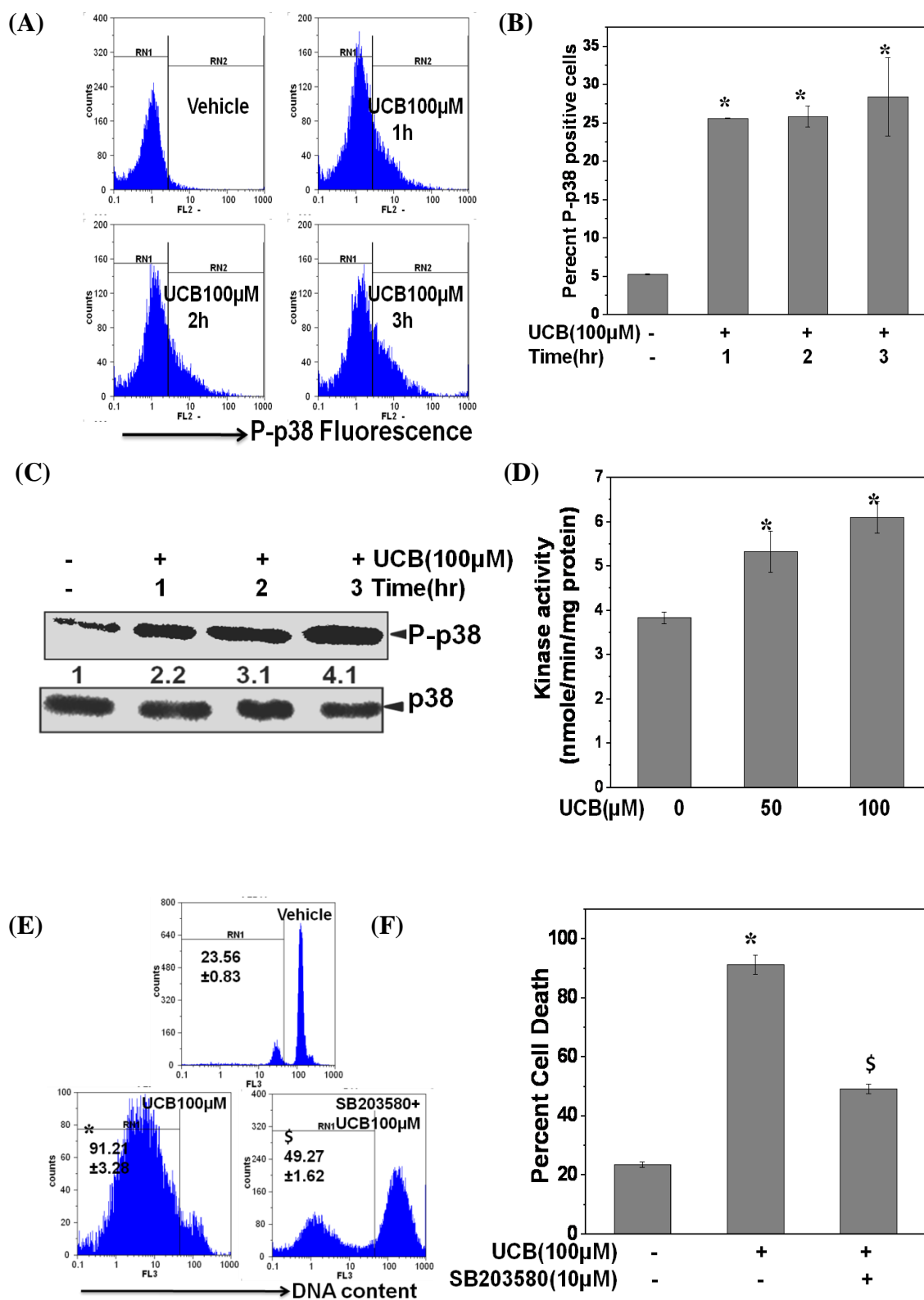
Fig. 3.10: UCB induced both extrinsic and intrinsic apoptotic pathways in lymphocytes: (A, B) Lymphocytes (1×10^6) were pretreated with inhibitors of caspase-8 (Caspase8i, 30μM), caspase-9 (Caspase9i, 30μM) caspase-3 (Caspase3i, 20μM) for 1h, followed by treatment with UCB (100μM) for 24h at 37°C and cell death was estimated by PI staining. (C, D) UCB increased the frequency of CD95 positive cells. Lymphocytes (1×10^6) were incubated with UCB (10-100μM) for 24h at 37°C and stained with PE labeled anti-CD95 antibody. Percent CD95 positive cells were estimated by flowcytometry. (E) UCB induced caspase-8 activation. Lymphocytes (1×10^6) were incubated with UCB (25-100μM) for 24h at 37°C and processed for caspase-8 colorimetric activity assay. (F, G) UCB increased the frequency of Bax positive cells. Lymphocytes (1×10^6) were incubated with UCB (10-100 μM) for 24h at 37°C and stained

with PE labeled anti-Bax antibody. Percent Bax positive cells were estimated by flowcytometry. **(H, I)** UCB treatment to lymphocytes induced release of calcium and MMP loss. Lymphocytes (1×10^6) were incubated with UCB (10-100 μ M) for 6h and cells were stained with **(H)** Fura 2-AM (2 μ M) for measurement of calcium or **(I)** JC-1 (5 μ M) for measurement of MMP. The data is the representative of two such independent experiments having similar results. Each bar represents mean \pm S.E.M. from three replicates. * $p < 0.05$, as compared to vehicle group. $^{\$}p < 0.05$, as compared to UCB group.

3.3.8 UCB induces apoptosis in lymphocytes by activating p38MAPK:

To identify the sequence of events contributing to UCB induced apoptosis, we examined the ability of UCB to activate p38MAPK in lymphocytes. For these studies, we selected the highest concentration of UCB (100 μ M), because it is still physiologically relevant and causes maximum immunosuppression and cell death and further this concentration corresponds to UCB/BSA molar ratio found in moderate to severe hyperbilirubinemia.

The results showed that UCB caused the phosphorylation of p38MAPK in a time dependent manner as demonstrated by flowcytometry and western blot analysis (Fig. 3.11 A-C). Since p38MAPK is activated by specific kinase via phosphorylation of threonine-180 and tyrosine-182, we also measured protein tyrosine kinase activity and it was found that UCB increased the kinase activity at both the concentrations tested (Fig. 3.11D). SB203580 (an inhibitor of p38MAPK) reduced UCB induced cell death confirming the involvement of p38MAPK activation in UCB induced cell death (Fig. 3.11E, F). The p38MAPK activation is known to induce apoptosis by activating both extrinsic and intrinsic pathways^{199,200}. The expression of markers of both extrinsic (CD95) and intrinsic (Bax) apoptotic pathways was significantly attenuated by p38MAPK inhibitor (Fig. 3.11 G-J). Taken together, these findings suggest a central role of p38MAPK in initiating UCB induced apoptosis.



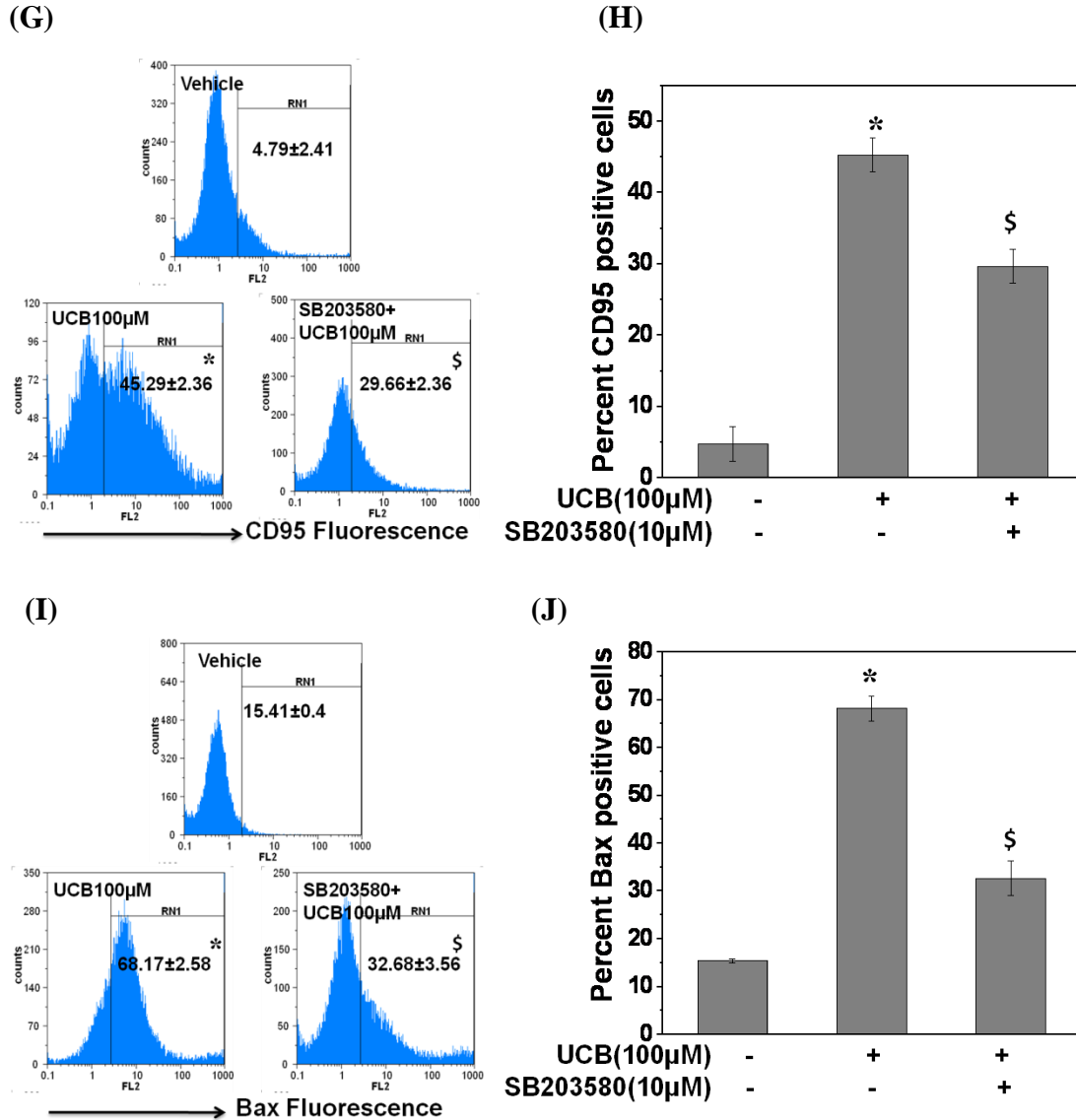


Fig. 3.11: UCB induced apoptosis in lymphocytes by activating p38MAPK: (A-C) Time-dependent phosphorylation of p38MAPK by UCB. (A-B) Lymphocytes (3×10^6) were treated with UCB (100µM) for indicated time and stained with PE labeled anti-phospho-p38 antibody and percent phospho-p38 positive cells were estimated using flowcytometry. (C) For Western blot analysis, equal amount of protein from cytoplasmic extracts of UCB (100µM) treated lymphocytes were fractionated on 10% SDS-PAGE, electro-transferred onto nitrocellulose membrane and probed with anti-phospho-p38MAPK antibody. Expression of p38MAPK in each group was used as loading control. (D) UCB treatment increased protein tyrosine kinase activity. Lymphocytes (10×10^6) were treated with UCB (50,100µM) for 3h and whole cell lysate was prepared and processed for tyrosine kinase colorimetric activity assay. (E-J) SB203580 (p38MAPK inhibitor) inhibited UCB induced death parameters. Lymphocytes (1×10^6) were pretreated with SB203580(10µM) for 1h followed by UCB(100µM) treatment for 24h at 37°C and processed for (E, F) PI staining or (G, H) PE labeled anti-CD95 antibody or (I, J) PE labeled anti-Bax antibody staining. The data is the representative of two such independent experiments having similar results. Each bar represents mean±S.E.M. from three replicates. *p<0.05, as compared to vehicle group. §p<0.05, as compared to UCB group.

3.3.9 UCB depleted cellular GSH levels in lymphocytes:

Earlier reports by Brito et al^{78,79} showed that UCB induced cytotoxicity in neuronal cells are mediated by induction of oxidative stress via GSH depletion. The role of oxidative stress in UCB induced immunotoxicity was thus investigated, by measuring the intracellular GSH and ROS levels in UCB treated lymphocytes. UCB decreased the basal levels of GSH in a concentration dependent manner in treated lymphocytes (Fig. 3.12A). A time kinetics study demonstrated that UCB completely suppressed the basal GSH level in splenic lymphocytes within 0.5h of incubation (Fig. 3.12B). These results were further confirmed by using confocal microscopy (Fig. 3.12C) and flowcytometry (Fig. 3.12D).

Cellular GSH exists predominantly in a reduced form, but small amounts of the oxidized disulfide form are also present, the GSH/GSSG ratio is, therefore, taken as a more appropriate indicator of the cellular redox status. Thus, we specifically measured the effect of UCB on GSH/GSSG ratio and GSt (total glutathione) levels. UCB decreased the cellular GSH/GSSG ratio and GSt levels (Fig. 3.12E, F).

To further investigate the role of UCB on the redox status of lymphocytes, we also measured its effect on intracellular ROS levels by using a redox sensitive dye H₂DCF-DA. Surprisingly, UCB treatment to splenic lymphocytes for 1h decreased the basal ROS levels in a concentration dependent manner (Fig. 3.13A). The result was confirmed by using another oxidation sensitive probe DHE (Fig. 3.13B) and mitochondrial specific redox sensitive dye DHR123 (Fig. 3.13C).

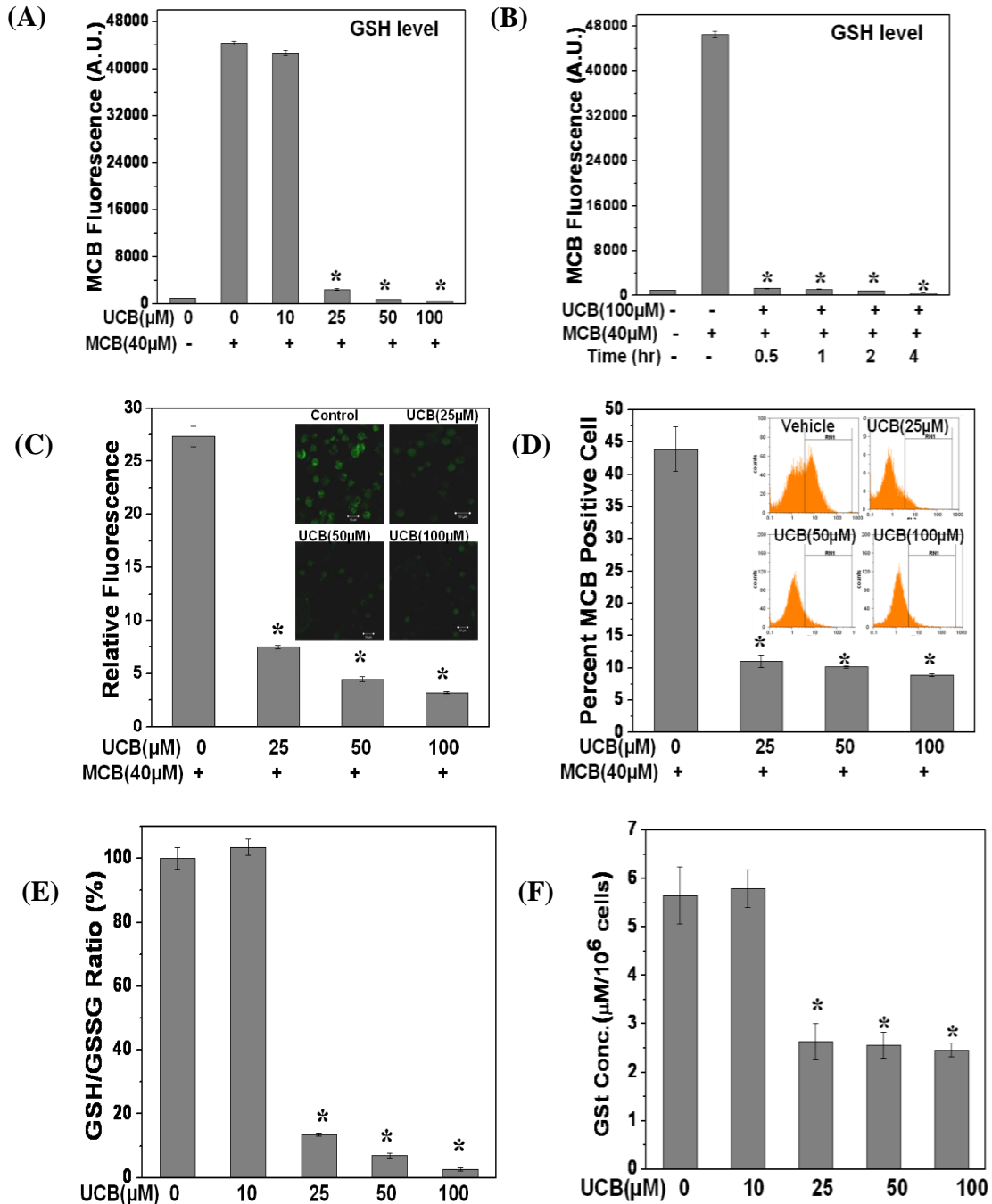


Fig. 3.12: UCB depleted cellular GSH levels in lymphocytes: (A-D) Lymphocytes (1×10^6) were incubated with UCB (10-100μM) for 1h or indicated time at 37°C and stained with MCB (40μM) for 0.5h. Fluorescence emission was recorded using (A, B) spectrofluorimeter at 490nm following excitation at 394nm (C) confocal microscopy and fluorescence intensity of images were quantified using LSM Image Browser software and representative images of the MCB-GSH conjugate in different treatment are shown in the inset. (D) flowcytometry and percent MCB positive cell were quantified by using Flowmax® software. (E, F) Lymphocytes (1×10^6) were incubated with UCB (10-100μM) for 1h at 37°C and cellular levels of GSH, GSSG and GSt were evaluated by an enzymatic recycling assay. The data is the representative of three such independent experiments having similar results. Each bar shows mean \pm SEM from hexareplicate. * $p < 0.05$, as compared to vehicle group.

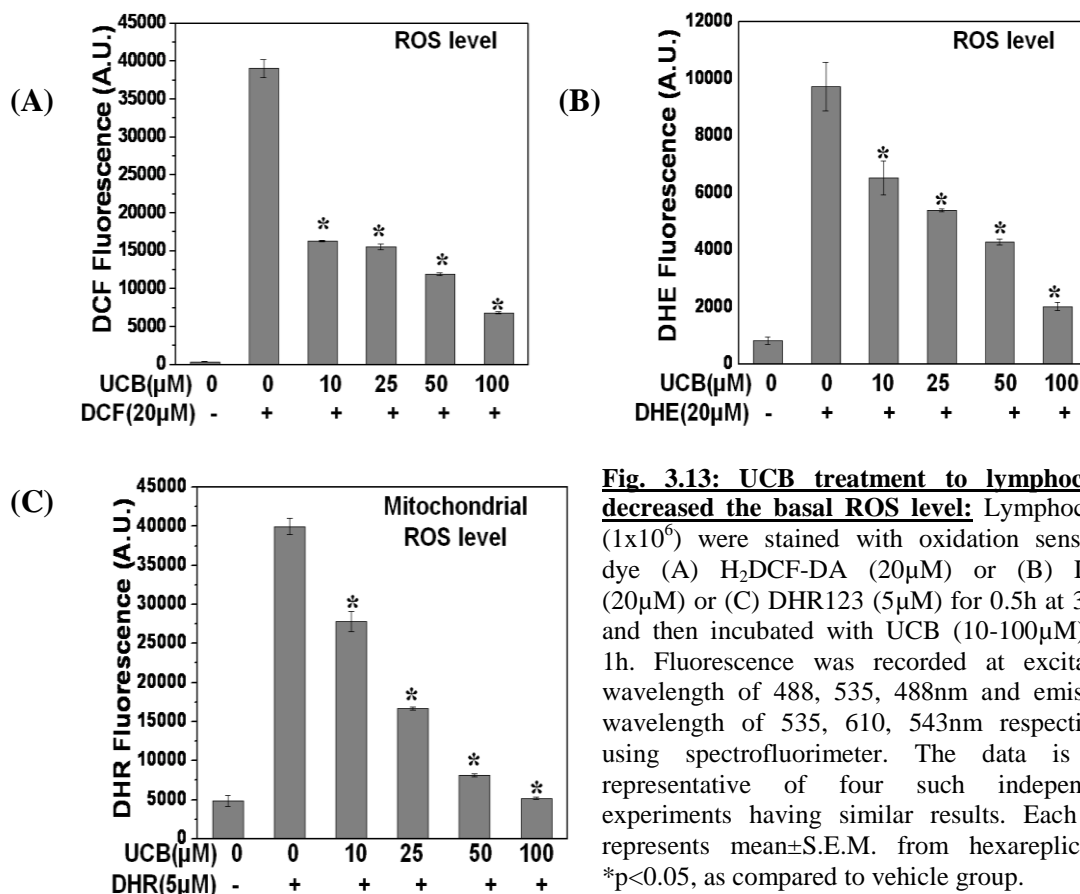


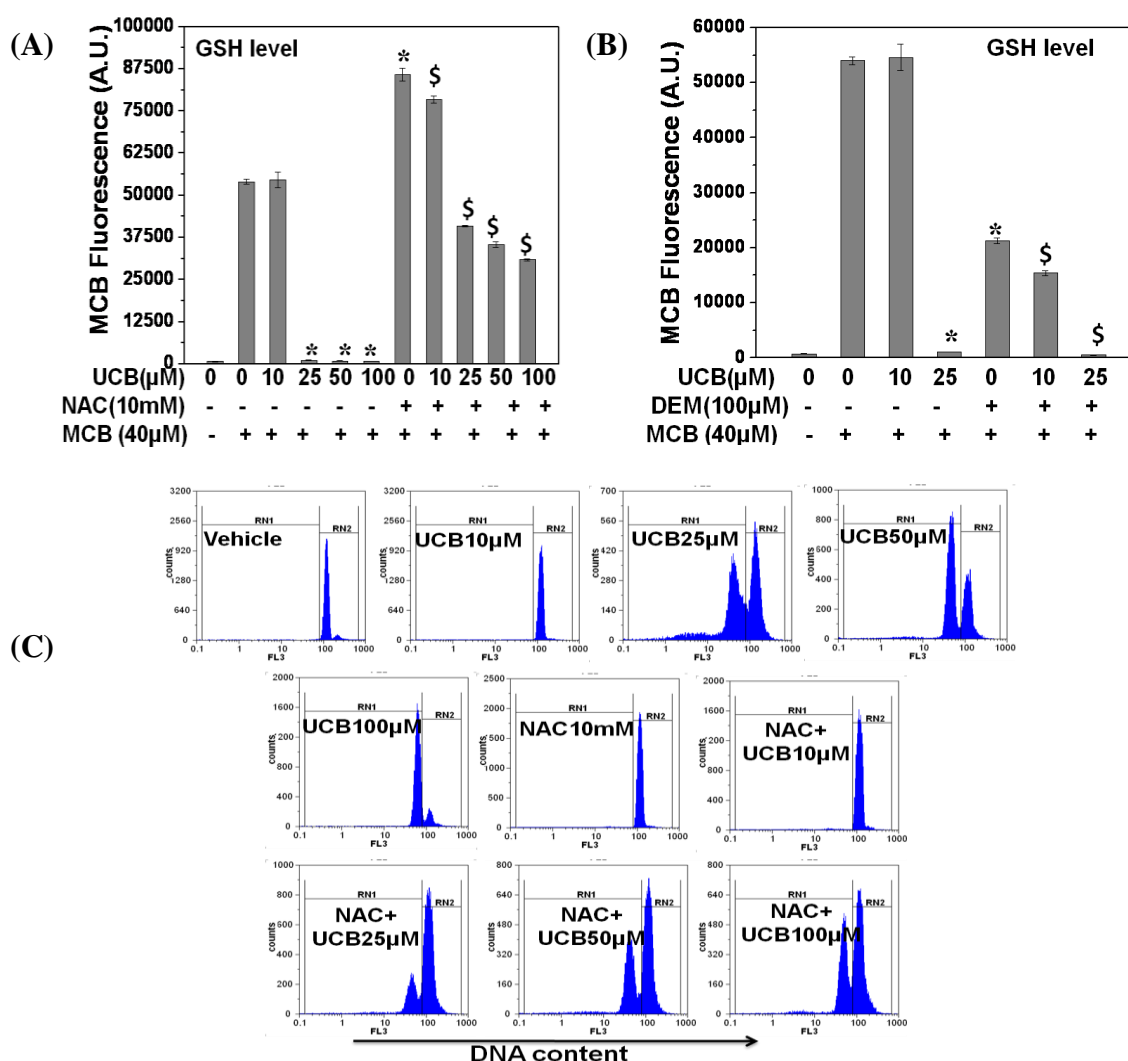
Fig. 3.13: UCB treatment to lymphocytes decreased the basal ROS level: Lymphocytes (1×10^6) were stained with oxidation sensitive dye (A) H_2DCF -DA (20μM) or (B) DHE (20μM) or (C) DHR123 (5μM) for 0.5h at 37°C and then incubated with UCB (10-100μM) for 1h. Fluorescence was recorded at excitation wavelength of 488, 535, 488nm and emission wavelength of 535, 610, 543nm respectively using spectrofluorimeter. The data is the representative of four such independent experiments having similar results. Each bar represents mean±S.E.M. from hexareplicates. *p<0.05, as compared to vehicle group.

3.3.10 Glutathione appeared a key molecule in the prevention of UCB induced cell death:

Since UCB depleted cellular GSH levels in lymphocytes, we hypothesized that glutathione might be a critical molecule in UCB induced immunotoxicity. To test our hypothesis, we evaluated the modulation of UCB induced cell death in conditions of both augmentation and depletion of GSH. For this purpose, lymphocytes were preincubated with NAC, a precursor of glutathione^{78,79,201}, or treated with DEM, a known GSH depletor¹⁰⁰, then were exposed to UCB and measured for the cellular GSH levels and cell death using PI staining and esterase activity.

Results showed that NAC treatment to lymphocytes for 1h increased GSH levels

and it also partially restored the GSH levels decreased by UCB treatment (Fig. 3.14A). Furthermore, DEM induced GSH depletion, was further augmented by UCB treatment to splenocytes (Fig. 3.14B). UCB (10 μ M) did not deplete GSH level alone; however in the presence of DEM it significantly decreased the cellular GSH levels (Fig. 3.14B). Lymphocytes were treated with NAC or DEM and/or UCB as mentioned above and were assessed for cell death at the end of 24h. As shown in Fig. 3.14C, D pretreatment of lymphocytes with non-toxic dose of NAC (10mM), reduced UCB induced cell death. UCB (10 μ M) is not toxic to lymphocytes, whereas in presence of non-toxic dose of DEM (100 μ M), it led to a significant increase in cell death (Fig. 3.14E).



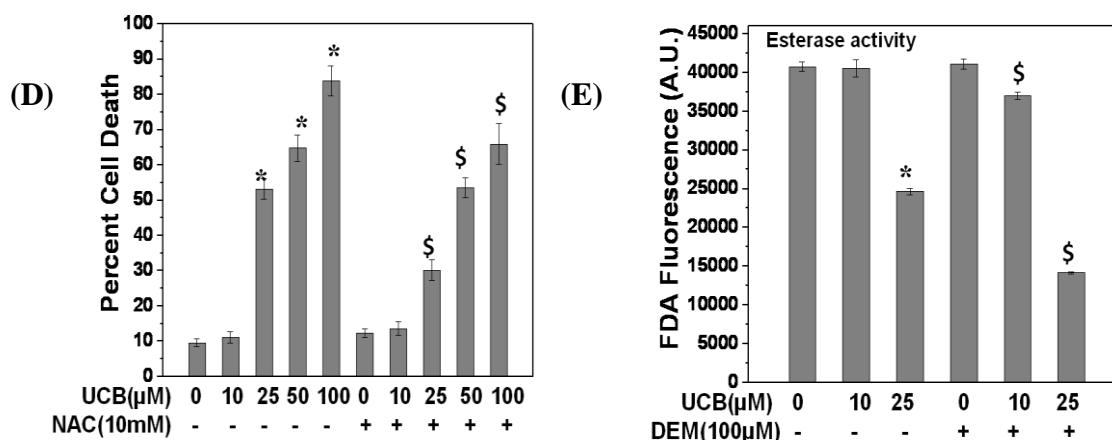


Fig. 3.14: Glutathione appeared a key molecule in the prevention of UCB induced cell death: (A, B) NAC increased and DEM decreased the GSH content in lymphocytes treated with UCB. Lymphocytes (1×10^6) were treated with (A) NAC or (B) DEM for 1h at 37 °C and further incubated with UCB (10-100μM) for 1h, stained with MCB (40μM) for 0.5h at 37°C and fluorescence emission was recorded at 490nm emission following excitation at 394nm. (C, D) NAC inhibited UCB induced cell death. Lymphocytes (1×10^6) were treated with NAC (10mM) for 1h prior to incubation of UCB (10-100μM) for 24h at 37°C and cell death was estimated by PI staining. (E) DEM augmented UCB induced cell death. Lymphocytes (1×10^6) were treated with DEM (100μM) for 1h prior to incubation of UCB (10-25μM) for 24h at 37°C and cell viability was estimated by esterase activity. The data is the representative of three such independent experiments having similar results. Each data point represents mean \pm S.E.M. from three replicates. * $p < 0.05$, as compared to vehicle group. \$ $p < 0.05$, as compared to corresponding UCB group.

3.3.11 UCB induced p38MAPK activation was mediated by depletion of GSH levels:

Several studies have reported the crucial role of intracellular glutathione in regulating the activation of p38MAPK^{197,202-204}. A report by Limon-Pacecho et al. had shown that GSH depletion activates p38MAPK in different organs of mice¹⁹⁷. Accordingly, we examined whether UCB induced p38MAPK activation in lymphocytes was associated with GSH depletion. It was observed that NAC treatment to lymphocytes 1h prior to UCB, significantly inhibited the phosphorylation of p38MAPK (Fig. 3.15 A, B). Taken together, these results suggest that glutathione depletion by UCB is a critical factor in mediating UCB induced p38MAPK activation and immunotoxicity.

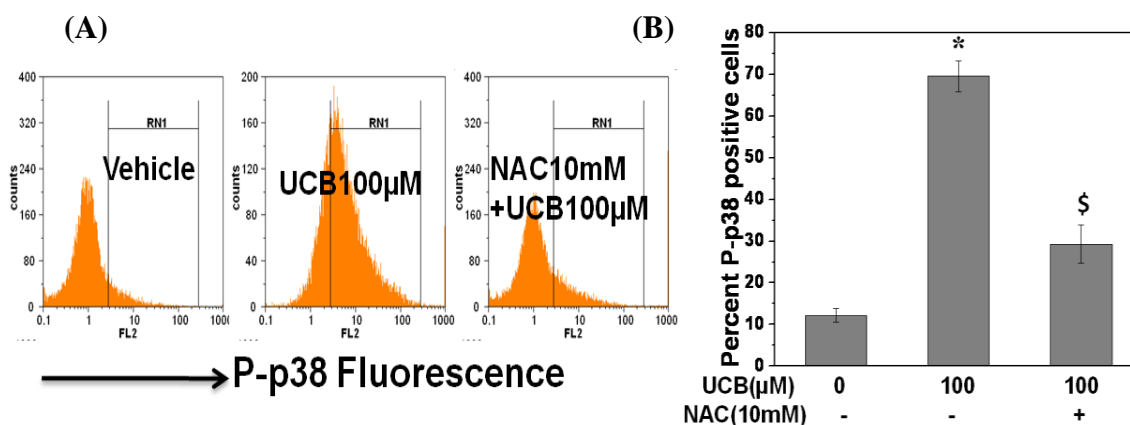


Fig. 3.15: UCB induced p38MAPK activation is mediated by depletion of GSH levels: NAC inhibited UCB induced activation of p38MAPK. Lymphocytes (3×10^6) were treated with NAC (10mM) for 1h prior to incubation of UCB (100µM, 3h) and stained with PE labeled anti-phospho-p38MAPK antibody. Percent P-p38 positive cells were estimated by flowcytometry. The data is the representative of three such independent experiments having similar results. Each data point represents mean \pm S.E.M. from three replicates. * $p < 0.05$, as compared to vehicle group. \$ $p < 0.05$, as compared to UCB group.

3.3.12 UCB caused immunotoxicity and immunosuppression *in vivo*:

In order to evaluate the relevance of *in vitro* methods for immunotoxicity assessment, we examined the consequence of UCB administration to the immune system *in vivo*. Since 30-100mg/kbw of UCB has been used in animal models^{169,170}, a dose of 25-50mg/kbw, to examine the immunotoxicity of UCB *in vivo*, was selected. UCB (≥ 25 mg/kbw) administration to mice, lead to a significant reduction in spleen weight, spleen index, and viability of spleen and bone marrow cells (Fig. 3.16A-D). Additionally, a significant decrease in erythrocyte counts, leucocyte counts, hemoglobin levels, percentage lymphocytes, monocytes and packed cell volume was also recorded in UCB administered mice as compared to vehicle administered mice (Fig. 3.16E).

Since, UCB exposure to mice lead to a significant reduction in the viable cell numbers in spleen, the ability of residual splenic lymphocytes to mount a proliferative immune response to T and B cell mitogens was examined. Fig. 3.16F showed that

lymphocytes taken from UCB ($\geq 25\text{mg/kbw}$) injected mice showed significantly depressed proliferative responses to both the mitogens, as compared to that obtained from control mice. Taken together, these results suggested that UCB administration altered the host immune response *in vivo*.

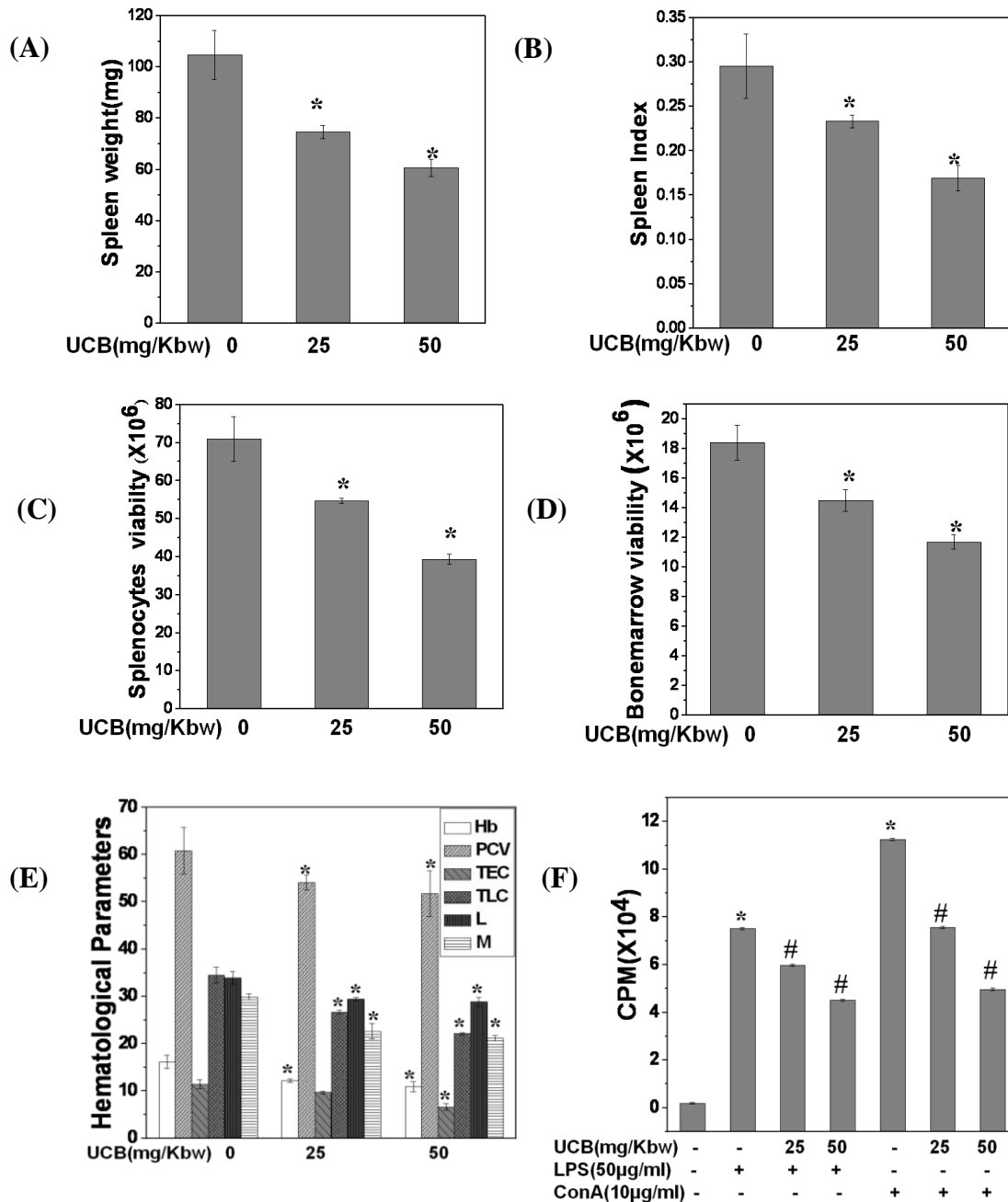


Fig. 3.16: UCB caused immunotoxicity and immunosuppression *in vivo*: Mice were injected with UCB (25-50mg/kbw) i.p. and sacrificed 24h UCB administration, spleen and femur bone marrow were removed and cell viability was enumerated by trypan blue dye exclusion methods. UCB (25, 50mg/Kbw) administration to mice decreased (A) spleen weight (B) spleen index (C) splenocyte viability (D) bone

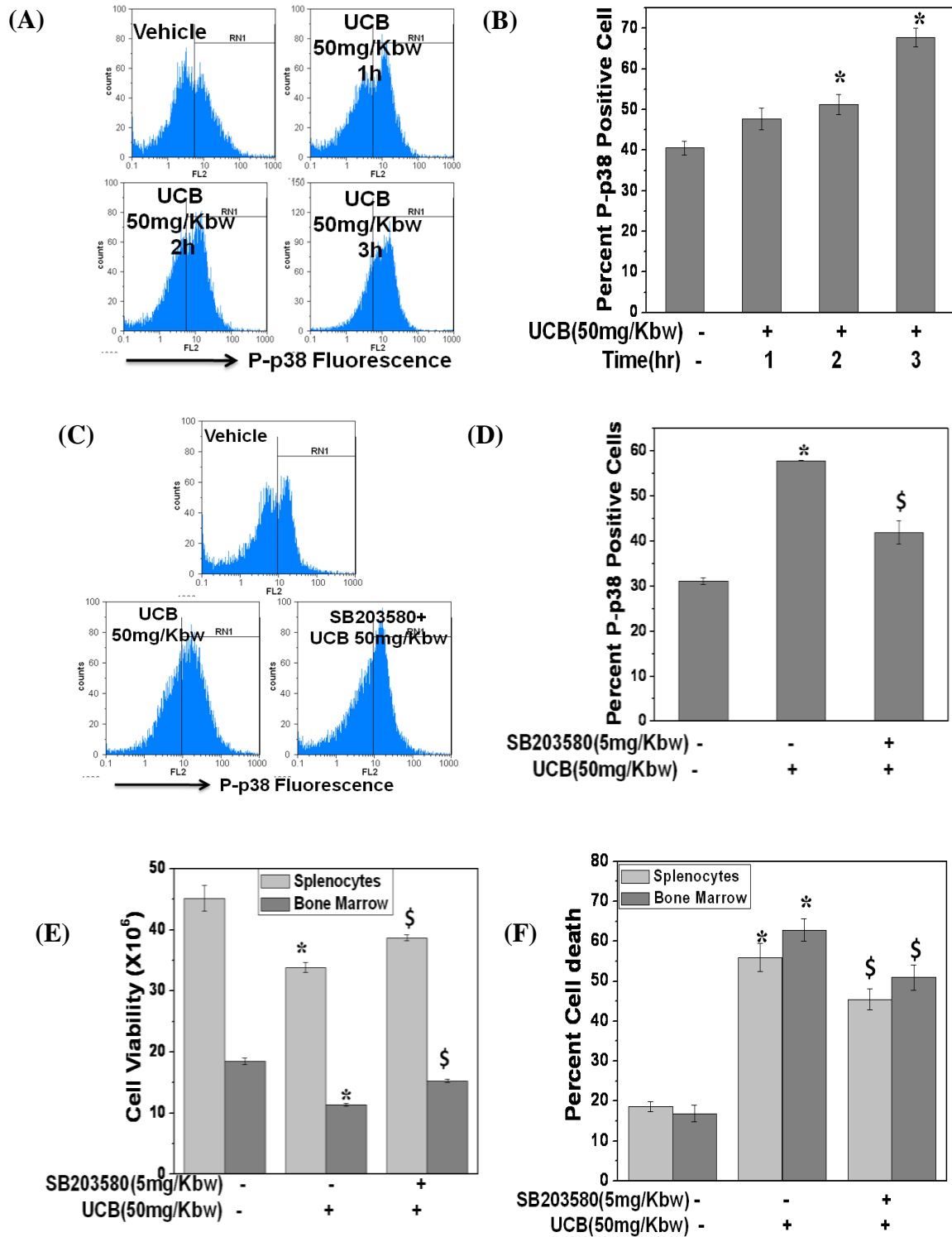
marrow viability and (E) Hematological parameters. Hb represents Hemoglobin (g/dl), PCV (packed cell volume in %), TEC (Total erythrocyte count in $\times 10^6/\text{mm}^3$), TLC (Total Leukocyte count in $\times 10^3/\text{mm}^3$), L (Lymphocyte %), M (Monocyte %). (F) UCB administration inhibited immune response of splenic lymphocytes to T cell and B cell mitogen. Lymphocytes ($1 \times 10^6/\text{ml}$) isolated from vehicle or UCB (25-50mg/Kbw, 24h) administered mice were simulated with ConA ($10 \mu\text{g}/\text{ml}$) or LPS ($50 \mu\text{g}/\text{ml}$) for 72 or 48h respectively and were pulsed with ^3H thymidine ($0.5 \mu\text{Ci}$) and the cells were harvested after 16h and incorporated radioactivity was measured by liquid scintillation counter. The data is derived from one of the four such independent experiments having similar results. In each experiment, data from five mice per group were assessed and each bar represents mean \pm S.E.M. * $p < 0.05$, as compared to vehicle group and # $p < 0.05$, as compared to either LPS or ConA control group.

3.3.13 UCB induced immunotoxicity was mediated by activation of p38MAPK in

vivo:

To elucidate the molecular mechanism of UCB mediated immunotoxicity *in vivo*, we examined p38MAPK activation in lymphocytes at various time after UCB administration to mice. A significant increase in phospho-p38MAPK was observed at 2h of UCB administration (Fig. 3.17A, B). To confirm p38MAPK activation in UCB mediated immunotoxicity, we analyzed whether selective inhibitor could inhibit the response observed during UCB challenge. Earlier reports using *in vivo* studies had demonstrated that i.p. administration of SB203580 (p38MAPK inhibitor) at 5mg/kbw 2h prior to chemical challenges inhibited p38MAPK activation^{197,205}. Using this strategy in our experimental model, we injected inhibitor (SB203580) 2h prior to UCB administration and result showed that SB203580 inhibited UCB induced p38MAPK activation (Fig. 3.17C, D) and significantly inhibited UCB induced decrease in the viability of splenocytes and bone marrow (Fig. 3.17E). UCB induced death in splenic lymphocytes and bone marrow were also inhibited by prior administration of p38MAPK inhibitor as measured by PI staining (Fig. 3.17F, G). Similarly, SB203580 administration attenuated the UCB induced decrease in proliferative response of splenocytes (Fig. 3.17 H, I). On the whole, these results suggested that *in vivo* response observed during UCB

administration was mediated by the activation of p38MAPK and could be attenuated by using a specific inhibitor.



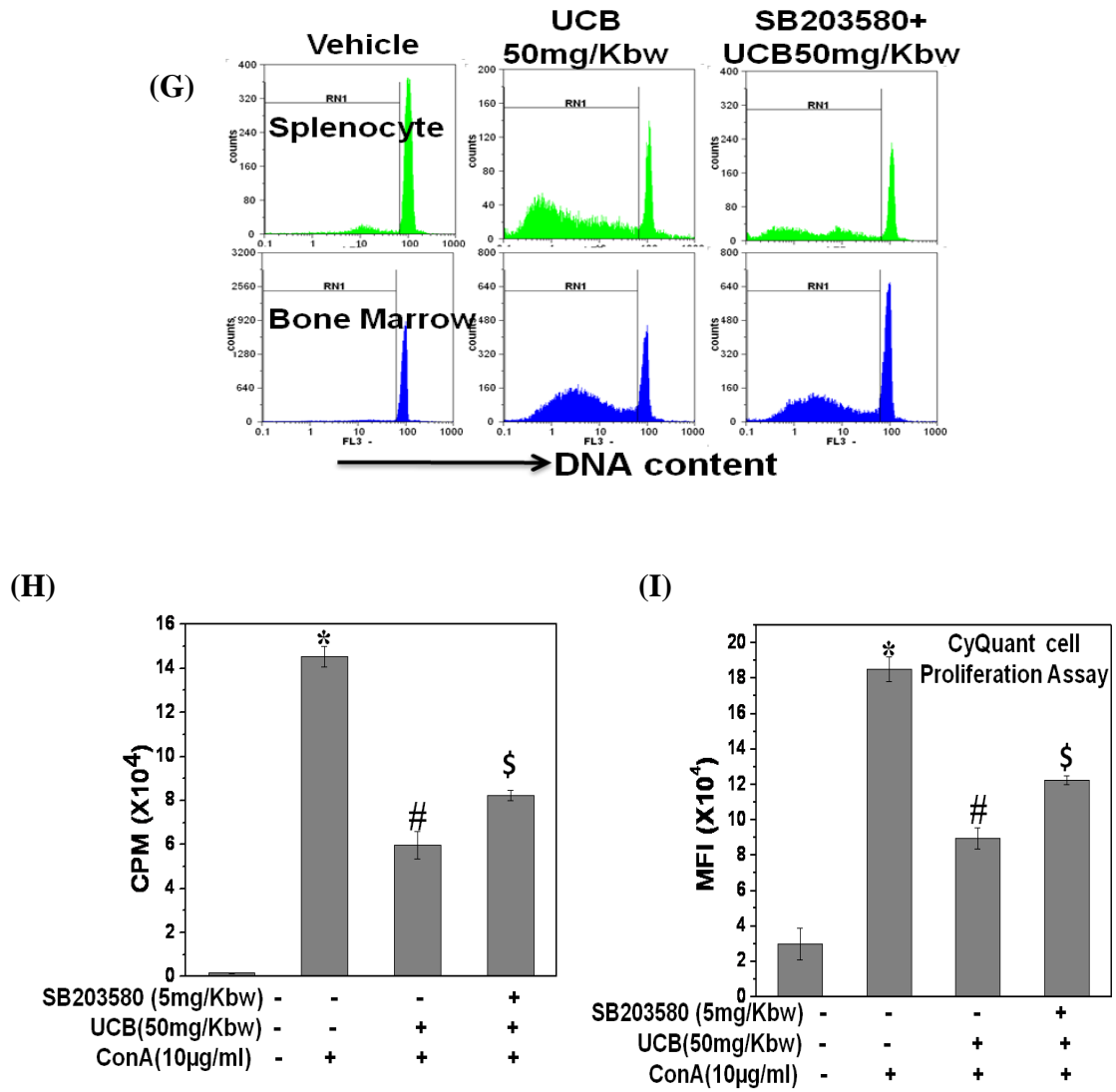
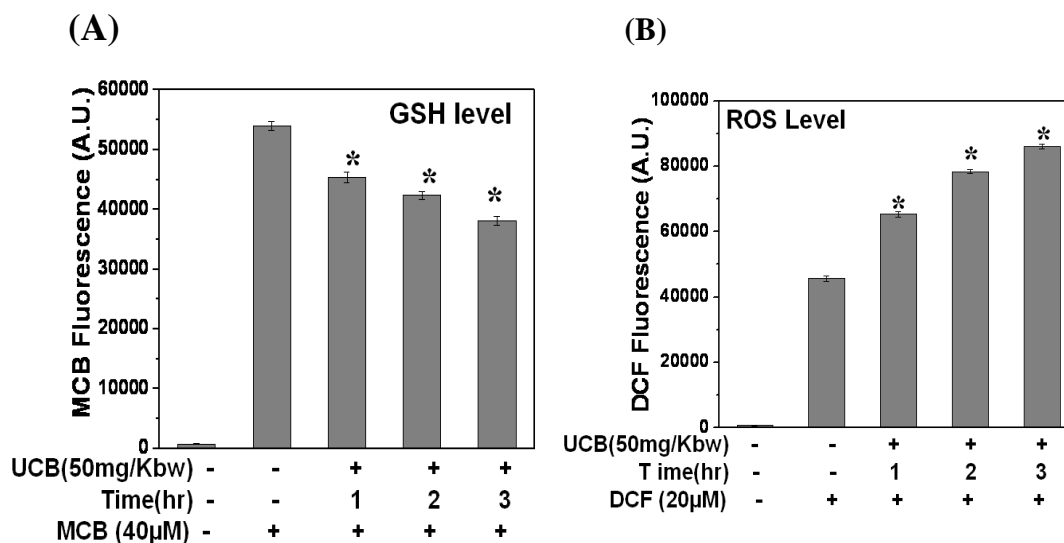


Fig. 3.17: UCB induced immunotoxicity was mediated by activation of p38MAPK *in vivo*: (A-B) UCB administration to mice activated p38MAPK in splenic lymphocytes in a time dependent manner. Lymphocytes (3×10^6), isolated at indicated time from vehicle or UCB (50mg/kbw) administered mice were stained with PE labeled anti-phospho-p38MAPK antibody and frequency of labeled cells were estimated using flowcytometer. (C-D) SB203580 administration inhibited UCB induced p38MAPK activation *in vivo*. SB203580 (5mg/Kbw) was injected into mice i.p. 2h before UCB treatment and splenic lymphocytes were isolated 3h after UCB administration and stained with PE labeled anti-phospho-p38MAPK antibody and frequency of phospho-p38MAPK positive cells were estimated by flowcytometer. (E-I) SB203580 administration attenuated UCB immunotoxicity *in vivo*. SB203580 (5mg/kbw) was injected into mice i.p. 2h before UCB administration and splenocytes and bone marrow were taken 24h after UCB injection, and (E) viability was enumerated by trypan blue dye exclusion test, (F,G) cell death was estimated by PI staining after culturing cells for 24h at 37°C. (H, I) Lymphocytes functionality in response to ConA was estimated by (H) ³H thymidine incorporation assay or (I) CyQuant cell proliferation assay. The data is derived from one of the three such independent experiments having similar results. In each experiment, data from five mice per group were assessed and each bar represents mean±S.E.M. *p<0.05, as compared to vehicle group and #p<0.05, as compared to as compared to Con A group, \$p<0.05, as compared to corresponding UCB group.

3.3.14 UCB administration caused oxidative stress *in vivo*:

To elucidate the role of oxidative stress *in vivo*, we measured the effect of UCB administration on cellular ROS and GSH levels. Results showed that UCB administration at 50mg/kbw significantly decreased GSH levels and concomitantly increased the ROS levels in a time dependent manner (Fig. 3.18A, B). To further confirm the role of oxidative stress in UCB induced death in splenic lymphocytes, experiments were carried out using NAC, an antioxidant and a GSH precursor^{78,79,201}. NAC administration inhibited UCB induced cellular GSH depletion and also the death in lymphocytes (Fig. 3.18C, D). Taken together these results demonstrated that UCB administration to mice caused oxidative stress by depleting cellular GSH and increasing intracellular ROS levels resulting into induction of cell death in splenic lymphocytes and these responses could be modified by prior administration of NAC.



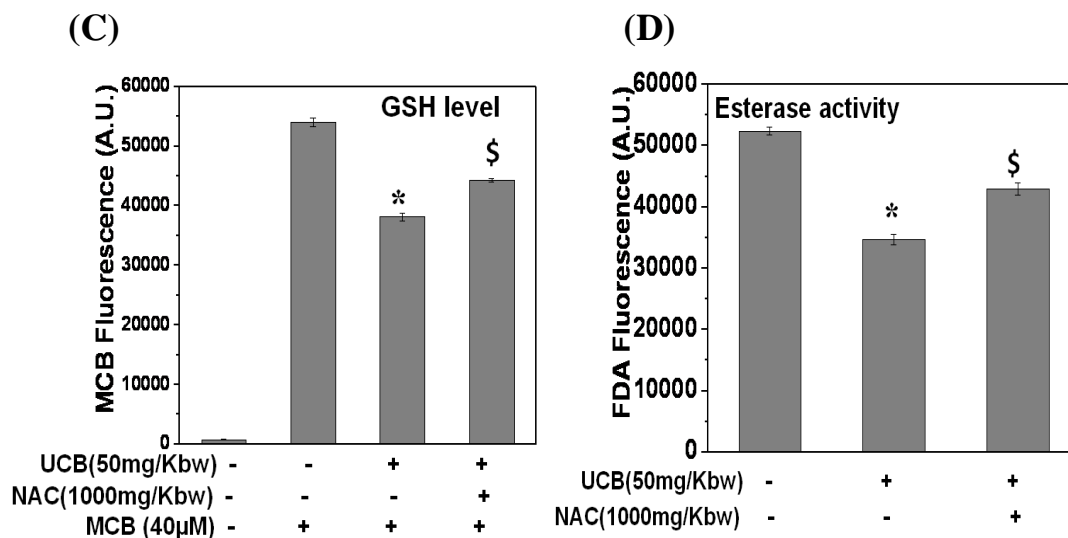


Fig. 3.18: UCB administration caused oxidative stress *in vivo*: Splenic lymphocytes (1×10^6), isolated at indicated time from vehicle or UCB (50mg/Kbw) injected mice were stained with MCB (40µM) or H₂DCF-DA (20µM) for 0.5h at 37°C and fluorescence emission were recorded using spectrofluorimeter for measurement of (A) GSH at 490nm following excitation at 394nm, or (B) ROS at 535nm following excitation at 485nm. (C-D) NAC administration inhibited UCB induced GSH depletion and cell death. NAC (100mg/kbw) was injected into mice i.p. 0.5h before UCB administration. (C) Splenic lymphocytes (1×10^6) were taken 3h after UCB administration and GSH level was estimated by MCB method (D) Splenic lymphocytes (1×10^6) were taken 24h after UCB administration and further cultured for 24h and esterase activity was estimated. The data is derived from one of the three such independent experiments having similar results. In each experiment, data from five mice per group were assessed and each bar represents mean±S.E.M. *p<0.05, as compared to vehicle group and \$p<0.05, as compared to UCB group.

3.4 DISCUSSION

Although UCB is known to induce toxic effects in developing nervous system, very few studies have been conducted in the past, to investigate the toxic effects of UCB on the immune system¹⁷²⁻¹⁷⁷. However, no studies have been directed towards examining the immunotoxic and radiomimetic effects of purified UCB at clinically relevant concentrations and molar ratios of UCB to BSA. We selected murine splenic lymphocytes as a model for screening of immunotoxic potential of UCB. The lymphocyte proliferation to a mitogen and the ability of immune cells to release cytokines after the stimulation are very relevant end points to establish the immunotoxic effects of UCB. The results indicated the ability of UCB to suppress the immune response both *in vitro* and *in vivo* by inducing apoptosis in these cells. The UCB immunotoxicity results closely resemble with the toxic effects of radiation in terms of induction of apoptosis and DNA strand breaks in lymphocytes and thus showing the potential of UCB as radiomimetic agent (Fig. 3.1A, B and Fig. 3.3A, B). Our data on the decreased levels of inflammatory cytokines from macrophages, toxicity of UCB on T cells, B cells and macrophages may explain the molecular mechanisms by which UCB reduces inflammation, iNOS expression, host immune response and prevents the solid-organ graft rejection^{169,171,206}. Our results suggest that the molecular mechanisms by which UCB may induce immunosuppression in the host is not due to cellular unresponsiveness but due to induction of necrosis and apoptosis in mature immune cells. The results suggest that UCB is toxic to cells involved in both adaptive and innate immune system. Splenic macrophages significantly contribute to the degradation of hemoglobin to UCB²⁰⁷. These results suggest that increased hemoglobin metabolism in the spleen could contribute to

the host immunosuppression. It is interesting to note that the cell which produces UCB is sensitive to pathological concentrations of UCB. Studies need to be carried out to see whether this feedback inhibition is operative in the host and whether it has any biological significance.

The immunotoxic effects of UCB were studied by multiple viability assays. However, MTT assay for viability testing is not an appropriate method under our experimental conditions, because, besides cells, other constituents of the media like, antioxidants, vitamins, albumin proteins with free SH groups are also able to reduce tetrazolium salt, leading to the underestimation of cytotoxicity of the compounds to be tested²⁰⁸. UCB has also been known to get deposited on the cell surface leading to underestimation of cytotoxicity of the tested compounds¹⁶⁸. Our studies demonstrate that both commercial and purified UCB kill resting lymphocytes at clinically relevant concentrations, and UCB to BSA molar ratios. This experimental data is very relevant to the health consequences of increased serum UCB. It is notable that our studies demonstrate significant cytotoxic effects of 25 μ M of UCB in immune cells, at molar ratios of UCB/BSA that are well below unity. All concentrations used by us correspond to UCB/BSA molar ratio found in moderate to severe hyperbilirubinemia. The estimated free concentrations of UCB used in the present study are below its maximum aqueous solubility and hence it is unlikely that the inhibitory effects of UCB observed in our studies were mediated by precipitation of UCB aggregates¹⁸. UCB binding variables for babies of different birth weight had indicated a mean B_T to albumin molar ratio of 0.26 to 0.61¹⁸⁰. To be clinically relevant, UCB levels should be selected such that B_f levels are

below its solubility i.e. 70nmol/L. At the molar ratios of UCB and albumin selected in our studies, the B_f levels are much lower than 70 nmol/L based on the earlier work¹⁶⁴.

Previous studies have demonstrated that UCB induced cell death in neural cells and astrocytes are mediated by both apoptosis and necrosis^{190,209}. Elevated concentrations of UCB are able to activate select components of stress pathway in Hepa 1c1c7 cells, which may contribute to UCB mediated apoptosis. The ability of UCB to bind to the plasma membrane, disrupt mitochondrial function and induce apoptosis in various cell lines has been demonstrated^{16-18,61,80,161,166-168}. The studies using rat brain neurons, have shown that UCB induced apoptosis is mediated via the mitochondrial pathway, as evidenced by the significant disruption in the MMP and the release of intracellular Ca²⁺ from calcium stores and specific activation of caspase-3¹⁶⁶. Thus UCB can initiate changes in mitochondria and contribute to the apoptotic cascade. The decreased MMP, increased cytoplasmic calcium and Bax activation observed in our experiments suggest that apoptosis of immune cells is also contributed by the perturbation of the mitochondrial membrane (Fig. 3.10F-I). In addition to activation of these intrinsic apoptotic events, UCB was found to upregulate the expression of CD95 (Fas) and increase caspase-8 activity (Fig. 3.10C-E), suggesting that UCB induces apoptosis in splenic lymphocytes via activation of both apoptotic pathways and therefore mimics the radiation effects because radiation exposure to lymphocytes is known to induce apoptosis via induction of both the pathways.

The role of p38MAPK in UCB induced neuronal death has been reported earlier^{13,80}. Activation of p38MAPK has been implicated in both extrinsic and intrinsic apoptotic response of the cell, as it is involved in FasL expression, Bax translocation to

the mitochondria, cytochrome-c release and caspase-3 activation^{199,200}. The early activation of p38MAPK in UCB treated lymphocytes suggests its contribution in the cell death by both the apoptotic pathways (Fig. 3.11A-C). The ability of p38MAPK inhibitor to attenuate the apoptotic markers and apoptosis induced by UCB further confirmed the role of p38MAPK activation in UCB induced cell death (Fig. 3.11E-J). Ours is the first report demonstrating the involvement of p38MAPK signaling cascade, in the immunotoxicity of UCB.

The p38MAPK is a stress activated protein kinase (SAPK) that transduces environmental signals to the nucleus in response to various cellular stresses. Furthermore, various inflammatory mediators that regulate redox status of cell activate p38MAPK in various cell types²¹⁰. Changes in intracellular redox status are crucial events that trigger activation of p38MAPK signaling pathways. GSH is an important protective antioxidant against oxidative stress. Dagmar Wilhelm et al (1997) have shown that induction of p38MAPK was almost completely blocked by pretreatment of the cells with reducing agents, such as GSH and NAC, and depletion of the intracellular pool of GSH resulted in superinduction of p38MAPK activity²¹¹. UCB induced GSH depletion in lymphocytes at an early time point may be contributing to the activation of p38MAPK (Fig. 3.13A-F). Furthermore, pretreatment of cells with NAC, a known GSH precursor^{78,79,201}, abolished the UCB induced activation of p38MAPK (Fig. 3.15A, B) and reduced the cell death (Fig. 3.14C, D), which suggests that, p38MAPK activation occurs via GSH depletion. Reports from earlier investigators showed that depletion of intracellular GSH activates p38MAPK signal transduction pathways through several mechanisms which include: (i) MAPK modulation by GSSG, (ii) oxidation of negative regulators of the MAPK kinase

kinase apoptosis signal-regulated kinase 1(ASK-1) (iii) reversible ROS oxidation of cysteines in ERK-directed phosphatases and iv) direct interaction with GSH or glutathionylation¹⁹⁷.

The levels of cellular glutathione (GSH+GSSG) are considered as markers of oxidative stress and GSH/GSSG ratio is taken as an indicator of cellular redox status. GSH constitutes the major intracellular redox buffer in the cells and has been implicated in the modulation of various signal transduction pathways²¹². UCB has been shown to decrease cellular GSH levels and contribute to the altered redox state, leading to apoptosis in neuronal cells^{78,79}. These results are in agreement with our results which demonstrate reduced GSH levels in UCB treated splenocytes (Fig. 3.12A-F). Our results indicate the absence of ROS production when lymphocytes were treated with UCB *in vitro*. On the contrary, UCB possessed significant antioxidant activity in the immune cells, when treated *in vitro* (Fig. 3.13A-C). These results are in agreement with the earlier studies showing antioxidant effects of UCB^{76,83,86,156-159}. Serum bilirubin levels, in premature neonates, comparable to the concentrations used in our studies, significantly correlated with total antioxidant status²¹³. UCB behaves like a metabolic “double edged sword” counteracting oxidative stress-mediated injury at low concentrations but becoming cytotoxic above a certain threshold¹³. UCB differentially affects the redox status of neuronal and astroglial cells⁷⁹. The final outcome of its cellular effects- toxicity or protection, pro or antioxidant will depend on: 1) UCB concentration, extent of binding to plasma albumin and time of incubation; 2) target cell/tissue involved; 3) cellular redox state; and 4) developmental stages of cells¹³. Recent studies suggest a necessary and critical role of GSH depletion in the execution of apoptosis in lymphoid cells,

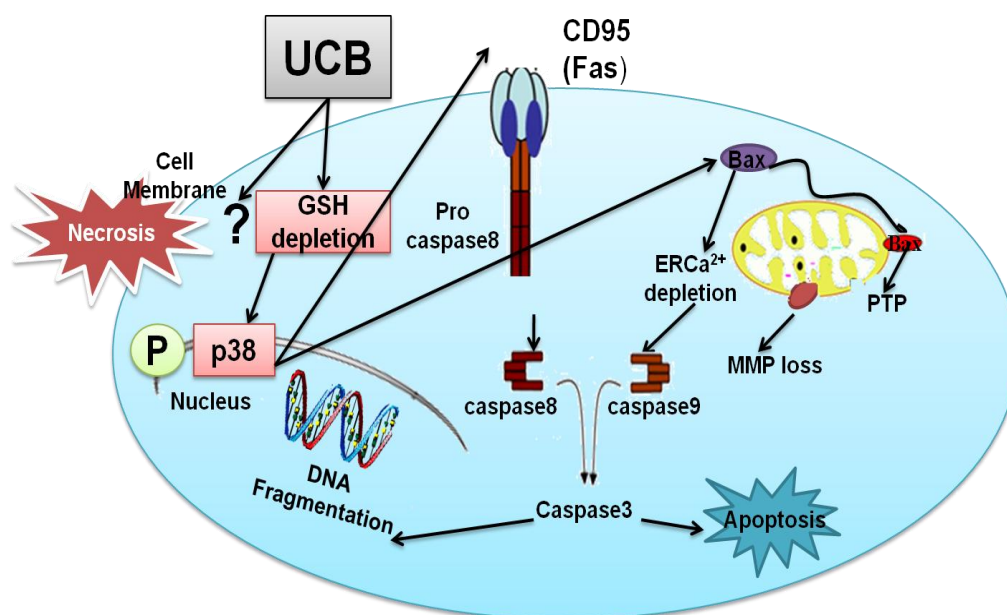
independent of ROS formation²¹⁴. Other studies have also shown that apoptosis seems to be actively regulated by GSH content and not by excessive ROS generation^{212,215}. Additionally, apoptosis has been suggested to occur under anaerobic conditions in the absence of ROS formation²¹⁶. We also observed the attenuation of UCB induced apoptosis by pretreatment of cells with NAC, a known GSH precursor (Fig. 3.14C-E). Protective effects of thiol compounds on apoptosis in the absence of excessive ROS formation have also been reported by others²¹⁵. These findings support the idea of a direct role of GSH in the regulation of the apoptotic machinery independent from ROS generation. These results imply a central role for GSH in the regulation of apoptosis rather than simply acting as an antioxidant/scavenger against ROS. Thus, it is time to look beyond GSH as a simple antioxidant and define its precise role in signaling and execution of programmed cell death.

UCB administration *in vivo* led to a significant depletion of cellular GSH levels and increased ROS levels, indicating the contribution of oxidative stress in UCB induced immunotoxicity (Fig. 3.18A, B). The difference in the *in vitro* and *in vivo* data regarding ROS formation seems to be due to the route of administration and metabolism of UCB inside the host. Our data in immune cells is very similar to the UCB toxicity of neuronal cells, astroglial cells and hepatoma cells, which had shown that alteration of the redox status are likely early events responsible for UCB induced cytotoxicity. UCB (50mg/kbw) administration to mice causes activation of p38MAPK in lymphocytes at an early time point and this activation was significantly reduced by a prior injection of mice with p38MAPK inhibitor (SB203580) or GSH precursor (NAC), which suggest that p38MAPK activation in lymphocytes of UCB injected mice occurs via depletion of

cellular GSH (Fig. 3.17A-D). Our results are in agreement with earlier findings of Limon-Pacecho et al which have shown the activation of p38MAPK in different organs of mice is associated with GSH depletion¹⁹⁷.

Our immunotoxicity data of UCB imitates with the radiation toxicity, as exposure of radiation to lymphocytes have been shown earlier to induce apoptotic death via induction of oxidative stress¹⁰⁰. UCB resembles ionizing radiation in several aspects i.e. induction of DNA strand breaks, depletion of total RNA content and cellular GSH levels, induction of necrosis and apoptosis by activation of both extrinsic and intrinsic pathways in exposed lymphocytes. However UCB differs from ionizing radiation in producing no ROS levels in lymphocytes *in vitro*. Since the list of criteria fulfilled by radiomimetic chemicals as compiled by Elson (1955), refer to the effects of chemicals upon cells *in vivo*, our *in vivo* immunotoxicity data of UCB strengthen the potential of UCB as radiomimetic chemical^{187,188}. The comparison of effects of UCB administration with the known effects of whole body radiation exposure to mice, have shown similarities in terms of induction of erythropenia, lymphopenia, leucopenia, splenic atrophy, bone marrow aplasia, decreased hemoglobin level, increased oxidative stress, depressed immune response upon mitogenic stimulation and increased cell death. If these had been the only parameters examined for a chemical to be radiomimetic then UCB can be described as a radiomimetic drug. Elson (1955) did not expect all the biological effects of radiation to be reproducible by all radiomimetic chemicals¹⁸⁷. He showed that some chemicals have a greater specificity of action than radiation, not only reproducing some biological effects and not others, but also producing a radiation like action on some cells and tissues, but lacking this radiomimetic action on others. On the other hand, since small radiobiological

differences are found between different forms of ionizing radiation, it is not unreasonable to apply the term "radiomimetic" to drugs whose effects show a number of similarities to those of radiation. These results indicate the potential of UCB as radiomimetic agent at least in splenic lymphocytes. The proposed model of UCB induced immunotoxic and radiomimetic effects by activating death pathways have been summarized in (Scheme 3.2).



Scheme 3.2: Proposed model of radiomimetic and immunotoxic effects of UCB: UCB perturbed plasma membrane integrity and depleted the cellular GSH levels which in turn phosphorylated p38MAPK, resulting in activation of CD95, mitochondrial translocation of Bax, and loss of MMP, leading to activation of caspases, DNA fragmentation and apoptosis.

The data on UCB toxicity to human PBMNCs is very relevant, as the increased UCB levels are seen mainly in the blood of hyperbilirubenimic patients⁶². Tissue levels of UCB in rodents is very low and is in the range of 10-50nM²¹⁷. In the case of human patients with hyperbilirubinemia, the PBMNCs are exposed to higher than 150μM of UCB. The death of immune cells by necrosis as indicated by our assays, clearly demonstrates the ability of UCB to cause plasma membrane damage (Fig. 3.9A, D, E)). Our data on

UCB toxicity to RBCs (Fig. 3.9F) is in agreement with the earlier work, where UCB has been shown to induce profound disturbance in erythrocyte membrane integrity^{81,82,163,165,185}. Considering the above, our results, which demonstrate UCB toxicity to RBCs and PBMNCs at concentrations of 25 μ M, become extremely important. *In vivo* UCB administration induced a significant decrease in erythrocyte, blood lymphocyte counts and splenic cellularity, which may contribute to the susceptibility of the host to infection. The decreased lymphocyte count is suggestive of active destruction of mature resting lymphocytes, as evidenced by the *in vitro* immunotoxicity of UCB (Fig. 3.1A, B). Since UCB causes bone marrow depletion it can be considered immunotoxic and radiomimetic, as progenitor cells are derived from pluripotent stem cells present in the bone marrow. The *in vivo* immunotoxicity correlates with the immune parameters like T cell mitogen response to Con A and B cell mitogen response to LPS, in an *ex vivo* set up (Fig. 3.16F). The *in vitro* immunotoxic effect of UCB suggests that the acute immunosuppression observed in mice might be, at least in part, due to direct cytotoxic effect of UCB on resting lymphocytes. Our results give direct support to the hypothesis that high plasma UCB levels found in hyperbilirubinemic patients has been shown to act as a negative immune regulator under physio-pathological situations including infection¹⁷⁹. Further studies on the levels of UCB in blood plasma and immune status of the patients will give valuable insights regarding the *in vivo* relevance of our results.

In conclusion, our results demonstrate the ability of UCB to cause immunotoxicity besides neurotoxicity. These findings should prove useful in understanding the immunosuppression associated with hyperbilirubinemia. The observations presented in this study provide a molecular basis for the immunoregulatory

and radiomimetic properties of this important endogenous molecule. Hyperbilirubinemia associated increased infection may be contributed by the immunosuppression caused by elevated plasma UCB levels. Results from our studies also reveal the potential use of UCB as an immunosuppressive and radiomimetic agent *in vivo*.

CHAPTER 4

RADIOMODIFYING

EFFECTS OF

BILIRUBIN

4.1 INTRODUCTION

The increased bilirubin levels in the body have been shown to suppress all the principal compartments of immune system: cellular immune response^{177,218-221}, humoral immune response^{176,181} and non-specific immune response, i.e. complement and phagocytes^{181,222-225}. The several *in vitro* and *in vivo* studies demonstrated that bilirubin may be considered to be a potential immunosuppressive agent^{170,226}. UCB decreases immune responses^{172,175-177} and increased rates of infection have been documented in hyperbilirubinemic patients^{179,227}. Our work presented in chapter 3 demonstrated that clinically relevant concentration of UCB induced both apoptosis and necrosis in immune cells via induction of oxidative stress²²⁶. An elevated level of bilirubin in blood is called hyperbilirubinemia. Although hyperbilirubinemia has been associated with overall poor outcomes in critical illness^{179,228,229}, the response of these individuals to radiation exposure remain largely unknown.

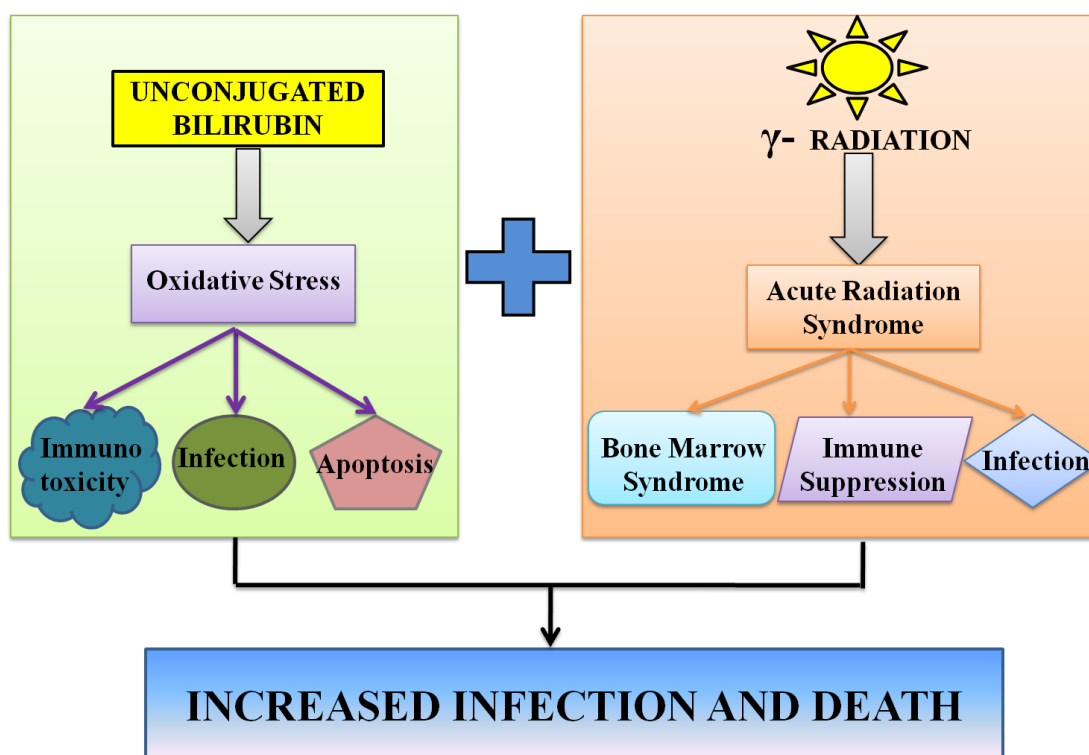
Hyperbilirubinemia is common in intensive care unit patients, occurring in as many as 40% of patients¹⁷⁹. It is very common in neonatal jaundice and in Crigler–Najjar syndrome at all ages⁶². The classical hyperbilirubinemia is clinically seen in jaundice, bilirubin encephalopathy and Gilbert syndrome⁷⁷. Besides, hyperbilirubinemia has been shown to be associated with inflammatory disorder and several types of cancer. In a prospective study of 45 patients with acute appendicitis, Khan S. (2006) has reported that acute inflammation of appendix and its complications is closely associated with hyperbilirubinemia²³⁰. Further, several carcinomas of pancreas and liver have been shown to have close association with hyperbilirubinemia. Pancreatic ductal cancer is frequently associated with obstructive jaundice which further complicates the diseased condition by

suppressing the immune responses²³¹. Uchida H. et al (2009) had demonstrated that obstructive jaundice generally reflects the advance stage of ampullary carcinoma²³². Additionally, obstructive jaundice with increased bilirubin level was found as major symptoms of pancreatic adenocarcinoma²³³⁻²³⁵. Recently, Chan-Kwon Park et al (2011) has reported that jaundice occurs in 19 to 40% of patients with hepatocellular carcinoma²³⁶. Radiation therapy is the widely recognized and most common treatment for these hepatocellular carcinoma²³⁶⁻²⁴⁰, pancreatic adenocarcinoma^{241,242}, cholangiocellular carcinoma with obstructive jaundice^{243,244} and ampullary carcinoma²⁴⁵. Although hyperbilirubinemic cancer patients were exposed to ionizing radiation for cancer therapy, the data concerning the effects of hyperbilirubinemia on exposure to ionizing radiation were completely lacking. Characterizing the radiomodifying effects of clinically relevant concentrations of UCB is critical for understanding the potential risk to hyperbilirubinemic patients during radiotherapy and exposure to acute radiation in the course of radiation accidents.

Exposure to ionizing radiation majorly occurs either through therapy and diagnosis or through occupational and environmental exposures. Individuals may get exposed to doses of radiation of 1-10Gy during the course of radiation therapy or as the result of radiation accidents or nuclear/radiological terrorism alone or in conjunction with bioterrorism²⁴⁶. Whole-body exposure to radiation greater than 1Gy induces acute radiation syndrome (ARS)²⁴⁷. The earliest presentation of ARS is the hematopoietic syndrome or bone marrow syndrome (BMS) that occurs in patients who have received 2-6Gy²⁴⁸. Infection is the primary cause of death during radiation exposure that induces BMS. The seriously affected patients with bone marrow aplasia experience reduced

defense against exogenous and endogenous factors, such as infection and inflammation, and consequently suffer from invasive infection and organ dysfunction²⁴⁹⁻²⁵².

Although ARS may be observed in patients who receive whole-body doses ~ 1 Gy, but generally it is not clinically significant at doses ~ 2 Gy unless other combined injuries including inflammation, stress and depressed immunity²⁵³. Morbidity and mortality associated with radiation injuries are highly aggravated by secondary complication of stress, inflammation, infection and trauma along with ARS²⁵⁴⁻²⁵⁶. Based on these findings, we hypothesize that hyperbilirubinemia during radiation exposure may worsen the radiation effects and increases the susceptibility of mice to develop infection (Scheme 4.1).



Scheme 4.1: Hypothesis of radiopotentiating effects of UCB

We chose a dose of 2Gy because at this dose BMS is prominent component of ARS and further this dose is used during radiation therapy of cancer. Radiopotentiating effects of UCB was studied using mouse as experimental model, because murine model are the best-characterized animal model for initial assessment radiation injury¹¹⁴. In the present report, we used a mouse model of ARS to study the effects of clinically relevant concentrations of UCB administration on suppression of immune responses in the irradiated host. Combination treatment protocol consisting of pretreatment of the mice with UCB followed by WBI was used to simulate hyperbilirubinemic conditions of patients exposed to radiation. We have also used an infection model of bacterial peritonitis to study the effects of clinically relevant concentrations of UCB on inflammatory cascade, infection susceptibility and death in mice exposed to radiation.

4.2 MATERIALS AND METHODS

4.2.1 Reagents and Chemicals:

FITC labeled E. coli was purchased from Sigma Chemical Co (St. Louis, MO, USA). In Situ Cell Death Detection Kit, Fluorescein was purchased from Roche Applied Science (Germany). Eosine methylene blue (EMB) agar media was procured from Himedia Labs Pvt. Ltd (Mumbai, India). All other chemicals used were described in chapter 3, section 3.2.1.

4.2.2 Animal maintenance:

As described in chapter 2, section 2.2.2.

4.2.3 Preparation and treatment schedule of UCB:

UCB was prepared as described in chapter 3, section 3.2.3. In all *in vitro* experiments, cells were treated with UCB (10-50 μ M) for 4h in RPMI-1640 medium without FCS and were irradiated 2Gy without washing the cells. Appropriate vehicle was for control or radiation group *in vitro*. Cells were then supplemented with 10% FCS and cultured at 37°C in a 95% air/5% CO₂ atmosphere.

For *in vivo* studies, mice were divided into four groups: The mice in first group (UCB group) were injected with UCB (50mg/kbw) intraperitoneally (i.p.). The second group received 2Gy whole body irradiation (WBI group) 0.5h after vehicle administration. Third group received 2Gy WBI, 0.5h after UCB (50mg/kbw) administration (Combination treatment group). Mice in fourth group were treated with an equal volume of vehicle (Vehicle group).

4.2.4 Irradiation schedule:

As described in chapter 2, section 2.2.5.

4.2.5 Bone marrow and spleen cell suspensions:

As described in chapter 2, section 2.2.6.

4.2.6 Human lymphocyte isolation:

As described in chapter 2, section 2.2.15.

4.2.7 Estimation of apoptosis:

As described in chapter 2, section 2.2.7.

4.2.8 Estimation of apoptosis using TUNEL assay:

To measure UCB (50 μ M) induced apoptosis in lymphocytes in presence or absence of radiation, TUNEL assay was performed according to manufacturer's protocols. The assays use an optimized terminal transferase (TdT) to label free 3'OH ends in genomic DNA with fluorescein-dUTP. Apoptotic death was estimated using flowcytometer by measuring the fluorescence of fluorescein-dUTP labeled DNA nicks.

4.2.9 Measurement of change in MMP and intracellular calcium levels:

As described in chapter 2, section 2.2.17 and 2.2.18.

4.2.10 Estimation of DNA strand breaks by alkaline single-cell gel electrophoresis (Comet assay):

As described in chapter 3, section 3.2.11.

4.2.11 Measurements of RBC hemolysis:

As described in chapter 3, section 3.2.12.

4.2.12 Administration of UCB to mice:

Mice (four animals per group) were administered i.p. with UCB (50mg/kbw) or vehicle, 0.5h before WBI (2Gy) and sacrificed 24h after irradiation. Viability of spleen cells, bone marrow cells and peritoneal exudate cells (PECs) were enumerated by trypan blue dye exclusion method. Hematological parameters were assessed 24h after WBI using autoanalyzer.

For apoptotic studies, mice were sacrificed immediately after WBI and cells (lymphocyte, bone marrow cells and PECs) were isolated and further cultured for 24h at 37°C and death was estimated by PI staining. To study the p38MAPK activation in PECs, mice were sacrificed 3h after WBI and antibody staining was performed as described in chapter 2, section 2.2.24. The studies involving use of p38MAPK inhibitor, SB203580 (5mg/kbw) was injected i.p., 2h prior to UCB administration. The cell death in PECs isolated from these mice was estimated by esterase activity assay using FDA as fluorescent probe as described in chapter 3, section 3.2.20.

4.2.13 Antibody staining:

As described in chapter 2, section 2.2.24.

4.2.14 ³H thymidine incorporation assay:

As described in chapter 3, section 3.2.17.

4.2.15 Measurement of cytokines:

As described in chapter 2, section 2.2.31.

4.2.16 Phagocytic activity of peritoneal exudate cells:

Phagocytic activity of PECs from WBI exposed mice injected with vehicle or

UCB (50mg/Kbw) was estimated using FITC-labeled *E. coli* as described earlier¹²⁸. PECs were isolated 24h after WBI exposure by injection of 4ml ice cold RPMI-1640 medium into the peritoneal cavity and viable cells were counted using trypan blue dye exclusion. Cells (1×10^6) were mixed with FITC labeled bacteria (1×10^7) in 1:10 effector to target ratio and centrifuged for 15seconds to increase their interaction. The mixtures were incubated at 37°C for 0.5h. Ice cold PBS was added to stop phagocytosis. Cells were acquired in a flowcytometer immediately with or without crystal violet to distinguish the fluorescence of surface bound *E. coli* from phagocytosed *E. coli*¹²⁸. A total of 20,000 PECs were acquired for each sample. The fraction of cells that had phagocytosed bacteria was calculated using Flowmax® software.

The uptake of labeled bacteria by PECs was also studied by confocal laser microscopy. Cells were centrifuged on coverslips and mounted on glass-slide with DABCO. Phagocytosed bacteria were observed using a LSM510 confocal microscope (Carl Zeiss, Jena GmbH, Germany) with a Krypton-Argon laser, coupled to an Orthoplan Zeiss photomicroscope using a 488nm laser line and a 530nm band pass filter.

4.2.17 Studies on mouse model of bacterial infection:

To study the susceptibility of mice to develop infection in treatment group, we have established intra-peritoneal bacterial infection model which is medically termed as bacterial peritonitis. Mice were exposed to WBI (2Gy) 0.5h after administration of UCB (50mg/kbw) or vehicle. To develop infection, these mice were injected i.p. with non-pathogenic *E. coli* K-12 strain (MG1655) 24h after WBI exposure as described earlier²⁵⁷.

MG1655 is an *E. coli* strain having fimbriae (pili), which are required for successful attachment and adhesion to the host tissues^{258,259} therefore in spite of being

non pathogenic, it is an excellent model system to simulate the bacterial infection in animal models²⁶⁰. For infection purpose, cells of log phase cultures ($OD_{600} \sim 0.5$) were collected by centrifugation, and resuspended in sterile normal saline at 4°C. About 4×10^8 CFU (determined by plating) were injected i.p. into mice in 400µl aliquots. For survival studies acute dose (1×10^9 CFU) were injected in treated mice to record mortality. These mice were monitored for presence of diarrhea and weight loss. Survival of mice was recorded for next 30days and mean survival time was calculated.

4.2.18 Quantification of bacterial load in peritoneal cavity:

Bacterial suspensions (4×10^8 CFU of MG1655) were injected 24h after WBI (2Gy) exposure to vehicle or UCB treated mice (50mg/Kbw). The animals were anaesthetized 24hr after bacterial injection and their intra peritoneal cavity was flushed using 5ml of chilled saline. The recovered peritoneal flush was 10 fold serially diluted and plated in duplicate on EMB agar, followed by overnight incubation at 37°C for enumeration of the bacterial counts in intra peritoneal cavity. The grown *E. coli* colonies give a distinctive metallic green sheen because of ability of *E. coli* to ferment lactose and acidify the medium, and under acidic conditions the dyes produce a dark purple complex which is usually associated with a green metallic sheen. The EMB agar plates with grown *E. coli* were photographed using a Sony digital camera. The bacterial counts thus obtained were compared across different treatments to assess the effect of UCB administration in presence of radiation on bacterial clearance from the given host.

4.2.19 Measurement of serum nitric oxide (NO) and cytokines:

Mice (4 animals per group) were exposed to WBI (2Gy) 0.5h after administration of UCB (50mg/kbw) or vehicle and were injected with *E. coli* (4×10^8 CFU) 24h after

WBI. The mice were sacrificed at 6h after bacterial injection and concentration of NO was measured in the serum by using Griess reagent and the levels of pro-inflammatory cytokines (IL-1 β , IL-6 and TNF- α) in the serum were estimated using cytokine ELISA sets as described in chapter 2, section 2.2.31.

4.2.20 Statistical analysis:

Data were presented as mean \pm SEM. Data from all the experiments were analyzed using one-way ANOVA followed by post hoc analyses using the Scheffe test. Significance was set at $p < 0.05$.

4.3 RESULTS

4.3.1 UCB potentiated radiation induced apoptosis in lymphocytes:

Since cellular constituents of immune system are highly sensitive to radiation, we examined the effects of UCB pretreatment on radiation induced apoptosis in murine splenic lymphocytes, the key players of adaptive immune response. Fig. 4.1A shows flow cytometric histograms of PI stained cells exposed to radiation in presence or absence of UCB. It was found that UCB at $\geq 25\mu\text{M}$ was toxic to lymphocytes, which is in agreement with our earlier findings²²⁶. The pretreatment of lymphocytes with UCB before radiation exposure significantly increased apoptosis, when compared to either UCB or radiation group ((Fig. 4.1B).

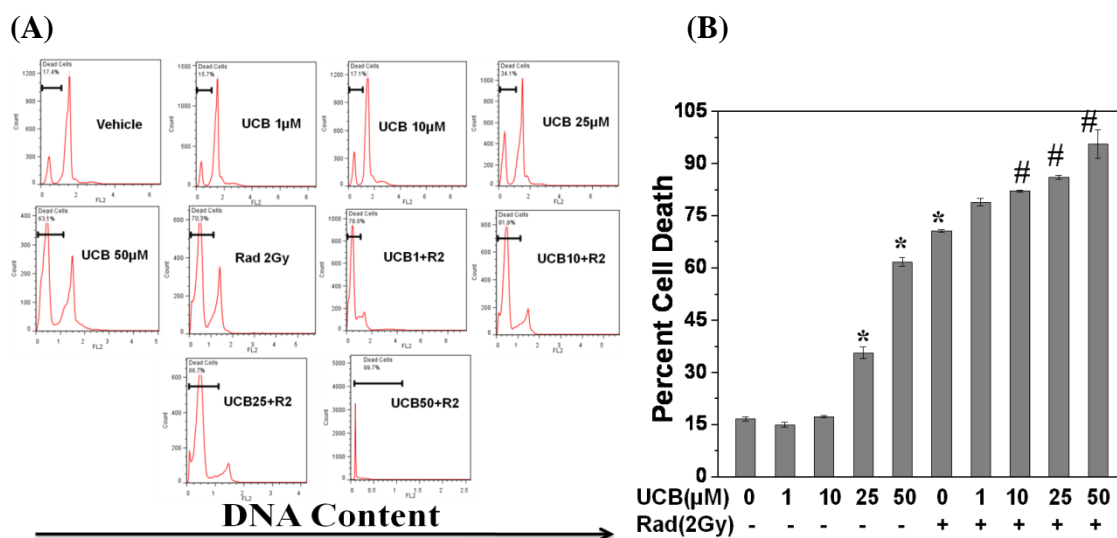


Fig. 4.1: UCB potentiated radiation induced apoptosis in lymphocytes: Splenic lymphocytes (1×10^6) were incubated with UCB (1-50 μM) for 4h at 37°C, exposed to 2Gy gamma irradiation and further cultured for 24h and cell death was estimated by PI staining. A total of 20,000 cells were acquired in Partec PAS III flowcytometer and percent apoptotic cells were determined by analyzing sub G1 population (less than 2n DNA content) using FlowJo software. Representative flowcytometric histograms (A) and corresponding bars graph (B) showing UCB induced radiopotential in lymphocytes. The data is the representative of two such independent experiments having similar results. Each bar represents mean \pm S.E.M. from three replicates. * $p < 0.05$, as compared to vehicle group. # $p < 0.05$, as compared to either UCB group or irradiated group.

The radiopotentiating effect of UCB was further confirmed by live and dead assay (Fig. 4.2A, B) TUNEL assay (Fig. 4.2C, D), changes in cell size (Fig 4.2E) and DNA-fragmentation assay (Fig. 4.2F).

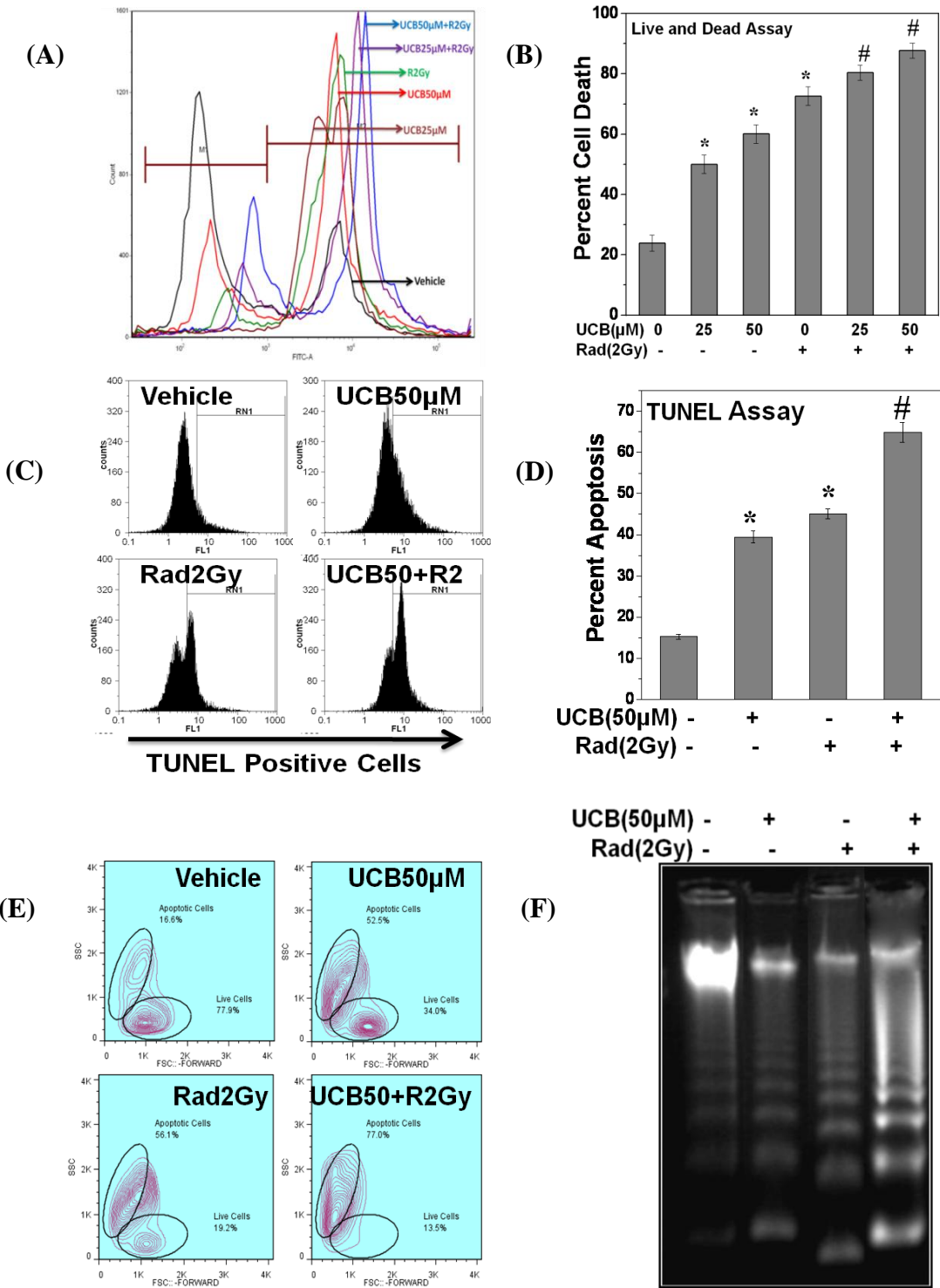


Fig. 4.2: UCB potentiated radiation induced cell death in lymphocytes: Splenic lymphocytes (1×10^6) were incubated with UCB (1-50 μ M) for 4h at 37°C, exposed to 2Gy gamma irradiation and further cultured for 24h and processed for (A-B) Live and Dead assay, (C-D) TUNEL assay, (E) changes in cell size and (F) DNA-fragmentation assay. Change in forward and side scatter was used to assess the size and density of cells. Cells undergoing apoptosis showed low FSC and increase in cell density having high SSC as analyzed using FlowJo software. The data is the representative of two such independent experiments having similar results. Each bar represents mean \pm S.E.M. from three replicates. *p<0.05, as compared to vehicle group. #p<0.05, as compared to either UCB group or irradiated group.

4.3.2 UCB potentiated radiation induced DNA strand breaks in lymphocytes:

Since DNA is the primary target of radiation, we studied the effects of UCB on radiation induced DNA strand breaks in lymphocytes by alkaline Comet assay. Results showed UCB (50 μ M) treatment to lymphocytes induced DNA strand breaks and further potentiated radiation induced DNA strand break (Fig. 4.3 A, B).

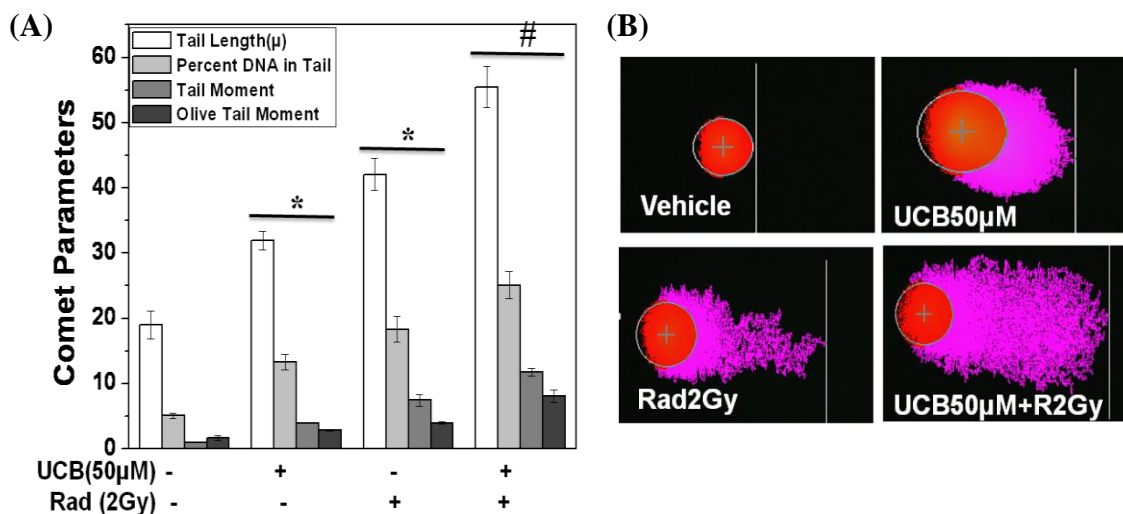


Fig. 4.3: UCB potentiated radiation induced DNA strand breaks in lymphocytes: Splenic lymphocytes (0.1×10^6) were incubated with UCB (1-50 μ M) for 4h at 37°C, exposed to 2Gy gamma irradiation and immediately kept in ice to prevent repair and processed for comet assay. (A) Bar graph and (B) representative images of comet assay showing UCB induced potentiation of radiation induced DNA strand breaks in lymphocytes. The data is the representative of two such independent experiments having similar results. Each value represents mean \pm S.E.M. from 50 cells *p<0.05, as compared to vehicle group. #p<0.05, as compared to either UCB group or irradiated group.

4.3.3 UCB potentiated radiation induced loss of MMP and calcium release in lymphocytes:

Since UCB showed radiopotentiating effect in lymphocytes by augmenting

radiation induced apoptosis, experiments were carried out to see the effects of UCB pretreatment on early events of radiation induced apoptosis. Alteration in intracellular Ca^{2+} homeostasis and mitochondrial membrane integrity leading to loss of MMP are early events of apoptosis. Results showed that treatment of lymphocytes with UCB (50 μM) induced loss of MMP and release of calcium into cytoplasm (Fig. 4.4A, B). Our results also revealed that radiation induced loss of MMP and calcium release were further augmented by pretreatment of lymphocytes with UCB (Fig. 4.4A, B). Taken together these results suggest that UCB potentiated the effects of radiation in lymphocytes by augmenting radiation induced early events of intrinsic apoptotic pathways.

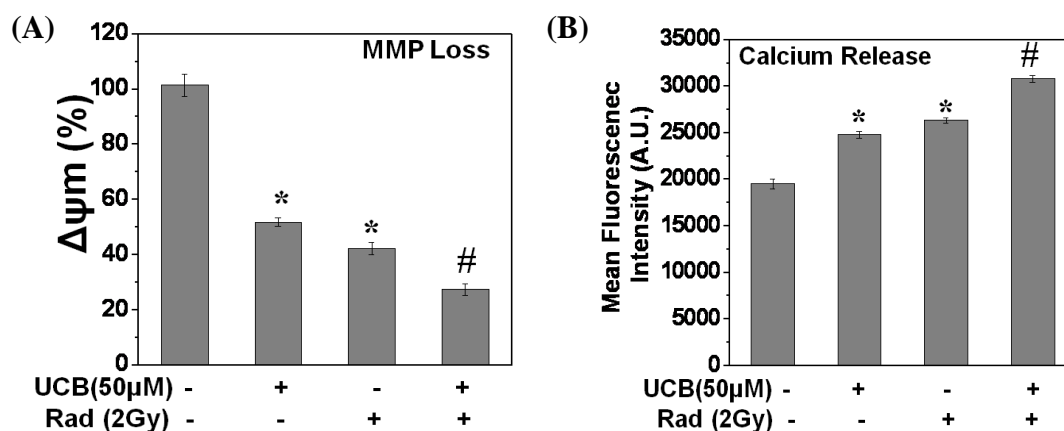


Fig. 4.4: UCB potentiated radiation induced loss of MMP and calcium release in lymphocytes: Splenic lymphocytes (1×10^6) incubated with UCB (50 μM , 4h) were exposed to radiation (2Gy) and further culture for 6h and cells were stained with (A) JC-1(5 μM) for measurement of MMP or (B) Fura 2-AM (2 μM) for measurement of calcium. The data is the representative of two such independent experiments having similar results. Each bar represents mean \pm S.E.M. from four replicates. * $p < 0.05$, as compared to vehicle group. # $p < 0.05$, as compared to either UCB group or irradiated group.

4.3.4 UCB potentiated radiation induced apoptosis of various immune cells:

To ascertain whether the radiopotentiating effects of UCB were of general importance for multiple cell types, similar experiments were performed in CD4+T cells, CD19+B cells, PECs and human PBMNCs. Results showed UCB induced significant apoptosis in all cell types and further augmented radiation induced apoptosis (Fig. 4.5A, B).

To see the radiomodifying effect of UCB in erythrocytes, we have studied RBC hemolysis by measuring the quantity of released hemoglobin. Since RBCs are devoid of nuclear effect of radiation, we used high dose of ionizing radiation (400Gy) to destabilize the membrane integrity of erythrocytes¹⁹⁴. Results showed that UCB treatment to RBCs induced significant hemolysis which was further increased in presence radiation exposure (Fig.4.5C). Exposure of erythrocytes to radiation alone induced minimal hemolysis (6.8% over control) which was in agreement with earlier published results from our laboratory¹⁹⁴.

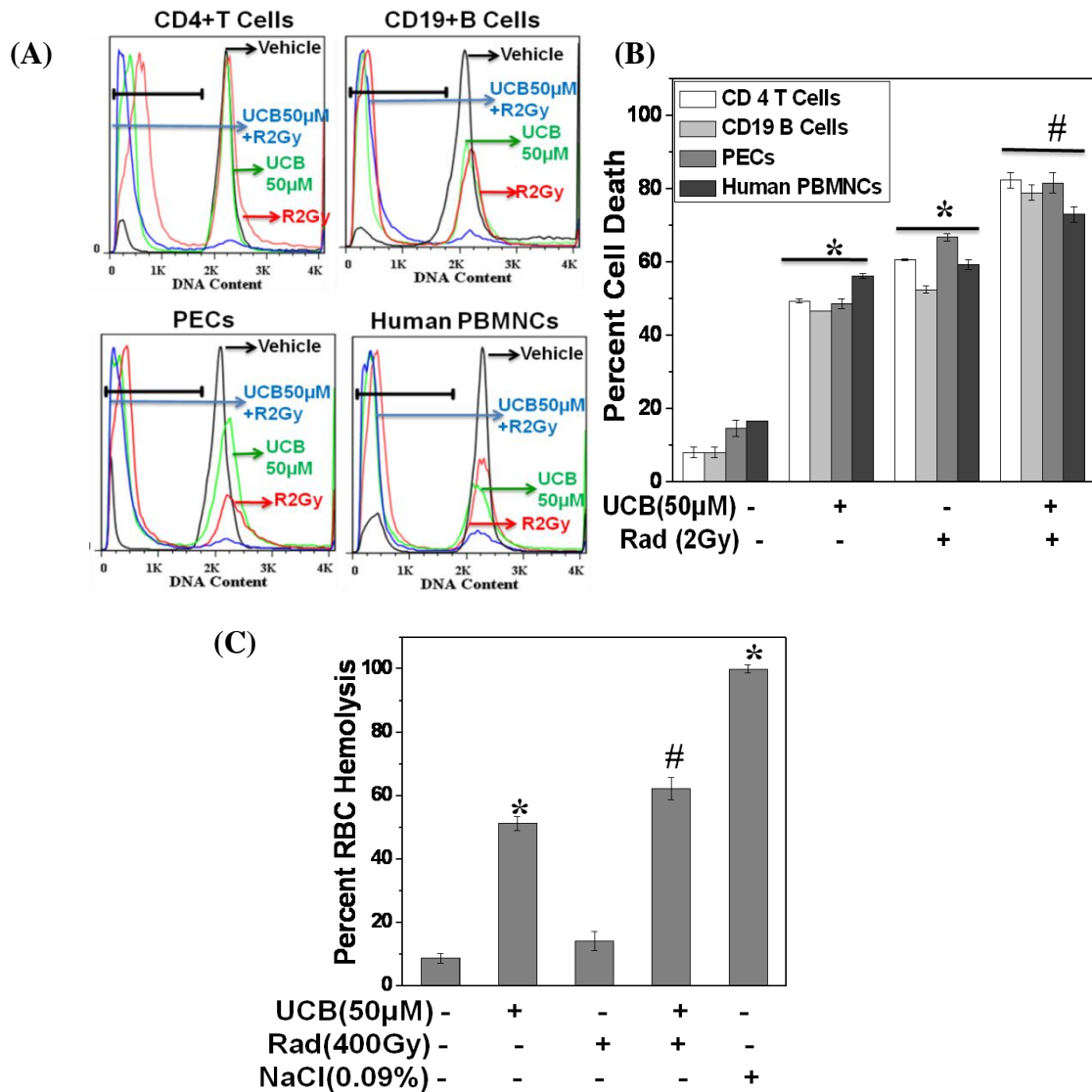


Fig. 4.5: UCB potentiated radiation induced apoptosis of various immune cells: (A, B) Purified mouse splenic CD4+T cells or CD19+B cells or PECs, or human PBMNCs (1×10^6 each) were treated with UCB ($50 \mu\text{M}$) for 4h before exposing them to radiation (2Gy) and further cultured for 24h at 37°C and cell death was estimated by PI staining. (C) UCB augmented radiation induced RBC hemolysis. Murine diluted blood treated with UCB ($50 \mu\text{M}$, 4h) were exposed to radiation (400Gy) and further incubated for 3h and RBC hemolysis was estimated. 100% hemolysis is represented by hemoglobin release in 0.09%NaCl. The data is the representative of two such independent experiments having similar results. Each bar represents mean \pm S.E.M. from three replicates. * $p < 0.05$, as compared to vehicle group. # $p < 0.05$, as compared to either UCB group or irradiated group.

4.3.5 UCB pretreatment of mice potentiated WBI induced immunosuppression:

To evaluate the relevance of *in vitro* radiopotentiating effect of UCB under *in vivo* condition, we administered the mice with immunotoxic dose of UCB (50mg/kbw) 0.5 h prior to WBI exposure and examined the ability of UCB to potentiate the WBI induced immunotoxicity in terms of loss of viability of splenocytes, bone marrow, PECs and various hematological parameters. The dose of 50 mg/kbw of UCB was selected because in earlier studies this dose was shown to have immunosuppressive and immunotoxic activity in mice²²⁶. WBI exposure to mice was given 0.5h after UCB administration because serum level of UCB reached the peak value, 30-45 minutes after UCB administration^{169,170}. WBI dose of 2Gy was selected since this dose caused acute immunosuppression¹¹⁴.

Results showed that UCB administration to mice reduced spleen weight, spleen index and viability of splenocytes suggesting its immunotoxic potential under *in vivo* conditions (Fig. 4.6A-C). The combination treatment of mice with UCB and WBI significantly decreased the above immune parameters, when compared to either UCB or WBI group (Fig. 4.6A-C). Additionally, UCB administration to mice further potentiated WBI induced loss in viable cell counts of bone marrow and PECs (Fig. 4.6D, E).

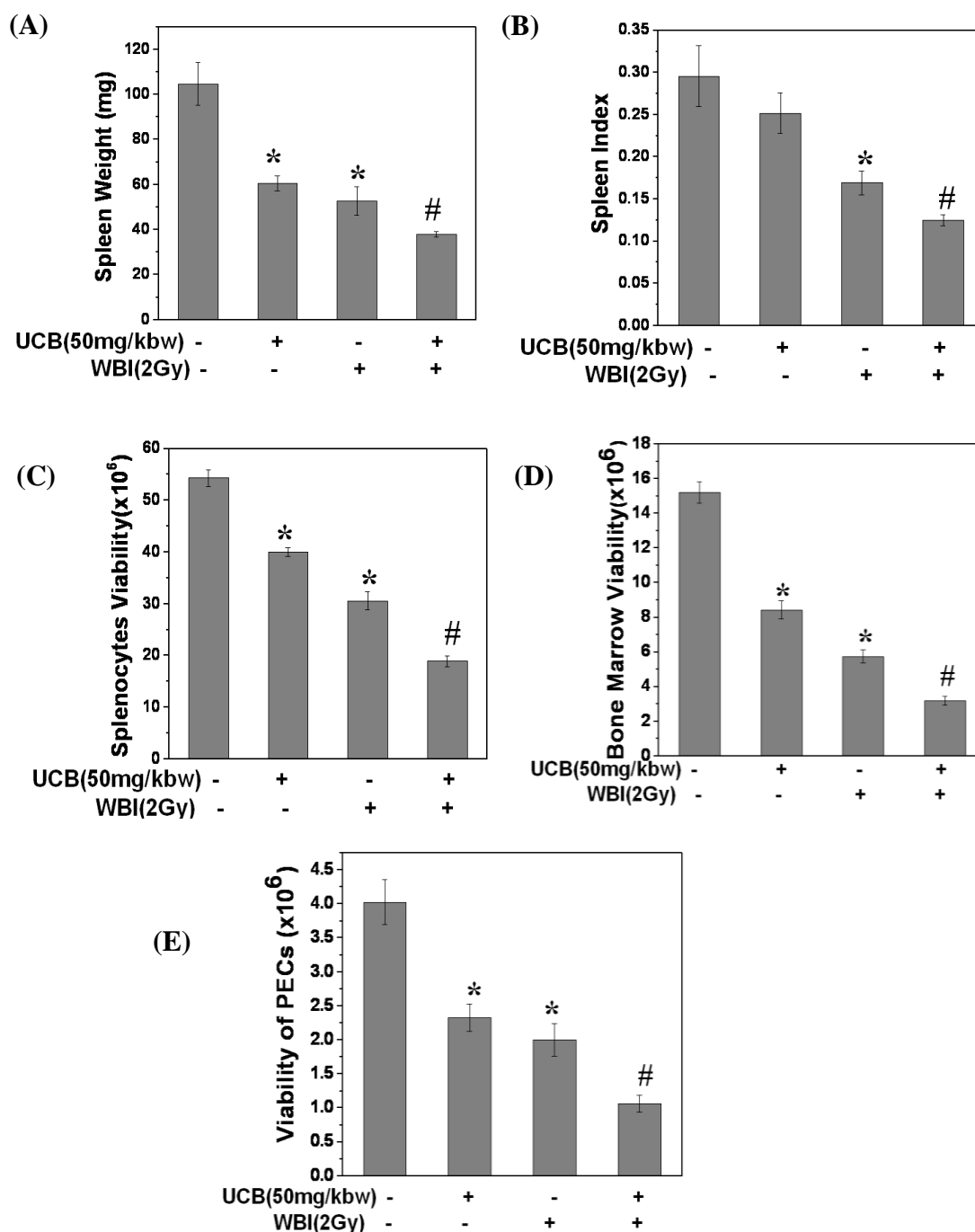


Fig. 4.6: UCB pretreatment of mice potentiated WBI induced immunosuppression: Mice were injected i.p. with UCB (50mg/kbw) or vehicle 0.5h prior to WBI (2Gy) exposure and sacrificed 24h after WBI and spleen, femur bone marrow and PECs were isolated. (A) Spleen weight, (B) spleen index were recorded and viable cell counts were enumerated by trypan blue dye exclusion method in (C) spleen, (D) Bone marrow, (E) PECs. The data is derived from one of the three such independent experiments having similar results. In each experiment, data from four mice per group were assessed and each bar represents mean \pm S.E.M. * $p < 0.05$, as compared to vehicle group and # $p < 0.05$, as compared to either UCB group or WBI group.

4.3.6 UCB pretreatment of mice potentiated WBI induced loss of splenocyte subsets:

Since UCB potentiated WBI induced splenic atrophy, we specifically monitored the effect of combination treatment of mice on various phenotypes of spleen cells. The results showed that combination treatment of mice significantly decreased the counts of different splenocyte subsets like CD3+T cells, CD4+T helper cells, CD8+T cytotoxic cells, CD19+ B cells and also CD14+ macrophages, when compared to either UCB or WBI group (Table 4.1).

Splenocyte Subsets	No. X10 ⁻⁶ per spleen			
	Control	UCB 50mg/kbw	WBI 2Gy	UCB 50mg/Kbw +WBI 2Gy
Lymphocytes	47.03±3.7	26.57±1.7*	19.49±0.7*	12.21±1.1 #
CD3+ T Cells	18.90±1.4	10.68±0.6 *	7.83±0.3 *	4.91±0.4 #
CD4+ T Cells	13.07±1.0	7.38±0.4 *	5.41±0.21*	3.39±0.3 #
CD8+ T Cells	1.88±0.1	1.06±0.06*	0.78±0.03*	0.49±0.04 #
CD19+ B Cells	14.67±1.1	8.29±0.5 *	6.08±0.24*	3.81±0.35 #
CD14+ Macrophages	2.16±0.17	1.22±0.07*	0.89±0.03*	0.56±0.05 #

Table 4.1: UCB administration to mice potentiated WBI induced loss of splenocytes subsets: Mice were administered with UCB (50mg/kbw) or vehicle 0.5h prior to WBI (2Gy) exposure and sacrificed 24h after WBI. The number of CD3+T cells, CD4+ helper T cells, CD8+ cytotoxic T cells, CD19+B cells and CD14+ macrophages in spleen of treated mice were determined by antibody staining. The total cell yield was calculated by multiplying the proportion of each cell subset by the total number of live cells obtained per spleen. The data is derived from one of the two such independent experiments having similar results. In each experiment, data from four mice per group were assessed and each bar represents mean±S.E.M. *p<0.05, as compared to vehicle group and #p<0.05, as compared to either UCB group or WBI group.

4.3.7 UCB pretreatment of mice potentiated WBI induced loss of hematological parameters:

Hematological studies showed that WBI induced leucopenia, erythropenia, lymphopenia, thrombocytopenia and neutropenia were further potentiated in mice from

combination treatment group (Table 4.2). Result showed that although relative percentage of neutrophil was increased in mice exposed to radiation in presence or absence of UCB administration as compared to nonirradiated control, the absolute neutrophil count was decreased suggesting that neutropenia occurred in irradiated mice administered with or without UCB (Table 4.2). Further, additional decrease in hemoglobin level, packed cell volume and mean corpuscular volume were seen in mice from combination treatment group when compared to either UCB or WBI group (Table 4.2). These results demonstrate that combination treatment of mice with UCB and WBI resulted in significant loss of viability of various murine immune cells suggesting that UCB possessed *in vivo* radiopotentiating effects.

Hematological Parameters	Control	UCB 50mg/kbw	WBI 2Gy	UCB 50mg/Kbw +WBI 2Gy
Platelet Counts (x10 ⁵ /ml)	3.86±0.20	2.46±0.12 *	2.39±0.11 *	1.53±0.17 #
WBCs (x10 ⁴ /ml)	1.18±0.12	0.85±0.07 *	0.65±0.02 *	0.38±0.01 #
Lymphocytes (%)	44.0±1.18	32.4±1.44 *	25.2±1.24 *	20.0±1.18 #
Neutrophils (%)	54.6±2.52	63.5±1.53 *	66.2±0.58 *	74.2±0.66 #
RBCs (x10 ⁶ /ml)	7.06±0.27	5.99±0.21 *	5.22±0.15 *	4.52±0.15 #
Hb (g/dl)	14.62±0.19	14.41±0.25 *	14.72±0.1 *	12.98±0.26 #
Packed Cell Volume (%)	40.76±0.49	31.18±0.22	28.04±0.9 *	22.62±1.25 #
Mean corpuscular Volume (fl)	72.08 ±1.77	61.72±0.46 *	60.4±1.36 *	51.02±0.7 #

Table 4.2: UCB administration to mice potentiated WBI induced loss of hematological parameters:

Mice were administered with UCB (50mg/kbw) or vehicle 0.5h prior to WBI (2Gy) exposure and 24h after WBI blood was collected in heparinised tube by retro orbital puncture and complete blood count was taken using auto-analyzer. The data is derived from one of the two such independent experiments having similar results. In each experiment, data from five mice per group were assessed and each bar represents mean±S.E.M. *p<0.05, as compared to vehicle group and #p<0.05, as compared to either UCB group or WBI group.

4.3.8 UCB pretreatment of mice potentiated WBI induced apoptosis in various immune cells:

Since WBI induced decrease in viable cell counts of various immune cells is mediated by induction of apoptosis in these cells, experiment was setup to see the effect of UCB administration on induction of WBI induced apoptosis. It was found that UCB administration alone to mice induced apoptosis in lymphocytes, bone marrow and PECs (Fig.4.7). Results also showed that mice from combination treatment group exhibited significantly increased apoptosis when compared to either UCB or WBI group (Fig. 4.7).

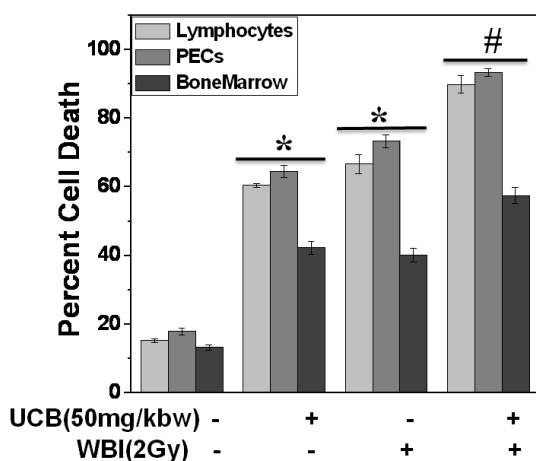


Fig. 4.7: UCB pretreatment of mice potentiated WBI induced apoptosis in various immune cells: Mice were administered with UCB (50mg/kbw) or vehicle 0.5h prior to WBI (2Gy) exposure and sacrificed immediately after WBI, and spleen, bone marrow and PECs were removed from different groups and cultured for 24h at 37°C and cell death in each group was estimated by PI staining. The data is derived from one of the two such independent experiments having similar results. In each experiment, data from three mice per group were assessed and each bar represents mean±S.E.M. *p<0.05, as compared to vehicle group and #p<0.05, as compared to either UCB group or WBI group.

4.3.9 UCB pretreatment of mice decreased WBI induced loss of functional response of lymphocytes:

Since, UCB administration to mice in presence or absence of WBI exposure lead to a significant reduction in the viable cell numbers in spleen, the ability of residual splenocytes to mount a proliferative immune response to T and B cell mitogens was examined. Results showed that lymphocytes taken from UCB (50mg/kbw) administered mice showed significantly depressed proliferative responses to both mitogens (LPS, Con A), as compared to that obtained from vehicle administered mice (Fig. 4.8A). It was found that lymphocytes obtained from combination treatment group were less responsive

to both the mitogens, as compared to either UCB or WBI group (Fig. 4.8A). Similar depressed responses of lymphocytes from combination treatment group as compared to either UCB or WBI group were obtained in terms of cytokine production (IL-2, IL-6 and IFN- γ) upon Con A stimulation (Fig. 4.8B).

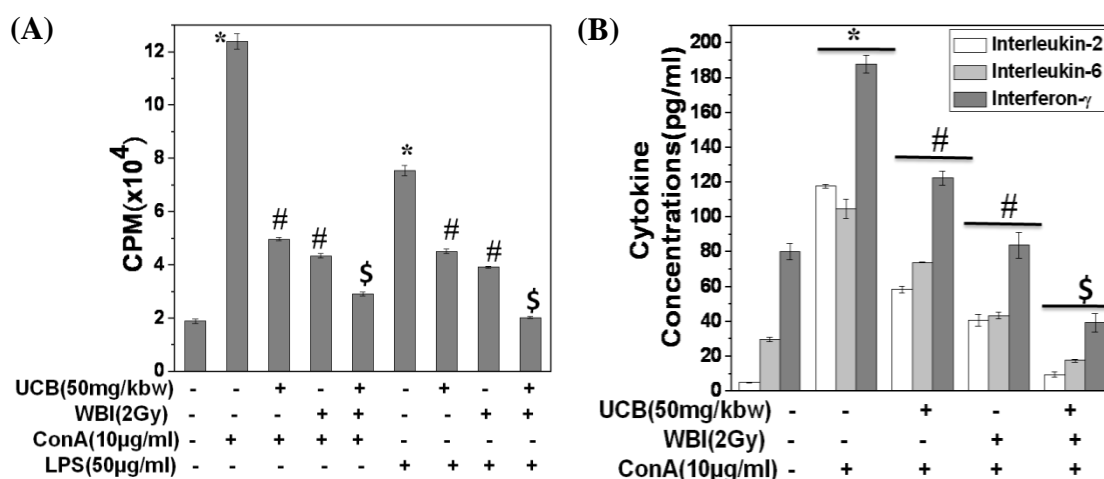


Fig. 4.8: UCB pretreatment of mice decreased WBI induced loss of functional response of lymphocytes: Mice were administered with UCB (50mg/kbw) or vehicle, 0.5h prior to WBI (2Gy). Mice were sacrificed 24h after WBI and spleen was isolated and their functional responses were evaluated. **(A)** Splenic lymphocytes (1x10⁶/ml) were stimulated with Con A (10 μ g/ml) or LPS (50 μ g/ml) for 72 or 48h respectively and were pulsed with ³H thymidine (0.5 μ Ci) and the cells were harvested after 16h. The incorporated radioactivity was counted using liquid scintillation counter. **(B)** Splenic lymphocytes (2x10⁶/2ml) were stimulated with Con A (10 μ g/ml) for 24h and cytokines (IL-2, IL-6 and IFN- γ) were estimated in culture supernatant using ELISA. The data is derived from one of the two such independent experiments having similar results. In each experiment, data from three mice per group were assessed and each bar represents mean \pm S.E.M. *p<0.05, as compared to vehicle group, #p<0.05, as compared to either ConA or LPS group, and \$p<0.05 as compared to either Con A+WBI group or Con A+UCB group or LPS+WBI group or LPS+UCB group.

4.3.10 UCB pretreatment of mice decreased WBI induced loss of functional response of PECs:

Since, UCB administration to mice prior to WBI exposure lead to a significant reduction in WBI induced loss of viable cell counts of PECs, functional response of residual PECs were monitored in terms of bacterial phagocytosis because PECs are highly rich in macrophage which are major offender against bacterial infection.

Flowcytometric analysis showed that PECs isolated from UCB administered mice showed significantly decreased phagocytosis as compared to that obtained from vehicle treated mice (Fig. 4.9A, B). Further, PECs obtained from combination treatment group showed significantly decreased phagocytosis as compared to that obtained from either UCB or WBI group (Fig. 4.9A, B). Confocal studies further confirmed these findings (Fig. 4.9C). Altogether these results demonstrate that increased serum bilirubin level during radiation exposure resulted in decreased functional response of cells involved in innate immunity.

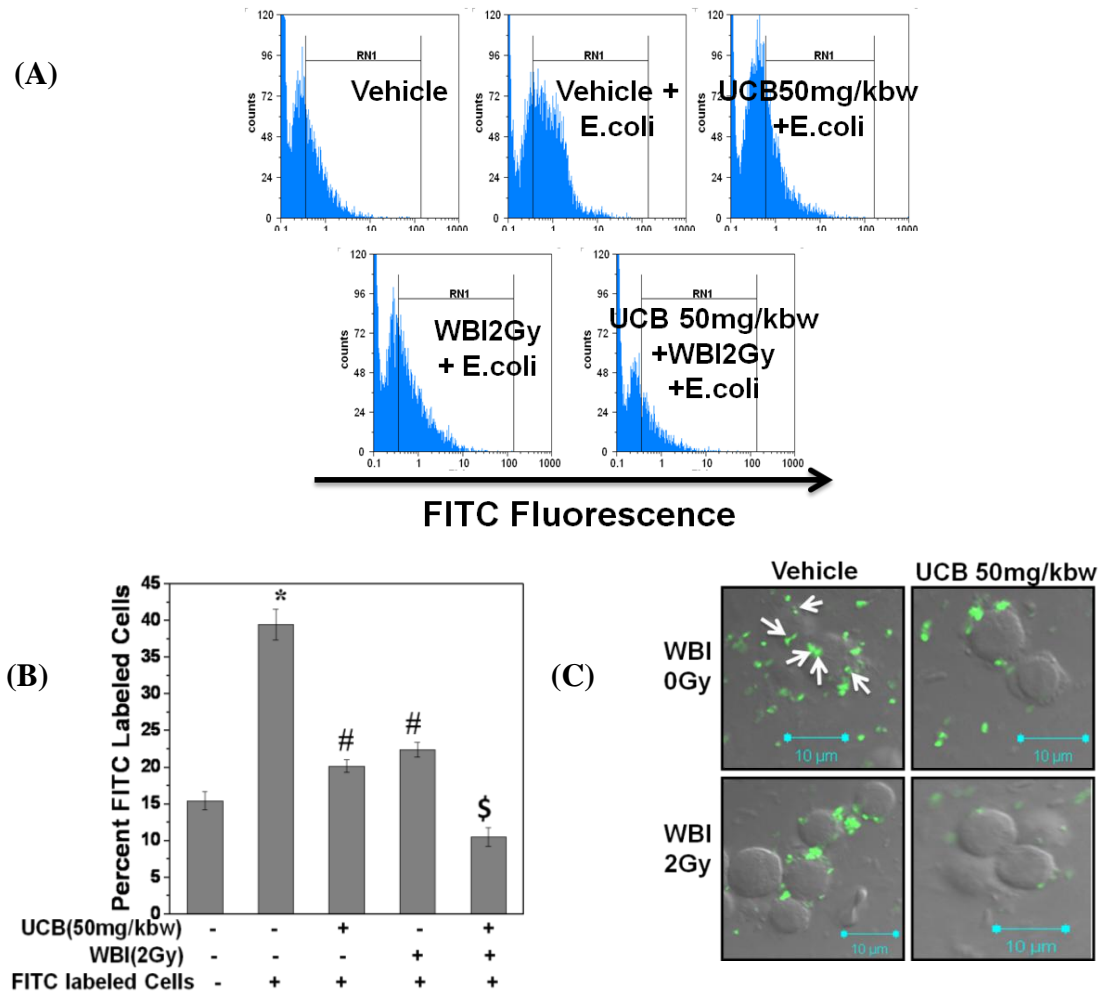


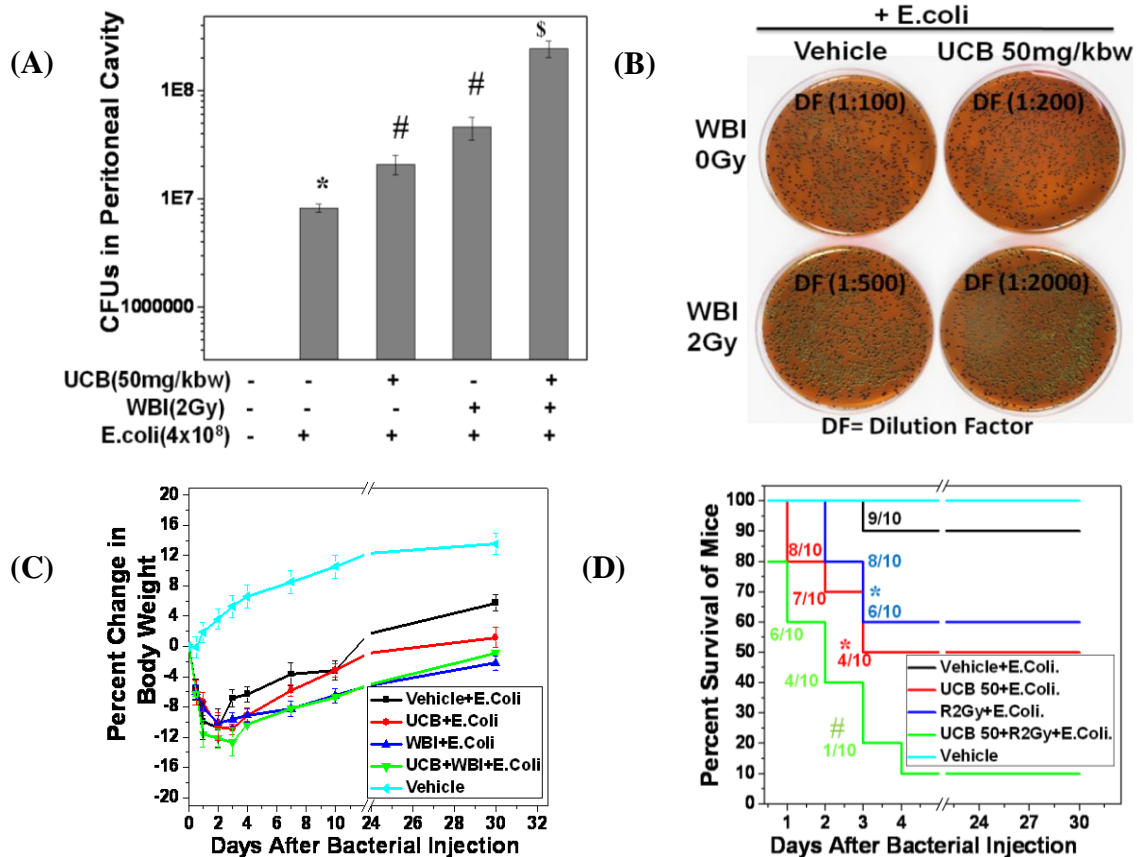
Fig. 4.9: UCB pretreatment of mice decreased WBI induced loss of functional response of PECs: Mice were administered with UCB (50mg/kbw) or vehicle, 0.5h prior to WBI (2Gy) and sacrificed 24h after WBI exposure and PECs were isolated. (A-C) PECs (1×10^6) from different groups were incubated with FITC labeled E. coli at 37°C for 0.5h. Surface fluorescence on cells was quenched by addition of

crystal violet. FITC positive cells were measured (**A, B**) using flowcytometer and (**C**) confocal microscopy. RN1 population represents FITC positive cells after quenching. The data is derived from one of the two such independent experiments having similar results. In each experiment, data from three mice per group were assessed and each bar represents mean \pm S.E.M. * $p < 0.05$, as compared to untreated control group, # $p < 0.05$, as compared to FITC labeled E. coli treated control group and § $p < 0.05$ as compared to either FITC labeled E. coli treated UCB group or FITC labeled E. coli treated WBI group.

4.3.11 UCB pretreated mice were more susceptible to WBI induced infection:

Since UCB administration to mice during radiation exposure induced increased apoptosis and decreased functional responses of lymphocytes and macrophages, the major responder against infection, we hypothesized that these mice might be more prone to infection. To test the hypothesis, mice from various groups were injected with E. coli (K-12 strain) 24h after WBI exposure. These mice were examined 24h after bacterial injection for incidence of bacterial peritonitis by quantifying the bacterial overload in the peritoneum of treated mice. As shown in the Fig. 4.10A, peritoneal cavity of mice from either UCB group or WBI group challenged with E. coli showed increased bacterial counts as compared to that of vehicle group, injected with E. coli. Further, combination treatment group injected with E. coli showed significantly increased bacterial counts as compared to that obtained from either UCB or WBI group injected with E. coli (Fig. 4.10 A, B). Further, experiments were designed to see the loss of body weight and survival of mice from various groups injected with E. coli. Results showed that mice from either UCB group or WBI group challenged with E. coli showed increased weight loss, diarrhea and mortality as compared to that of vehicle group, injected with E. coli (Fig. 4.10C, D). Further, mice from combination treatment group injected with E. coli showed significantly increased weight loss, diarrhea and mortality as compared to that obtained from either UCB or WBI group injected with E. coli (Fig. 4.10C, D and Table 4.3). These results indicate that UCB administration before WBI potentiated the WBI induced susceptibility of mice to develop infection and death.

Proinflammatory cytokines (TNF- α , IL-1 β , and IL-6) are important mediators of establishment of bacterial peritonitis^{261,262}. It is well documented that release of NO is one of the primary events of bacterial peritonitis, which led to increased production of TNF- α . To study the effect of UCB administration on the release of proinflammatory cytokines and NO in mice challenged with bacteria, serum cytokines and NO were measured at +6 h after bacterial injection. Results demonstrated that mice from either UCB group or WBI group challenged with *E. coli* showed increased level proinflammatory cytokine (TNF- α , IL-1 β , and IL-6) and NO as compared to that of vehicle group, injected with *E. coli* (Fig. 4.10E, F). Further, mice from combination treatment group injected with *E. coli* showed significantly increased level proinflammatory cytokine and NO as compared to that obtained from either UCB or WBI group injected with *E. coli* (Fig. 4.10E, F).



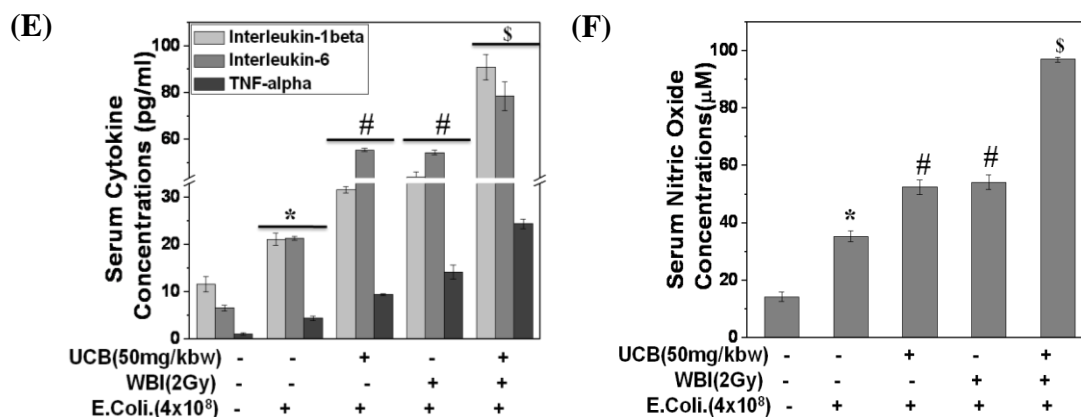


Table 4.3

Groups	Survival Rate (%)	Mean Survival Time (Days)
Vehicle+E.coli	90	27.2±2.8
UCB 50 mg/kg b wt +E.coli	50 *	12.8±4.68 *
WBI 2Gy+E.coli	60 *	18.6±4.66 *
UCB 50 mg/kg b wt+ WBI 2Gy +E.coli	10 #	4±2.9 #

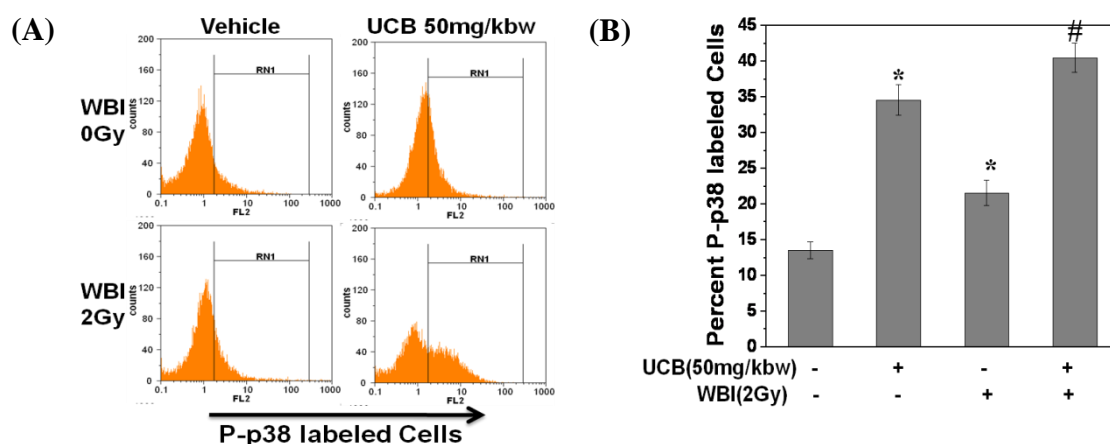
Fig. 4.10 and Table 4.3: UCB pretreated mice were more susceptible to WBI induced infection: Mice were administered with UCB (50mg/kbw) or vehicle 0.5h prior to WBI (2Gy) exposure. Mice were challenged i.p. with bacterial inoculums (4×10^8 - 10^9 CFU/ml) 24h after WBI exposure. **(A-B)** Mice were sacrificed 24h after bacterial challenge and peritoneal flush isolated from different groups were serially diluted and plated on EMB agar in duplicate and incubated for 37°C overnight and visible colonies were enumerated and photographed. * $p < 0.05$, as compared to vehicle group, # $p < 0.05$, as compared to vehicle+E. coli group and \$ $p < 0.05$ as compared to either UCB+ E. coli group or WBI+E. coli group. **(C-D)** Weight loss and mortality of treated mice were monitored for period of 30 days. Percent mortality and mean survival time were recorded (**Table 4.3**). Total ten mice per group were used for assessment of mortality * $p < 0.05$, as compared to vehicle+ E. coli group, # $p < 0.05$, as compared to either UCB+ E. coli group or WBI+E. coli group. **(E-F)** Blood was collected by retro-orbital puncture at 6h after bacterial challenge and serum were separated. **(E)** Level of pro-inflammatory cytokines (TNF- α , IL-1 β , and IL-6) were estimated by ELISA. **(F)** NO level was estimated by Griess reagent. The data is derived from one of the two such independent experiments having similar results. In each experiment, data from three mice per group were assessed and each bar represents mean \pm S.E.M.* $p < 0.05$, as compared to vehicle group, # $p < 0.05$, as compared to vehicle+E. coli group and \$ $p < 0.05$ as compared to either UCB+ E. coli group or WBI+E. coli group.

4.3.12 UCB pretreatment of mice potentiated WBI induced p38MAPK activation in

PECs:

The p38MAPK has been implicated to play a critical role in the activation and function of immune cells, release of cytokines by immunocompetent cells and also in the

pathogenesis of peritonitis²⁶³. To elucidate the role of p38MAPK in radiopotentiating effects of UCB, we examined the ability of UCB administration in presence or absence of WBI to activate p38MAPK in PECs. Results showed that UCB administration to mice activated p38MPAK in PECs and combination treatment of mice with UCB and WBI significantly potentiated the phosphorylation of p38MAPK when compared to that obtained from either UCB or WBI group (Fig. 4.11A, B). To confirm the involvement of p38MAPK in radiopotentiating effects of UCB, we have administered mice with pharmacological inhibitor of p38MPAK (SB203580) prior to combination treatment and analyzed whether selective inhibitor could inhibit the responses observed during UCB challenge in presence of WBI exposure. Results showed that SB203580 administration to mice significantly inhibited the combination treatment induced loss of viable cell counts (Fig. 4.11C) and cell death in PECs (Fig. 4.11D). We also examined the effects of SB203580 administration on induction of peritonitis and various inflammatory mediators in mice from combination treatment group injected with *E. coli*. Results showed that prior administration of SB203580 to combination treated mice injected with *E. coli*, significantly decreased the peritoneal bacterial counts (Fig. 4.11E), serum TNF- α and NO production (Fig. 4.11F).



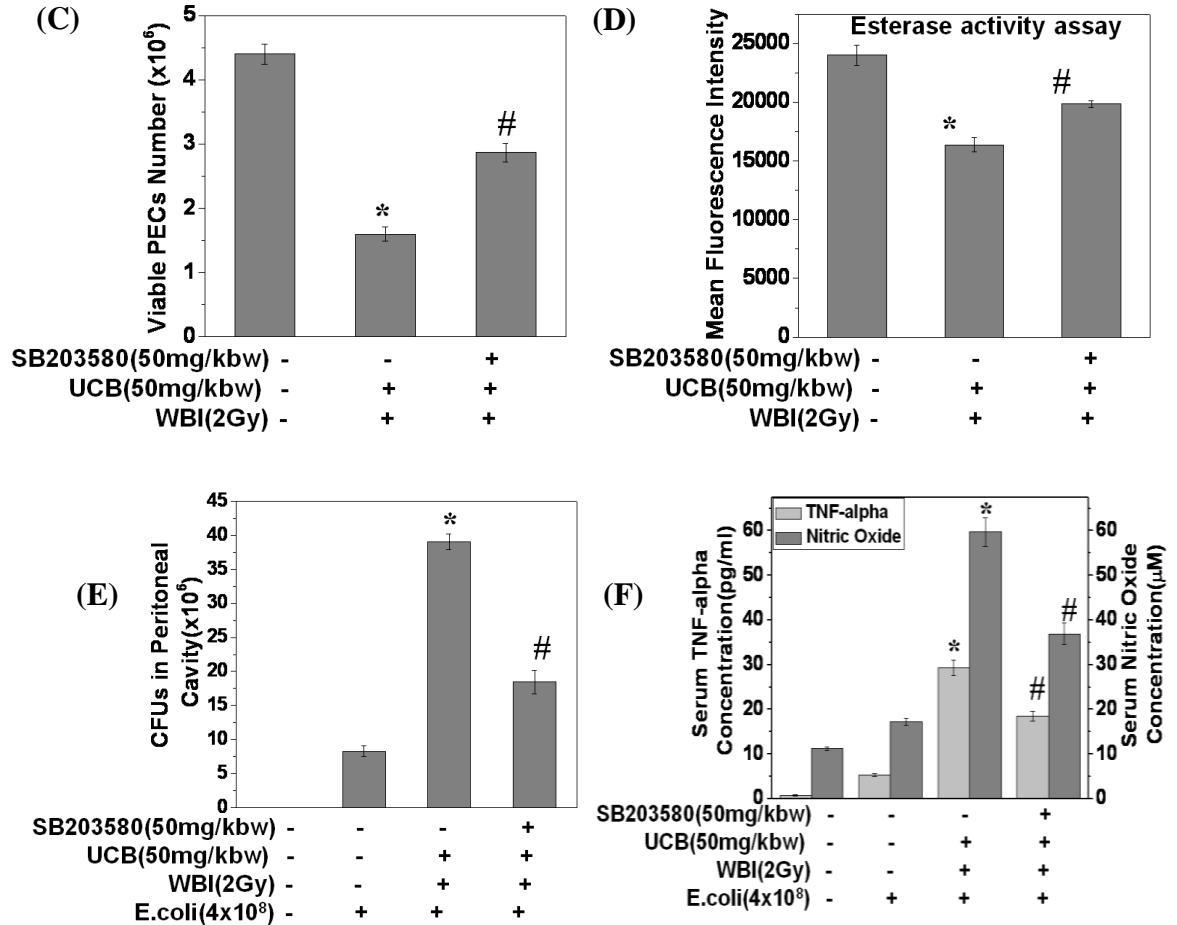


Fig. 4.11: UCB pretreatment of mice potentiated WBI induced p38MPAK activation in PECs: (A-B) Mice were administered with UCB (50mg/kbw) or vehicle 0.5h prior to WBI (2Gy) exposure and sacrificed 3h after WBI exposure. PECs were isolated and processed for intracellular staining with anti-phospho-p38MAPK. *p<0.05, as compared to vehicle group and #p<0.05, as compared to either UCB group or WBI group. (C-F) Mice were injected i.p. with SB203580 (5mg/kbw) 2h prior to UCB administration and were exposed to WBI 0.5h after UCB administration. (C) Mice were sacrificed 24h after WBI and viable PECs were enumerated by trypan blue dye exclusion method. (D) Mice were sacrificed immediately after WBI, PECs were isolated and further cultured for 24h and death was estimated by esterase activity assay. *p<0.05, as compared to vehicle group and #p<0.05, as compared to combination treatment group. (E-F) These mice were injected with *E. coli* (4x10⁸ CFU) 24h after WBI exposure. (E) Peritoneal flush isolated 24h after bacterial challenge were plated on EMB agar in duplicate and incubated for 37°C overnight and visible colonies were enumerated. (F) Blood was collected by retro-orbital puncture at 6h after bacterial challenge and serum were separated. Level of TNF-α was estimated by ELISA and NO level was estimated by Griess reagent. The data is derived from one of the two such independent experiments having similar results. In each experiment, data from three mice per group were assessed and each bar represents mean±S.E.M. *p<0.05, as compared to vehicle+E. coli group and #p<0.05, as compared to combination treatment +E. coli group.

4.4 DISCUSSION

The effect of ionizing radiation exposure in individuals with elevated levels of UCB has not been studied so far. Therefore, there is a great need to understand how increased UCB can modify the host response to WBI. In light of this background, we attempted to underscore radiopotentiating effects of UCB using mouse as experimental model. Our results demonstrate that UCB is immunotoxic and has ability to potentiate the toxic effects of radiation in various immune cells both *in vitro* and *in vivo*. Decreased functional responses of lymphocytes and PECs observed in our study revealed that UCB has radiopotentiating effects in cells involved in both innate and adaptive immunity.

Treatment of immune cells with clinically relevant UCB concentration (50 μ M) prior to radiation exposure augmented radiation induced apoptosis in T cells, B cells, macrophages and human PBMCs (Fig. 4.5). Further, increased release of calcium in cytoplasm and loss of MMP in UCB treated lymphocytes exposed to radiation suggest that UCB exhibited radiopotentiating effects by involvement intrinsic pathway of apoptosis (Fig.4.4). Our data showing decreased viable counts in splenocytes, bone marrow and PECs in UCB administered mice exposed to WBI demonstrates that in addition to its *in vitro* effect, UCB also possess *in vivo* radiopotentiating effects in various immune cells.

Our results are first one to suggest that bilirubin treatment prior to exposure of ionizing radiation intensified the cytotoxic effects of ionizing radiation (gamma rays). Although, there were no other reports available in the literature describing the effects of exposure of ionizing radiation in presence of increased levels of UCB, only few reports

are available demonstrating the effects of ultraviolet (UV) radiation exposure during phototherapy of newborn jaundiced infants with elevated UCB levels^{264,265}. Although phototherapy utilizes blue light of visible region, emissions from the adjacent UV region present a possible hazard if the exposure is of sufficient duration and used without plexiglass shields. Exposure of UV light to neonates induced UV burn which includes erythema and transient rashes on the skin²⁶⁴. Recent studies have demonstrated that phototherapy of hyperbilirubinemic neonates induced sister chromatid exchange²⁶⁶ and DNA strand breaks²⁶⁷⁻²⁶⁹. Aycicek A et al (2007) had reported a negative impact of phototherapy on numerous parts of the oxidant/antioxidant defense system in jaundiced full-term newborns²⁷⁰. Phototherapy of neonatal hyperbilirubinemia affects cytokine production and lymphocyte subsets^{271,272}. The studies collectively suggested that hyperbilirubinemia aggravated the genotoxic effects of UV radiation exposure in neonatal jaundiced with elevated levels of bilirubin.

Exposure of mice to radiation induces severe damage to immune system as its cellular constituents are highly vulnerable to radiation induced apoptosis¹⁰⁰. Our results demonstrate that WBI exposure to mice induces myelosuppression by decreasing the viable bone marrow counts (Fig.4.6D). UCB administration to mice prior to WBI exposure leads to augmented suppression of viability of bone marrow cells. Earlier report by Yong Wang et al (2006) demonstrated that myelosuppression induced by ionizing radiation is the result of induction of apoptosis in hematopoietic progenitor and hematopoietic stem cells of bone marrow²⁷³. In agreement with this study, we also found that WBI exposed mice showed increased apoptosis in bone marrow cells and combination treatment further potentiated the apoptosis in these cells (Fig. 4.7) and

thereby, exacerbated the WBI induced myelosuppression. Acute myelosuppression is an immediate concern for the radiation victims as it could cause high mortality and morbidity in exposed individual²⁷³. In accordance with our earlier published work¹⁰⁰, exposure of mice to WBI induces splenic atrophy and decreases spleen weight, spleen index, viable counts of total splenocytes and its various subsets like CD3+ T cells, CD4+ helper T cell, CD8+ cytotoxic T cells, CD19+ B cells and CD14+ macrophages (Fig. 4.6A-C and Table 4.1). UCB administration to mice potentiated WBI induced splenic atrophy by inducing increased apoptosis in splenocytes (Fig.4.7). The increased apoptosis in splenic lymphocyte obtained UCB administered mice exposed to radiation is well correlated with decreased number of viable spleen cells. The earlier published studies from our laboratories had indicated that splenocytes from irradiated mice were suppressed in their ability to mount a proliferative immune response to T cell mitogen¹¹⁴. Further, decreased proliferative response and cytokine production upon mitogenic stimulation were found in lymphocytes obtained from mice administered with UCB and exposed to radiation mice (Fig.4.8). The observed hypo-responsiveness in lymphocytes from combination treatment group is suggestive of induction of increased anergy compared to group treated with either of the treatments. The increased hypo-responsiveness is associated with increased risk of infection and death. Thus the presence of elevated levels of UCB during radiation exposure of patients should be considered in clinical situation.

Our present study further probed the radiation sensitivity of PECs in UCB treated mice. In consistent with recent reports by Xiaogang Du (2010), we found that radiation exposure to mice reduces the viability of PECs²⁷⁴. UCB administration further depleted

radiation induced loss of the viability in these cells. Further, the decreased PECs obtained in mice from combination treatment group is suggestive of active destruction of mature PECs, as evidenced by the increased apoptosis in these cells (Fig.4.7). Since PECs are highly rich in macrophages which are considered as the most efficient phagocytes, and can phagocytose substantial numbers of bacteria or other cells or microbes, functional response was studied by phagocytosis of FITC labeled bacteria using flowcytometry. Earlier report by Sablonnière B (1983) demonstrated that whole body gamma radiation exposure to rat decreased phagocytic activity of alveolar macrophages on first day post-irradiation²⁷⁵. In agreement with this study, we found that WBI exposure to mice reduced the phagocytic activity of PECs at 24h post-irradiation and combination treatment further decreased bacterial phagocytosis (Fig.4.9). Therefore combination treatment significantly decreases the innate immunity of host, which may contribute to the increased susceptibility to infection in these mice.

Our studies pertaining to hematological parameters revealed that exposure of mice to WBI induces thrombocytopenia, leucopenia, neutropenia, lymphopenia and erythropenia and further UCB administration exacerbated effects of radiation exposure (Table 4.2). Radiation exposure to mice is known to induce hematopoietic suppression by dropping the peripheral blood counts. Additionally, ML Patchen et al (1991) in his murine studies demonstrated that radiation induced neutropenia and thrombocytopenia lead to hemorrhagic complications and life threatening opportunistic infection and thus appeared as major factors contributing to morbidity and mortality after radiation exposure¹⁵². Importantly a recent study showed that, there is a quantitative relationship between the degree of neutropenia and the increased risk of infectious complications. As

the duration of neutropenia increases, the risk of secondary infections such as invasive mycoses also increases²⁷⁶. However, preclinical studies involving large animals have demonstrated that hemorrhage due to radiation induced loss of platelets remains a life-threatening problem²⁷⁷. In addition, hemorrhage exacerbates anemia, which also occurs following radiation induced hematopoietic injury¹⁵². The *in vitro* RBC hemolysis data suggests that decreased hemoglobin level observed in UCB administered mice prior to WBI exposure might be, at least in part, due to increased cytotoxic effect of UCB during radiation exposure in erythrocytes (Fig. 4.5C). Increased hemolysis in radiation exposed UCB treated RBCs may also provide plausible explanation of decreased hematocrit (packed cell volume) and decreased mean corpuscular volume observed in UCB administered mice exposed to WBI. Results obtained from our murine model of radiation injury clearly showed that combination treatment of mice potentiated WBI induced hematopoietic injury.

Suppressing the functionality of the important immune cells involved in both innate and adaptive immunity by combination treatment of mice may pose the organism at serious risk of opportunistic pathogens. Lymphocytes are key player of adaptive immunity where as macrophages are important mediator of innate immunity and provide immediate defense against infection. Spleen is secondary lymphoid organ that is involved in fighting the systemic infections and contains both multipotential stem cells and a variety of committed progenitor cells. Bone marrow is major hematopoietic organ and comprised of rapidly proliferating HPCs and relatively quiescent HSCs. Self renewing properties of HSCs maintain hematopoietic homeostasis.

To study the effects of combination treatment on host susceptibility to infection, we experimentally induced acute bacterial peritonitis as an infection model by injecting *E. coli* cells through intra-peritoneal route. Intra-peritoneal infections are one of the prominent reasons for morbidity and mortality in humans²⁷⁸. Among diverse known pathogens, *E. coli* emerge as the predominant causative agent for intra-peritoneal infections^{278,279}. As reported earlier by Billips et. al., (2007), we found that intra-peritoneal injection of *E. coli* cells in vehicle administered mice induce bacterial infection as evinced by increased levels of NO and pro-inflammatory cytokines (IL-1 β , IL-6, and TNF- α) and incidence of bacterial overload (Fig. 4.10A, E, F)²⁶⁰. These findings were in agreement with earlier independent reports where levels of pro-inflammatory cytokines had been reported to increase during establishment of bacterial peritonitis^{261,262}. Clinical study involving patients with septic shock secondary to generalized peritonitis showed that systemic release of TNF- α and IL-6 was found to be maximal on day1²⁸⁰. A recent study suggests that systemic inflammatory response syndrome (SIRS) accompanies severe forms of peritonitis and proinflammatory cytokines mediate systemic inflammatory reaction²⁸¹. Exaggeration of these inflammatory cytokines leads to tissue damage and organ failure. Excessive production of TNF and IL-1 β causes shock and high plasma level of TNF, IL-1 β and IL-6 are associated with high mortality rates²⁸². Increased mortality (20%) due to establishment of peritonitis in vehicle administered mice may be due to increased production of these pro-inflammatory cytokines (Fig.4.10D and Table 4.3). The study further revealed that serum levels of pro-inflammatory cytokines, occurrence of bacterial peritonitis and associated mortality was significantly higher in mice from UCB group as compared to mice from vehicle group (Fig.4.10). The increased bacterial counts found in the peritoneum of UCB administered mice could be

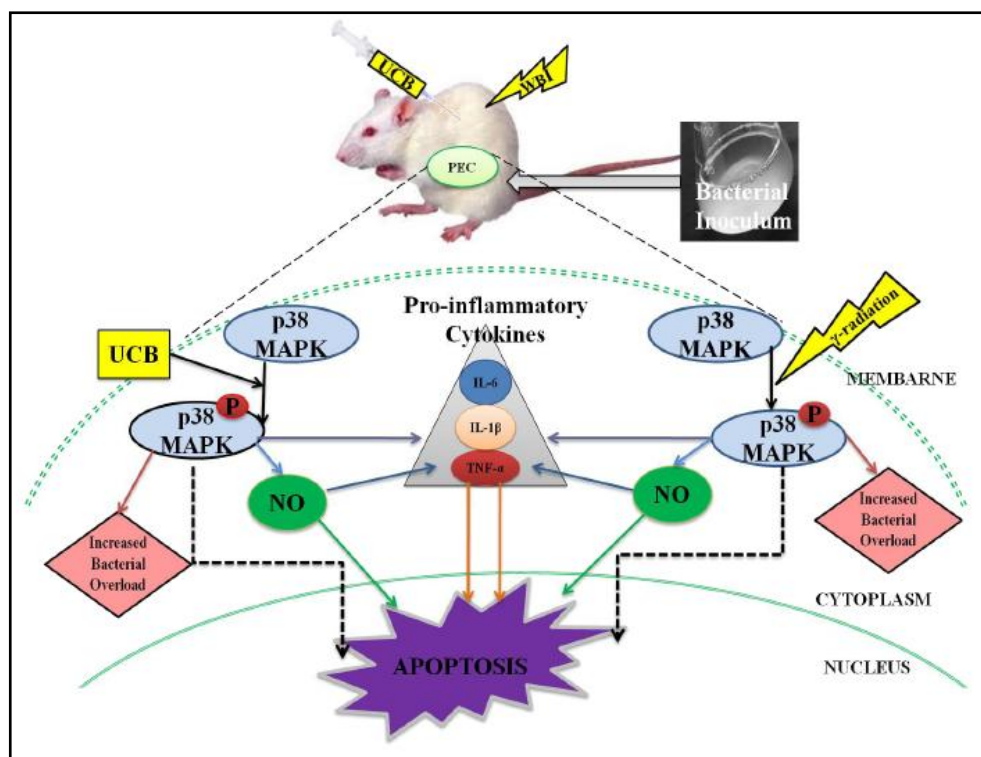
consequence of depressed phagocytosis by peritoneal macrophages. Our data may provide molecular basis by which hyperbilirubinemia predisposes the surgical ICU patients to infection and contributes to sepsis related acute respiratory distress syndrome development and mortality²²⁷. Further, our data give direct explanation of findings of Field, E et al (2008) who have reported that hyperbilirubinemic patients are at increased risk of subsequent infection and the infection risk increases as bilirubin level increases¹⁷⁹. Nisha Chand et al (2007) has reported that jaundice has been associated with infections caused by several gram-negative and gram-positive bacteria²⁸³. The primary site of infection is most often intra-abdominal, but infections of various other sites such as urinary tract infection, pneumonia, endocarditis, and meningitis have been associated with this complication. Our results confirm the findings of Paul van den Broek (2011) showing that unconjugated hyperbilirubinemia may precede bacteremia²⁸⁴. Recently Chamdine Omar et al (2011) in his case study of asymptomatic jaundiced neonates reported that 32 newborns (21%) out of 152 cases had urinary tract infection²⁸⁵. Our data suggest molecular mechanism of unanswered question why hyperbilirubinemia has been associated with overall poor outcomes in critical illness.

Additionally our results demonstrate that mice from combination treatment group injected with *E. coli* has increased occurrence of peritonitis characterized by increased peritoneal bacterial overload, increased pro-inflammatory cytokines (TNF- α , IL-6 and IL-1 β), increased NO production, decreased body weight and increased mortality (Fig.4.10 and Table 4.3). Plum J et al (1999) had reported that in case of acute peritonitis, inflammatory mediators (especially IL-1 and bacterial LPS) induced expression of iNOS in macrophages and increased levels of NO²⁸⁶. Armin K. Moshayed et

al (1998) suggested that during acute inflammation, proinflammatory cytokines such as TNF- α may induce anorexia and weight loss in mice²⁸⁷. Martineau L et al (2000), in his randomized, controlled study using rat model of peritonitis, reported that peritoneal pro-inflammatory cytokines (TNF- α , IL-1 β and IL-6) were adversely correlated with survival outcome²⁸⁸. The decreased body weight and increased mortality found in our experimental model was well correlated with increased cytokine profile (Fig.4.10).

The p38MAPK activation has been shown to play a key role in the immune dysfunction seen during murine peritonitis induced by cecal ligation and puncture²⁸⁹. The activation of p38MAPK has been implicated as an important regulator of the coordinated release various inflammatory mediators (proinflammatory cytokine, NO) by host defense cells like macrophage²⁹⁰. Lu J et al (2001) showed the regulative effects of p38MAPK on release of TNF- α and NO from alveolar macrophages under endotoxin stimulation²⁹¹. The increased cytokine profile and NO seen in the serum of combination treatment mice injected with E. coli is well correlated with increased p38MAPK activation in these mice (Fig.4.10E,F and 4.11A,B). Further, studies using pharmacological inhibitor confirmed the involvement of p38MPAK in the inflammatory cascade of peritonitis (Fig.4.11C-E). Recent studies using Mkp-1^{-/-}(MAPK phosphatase1) mice having increased p38MAPK activation showed that knockout of Mkp-1, sensitized mice to sepsis caused by cecal ligation and puncture²⁹². Further, Konstantin V. Salojin et al (2006) demonstrated that MKP-1^{-/-} mice showed enhanced constitutive activation of p38MAPK and were hyper-responsive to bacterial endotoxin (LPS) induced toxicity and exhibit significantly increased serum TNF- α , IL-6, IL-12, IFN- γ , and IL-10 levels after systemic administration of LPS²⁹³. Additionally, Mkp-1 deficiency predisposed animals to

accelerated mortality and was associated with greater bacterial burden²⁹². The increased bacterial overload found in combination treatment group injected with *E. coli* and further decreased bacterial counts due to prior administration of SB203580 in these mice showed that p38MAPK activation play key role in the pathogenesis of bacterial peritonitis in mice treated with UCB and WBI (Fig.4.11E). The proposed model of UCB induced radiopotentiating effects in mice has been summarized in scheme 4.2.



Scheme 4.2: Schematic representation of radiopotentiating effects of UCB: UCB pretreatment of mice potentiated WBI induced apoptosis by augmenting radiation induced p38MAPK activation and NO and proinflammatory cytokine (TNF- α , IL-1 β , IL-6) production in response to bacterial challenge. Further, p38MAPK activation in combination treatment mice increased bacterial overload leading to increased peritonitis.

To the best of our knowledge, this is the first study demonstrating the role of increased UCB, in exacerbating the effects of radiation exposure and increasing the infection susceptibility by suppressing the host defense against microbial infection. In conclusion, our results collectively proved that administration of the physiologically and

clinically relevant dose of UCB (50mg/kgbw) prior to exposure of 2Gy ionizing radiation (the dose typically used during radiotherapy) to mice, deteriorate the host innate and adaptive immune response and in response to subsequent bacterial challenge, heightened the immediate inflammatory reaction by inducing increased production of NO and pro-inflammatory cytokines and thus make the host more susceptible to infection, sepsis and mortality.

These experimental data sets are very relevant to human health especially in understanding the potential risk to hyperbilirubinemic patients during radiotherapy and understanding the radiopotentiating effect of UCB in ARS patients. The prevention and management of infection is the mainstay of therapy. Therefore, it is important to recognize the presence of hyperbilirubinemia during radiotherapy in order to minimize the potential side effect of radiation on normal sensitive tissue of immune system and to reduce the infection risk in the irradiated host.

CHAPTER 5

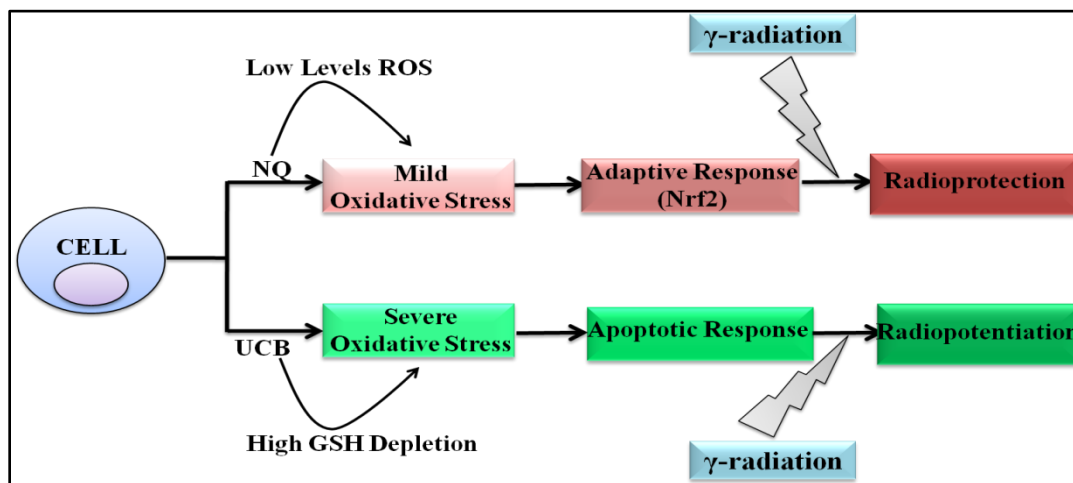
SUMMARY AND CONCLUSIONS

5.1 SUMMARY

The redox system is essential in maintaining cellular homeostasis. Under physiologic conditions, the balance between generation and elimination of ROS/RNS maintains the cellular redox homeostasis which is considered as first line of defense against diverse stimuli including various pathogens and diseased conditions. Alterations in redox homeostasis can promote cell death or cell survival, depending on the magnitude of the stimuli. The final outcomes of cell fates (survival or death) under oxidative stress depend largely on the levels and types of ROS. Also, the functional status of cellular antioxidant systems and the redox-sensitive survival-signaling pathways can significantly influence the cell-fate decision. Therefore, the redox-based therapeutic/preventive strategies should include manipulations of redox homeostasis and modulations of the redox-sensitive factors that regulate cell survival and apoptosis.

In the present study, we have employed a novel strategy of cellular redox alteration in the modulation of radiation injury. We proposed that alterations in cellular redox homeostasis can modulate the response of cell to ionizing radiation. Alteration in homeostasis of cellular redox can elicit oxidative stress which can either enhance cell survival or promote cell death upon subsequent radiation exposure, depending on the magnitude and duration of the stress and the genetic background and redox states of the cells. Oxidative stress not only serves as a type of stimulus to trigger stress-response signal-transduction pathways but also can modulate cell death/survival through direct oxidative modifications of the execution molecules. The final decision, whether the cells will survive or die due to radiation exposure, is the overall outcome of the integration of signals from redox-sensitive factors and other regulatory mechanisms.

In the present thesis work, two different approaches were used to modulate the redox status of cell and role of these alterations of cellular redox in the modulation of radiation injury were examined. We have used NQ an exogenous molecule and UCB an endogenous molecule to modulate the redox homeostasis by inducing different levels of oxidative stress in the cells. NQ (1 μ M) treatment to cells induced mild oxidative stress by generating low levels of ROS, whereas treatment of cells with physiologically relevant doses of UCB resulted in induction of severe oxidative stress via depletion of cellular GSH. Further effects of these oxidative stress generations on modulation of radiation injury were studied in the cellular system as well as in the animal model. Mild oxidative stress by treatment of cells with NQ induced the expression of a battery of phase II enzymes under regulation of Nrf2, which detoxify ROS and electrophilic chemicals induced by subsequent radiation exposure to cells. Whereas, severe oxidative stress due to UCB treatment, depleted cellular GSH and perturbed mitochondrial membrane potential, which further deteriorated the host condition after subsequent radiation exposure. Therefore, mild oxidative stressor like NQ can be used as radioprotector and severe oxidative stressor like UCB behave as radiopotentiating agent (Scheme5.1).



Scheme 5.1: Role of oxidative stress in the modulation of radiation response of cell

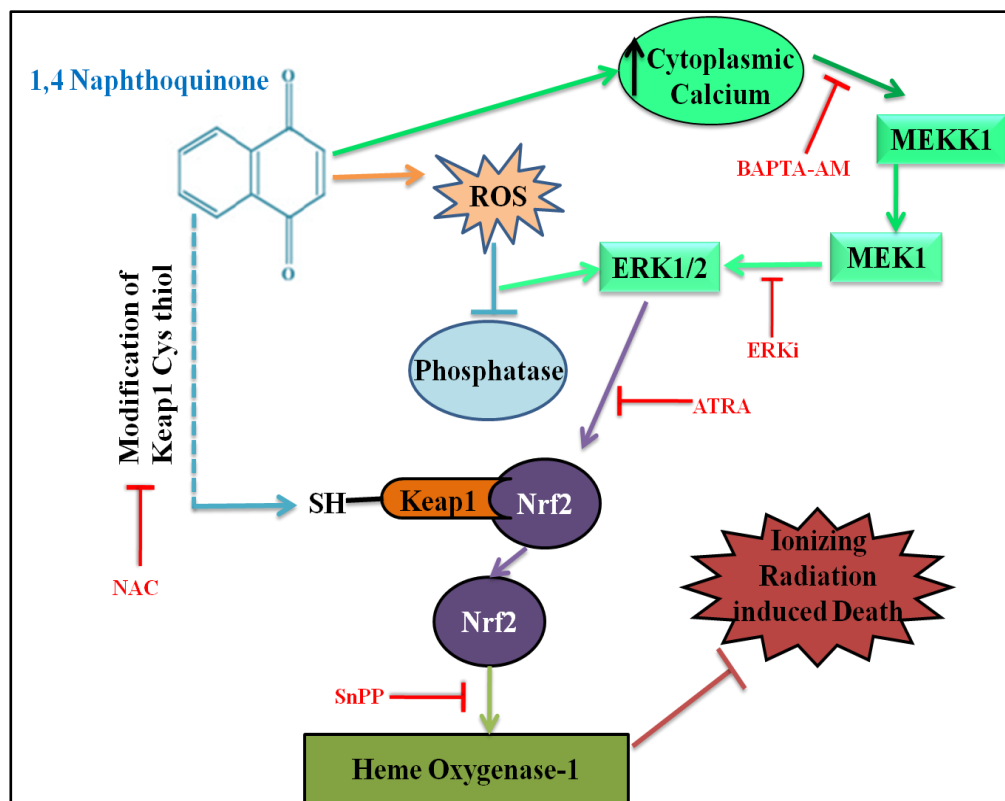
In the present study signaling pathways involved in radiation injury and molecular mechanisms implicated in the modulation (protection or potentiation) of cellular response to exposure of ionizing radiation have been delineated. Alteration in cellular redox homeostasis is a common denominator of the modulation of radiation injury. The results presented in this thesis have identified “manipulations of cellular redox homeostasis” as a molecular switch to modify the radiation injury. Oxidative stress induced by perturbation of cellular redox behaves like “double edge sword” in the modulation of radiation injury- where low levels of oxidative stress are protective at one end, on the other end high levels of oxidative stress are detrimental to the radiation exposure.

Exposure to ionizing radiation affected the host immune surveillance to a great extent because its cellular constituents are very sensitive to radiation. An acute radiation exposure caused severe damage to hematopoietic and gastrointestinal systems. Hematopoietic syndrome induced depletion of hematopoietic cells and tissues present in the bone marrow and spleen leading to immunosuppression and infection. This thesis focused on effects of NQ on amelioration of radiation induced hematopoietic syndrome and further described the molecular mechanism of action of NQ in mitigating radiation injury. Results indicated that presence of NQ (1 μ M) during radiation (4Gy) exposure to lymphocytes inhibited radiation induced apoptosis. Further, NQ inhibited early and late events associated with apoptosis for example loss of MMP, Ca⁺² release in cytoplasm and activation of caspases and fragmentation of DNA. NQ treatment to lymphocytes upregulated the expression of antiapoptotic proteins Bcl-2 and Bcl-xl. Interestingly, NQ offered protection to lymphocytes even when added to cells post-irradiation.

NQ treatment to lymphocytes was found to increase the intracellular ROS levels and decrease the cellular GSH levels. Radioprotective effect of NQ was sensitive to presence of thiol containing antioxidant N-acetyl cysteine. Whereas, non-thiol antioxidant MnTBAP failed to abrogate the radioprotective efficacy of NQ suggesting that depletion of thiol levels by NQ may be playing a role in the observed radioprotection. Further, HPLC separation and MS analysis revealed that NQ reacted with NAC and formed an adduct. Exposure of lymphocytes to NQ activated Nrf2 and increased the expression of cytoprotective gene HO-1. On knockdown of Nrf2, lymphocytes showed sensitivity to radiation suggesting that Nrf2 activation play critical role in radioprotection. For the first time, our results highlighted the role of Nrf2 in radioprotection of lymphocytes.

NQ increased ERK phosphorylation which is upstream to Nrf2 and this ERK activation was accompanied by phosphorylation of several upstream kinases like MEK1, and MEKK1 in lymphocytes. Further, addition of NQ to lymphocytes increased the intracellular calcium levels that may be responsible for activation of ERK via Raf/MEK/ERK pathway. Calcium chelators or inhibitors of ERK or Nrf2 or HO-1 abrogated the radioprotective action of NQ. These results demonstrated that a prooxidant like NQ has multiple targets in cells and can protect against radiation-induced apoptosis by activation of multiple prosurvival mechanisms including upregulation of calcium-ERK1/2-Nrf2/HO-1 pathway (Scheme5.2).

To the best of our knowledge, the results presented this thesis is the first report showing a prooxidant and a GSH depletor offering radioprotection at such low concentrations. Our proposed concept of radioprotection by prooxidant was strengthened by radioprotective effects of other well known prooxidants like H₂O₂, t-BHQ and DEM.



Scheme 5.2: NQ induced activation of prosurvival pathways for radioprotection

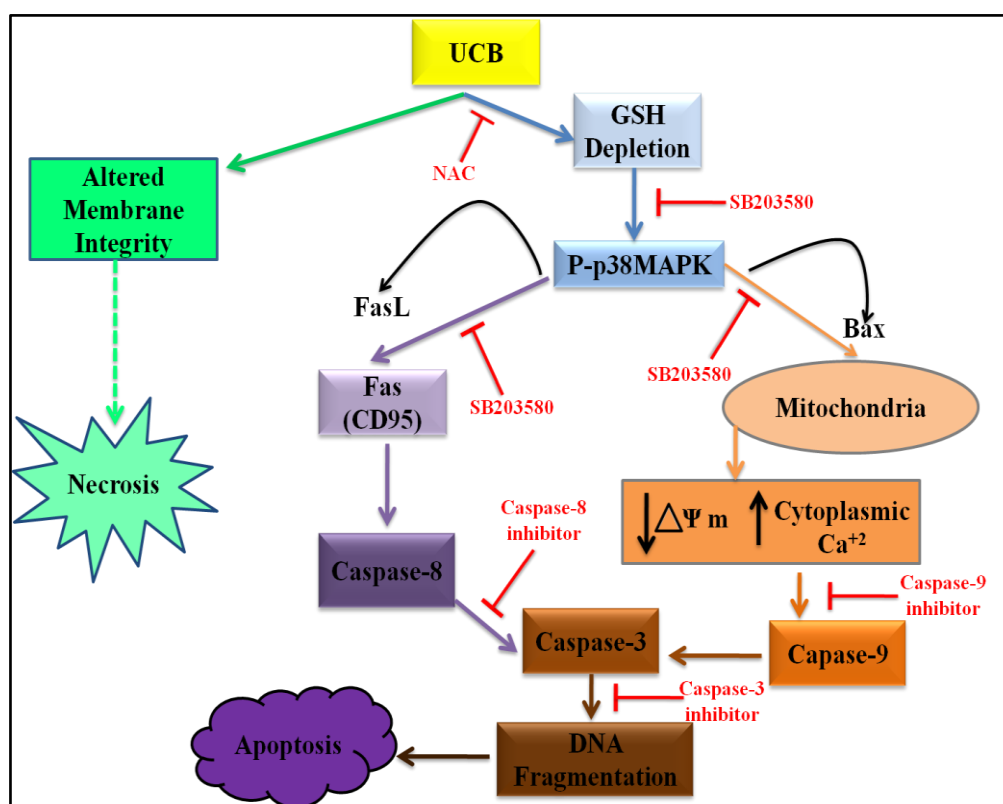
The administration of NQ (2mg/kbw) to mice offered protection against WBI (4Gy) induced splenic atrophy, hypoplasia, hemosiderosis, bone marrow aplasia and apoptosis in lymphocytes. It restored WBI mediated loss of functional responses of lymphocytes. NQ administration prevented WBI induced lymphopenia, neutropenia, erythropenia and leucopenia and other various changes in hematological parameters. NQ administration was found to be effective in stimulating the regeneration of hematopoietic stem cells as evidenced by the increase in the endogenous spleen colonies. NQ administration to mice elevated the plasma levels of radioprotective cytokine IL-1 β and IL-6. Importantly, NQ rescued mice against WBI induced mortality and prevented WBI induced loss of body weight. An increase in the LD50/30 from 6.67Gy for vehicle injection to 7.86Gy in NQ treated group was observed, which corresponds to a dose

modification factor (DMF) of 1.18. These results suggested that NQ has potential to ameliorate radiation injury both *in vitro* and *in vivo*. The key finding of present work is low levels of oxidative stress induced by alteration in cellular redox homeostasis by treatment with mild oxidative stressor is radioprotective via induction of redox sensitive transcription factor Nrf2 which can protect against radiation injury by upregulating downstream cytoprotective gene HO-1.

Although mild oxidative stress induced by low levels of ROS act as signaling molecules that protect against radiation insult, severe oxidative stress induced cell death and in combination with radiation further deteriorated the host condition. In the present thesis, we have used UCB an endogenous molecule at physiologically relevant dose, as a severe oxidative stressor. Treatment with UCB alone, induced apoptosis in the cells of immune system showing its immunotoxic potential. The immunotoxic effects of UCB imitate cytotoxic effects of ionizing radiation in various aspects. Therefore UCB behave as radiomimetic agent. Further exposure of ionizing radiation to various immune cells pretreated with UCB showed increased cytotoxicity demonstrating UCB as radiopotentiating agent.

Multiple cell viability assays demonstrated that UCB($\geq 25\mu\text{M}$) was toxic to unfractionated splenocytes, splenic T cells, B cells, macrophages or LPS stimulated CD19+B cells, human PBMNCs and red blood cells. Treatment of lymphocytes with UCB inhibited the proliferation of B cells in response to LPS and also inhibited the cytokine production from splenic macrophages. UCB induced cell death was mediated by induction of necrosis and apoptosis in splenocytes as revealed by annexin-V/PI staining. UCB activated both the extrinsic and intrinsic pathways of apoptosis as reflected by the upregulation of CD95, activation of caspase-8 and Bax, loss of MMP, Ca^{+2} release into

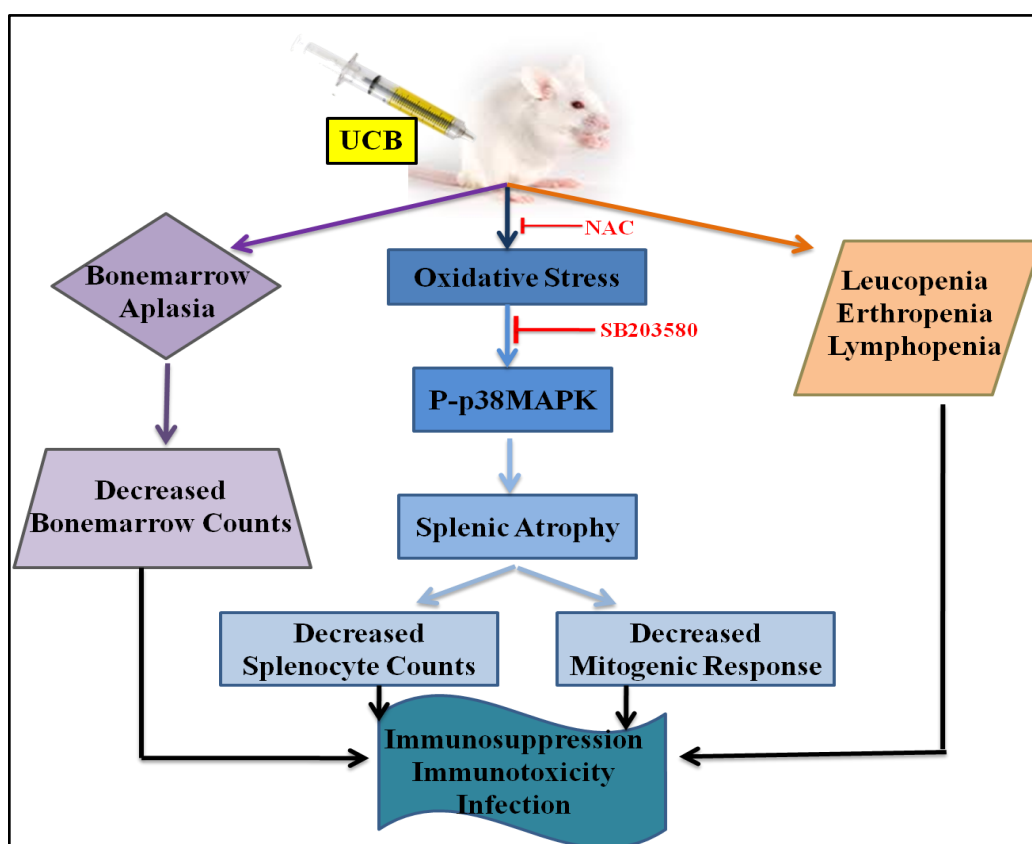
cytoplasm, caspase-3 activation and DNA ladder formation. UCB induced upregulation of CD95 expression and Bax activation was mediated by phosphorylation of p38MAPK. Inhibitors of caspases and p38MAPK significantly attenuated the UCB induced apoptosis. Further, UCB induced p38MAPK activation was found to be dependent on GSH depletion in lymphocytes. NAC, a known precursor of GSH abrogated UCB induced apoptosis (Scheme5.3).



Scheme 5.3: Molecular pathways involved in immunotoxic effects of UCB

The administration of UCB ≥ 25 mg/Kbw induced atrophy of spleen, depletion of bone marrow cells, leucopenia and decreased lymphocyte counts, which correlated with a significant decrease in T and B cell response *ex vivo* to mitogens. UCB administration to mice led to induction of oxidative stress, activation of p38MAPK and cell death in lymphocytes. These parameters were attenuated by the injection of NAC and p38MAPK

inhibitor. Our results presented in the thesis demonstrated for the first time that clinically relevant concentrations of UCB induced both apoptosis and necrosis in the cells of immune system by depleting cellular GSH. The observations presented in this study provide a molecular basis for the immunosuppressive effects of this important endogenous molecule. These findings should prove useful in understanding the immunosuppression associated with hyperbilirubinemia. Hyperbilirubinemia associated increased infection may be contributed by the immunosuppression caused by elevated plasma UCB levels (Scheme5.4). Results from our studies also reveal the potential use of UCB as an immunosuppressive agent *in vivo*.

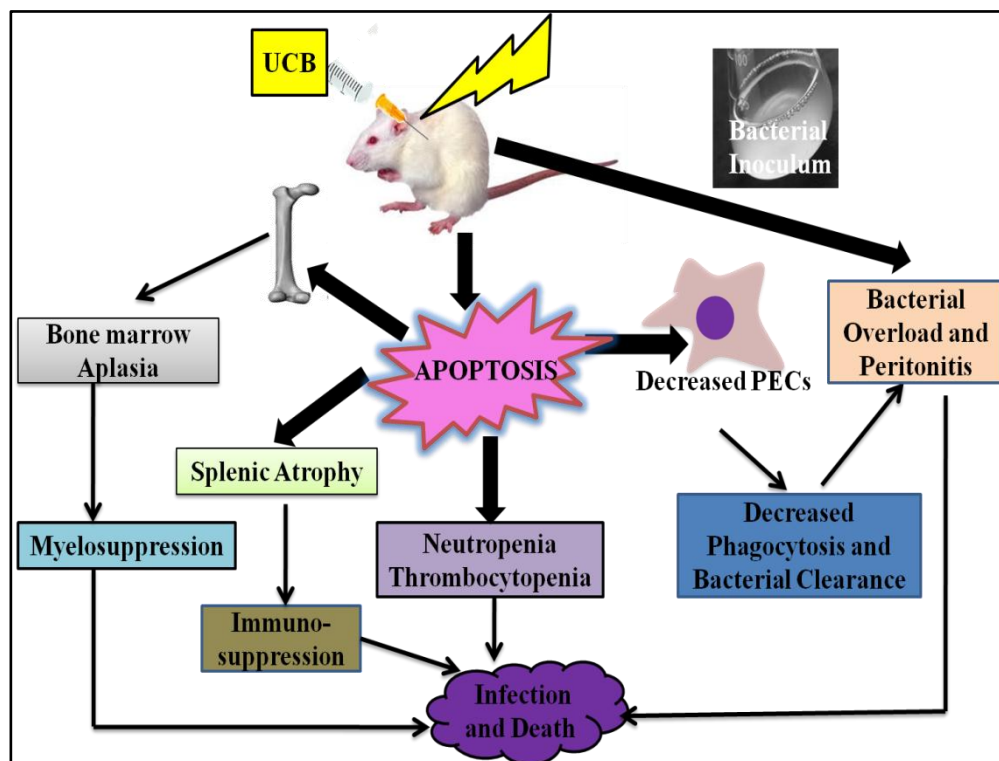


Scheme 5.4: Pathways involved in UCB induced immunosuppression and infection

Further radiation exposure to UCB treated lymphocytes showed increased DNA strand breaks, MMP loss, Ca^{+2} release and apoptosis demonstrating its radiopotentiating effect. Combination treatment of mice with UCB followed by WBI, resulted in significantly increased splenic atrophy, bone marrow aplasia, decreased counts of peritoneal exudate cells and different splenocyte subsets like CD3+T, CD4+T, CD8+T, CD19+B and CD14+macrophages as compared to either UCB or WBI treatment. Hematological studies showed that WBI-induced lymphopenia, thrombocytopenia and neutropenia was further aggravated in combination treatment group.

UCB pretreatment of mice potentiated WBI induced apoptosis and decreased WBI induced loss of functional response of various immune cells leading to potentiation of immunosuppression and infection susceptibility caused by WBI (Scheme 5.5). In an acute bacterial peritonitis model, UCB pretreatment of mice significantly increased WBI induced proinflammatory cytokines, nitric oxide and peritoneal bacterial load resulting in increased infection and death (Scheme 5.5). Studies using pharmacological inhibitor of p38MAPK, demonstrated the involvement of p38MAPK activation in the inflammatory cascade of peritonitis.

These findings should be very helpful in understanding the potential risk to hyperbilirubinemic patients during radiotherapy and victims of acute radiation exposure in the course of radiation accidents. To the best of our knowledge, this is the first study demonstrating the role of increased UCB, in exacerbating the effects of radiation exposure and increasing the infection susceptibility by suppressing the host defense against microbial infection.



Scheme 5.5: Pathways involved in UCB induced radiopotential leading to increased infection and death

The results presented in this thesis identified concept of alteration in cellular redox homeostasis as a novel strategy to modulate (protect or potentiate) radiation injury. Modulation of cellular redox elicits oxidative stress and depending on the magnitude of oxidative stress it can activate either prosurvival or proapoptotic pathways which in turn can be either radioprotective (like NQ) or radiopotentiative (like UCB). Strategies to modulate cellular redox status, either by prooxidants and antioxidants or by affecting redox-sensitive signaling pathways, may find significant clinical applications in modulation of radiation injury. A comprehensive understanding of the redox biology underlying cellular redox modulation and the mechanisms of action of radiation injury is essential for developing effective radiomodifiers.

5.2 CONCLUSIONS

The major conclusions drawn from this study are:

1. Mild oxidative stressor can be used as potential radioprotector where as severe oxidative stressor behave as cytotoxic agent and potentiate the effect of radiation.
2. Besides antioxidants, prooxidants like NQ, H₂O₂, t-BHQ and DEM showed radioprotective effects in lymphocytes.
3. NQ, the parent molecule of many clinically approved anticancer drugs opened a new class of quinonoid radioprotector.
4. NQ at 1μM protected murine splenic lymphocytes against radiation induced apoptosis by activation of Ca⁺²-ERK1/2-Nrf2-HO-1 pathway.
5. Nrf2 knockdown lymphocytes were sensitive to radiation induced apoptosis.
6. Activation of Nrf2 played a key role in protecting lymphocytes against radiation induced apoptosis.
7. NQ administration at 2mg/kgbw i.p. to mice inhibited WBI induced splenic atrophy, hypoplasia, hemosiderosis, bone marrow aplasia and apoptosis in lymphocytes.
8. NQ administration at same dose restored WBI mediated changes in various hematological parameters.
9. NQ administration prior to WBI exposure stimulated the regeneration of hematopoietic stem cells as evidenced by the increase in the endogenous spleen colonies.

10. NQ administration at 2mg/kbw i.p. improved 30 days survival of mice upon exposure of lethal dose (7Gy) of radiation by 50% and the dose modification factor was found to be 1.18.
11. UCB at clinically relevant concentrations and relevant UCB to BSA molar ratio showed immunotoxic and radiomimetic effects in murine splenic lymphocytes.
12. UCB ($\geq 25\mu\text{M}$) was toxic to unfractionated splenocytes, splenic T cells, B cells, macrophages or LPS stimulated CD19+B cells, human PBMNCs and red blood cells.
13. UCB induced cell death was mediated by induction of both necrosis and apoptosis.
14. UCB activated both the extrinsic and intrinsic pathways of apoptosis in lymphocytes.
15. UCB induced apoptosis in lymphocyte was mediated by depletion of cellular GSH and phosphorylation of p38MAPK.
16. The administration of UCB $\geq 25\text{mg/kbw}$ induced atrophy of spleen, depletion of bone marrow cells, leucopenia, decreased lymphocyte counts and decreased mitogenic response of lymphocytes.
17. UCB administration to mice at same dose led to induction of oxidative stress, activation of p38MAPK and cell death in lymphocytes.
18. UCB induced immunotoxic effects and decreased functional responses of various immune cells provided the molecular basis of increased infection rate during hyperbilirubinemia.
19. UCB ($\geq 25\mu\text{M}$) showed radiopotentiating effects in lymphocytes as demonstrated by increased DNA strand breaks, MMP loss, Ca^{+2} release and apoptosis.

20. Administration of UCB (50mg/kbw) to mice prior to radiation exposure, potentiated WBI induced splenic atrophy, bone marrow aplasia, decreased counts of peritoneal exudate cells and different splenocyte subsets like CD3+T, CD4+T, CD8+T, CD19+B and CD14+macrophages.
21. UCB administration to mice potentiated WBI induced lymphopenia, neutropenia, thrombocytopenia and various other hematological parameters.
22. UCB pretreatment of mice potentiated WBI induced apoptosis and decreased WBI induced loss of functional response of lymphocytes (measured in terms of cell proliferation and cytokine production upon mitogenic stimulation) and macrophages (measured in terms of bacterial phagocytosis).
23. UCB pretreatment of mice significantly increased WBI induced production of proinflammatory cytokines (IL-1 β , IL-6 and TNF- α) and nitric oxide in response to bacterial challenge.
24. In an acute bacterial peritonitis model, UCB pretreatment of mice significantly increased WBI induced peritoneal bacterial overload resulting in increased susceptibility to infection, sepsis and mortality.
25. UCB administration prior to WBI exposure deteriorated the host innate and adaptive immune response and in response to subsequent bacterial challenge, heightened the immediate inflammatory reaction by activation of p38MAPK in peritoneal macrophages.

5.3 FUTURE PROSPECTS

1. Further detailed studies would require a better understanding of the molecular, cellular and physiological mechanisms of *in vivo* radioprotective effects of NQ.
2. A logical extension of these studies would require the evaluation of NQ in ameliorating radiation induced gastrointestinal syndrome.
3. Since increased UCB levels during radiation exposure, exacerbated the toxic effects of radiation, further detailed studies in hyperbilirubinemic patients would require for assessing the potential risk during radiotherapy.

CHAPTER 6

BIBLIOGRAPHY

- (1) Landriscina, M.; Maddalena, F.; Laudiero, G.; Esposito, F. *Antioxid Redox Signal* **2009**, *11*, 2701-16.
- (2) Li, N.; Nel, A. E. *Antioxid Redox Signal* **2006**, *8*, 88-98.
- (3) Trachootham, D.; Lu, W.; Ogasawara, M. A.; Nilsa, R. D.; Huang, P. *Antioxid Redox Signal* **2008**, *10*, 1343-74.
- (4) Nakashima, I.; Kato, M.; Akhand, A. A.; Suzuki, H.; Takeda, K.; Hossain, K.; Kawamoto, Y. *Antioxid Redox Signal* **2002**, *4*, 517-31.
- (5) Masutani, H. *Int J Hematol* **2000**, *71*, 25-32.
- (6) Sarsour, E. H.; Kumar, M. G.; Chaudhuri, L.; Kalen, A. L.; Goswami, P. C. *Antioxid Redox Signal* **2009**, *11*, 2985-3011.
- (7) Ciriolo, M. R. *Antioxid Redox Signal* **2005**, *7*, 432-5.
- (8) Ueda, S.; Masutani, H.; Nakamura, H.; Tanaka, T.; Ueno, M.; Yodoi, J. *Antioxid Redox Signal* **2002**, *4*, 405-14.
- (9) Karin, M.; Smeal, T. *Trends Biochem Sci* **1992**, *17*, 418-22.
- (10) Moi, P.; Chan, K.; Asunis, I.; Cao, A.; Kan, Y. W. *Proc Natl Acad Sci U S A* **1994**, *91*, 9926-30.
- (11) Jozkiewicz, A.; Was, H.; Dulak, J. *Antioxid Redox Signal* **2007**, *9*, 2099-117.
- (12) Wang, X.; Thomas, B.; Sachdeva, R.; Arterburn, L.; Frye, L.; Hatcher, P. G.; Cornwell, D. G.; Ma, J. *Proc Natl Acad Sci U S A* **2006**, *103*, 3604-9.
- (13) Kapitulnik, J. *Mol Pharmacol* **2004**, *66*, 773-9.
- (14) Seubert, J. M.; Darmon, A. J.; El-Kadi, A. O.; D'Souza, S. J.; Bend, J. R. *Mol Pharmacol* **2002**, *62*, 257-64.
- (15) Rao, P.; Suzuki, R.; Mizobuchi, S.; Yamaguchi, T.; Sasaguri, S. *Biochem Biophys Res Commun* **2006**, *342*, 1279-83.
- (16) Keshavan, P.; Schwemberger, S. J.; Smith, D. L.; Babcock, G. F.; Zucker, S. D. *Int J Cancer* **2004**, *112*, 433-45.
- (17) Akin, E.; Clower, B.; Tibbs, R.; Tang, J.; Zhang, J. *Brain Res* **2002**, *931*, 168-75.
- (18) Rodrigues, C. M.; Sola, S.; Brites, D. *Hepatology* **2002**, *35*, 1186-95.
- (19) Von Sonntag, C. *The chemical basis of radiation biology*; Taylor and Francis, : New York, 1987.
- (20) Kogelnik, H. D. *Int J Radiat Oncol Biol Phys* **1996**, *35*, 219-26.
- (21) Walker R. I.; Cervený, R. J. "Medical Consequences of Nuclear Warfare, Falls Church, VA: Office of the Surgeon General," 1989.
- (22) Tak, J. K.; Park, J. W. *Free Radic Biol Med* **2009**, *46*, 1177-85.
- (23) Buxton, G. V. G., C. L.; Helman, W. P.; Ross, A. B. *J. Phys. Chem. Ref. Data* **1988**, *17*, 513-88.
- (24) Riley, P. A. *Int. J. Radiat. Biol* **1994**, *65*, 27-33.
- (25) Symons M. C. R.; Gutteridge *Free Radicals and Ion, Chemistry Biology and Medicine* ; Oxford University Press, Oxford,, 1998.
- (26) Ainsworth, E. J. A., S. M.; Crouse, D. A.; Hanson, W. R.; Fry, R. *J. Adv. Space Res.* **1989**, *9*, 299-313.
- (27) Dizdaroglu, M. J., P.; Birincioglu, M.; Rodriguez, H. *Free Radic. Biol. Med.* **2002**, *32*, 1102-1115.
- (28) Beckman, K. B. A., B. N. *J. Biol. Chem.* **1997**, *272*, 19633-19636.

-
- (29) Devasagayam, T. P.; Steenken, S.; Obendorf, M. S.; Schulz, W. A.; Sies, H. *Biochemistry* **1991**, *30*, 6283-9.
- (30) Weiss, J. F.; Landauer, M. R.; Hogan, J. B.; Gunter-Smith, P. J.; Benson, K. A.; Neta, R.; Hanson, W. R. *Adv Exp Med Biol* **1997**, *400B*, 865-72.
- (31) Kumar, K. S.; Vaishnav, Y. N.; Weiss, J. F. *Pharmacol Ther* **1988**, *39*, 301-9.
- (32) Maisin, J. R. *Int J Radiat Biol* **1998**, *73*, 443-50.
- (33) Weiss, J. F.; Landauer, M. R. *Toxicology* **2003**, *189*, 1-20.
- (34) Patt, H. M.; Tyree, E. B.; Straube, R. L.; Smith, D. E. *Science* **1949**, *110*, 213-4.
- (35) Bacq, Z. M.; Herve, A. *Nature* **1951**, *168*, 1126.
- (36) Sweeney, T. R. "Survey of Compounds from the Antiradiation Drug Development Program of the U.S. Army Medical Research and Development Command," 1979.
- (37) Capizzi, R. L. O., W. *Int. J. Hematol* **2000**, *72*, , 425-435.
- (38) Andreassen, C. N. G., C.; Lindegaard, J. C. , *Seminars in Radiation Oncology* **2008**, *13*,, 62-72.
- (39) Brown, P. E. *Nature* **1967**, *213*, 363-364.
- (40) Landauer, M. R. D., H. D.; Dominitz, J. A.; Weiss, J. F. *Pharmacol. Ther.* **1988**, *39*, 97-100.
- (41) Nair, C. K.; Parida, D. K.; Nomura, T. *J Radiat Res* **2001**, *42*, 21-37.
- (42) Burdelya, L. G.; Krivokrysenko, V. I.; Tallant, T. C.; Strom, E.; Gleiberman, A. S.; Gupta, D.; Kurnasov, O. V.; Fort, F. L.; Osterman, A. L.; Didonato, J. A.; Feinstein, E.; Gudkov, A. V. *Science* **2008**, *320*, 226-30.
- (43) Babula, P.; Adam, V.; Havel, L.; Kizek, R. *Current Pharmaceutical Analysis* **2009**, *5*, 47-68.
- (44) Kishikawa, N.; Ohkubo, N.; Ohyama, K.; Nakashima, K.; Kuroda, N. *Anal Bioanal Chem* **2009**, *393*, 1337-43.
- (45) Yamashita, Y.; Kawada, S.; Fujii, N.; Nakano, H. *Biochemistry* **1991**, *30*, 5838-45.
- (46) Rowley, D. A.; Halliwell, B. *Biochim Biophys Acta* **1983**, *761*, 86-93.
- (47) Baggish, A. L.; Hill, D. R. *Antimicrob Agents Chemother* **2002**, *46*, 1163-73.
- (48) Looareesuwan, S.; Chulay, J. D.; Canfield, C. J.; Hutchinson, D. B. *Am J Trop Med Hyg* **1999**, *60*, 533-41.
- (49) Tanaka, Y.; Kamei, K.; Otoguro, K.; Omura, S. *J Antibiot (Tokyo)* **1999**, *52*, 880-8.
- (50) Ray, S.; Hazra, B.; Mittra, B.; Das, A.; Majumder, H. K. *Mol Pharmacol* **1998**, *54*, 994-9.
- (51) Thor, H.; Smith, M. T.; Hartzell, P.; Bellomo, G.; Jewell, S. A.; Orrenius, S. *J Biol Chem* **1982**, *257*, 12419-25.
- (52) Kappus, H. *Biochem Pharmacol* **1986**, *35*, 1-6.
- (53) Watanabe, N.; Forman, H. J. *Arch Biochem Biophys* **2003**, *411*, 145-57.
- (54) Bachur, N. R. *Cancer Treat Rep* **1979**, *63*, 817-20.
- (55) Giulivi, C.; Cadenas, E. *Biochem J* **1994**, *301* (Pt 1), 21-30.

- (56) Kayashima, T.; Mori, M.; Yoshida, H.; Mizushima, Y.; Matsubara, K. *Cancer Lett* **2009**, *278*, 34-40.
- (57) Kumar, M. R.; Aithal, K.; Rao, B. N.; Udupa, N.; Rao, B. S. *Toxicol In Vitro* **2009**, *23*, 242-50.
- (58) Klaus, V.; Hartmann, T.; Gambini, J.; Graf, P.; Stahl, W.; Hartwig, A.; Klotz, L. O. *Arch Biochem Biophys* **2010**, *496*, 93-100.
- (59) Coelho Cerqueira, E.; Netz, P. A.; Diniz, C.; Petry do Canto, V.; Follmer, C. *Bioorg Med Chem* **2011**, *19*, 7416-24.
- (60) Sherif, E. M.; Park, S.-M. *Electrochimica Acta* **2006**, *51*, 1313-1321.
- (61) Ostrow, J. D.; Pascolo, L.; Brites, D.; Tiribelli, C. *Trends Mol Med* **2004**, *10*, 65-70.
- (62) wang, X. *Current Paediatrics* **2006**, *16*, 70.
- (63) Bonnett, R.; Davies, J. E.; Hursthouse, M. B. *Nature* **1976**, *262*, 327-8.
- (64) Ostrow, J. D.; Mukerjee, P.; Tiribelli, C. *J Lipid Res* **1994**, *35*, 1715-37.
- (65) Drummond, G. S.; Kappas, A. *Semin Perinatol* **2004**, *28*, 365-8.
- (66) Aziz, S.; Kotal, P.; Leroy, P.; Servaes, R.; Eggermont, E.; Fevery, J. *Acta Paediatr* **2001**, *90*, 81-7.
- (67) Blanckaert, N.; Fevery, J.; Heirwegh, K. P.; Compennolle, F. *Biochem J* **1977**, *164*, 237-49.
- (68) Fevery, J. *Liver Int* **2008**, *28*, 592-605.
- (69) Berk, P. D.; Howe, R. B.; Bloomer, J. R.; Berlin, N. I. *J Clin Invest* **1969**, *48*, 2176-90.
- (70) Brodersen, R. *J Biol Chem* **1979**, *254*, 2364-9.
- (71) Zucker, S. D.; Goessling, W.; Hoppin, A. G. *J Biol Chem* **1999**, *274*, 10852-62.
- (72) Campbell, S. D.; de Morais, S. M.; Xu, J. J. *Chem Biol Interact* **2004**, *150*, 179-87.
- (73) Bosma, P. J.; Seppen, J.; Goldhoorn, B.; Bakker, C.; Oude Elferink, R. P.; Chowdhury, J. R.; Chowdhury, N. R.; Jansen, P. L. *J Biol Chem* **1994**, *269*, 17960-4.
- (74) Huang, W.; Zhang, J.; Chua, S. S.; Qatanani, M.; Han, Y.; Granata, R.; Moore, D. D. *Proc Natl Acad Sci U S A* **2003**, *100*, 4156-61.
- (75) Jansen, P. L.; Strautnieks, S. S.; Jacquemin, E.; Hadchouel, M.; Sokal, E. M.; Hooiveld, G. J.; Koning, J. H.; De Jager-Krikken, A.; Kuipers, F.; Stellaard, F.; Bijleveld, C. M.; Gouw, A.; Van Goor, H.; Thompson, R. J.; Muller, M. *Gastroenterology* **1999**, *117*, 1370-9.
- (76) Stocker, R.; Yamamoto, Y.; McDonagh, A. F.; Glazer, A. N.; Ames, B. N. *Science* **1987**, *235*, 1043-6.
- (77) Shapiro, S. M. *Pediatr Neurol* **2003**, *29*, 410-21.
- (78) Brito, M. A.; Lima, S.; Fernandes, A.; Falcao, A. S.; Silva, R. F.; Butterfield, D. A.; Brites, D. *Neurotoxicology* **2008**, *29*, 259-69.
- (79) Brito, M. A.; Rosa, A. I.; Falcao, A. S.; Fernandes, A.; Silva, R. F.; Butterfield, D. A.; Brites, D. *Neurobiol Dis* **2008**, *29*, 30-40.
- (80) Lin, S.; Yan, C.; Wei, X.; Paul, S. M.; Du, Y. *Neurosci Lett* **2003**, *353*, 209-12.
- (81) Brito, M. A.; Silva, R.; Tiribelli, C.; Brites, D. *Eur J Clin Invest* **2000**, *30*, 239-47.

- (82) Brito, M. A.; Silva, R. F.; Brites, D. *Cell Biol Toxicol* **2002**, *18*, 181-92.
- (83) Stocker, R.; Glazer, A. N.; Ames, B. N. *Proc Natl Acad Sci U S A* **1987**, *84*, 5918-22.
- (84) Neuzil, J.; Stocker, R. *FEBS Lett* **1993**, *331*, 281-4.
- (85) Dennery, P. A.; McDonagh, A. F.; Spitz, D. R.; Rodgers, P. A.; Stevenson, D. K. *Free Radic Biol Med* **1995**, *19*, 395-404.
- (86) Neuzil, J.; Stocker, R. *J Biol Chem* **1994**, *269*, 16712-9.
- (87) Wu, T. W.; Fung, K. P.; Wu, J.; Yang, C. C.; Weisel, R. D. *Biochem Pharmacol* **1996**, *51*, 859-62.
- (88) Novotny, L.; Vitek, L. *Exp Biol Med (Maywood)* **2003**, *228*, 568-71.
- (89) Vitek, L.; Jirsa, M.; Brodanova, M.; Kalab, M.; Marecek, Z.; Danzig, V.; Novotny, L.; Kotal, P. *Atherosclerosis* **2002**, *160*, 449-56.
- (90) Granato, A.; Gores, G.; Vilei, M. T.; Tolando, R.; Ferraresso, C.; Muraca, M. *Gut* **2003**, *52*, 1774-8.
- (91) Liu, Y.; Zhu, B.; Wang, X.; Luo, L.; Li, P.; Paty, D. W.; Cynader, M. S. *J Neuroimmunol* **2003**, *139*, 27-35.
- (92) Surh, Y. J.; Kundu, J. K.; Na, H. K. *Planta Med* **2008**, *74*, 1526-39.
- (93) Groeger, G.; Quiney, C.; Cotter, T. G. *Antioxid Redox Signal* **2009**, *11*, 2655-71.
- (94) Son, T. G.; Camandola, S.; Arumugam, T. V.; Cutler, R. G.; Telljohann, R. S.; Mughal, M. R.; Moore, T. A.; Luo, W.; Yu, Q. S.; Johnson, D. A.; Johnson, J. A.; Greig, N. H.; Mattson, M. P. *J Neurochem* **2010**, *112*, 1316-26.
- (95) Haskew-Layton, R. E.; Payappilly, J. B.; Smirnova, N. A.; Ma, T. C.; Chan, K. K.; Murphy, T. H.; Guo, H.; Langley, B.; Sultana, R.; Butterfield, D. A.; Santagata, S.; Alldred, M. J.; Gazaryan, I. G.; Bell, G. W.; Ginsberg, S. D.; Ratan, R. R. *Proc Natl Acad Sci U S A* **2010**, *107*, 17385-90.
- (96) Li, J.; Johnson, D.; Calkins, M.; Wright, L.; Svendsen, C.; Johnson, J. *Toxicol Sci* **2005**, *83*, 313-28.
- (97) Checker, R.; Sharma, D.; Sandur, S. K.; Khanam, S.; Poduval, T. B. *Int Immunopharmacol* **2009**, *9*, 949-58.
- (98) Kim, B. H.; Yoo, J.; Park, S. H.; Jung, J. K.; Cho, H.; Chung, Y. *Arch Pharm Res* **2006**, *29*, 123-30.
- (99) Lehnert, S.; Greene, D.; Batist, G. *Radiat Res* **1990**, *124*, 208-15.
- (100) Khan, N. M.; Sandur, S. K.; Checker, R.; Sharma, D.; Poduval, T. B.; Sainis, K. B. *Free Radic Biol Med* **2011**, *51*, 115-28.
- (101) Maurya, D. K.; Adhikari, S.; Nair, C. K.; Devasagayam, T. P. *Mutat Res* **2007**, *634*, 69-80.
- (102) Uma Devi, P.; Ganasoundari, A.; Vrinda, B.; Srinivasan, K. K.; Unnikrishnan, M. K. *Radiat Res* **2000**, *154*, 455-60.
- (103) Checker, R.; Chatterjee, S.; Sharma, D.; Gupta, S.; Variyar, P.; Sharma, A.; Poduval, T. B. *Int Immunopharmacol* **2008**, *8*, 661-9.
- (104) Kumar, S. S.; Shankar, B.; Sainis, K. B. *Biochim Biophys Acta* **2004**, *1672*, 100-11.

- (105) Kunwar, A.; Bansal, P.; Kumar, S. J.; Bag, P. P.; Paul, P.; Reddy, N. D.; Kumbhare, L. B.; Jain, V. K.; Chaubey, R. C.; Unnikrishnan, M. K.; Priyadarsini, K. I. *Free Radic Biol Med* **2010**, *48*, 399-410.
- (106) Kunwar, A.; Bansal, P.; Kumar, S. J.; Bag, P. P.; Paul, P.; Reddy, N. D.; Kumbhare, L. B.; Jain, V. K.; Chaubey, R. C.; Unnikrishnan, M. K.; Priyadarsini, K. I. *Free Radic Biol Med*, *48*, 399-410.
- (107) Kang, K. W.; Lee, S. J.; Kim, S. G. *Antioxid Redox Signal* **2005**, *7*, 1664-73.
- (108) Kensler, T. W.; Wakabayashi, N.; Biswal, S. *Annu Rev Pharmacol Toxicol* **2007**, *47*, 89-116.
- (109) Jeong, W. S.; Jun, M.; Kong, A. N. *Antioxid Redox Signal* **2006**, *8*, 99-106.
- (110) Zhang, D. D. *Antioxid Redox Signal*.
- (111) Kim, J. W.; Li, M. H.; Jang, J. H.; Na, H. K.; Song, N. Y.; Lee, C.; Johnson, J. A.; Surh, Y. J. *Biochem Pharmacol* **2008**, *76*, 1577-89.
- (112) Kang, K. W.; Lee, S. J.; Park, J. W.; Kim, S. G. *Mol Pharmacol* **2002**, *62*, 1001-10.
- (113) Singh, A.; Bodas, M.; Wakabayashi, N.; Bunz, F.; Biswal, S. *Antioxid Redox Signal*.
- (114) Shukla, J.; Chatterjee, S.; Thakur, V. S.; Premachandran, S.; Checker, R.; Poduval, T. B. *Radiat Res* **2009**, *171*, 180-7.
- (115) Grahn, D.; Hamilton, K. F. *Genetics* **1957**, *42*, 189-98.
- (116) Okayasu, R.; Suetomi, K.; Yu, Y.; Silver, A.; Bedford, J. S.; Cox, R.; Ullrich, R. L. *Cancer Res* **2000**, *60*, 4342-5.
- (117) Sharma, D.; Sandur, S. K.; Rashmi, R.; Maurya, D. K.; Suryavanshi, S.; Checker, R.; Krishnan, S.; Sainis, K. B. *Mutat Res* **2010**, *703*, 149-57.
- (118) Arends, M. J.; Morris, R. G.; Wyllie, A. H. *Am J Pathol* **1990**, *136*, 593-608.
- (119) Ormerod, M. G.; Sun, X. M.; Brown, D.; Snowden, R. T.; Cohen, G. M. *Acta Oncol* **1993**, *32*, 417-24.
- (120) Elmore, S. *Toxicol Pathol* **2007**, *35*, 495-516.
- (121) Bortner, C. D.; Cidlowski, J. A. *J Biol Chem* **1999**, *274*, 21953-62.
- (122) Franken, N. A.; Rodermond, H. M.; Stap, J.; Haveman, J.; van Bree, C. *Nat Protoc* **2006**, *1*, 2315-9.
- (123) Wysocki, L. J.; Sato, V. L. *Proc Natl Acad Sci U S A* **1978**, *75*, 2844-8.
- (124) Mage, M. G.; McHugh, L. L.; Rothstein, T. L. *J Immunol Methods* **1977**, *15*, 47-56.
- (125) Cohen, G. M. *Biochem J* **1997**, *326* (Pt 1), 1-16.
- (126) Rai, N. K.; Tripathi, K.; Sharma, D.; Shukla, V. K. *Int J Low Extrem Wounds* **2005**, *4*, 138-44.
- (127) Krutzik, P. O.; Nolan, G. P. *Cytometry A* **2003**, *55*, 61-70.
- (128) Sharma, D.; Kumar, S. S.; Sainis, K. B. *Mol Immunol* **2007**, *44*, 347-59.
- (129) Checker, R.; Sandur, S. K.; Sharma, D.; Patwardhan, R. S.; Jayakumar, S.; Kohli, V.; Sethi, G.; Aggarwal, B. B.; Sainis, K. B. *PLoS One* **2012**, *7*, e31318.
- (130) Till, J. E.; Mc, C. E. *Radiat Res* **1961**, *14*, 213-22.

- (131) Mantena, S. K.; Unnikrishnan, M. K.; Uma Devi, P. *Mutagenesis* **2008**, *23*, 285-92.
- (132) Checker, R.; Sharma, D.; Sandur, S. K.; Subrahmanyam, G.; Krishnan, S.; Poduval, T. B.; Sainis, K. B. *J Cell Biochem* **2010**, *110*, 1082-93.
- (133) Shankar, B.; Kumar, S. S.; Sainis, K. B. *Radiat Res* **2003**, *160*, 478-87.
- (134) Reisner, Y.; Itzicovitch, L.; Meshorer, A.; Sharon, N. *Proc Natl Acad Sci U S A* **1978**, *75*, 2933-6.
- (135) Prabhakar, K. R.; Veerapur, V. P.; Bansal, P.; Parihar, V. K.; Reddy Kandadi, M.; Bhagath Kumar, P.; Priyadarsini, K. I.; Unnikrishnan, M. K. *Chem Biol Interact* **2007**, *165*, 22-32.
- (136) Maurya, D. K.; Balakrishnan, S.; Salvi, V. P.; Nair, C. K. *Mol Cell Biochem* **2005**, *280*, 57-68.
- (137) Kansra, V.; Groves, C.; Gutierrez-Ramos, J. C.; Polakiewicz, R. D. *J Biol Chem* **2001**, *276*, 31831-8.
- (138) Schmitt, J. M.; Wayman, G. A.; Nozaki, N.; Soderling, T. R. *J Biol Chem* **2004**, *279*, 24064-72.
- (139) Kumar, B.; Kumar, A.; Ghosh, S.; Pandey, B. N.; Mishra, K. P.; Hazra, B. *Biochem Biophys Res Commun* **2012**, *417*, 903-9.
- (140) Maurya, D. K.; Devasagayam, T. P.; Nair, C. K. *Indian J Exp Biol* **2006**, *44*, 93-114.
- (141) Sudheer Kumar, M.; Unnikrishnan, M. K.; Uma Devi, P. *Mutat Res* **2003**, *527*, 7-14.
- (142) Chawla, R.; Arora, R.; Singh, S.; Sagar, R. K.; Sharma, R. K.; Kumar, R.; Sharma, A.; Tripathi, R. P.; Puri, S. C.; Khan, H. A.; Shawl, A. S.; Sultan, P.; Krishan, T.; Qazi, G. N. *Evid Based Complement Alternat Med* **2006**, *3*, 503-11.
- (143) Tannehill, S. P.; Mehta, M. P. *Semin Oncol* **1996**, *23*, 69-77.
- (144) Neta, R.; Oppenheim, J. J. *Blood* **1988**, *72*, 1093-5.
- (145) Mazur, L. *Mutat Res* **2000**, *468*, 27-33.
- (146) Clark, E. P.; Epp, E. R.; Morse-Gaudio, M.; Biaglow, J. E. *Radiat Res* **1986**, *108*, 238-50.
- (147) Osburn, W. O.; Kensler, T. W. *Mutat Res* **2008**, *659*, 31-9.
- (148) Zhang, P.; Singh, A.; Yegnasubramanian, S.; Esopi, D.; Kombairaju, P.; Bodas, M.; Wu, H.; Bova, S. G.; Biswal, S. *Mol Cancer Ther*, *9*, 336-46.
- (149) Surh, Y. J. *Nat Rev Cancer* **2003**, *3*, 768-80.
- (150) Schmidt, M.; Goebeler, M.; Posern, G.; Feller, S. M.; Seitz, C. S.; Brocker, E. B.; Rapp, U. R.; Ludwig, S. *J Biol Chem* **2000**, *275*, 41011-7.
- (151) Kim, A. N.; Jeon, W. K.; Kim, B. C. *Free Radic Biol Med*.
- (152) Patchen, M. L.; MacVittie, T. J.; Williams, J. L.; Schwartz, G. N.; Souza, L. M. *Blood* **1991**, *77*, 472-80.
- (153) Zhou, Y.; Mi, M. T. *J Radiat Res* **2005**, *46*, 425-33.
- (154) Song, J. Y.; Han, S. K.; Bae, K. G.; Lim, D. S.; Son, S. J.; Jung, I. S.; Yi, S. Y.; Yun, Y. S. *Radiat Res* **2003**, *159*, 768-74.
- (155) Zheng, L.; Asprodites, N.; Keene, A. H.; Rodriguez, P.; Brown, K. D.; Davila, E. *Blood* **2008**, *111*, 2704-13.
- (156) Stocker, R.; Peterhans, E. *Free Radic Res Commun* **1989**, *6*, 57-66.
- (157) Hatfield, G. L.; Barclay, L. R. *Org Lett* **2004**, *6*, 1539-42.

- (158) Dudnik, L. B.; Khrapova, N. G. *Membr Cell Biol* **1998**, *12*, 233-40.
- (159) MacLean, P. D.; Drake, E. C.; Ross, L.; Barclay, C. *Free Radic Biol Med* **2007**, *43*, 600-9.
- (160) Ostrow, J. D.; Tiribelli, C. *J Hepatol* **2001**, *34*, 467-70.
- (161) Ostrow, J. D.; Pascolo, L.; Tiribelli, C. *Hepatology* **2002**, *35*, 1277-80.
- (162) Corich, L.; Aranda, A.; Carrassa, L.; Bellarosa, C.; Ostrow, J. D.; Tiribelli, C. *Biochem J* **2009**, *417*, 305-12.
- (163) Brito, M. A.; Brites, D. *Mol Cell Biochem* **2003**, *247*, 155-62.
- (164) Chuniaud, L.; Dessante, M.; Chantoux, F.; Blondeau, J. P.; Francon, J.; Trivin, F. *Clin Chim Acta* **1996**, *256*, 103-14.
- (165) Alexandra Brito, M.; Silva, R. F.; Brites, D. *Clin Chim Acta* **2006**, *374*, 46-56.
- (166) Rodrigues, C. M.; Sola, S.; Brito, M. A.; Brites, D.; Moura, J. J. *J Hepatol* **2002**, *36*, 335-41.
- (167) Grojean, S.; Koziel, V.; Vert, P.; Daval, J. L. *Exp Neurol* **2000**, *166*, 334-41.
- (168) Ngai, K. C.; Yeung, C. Y.; Karlberg, J. *Acta Paediatr Jpn* **1998**, *40*, 313-7.
- (169) Wang, W. W.; Smith, D. L.; Zucker, S. D. *Hepatology* **2004**, *40*, 424-33.
- (170) Liu, Y.; Li, P.; Lu, J.; Xiong, W.; Oger, J.; Tetzlaff, W.; Cynader, M. *J Immunol* **2008**, *181*, 1887-97.
- (171) Ollinger, R.; Wang, H.; Yamashita, K.; Wegiel, B.; Thomas, M.; Margreiter, R.; Bach, F. H. *Antioxid Redox Signal* **2007**, *9*, 2175-85.
- (172) Vetvicka, V.; Sima, P.; Miler, I.; Bilej, M. *Folia Microbiol (Praha)* **1991**, *36*, 112-9.
- (173) Haga, Y.; Tempero, M. A.; Kay, D.; Zetterman, R. K. *Dig Dis Sci* **1996**, *41*, 1468-74.
- (174) Haga, Y.; Tempero, M. A.; Zetterman, R. K. *Biochim Biophys Acta* **1996**, *1317*, 65-70.
- (175) Miler, I.; Sima, P.; Vetvicka, V.; Indrova, M.; Slavikova, M. *Allerg Immunol (Leipz)* **1988**, *34*, 177-84.
- (176) Sima, P.; Mala, J.; Miler, I.; Hodr, R.; Truxova, E. *Folia Microbiol (Praha)* **1980**, *25*, 483-90.
- (177) Rola-Plezczyński, M.; Hensen, S. A.; Vincent, M. M.; Bellanti, J. A. *J Pediatr* **1975**, *86*, 690-6.
- (178) Wu, J. F.; Chiang, B. L.; Chen, H. L.; Lai, H. S.; Chang, M. H.; Ni, Y. H. *Pediatr Res* **2006**, *60*, 602-6.
- (179) Field, E.; Horst, H. M.; Rubinfeld, I. S.; Copeland, C. F.; Waheed, U.; Jordan, J.; Barry, A.; Brandt, M. M. *Am J Surg* **2008**, *195*, 304-6; discussion 306-7.
- (180) Ahlfors, C. E.; Wennberg, R. P.; Ostrow, J. D.; Tiribelli, C. *Clin Chem* **2009**, *55*, 1288-99.
- (181) Nejedla, Z. *Pediatrics* **1970**, *45*, 102-4.
- (182) Vetvicka, V.; Miler, I.; Sima, P.; Taborsky, L.; Fornusek, L. *Folia Microbiol (Praha)* **1985**, *30*, 373-80.
- (183) McDonagh, A. F. *Pediatrics* **2007**, *120*, 175-8.
- (184) Malik, S. G.; Irwanto, K. A.; Ostrow, J. D.; Tiribelli, C. *BMC Res Notes* **2010**, *3*, 162.

- (185) Mireles, L. C.; Lum, M. A.; Dennery, P. A. *Pediatr Res* **1999**, *45*, 355-62.
- (186) Miler, I. *Cesk Pediatr* **1980**, *35*, 351-5.
- (187) Elson, L. A. *Br J Haematol* **1955**, *1*, 104-16.
- (188) Connors, T. A.; Elson, L. A. *Biochem Pharmacol* **1962**, *11*, 1221-32.
- (189) Bulmer, A. C.; Ried, K.; Blanchfield, J. T.; Wagner, K. H. *Mutat Res* **2008**, *658*, 28-41.
- (190) Ostrow, J. D.; Pascolo, L.; Tiribelli, C. *Pediatr Res* **2003**, *54*, 98-104.
- (191) McDonagh, A. F.; Assisi, F. *Biochem J* **1972**, *129*, 797-800.
- (192) Lyons, A. B.; Hasbold, J.; Hodgkin, P. D. *Methods Cell Biol* **2001**, *63*, 375-98.
- (193) Sharma, D.; Sandur, S. K.; Rashmi, R.; Maurya, D. K.; Suryavanshi, S.; Checker, R.; Krishnan, S.; Sainis, K. B. *Mutat Res* **2010**.
- (194) Chatterjee, S.; Premachandran, S.; Bagewadikar, R. S.; Poduval, T. B. *Radiat Res* **2005**, *163*, 351-5.
- (195) Sandur, S. K.; Ichikawa, H.; Pandey, M. K.; Kunnumakkara, A. B.; Sung, B.; Sethi, G.; Aggarwal, B. B. *Free Radic Biol Med* **2007**, *43*, 568-80.
- (196) Sandur, S. K.; Ichikawa, H.; Sethi, G.; Ahn, K. S.; Aggarwal, B. B. *J Biol Chem* **2006**, *281*, 17023-33.
- (197) Limon-Pacheco, J. H.; Hernandez, N. A.; Fanjul-Moles, M. L.; Gonshebat, M. E. *Free Radic Biol Med* **2007**, *43*, 1335-47.
- (198) Kusnierczyk, P.; Czarnomska, A.; Opolski, A.; Seshadri, M.; Zborowska, E.; Radzikowski, C.; Kisielow, P.; Pajtasz, E.; Steuden, I. *Arch Immunol Ther Exp (Warsz)* **1987**, *35*, 423-30.
- (199) Van Laethem, A.; Van Kelst, S.; Lippens, S.; Declercq, W.; Vandenabeele, P.; Janssens, S.; Vandenheede, J. R.; Garmyn, M.; Agostinis, P. *FASEB J* **2004**, *18*, 1946-8.
- (200) Hsu, S. C.; Gavrilin, M. A.; Tsai, M. H.; Han, J.; Lai, M. Z. *J Biol Chem* **1999**, *274*, 25769-76.
- (201) McLellan, L. I.; Lewis, A. D.; Hall, D. J.; Ansell, J. D.; Wolf, C. R. *Carcinogenesis* **1995**, *16*, 2099-106.
- (202) Cuadrado, A.; Garcia-Fernandez, L. F.; Gonzalez, L.; Suarez, Y.; Losada, A.; Alcaide, V.; Martinez, T.; Fernandez-Sousa, J. M.; Sanchez-Puelles, J. M.; Munoz, A. *J Biol Chem* **2003**, *278*, 241-50.
- (203) Wu, D.; Cederbaum, A. *Mol Pharmacol* **2004**, *66*, 749-60.
- (204) Kim, S. M.; Park, J. G.; Baek, W. K.; Suh, M. H.; Lee, H.; Yoo, S. K.; Jung, K. H.; Suh, S. I.; Jang, B. C. *Neurosci Lett* **2008**, *440*, 289-93.
- (205) Ward, K. W.; Prokscht, J. W.; Azzaranot, L. M.; Mumawa, J. A.; Roethke, T. J.; Stelman, G. J.; Walsh, M. J.; Zeigler, K. S.; McSurdy-Freed, J. E.; Kehlert, J. R.; Chokshi, J.; Levy, M. A.; Smith, B. R. *Xenobiotica* **2001**, *31*, 783-97.
- (206) Mazzone, G. L.; Rigato, I.; Ostrow, J. D.; Bossi, F.; Bortoluzzi, A.; Sukowati, C. H.; Tedesco, F.; Tiribelli, C. *Biochem Biophys Res Commun* **2009**, *386*, 338-44.
- (207) Pimstone, N. R.; Tenhunen, R.; Seitz, P. T.; Marver, H. S.; Schmid, R. *J Exp Med* **1971**, *133*, 1264-81.
- (208) Funk, D.; Schrenk, H. H.; Frei, E. *Biotechniques* **2007**, *43*, 178, 180, 182 passim.

- (209) Silva, R. F.; Rodrigues, C. M.; Brites, D. *J Hepatol* **2001**, *34*, 402-8.
- (210) Haddad, J. J. *Biochem Pharmacol* **2002**, *63*, 305-20.
- (211) Wilhelm, D.; Bender, K.; Knebel, A.; Angel, P. *Mol Cell Biol* **1997**, *17*, 4792-800.
- (212) Franco, R.; Cidlowski, J. A. *Cell Death Differ* **2009**, *16*, 1303-14.
- (213) Hammermann, C.; Goldstein, R.; Kaplan, M.; Eran, M.; Goldschmidt, D.; Eidelman, A. I. *Clin Chem* **1998**, *44*, 2551-3.
- (214) Franco, R.; Panayiotidis, M. I.; Cidlowski, J. A. *J Biol Chem* **2007**, *282*, 30452-65.
- (215) Han, Y. H.; Kim, S. H.; Kim, S. Z.; Park, W. H. *J Cell Biochem* **2008**, *104*, 862-78.
- (216) Jacobson, M. D.; Raff, M. C. *Nature* **1995**, *374*, 814-6.
- (217) Sedlak, T. W.; Snyder, S. H. *Pediatrics* **2004**, *113*, 1776-82.
- (218) De Sanctis, C.; Malandra, C.; Zanetti, P.; Fabris, C.; Ponzzone, A. *Minerva Pediatr* **1968**, *20*, 2010-3.
- (219) XANTHOU M., M.-S. E., CAMPBELL A.C., WALLSR C.A., ECONOMOU-MAYROV C., MATSANIOTIS N *Intensive Care in the Newborn* **1976**, 139.
- (220) Rubaltelli, F. F.; Piovesan, A. L.; Semenzato, G.; Barbato, A.; Ongaro, G. *Helv Paediatr Acta* **1977**, *32*, 129-33.
- (221) Svejcar, J.; Miler, I.; Pekarek, J. *J Clin Lab Immunol* **1984**, *13*, 145-9.
- (222) Thong, Y. H.; Rencis, V. *Acta Paediatr Scand* **1977**, *66*, 757-9.
- (223) Miler, I.; Vondracek, J.; Hromadkova, L. *Czech Med* **1979**, *2*, 29-40.
- (224) Miler, I.; Vondracek, J.; Hromadkova, L. *Folia Microbiol (Praha)* **1981**, *26*, 413-6.
- (225) Rubaltelli, F. F.; Granati, B.; Fortunato, A.; Piovesan, A.; Casara, G.; Colleselli, P.; Semenzato, G. *Biol Neonate* **1982**, *42*, 152-8.
- (226) Khan, N. M.; Poduval, T. B. *J Leukoc Biol* **2011**, *90*, 997-1015.
- (227) Zhai, R.; Sheu, C. C.; Su, L.; Gong, M. N.; Tejera, P.; Chen, F.; Wang, Z.; Convery, M. P.; Thompson, B. T.; Christiani, D. C. *Thorax* **2009**, *64*, 784-90.
- (228) Brienza, N.; Dalfino, L.; Cinnella, G.; Diele, C.; Bruno, F.; Fiore, T. *Intensive Care Med* **2006**, *32*, 267-74.
- (229) Harbrecht, B. G.; Zenati, M. S.; Doyle, H. R.; McMichael, J.; Townsend, R. N.; Clancy, K. D.; Peitzman, A. B. *J Trauma* **2002**, *53*, 517-23.
- (230) Khan, S. *Kathmandu Univ Med J (KUMJ)* **2006**, *4*, 281-9.
- (231) Monson, J. R.; Guillou, P. J. *Hepatogastroenterology* **1989**, *36*, 437-41.
- (232) Uchida, H.; Shibata, K.; Iwaki, K.; Kai, S.; Ohta, M.; Kitano, S. *Hepatogastroenterology* **2009**, *56*, 1194-8.
- (233) Guglielmi, A.; De Manzoni, G.; Girlanda, R.; Frameglia, M.; Cordiano, C. *Ann Ital Chir* **1997**, *68*, 635-41.
- (234) Mazza, E.; Carmignani, L.; Stecco, A.; Lucibello, P. *Tumori* **1999**, *85*, S54-9.
- (235) Dumanskii Iu, V.; Khaletskii, I. V. *Klin Khir* **2010**, 24-9.
- (236) Park, C. K.; Bae, S. H.; Yang, H. J.; Chun, H. J.; Choi, I. B.; Choi, J. Y.; Yoon, S. K. *Korean J Intern Med* **2011**, *26*, 94-8.

- (237) Herfarth, K. K.; Debus, J.; Lohr, F.; Bahner, M. L.; Rhein, B.; Fritz, P.; Hoss, A.; Schlegel, W.; Wannenmacher, M. F. *J Clin Oncol* **2001**, *19*, 164-70.
- (238) Kwon, J. H.; Bae, S. H.; Kim, J. Y.; Choi, B. O.; Jang, H. S.; Jang, J. W.; Choi, J. Y.; Yoon, S. K.; Chung, K. W. *BMC Cancer* **2010**, *10*, 475.
- (239) Seong, J.; Keum, K. C.; Han, K. H.; Lee, D. Y.; Lee, J. T.; Chon, C. Y.; Moon, Y. M.; Suh, C. O.; Kim, G. E. *Int J Radiat Oncol Biol Phys* **1999**, *43*, 393-7.
- (240) Choi, B. O.; Choi, I. B.; Jang, H. S.; Kang, Y. N.; Jang, J. S.; Bae, S. H.; Yoon, S. K.; Chai, G. Y.; Kang, K. M. *BMC Cancer* **2008**, *8*, 351.
- (241) Yamaguchi, K.; Kobayashi, K.; Ogura, Y.; Nakamura, K.; Nakano, K.; Mizumoto, K.; Tanaka, M. *Hepatogastroenterology* **2005**, *52*, 1605-12.
- (242) Nishimura, Y.; Hosotani, R.; Shibamoto, Y.; Kokubo, M.; Kanamori, S.; Sasai, K.; Hiraoka, M.; Ohshio, G.; Imamura, M.; Takahashi, M.; Abe, M. *Int J Radiat Oncol Biol Phys* **1997**, *39*, 39-49.
- (243) Nakayama, H.; Tsuji, K.; Matsui, R.; Shiotani, S.; Atake, S.; Isaka, N.; Wada, M.; Tokuuye, K.; Ishikawa, A.; Akine, Y. *Radiat Med* **2001**, *19*, 297-301.
- (244) Kuvshinoff, B. W.; Armstrong, J. G.; Fong, Y.; Schupak, K.; Getradjman, G.; Heffernan, N.; Blumgart, L. H. *Br J Surg* **1995**, *82*, 1522-5.
- (245) Saito, H.; Takada, T.; Miyazaki, M.; Miyakawa, S.; Tsukada, K.; Nagino, M.; Kondo, S.; Furuse, J.; Tsuyuguchi, T.; Kimura, F.; Yoshitomi, H.; Nozawa, S.; Yoshida, M.; Wada, K.; Amano, H.; Miura, F. *J Hepatobiliary Pancreat Surg* **2008**, *15*, 63-8.
- (246) Coleman, C. N.; Blakely, W. F.; Fike, J. R.; MacVittie, T. J.; Metting, N. F.; Mitchell, J. B.; Moulder, J. E.; Preston, R. J.; Seed, T. M.; Stone, H. B.; Tofilon, P. J.; Wong, R. S. *Radiat Res* **2003**, *159*, 812-34.
- (247) Pellmar, T. C.; Rockwell, S. *Radiat Res* **2005**, *163*, 115-23.
- (248) Greenberger, J. S. *In Vivo* **2009**, *23*, 323-36.
- (249) Fauci AS, B. E., Kasper DL *Radiation injury In: editors Harrison's Principles of Internal Medicine*, 2008; Vol. 17th ed. New York, NY.
- (250) EJ, H. *Radiobiology for the Radiologist*; Lippincott Williams and Wilkins, 2000.
- (251) Cervený TJ, M. T., Young RW *Acute radiation syndrome in humans*; TMM Publications, 1989.
- (252) Anno, G. H.; Baum, S. J.; Withers, H. R.; Young, R. W. *Health Phys* **1989**, *56*, 821-38.
- (253) Waselenko, J. K.; MacVittie, T. J.; Blakely, W. F.; Pesik, N.; Wiley, A. L.; Dickerson, W. E.; Tsu, H.; Confer, D. L.; Coleman, C. N.; Seed, T.; Lowry, P.; Armitage, J. O.; Dainiak, N. *Ann Intern Med* **2004**, *140*, 1037-51.
- (254) DiCarlo, A. L.; Hatchett, R. J.; Kaminski, J. M.; Ledney, G. D.; Pellmar, T. C.; Okunieff, P.; Ramakrishnan, N. *Radiat Res* **2008**, *169*, 712-21.
- (255) Palmer, J. L.; Deburghgraeve, C. R.; Bird, M. D.; Hauer-Jensen, M.; Kovacs, E. J. *J Burn Care Res* **2011**, *32*, 317-23.
- (256) Shah, K. G.; Wu, R.; Jacob, A.; Blau, S. A.; Ji, Y.; Dong, W.; Marini, C. P.; Ravikumar, T. S.; Coppa, G. F.; Wang, P. *Mol Med* **2009**, *15*, 407-14.

- (257) Tan, X. X.; Actor, J. K.; Chen, Y. *Antimicrob Agents Chemother* **2005**, *49*, 3203-7.
- (258) Krogfelt, K. A.; Bergmans, H.; Klemm, P. *Infect Immun* **1990**, *58*, 1995-8.
- (259) Muller, C. M.; Aberg, A.; Straseviciene, J.; Emody, L.; Uhlin, B. E.; Balsalobre, C. *PLoS Pathog* **2009**, *5*, e1000303.
- (260) Billips, B. K.; Forrestal, S. G.; Rycyk, M. T.; Johnson, J. R.; Klumpp, D. J.; Schaeffer, A. J. *Infect Immun* **2007**, *75*, 5353-60.
- (261) Montravers, P.; Mohler, J.; Saint Julien, L.; Carbon, C. *Infect Immun* **1997**, *65*, 144-9.
- (262) Sterns, T.; Pollak, N.; Echtenacher, B.; Mannel, D. N. *Infect Immun* **2005**, *73*, 4905-12.
- (263) Branger, J.; van den Blink, B.; Weijer, S.; Madwed, J.; Bos, C. L.; Gupta, A.; Yong, C. L.; Polmar, S. H.; Olszyna, D. P.; Hack, C. E.; van Deventer, S. J.; Peppelenbosch, M. P.; van der Poll, T. *J Immunol* **2002**, *168*, 4070-7.
- (264) Siegfried, E. C.; Stone, M. S.; Madison, K. C. *Pediatr Dermatol* **1992**, *9*, 278-82.
- (265) Gies, H. P.; Roy, C. R. *Health Phys* **1990**, *58*, 313-20.
- (266) Karadag, A.; Yesilyurt, A.; Unal, S.; Keskin, I.; Demirin, H.; Uras, N.; Dilmen, U.; Tatli, M. M. *Mutat Res* **2009**, *676*, 17-20.
- (267) Tatli, M. M.; Minnet, C.; Kocyigit, A.; Karadag, A. *Mutat Res* **2008**, *654*, 93-5.
- (268) Christensen, T.; Reitan, J. B.; Kinn, G. *J Photochem Photobiol B* **1990**, *7*, 337-46.
- (269) Aycicek, A.; Kocyigit, A.; Erel, O.; Senturk, H. *J Pediatr (Rio J)* **2008**, *84*, 141-6.
- (270) Aycicek, A.; Erel, O. *J Pediatr (Rio J)* **2007**, *83*, 319-22.
- (271) Kurt, A.; Aygun, A. D.; Kurt, A. N.; Godekmerdan, A.; Akarsu, S.; Yilmaz, E. *Neonatology* **2009**, *95*, 262-6.
- (272) Sirota, L.; Straussberg, R.; Gurary, N.; Aloni, D.; Bessler, H. *Eur J Pediatr* **1999**, *158*, 910-3.
- (273) Wang, Y.; Schulte, B. A.; LaRue, A. C.; Ogawa, M.; Zhou, D. *Blood* **2006**, *107*, 358-66.
- (274) Xiaogang Du, H. P., Chengyun Zhang, Huaiyu Zhang, Hanmei Liu, Zhiyu Chen and Xianyin Zeng *Journal of Medicinal Plants Research* **2010**, *4*, 1647-1655.
- (275) Sablonniere, B.; Nicolas, J.; Neveux, Y.; Drouet, J. *Int J Radiat Biol Relat Stud Phys Chem Med* **1983**, *44*, 575-84.
- (276) Heslet, L.; Bay, C.; Nepper-Christensen, S. *Int J Gen Med* **2012**, *5*, 105-15.
- (277) MacVittie, T. J.; Monroy, R. L.; Patchen, M. L.; Souza, L. M. *Int J Radiat Biol* **1990**, *57*, 723-36.
- (278) May, A. K.; Gleason, T. G.; Sawyer, R. G.; Pruett, T. L. *Infect Immun* **2000**, *68*, 176-83.
- (279) Hau, T. *World J Surg* **1990**, *14*, 167-75.
- (280) Riche, F. C.; Cholley, B. P.; Panis, Y. H.; Laisne, M. J.; Briard, C. G.; Graulet, A. M.; Gueris, J. L.; Valleur, P. D. *Crit Care Med* **2000**, *28*, 433-7.

-
- (281) Badiu, D. C.; Paunescu, V.; Aungurenci, A.; Pasarica, D. *J Med Life* **2011**, *4*, 158-62.
- (282) Rodriguez-Ramos, C.; Galan, F.; Diaz, F.; Elvira, J.; Martin-Herrera, L.; Giron-Gonzalez, J. A. *Dig Dis Sci* **2001**, *46*, 1668-76.
- (283) Chand, N.; Sanyal, A. J. *Hepatology* **2007**, *45*, 230-41.
- (284) van den Broek, P.; Verkade, H. J.; Hulzebos, C. V. *Early Hum Dev* **2011**, *87*, 515-9.
- (285) Omar, C.; Hamza, S.; Bassem, A. M.; Mariam, R. *N Am J Med Sci* **2011**, *3*, 544-7.
- (286) Plum, J.; Tabatabaei, M. M.; Lordnejad, M. R.; Pipinika, O.; Razeghi, P.; Huang, C.; Meyer-Kirchrath, J.; Grabensee, B. *Perit Dial Int* **1999**, *19 Suppl 2*, S378-83.
- (287) Moshyedi, A. K.; Josephs, M. D.; Abdalla, E. K.; Mackay, S. L.; Edwards, C. K., 3rd; Copeland, E. M., 3rd; Moldawer, L. L. *Infect Immun* **1998**, *66*, 1800-2.
- (288) Martineau, L.; Shek, P. N. *Crit Care Med* **2000**, *28*, 788-94.
- (289) Song, G. Y.; Chung, C. S.; Chaudry, I. H.; Ayala, A. *Am J Physiol Cell Physiol* **2001**, *281*, C662-9.
- (290) Nick, J. A.; Young, S. K.; Brown, K. K.; Avdi, N. J.; Arndt, P. G.; Suratt, B. T.; Janes, M. S.; Henson, P. M.; Worthen, G. S. *J Immunol* **2000**, *164*, 2151-9.
- (291) Lu, J.; Yang, Z.; Jiang, J.; Wang, Z.; Zhu, P. *Chin J Traumatol* **2001**, *4*, 75-7.
- (292) Frazier, W. J.; Wang, X.; Wancket, L. M.; Li, X. A.; Meng, X.; Nelin, L. D.; Cato, A. C.; Liu, Y. *J Immunol* **2009**, *183*, 7411-9.
- (293) Salojin, K. V.; Owusu, I. B.; Millerchip, K. A.; Potter, M.; Platt, K. A.; Oravec, T. *J Immunol* **2006**, *176*, 1899-907.

ANNEXURE

Trypan blue dye solution: 0.5% Trypan Blue+ 0.9% NaCl in 1X PBS, For 100ml:

Trypan Blue 0.5g+ NaCl 0.9g+ 1X PBS 100ml

Methylene blue solution: 1% methylene blue in 1% Glacial acetic acid prepared in Distilled Water

Mitogen dilutions: Concanavalin A: Stock solution 25mg/ml in RPMI. For working solution of 200µg/ml, add 40µl of stock solution and 4.960ml RPMI.

Lipopolysaccharide: Stock solution 5mg/ml in RPMI. For working solution of 50µg/ml add 0.2ml of stock solution and 9.8ml RPMI

Propidium Iodide (PI) Staining Solution: 50µg /ml PI in 0.1 % Na-citrate + 0.1 % Triton X-100, For 100 ml: Na Citrate 0.1g+Triton X-100, 0.1 ml+ PI 5mg+ 1X PBS 100ml

Phosphate Buffer Saline (PBS): 10mM, pH 7.4, For 100ml: NaCl 0.9g+ Na₂HPO₄ 0.126 g+ NaH₂PO₄ 0.0451g+ Distilled Water 100ml

Tris-Borate EDTA (5X): TRIZMA base 54g+ Boric acid 27.5g+0.5M EDTA 20ml (pH: 8.0)+ Distilled Water 1000 ml

Ethidium bromide: 10mg/ml in Distilled Water

Gel Loading Dye: Bromophenol Blue 0.25 % W/V+ Sucrose 40 % W/V in Distilled Water

Agarose Gel (1.8%): Agarose 1.8 g + 0.5X TBE 100ml + Ethidium Bromide (10mg/ml) 10µl

Lysis Buffer for DNA Ladder: 50mM Tris-Cl pH 8.0+ 10mM EDTA+ 5 L-Sarcosine 0.5 % + Proteinase-K 0.5 mg /ml, For 100ml: Tris-Cl 0.605 gm + EDTA 0.372g + S L-Sarcosine 0.5g + Proteinase-K 0.05g + Distilled Water 100ml

Griess Reagent: Sulphanilamide 500mg+ Naphthylethylene diamine dihydrochloride (NEDDH) 50mg + H₃PO₄ 1.25ml+ Distilled Water 50ml

Neutral Buffered Formalin For Tissue Fixation: NaH₂PO₄ 4g+ Na₂HPO₄ 6.5g+ 40% Formaldehyde 100ml+ Distilled Water 900ml

Coating Buffer (0.1 M Sodium Carbonate): NaHCO₃ 8.4g+ Na₂CO₃ 3.56g+ Distilled Water 1000ml and adjust pH to 9.5

Assay Diluent: 1X PBS + 10% FCS

Wash Buffer: 1X PBS + 0.05% Tween 20

Stop solution: 0.1N HCl

LIST OF PUBLICATIONS

(A) In International Peer Reviewed Journal

1. **Nazir M Khan**, Sandur SK, Checker R, Sharma D, Poduval TB, Sainis KB. Pro-oxidants ameliorate radiation-induced apoptosis through activation of the calcium-ERK1/2-Nrf2 pathway. **Free Radic Biol Med.** 2011 Jul 1; 51(1):115-28. Epub 2011 Apr 8. PubMed PMID: 21530647.
2. **Nazir M Khan**, Poduval T.B. Immunomodulatory and Immunotoxic effects of bilirubin: Molecular mechanism. **J. leuk. Biol.** 2011 Nov; 90(5):997-1015. Epub 2011 Aug 1. PMID: 21807743.
3. **Nazir M. Khan**, Poduval T. B. Bilirubin augments radiation injury and leads to increased infection and mortality in mice: Molecular mechanisms. **Free Radic Biol Med.** (Accepted), 2012
4. Premachandran S, **Nazir M. Khan**, Thakur VS, Shukla J, Poduval T. B. Differential immunotoxic effects of ethanol on murine EL-4 lymphoma and normal lymphocytes is mediated through increased ROS production and activation of p38MAPK. **Immunopharmacology and Immunotoxicology**, 2012 Aug; 34(4):616-26.
5. Wilankar C, **Nazir M. Khan**, Checker R., Sharma D., Patwardhan R.S., Gota V., Sandur S.K., Devasagayam T. P. A. γ -Tocotrienol Induces Apoptosis in Human T Cell Lymphoma through Activation of Both Intrinsic and Extrinsic Pathways: **Curr Pharm Des**, 2011, 17 (21) : 2176-89. PMID: 21774779.
6. Shukla J, **Nazir M. Khan**, Thakur VS, Poduval TB. L-Arginine Mitigates Radiation-Induced Early Changes in Cardiac Dysfunction: The Role of Inflammatory Pathways. **Radiat Res.** 2011 Aug; 176(2):158-69. Epub 2011 Jun 10. PMID: 2166339.
7. Checker R, Sharma D, Sandur SK, **Nazir M. Khan**, Patwardhan RS, Kohli V, Sainis KB. Vitamin K3 suppressed inflammatory and immune responses in a redox-dependent manner. **Free Radic Res.** 2011 Aug; 45(8):975-85. Epub 2011 Jun 9. PMID: 21651451.
8. Wilankar C, Sharma D, Checker R, **Nazir M. Khan**, Patwardhan R, Patil A, Sandur SK, Devasagayam TP. Role of immunoregulatory transcription factors in differential immunomodulatory effects of tocotrienols. **Free Radic Biol Med.** 2011 Jul;51(1):129-43. Epub 2011 Apr 8. PubMed PMID: 21536125.

(B) In National Journal

1. **Mohd Nazir Khan**, Santosh Kumar Sandur, Rahul Checker, Deepak Sharma, T. B. Poduval and K.B. Sainis. Radioprotective Effects of Pro-oxidants. **Advanced Biotech, Journal of Biotechnology** (ISSN:0973-0109) 2010, Nov; 10(05): 100

(C) In Conference/Symposia

1. **Nazir M. Khan**, Santosh Kumar Sandur, Rahul Checker, Deepak Sharma, and T. B. Poduval. 1,4 Naphthoquinone protect radiation induced death and DNA damage in lymphocyte by enhancement in DNA repair. International Conference on Emerging Frontiers and Challenges in Radiation Biology. Bikaner, India, January 24th – 25th, 2012.
2. **Nazir M. Khan**, H. N. Bhilwade, Rahul Checker, Deepak Sharma, Vikram Gota and Santosh K. Sandur. Withaferin- α offers radioprotection via activation of repair of radiation induced DNA strand breaks in lymphocytes. International Conference on “Emerging Trends in Free Radicals, Antioxidants and nutraceuticals on Health, Disease and Radiation Biology. Kolkata, India, January 12th -14th, 2012.
3. Chandan Wilankar C, **Nazir M. Khan**, Rahul Checker R., Deepak Sharma, Patwardhan R.S., Gota V., Sandur S.K., Devasagayam T. P. A. γ -Tocotrienol Induces Apoptosis in Human T Cell Lymphoma through Activation of Both Intrinsic and Extrinsic Pathways. International Conference on “Emerging Trends in Free Radicals, Antioxidants and nutraceuticals on Health, Disease and Radiation Biology. Kolkata, India, January 12th-14th, 2012.
4. Sudha Premachandran, **Nazir M. Khan**, Vikas S. Thakur, Jyoti Shukla, and T. B. Poduval. Differential immunotoxic effects of ethanol on murine EL-4 lymphoma and normal lymphocytes is mediated through increased ROS production and activation of p38MAPK. International Symposium on Innovation in Free Radical Research and Experimental Therapeutics, Coimbatore, India, December 7th-9th, 2011.
5. Goswami M, Deepak Sharma, **Nazir M. Khan**, Shweta Suryavanshi, Santosh Kumar Sandur, Narendra Jawali. Effects of Antioxidant on Streptomycin Mediated Clearance of Acute Bacterial Peritonitis in Swiss Albino Mice. International Conference on Recent Trends on Therapeutic Advancement of Free Radical Science, Chennai, India, January 9th-11th, 2011.
6. **Mohd Nazir Khan**, Santosh Kumar Sandur, Rahul Checker, Deepak Sharma, T. B. Poduval and K.B. Sainis. Radioprotective Effects of Pro-oxidants. International Conference on Radiation Biology: Nanotechnology, Imaging and Stem Cells in Radiation Oncology. Chennai, India, November 15th-17th, 2010.
7. Shweta Suryavanshi, **Mohd Nazir Khan**, Rahul Checker, Deepak Sharma, S. Santosh Kumar and K. B. Sainis Radioprotective Effects of Chlorophyllin on Hematopoietic System. International Conference on Advances in Free Radical Research: Natural Products, Antioxidants and Radioprotectors. Hyderabad, India, January 11th-13th, 2010.
8. **Mohd Nazir Khan**, Shweta Suryavanshi, Deepak Sharma, Rahul Checker, Sandur Santosh Kumar, T. B. Poduval. Investigation of the radioprotective efficacy of 1, 4-Naphthoquinone against gamma-radiation induced cellular damage in murine lymphocytes. International Conference on Advances in Free Radical Research: Natural Products, Antioxidants and Radioprotectors. January 11th-13th, 2010.
9. **Mohd Nazir Khan**, Rahul Checker, Deepak Sharma, Rashmi Raghu, S. Santosh Kumar and T. Balakrishna Poduval. Immunomodulation by NF-kappaB inhibitors

from natural sources. International Conference on Advances in Free Radical Research: Natural Products, Antioxidants and Radioprotectors. Lucknow, India, March 19th-21th, 2009.

10. **Mohd Nazir Khan**, Deepak Sharma, Rahul Checker, Rashmi Raghu, T. B. Poduval Radioprotective and Immunomodulatory Properties of Bilirubin. Life Sciences Symposium on Recent Advances in Immunomodulation in Stress and Cancer. Mumbai, India December 22th-24th, 2008.

(D) In News Letter

1. **Nazir M. Khan**, T. B. Poduval. Is antioxidant property, a better approach to find a radioprotector? **Radiation Science Today**, 2012, Issue 19, July, 4-6.

Oral Presentation:

1. **Nazir M. Khan**, Santosh Kumar Sandur, Rahul Checker, Deepak Sharma, and T. B. Poduval. 1,4 Naphthoquinone protect radiation induced death and DNA damage in lymphocyte by enhancement in DNA repair. International Conference on Emerging Frontiers and Challenges in Radiation Biology. Bikaner, India, January 24th-25th, 2012.
2. **Mohd Nazir Khan**, Santosh Kumar Sandur, Rahul Checker, Deepak Sharma, T. B. Poduval and K.B. Sainis. Radioprotective Effects of Pro-oxidants. International Conference on Radiation Biology: Nanotechnology, Imaging and Stem Cells in Radiation Oncology. Chennai, India, November 15th-17th, 2010.

Awards Received:

1. My paper (**J. leuk. Biol. 2011 Nov; 90(5):997-1015**) was enlisted in the series publication by **Global Medical Discovery**, a **Canadian based company** serving alerts the scientific community to **breaking journal articles** considered to be of importance to the **drug discovery Process**.
2. **Travel award** from Indian Society of Radiation Biology for Oral presentation at International Conference on Emerging Frontiers and Challenges in Radiation Biology. Bikaner, India, January 24th – 25th, 2012.
3. **Best Poster Award** in International Conference on “Emerging Trends in Free Radicals, Antioxidants and Nutraceuticals on Health, Disease and Radiation Biology held in Kolkata, India, January 12th -14th, 2012.



Original Contribution

Pro-oxidants ameliorate radiation-induced apoptosis through activation of the calcium–ERK1/2–Nrf2 pathway

Nazir M. Khan, Santosh K. Sandur, Rahul Checker, Deepak Sharma¹, T.B. Poduval, Krishna B. Sainis^{*}

Bio-Medical Group, Radiation Biology & Health Sciences Division, Bhabha Atomic Research Centre, Mumbai 400085, India

ARTICLE INFO

Article history:

Received 25 October 2010

Revised 18 March 2011

Accepted 28 March 2011

Available online 8 April 2011

Keywords:

Naphthoquinone

ERK

Nrf2

Radioprotection

Heme oxygenase-1

Free radicals

ABSTRACT

There are no reports describing the ability of pro-oxidants to protect against radiation-induced apoptosis. Activation of the redox-sensitive transcription factor Nrf2 by low levels of ROS is known to protect against oxidative stress-induced cell death. In this study, hydrogen peroxide, diethylmaleate, and 1,4-naphthoquinone (NQ) exhibited complete protection against radiation-induced cell death in lymphocytes as estimated by propidium iodide staining. Radioprotection by NQ was demonstrated by inhibition of caspase activation, decrease in cell size, DNA fragmentation, nuclear blebbing, and clonogenic assay. Interestingly, NQ offered protection to lymphocytes even when added to cells postirradiation. NQ increased intracellular ROS levels and decreased GSH levels. NQ activated Nrf2 and increased the expression of the cytoprotective gene heme oxygenase-1 in lymphocytes. NQ increased ERK phosphorylation, which is upstream of Nrf2, and this ERK activation was through increased intracellular calcium levels. Administration of NQ to mice offered protection against whole-body irradiation (WBI)-induced apoptosis in splenic lymphocytes and loss of viability of spleen and bone marrow cells. It restored WBI-mediated changes in hematological parameters and functional responses of lymphocytes. Importantly, NQ rescued mice against WBI-induced mortality. These results demonstrated that a pro-oxidant such as NQ can protect against radiation-induced apoptosis by activation of multiple prosurvival mechanisms including activation of the calcium–ERK1/2–Nrf2 pathway.

© 2011 Elsevier Inc. All rights reserved.

Reactive oxygen species (ROS) are known to play a dual role as both deleterious and beneficial molecules [1]. Under normal physiologic conditions, the balance between the generation and the elimination of ROS maintains redox homeostasis. High amounts of ROS are known to induce cell death, whereas low levels are shown to activate prosurvival pathways such as nuclear factor E2-related factor-2 (Nrf2). There are several reports in the literature demonstrating protection by pro-oxidants in neuronal cell lines against oxidative insults [2–4]. Based on these reports this study was undertaken to investigate the radioprotective ability of pro-oxidants such as hydrogen peroxide (H₂O₂), diethylmaleate (DEM), and 1,4-naphthoquinone (NQ) in lymphocytes. Detailed mechanistic studies on radioprotection by pro-oxidants were carried out using NQ.

1,4-Naphthoquinone, the parent molecule of many clinically approved anticancer, anti-infective, and antiparasitic drugs such as anthracycline, mitomycin, daunorubicin, doxorubicin, diospyrin, and malarone, has been studied as a model molecule for biologically important quinones [5–9]. Quinones, such as phyloquinone (vitamin K1) and menadione (vitamin K3), take part in the blood clotting process, and ubiquinone (coenzyme Q10) acts as an electron carrier in the mitochondrial electron transport chain. In general, the biological activity of a quinone has been attributed to its ability to undergo reversible oxidation–reduction reactions, as well as its electrophilic nature leading to arylation of cellular nucleophiles such as thiols in cysteine residues of proteins and glutathione (GSH) [10]. The pro-oxidant property of naphthoquinones is responsible for initiation of tissue damage selectively in tumor cells [11,12].

Acute radiation injury is associated with severe damage to the immune system. In lymphoid organs such as spleen and thymus, radiation induces massive apoptosis. Conventional radioprotectors such as amifostine, N-acetylcysteine, and other antioxidants are free radical scavengers [13–16]. Recent studies suggest that exposure of cells to pro-oxidants, which are key inducers of the redox-sensitive transcription factor Nrf2, results in activation of cytoprotective genes encoding phase 2 detoxifying and antioxidant defense enzymes such as heme oxygenase-1, MnSOD, and GPx [17,18]. Activation of the Nrf2–antioxidant response element (ARE) pathway by natural compounds has been implicated in the prevention of cancer, ischemia,

Abbreviations: BAPTA-AM, 1,2-bis(*o*-aminophenoxy)ethane-*N,N,N',N'*-tetraacetic acid tetra(acetoxymethyl) ester; DCFH₂-DA, dichlorodihydrofluorescein diacetate; DEM, diethylmaleate; ERK, extracellular signal-regulated kinase; MnTBAP, Mn(III) tetrakis(4-benzoic acid)porphyrin chloride; MMP, mitochondrial membrane potential; NAC, N-acetylcysteine; NQ, 1,4-naphthoquinone; Nrf2, nuclear factor E2-related factor-2; ROS, reactive oxygen species.

^{*} Corresponding author. Fax: +91 22 25505326.

E-mail address: kbsainis@barc.gov.in (K.B. Sainis).

¹ Present address: McArdle Laboratory for Cancer Research, University of Wisconsin at Madison, Madison, WI 53706, USA.

and inflammatory diseases [19,20]. Kim et al. reported that activation of the Nrf2–ARE pathway led to protection against hydrogen peroxide-induced cell death in rat PC12 cells [21]. Sulfur amino acid deprivation and *tert*-butylhydroquinone, a representative pro-oxidant, induce glutathione S-transferase A2 primarily through binding of Nrf2 to the antioxidant response element in the promoter region [22]. Using genetically modified gain- and loss-of-function mutants of Nrf2, it has been established that constitutive activation of Nrf2 confers radioresistance in non-small-cell lung cancer cells [23]. Considering the ability of low levels of ROS to initiate an adaptive response against further oxidative challenge we hypothesized that pro-oxidants might protect against radiation-induced damage via activation of the Nrf2–ARE pathway. Our results, reported herein, clearly demonstrate activation of the Nrf2–Keap1 signaling pathway by NQ and subsequent expression of the cytoprotective gene heme oxygenase-1 (HO-1), which confers protection against radiation-induced apoptosis.

Materials and methods

Reagents

NQ, RPMI 1640 medium, ethylene glycol tetraacetic acid (EGTA), *N*-acetylcysteine (NAC), propidium iodide (PI), Hoechst-33258, DEM, dimethyl sulfoxide (DMSO), Fura-2AM, JC-1, thapsigargin, BAPTA-AM, all-*trans*-retinoic acid (ATRA), crystal violet, protein tyrosine phosphatase assay kit, glutathione assay kit, and Alexa532-labeled anti-rabbit secondary antibody were purchased from Sigma Chemical Co. (USA). Tin protoporphyrin (SnPP) was purchased from Tocris UK. Fetal calf serum (FCS) and Dulbecco's modified Eagle medium were obtained from GIBCO BRL. Mn(III)tetrakis(4-benzoic acid)porphyrin (MnTBAP) and ERK inhibitor (Cat. No. 328006) were purchased from Calbiochem (USA). Mouse CD4⁺ and CD19⁺ cell sorting kits were purchased from Stem Cell Technology (USA). Homogeneous caspase assay kit was obtained from Roche Applied Science (Germany). Live/Dead Cell Assay kit and Lipofectamine were obtained from Invitrogen. Mouse methylcellulose complete medium was obtained from R&D Systems. Monoclonal antibodies against pERK, CD3, CD4, CD14, and Bax labeled with phycoerythrin (PE) and monoclonal antibodies against CD19 and CD8 labeled with FITC were obtained from BD Biosciences (USA). Nrf2 short hairpin RNA (shRNA) plasmids were obtained from Santa Cruz Biotechnology (USA). Antibodies against Nrf2 and PE-labeled anti-HO-1 were purchased from Abcam (USA).

Animal maintenance

Six- to eight-week-old inbred BALB/c male mice, weighing approximately 20–25 g, reared in the animal house of the Bhabha Atomic Research Centre were used. The guidelines issued by the Institutional Animal Ethics Committee of the Bhabha Atomic Research Centre, Government of India, regarding the maintenance and dissection of small animals were strictly followed.

Cell line and culture

Int407, a human embryonic intestinal epithelial cell line, was grown in RPMI 1640 medium supplemented with 10% FCS.

Preparation of splenic lymphocytes and treatment with NQ

Spleens were aseptically removed and placed in sterile dishes containing RPMI 1640 medium. Single-cell suspensions were prepared by gently teasing the spleen on a sterile nylon mesh placed in the dish. Splenocytes were centrifuged and red blood cells were lysed by brief hypotonic shock. In all in vitro experiments, cells were

pretreated with NQ (1 μ M) for 2 h in RPMI medium before irradiation. DMSO was used as vehicle control in vitro.

Irradiation schedule

BALB/c mice, their spleen cells, and Int407 cells suspended in medium were exposed to radiation using a ⁶⁰Co γ -irradiator at a dose rate of 2.93 Gy/min (Gamma Cell220; AECL, Canada). Nrf2 shRNA plasmid-transfected cells were irradiated at a dose rate of 1.98 Gy/min in a blood irradiator (BRIT, Mumbai, India).

Estimation of cell death by PI staining

Lymphocytes (1×10^6) were incubated with or without NQ (1 μ M) for 2 h or H₂O₂ (10 min) or DEM for 1 h before irradiation (4 Gy) and cultured for 24 h at 37 °C. Cells treated with H₂O₂ were washed with medium before irradiation to eliminate its potential toxicity and PI staining was done as reported earlier [7].

Live and dead assay

To measure radiation-induced cell death, the Live/Dead Cell Assay kit was used as per the manufacturer's protocol.

Colony-forming unit (CFU) assay

To measure the proliferating capacity of hematopoietic stem cells present in the spleen, an in vitro colony-forming cell assay was performed using mouse methyl cellulose-complete medium according to the manufacturer's protocols. Characterization and enumeration of multipotential progenitors (e.g., CFU-GEMM) and lineage-committed progenitors (e.g., CFU-GM) representing the various stages along the differentiation pathway was done using an inverted microscope and scoring grid.

Clonogenic cell survival assay

One thousand Int407 cells were seeded in 100-mm culture dishes, treated with NQ (1 μ M) for 2 h, and then irradiated at 4 or 6 Gy. Cells were allowed to grow for 14 days to form colonies, which were then stained with crystal violet (0.4 g/L; Sigma), and colonies were counted [24].

Estimation of apoptosis and nuclear Nrf2 levels by confocal microscopy

Lymphocytes (1×10^6) pretreated with or without NQ (1 μ M) for 2 h were exposed to radiation (4 Gy) and cultured for 24 h. The cells were centrifuged on coverslips, fixed with paraformaldehyde (4%), and stained with Hoechst dye. Nuclear condensation and fragmentation were counted in 10 randomly selected fields. Approximately 300 nuclei were examined for each sample and results were expressed as the number of apoptotic nuclei divided by the total number of nuclei counted.

In another experiment, lymphocytes were treated with NQ (1 μ M) for various time intervals. These cells were labeled with Nrf2 antibody as described previously [25]. Further, these cells were stained with Alexa532-labeled secondary antibody followed by Hoechst staining. Slides were examined using an LSM510 confocal microscope (Carl Zeiss, Jena, Germany) with a krypton–argon laser coupled to an Orthoplan Zeiss photomicroscope using a 488-nm laser line and a 530-nm band-pass filter.

Transfection of lymphocytes with Nrf2 shRNA plasmid

Lymphocytes (1.5×10^6) were plated in 24-well plates in triplicate. Nrf2 shRNA plasmid (2 μ g) or an equivalent amount of scrambled

plasmid was transfected using Lipofectamine transfection reagent. After 6 h of transfection, the cells were cultured in complete medium for the next 18 h and then washed once and exposed to 2 Gy. Cells were then cultured for 24 h at 37 °C and cell death was estimated by PI staining, live and dead assay, and DNA fragmentation assay.

Estimation of radiation-induced apoptosis using DNA ladder assay

Lymphocytes (1×10^6 cells) were incubated with NQ (1 μ M) for 2 h and irradiated in vitro (4 Gy). These cells were further cultured overnight at 37 °C. Then the cells were lysed and their DNA was loaded on an agarose gel as described earlier [13].

Measurement of intracellular calcium levels

Lymphocytes (1×10^6 cells) were stained with Fura-2AM (2 μ M) for 30 min and treated with or without NQ (1 μ M) for the indicated time intervals. The fluorescence was measured in a spectrofluorimeter (BMG Labtech Optima) using 335 nm excitation and 500 nm emission [26].

Antibody staining

Lymphocytes (3×10^6 cells) were incubated for the indicated time intervals in the presence or absence of NQ (1 μ M). Cultured cells were stained with PE-labeled anti-Bax or anti-HO-1 or anti-phosphoERK-1 antibodies according to the method described earlier [27]. For surface staining, splenocytes (1×10^6) obtained from treated animals were stained with PE-conjugated antibodies to CD3, CD4, or CD14 or with FITC-conjugated antibodies to CD8 or CD19 as described earlier [7].

Pro-oxidant measurements

To detect intracellular ROS, lymphocytes were preincubated with 20 μ M oxidation-sensitive dichlorodihydrofluorescein diacetate (DCFH₂-DA) or its oxidation-insensitive analogue fluorescein diacetate for 0.5 h at 37 °C and were further treated with NQ (1 μ M) or vehicle [28]. DMSO (0.1%) was used as vehicle. To ascertain the contribution of H₂O₂ to NQ-mediated increase in ROS, lymphocytes were treated with PEG-catalase (50 units/ml) for 2 h before the addition of NQ (1 μ M). After 1 h of incubation, the increase in fluorescence resulting from

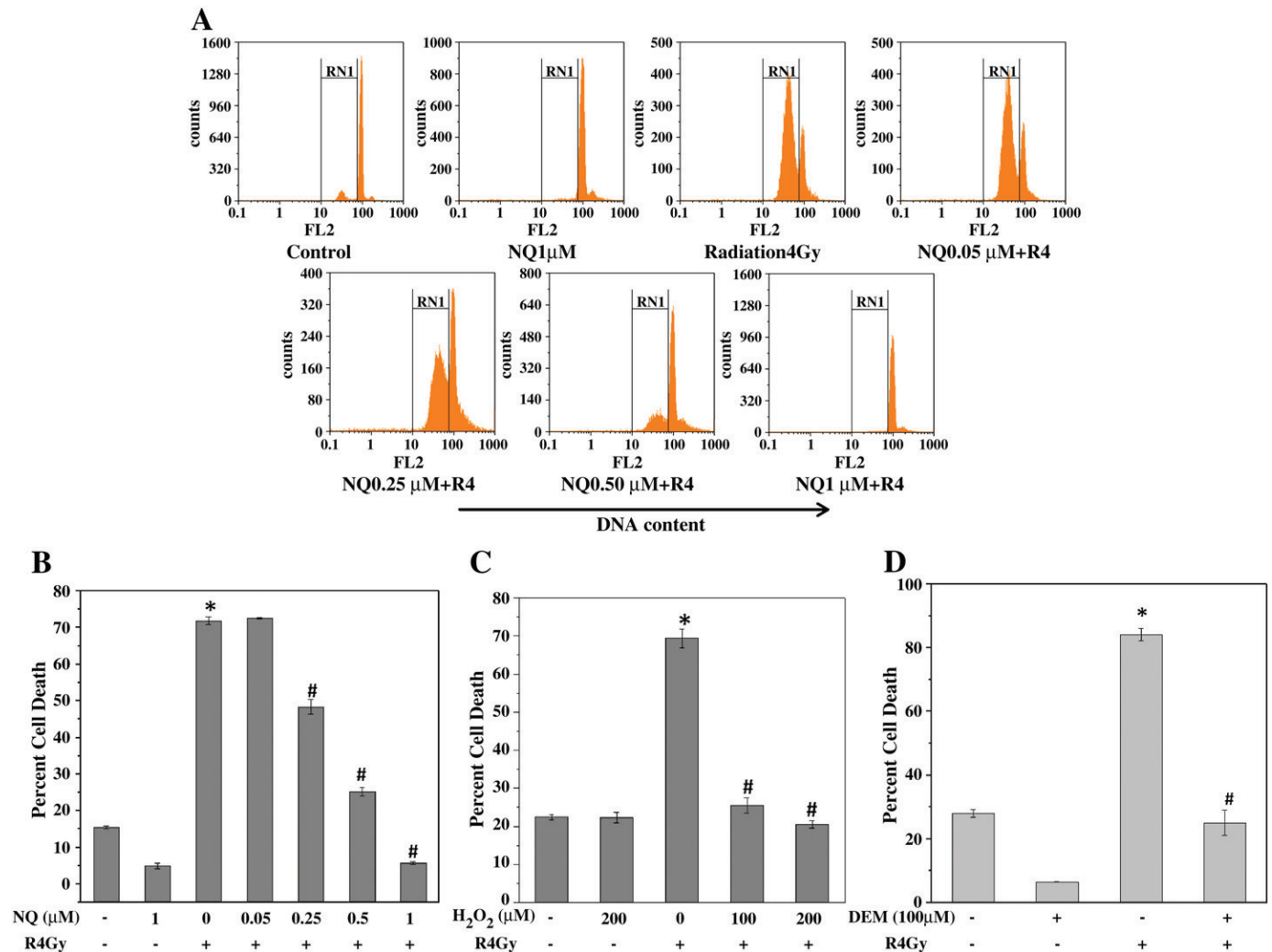


Fig. 1. (A) Flow cytometric histograms of NQ-treated cells exposed to radiation and stained with PI. Murine splenic lymphocytes were incubated with NQ (0.05–1 μ M) for 2 h at 37 °C, exposed to 4 Gy γ -irradiation, and further cultured for 24 h. Cells were harvested and stained with PI. Twenty thousand cells in each group were acquired using a flow cytometer. The Sub-G1 region (RN1) represents the percentage of cells undergoing apoptosis. (B–D) Bar diagrams showing radiation-induced percentage of apoptotic cells estimated by PI staining and its amelioration by treatment with (B) NQ, (C) H₂O₂, and (D) diethylmaleate. Each bar shows the mean \pm SEM from three replicates, and two such independent experiments were carried out. * p < 0.05, compared to vehicle-treated control, and # p < 0.05, compared to irradiated group.

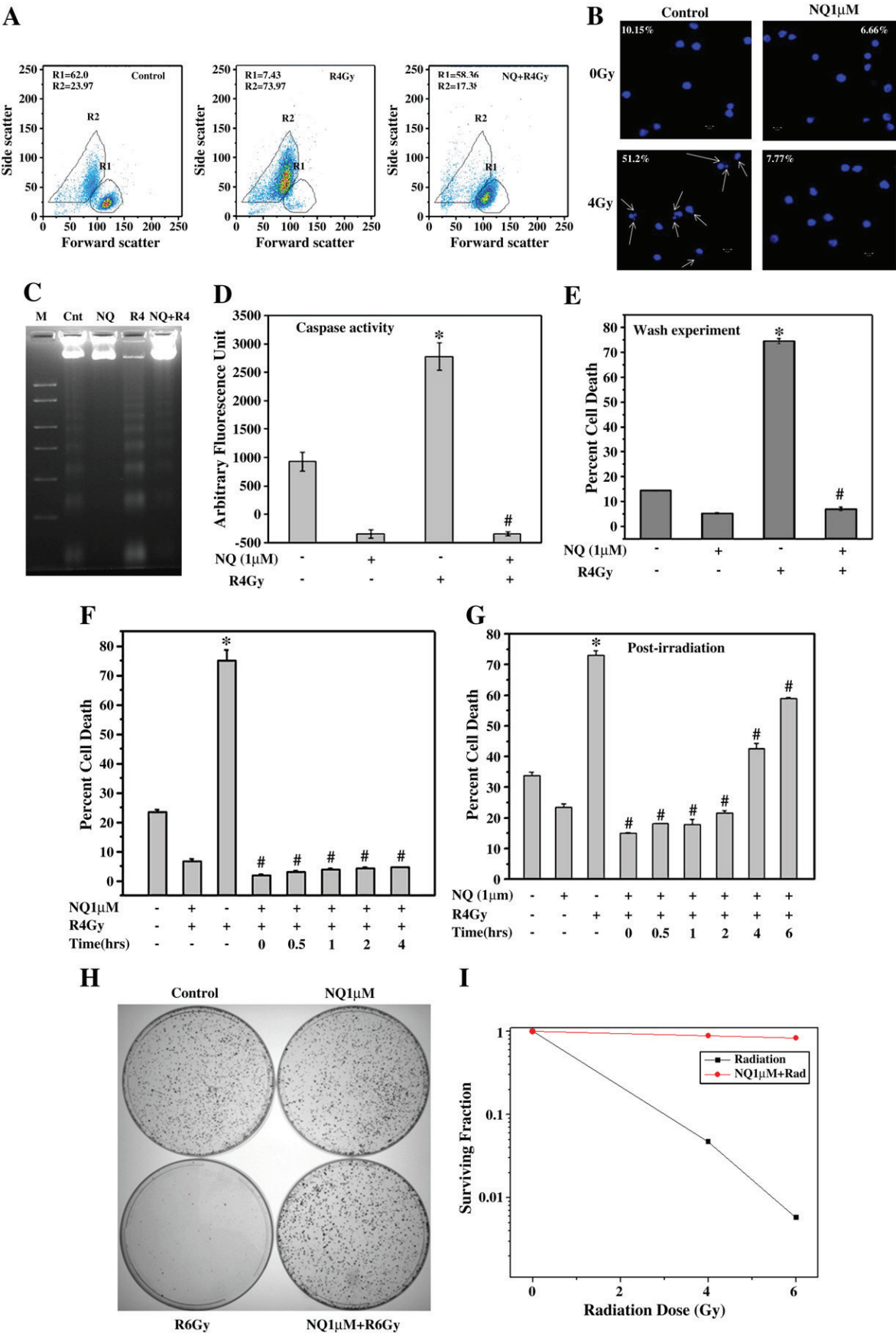


Table 1

NQ treatment prevented radiation-induced loss of proliferative capacity of various hematopoietic progenitor cells present in the spleen.

Treatment	Progenitor cells per 0.2×10^6 splenocytes plated				
	BFU-E	CFU-G	CFU-M	CFU-GM	CFU-GEMM
Control	27 ± 2.7	17 ± 2.0	10.5 ± 4.5	21 ± 2.3	1.5 ± 0.5
NQ	26 ± 1.0	19 ± 3.0	3.5 ± 2.5	24 ± 8.0	8.5 ± 0.5
R 4 Gy	4 ± 1.0*	2 ± 1.0*	1.5 ± 0.5*	0	0
NQ + R 4 Gy	43 ± 9.5#	4.5 ± 0.5#	8.5 ± 3.5#	35 ± 9.0	17.5 ± 0.5

Splenocytes were treated with NQ (1 μ M) for 2 h before being exposed to radiation of 4 Gy and cultured in methyl-cellulose-complete medium for 11 days. Colonies were enumerated under an inverted microscope using a scoring grid. Data are means \pm SEM. NQ, 1,4-naphthoquinone; R, radiation; CFU, colony-forming unit; G, granulocyte; M, macrophage; GM, granulocyte/macrophage; Granulocyte-Erythrocyte-Macrophage-Megakaryocyte, Burst Forming Unit-Erythroid.

* $p < 0.05$, compared to vehicle-treated controls.

$p < 0.05$, compared to irradiated group.

oxidation of DCFH₂ to DCF was measured using a spectrofluorimeter (BMG Labtech Optima) using 485 nm excitation and 535 nm emission.

Intracellular GSH assay

To measure intracellular GSH, lymphocytes were incubated with DEM (100 μ M) or treated with NQ (1 μ M) for the indicated times at 37 °C. DEM was used as a positive control for GSH depletion. GSH was measured by colorimetric assay using a glutathione assay kit as per the manufacturer's protocol.

Mass spectrometry (MS)

To characterize the products of reaction of NQ with NAC, MS analysis was carried out. MS was performed using a triple-quadrupole mass spectrometer with an electrospray ionization (ESI) source (Varian, Inc., USA). The ESI source operated in positive ionization mode.

RT-PCR

Total RNA from lymphocytes (5×10^6) cultured with and without NQ (1 μ M for 24 h) was isolated and reverse transcribed. The gene of interest was amplified from cDNA using primers for HO-1 (forward, 5'-AACAAGCAGAACCCAGTC-3', and reverse, 5'-TGTCATCTCCAGAGTGTTC-3') and β -actin (forward, 5'-CATCACTATTGGCAACGAGC-3', and reverse, 5'-GGACTGTTACTGAGTCGCT-3').

Protein tyrosine phosphatase assay

Lymphocytes were incubated with NQ for 2 h, whole-cell lysates were prepared, and phosphatase activity was estimated according to the manufacturer's protocol.

Administration of NQ to mice

BALB/c mice (five per group) were administered NQ (2 mg/kg body wt) intraperitoneally (ip) and were given whole-body irradiation (WBI; 4 Gy) after 0.5 h. These mice were sacrificed on day 5 after WBI and living spleen cells and bone marrow cells were enumerated by trypan blue dye exclusion. Hematological profiles were assessed by autoanalyzer. Plasma was isolated from blood and used for measure-

ment of cytokines (IL-1 β and IL-6) by ELISA and nitric oxide using the Griess reagent as described earlier [29].

Cytokine measurement

Splenic lymphocytes obtained from NQ-treated animals were cultured for 24 h in the presence or absence of concanavalin A (10 μ g/ml) and the concentrations of IL-2, IL-4, IL-6, and IFN- γ in their supernatants were evaluated [7].

Endogenous spleen colony assay

Mice (seven per group) treated with NQ or vehicle were sacrificed on day 9 after irradiation at 6 Gy and the spleens were removed immediately. Subsequently, the spleens were fixed in 10% buffered formalin and the spleen CFUs were counted manually as described previously [15].

In vivo radioprotection studies

Mice (five per group) were subjected to NQ (2 mg/kg body wt) treatment 0.5 h before WBI (4 Gy) and immediately sacrificed, and lymphocytes were cultured for 24 h at 37 °C. The cells were processed for homogeneous caspase activity, DNA fragmentation, nuclear blebbing, PI staining, Bax staining, and change in mitochondrial membrane potential using JC-1 (10 μ M) by spectrofluorimetry [30].

Survival studies

Mice were administered NQ (2 mg/kg body wt) ip and were given WBI (7 Gy) after 0.5 h. To estimate the dose modification factor (DMF), radiation doses between 6 and 8.5 Gy were used. Groups of 10 animals each were pretreated with a single ip injection of NQ (2 mg/kg body wt) and after 0.5 h irradiated with 6, 6.5, 7, 7.5, 8, or 8.5 Gy. The animals were monitored daily for 30 days after irradiation, and mortality and body weights were recorded. The average percentage mortality was converted into probit value as reported earlier [15] and DMF was calculated by taking the ratio of LD₅₀/30 days in the presence and absence of NQ.

Statistical analysis

Data are presented as means \pm SEM. The statistical significance of the differences with respect to all parameters studied between untreated and irradiated groups in the presence or absence of NQ was assessed by one-way ANOVA with Microcal Origin 7.5 software followed by post hoc analysis using Scheffe's test. Values of $p < 0.05$ were considered statistically significant.

Results

Exposure to radiation is thought to affect the host immune system to a great extent, because its cellular constituents are sensitive to radiation. In this study, amelioration of radiation-induced damage in murine splenic lymphocytes by pro-oxidants was assessed and the mechanism of action of NQ was investigated.

Fig. 2. (A) Change in forward and side scatter was used to assess the size and density of cells. Cells undergoing apoptosis showed low forward scatter and increases in cell density, (B) nuclear blebbing, (C) DNA fragmentation, and (D) homogeneous caspase (2, 3, 6, 7, and 9) activity. (E) Radioprotective effect of NQ is not reversible. Lymphocytes were washed twice with RPMI after 2 h of incubation with NQ and then irradiated with 4 Gy and cultured for 24 h. Cell death was estimated by PI staining. (F) Cells were treated with NQ for various time intervals (0 to 240 min) before being exposed to radiation, and percentage cell death was measured by PI staining. (G) Therapeutic potential of NQ in inhibiting radiation-induced cell death. NQ was added to lymphocytes at various time intervals after irradiation and cultured for 24 h. (H and I) Int407 cells were pretreated with NQ for 2 h before being exposed to 4 or 6 Gy and cultured for 14 days. Visible colonies were enumerated after staining with crystal violet. Each bar shows the mean \pm SEM from three replicates, and two such independent experiments were carried out. * $p < 0.05$, compared to vehicle-treated control, and # $p < 0.05$, compared to irradiated group.

NQ, H₂O₂, and DEM protected lymphocytes against radiation-induced cell death

Fig. 1A shows flow cytometric histograms of PI-stained cells exposed to radiation in the presence or absence of NQ. NQ (1 μ M) reduced basal cell death in lymphocytes, suggesting that it is not toxic to cells at this concentration (Fig. 1A). Exposure of cells to radiation (4 Gy) induced about 60% apoptotic cell death over control. NQ significantly inhibited radiation-induced apoptosis in a concentration-dependent manner (Fig. 1B). Other well-known pro-oxidants, H₂O₂ and DEM (thiol depletor), also offered complete protection against radiation-induced apoptosis (Figs. 1C and D).

The observed radioprotection by NQ was further confirmed by various assays such as changes in cell size (Fig. 2A), nuclear blebbing (Fig. 2B), DNA fragmentation (Fig. 2C), and caspase activity (Fig. 2D). To understand whether NQ is required to be present throughout to exhibit radioprotection, cells were washed 2 h after NQ addition and exposed to radiation. NQ offered complete protection against radiation-induced cell death despite the cells being washed (Fig. 2E). Incubation of cells with NQ (1 μ M) for various time intervals (0 to 240 min) before exposing them to radiation revealed 100% protection against radiation-induced cell death at all the time points used in our study (Fig. 2F). Supplementary Fig. S1A shows that NQ (1 μ M) mitigated radiation-induced cell death even up to a dose of 25 Gy. Radiation doses more than 8 Gy showed a significant decline in percentage apoptosis, suggesting that necrosis may be predominant at higher doses of radiation over apoptosis (Supplementary Fig. S1A). These results were in agreement with an earlier report from our laboratory [30]. It was also found that NQ protected significantly against radiation-induced cell death even when added after irradiation. Complete protection was observed by addition of NQ up to 2 h after irradiation. However, percentage protection decreased with increasing time interval (Fig. 2G). Colony-forming cell assay was performed to assess the proliferating ability of hematopoietic spleen cells in the presence of appropriate growth factors. NQ treatment before radiation prevented radiation-induced loss of proliferative capacity of various hematopoietic progenitor cells present in the spleen (Table 1). NQ protected multiple progenitors (e.g., CFU-GEMM) and lineage-committed progenitors, which form BFU-E and CFU-GM (Table 1). Further, clonogenic assay was also performed on a normal human intestinal cell line (Int407) and NQ also abrogated the loss of colony-forming ability of these cells exposed to 4 or 6 Gy of radiation (Figs. 2H and I).

NQ protected CD4⁺ T cells and B cells against radiation-induced death

Protecting CD4⁺ T cells against radiation-induced cell death may aid in effective antitumor immune responses after radiotherapy. Purified CD4⁺ T cells or CD19⁺ B cells were exposed to radiation in the presence or absence of NQ. NQ completely protected against radiation-induced death in CD4⁺ T cells as estimated by the increase in pre-G1 population and DNA fragmentation (Supplementary Figs. S1B and S1C). The radioprotective effect of NQ was not limited to CD4⁺ T cells. It also protected CD19⁺ B cells to the same extent at 1 μ M (Supplementary Fig. S1D).

NQ perturbed intracellular redox balance

Most of the radioprotectors from natural sources have been shown to act by scavenging radiation-derived free radicals [31–33]. Surprisingly, NQ elevated the basal ROS levels in splenic lymphocytes in a concentration-dependent manner as measured using DCFH₂-DA (Fig. 3A). It also increased mitochondrial ROS as measured by oxidation of dihydrorhodamine 123 (data not shown). NQ did not increase the fluorescence of the oxidation-insensitive dye fluorescein diacetate, suggesting that increased

fluorescence intensity seen with DCFH₂-DA could be attributed to its oxidation by ROS that are generated by NQ (Supplementary Fig. S2A). To identify the nature of the ROS induced by NQ, PEG-catalase was used before addition of NQ and it was observed that the NQ-mediated increase in fluorescence was significantly suppressed in the presence of PEG-catalase (Supplementary Fig. S2B). Fig. 3B shows that NQ exhibited marginal scavenging (14.67%) of radiation-derived ROS. NQ depleted intracellular GSH levels significantly in lymphocytes 2 h after treatment (Fig. 3C). Here DEM served as a positive control for GSH depletion.

NQ-mediated radioprotection was abrogated by thiol-containing antioxidants

To understand the involvement of NQ-mediated changes in ROS and GSH levels in the observed radioprotection, thiol and nonthiol antioxidants were used in combination with NQ. Fig. 3D shows that MnTBAP (nonthiol antioxidant) failed to abrogate the radioprotective efficacy of NQ, but NAC (thiol antioxidant) completely inhibited the action of NQ. However, when NAC was added to cells 2 h after NQ treatment, it failed to abrogate the radioprotective effect of NQ (Supplementary Fig. S3A). Both NAC and MnTBAP by themselves did not protect against radiation-induced cell death at the concentrations used (Fig. 3D). This suggested that depletion of thiol levels by NQ may play a role in the observed radioprotection.

Because the radioprotective effect of NQ was sensitive to the presence of thiol antioxidants, experiments were carried out to determine whether NQ physically interacted with a thiol group. NQ was incubated with NAC and subjected to HPLC separation. The retention time of pure NQ on a C18 column was 3.2 min (Supplementary Fig. S3B, black line). This peak height was attenuated when NQ was preincubated with NAC (blue line). These results indicate that NQ indeed reacts with NAC. To characterize the products, MS analysis was carried out. Molecular mass analysis revealed that the major peak corresponded to an NQ–NAC adduct ($M = 323.1$; Fig. 3E). In addition to NQ–NAC complex, another peak corresponding to m/z 162 was observed, which could be that of unreacted NAC.

NQ activated Nrf2 in lymphocytes and increased HO-1 expression

Because scavenging of radiation-derived ROS by NQ was a minor contributor to the observed radioprotection, it may be acting through activation of adaptive response pathways. One of them could be activation of a redox-sensitive transcription factors such as Nrf2. Fig. 4A shows the direct activation of Nrf2 by addition of NQ to lymphocytes. A significant accumulation of Nrf2 in the nucleus was seen after 4 h of addition of NQ to the lymphocytes. ATRA, an inhibitor of Nrf2, completely inhibited the radioprotection offered by NQ (Fig. 4B). To further substantiate the role of Nrf2 in radioprotection, Nrf2-knockdown cells were exposed to radiation. Figs. 4C–E show that cells transfected with Nrf2 shRNA plasmid were more sensitive to radiation than lymphocytes transfected with control shRNA as estimated by pre-G1 peak, live and dead cell assay, and DNA fragmentation assay. Expression of the Nrf2-dependent cytoprotective gene HO-1 was also upregulated by NQ in a dose- and time-dependent manner (Figs. 4F–H). As a corollary to this observation, addition of an inhibitor of HO-1 (SnPP) to lymphocytes suppressed the radioprotection offered by NQ (Fig. 4I).

NQ induced phosphorylation of ERK

Because Nrf2 is reported to be activated by ERK [34,35], we examined whether NQ induces phosphorylation of ERK in lymphocytes. We observed that addition of NQ to lymphocytes increased phosphorylation of ERK significantly in a time-dependent manner (Fig. 5A). A pharmacological inhibitor of ERK completely abolished

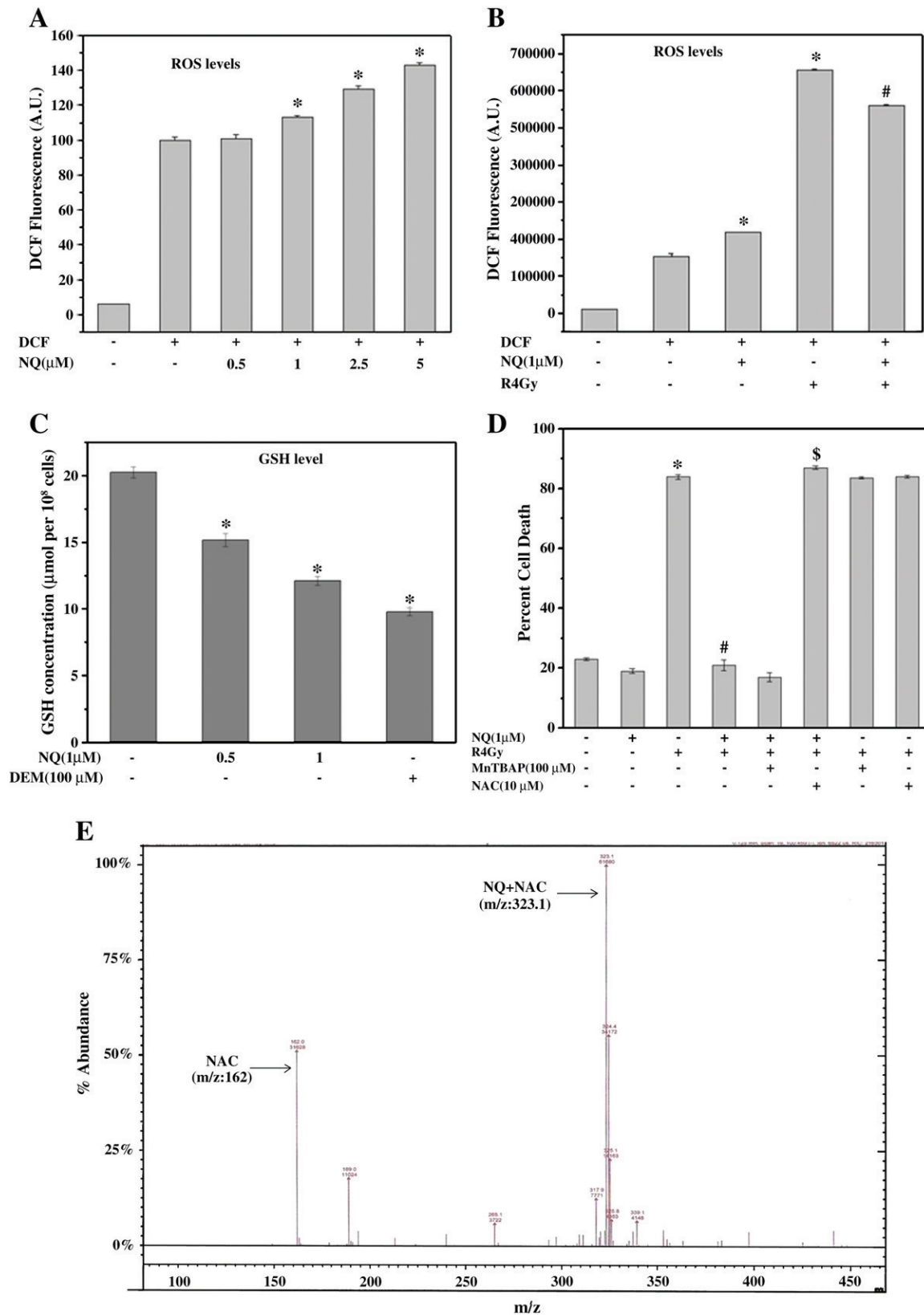
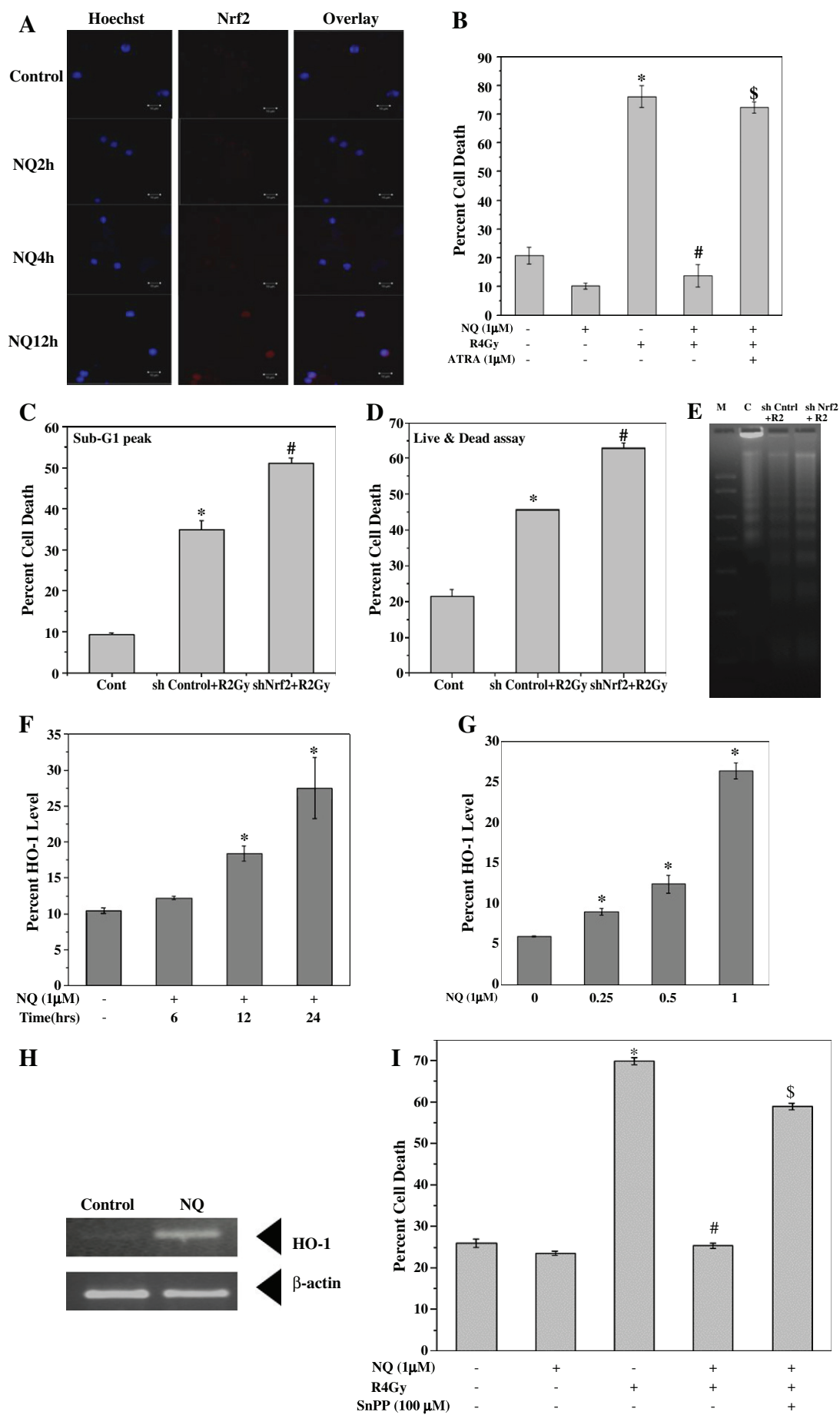


Fig. 3. (A) NQ increased ROS levels in lymphocytes. DCFH₂-DA-stained lymphocytes were treated with NQ for 2 h at 37 °C and fluorescence emission was measured at 535 nm. (B) NQ scavenged radiation-induced ROS marginally. Lymphocytes were treated with NQ for 2 h, stained with DCFH₂-DA, and irradiated with 4 Gy. (C) NQ depleted intracellular thiols. Lymphocytes were treated with NQ for 2 h and GSH level was measured using a glutathione assay kit. (D) Radioprotective effects of NQ were abrogated by thiol-containing antioxidant. Lymphocytes were incubated with NAC or MnTBAP for 1 h followed by treatment with NQ for 2 h. Cells were irradiated at 4 Gy and cultured for 24 h and stained with PI. Each bar represents the mean \pm SEM from three replicates, and three such independent experiments were carried out. * p < 0.05, compared to vehicle-treated control; # p < 0.05, compared to irradiated group; \$ p < 0.05, compared to major group in presence of NQ. (E) Identification of products of reaction of NQ with NAC by mass spectrometry. The samples were subjected to MS analysis using an ESI ion trap detector. Major peak at m/z 323.1 corresponds to NQ-NAC adduct and the other at m/z 162 may correspond to unreacted NAC.



NQ-mediated radioprotection (Fig. 5B). NQ-induced phosphorylation of ERK was accompanied by inhibition of cellular phosphatases (Fig. 5C).

NQ increased intracellular calcium levels

An earlier report by Schmidt et al. has shown that calcium activates the Raf–MEK–ERK pathway [35]. It was observed that treatment with NQ resulted in immediate elevation of intracellular Ca^{2+} , which peaked at 3 min, followed by a slow decline (Fig. 5D). To substantiate the role of calcium in radioprotection elicited by NQ, lymphocytes were incubated with BAPTA-AM (intracellular calcium chelator) or EGTA before the addition of NQ. The cells were then exposed to radiation and cultured for 24 h. BAPTA-AM and EGTA significantly abrogated NQ-mediated radioprotection (Fig. 5E). Thapsigargin, which elevated cytosolic calcium concentration similar to NQ, also offered significant protection against radiation-induced cell death (Fig. 5E). Further, incubation of lymphocytes with BAPTA-AM before treatment with NQ resulted in abrogation of phosphorylation of ERK, indicating that NQ offered radioprotection in lymphocytes via the Ca^{2+} –ERK–Nrf2 pathway (Fig. 5F).

In vivo radioprotection by NQ

To evaluate the relevance of our in vitro results, we examined the ability of NQ administration to ameliorate WBI-induced immunosuppression and myelosuppression. Administration of NQ (2 mg/kg body wt) to mice protected against WBI-induced loss of splenic lymphocytes and bone marrow viability as observed on day 5 (Figs. 6A and B). Because WBI-induced splenic atrophy was inhibited by NQ, we specifically monitored its effect on various phenotypes of spleen cells. NQ restored the counts of various lymphocyte subsets such as CD3^{+} T cells, CD4^{+} T helper cells, CD8^{+} T cytotoxic cells, CD19^{+} B cells, and also CD14^{+} macrophages (Table 2). NQ treatment protected the mice against WBI-induced leukopenia, lymphopenia, neutrophilia, thrombocytopenia, and erythropenia. It also protected the mice from WBI-induced decrease in hemoglobin level, packed cell volume, and mean corpuscular volume (Table 3). NQ administration to mice completely inhibited the WBI-induced increase in nitric oxide level (Supplementary Fig. S4A). To understand the in vivo radioprotective action of NQ, the plasma levels of IL-1 β and IL-6 were estimated. Administration of these cytokines to mice has been reported to stimulate bone marrow stem cells and offer radioprotection. The plasma levels of IL-1 β and IL-6 were significantly elevated with NQ administration to mice (Fig. 6C).

Because NQ rescued WBI-mediated loss of lymphocyte numbers, an experiment was set up to evaluate the functional response of the remnant lymphocytes upon stimulation with a mitogen. It was found that residual T cells from the NQ + WBI group responded significantly better than those from the vehicle + WBI group to concanavalin A as measured in terms of production of cytokines such as IL-2, IL-4, IL-6, and IFN- γ (Supplementary Fig. S4B). Importantly, NQ restored the proliferative potential of stem cells in mice after WBI, estimated in terms of endogenous spleen colony formation. The number of spleen

CFUs was significantly higher in the NQ + WBI group compared to the vehicle + WBI group (Fig. 6D).

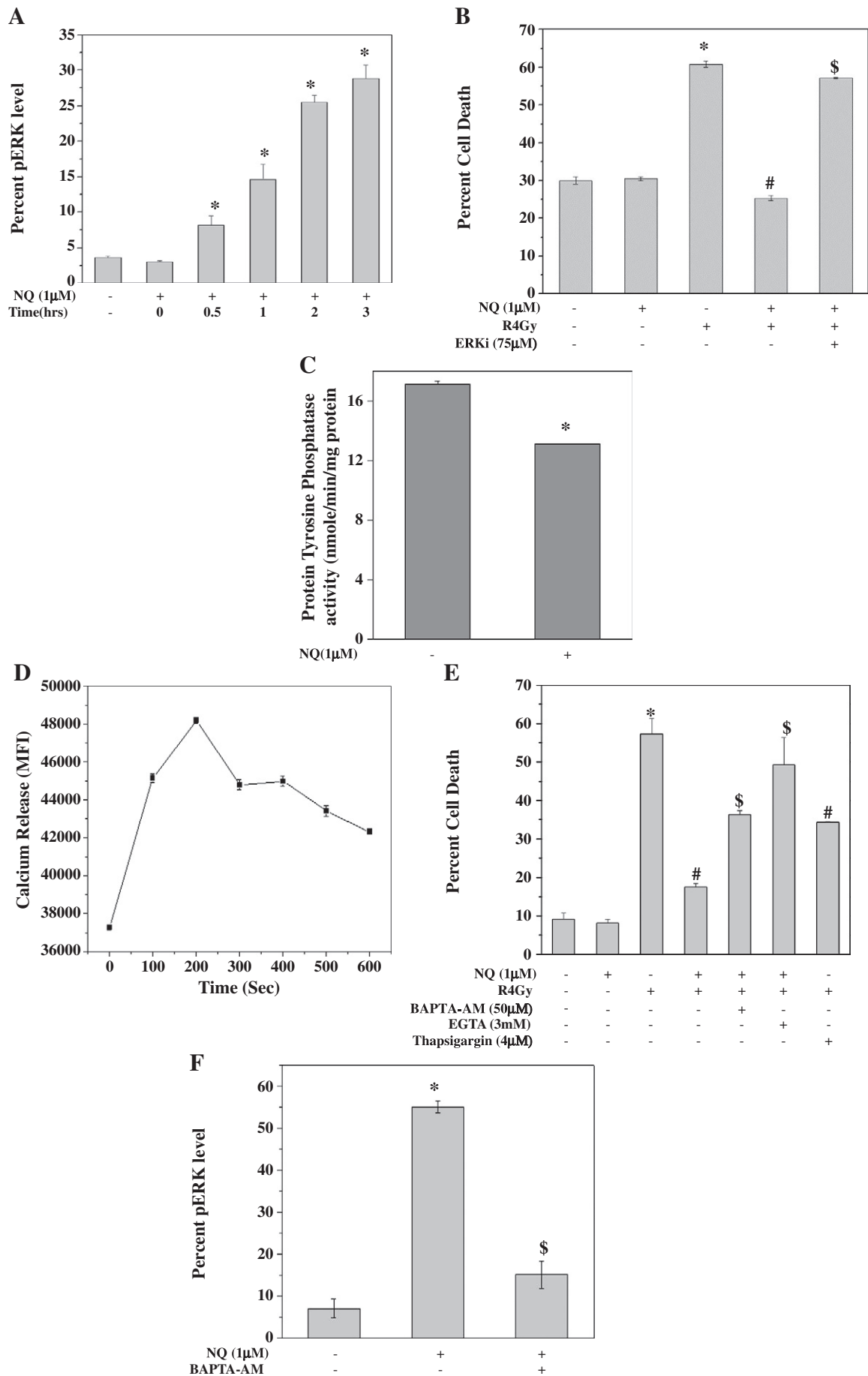
Administration of NQ (2 mg/kg body wt) to mice 0.5 h before WBI (4 Gy) protected against WBI-induced apoptosis (pre-G1 cells), nuclear blebbing, and DNA fragmentation (Figs. 7A–C). It was also observed that NQ ameliorated both early (loss of MMP) and late events (caspase activation and Bax expression) associated with radiation-induced apoptosis (Figs. 7D–F). Finally, NQ administration 0.5 h before 7 Gy WBI was able to significantly prevent radiation-induced mortality and weight loss (Figs. 7G and H). To determine the dose-reduction factor (DRF) of NQ, mortality was recorded up to 30 days after graded doses of radiation (6–8.5 Gy). An increase in the $\text{LD}_{50}/30$ days from 6.67 Gy for vehicle injection to 7.86 Gy in the NQ-treated group was observed; the DRF was calculated to be 1.18 (Fig. 7I).

Discussion

These studies were undertaken to test the hypothesis that pro-oxidants would protect murine splenic lymphocytes against toxic effects of radiation by initiating an adaptive response through the activation of the Nrf2–ARE pathway. NQ, a well-known pro-oxidant [12], offered complete protection to lymphocytes against radiation-induced cell death (Figs. 1 and 2). To the best of our knowledge, this is the first report showing radioprotection by any compound at such a low concentration as 250 nM. Interestingly, when NQ was added to cells after irradiation at various time intervals, it offered significant protection to cells. Colony-forming-cell assay in splenocytes and normal human cells (Int407) demonstrated that NQ was able to prevent the loss of proliferative capacity of cells exposed to radiation (Table 1, Fig. 2I). These results clearly demonstrated the potent radioprotective potential of NQ in vitro.

The molecular mechanism of NQ-mediated radioprotection was examined. Addition of NQ to lymphocytes generated significant levels of ROS and failed to completely scavenge radiation-derived free radicals, suggesting that NQ did not act by antioxidant action (Figs. 3A and B). Conventional radioprotectors are known to act by various mechanisms, such as detoxifying radiation-induced ROS; elevating endogenous defense molecules such as SOD, catalase, GPX, and GSH; enhancing DNA repair; and delaying cell division to allow the repair [36]. Several antioxidants and also plant extracts containing antioxidants have been evaluated in in vitro and in vivo models [31–33,37–39]. Amifostine, which is currently used as an adjuvant in radiotherapy, has been proposed to act as a radioprotector by scavenging radiation-derived free radicals [40]. Activators of the prosurvival transcription factor NF- κ B or its dependent gene products such as cytokines are also shown to offer resistance against radiation-induced toxicity [41,42]. Administration of glutathione to mice inhibited radiation-induced cytogenetic damage [43]. Radioprotective effects of thiol compounds include free radical scavenging, hydrogen atom donation, repair of free radicals in target molecules, mixed disulfide formation, and target stabilization by binding to DNA. Conversely, depletion of cellular thiols would lead to increased sensitivity of cells to radiation-induced damage [44].

Fig. 4. (A) Direct activation of Nrf2 by NQ. Lymphocytes were treated with NQ for the indicated times and then harvested, fixed, permeabilized, and stained with anti-Nrf2 (red). Nuclei were stained with Hoechst (blue). Nuclear translocation of Nrf2 from cytoplasm was analyzed by confocal laser microscopy. (B) ATRA, an Nrf2 inhibitor, abrogated the radioprotective action of NQ. NQ was added to ATRA-pretreated (6 h) lymphocytes and cells were exposed to 4 Gy γ -irradiation. Cell death was measured by PI staining. (C–E) Nrf2 knockdown lymphocytes were sensitive to radiation. Lymphocytes were transfected with control shRNA or Nrf2 shRNA plasmid for 24 h and then irradiated at 2 Gy. Further, cells were cultured for 24 h and cell death was assessed by PI staining, live and dead assay, and DNA fragmentation. (F and G) NQ upregulated the expression of the cytoprotective gene HO-1. NQ activated HO-1 expression in a time- and dose-dependent manner. Cells were treated with NQ at the indicated concentrations and for the indicated times and harvested, fixed, permeabilized, and stained with PE-labeled anti-HO-1. Bar graphs show the upregulation HO-1. (H) Total RNA isolated from NQ-treated (24 h) lymphocytes was reverse transcribed. RT-PCR analysis of the HO-1 gene was carried out. PCR products were resolved on 2% agarose gels containing ethidium bromide. β -Actin gene expression was used as an internal control. (I) SnPP, an inhibitor of HO-1, abrogated the radioprotective action of NQ. NQ was added to SnPP-pretreated (1 h) lymphocytes, which were irradiated at 4 Gy and cultured for 24 h. Cell death was estimated by PI staining. Each bar shows the mean \pm SEM from three replicates, and two such independent experiments were carried out. * $p < 0.05$, compared to vehicle-treated control; # $p < 0.05$, compared to irradiated group; \$ $p < 0.05$, compared to irradiated group in the presence of NQ.



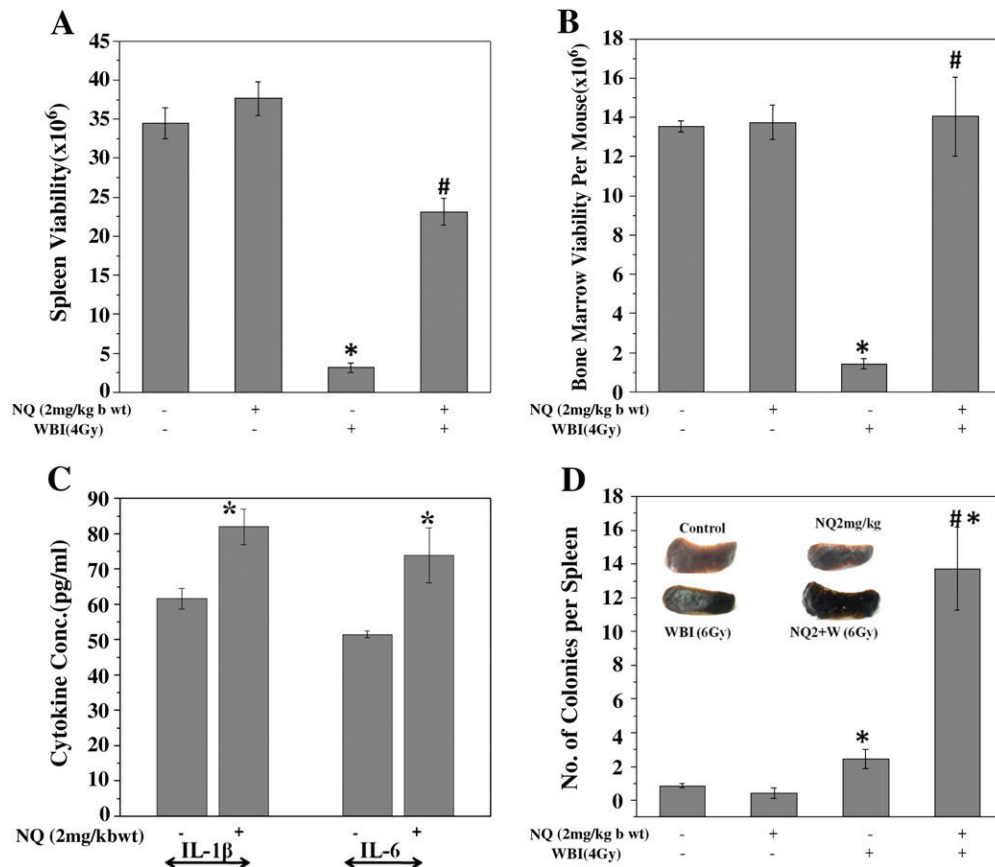


Fig. 6. Mice were administered NQ (2 mg/kg body wt) and after 0.5 h they were exposed to WBI (4 Gy) and sacrificed on day 5. (A, B) Spleen and bone marrow viability was assessed by trypan blue dye exclusion method. (C) NQ activated radioprotective cytokines, IL-1β and IL-6 in blood plasma were estimated by ELISA. (D) NQ treatment offered improvement of hematopoietic ability as demonstrated by number of macroscopic colonies appearing on the spleen (measured as CFUs) as monitored on day 9 after irradiation at 6 Gy. A total of seven mice were used per group for measurement of CFUs and five mice were taken per group for other experiments. Each bar shows the mean ± SEM from three replicates, and two such independent experiments were carried out. **p* < 0.05, compared to vehicle-treated control; #*p* < 0.05, compared to irradiated group.

NQ appeared to act as a radioprotector by altering cellular redox status. NQ significantly depleted GSH levels, and NAC, a thiol-containing antioxidant, could abrogate NQ mediated radioprotection, suggesting that NQ may be directly reacting with thiol groups (Fig. 3D). HPLC and MS analysis demonstrated the direct reaction and adduct formation between NQ and NAC (Supplementary Fig. S3B and Fig. 3E). Our findings, for the first time, prove that a thiol-depleting pro-oxidant can exhibit radioprotection in normal lymphocytes. DEM, a known GSH depletor, also offered complete protection against radiation-induced cell death, which further supports our hypothesis (Fig. 1D).

One of the redox-sensitive transcription factors, Nrf2 is bound to Keap1, which has two critical cysteine residues, and modulation of these residues has been shown to activate Nrf2 [45,46]. NQ activated Nrf2, as its nuclear translocation was observed 4 h after incubation of lymphocytes with NQ (Fig. 4A). ATRA, an inhibitor of Nrf2, completely abrogated NQ-mediated radioprotection in lymphocytes, indicating

the involvement of Nrf2 (Fig. 4B). To further substantiate the involvement of Nrf2, Nrf2-knockdown lymphocytes were found to be more sensitive to radiation than lymphocytes transfected with control shRNA plasmid (Figs. 4C–E). These results are in agreement with earlier reports by D.D. Zhang and P. Zhang et al., which showed that constitutive activation of Nrf2 in tumor cells led to radiation resistance [20,47]. NQ activated the Nrf2-dependent gene HO-1. SnPP, an inhibitor of HO-1, abrogated NQ-mediated radioprotection (Fig. 4I) to about 75%, suggesting that along with HO-1 other Nrf2-dependent cytoprotective proteins, such as MnSOD, NQO1, and catalase, may be responsible for the observed radioprotection.

NQ may be activating Nrf2 directly through modulation of critical cysteine residues present on Keap1 or through activation of ERK, which is upstream of Nrf2. There are several reports implicating ERK in the activation of Nrf2 [48]. We observed that treatment with NQ indeed resulted in phosphorylation of ERK in lymphocytes and a

Fig. 5. (A, B) Cells were treated with NQ for the indicated times and harvested, fixed, permeabilized, and stained with PE-labeled anti-pERK. Bar graph shows the upregulation of pERK. (B) ERK inhibitor abrogated the radioprotective action of NQ. Lymphocytes were treated with ERK inhibitor (1 h) before addition of NQ, irradiated at 4 Gy, and cultured for 24 h. Cell death was estimated by PI staining. (C) NQ suppressed protein tyrosine phosphatase activity. Whole-cell lysates of NQ-treated (2 h) lymphocytes were prepared and phosphatase activity was measured as per the manufacturer's protocol. (D) NQ increased intracellular calcium levels. Fura-2AM was added 0.5 h before NQ addition. The data represent intracellular changes in calcium levels with time. (E) Chelators of calcium inhibited the radioprotective action of NQ. Cells were cultured for 24 h and cell death was estimated by PI staining. Thapsigargin, a calcium mobilizer, offered significant radioprotection to lymphocytes. (F) BAPTA-AM abrogated NQ-mediated ERK phosphorylation. Lymphocytes were incubated with BAPTA-AM for 0.5 h, followed by treatment with NQ for 3 h, and then processed for intracellular staining with PE-labeled pERK antibody. Each bar shows the mean ± SEM from three replicates, and two such independent experiments were carried out. **p* < 0.05, compared to vehicle-treated control, #*p* < 0.05, compared to irradiated group; \$*p* < 0.05, compared to irradiated group in the presence of NQ.

Table 2

NQ administration to mice prevents WBI-induced suppression of subsets of splenocytes.

Splenocyte subset	$N \times 10^6$ per spleen			
	Control	NQ 2 mg/kg	WBI 4 Gy	NQ 2 mg/kg + WBI 4 Gy
Lymphocytes	37.5 ± 0.09	40.45 ± 0.21	4.2 ± 0.02*	20.18 ± 0.36#
CD3 ⁺ T cells	14.71 ± 1.49	17.82 ± 0.33	2.34 ± 0.11*	10.20 ± 0.91#
CD4 ⁺ T cells	10.37 ± 0.31	13.82 ± 0.26	2.20 ± 0.01*	6.56 ± 0.56#
CD8 ⁺ T cells	1.60 ± 0.09	2.34 ± 0.19	0.104 ± 0.006*	1.08 ± 0.60#
CD19 ⁺ B cells	11.60 ± 0.84	13.23 ± 0.26	0.53 ± 0.07*	5.50 ± 0.46#
CD14 ⁺ macrophages	1.74 ± 0.20	1.60 ± 0.16	0.32 ± 0.03*	0.96 ± 0.11#

The numbers of CD3⁺ T cells, CD4⁺ T helper cells, CD8⁺ T cytotoxic cells, CD19⁺ B cells, and CD14⁺ macrophages in spleen of vehicle- and NQ- (2 mg/kg body wt) treated mice were determined by flow cytometry. The total cell yield was calculated by multiplying the proportion of each cell subset by the total number of live cells obtained per spleen. NQ, 1,4-naphthoquinone; WBI, whole-body irradiation.

* $p < 0.05$, compared to vehicle-treated controls.

$p < 0.05$, compared to irradiated group.

pharmacological inhibitor of ERK suppressed NQ-mediated radioprotection (Figs. 5A and B). NQ-mediated increase in phosphorylation of ERK may occur through elevation of calcium levels [49] and/or by decreased phosphatase activity. NQ increased intracellular calcium levels within seconds of addition to lymphocytes and also decreased protein tyrosine phosphatase activity (Figs. 5C and D). These results are in corroboration with a recent report by Kim et al. demonstrating that bisdemethoxycurcumin increased intracellular calcium levels leading to activation of ERK [50]. Another cysteine-containing protein target of NQ could be caspases, especially postirradiation. Our results, thus, indicate that NQ may activate multiple mechanisms in upregulating prosurvival molecules.

Exposure of mice to radiation elevated the plasma levels of nitric oxide (Supplementary Fig. S4A). This was in agreement with our recent study [28]. Nitric oxide is a potent inhibitor of lymphocyte proliferation and has been reported to increase radiation-induced damage through inhibition of the activity of DNA repair enzymes [28]. Administration of NQ resulted in complete abrogation of WBI-mediated increase in plasma nitric oxide levels (Supplementary Fig. S4A). Further, NQ augmented the plasma levels of radioprotective IL-1 β and IL-6 (Fig. 6C). IL-1 β induces neutrophilia by mobilizing polymorphonuclear cells from bone marrow and promotes the formation of microthrombi by stimulating increased levels of fibrinogen in the circulation and thus induces hypoxic conditions, which protect the cell from radiation damage [42]. The increased IL-6 level is known to accelerate hematopoietic regeneration, splenic CFUs, and recovery of peripheral white and red blood cells [49].

Lymphocytes obtained from WBI-treated mice secreted significantly decreased levels of IL-2, IL-4, IL-6, and IFN- γ in response to a mitogen, concanavalin A, compared to controls (Supplementary Fig. S4B). However, a significant increase in cytokine secretion was observed in lymphocytes taken from NQ-administered mice followed by WBI. Further, spleen colony-forming units were enumerated on the 9th day after WBI. A significant increase in number of colonies was observed in NQ + WBI-treated mice compared to the vehicle + WBI group (Fig. 6D). These endogenous

Table 3

NQ administration to mice inhibited WBI-induced changes in hematological parameters.

Hematological parameter	Control	NQ 2 mg/kg	WBI 4 Gy	NQ 2 mg/kg + WBI 4 Gy
WBCs ($\times 10^4$ /ml)	1.05 ± 0.07	1.02 ± 0.1	0.28 ± 0.1*	0.83 ± 0.02#
Platelets ($\times 10^6$ /ml)	3.34 ± 0.3	3.64 ± 0.2	4.9 ± 0.10*	2.99 ± 0.2#
Neutrophils (%)	46.2 ± 1.2	43.8 ± 1.6	59.6 ± 0.9*	43.4 ± 2.8#
Lymphocytes (%)	54.8 ± 1.6	54.8 ± 1.6	36.4 ± 0.9*	55.5 ± 2.9#
Packed cell volume (%)	41.44 ± 0.5	41.36 ± 0.3	32.72 ± 0.4*	40.52 ± 0.5#
Mean corpuscular volume	73.66 ± 1.7	75.55 ± 0.6	57.2 ± 1.3*	71.52 ± 0.9#
RBCs ($\times 10^6$ /ml)	6.14 ± 0.2	5.88 ± 0.2	4.76 ± 0.3*	6.63 ± 0.3#
Hemoglobin (g/dl)	15.7 ± 0.2	15.4 ± 0.1	13.28 ± 0.5*	15.4 ± 0.1#

Blood was collected in heparinized tubes by retro-orbital puncture and complete blood count was done by autoanalyzer. NQ, 1,4-naphthoquinone; WBI, whole-body irradiation; WBCs, white blood cells; RBCs, red blood cells.

* $p < 0.05$, compared to vehicle-treated controls.

$p < 0.05$, compared to irradiated group.

spleen colonies appeared as nodules that represent the rapidly proliferating hematopoietic stem cells [51]. Finally, the protection conferred on radiosensitive cells such as lymphocytes and bone marrow by NQ manifested as an improvement in the survival of irradiated animals. NQ (2 mg/kg body wt) clearly enhanced the survival of mice exposed to a lethal whole-body irradiation dose of 7 Gy by 50% and prevented the loss of weight (Figs. 7G and H). The DMF of NQ was 1.18 (Fig. 7I) compared to 1.33 for amifostine, which is a well-known radioprotector [52].

In addition to protecting lymphocytes in vitro, NQ offered in vivo radioprotection to lymphocytes evaluated in terms of inhibition of increase in pre-G1 population, nuclear blebbing, DNA fragmentation, Bax levels, MMP loss, and activation of caspases (Fig. 7). Importantly, loss of bone marrow and spleen viability as a result of exposure to WBI was significantly abrogated in the presence of NQ (Figs. 6A and B). There was significant recovery of lymphocyte subsets obtained from NQ-administered mice followed by WBI compared to only WBI mice (Table 2).

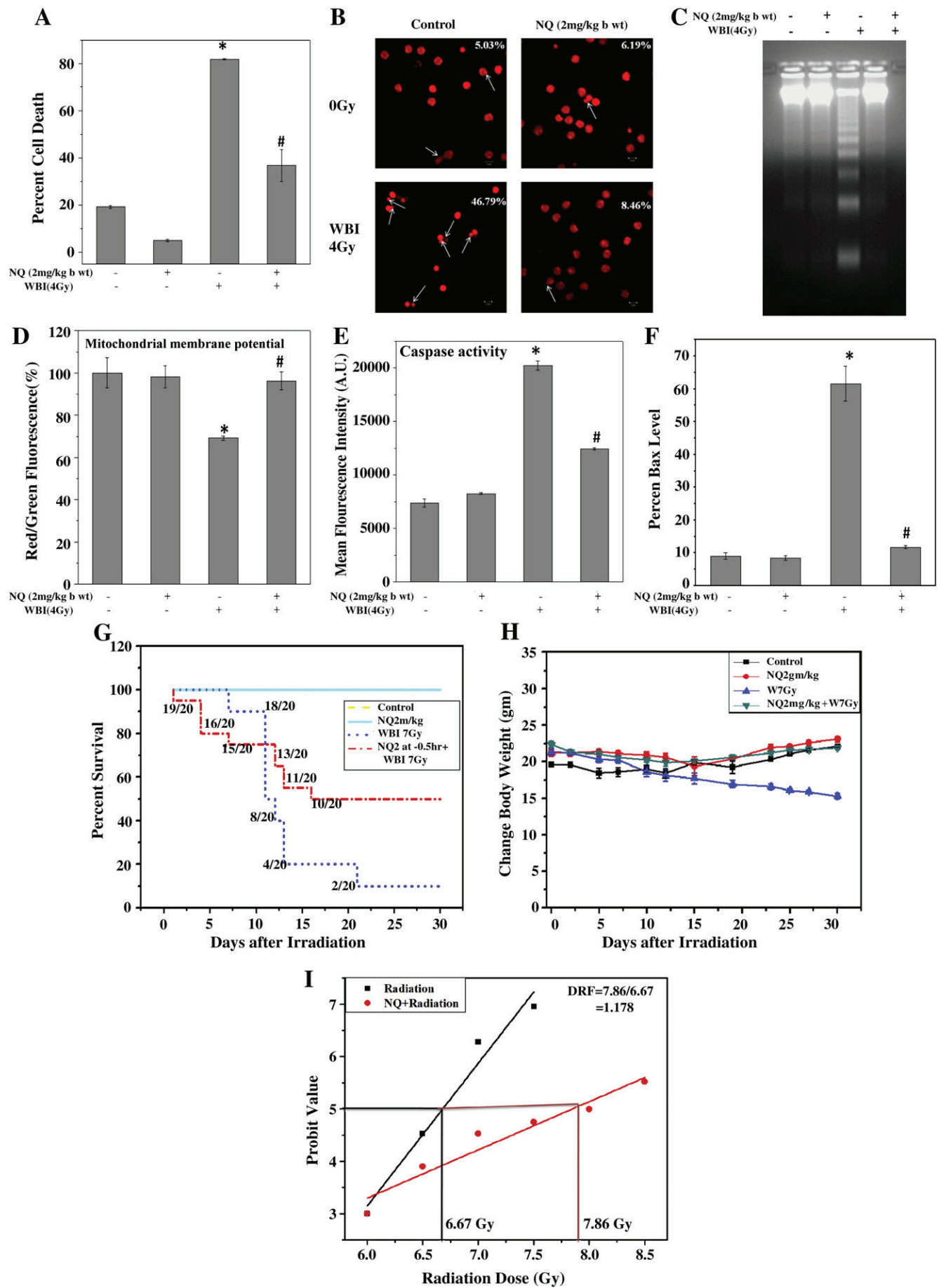
In conclusion, NQ offered radioprotection to lymphocytes due to activation of multiple prosurvival mechanisms including upregulation of the Ca²⁺-ERK-Nrf2 pathway. Further, our results indicate a possible radiation hematopoietic syndrome-specific radioprotective role for NQ. To the best of our knowledge, this is the first report showing a pro-oxidant and a GSH depletor offering radioprotection at such low concentrations.

Supplementary materials related to this article can be found online at doi:10.1016/j.freeradbiomed.2011.03.037.

Acknowledgments

The authors thank Dr. B.S. Patro for his help. The authors also acknowledge the technical assistance of Mr. Prayag Amin, Mr. Manjoor Ali, Mr. Narendra Sidnalkar, Mr. Kashinath Munankar, and Mr. Deepak Kathole. Support from the Department of Atomic Energy, India, in the form of a research grant is acknowledged.

Fig. 7. Mice were administered NQ (2 mg/kg body wt) and after 0.5 h they were exposed to WBI (4 Gy) and sacrificed immediately. Splenic lymphocytes were cultured from the various groups for 24 h. (A) Bar diagram showing percentage apoptotic cells estimated by PI staining. (B, C) NQ treatment inhibited WBI-induced apoptosis as demonstrated by (B) nuclear blebbing and (C) DNA fragmentation. (D) NQ inhibited WBI-induced loss of mitochondrial membrane potential as shown by loss of mean (red/green) fluorescence of JC-1. (E) NQ inhibited WBI-induced activation of homogeneous caspase (2, 3, 6, 7, and 9) activity. (F) NQ inhibited WBI-induced activation of proapoptotic protein Bax. Lymphocytes obtained from mice treated as above were cultured for 24 h and then processed for intracellular staining with PE-labeled Bax antibody. * $p < 0.05$, compared to vehicle-treated control; # $p < 0.05$, compared to irradiated group. (G) NQ treatment significantly improved 30-day survival rate of mice exposed to lethal dose of ionizing radiation (7 Gy). (H) NQ treatment provided protection against WBI (7 Gy)-induced loss of body weight of mice. (I) NQ administration to mice exposed to various doses of radiation gives a DMF of 1.178. Each data point shows the mean \pm SEM, and two such independent experiments were carried out. A total of 20 mice were taken per group for monitoring the survival and 10 mice for determining DMF.



References

- [1] Feinendegen, L. E. Evidence for beneficial low level radiation effects and radiation hormesis. *Br. J. Radiol.* **78**:3–7; 2005.
- [2] Son, T. G.; Camandola, S.; Arumugam, T. V.; Cutler, R. G.; Telljohann, R. S.; Mughal, M. R.; Moore, T. A.; Luo, W.; Yu, Q. S.; Johnson, D. A.; Johnson, J. A.; Greig, N. H.; Mattson, M. P. Plumbagin, a novel Nrf2/ARE activator, protects against cerebral ischemia. *J. Neurochem.* **112**:1316–1326; 2010.
- [3] Haskew-Layton, R. E.; Payappilly, J. B.; Smirnova, N. A.; Ma, T. C.; Chan, K. K.; Murphy, T. H.; Guo, H.; Langley, B.; Sultana, R.; Butterfield, D. A.; Santagata, S.; Alldred, M. J.; Gazaryan, I. G.; Bell, G. W.; Ginsberg, S. D.; Ratan, R. R. Controlled enzymatic production of astrocytic hydrogen peroxide protects neurons from oxidative stress via an Nrf2-independent pathway. *Proc. Natl. Acad. Sci. USA* **107**:17385–17390; 2010.
- [4] Li, J.; Johnson, D.; Calkins, M.; Wright, L.; Svendsen, C.; Johnson, J. Stabilization of Nrf2 by tBHQ confers protection against oxidative stress-induced cell death in human neural stem cells. *Toxicol. Sci.* **83**:313–328; 2005.
- [5] Rowley, D. A.; Halliwell, B. DNA damage by superoxide-generating systems in relation to the mechanism of action of the anti-tumour antibiotic adriamycin. *Biochim. Biophys. Acta* **761**:86–93; 1983.
- [6] Yamashita, Y.; Kawada, S.; Fujii, N.; Nakano, H. Induction of mammalian DNA topoisomerase I and II mediated DNA cleavage by saintopin, a new antitumor agent from fungus. *Biochemistry* **30**:5838–5845; 1991.
- [7] Checker, R.; Sharma, D.; Sandur, S. K.; Khanam, S.; Poduval, T. B. Anti-inflammatory effects of plumbagin are mediated by inhibition of NF-kappaB activation in lymphocytes. *Int. Immunopharmacol.* **9**:949–958; 2009.
- [8] Kim, B. H.; Yoo, J.; Park, S. H.; Jung, J. K.; Cho, H.; Chung, Y. Synthesis and evaluation of antitumor activity of novel 1,4-naphthoquinone derivatives (IV). *Arch. Pharm. Res.* **29**:123–130; 2006.
- [9] Looaresuwan, S.; Chulay, J. D.; Canfield, C. J.; Hutchinson, D. B. Malarone (atovaquone and proguanil hydrochloride): a review of its clinical development for treatment of malaria: Malarone Clinical Trials Study Group. *Am. J. Trop. Med. Hyg.* **60**:533–541; 1999.
- [10] Wang, X.; Thomas, B.; Sachdeva, R.; Arterburn, L.; Frye, L.; Hatcher, P. G.; Cornwell, D. G.; Ma, J. Mechanism of arylating quinone toxicity involving Michael adduct formation and induction of endoplasmic reticulum stress. *Proc. Natl. Acad. Sci. USA* **103**:3604–3609; 2006.
- [11] Lehnert, S.; Greene, D.; Batist, G. Radiation response of drug-resistant variants of a human breast cancer cell line: the effect of glutathione depletion. *Radiat. Res.* **124**:208–215; 1990.
- [12] Kayashima, T.; Mori, M.; Yoshida, H.; Mizushima, Y.; Matsubara, K. 1,4-Naphthoquinone is a potent inhibitor of human cancer cell growth and angiogenesis. *Cancer Lett.* **278**:34–40; 2009.
- [13] Checker, R.; Chatterjee, S.; Sharma, D.; Gupta, S.; Variyar, P.; Sharma, A.; Poduval, T. B. Immunomodulatory and radioprotective effects of lignans derived from fresh nutmeg mace (*Myristica fragrans*) in mammalian splenocytes. *Int. Immunopharmacol.* **8**:661–669; 2008.
- [14] Kumar, S. S.; Shankar, B.; Sainis, K. B. Effect of chlorophyllin against oxidative stress in splenic lymphocytes in vitro and in vivo. *Biochim. Biophys. Acta* **1672**:100–111; 2004.
- [15] Kunwar, A.; Bansal, P.; Kumar, S. J.; Bag, P. P.; Paul, P.; Reddy, N. D.; Kumbhare, L. B.; Jain, V. K.; Chaubey, R. C.; Unnikrishnan, M. K.; Priyadarsini, K. I. In vivo radioprotection studies of 3,3'-diselenodipropionic acid, a selenocystine derivative. *Free Radic. Biol. Med.* **48**:399–410; 2010.
- [16] Uma Devi, P.; Ganasoundari, A.; Vrinda, B.; Srinivasan, K. K.; Unnikrishnan, M. K. Radiation protection by the ocimum flavonoids orientin and vicenin: mechanisms of action. *Radiat. Res.* **154**:455–460; 2000.
- [17] Kang, K. W.; Lee, S. J.; Kim, S. G. Molecular mechanism of nrf2 activation by oxidative stress. *Antioxid. Redox Signal.* **17**:1664–1673; 2005.
- [18] Kensler, T. W.; Wakabayashi, N.; Biswal, S. Cell survival responses to environmental stresses via the Keap1–Nrf2–ARE pathway. *Annu. Rev. Pharmacol. Toxicol.* **47**:89–116; 2007.
- [19] Jeong, W. S.; Jun, M.; Kong, A. N. Nrf2: a potential molecular target for cancer chemoprevention by natural compounds. *Antioxid. Redox Signal.* **8**:99–106; 2006.
- [20] Zhang, D. D. The Nrf2–Keap1–ARE signaling pathway: the regulation and dual function of Nrf2 in cancer. *Antioxid. Redox Signal.* **13**:1623–1626; 2010.
- [21] Kim, J. W.; Li, M. H.; Jang, J. H.; Na, H. K.; Song, N. Y.; Lee, C.; Johnson, J. A.; Surh, Y. J. 15-Deoxy-Delta(12,14)-prostaglandin J(2) rescues PC12 cells from H₂O₂-induced apoptosis through Nrf2-mediated upregulation of heme oxygenase-1: potential roles of Akt and ERK1/2. *Biochem. Pharmacol.* **76**:1577–1589; 2008.
- [22] Kang, K. W.; Lee, S. J.; Park, J. W.; Kim, S. G. Phosphatidylinositol 3-kinase regulates nuclear translocation of NF-E2-related factor 2 through actin rearrangement in response to oxidative stress. *Mol. Pharmacol.* **62**:1001–1010; 2002.
- [23] Singh, A.; Bodas, M.; Wakabayashi, N.; Bunz, F.; Biswal, S. Gain of Nrf2 function in non-small-cell lung cancer cells confers radioresistance. *Antioxid. Redox Signal.* **13**:1627–1637; 2010.
- [24] Franken, N. A.; Rodermond, H. M.; Stap, J.; Haveman, J.; van Bree, C. Clonogenic assay of cells in vitro. *Nat. Protoc.* **1**:2315–2319; 2006.
- [25] Sandur, S. K.; Ichikawa, H.; Sethi, G.; Ahn, K. S.; Aggarwal, B. B. Plumbagin (5-hydroxy-2-methyl-1,4-naphthoquinone) suppresses NF-kappaB activation and NF-kappaB-regulated gene products through modulation of p65 and I-kappaB-alpha kinase activation, leading to potentiation of apoptosis induced by cytokine and chemotherapeutic agents. *J. Biol. Chem.* **281**:17023–17033; 2006.
- [26] Rosales, C.; Brown, E. J. Calcium channel blockers nifedipine and diltiazem inhibit Ca²⁺ release from intracellular stores in neutrophils. *J. Biol. Chem.* **267**:1443–1448; 1992.
- [27] Krutzik, P. O.; Nolan, G. P. Intracellular phospho-protein staining techniques for flow cytometry: monitoring single cell signaling events. *Cytometry A* **55**:61–70; 2003.
- [28] Sandur, S. K.; Ichikawa, H.; Pandey, M. K.; Kunnumakara, A. B.; Sung, B.; Sethi, G.; Aggarwal, B. B. Role of pro-oxidants and antioxidants in the anti-inflammatory and apoptotic effects of curcumin (diferuloylmethane). *Free Radic. Biol. Med.* **43**:568–580; 2007.
- [29] Shukla, J.; Chatterjee, S.; Thakur, V. S.; Premachandran, S.; Checker, R.; Poduval, T. B. L-Arginine reverses radiation-induced immune dysfunction: the need for optimum treatment window. *Radiat. Res.* **171**:180–187; 2009.
- [30] Bortner, C. D.; Cidlowski, J. A. Caspase independent/dependent regulation of K⁺, cell shrinkage, and mitochondrial membrane potential during lymphocyte apoptosis. *J. Biol. Chem.* **274**:21953–21962; 1999.
- [31] Maurya, D. K.; Adhikari, S.; Nair, C. K.; Devasagayam, T. P. DNA protective properties of vanillin against gamma-radiation under different conditions: possible mechanisms. *Mutat. Res.* **634**:69–80; 2007.
- [32] Prabhakar, K. R.; Veerapur, V. P.; Bansal, P.; Parihar, V. K.; Reddy Kandadi, M.; Bhagath Kumar, P.; Priyadarsini, K. I.; Unnikrishnan, M. K. Antioxidant and radioprotective effect of the active fraction of *Pilea microphylla* (L.) ethanolic extract. *Chem. Biol. Interact.* **165**:22–32; 2007.
- [33] Maurya, D. K.; Balakrishnan, S.; Salvi, V. P.; Nair, C. K. Protection of cellular DNA from gamma-radiation-induced damages and enhancement in DNA repair by trolox. *Mol. Cell. Biochem.* **280**:57–68; 2005.
- [34] Kansra, V.; Groves, C.; Gutierrez-Ramos, J. C.; Polakiewicz, R. D. Phosphatidylinositol 3-kinase-dependent extracellular calcium influx is essential for CX(3)CR1-mediated activation of the mitogen-activated protein kinase cascade. *J. Biol. Chem.* **276**:31831–31838; 2001.
- [35] Schmidt, J. M.; Wayman, G. A.; Nozaki, N.; Soderling, T. R. Calcium activation of ERK mediated by calmodulin kinase I. *J. Biol. Chem.* **279**:24064–24072; 2004.
- [36] Maurya, D. K.; Devasagayam, T. P.; Nair, C. K. Some novel approaches for radioprotection and the beneficial effect of natural products. *Indian J. Exp. Biol.* **44**:93–114; 2006.
- [37] Sudheer Kumar, M.; Unnikrishnan, M. K.; Uma Devi, P. Effect of 5-aminosalicylic acid on radiation-induced micronuclei in mouse bone marrow. *Mutat. Res.* **527**:7–14; 2003.
- [38] Chawla, R.; Arora, R.; Singh, S.; Sagar, R. K.; Sharma, R. K.; Kumar, R.; Sharma, A.; Tripathi, R. P.; Puri, S. C.; Khan, H. A.; Shawl, A. S.; Sultan, P.; Krishan, T.; Qazi, G. N. Podophyllum hexandrum offers radioprotection by modulating free radical flux: role of aryl-tetralin lignans. *Evid. Based Complement. Altern. Med.* **3**:503–511; 2006.
- [39] Weiss, J. F.; Landauer, M. R. Protection against ionizing radiation by antioxidant nutrients and phytochemicals. *Toxicology* **189**:1–20; 2003.
- [40] Tannehill, S. P.; Mehta, M. P. Amifostine and radiation therapy: past, present, and future. *Semin. Oncol.* **23**:69–77; 1996.
- [41] Burdelya, L. G.; Krivokrysenko, V. I.; Tallant, T. C.; Strom, E.; Gleiberman, A. S.; Gupta, D.; Kurnasov, O. V.; Fort, F. L.; Osterman, A. L.; Didonato, J. A.; Feinstein, E.; Gudkov, A. V. An agonist of toll-like receptor 5 has radioprotective activity in mouse and primate models. *Science* **320**:226–230; 2008.
- [42] Neta, R.; Oppenheim, J. J. Cytokines in therapy of radiation injury. *Blood* **72**:1093–1095; 1988.
- [43] Mazur, L. Radioprotective effects of the thiols GSH and WR-2721 against X-ray-induction of micronuclei in erythroblasts. *Mutat. Res.* **468**:27–33; 2000.
- [44] Clark, E. P.; Epp, E. R.; Morse-Gaudin, M.; Biaglow, J. E. The role of glutathione in the aerobic radioresponse. I. Sensitization and recovery in the absence of intracellular glutathione. *Radiat. Res.* **108**:238–250; 1986.
- [45] Osburn, W. O.; Kensler, T. W. Nrf2 signaling: an adaptive response pathway for protection against environmental toxic insults. *Mutat. Res.* **659**:31–39; 2008.
- [46] Surh, Y. J.; Kundu, J. K.; Na, H. K. Nrf2 as a master redox switch in turning on the cellular signaling involved in the induction of cytoprotective genes by some chemopreventive phytochemicals. *Planta Med.* **74**:1526–1539; 2008.
- [47] Zhang, P.; Singh, A.; Yegnasubramanian, S.; Esopi, D.; Kombairaju, P.; Bodas, M.; Wu, H.; Bova, S. G.; Biswal, S. Loss of Kelch-like ECH-associated protein 1 function in prostate cancer cells causes chemoresistance and radioresistance and promotes tumor growth. *Mol. Cancer Ther.* **9**:336–346; 2010.
- [48] Surh, Y. J. Cancer chemoprevention with dietary phytochemicals. *Nat. Rev. Cancer* **3**:768–780; 2003.
- [49] Schmidt, M.; Goebeler, M.; Posern, G.; Feller, S. M.; Seitz, C. S.; Brocker, E. B.; Rapp, U. R.; Ludwig, S. Ras-independent activation of the Raf/MEK/ERK pathway upon calcium-induced differentiation of keratinocytes. *J. Biol. Chem.* **275**:41011–41017; 2000.
- [50] Kim, A. N.; Jeon, W. K.; Kim, B. C. Up-regulation of heme oxygenase-1 expression through CaMKII–ERK1/2–Nrf2 signaling mediates the anti-inflammatory effect of bisdemethoxycurcumin in LPS-stimulated macrophages. *Free Radic. Biol. Med.* **49**:323–331; 2010.
- [51] Zheng, L.; Aspridites, N.; Keene, A. H.; Rodriguez, P.; Brown, K. D.; Davila, E. TLR9 engagement on CD4 T lymphocytes represses gamma-radiation-induced apoptosis through activation of checkpoint kinase response elements. *Blood* **111**:2704–2713; 2008.
- [52] Song, J. Y.; Han, S. K.; Bae, K. G.; Lim, D. S.; Son, S. J.; Jung, I. S.; Yi, S. Y.; Yun, Y. S. Radioprotective effects of ginsan, an immunomodulator. *Radiat. Res.* **159**:768–774; 2003.

Immunomodulatory and immunotoxic effects of bilirubin: molecular mechanisms

Nazir M. Khan and T. B. Poduval¹

Immunology and Hyperthermia Section, Radiation Biology and Health Sciences Division, Bhabha Atomic Research Centre, Trombay, Mumbai, India

RECEIVED FEBRUARY 9, 2011; REVISED JULY 10, 2011; ACCEPTED JULY 11, 2011. DOI: 10.1189/jlb.0211070

ABSTRACT

The immunomodulatory and immunotoxic effects of purified UCB have not been evaluated previously at clinically relevant UCB concentrations and UCB:BSA ratios. To delineate the molecular mechanism of UCB-induced immunomodulation, immune cells were exposed to clinically relevant concentrations of UCB. It inhibited LPS-induced B cell proliferation and cytokine production from splenic macrophages. UCB ($\geq 25 \mu\text{M}$) was toxic to unfractionated splenocytes, splenic T cells, B cells, macrophages, LPS-stimulated CD19⁺ B cells, human PBMCs, and RBCs. Purified UCB also was found to be toxic to splenocytes and human PBMCs. UCB induced necrosis and apoptosis in splenocytes. UCB activated the extrinsic and intrinsic pathways of apoptosis, as reflected by the markers, such as CD95, caspase-8, Bax, MMP, cytoplasmic Ca²⁺, caspase-3, and DNA fragmentation. UCB depleted GSH and activated p38MAPK. NAC, caspase inhibitors, and p38MAPK inhibitor attenuated the UCB-induced apoptosis. In vivo administration of $\geq 25 \text{ mg/kgbw}$ UCB induced atrophy of spleen, depletion of bone marrow cells, and leukopenia and decreased lymphocyte count and the T and B cell response to mitogens. UCB administration to mice led to induction of oxidative stress, activation of p38MAPK, and cell death in splenocytes. These parameters were attenuated by the injection of NAC and the p38MAPK inhibitor. Our results demonstrate for the first time that clinically relevant concentrations of UCB induce apoptosis and necrosis in immune cells by depleting cellular GSH. These findings should prove useful in understanding the immunosuppression associated with

hyperbilirubinemia. *J. Leukoc. Biol.* 90: 997–1015; 2011.

Introduction

Although physiological levels of UCB act as an antioxidant, increasing evidences have demonstrated that at high concentrations, it may be an active participant in the disease process [1, 2]. In vitro and in vivo studies in humans and rodents have demonstrated that elevated UCB is neurotoxic [1, 3–10]. UCB is a potentially toxic molecule to erythrocytes, cultured neurons, neuroblastoma cells, hepatoma cells, colon cancer cells, and fibroblast cells [1, 3, 5, 6, 11–14]. The ability of UCB to damage mitochondria and induce apoptosis in various cell lines has been demonstrated [4–6, 14–19]. In vitro studies have demonstrated the multiple toxic effects of UCB on cell response, membrane integrity, respiration, and transport functions [5].

Several studies suggest that UCB possesses multiple biological activities, including potential immunomodulatory and anti-inflammatory properties [20–23]. UCB decreases immune responses [22, 24–30], and increased rates of infection have been documented in hyperbilirubinemic patients [31–33]. The decreased immune response has been attributed to the immunological anergy induced by UCB. Direct interaction of a high concentration of UCB with the plasma membrane of immune cells, at greater than or equal to three UCB:albumin molar ratios, has been demonstrated [24]. The cytotoxicity of UCB at clinically relevant concentrations and molar ratios of UCB:albumin has not been evaluated using cells of the immune system. In contrast to the great interest in elucidating the molecular mechanisms of UCB-induced neurotoxicity, fewer studies addressed the possibility of UCB also being toxic for non-neural cells [34–40]. Characterizing the potential immunotoxicity of UCB is critical for understanding the potential risk of elevated UCB in hyperbilirubinemic patients. The probable molecular mechanisms by which UCB induces immunosuppression in the host have also not been investigated and may in-

Abbreviations: BARC=Bhabha Atomic Research Centre, B_f=free (unbound) bilirubin fraction, bw=body weight, DEM=diethylmaleate, DHE=dihydroethidium, DHR123=dihydrorhodamine-123, DTNB=dithiobis 2-nitrobenzoic acid, FDA=fluorescein diacetate, GR=glutathione reductase, GSSG=oxidized GSH, GSt=total glutathione, H₂DCF-DA=2,7-dichlorodihydrofluorescein-diacetate, JC-1=5,5',6,6'-tetrachloro-1,1',3,3'-tetraethylbenzimidazolyl carbocyanine iodide, MCB=monochlorobimane, MFI=mean fluorescence intensity, MMP=mitochondrial membrane potential, NAC=N-acetyl cysteine, p=phosphorylated, SH=sulfhydryl, TNB=5-thio-2-nitrobenzoic acid, UCB=unconjugated bilirubin

The online version of this paper, found at www.jleukbio.org, includes supplemental information.

1. Correspondence: Immunology and Hyperthermia Section, Radiation Biology and Health Sciences Division, Bhabha Atomic Research Centre, Trombay, Mumbai-400 085, India. E-mail: tbodu@barc.gov.in

volve proliferative arrest in lymphocytes or alternatively, induction of necrosis and apoptosis in mature immune cells.

Survey of literature indicates that the toxicity of UCB depends on the B_p concentration of UCB used, cell type studied, source of UCB/impurities present in the commercial preparations, and end-point selected for the studies [1]. Considering the importance of immunotoxicity data of UCB in human health, we carried out exhaustive studies to delineate the cellular and molecular mechanism by which a pathologically relevant concentration of UCB can cause immunotoxicity in murine splenic resting immune cells such as T cells, B cells, macrophages, and human PBMCs. As in humans, the normal plasma level of UCB is $\sim 20 \mu\text{M}$, and levels as high as $170 \mu\text{M}$ in neonates are still considered physiological, we chose clinically relevant concentrations of UCB between 10 and $100 \mu\text{M}$ for the present studies [21]. These concentrations have been used previously for the study of apoptotic, anti-inflammatory, antimutagenic, antioxidant, and anticancer properties of UCB [14, 20–22, 25, 40]. As toxicity of UCB is determined by the plasma B_p , which is not bound to plasma proteins and lipoproteins [12, 33, 41], we used molar ratios of UCB:BSA < 0.7 to make the studies physiologically more relevant. The effect of in vivo administration of UCB on the host immune competence was also studied. Purified UCB and UCB sourced from different manufacturers were also used to see the toxicity, if any, contributed by the impurities present in the commercial preparations.

MATERIALS AND METHODS

Reagents

UCB, BSA (fraction V), PI, Fura 2-AM, JC-1, LPS, RPMI 1640, Nonidet P-40, EDTA, PMSF, HEPES, EGTA, sodium chloride, sodium hydrogen phosphate, disodium-hydrophosphate, trizma base, sodium azide, Triton X-100, Tween-20, 5-sulfosalicylic acid, DTNB, NADPH, GR, GSH, GSSG, triethanolamine, 2-vinylpyridine, DEM, MCB, $H_2DCF\text{-DA}$, DHR123, DHE, NAC, Caspase-3,8 colorimetric assay kit, Annexin V-FITC/PI staining assay kit, and protein tyrosine kinase assay kit were purchased from Sigma Chemical Co. (St. Louis, MO, USA). FCS was obtained from Gibco-BRL (Grand Island, NY, USA). ELISA sets for detection of cytokines (IL-1 β , IL-6, and TNF- α) and mAb against anti-p-p38, Bax, and CD95, labeled with PE, were obtained from BD Biosciences (San Jose, CA, USA). CyQUANT NF cell proliferation assay kit and Live/Dead assay kit were purchased from Molecular Probes, Invitrogen (Eugene, OR, USA). Caspase-3,8,9 inhibitor SB203580 and UCB were purchased from Calbiochem (San Diego, CA, USA). Mouse CD4,19 positive selection kits were purchased from Stemcell Technologies (Vancouver, BC, Canada). FDA was purchased from MP Biochemicals (Irvine, CA, US). Antibodies to mouse anti-p-p38 and anti-p38 for Western blotting were purchased from Cell Signaling Technology (Beverly, MA, USA). HRP-conjugated secondary antibody and Western blotting kits were obtained from Roche (Germany).

Preparation of UCB

All preparations of UCB and experiments in vitro as well as in vivo were performed with minimal light to prevent its photo degradation. To ensure its chemical integrity, UCB stock solution was prepared just before the experiment, as described previously [42]. Briefly, a stock solution of $900 \mu\text{M}$ UCB was prepared by dissolving 1.05 mg UCB in 2 ml 0.1 N NaOH. After complete dissolution, 4 ml BSA ($450 \mu\text{M}$) was added to UCB stock to get a final concentration of $300 \mu\text{M}$ UCB and BSA. The culture medium con-

tained 10% FCS, which corresponds to a BSA concentration of $\sim 45 \mu\text{M}$ and was considered for calculating the molar ratios of UCB:BSA [14]. The bilirubin:albumin molar ratios in the different UCB concentrations are shown in **Table 1**. For in vivo studies, UCB was dissolved in 0.1 N NaOH solution, and final concentration was adjusted to 2.5–5 mg/ml with 5% BSA. The solution was ($10 \mu\text{l/gbw}$) injected i.p. to mice.

Experiments involving purified UCB were performed after further purifying the commercial preparation, according to the method of McDonagh and Assisi [43], to eliminate potential lipid contaminants. Briefly, 40 mg UCB was dissolved in 50 ml chloroform and heated to boiling, and then it was kept until it was room temperature. The solution (which contains some undissolved solid) was washed with 0.1 M NaHCO_3 ($3 \times 30 \text{ ml}$), dried over anhydrous Na_2SO_4 (2 g), and filtered. About one-third of the volume of chloroform was removed by distillation, and methanol was added by parts in a small volume to the boiling solution until a faint turbidity appeared. The solution was cooled to room temperature, and precipitate was filtered after 2 h. The crystalline precipitate was washed with chloroform:methanol mixture (1:1), dried at room temperature, and used as purified bilirubin.

Animals

Six- to 8-week-old inbred Swiss, Balb/c male mice, weighing 20–25 g, reared in the animal house of BARC (Mumbai, India), were used. The guidelines issued by the Institutional Animal and Human Ethics Committee of BARC, Government of India, were followed strictly.

Bone marrow and spleen cell suspensions

Bone marrow cell suspensions were prepared by injecting RPMI-1640 tissue-culture medium through the marrow of the femur. Cells from both femurs of each mouse were centrifuged and suspended in a known volume of medium. Spleen was aseptically removed and placed in sterile dishes containing RPMI-1640 medium. Splenocytes were obtained by squeezing the spleen through a nylon mesh in a petriplate-containing medium. The RBCs were lysed by brief hypotonic shock. Absolute cell count was taken by staining with methylene blue, and viable cells were counted using trypan blue [44].

^3H Thymidine incorporation assay

The assay was carried out as reported earlier [44]. Briefly, splenocytes ($1 \times 10^6/\text{ml}$) suspended in RPMI-1640 medium containing 10% FCS were treated with UCB (10– $100 \mu\text{M}$, 4 h) and stimulated with the B cell mitogen LPS ($50 \mu\text{g}/\text{ml}$) for 48 h at 37°C in a 95% air/5% CO_2 atmosphere in a 96-well plate. For ex vivo assay of proliferation, splenocytes isolated from vehicle or UCB-treated mice (25, 50 mg/kgbw, 24 h) were stimulated with LPS or Con A for 48 h or 72 h, respectively. Cells were pulsed with ^3H thymidine ($0.5 \mu\text{Ci}/\text{well}$, specific activity $6500 \text{ mCi}/\text{mM}$, Board of Radiation and Isotope Technology, Department of Atomic Energy, Mumbai, India) and cultured further for the next 16 h. Cells were harvested on glass fiber filters using a Multimash-2000 harvester (Dynatech Laboratories, Chantilly, VA, USA). The incorporated radioactivity was counted in a liquid scintillation counter (LKB Instruments, Australia) and was expressed as cpm.

CyQUANT NF cell proliferation assay

Splenocytes (1×10^6) were treated with UCB (10– $100 \mu\text{M}$, 4 h) and then stimulated with LPS ($50 \mu\text{g}/\text{ml}$) for 48 h at 37°C . Proliferation was esti-

TABLE 1. Molar Ratio of UCB:BSA Used in the Study

UCB concentration	BSA concentration	Molar ratio of UCB:BSA
10 μM	55 μM	0.18
25 μM	70 μM	0.36
50 μM	95 μM	0.53
100 μM	145 μM	0.69

mated by the changes in the total DNA content using the CyQUANT NF cell proliferation assay, according to the manufacturer's protocol. Fluorescence signals were recorded using a plate reader (Fluostar Optima, BMG Labtech, Germany) with excitation at 485 nm and emission at 530 nm and expressed as MFI.

Measurement of cytokines

Splenocytes (5×10^6 /well) were seeded in a 24-well plate for 4 h at 37°C in a 5% CO₂ atmosphere for adherence. The medium was aspirated, and the adherent cells, which are mainly macrophages, were washed with medium and incubated with UCB for 4 h and then stimulated with LPS for 6 h. The concentration of IL-1 β , IL-6, and TNF- α in the supernatant was estimated using cytokine ELISA sets.

Estimation of cell death by PI staining

Splenocytes (1×10^6) were incubated with UCB (10–100 μ M) for 24 h at 37°C in RPMI-1640 medium supplemented with 10% FCS in a 5% CO₂ atmosphere. These cells were washed with 10 mM PBS and incubated with 1 ml staining solution containing 0.5 μ g/ml PI, 0.1% sodium citrate, and 0.1% Triton X-100 overnight at 4°C. A total of 20,000 cells was acquired in a Partec PAS III flow cytometer, and percent dead cells were determined by analyzing a sub-G1 population (<2 n DNA content) using FloMax software [45].

Estimation of cell death by esterase activity assay

Splenocytes (1×10^6), isolated 24 h after UCB (25 mg/kbw) injection, were cultured for 24 h at 37°C in complete medium. The cells were stained with FDA (20 μ M) for 0.5 h at 37°C. Fluorescence intensity of FDA-stained cells was measured at an excitation wavelength of 485 nm and emission wavelength of 533 nm. A decrease in fluorescence intensity was taken as a decrease in the viability of the cell.

Estimation of DNA strand breaks by alkaline single-cell gel electrophoresis (Comet assay)

Splenocytes (0.1×10^6 cells/ml) were cultured for 24 h in the presence or absence of UCB, and two microscopy slides from each group were prepared and processed for Comet assay [46]. The slides were immersed in lysis buffer for 1 h at 4°C and equilibrated in alkaline solution for 20 min, followed by electrophoresis for 0.5 h at 25 V, 399 mA. After electrophoresis, the slides were neutralized and stained by 5 \times SYBR Green-II dye. The images were captured using a Carl Zeiss Axioplan fluorescence microscope (Germany). Fifty images/slide were analyzed for percentage DNA content in the tail, tail length, tail moment, and olive tail moment using Comet assay project software.

Annexin V-FITC/PI staining

To measure UCB-induced necrotic and apoptotic death, Annexin V-FITC/PI staining was performed, according to the manufacturer's protocol. A total of 20,000 cells was acquired in the flow cytometer and analyzed using FloMax software.

Live/Dead assay

To measure UCB-induced necrotic death, the Live/Dead assay (Molecular Probes, Invitrogen) was performed, according to the manufacturer's protocol. Necrotic death was measured by an increase in the fluorescence of dye bound to polyamine groups present in the inner surface of a membrane using a flow cytometer.

Estimation of apoptosis using DNA ladder assay

DNA fragmentation is the hallmark of apoptosis and was done as reported earlier [45]. In brief, splenocytes (1×10^6 cells) were cultured with UCB (10–100 μ M) for 24 h at 37°C. The cells were washed with PBS, and the pellet was suspended in 50 μ l lysis buffer (50 mM Tris HCl, pH 8.0, 10 mM

EDTA, 0.5% N-lauroyl sarcosine, 0.5 mg/ml proteinase K) and incubated for 1 h at 50°C. RNase (10 μ l) was added to the lysate and incubated further for 1 h at 50°C. The DNA sample (10 μ l) was mixed with 2 μ l gel-loading buffer and electrophoresed in 1.8% agarose gel in TBE buffer (pH 8.0) containing ethidium bromide. The bands were visualized and photographed under UV light using Geldoc (Syngene, UK).

Caspase-3,8 colorimetric assay

To measure the activation of caspase-3,8 in the cell treated with or without UCB (24 h), a colorimetric assay kit was used, as per the manufacturer's protocol. The assays were performed in a 96-well plate, which measured the cleavage product p-nitro aniline, released from the C-terminal peptide bond at 405 nm.

Measurement of change in MMP and intracellular calcium levels

Change in MMP and intracellular calcium levels is considered as an early event associated with apoptosis and thus, was monitored in splenocytes incubated with UCB for 6 h. Change in MMP was assessed using the mitochondrial-specific fluorescent probe JC-1 by a spectrofluorimetric method [45]. JC-1 (5 μ M) was incubated with the cells for 0.5 h at 37°C, prior to analysis. JC-1 has dual emission, depending on the state of the MMP. JC-1 forms aggregates in cells with a high red fluorescence, indicating a normal MMP. Loss of the MMP results in a reduction in the red fluorescence with a concurrent gain in green fluorescence as the dye shifts from an aggregate to monomeric state. Ratio of red:green fluorescence was used as an indicator of loss of MMP.

Fura 2-AM was used to measure the intracellular Ca²⁺ levels as described previously [45]. Fura 2-AM fluorescence changes when it is bound to Ca²⁺. Splenocytes (1×10^6) were incubated with UCB (10–100 μ M) for 6 h at 37°C and then stained with Fura 2-AM (2 μ M) for 0.5 h and analyzed in a spectrofluorimeter (BMG Labtech, Optima) at 335 nm excitation and 500 nm emission.

Intracellular and surface antibody staining

The various apoptotic markers, 24 h after UCB treatment to splenocytes, were monitored by antibody staining, as illustrated earlier [45]. Briefly, splenocytes (3×10^6) were cultured in the presence or absence of UCB (100 μ M) for the indicated time at 37°C. Cultured cells were fixed with 4% paraformaldehyde for 10 min at room temperature, and excess of paraformaldehyde was removed by washing once with wash buffer (PBS containing 1% BSA). Cells were permeabilized with PBS containing 0.02% Tween-20, thrice for 5 min each at room temperature, followed by two washes with wash buffer and then incubated with PE-labeled anti-Bax or anti-p38 mAb for 0.5 h at room temperature. Further cells were washed twice and analyzed on a FACS Calibur.

Surface staining with PE-labeled anti-CD95 (Fas) antibody was performed by the procedure described earlier [46]. Splenocytes (1×10^6), cultured in presence or absence of UCB (100 μ M) for 24 h, were resuspended in 50 μ l buffer (PBS containing 10% serum, 0.1% sodium azide) and were incubated on ice for 10 min for blocking FcRs. The cells were incubated further with 1 μ g PE-labeled anti-CD95 in 50 μ l buffer for 0.5 h on ice in the dark and washed three times with the buffer, and 20,000 cells were acquired in the flow cytometer.

Protein tyrosine kinase assay

Splenocytes (10×10^6) were incubated with UCB (100 μ M) for 3 h, whole cell lysates were prepared, and kinase activity was estimated, according to the manufacturer's protocol.

Western blot analysis

To determine the levels of p-p38, cytoplasmic extracts were prepared from UCB (100 μ M)-treated splenocytes [47] and fractionated by SDS-PAGE. After electrophoresis, the proteins were electrotransferred to nitrocellulose

membranes, probed with anti-p-p38 antibody, and detected by ECL (Roche). The membrane was stripped and reprobed with anti-p38 antibody as a loading control.

Measurements of ROS level

To monitor intracellular ROS level, H₂DCF-DA, DHE, and DHR123 were used. To detect ROS level, splenocytes (1×10^6) were preincubated with H₂DCF-DA (20 μ M), DHE (20 μ M), or DHR123 (5 μ M) for 20 min at 37°C before treating with various concentrations of UCB. After 1 h of incubation, the change in fluorescence intensities of DCF, DHE, and Rhodamine123 was recorded at excitation wavelengths of 488, 535, 488 nm and emission wavelengths of 535, 610, 543 nm, respectively, using a spectrofluorimeter [9, 45, 47]. The oxidized form of the dye acts as a control for changes in uptake, ester cleavage, and efflux.

Intracellular GSH assay

MCB was used to measure intracellular GSH [48]. Splenocytes (1×10^6) were incubated with UCB for the indicated time at 37°C, and MCB (40 μ M, 0.5 h at 37°C) was loaded into the cell suspension. Fluorescence emission from cellular SH-reacted monochlorobimane was measured using a spectrofluorimeter (BMG Labtech, Optima), flow cytometer, and confocal microscope. DEM was used as positive control for GSH depletion [45]. MCB is also known to react with small MW thiols other than GSH, but GSH forms the major monochlorobimane-reactive thiol [48].

Cellular GSH exists predominantly in the reduced form, but small amounts of the oxidized disulfide form GSSG can also be detected. The GSH:GSSG ratio is often taken as an indicator of cellular redox status. GSH and GSSG levels were also determined by an enzymatic recycling procedure using the Tietze method [8]. The SH group of the molecule reacts with DTNB, producing a yellow-colored TNB, and the disulfide is reduced by NADPH in the presence of GR. GSSG was determined by derivatization of GSH by reaction with 2-vinylpyridine for 1 h at 4°C. Supernatants were assayed in 100 mM sodium phosphate buffer, containing 0.62 mM EDTA, 1.7 mM NADPH, and 20.2 mM DTNB. The rate of TNB formation was monitored following addition of 1.2 U GR at 420 nm. Glutathione concentrations were calculated using appropriate standards.

Administration of UCB to mice

Mice (five/group) were administered with UCB (25, 50 mg/kgbw) i.p. and killed 24 h after injection. The viability of spleen and bone marrow cells was enumerated by the trypan blue dye exclusion method. Spleen index was calculated [spleen index = (spleen weight/bw) \times 100], as described previously [44].

In experiments involving p38MAPK activation and GSH estimation, mice were killed at 1, 2, and 3 h following UCB administration. SB203580 (p38MAPK inhibitor) was dissolved in DMSO and administered i.p. at a dose of 5 mg/kgbw, 2 h prior to challenge with UCB. In experiments to determine the effect of altered GSH levels, mice were treated with NAC (1000 mg/kgbw), dissolved in PBS solution, 0.5 h prior to UCB administration [49].

Statistical analysis

Data were presented as mean \pm SEM. Data from all of the experiments were analyzed using one-way ANOVA, followed by post hoc analyses using the Scheffe test. Significance was set at $P < 0.05$.

RESULTS

UCB possesses significant immunomodulatory activity

As effects of UCB on B cells and macrophages have not been studied so far, we investigated the effects of UCB on the proliferative responses of Swiss splenocytes and purified CD19⁺ B cells to LPS stimulation. Studies were also performed to assess

the effects of UCB on cytokine release from macrophages in response to LPS stimulation. UCB inhibited LPS-induced B cell proliferation and cytokine release from macrophages in a concentration-dependent manner starting from 25 μ M (Fig. 1A–F). The results clearly indicate that UCB, at a clinically relevant concentration of 25 μ M, significantly compromises the immune function of B cells and macrophages.

UCB induces cell death in immune cells

The inhibitory effect of UCB on B cell proliferation after LPS stimulation could be a result of proliferative arrest in the lymphocyte or induction of necrosis and apoptosis in mature immune cells. To address this question, naïve and LPS-activated splenocytes were cultured for 24 h in the presence or absence of UCB (10–100 μ M), and cell death was determined. The results shown in Fig. 2A–D clearly indicate that the UCB concentration \geq 25 μ M induces cell death in naïve splenocytes and LPS-activated CD19⁺ B cells. UCB was found to induce DNA strand breaks in splenocytes, as indicated by Comet parameters (Fig. 2B). Results (Fig. 2C and D) also indicated the ability of UCB to arrest the cell population at a pre-G1 phase of the cell cycle and to reduce the LPS-induced increase in S + G2/M cells. These findings were supported further by CFSE staining of UCB-treated splenocytes, which demonstrated a significant increase in the dead population after exposure to \geq 25 μ M UCB (Supplemental Fig. 1). A purified population of CD4⁺ T cell, CD19⁺ B cell, adherent macrophage, and human PBMCs was equally susceptible to UCB-induced cell death (Fig. 2E). UCB was found to be equally toxic to Balb/c splenocytes, which have a different genetic background (data not shown).

To eliminate the possible effect of surface-active contaminants, usually present in the commercial UCB preparations [43], experiments were conducted using purified UCB, which was found to be equally toxic to splenocytes and human PBMCs (Fig. 2F). UCB sourced from a different manufacturer (Calbiochem) was also toxic to splenocytes (data not shown). Taken together, these results demonstrated that the immunosuppressive effects of UCB were mediated by induction of cell death.

Considering the above, further experiments were conducted using UCB from Sigma Chemical Co. The experiments used unfractionated splenocytes from Swiss mice as the source of immune cells, as the whole population mimics the in vivo situation more closely compared with the use of an enriched cell population.

UCB induces necrotic and apoptotic death in splenocytes

To find out the mode of cell death induced by UCB, annexin V/PI staining was done, and the results showed that UCB (\geq 25 μ M) induces necrosis and apoptosis (Fig. 3A). Results of the Live/Dead assay, trypan blue dye exclusion test, and methylene blue staining confirmed that UCB, at a concentration of \geq 25 μ M, led to a significant increase in necrotic death (Fig. 3B and C). UCB induced hemolysis of murine and human RBCs, which further confirmed the ability of UCB to cause

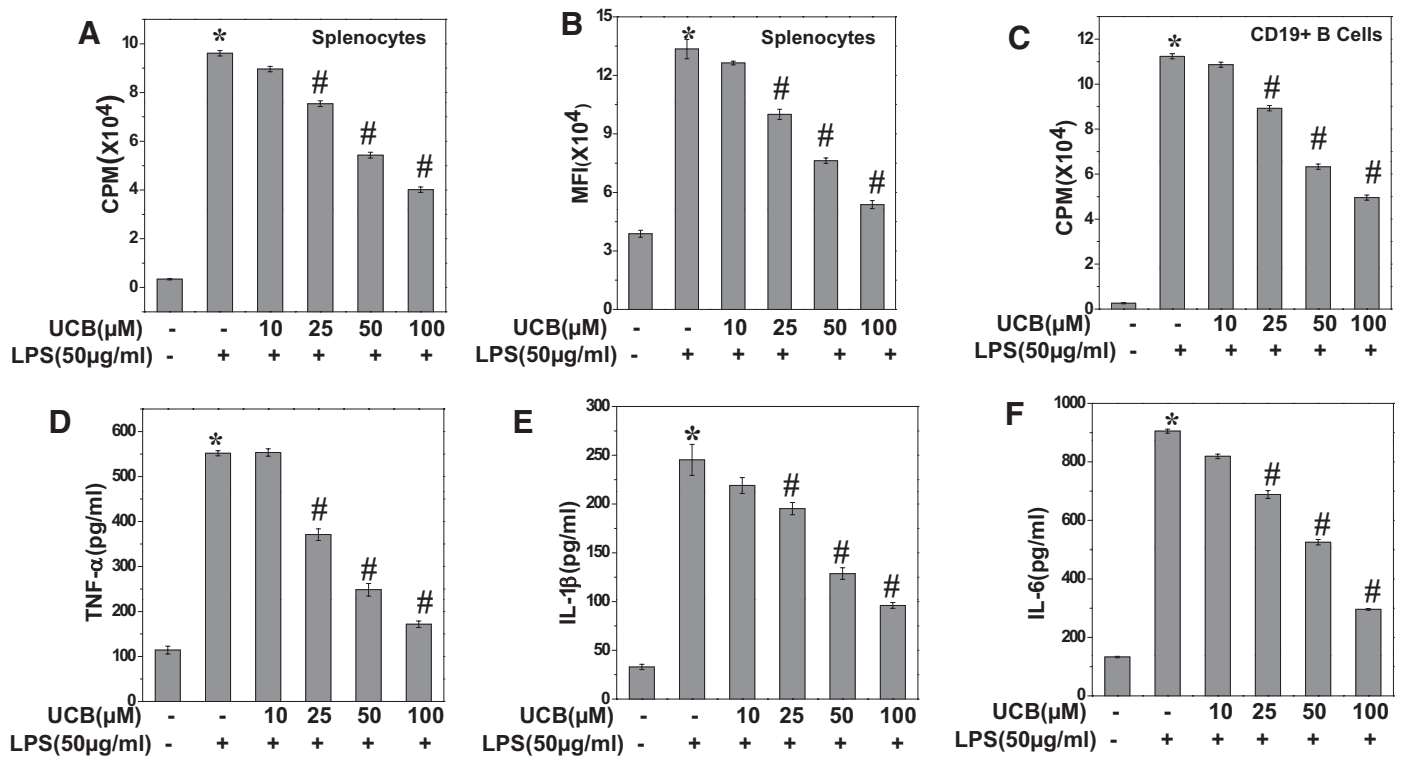


Figure 1. UCB possessed significant immunomodulatory activity. (A–C) UCB inhibited LPS-induced immune cell proliferation as assessed by (A and C) the ³H thymidine incorporation assay and (B) CyQUANT NF cell proliferation assay. Splenocytes (1 million/ml; A and B) or CD19 B cells (C) were treated with UCB (10–100 μM, 4 h) and stimulated with LPS (50 μg/ml) for 48 h at 37°C. Cell proliferation was monitored, as mentioned in Materials and Methods. (D–F) UCB inhibited LPS-induced production of TNF-α, IL-1β, and IL-6 from splenic adherent macrophages. Five million splenocytes were allowed to adhere in a 24-well plate for 4 h at 37°C. The adherent macrophages were incubated with UCB (10–100 μM) for 4 h and then stimulated with LPS (50 μg/ml) for 6 h. The levels of TNF-α, IL-1β, and IL-6 in the culture supernatants were determined by ELISA. The data are representative of three such independent experiments having similar results. Each bar represents mean ± SEM from three replicates. **P* < 0.05, as compared with vehicle group; #*P* < 0.05, as compared with LPS control group.

plasma membrane damage (Supplemental Fig. 2A and B). UCB-induced apoptotic death was confirmed by DNA fragmentation and a caspase-3 activation assay (Fig. 3D and E).

UCB induces extrinsic and intrinsic apoptotic pathways

As caspase-8,9 are involved in the extrinsic and intrinsic apoptotic pathways, respectively, and caspase-3 is common to both of the pathways, the inhibitors of these enzymes were used to find out the mode of apoptotic death. The results showed that these inhibitors attenuated the UCB-induced apoptosis, suggesting the involvement of both of the apoptotic pathways in UCB-induced cell death (Fig. 4A). The up-regulation of CD95 expression and the increase in caspase-8 activity by UCB treatment to splenocytes in a concentration-dependent manner suggested the contribution of the extrinsic apoptotic pathway (Fig. 4B and C). The exposure of UCB to splenocytes activated Bax, increased cytoplasmic calcium, and induced loss of MMP in a concentration-dependent manner, indicating the involvement of an intrinsic apoptotic pathway as well (Fig. 4D–F). Taken together, these results suggest that UCB-induced apoptosis in splenocytes is mediated by activation of both of the apoptotic pathways.

UCB induces apoptosis by activating p38MAPK

To identify the sequence of events contributing to UCB-induced apoptosis, we examined the ability of UCB to activate p38MAPK in splenocytes. For these studies, we selected the highest concentration of UCB, as it is still physiologically relevant and causes maximum immunosuppression and cell death. The results showed that UCB causes the phosphorylation of p38MAPK in a time-dependent manner, as demonstrated by flow cytometry and Western blot analysis (Fig. 5A–C). As p38MAPK is activated by specific kinase via phosphorylation of threonine-180 and tyrosine-182, we also measured protein tyrosine kinase activity, and it was found that UCB increased the kinase activity at both of the concentrations tested (Fig. 5D). SB203580 (an inhibitor of p38MAPK) reduced UCB-induced cell death, confirming the involvement of p38MAPK activation in UCB-induced cell death (Fig. 5E). p-p38MAPK is known to induce apoptosis by activating extrinsic and intrinsic pathways [50, 51]. The expression of markers of extrinsic (CD95) and intrinsic (Bax) apoptotic pathways was reduced significantly by the p38MAPK inhibitor (Fig. 5F and G). Taken together, these findings suggest a central role of p38MAPK in initiating UCB-induced apoptosis.

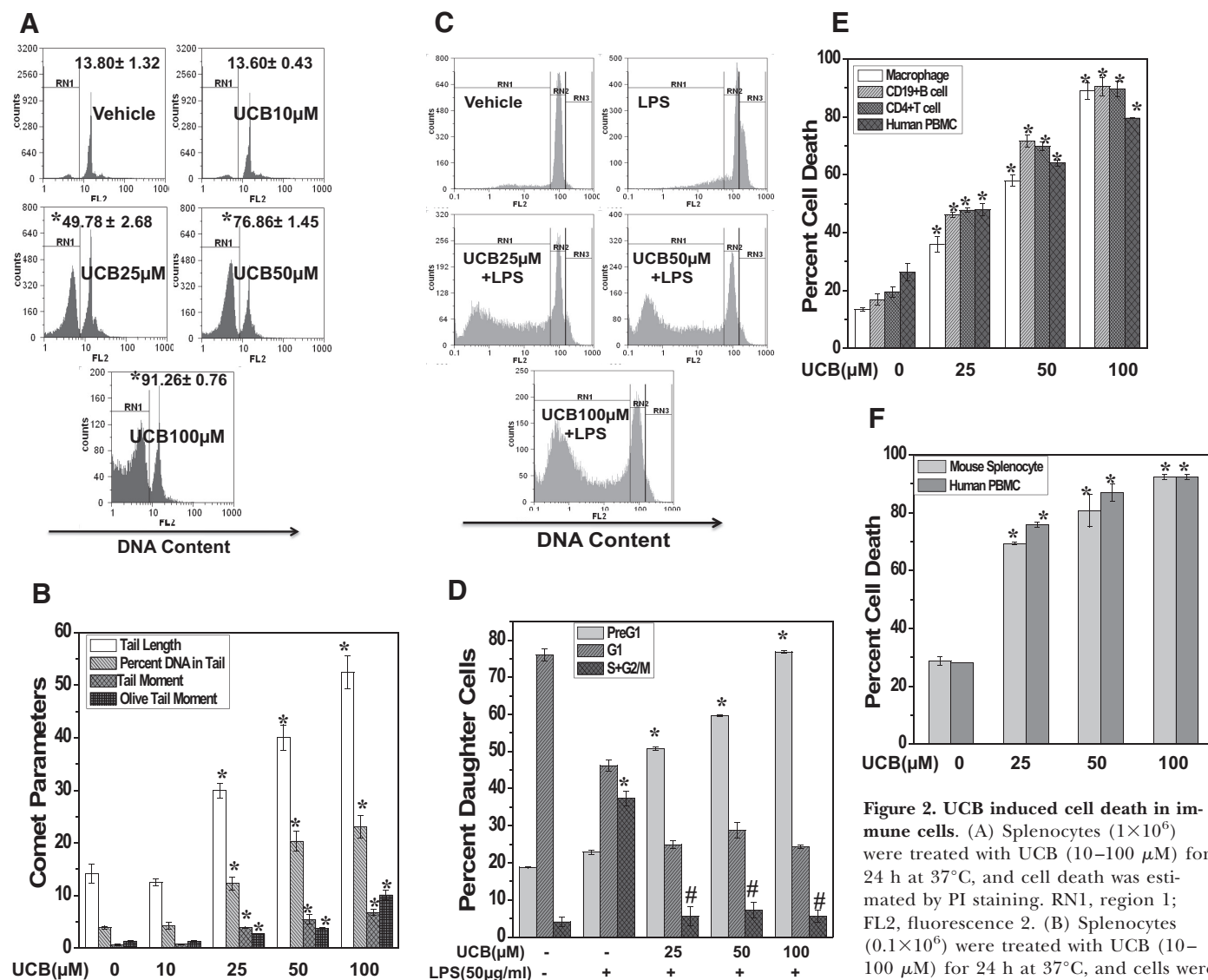


Figure 2. UCB induced cell death in immune cells. (A) Splenocytes (1×10^6) were treated with UCB (10–100 μ M) for 24 h at 37°C, and cell death was estimated by PI staining. RN1, region 1; FL2, fluorescence 2. (B) Splenocytes (0.1×10^6) were treated with UCB (10–100 μ M) for 24 h at 37°C, and cells were processed for the Comet assay to measure DNA strand breaks, as described in Materials and Methods. (C and D) UCB-induced death in LPS-activated CD19⁺ B cells. Purified mouse CD19⁺ B cells (1×10^6) were pretreated with UCB (25–100 μ M) for 4 h before stimulation with LPS (50 μ g/ml) for 48 h at 37°C, and cell death was estimated by PI staining. RN2/3, region 2/3. (E) UCB-induced cell death in multiple cell types. Splenic adherent macrophages, CD19⁺ B cells, CD4⁺ T cells, or human PBMCs (1×10^6 each) were treated with UCB (25–100 μ M) for 24 h at 37°C, and cell death was estimated by PI staining. (F) Purified UCB-induced cell death in murine splenocytes and human PBMCs. Murine splenocytes (1×10^6) or human PBMCs (1×10^6) were treated with purified UCB (25–100 μ M) for 24 h at 37°C, and cell death was estimated by PI staining. The data are representative of three such independent experiments having similar results. Each bar represents mean \pm SEM from three replicates. * $P < 0.05$, as compared with vehicle group; # $P < 0.05$, as compared with LPS control group.

measure DNA strand breaks, as described in Materials and Methods. (C and D) UCB-induced death in LPS-activated CD19⁺ B cells. Purified mouse CD19⁺ B cells (1×10^6) were pretreated with UCB (25–100 μ M) for 4 h before stimulation with LPS (50 μ g/ml) for 48 h at 37°C, and cell death was estimated by PI staining. RN2/3, region 2/3. (E) UCB-induced cell death in multiple cell types. Splenic adherent macrophages, CD19⁺ B cells, CD4⁺ T cells, or human PBMCs (1×10^6 each) were treated with UCB (25–100 μ M) for 24 h at 37°C, and cell death was estimated by PI staining. (F) Purified UCB-induced cell death in murine splenocytes and human PBMCs. Murine splenocytes (1×10^6) or human PBMCs (1×10^6) were treated with purified UCB (25–100 μ M) for 24 h at 37°C, and cell death was estimated by PI staining. The data are representative of three such independent experiments having similar results. Each bar represents mean \pm SEM from three replicates. * $P < 0.05$, as compared with vehicle group; # $P < 0.05$, as compared with LPS control group.

UCB depletes GSH levels in splenocytes

Earlier reports by Brites and co-workers [8, 9] showed that UCB-induced cytotoxicity in neuronal cells is mediated by induction of oxidative stress via GSH depletion. The role of oxidative stress in UCB-induced immunotoxicity was thus investigated by measuring the intracellular GSH and ROS levels in UCB-treated splenocytes. UCB decreased the basal levels of GSH in a concentration-dependent manner in treated splenocytes (Fig. 6A). A time kinetics study demonstrated that UCB completely suppressed the basal GSH level in splenocytes within 0.5 h of incubation (Supplemen-

tal Fig. 3A). These results were confirmed further by using confocal microscopy (Fig. 6B) and flow cytometry (Fig. 6C).

Cellular GSH exists predominantly in a reduced form, but small amounts of the oxidized disulfide form are also present; the GSH:GSSG ratio is, therefore, taken as a more appropriate indicator of the cellular redox status. Thus, we specifically measured its effect on intracellular levels of GSH, GSSG, GSt, and the GSH:GSSG ratio. UCB decreased the cellular GSH (Supplemental Fig. 3B), GSt levels (Supplemental Fig. 3C), and GSH:GSSG ratio (Fig. 6D),

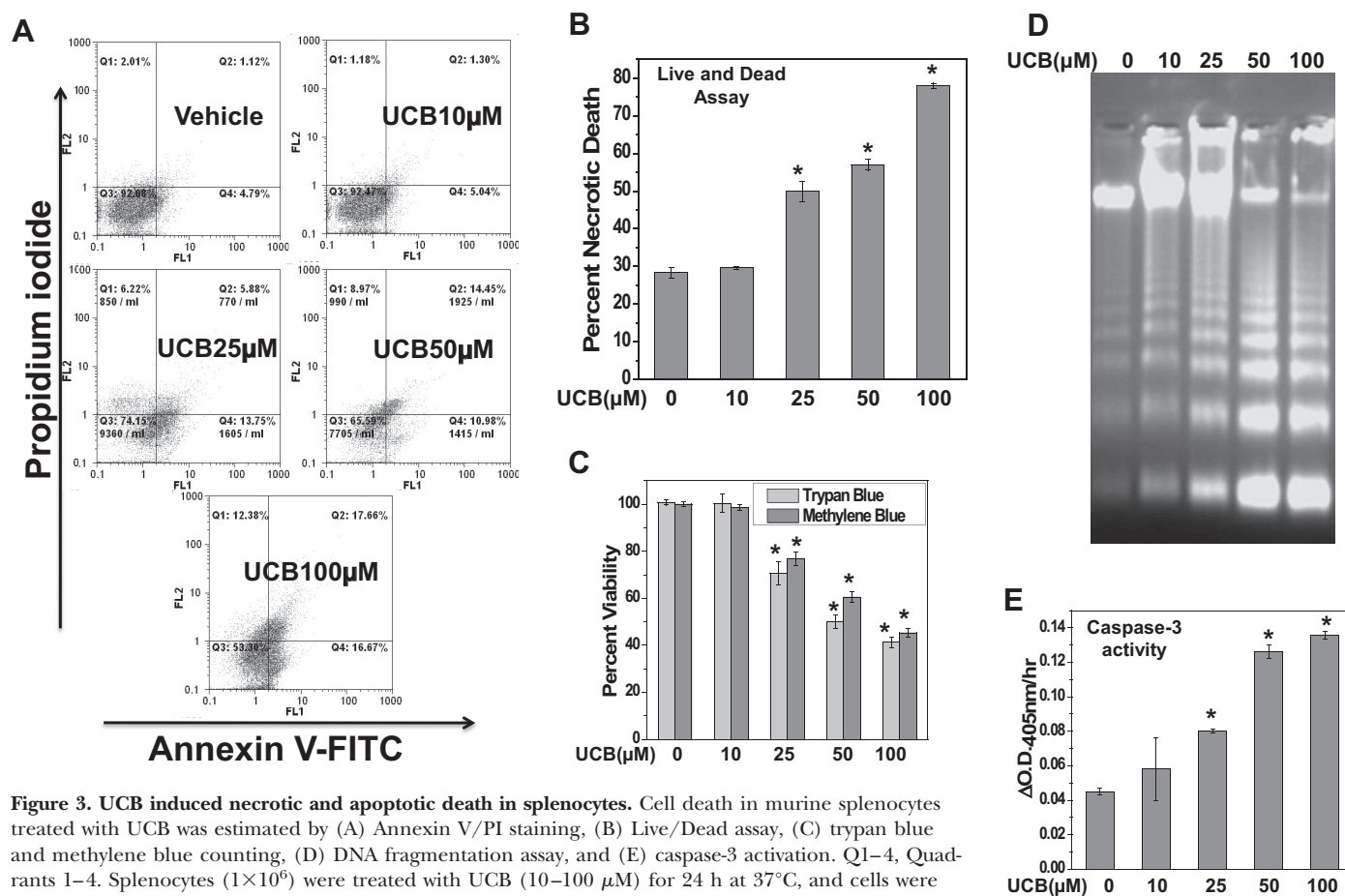


Figure 3. UCB induced necrotic and apoptotic death in splenocytes. Cell death in murine splenocytes treated with UCB was estimated by (A) Annexin V/PI staining, (B) Live/Dead assay, (C) trypan blue and methylene blue counting, (D) DNA fragmentation assay, and (E) caspase-3 activation. Q1–4, Quadrants 1–4. Splenocytes (1×10^6) were treated with UCB (10–100 μ M) for 24 h at 37°C, and cells were processed as described in Materials and Methods. The data are representative of three such independent experiments having similar results. Each bar represents mean \pm SEM. * $P < 0.05$, as compared with vehicle group.

whereas it increased the levels of GSSG (Supplemental Fig. 3D).

To further investigate the role of UCB on the redox status of splenocytes, we also measured its effect on intracellular ROS levels by using a redox-sensitive dye, H_2DCF -DA. Surprisingly, UCB treatment to splenocytes for 1 h decreased the basal ROS levels in a concentration-dependent manner (Supplemental Fig. 4A). This was confirmed by using another oxidation-sensitive probe, DHE (Supplemental Fig. 4B), and mitochondrial-specific redox-sensitive dye, DHR123 (Supplemental Fig. 4C).

Glutathione is a key molecule in the prevention of cell death induced by UCB

As UCB depleted cellular GSH levels in splenocytes, we hypothesized that glutathione is a critical molecule in UCB-induced immunotoxicity. To test our hypothesis, we evaluated the modulation of UCB-induced cell death in conditions of augmentation and depletion of GSH. For this purpose, splenocytes were preincubated with NAC, a precursor of glutathione [8, 9, 52], or treated with DEM, a known GSH depletor [45], then were exposed to UCB, and measured for the cellular GSH levels and cell death using PI staining and esterase activity.

Results showed that NAC treatment to splenocytes for 1 h increased GSH levels, and it also partially restored the GSH levels decreased by UCB treatment (Supplemental Fig. 5A). Furthermore, DEM induced GSH depletion and was augmented further by UCB treatment to splenocytes (Supplemental Fig. 5B). UCB (10 μ M) did not deplete GSH level alone; however, in the presence of DEM, it decreased the cellular GSH levels significantly (Supplemental Fig. 5B).

Splenocytes were treated with NAC or DEM and/or UCB, as mentioned above, and were assessed for cell death by PI staining at the end of 24 h. As shown in Fig. 6E and F, pretreatment of splenocytes with a nontoxic dose of NAC (10 mM) reduced UCB-induced cell death. UCB (10 μ M) is not toxic to splenocytes, whereas in the presence of a nontoxic dose of DEM (100 μ M), it led to a significant increase in cell death (Fig. 6G).

UCB-induced p38MAPK activation is mediated by depletion of GSH levels

Several studies have reported the crucial role of intracellular glutathione in regulating the activation of p38MAPK [49, 53–55]. A report by Limón-Pacheco et al. [49] has shown that GSH depletion activates p38MAPK in different organs of mice. Accordingly, we examined whether UCB-induced p38MAPK

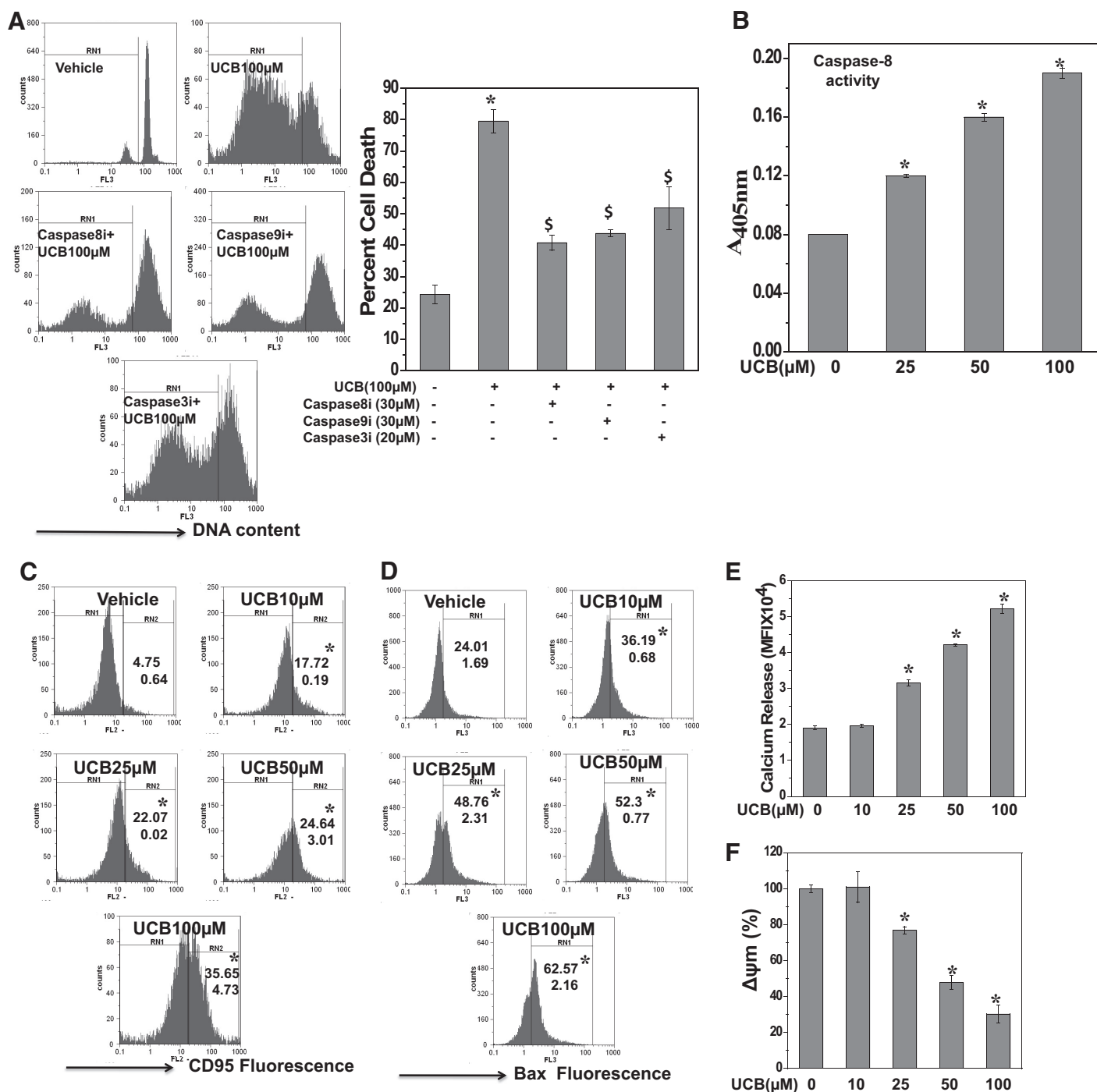


Figure 4. UCB induced extrinsic and intrinsic apoptotic pathways in splenocytes. (A) Splenocytes (1×10^6) were pretreated with inhibitors of caspase-8 (Caspase8i, 30 μ M), caspase-9 (Caspase9i, 30 μ M), and caspase-3 (Caspase3i, 20 μ M) for 1 h, followed by treatment with UCB (100 μ M) for 24 h at 37°C, and cell death was estimated by PI staining. (B) UCB induced caspase-8 activation. Splenocytes (1×10^6) were incubated with UCB (25–100 μ M) for 24 h at 37°C and processed for the caspase-8 colorimetric activity assay, as described in Materials and Methods. (C and D) UCB increased the frequency of CD95- and Bax-positive cells. Splenocytes (1×10^6) were incubated with UCB (10–100 μ M) for 24 h at 37°C and stained with PE-labeled anti-CD95 antibody or PE-labeled anti-Bax antibody. (E and F) UCB treatment to splenocyte caused release of calcium and MMP ($\Delta\psi$ m) loss. Splenocytes (1×10^6) were incubated with UCB (10–100 μ M) for 6 h, and cells were stained with Fura 2-AM (2 μ M) or JC-1 (5 μ M), as described in Materials and Methods. The data are representative of three such independent experiments having similar results. Each bar represents mean \pm SEM from three replicates. * $P < 0.05$, as compared with vehicle group; \$ $P < 0.05$, as compared with UCB group.

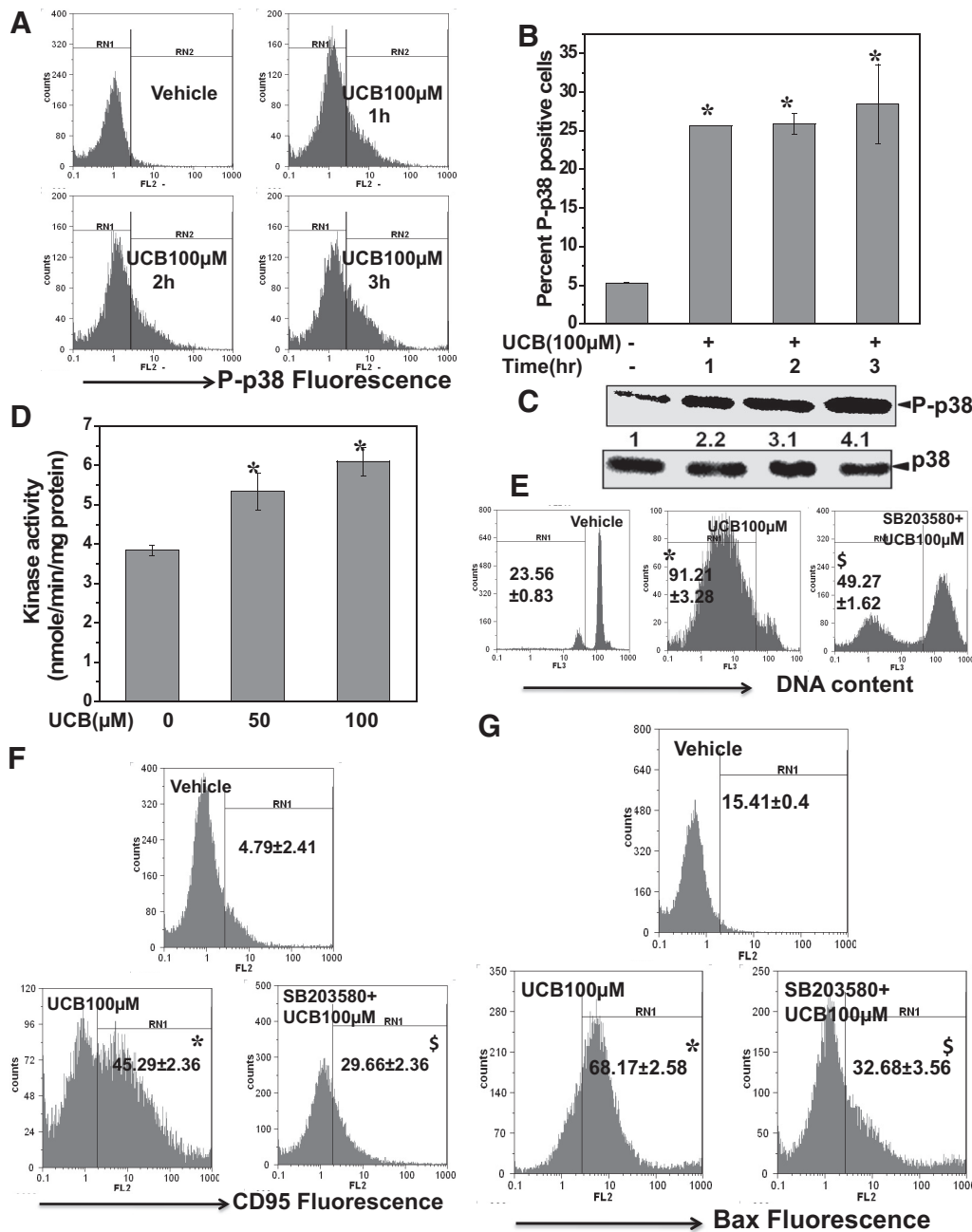


Figure 5. UCB induced apoptosis by activating p38MAPK pathways in splenocytes.

(A–C) Time-dependent phosphorylation of p38MAPK by UCB. (A and B) Splenocytes (3×10^6) were treated with UCB (100 µM) for an indicated time and stained with PE-labeled anti-p38 antibody, and percent p-p38-positive cells were estimated using flow cytometry. (C) For Western blot analysis, an equal amount of protein from cytoplasmic extracts of splenocytes was fractionated on 10% SDS-PAGE, electrotransferred onto a nitrocellulose membrane, and probed with an anti-p-p38MAPK antibody. Expression of p38MAPK in each group was used as a loading control. (D) UCB treatment increased protein tyrosine kinase activity. Splenocytes (10×10^6) were treated with UCB (50, 100 µM) for 3 h, and a whole cell lysate was prepared and processed for a tyrosine kinase colorimetric activity assay, as per the manufacturer's protocol. (E–G) SB203580 (p38MAPK inhibitor) inhibited UCB-induced death parameters. Splenocytes (1×10^6) were pretreated with SB203580 (10 µM) for 1 h, followed by UCB (100 µM) treatment for 24 h at 37°C, and processed for (E) PI staining, (F) PE-labeled anti-CD95 antibody, or (G) PE-labeled anti-Bax antibody. The data are representative of three such independent experiments having similar results. Each bar represents mean \pm SEM from three replicates. * $P < 0.05$, as compared with vehicle group; \$ $P < 0.05$, as compared with UCB group.

activation in splenocytes was associated with GSH depletion. It was observed that NAC treatment to splenocytes, 1 h prior to UCB, significantly inhibited the phosphorylation of p38MAPK (Fig. 6H and I). Collectively, these results suggest that glutathione depletion by UCB is a critical factor in mediating UCB-induced p38MAPK activation and immunotoxicity.

UCB causes immunotoxicity and immunomodulation in vivo

To evaluate the relevance of in vitro methods for immunotoxicity assessment, we examined the consequence of UCB

administration to the immune system in vivo. As 30–100 mg/kgbw UCB has been used in animal models [20, 21], a dose of 25–50 mg/kgbw to examine the immunotoxicity of UCB in vivo was selected. UCB (≥ 25 mg/kgbw) administration to mice led to a significant reduction in spleen weight, spleen index, and viability of spleen and bone marrow cells (Fig. 7A–D). Additionally, a significant decrease in erythrocytes, leukocytes, hemoglobin levels, percentage lymphocytes, monocytes, and packed cell volume was also recorded in UCB-administered mice, as compared with vehicle-administered mice (Fig. 7E).

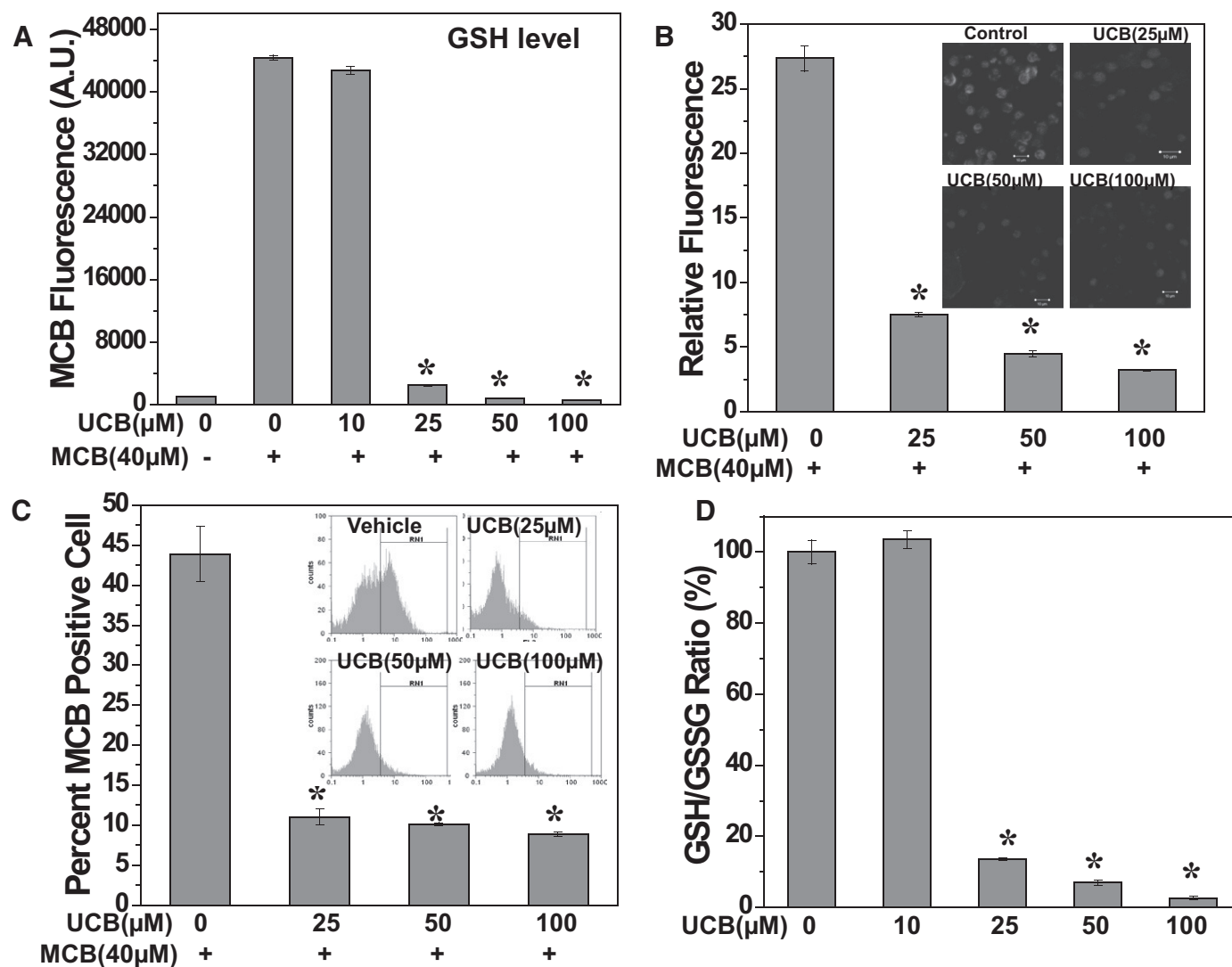


Figure 6. UCB depleted GSH levels in splenocytes. (A–D) UCB depleted cellular GSH levels. Splenocytes (1×10^6) were incubated with UCB (10–100 μ M) for 1 h at 37°C and stained with MCB (40 μ M) for 0.5 h. Fluorescence emission was recorded using (A) a spectrofluorimeter at 490 nm, following excitation at 394 nm; (B) confocal microscopy and fluorescence intensity of images were quantified using LSM Image Browser software, and representative images of the MCB-GSH conjugate in different treatments are shown in the inset. (C) Flow cytometry. (D) Splenocytes (1×10^6) were incubated with UCB (10–100 μ M) for 1 h at 37°C, and cellular levels of GSH and GSSG were evaluated by an enzymatic recycling assay. The data are representative of four such independent experiments having similar results. Each bar shows mean \pm SEM from hexareplicate.

(Continued on next page)

As UCB exposure to mice led to a significant reduction in the viable cell numbers in spleen, the ability of residual splenocytes to mount a proliferative immune response to T and B cell mitogens was examined. Fig. 7F showed that splenocytes taken from UCB (≥ 25 mg/kbw)-injected mice showed significantly depressed proliferative responses to both of the mitogens, as compared with that obtained from control mice. In all, these results suggest that UCB administration alters the host immune response in vivo.

UCB-induced immunotoxicity is mediated by activation of p38MAPK in vivo

To elucidate the molecular mechanism of UCB-mediated immunotoxicity in vivo, we examined p38MAPK activation in

splenocytes at various times after UCB administration to mice. A significant increase in p-p38MAPK was observed at 2 h of UCB administration (Fig. 8A and B). To confirm p38MAPK activation, we analyzed whether a selective inhibitor could inhibit the response observed during UCB challenge. In vivo studies have demonstrated that i.p. administration of SB203580 (p38MAPK inhibitor) at 5 mg/kbw, 2 h prior to chemical challenges, inhibited p38MAPK activation [49, 56]. Using this strategy in our experimental model, we injected inhibitor (SB203580) 2 h prior to UCB administration, and the result showed that SB203580 inhibited UCB-induced p38MAPK activation (Supplemental Fig. 6A and B) and significantly inhibited an UCB-induced decrease in the viability of splenocytes and bone marrow (Fig. 8C). UCB-induced death in splenocyte

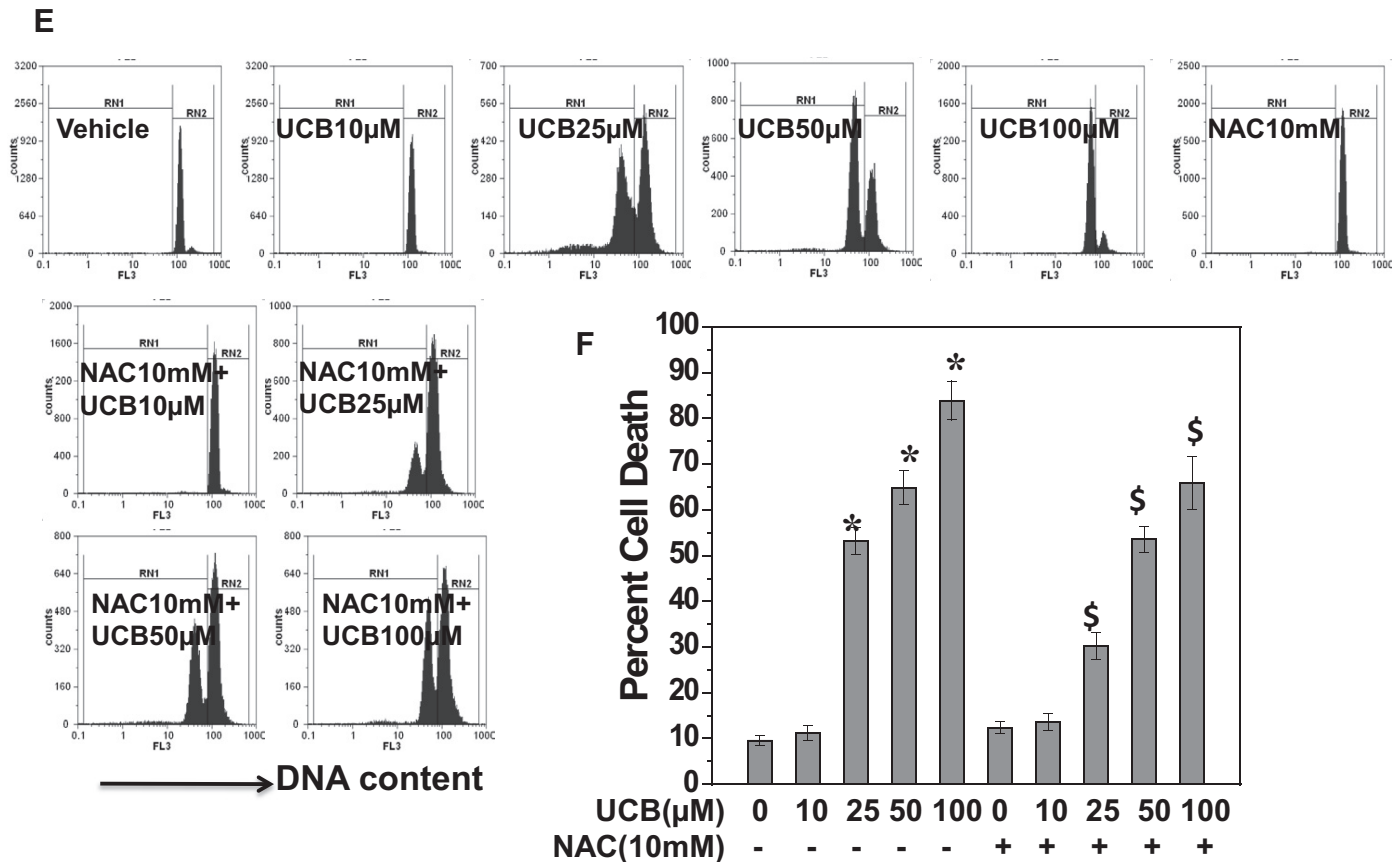


Figure 6. (E and F) NAC inhibited UCB-induced cell death. Splenocytes (1×10^6) were treated with NAC (10 mM) for 1 h prior to incubation of UCB (10–100 μ M) for 24 h at 37°C, and cell death was estimated by PI staining.

(Continued on next page)

and bone marrow was also inhibited by prior administration of the p38MAPK inhibitor, as measured by PI staining (Fig. 8D and E). Similarly, SB203580 administration attenuated the UCB-induced decrease in a proliferative response of splenocytes (Fig. 8F and G). On the whole, these results suggest that an in vivo response, observed during UCB administration, is mediated by the activation of p38MAPK and could be attenuated by using a specific inhibitor.

UCB administration causes oxidative stress in vivo

To elucidate the role of oxidative stress in vivo, we measured the effect of UCB administration on cellular ROS and GSH levels. Results showed that UCB administration at 50 mg/kgbw decreased GSH levels significantly and concomitantly increased the ROS levels in a time-dependent manner (Fig. 9A and B). To further confirm the role of oxidative stress in UCB-induced death in splenocytes, experiments were performed using NAC, an antioxidant and a GSH precursor [8, 9, 52]. NAC administration inhibited UCB-induced cellular GSH depletion and also the death in splenocytes (Fig. 9C and D). Taken together, these results demonstrated that UCB administration caused oxidative stress, and this response could be modified by prior administration of NAC.

DISCUSSION

Few studies have been conducted in the past to investigate the toxic effects of UCB on the immune system [21, 24, 26–31]. However, no studies have been directed toward examining the immunotoxicity of purified UCB at clinically relevant concentrations and molar ratios of UCB:BSA. We selected murine splenocytes as a model for screening of the immunotoxic potential of UCB. The lymphocyte proliferation to a mitogen and the ability of immune cells to release cytokines after the stimulation are relevant end-points to establish the immunotoxic effects of UCB. The results indicated the ability of UCB to suppress the immune response in vitro and in vivo. Our data about the decreased levels of inflammatory cytokines from macrophages and toxicity of UCB on T cells, B cells, and macrophages may explain the molecular mechanisms by which UCB reduces inflammation, iNOS expression, and host immune response and prevents the solid-organ graft rejection [20, 22, 57, 58]. Our results suggest that the molecular mechanisms by which UCB may induce immunosuppression in the host are not a result of cellular unresponsiveness but of induction of necrosis and apoptosis in mature immune cells. The results suggest that UCB is toxic to cells involved in the adap-

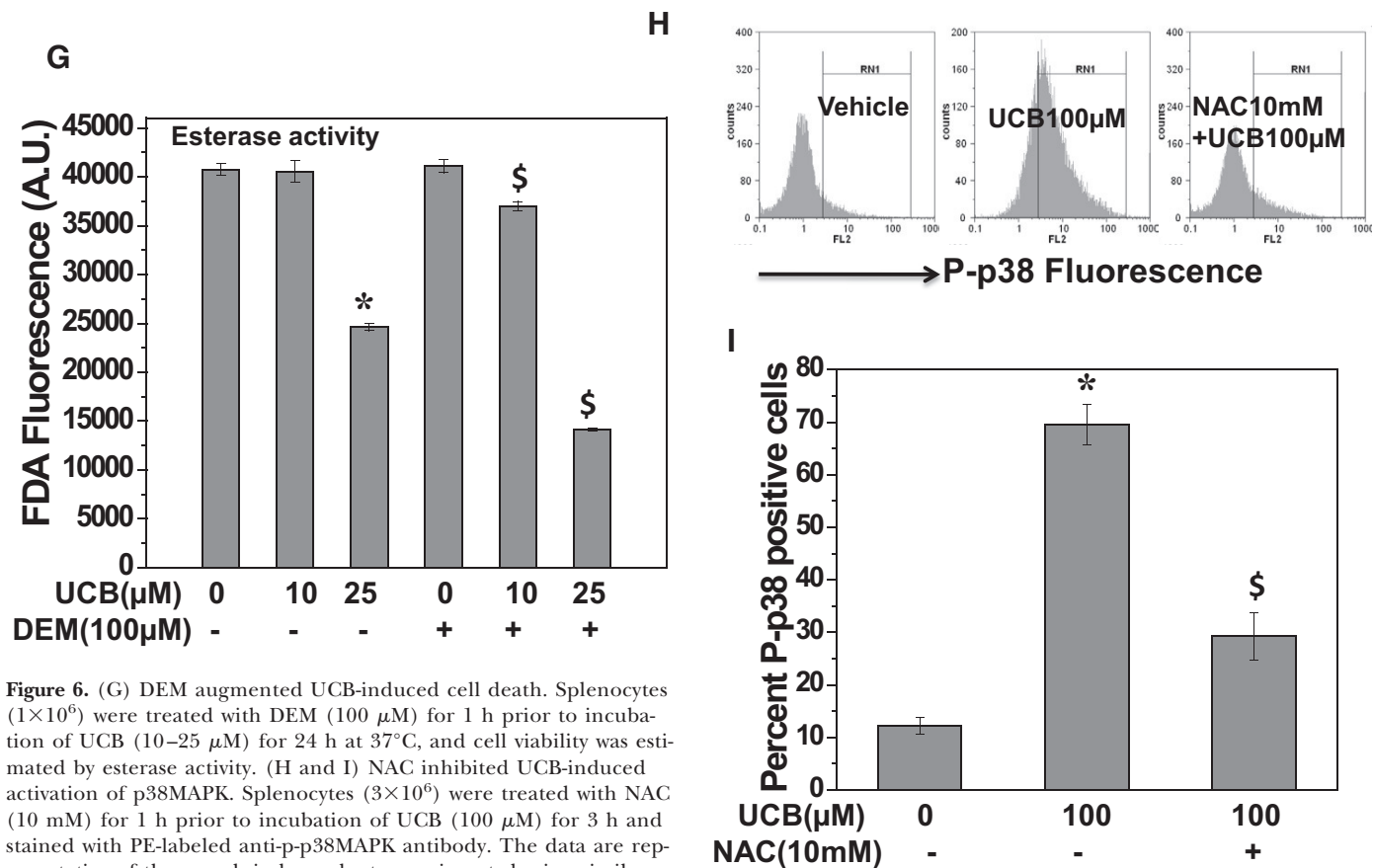


Figure 6. (G) DEM augmented UCB-induced cell death. Splenocytes (1×10^6) were treated with DEM (100 μ M) for 1 h prior to incubation of UCB (10–25 μ M) for 24 h at 37°C, and cell viability was estimated by esterase activity. (H and I) NAC inhibited UCB-induced activation of p38MAPK. Splenocytes (3×10^6) were treated with NAC (10 mM) for 1 h prior to incubation of UCB (100 μ M) for 3 h and stained with PE-labeled anti-p-p38MAPK antibody. The data are representative of three such independent experiments having similar results. Each data point represents mean \pm SEM from three replicates. * $P < 0.05$, as compared with vehicle group; \$ $P < 0.05$, as compared with corresponding UCB group.

tive and innate immune system. Splenic macrophages contribute significantly to the degradation of hemoglobin to UCB [59]. These results suggest that increased hemoglobin metabolism in the spleen could contribute to the host immunosuppression. It is interesting to note that the cell that produces UCB is sensitive to pathological concentrations of UCB. Studies need to be carried out to see whether this feedback inhibition is operative in the host and whether it has any biological significance.

The immunotoxic effects of UCB were studied by multiple viability assays. However, MTT assay for viability testing is not an appropriate method under our experimental conditions, as besides cells, other constituents of the media, such as antioxidants, vitamins, and albumin proteins with free SH groups, are also able to reduce tetrazolium salt, leading to the underestimation of cytotoxicity of the compounds to be tested [60]. UCB has also been known to get deposited on the cell surface, leading to underestimation of cytotoxicity of the tested compounds [19]. Our studies demonstrate that commercial and purified UCB kill resting lymphocytes at clinically relevant concentrations and UCB:BSA molar ratios. These experimental data are relevant to the health consequences of increased serum UCB. It is notable that our studies demonstrate significant cytotoxic effects of 25 μ M UCB in immune cells at molar ratios of UCB:BSA, which are well below unity. All concentra-

tions used by us correspond to an UCB:BSA molar ratio found in moderate-to-severe hyperbilirubinemia. The estimated free concentrations of UCB used in the present study are below its maximum aqueous solubility, and hence, it is unlikely that the inhibitory effects of UCB observed in our studies were mediated by precipitation of UCB aggregates [6]. UCB-binding variables for babies of different birthweight had indicated a mean total bilirubin concentration:albumin molar ratio of 0.26:0.61 [33]. To be clinically relevant, UCB levels should be selected such that B_f levels are below its solubility, i.e., 70 nmol/L. At the molar ratios of UCB and albumin, selected in our studies, the B_f levels are much lower than 70 nmol/L, based on the earlier work [12].

Previous studies have demonstrated that UCB-induced cell death in neural cells and astrocytes is mediated by apoptosis and necrosis [5, 41, 61]. Our results on UCB-induced immunotoxicity are in agreement with these findings. Elevated concentrations of UCB are able to activate select components of the stress pathway in Hepa 1c1c7 cells, which may contribute to UCB-mediated apoptosis [62]. The ability of UCB to bind to the plasma membrane, disrupt mitochondrial function, and induce apoptosis in various cell lines has been demonstrated [4–6, 12, 14–19, 35, 37, 38, 40]. The studies using rat brain neurons have shown that UCB-induced apoptosis is mediated via the mitochondrial pathway, as evidenced by the significant

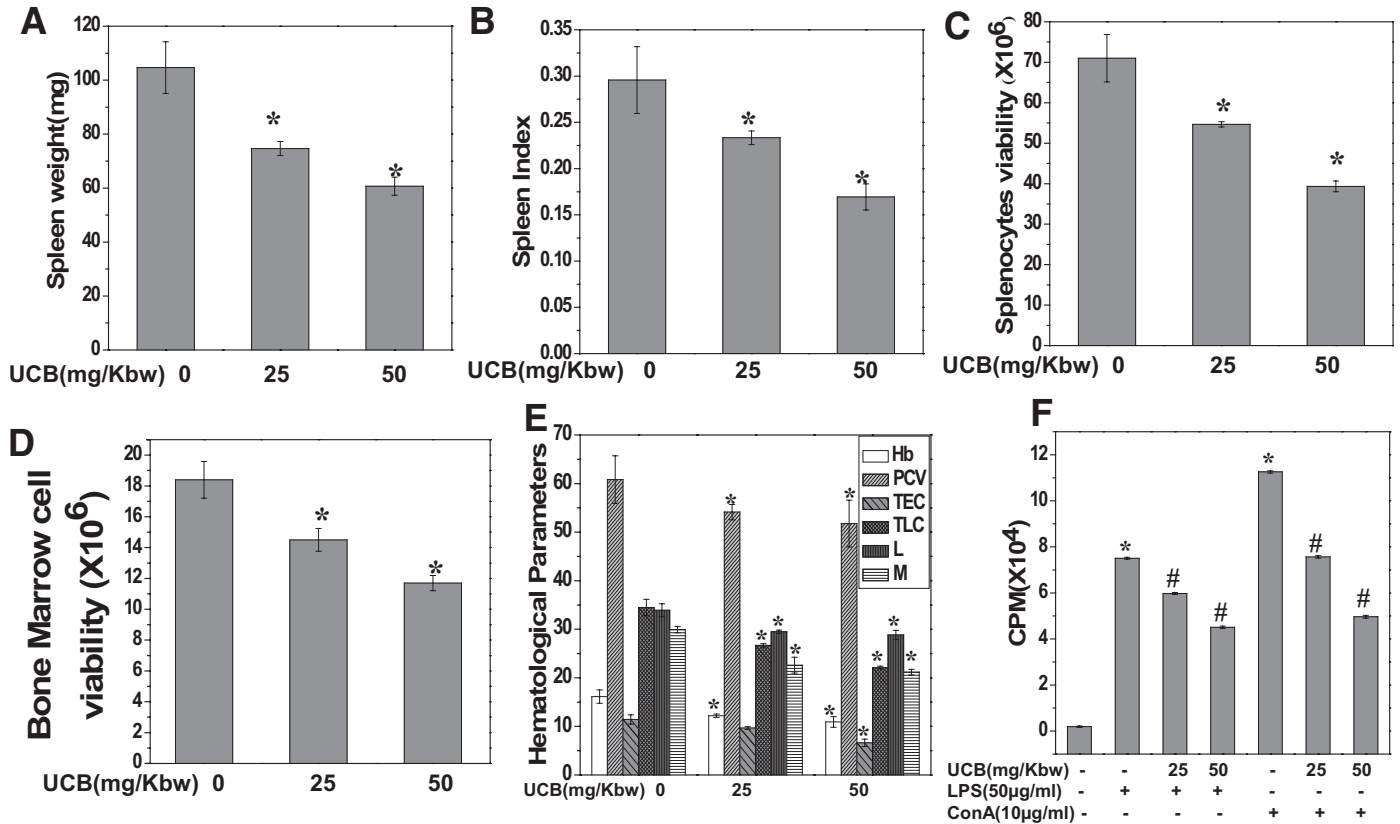


Figure 7. UCB caused immunotoxicity and immunomodulation in vivo. UCB (25, 50 mg/kbw) administration to mice decreased (A) spleen weight, (B) spleen index, (C) splenocyte viability, (D) bone marrow viability, and (E) hematological parameters. Hb, Hemoglobin (g/dl); PCV, packed cell volume in percent; TEC, total erythrocyte count in $\times 10^6/\text{mm}^3$; TLC, total leukocyte count in $\times 10^3/\text{mm}^3$; L, lymphocyte percent; M, monocyte percent. Mice were injected i.p. with UCB (25–50 mg/kbw), and after 24 h, spleen and femur bone marrow were removed, and cell viability was enumerated by trypan blue dye exclusion methods. Control mice were injected with vehicle only. (F) UCB administration inhibited the immune response of splenocytes to T cell and B cell mitogen. Splenocytes ($1 \times 10^6/\text{ml}$) isolated from vehicle or UCB (25–50 mg/kbw, 24 h)-administered mice were simulated with Con A (10 $\mu\text{g}/\text{ml}$) or LPS (50 $\mu\text{g}/\text{ml}$) for 72 h or 48 h, respectively, and were pulsed with ^3H thymidine (0.5 μCi); the cells were harvested after 16 h. The data are derived from one of the four such independent experiments having similar results. In each experiment, data from five mice/group were assessed, and each bar represents mean \pm SEM. * $P < 0.05$, as compared with vehicle group; # $P < 0.05$, as compared with LPS or Con A control group.

disruption in the MMP and the release of intracellular Ca^{2+} from calcium stores and specific activation of caspase-3 [16]. Thus, UCB can initiate changes in mitochondria and contribute to the apoptotic cascade. The decreased MMP observed in our experiments suggests that apoptosis of immune cells is also contributed by the perturbation of the mitochondrial membrane. In addition to activation of these intrinsic apoptotic events, UCB was found to up-regulate the expression of CD95 (Fas) and increase caspase-8 activity, suggesting that UCB induces apoptosis in splenocytes via activation of both apoptotic pathways.

The role of p38MAPK in UCB-induced neuronal death has been reported earlier [1, 17]. Activation of p38MAPK has been implicated in an extrinsic and intrinsic apoptotic response of the cell, as it is involved in Fas ligand expression, Bax translocation to the mitochondria, cytochrome c release, and caspase-3 activation [50, 51]. The early activation of p38MAPK in UCB-treated splenocytes suggests its contribution in cell death by the apoptotic pathways. The ability of the

p38MAPK inhibitor to attenuate the apoptotic markers and apoptosis induced by UCB further confirmed the role of p38MAPK activation in UCB-induced cell death. Ours is the first report demonstrating the involvement of the p38MAPK signaling cascade in the immunotoxicity of UCB.

The enzyme p38MAPK is a stress-activated protein kinase, which transduces environmental signals to the nucleus in response to various cellular stresses. Furthermore, various inflammatory mediators that regulate the redox status of cells activate p38MAPK in various cell types [63]. Changes in intracellular redox status are crucial events that trigger activation of p38MAPK signaling pathways. GSH is an important, protective antioxidant against oxidative stress. Wilhelm et al. [64] have shown that induction of p38MAPK was blocked almost completely by pretreatment of the cells with reducing agents, such as GSH and NAC, and depletion of the intracellular pool of GSH resulted in superinduction of p38MAPK activity. UCB-induced GSH depletion in splenocytes at an early time-point may be contributing to the activation of p38MAPK. Further-

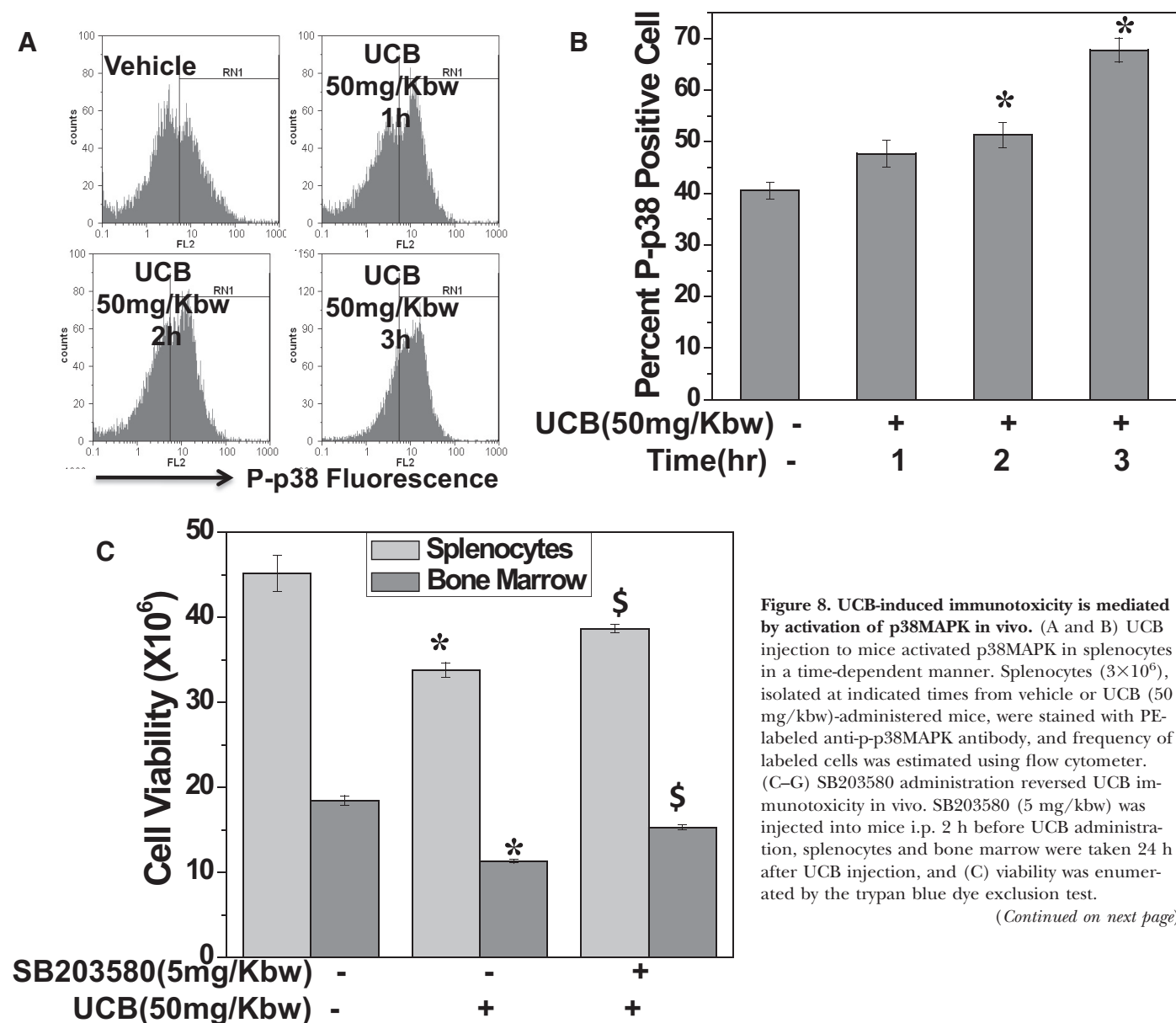


Figure 8. UCB-induced immunotoxicity is mediated by activation of p38MAPK in vivo. (A and B) UCB injection to mice activated p38MAPK in splenocytes in a time-dependent manner. Splenocytes (3×10^6), isolated at indicated times from vehicle or UCB (50 mg/kbw)-administered mice, were stained with PE-labeled anti-p-p38MAPK antibody, and frequency of labeled cells was estimated using flow cytometer. (C–G) SB203580 administration reversed UCB immunotoxicity in vivo. SB203580 (5 mg/kbw) was injected into mice i.p. 2 h before UCB administration, splenocytes and bone marrow were taken 24 h after UCB injection, and (C) viability was enumerated by the trypan blue dye exclusion test.

(Continued on next page)

more, pretreatment of cells with NAC, a known GSH precursor [8, 9, 52], abolished the UCB-induced activation of p38MAPK and reduced the cell death, which suggests that p38MAPK activation occurs via GSH depletion. Reports from earlier investigators showed that depletion of intracellular GSH activates p38MAPK signal transduction pathways through several mechanisms that include MAPK modulation by GSSG, oxidation of negative regulators of the MEK kinase apoptosis signal-regulated kinase 1, reversible ROS oxidation of cysteines in ERK-directed phosphatases, and direct interaction with GSH or glutathionylation [49].

The levels of cellular glutathione (GSH + GSSG) are considered as markers of oxidative stress, and the GSH:GSSG ratio is taken as an indicator of cellular redox status. GSH constitutes the major intracellular redox buffer in the cells and has been implicated in the modulation of various signal transduc-

tion pathways [65]. UCB has been shown to decrease cellular GSH levels and contribute to the altered redox state, leading to apoptosis in neuronal cells [8, 9]. These results are in agreement with our results, which demonstrate reduced GSH levels in UCB-treated splenocytes. Our results indicate the absence of ROS production when splenocytes were treated with UCB in vitro. On the contrary, UCB possessed significant antioxidant activity in immune cells when treated in vitro. These results are in agreement with the earlier studies [66–68]. Serum bilirubin levels in premature neonates, comparable with the concentrations used in our studies, correlated significantly with total antioxidant status [69]. UCB behaves like a metabolic “double-edged sword”, counteracting oxidative stress-mediated injury at low concentrations but becoming cytotoxic above a certain threshold [1, 62, 70]. UCB differentially affects the redox status of neuronal and astroglial cells [9]. The final

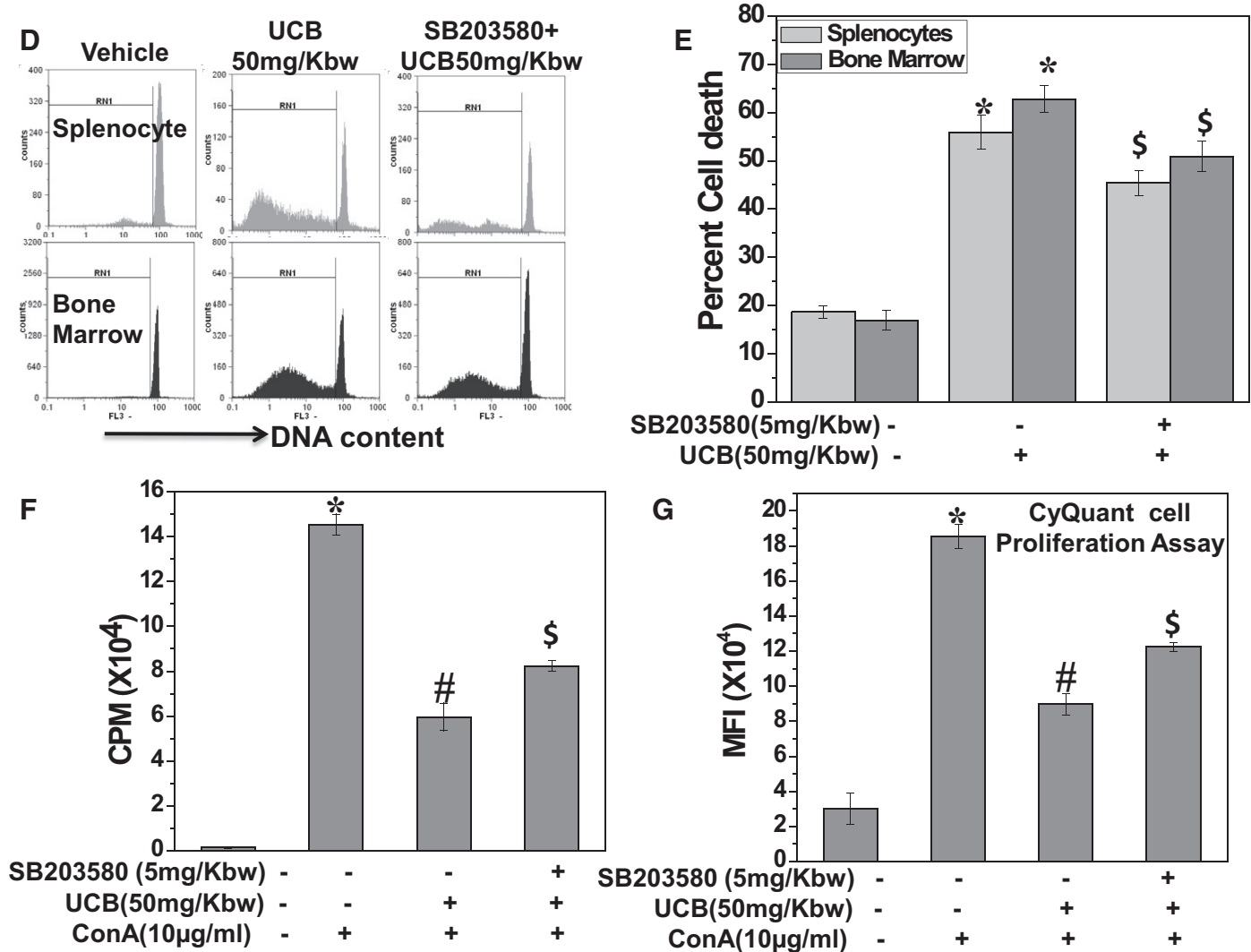


Figure 8. (D and E) Cell death was estimated by PI staining after culturing cells for 24 h at 37°C. (F and G) Splenocyte functionality, in response to Con A, was estimated by (F) ³H thymidine incorporation assay or (G) CyQuant cell proliferation assay. The data are derived from one of the three such independent experiments having similar results. In each experiment, data from five mice/group were assessed, and each bar represents mean ± SEM. * $P < 0.05$, as compared with vehicle group; # $P < 0.05$, as compared with Con A control group; \$ $P < 0.05$, as compared with corresponding UCB group.

outcome of its cellular effects—toxicity or protection, pro- or antioxidant—will depend on UCB concentration, extent of binding to plasma albumin, and time of incubation; target cell/tissue involved; cellular redox state; and developmental stages of cells [1]. Recent studies suggest a necessary and critical role of GSH depletion in the execution of apoptosis in lymphoid cells, independent of ROS formation [71]. Other studies have also shown that apoptosis seems to be actively regulated by GSH content and not by excessive ROS generation [65, 72]. Additionally, apoptosis has been suggested to occur under anaerobic conditions in the absence of ROS formation [73]. We have also observed the attenuation of UCB-induced apoptosis by pretreatment of cells with NAC, a known GSH donor. Protective effects of thiol compounds on apoptosis in the absence of excessive ROS formation have also been re-

ported by others [74]. These findings support the idea of a direct role of GSH in the regulation of the apoptotic machinery independent from ROS generation. These results imply a central role for GSH in the regulation of apoptosis rather than simply acting as an antioxidant/scavenger against ROS. Thus, it is time to look beyond GSH as a simple antioxidant and define its precise role in the signaling and execution of programmed cell death.

UCB administration in vivo led to a significant depletion of cellular GSH levels and increased ROS levels, indicating the contribution of oxidative stress in UCB-induced immunotoxicity. The difference in the in vitro and in vivo data regarding ROS formation seems to be a result of the route of administration and metabolism of UCB inside the host. Our data in immune cells are similar to the UCB toxicity of

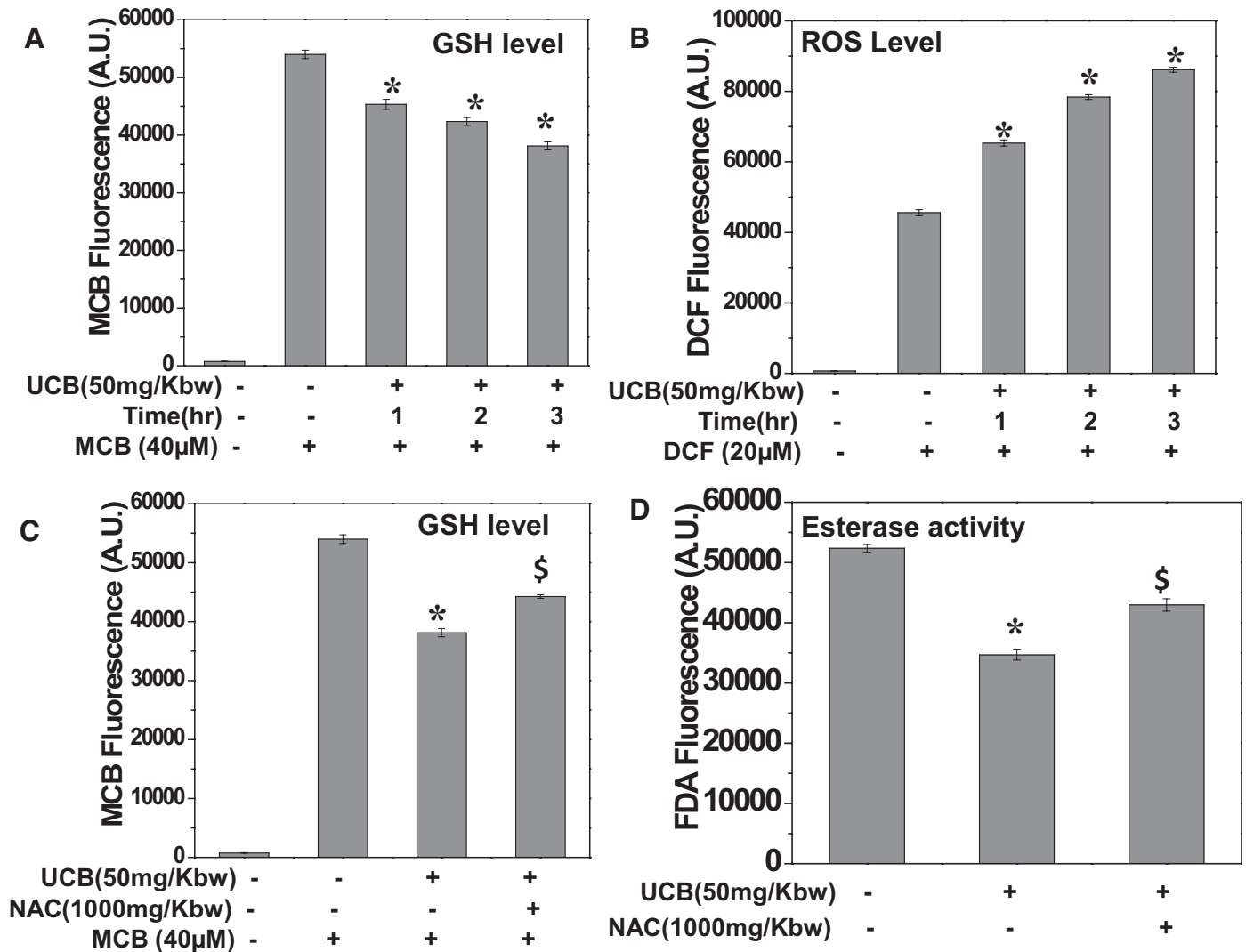


Figure 9. UCB administration caused oxidative stress in vivo. Splenocytes (1×10^6), isolated at indicated times from vehicle or UCB (50 mg/kbw)-injected mice, were stained with MCB (40 μ M) or H₂DCF-DA (DCF; 20 μ M) for 0.5 h at 37°C, and fluorescence emissions were recorded using a spectrofluorimeter for measurement of (A) GSH at 490 nm, following excitation at 394 nm, and (B) ROS at 535 nm, following excitation at 485 nm. (C and D) NAC administration inhibited UCB-induced GSH depletion and cell death. NAC (1000 mg/kbw) was injected into mice i.p., 0.5 h before UCB administration. (C) Splenocytes (1×10^6) were taken 3 h after UCB administration, and GSH level was estimated by the MCB method. (D) Splenocytes (1×10^6) were taken 24 h after UCB administration and cultured further for 24 h, and esterase activity was estimated. The data are derived from one of the three such independent experiments having similar results. In each experiment, data from five mice/group were assessed, and each bar represents mean \pm SEM. * $P < 0.05$, as compared with vehicle group; \$ $P < 0.05$, as compared with UCB group.

neuronal cells, astroglial cells, and hepatoma cells, which had shown that alteration of the redox status is a likely, early event responsible for UCB-induced cytotoxicity. UCB (50 mg/kbw) administration to mice causes activation of p38MAPK in splenocytes at an early time-point, and this activation was reduced significantly by a prior injection of mice with the p38MAPK inhibitor (SB203580) or GSH precursor (NAC), which suggests that p38MAPK activation in splenocytes of UCB-injected mice occurs via depletion of cellular GSH. Our results are in agreement with earlier findings of Limón-Pacheco et al. [49], which have shown that the activation of p38MAPK in different organs of mice

is associated with GSH depletion. The proposed model of UCB-induced activation of death pathways has been summarized in (Fig. 10).

The data about UCB toxicity to human PBMCs are very relevant, as the increased UCB levels are seen mainly in the blood of hyperbilirubinemic patients [2]. Tissue levels of UCB in rodents are low and in the range of 10–50 nM [75]. In the case of human patients with hyperbilirubinemia, the PBMCs are exposed to >150 μ M UCB. The death of immune cells by necrosis, as indicated by our assays, clearly demonstrates the ability of UCB to cause plasma membrane damage. Our data about UCB toxicity to RBCs are in agree-

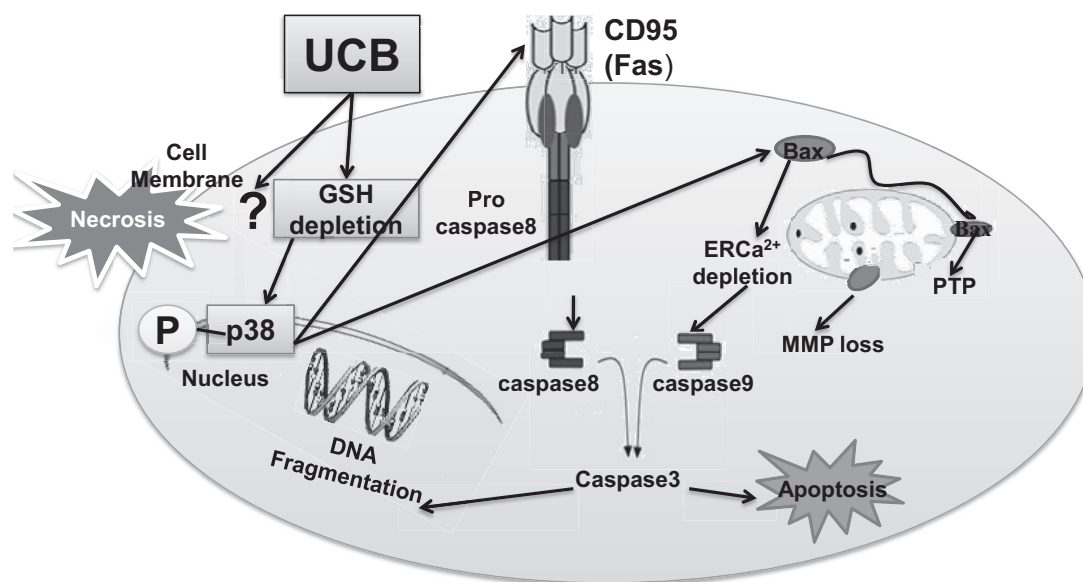


Figure 10. Proposed model of UCB-induced apoptosis and necrosis. UCB perturbed plasma membrane integrity and depleted the cellular GSH level, which in turn, phosphorylated p38MAPK (p38), resulting in activation of CD95, nuclear translocation of Bax, and loss of MMP, leading to activation of caspases and apoptosis. PTP, Permeability transition pore.

ment with the earlier work, where UCB has been shown to induce a profound disturbance in erythrocyte membrane integrity [13, 35, 36, 39]. Considering the above, our results, which demonstrate UCB toxicity to RBCs and PBMCs at concentrations of 25 μ M, become extremely important. In vivo, UCB administration induced a significant decrease in erythrocyte, blood lymphocyte count, and splenic cellularity, which may contribute to the susceptibility of the host to infection. The decreased lymphocyte count is suggestive of active destruction of mature, resting lymphocytes, as evidenced by the in vitro immunotoxicity of UCB. As UCB causes bone marrow depletion, it can be considered immunotoxic, because progenitor cells are derived from pluripotent stem cells present in the bone marrow. The in vivo immunotoxicity correlates with the immune parameters such as the T cell mitogen response to Con A and the B cell mitogen response to LPS in an ex vivo set-up. The in vitro immunotoxic effect of UCB suggests that the acute immunosuppression observed in mice might be, at least in part, a result of the direct cytotoxic effect of UCB on resting lymphocytes. Our results give direct support to the hypothesis that high-plasma UCB levels found in hyperbilirubinemic patients have been shown to act as a negative immune regulator under physiopathological situations including infection [31–33]. Further studies about the levels of UCB in blood plasma and immune status of the patients will give valuable insights regarding the in vivo relevance of our results.

In conclusion, our results demonstrate the ability of UCB to cause immunotoxicity besides neurotoxicity. These findings should prove useful in understanding the immunosuppression associated with hyperbilirubinemia. The observations presented in this study provide a molecular basis for the immunoregulatory properties of this important endoge-

nous molecule. Hyperbilirubinemia-associated, increased infection may be contributed by the immunosuppression caused by elevated plasma UCB levels. Results from our studies also reveal the potential use of UCB as an immunosuppressive agent in vivo.

AUTHORSHIP

N.M.K. designed and performed the research, and T.B.P. designed the research and wrote the manuscript.

ACKNOWLEDGMENTS

The authors acknowledge the Department of Atomic Energy (Mumbai, India) for financial support. We thank Dr. S. Adhikari, Radiation and Photochemistry Division, BARC, for his help in purifying the UCB. The authors also acknowledge the technical assistance of Mr. Prayag J. Amin, Mr. Narendra Sidnalkar, Mr. Kashinath Munankar, and Mr. Deepak Kathole.

REFERENCES

1. Kapitulnik, J. (2004) Bilirubin: an endogenous product of heme degradation with both cytotoxic and cytoprotective properties. *Mol. Pharmacol.* **66**, 773–779.
2. Wang, X., Chowdhury, J. R., Chowdhury, N. R. (2006) Bilirubin metabolism: applied physiology. *Curr. Paediatr.* **16**, 70–74.
3. Ostrow, J. D., Tiribelli, C. (2001) New concepts in bilirubin neurotoxicity and the need for studies at clinically relevant bilirubin concentrations. *J. Hepatol.* **34**, 467–470.
4. Ostrow, J. D., Pascolo, L., Tiribelli, C. (2002) Mechanisms of bilirubin neurotoxicity. *Hepatology* **35**, 1277–1280.
5. Ostrow, J. D., Pascolo, L., Brites, D., Tiribelli, C. (2004) Molecular basis of bilirubin-induced neurotoxicity. *Trends Mol. Med.* **10**, 65–70.

6. Rodrigues, C. M., Sola, S., Brites, D. (2002) Bilirubin induces apoptosis via the mitochondrial pathway in developing rat brain neurons. *Hepatology* **35**, 1186–1195.
7. Corich, L., Aranda, A., Carrassa, L., Bellarosa, C., Ostrow, J. D., Tiribelli, C. (2009) The cytotoxic effect of unconjugated bilirubin in human neuroblastoma SH-SY5Y cells is modulated by the expression level of MRP1 but not MDR1. *Biochem. J.* **417**, 305–312.
8. Brito, M. A., Lima, S., Fernandes, A., Falcao, A. S., Silva, R. F. M., Butterfield, D. A., Brites, D. (2008a) Bilirubin injury to neurons: contribution of oxidative stress and rescue by glycoconjugated bilirubin. *Neurotoxicology* **29**, 259–269.
9. Brito, M. A., Rosa, A. I., Falcao, A. S., Fernandes, A., Silva, R. F. M., Butterfield, D. A., Brites, D. (2008b) Unconjugated bilirubin differentially affects the redox status of neuronal and astroglial cells. *Neurobiol. Dis.* **29**, 30–40.
10. Silva, R. F. M., Rodrigues, C. M. P., Brites, D. (2002) Rat cultured neuronal and glial cells respond differently to toxicity of unconjugated bilirubin. *Pediatr. Res.* **51**, 535–541.
11. Seubert, J. M., Darmon, A. J., El-Kadi, A. O., D'Souza, S. J., Bend, J. R. (2002) Apoptosis in murine hepatoma hepa 1c1c7 wild-type, C12, and C4 cells mediated by bilirubin. *Mol. Pharmacol.* **62**, 257–264.
12. Chumiaud, L., Dessante, M., Chantoux, F., Blondeau, J. P., Francon, J., Trivin, F. (1996) Cytotoxicity of bilirubin for human fibroblasts and rat astrocytes in culture. Effect of the ratio of bilirubin to serum albumin. *Clin. Chim. Acta* **256**, 103–114.
13. Alexandra Brito, M., Silva, R. F., Brites, D. (2006) Bilirubin toxicity to human erythrocytes: a review. *Clin. Chim. Acta* **374**, 46–56.
14. Keshavan, P., Schwemmer, S. J., Smith, D. L., Babcock, G. F., Zucker, S. D. (2004) Unconjugated bilirubin induces apoptosis in colon cancer cells by triggering mitochondrial depolarization. *Int. J. Cancer* **112**, 433–445.
15. Akin, E., Clower, B., Tibbs, R., Tang, J., Zhang, J. (2002) Bilirubin produces apoptosis in cultured bovine brain endothelial cells. *Brain Res.* **931**, 168–175.
16. Rodrigues, C. M., Sola, S., Brito, M. A., Brites, D., Moura, J. J. (2002) Bilirubin directly disrupts membrane lipid polarity and fluidity, protein order, and redox status in rat mitochondria. *J. Hepatol.* **36**, 335–341.
17. Lin, S., Yan, C., Wei, X., Paul, S. M., Du, Y. (2003) p38 MAP kinase mediates bilirubin-induced neuronal death of cultured rat cerebellar granule neurons. *Neurosci. Lett.* **353**, 209–212.
18. Grojean, S., Koziel, V., Vert, P., Daval, J. L. (2000) Bilirubin induces apoptosis via activation of NMDA receptors in developing rat brain neurons. *Exp. Neurol.* **166**, 334–341.
19. Ngai, K. C., Yeung, C. Y., Karlberg, J. (1998) Modification of the MTT method for the study of bilirubin cytotoxicity. *Acta Paediatr. Jpn.* **40**, 313–317.
20. Wang, W. W., Smith, D. L., Zucker, S. D. (2004) Bilirubin inhibits iNOS expression and NO production in response to endotoxin in rats. *Hepatology* **40**, 424–433.
21. Liu, Y., Li, P., Lu, J., Xiong, W., Oger, J., Tetzlaff, W., Cynader, M. (2008) Bilirubin possesses powerful immunomodulatory activity and suppresses experimental autoimmune encephalomyelitis. *J. Immunol.* **181**, 1887–1897.
22. Ollinger, R., Wang, H., Yamashita, K., Wegiel, B., Thomas, M., Margreiter, R. (2007) Therapeutic applications of bilirubin and biliverdin in transplantation. *Antioxid. Redox Signal.* **9**, 2175–2185.
23. Kirkby, K. A., Adin, C. A. (2006) Products of heme oxygenase and their potential therapeutic applications. *Am. J. Physiol. Renal Physiol.* **290**, F563–F571.
24. Větvicka, V., Sima, P., Miler, I., Bilej, M. (1991) The immunosuppressive effects of bilirubin. *Folia Microbiol. (Praha)* **36**, 112–119.
25. Bulmer, A. C., Ried, K., Blanchfield, J. T., Wagner, K. H. (2008) The anti-mutagenic properties of bile pigments. *Mutat. Res.* **658**, 28–41.
26. Haga, Y., Tempero, M. A., Kay, D., Zetterman, R. K. (1996) Intracellular accumulation of unconjugated bilirubin inhibits phytohemagglutinin-induced proliferation and interleukin-2 production of human lymphocytes. *Dig. Dis. Sci.* **41**, 1468–1474.
27. Haga, Y., Tempero, M. A., Zetterman, R. K. (1996) Unconjugated bilirubin inhibits in vitro cytotoxic T lymphocyte activity of human lymphocyte. *Biochim. Biophys. Acta* **1317**, 65–70.
28. Miler, I., Sima, P., Větvicka, V. (1988) The potential immunosuppressive effects of bilirubin. *Allerg. Immunol. (Leipz.)* **34**, 177–184.
29. Sima, P., Mala, J., Miler, I., Hodr, R., Truxova, E. (1980) The suppressive effects of continuous infusion of bilirubin on immune response in mice. *Folia Microbiol. (Praha)* **25**, 483–490.
30. Rola-Plezczyński, M., Hensen, S. A., Vincent, M. M., Bellanti, J. A. (1975) Inhibitory effect of bilirubin on cellular immune response in man. *J. Pediatr.* **86**, 690–696.
31. Wu, J. F., Chiang, B. L., Chen, H. L., Lai, H. S., Chang, M. H., Ni, Y. H. (2006) Impaired T-lymphocyte proliferation function in biliary atresia patients with chronic cholestatic jaundice after a Kasai operation. *Pediatr. Res.* **60**, 602–606.
32. Field, E., Horst, H. M., Rubinfeld, I. S., Copeland, C. F., Waheed, U., Jordan, J. (2008) Hyperbilirubinemia: a risk factor for infection in the surgical intensive care unit. *Am. J. Surg.* **195**, 304–306.
33. Ahlfors, C. E., Wennberg, R. P., Ostrow, J. D., Tiribelli, C. (2009) Unbound (free) bilirubin: improving the paradigm for evaluating neonatal jaundice. *Clin. Chem.* **55**, 1288–1299.
34. McDonagh, A. F. (2007) Bilirubin toxicity to human erythrocytes: a more sanguine view. *Pediatrics* **120**, 175–178.
35. Brito, M. A., Silva, R. F. M., Brites, D. (2002) Bilirubin induces loss of membrane lipids and exposure of phosphatidylserine in human erythrocytes. *Cell Biol. Toxicol.* **18**, 181–192.
36. Alexandra Brito, M., Silva, R. F. M., Brites, D. (2006) Bilirubin toxicity to human erythrocytes: a review. *Clin. Chim. Acta* **374**, 46–56.
37. Malik, S. G., Irwanto, K. A., Ostrow, J. D., Tiribelli, C. (2010) Effect of bilirubin on cytochrome c oxidase activity of mitochondria from mouse brain and liver. *BMC Res. Notes* **3**, 162.
38. Amato, M. (1995) Mechanisms of bilirubin toxicity. *Eur. J. Pediatr.* **154** (Suppl. 4), S54–S59.
39. Mireles, L. C., Lum, M. A., Dennery, P. A. (1999) Antioxidant and cytotoxic effects of bilirubin on neonatal erythrocytes. *Pediatr. Res.* **45**, 355–362.
40. Rao, P., Suzuki, R., Mizobuchi, S., Yamaguchi, T., Sasaguri, S. (2006) Bilirubin exhibits a novel anti-cancer effect on human adenocarcinoma. *Biochem. Biophys. Res. Commun.* **342**, 1279–1283.
41. Ostrow, J. D., Pascolo, L., Tiribelli, C. (2003) Reassessment of the unbound concentrations of unconjugated bilirubin in relation to neurotoxicity in vitro. *Pediatr. Res.* **54**, 98–104.
42. Granato, A., Gores, G., Vilei, M. T., Tolando, R., Ferrareso, C., Muraca, M. (2003) Bilirubin inhibits bile acid induced apoptosis in rat hepatocytes. *Gut* **52**, 1774–1778.
43. McDonagh, A. F., Assisi, F. (1972) The ready isomerization of bilirubin IX- α in aqueous solution. *Biochem. J.* **129**, 797–800.
44. Shukla, J., Chatterjee, S., Thakur, V. S., Premachandran, S., Checker, R., Poduval, T. B. (2009) L-Arginine reverses radiation-induced immune dysfunction: the need for optimum treatment window. *Radiat. Res.* **171**, 180–187.
45. Khan, N. M., Sandur, S. K., Checker, R., Sharma, D., Poduval, T. B., Sainis, K. B. (2011) Pro-oxidants ameliorate radiation-induced apoptosis through activation of the calcium-ERK1/2-Nrf2 pathway. *Free Radic. Biol. Med.* **51**, 115–128.
46. Sharma, D., Sandur, S. K., Rashmi, R., Maurya, D. K., Suryavanshi, S., Checker, R., Sainis, K. B. (2010) Differential activation of NF- κ B and nitric oxide in lymphocytes regulates in vitro and in vivo radiosensitivity. *Mutat. Res.* **703**, 149–157.
47. Wilankar, C., Sharma, D., Checker, R., Khan, N. M., Patwardhan, R., Patil, A., Sandur, S. K., Devasagayam, T. P. A. (2011) Role of immunoregulatory transcription factors in differential immunomodulatory effects of tocotrienols. *Free Radic. Biol. Med.* **51**, 129–143.
48. Checker, R., Sharma, D., Sandur, S. K., Subrahmanyam, G., Krishnan, S., Poduval, T. B., Sainis, K. B. (2010) Plumbagin inhibits proliferative and inflammatory responses of T cells independent of ROS generation but by modulating intracellular thiols. *J. Cell. Biochem.* **110**, 1082–1093.
49. Limón-Pacheco, J. H., Hernández, N. A., Fanjul-Moles, M. L., Gonsébat, M. E. (2007) Glutathione depletion activates mitogen-activated protein kinase (MAPK) pathways that display organ-specific responses and brain protection in mice. *Free Radic. Biol. Med.* **43**, 1335–1347.
50. Hsu, S. C., Gavrilin, M. A., Tsai, M. H., Hani, J., Lai, M. Z. (1999) p38 Mitogen-activated protein kinase is involved in Fas ligand expression. *J. Biol. Chem.* **274**, 25769–25776.
51. Van Laethem, A., Kelst, S. V., Lippens, S., Declercq, W., Vandenaebroe, P., Janssens, S. (2004) Activation of p38 MAPK is required for Bax translocation to mitochondria, cytochrome c release and apoptosis induced by UVB irradiation in human keratinocytes. *FASEB J.* **18**, 1946–1948.
52. McLellan, L. I., Lewis, A. D., Hall, D. J., Ansell, J. D., Wolf, C. R. (1995) Uptake and distribution of N-acetylcysteine in mice: tissue-specific effects on glutathione concentrations. *Carcinogenesis* **16**, 2099–2106.
53. Cuadrado, A., Garcia-Fernandez, L. F., Gonzalez, L., Suarez, Y., Losada, A., Alcáide, V., Martínez, T., Fernandez-Sousa, J. M., Sanchez-Puelles, J. M., Muñoz, A. (2003) Aplidin induces apoptosis in human cancer cells via glutathione depletion and sustained activation of the epidermal growth factor receptor, Src, JNK, and p38 MAPK. *J. Biol. Chem.* **278**, 241–250.
54. Kim, S. M., Jong, G. P., Won, K. B., Min, H. S., Hyung, L., Yooc, S. K., Kyung, H. J., Seong, I. S., Byeong, C. J. (2008) Cadmium specifically induces MKP-1 expression via the glutathione depletion-mediated p38 MAPK activation in C6 glioma cells. *Neurosci. Lett.* **440**, 289–293.
55. Wu, D., Arthur, C. (2004) Glutathione depletion in CYP2E1-expressing liver cells induces toxicity due to the activation of p38 mitogen-activated protein kinase and reduction of nuclear factor- κ B DNA binding activity. *Mol. Pharmacol.* **66**, 749–760.
56. Ward, K. W., Prokscht, J. W., Azzarano, L. M., Mumawa, J. A., Roethke, T. J., Stelman, G. J., Walsh, M. J., Zeigler, K. S., McSurdy-Freed, J. E., Kehrlert, J. R., Chokshi, J., Levy, M. A., Smith, B. R. (2001) Preclinical

- pharmacokinetics of SB-203580, a potent inhibitor of p38 mitogen-activated protein kinase. *Xenobiotica* **31**, 783–797.
57. Kato, Y., Shimazu, M., Kondo, M., Uchida, K., Kumamoto, Y., Wakabayashi, G. (2003) Bilirubin rinse: a simple protectant against the rat liver graft injury mimicking heme oxygenase-1 preconditioning. *Hepatology* **38**, 364–373.
 58. Mazzone, G. L., Rigato, I., Ostrow, J. D., Bossi, F., Bortoluzzi, A., Sukowati, C. H. (2009) Bilirubin inhibits the TNF α -related induction of three endothelial adhesion molecules. *Biochem. Biophys. Res. Commun.* **386**, 338–344.
 59. Pimstone, N. R., Tenhunen, R., Seitz, P. T., Marver, H. S., Schmid, R. (1971) The enzymatic degradation of hemoglobin to bile pigments by macrophages. *J. Exp. Med.* **133**, 1264–1281.
 60. Funk, D., Schrenk, H. H., Frei, E. (2007) Serum albumin leads to false-positive results in the XTT and the MTT assay. *Biotechniques* **43**, 178–186.
 61. Silva, R. F., Rodrigues, C. M., Brites, D. (2001) Bilirubin-induced apoptosis in cultured rat neural cells is aggravated by chenodeoxycholic acid but prevented by ursodeoxycholic acid. *J. Hepatol.* **34**, 402–408.
 62. Oakes, G. H., Bend, J. R. (2010) Global changes in gene regulation demonstrate that unconjugated bilirubin is able to upregulate and activate select components of the endoplasmic reticulum stress response pathway. *J. Biochem. Mol. Toxicol.* **24**, 73–88.
 63. Haddad, J. J. (2002) The involvement of L- γ -glutamyl-L-cysteinyl-glycine (glutathione/GSH) in the mechanism of redox signaling mediating MAPK^{p38}-dependent regulation of cytokine production. *Biochem. Pharmacol.* **63**, 305–320.
 64. Wilhelm, D., Bender, K., Knebel, A., Angel, P. (1997) The level of intracellular glutathione is a key regulator for the induction of stress-activated signal transduction pathways including Jun N-terminal protein kinases and p38 kinase by alkylating agents. *Mol. Cell. Biol.* **17**, 4792–4800.
 65. Franco, R., Cidlowski, J. A. (2009) Apoptosis and glutathione: beyond an antioxidant. *Cell Death Differ.* **16**, 1303–1314.
 66. Stocker, R., Yamamoto, Y., McDonagh, A. F., Glazer, A. N., Ames, B. N. (1987) Bilirubin is an antioxidant of possible physiological importance. *Science* **235**, 1043–1046.
 67. MacLean, P. D., Drake, E. C., Ross, L., Barclay, C. (2007) Bilirubin as an antioxidant in micelles and lipid bilayers: its contribution to the total antioxidant capacity of human blood plasma. *Free Radic. Biol. Med.* **43**, 600–609.
 68. Tell, G., Gustincich, S. (2009) Redox state, oxidative stress, and molecular mechanisms of protective and toxic effects of bilirubin on cells. *Curr. Pharm. Des.* **15**, 2908–2914.
 69. Hammerman, C., Goldstein, R., Kaplan, M., Eran, M., Goldschmidt, D., Eidelman, A. I., Gartner, L. M. (1998) Bilirubin in the premature: toxic or natural waste. *Clin. Chem.* **44**, 2551–2553.
 70. Doré, S., Takahashi, M., Ferris, C. D., Hester, L. D., Guastella, D., Snyder, S. H. (1999) Bilirubin, formed by activation of heme oxygenase-2, protects neurons against oxidative stress injury. *Proc. Natl. Acad. Sci. USA* **96**, 2445–2450.
 71. Franco, R., Mihalics, I. P., John, A. C. (2007) Glutathione depletion is necessary for apoptosis in lymphoid cells independent of reactive oxygen species formation. *J. Biol. Chem.* **282**, 30452–30465.
 72. Han, Y. H., Kim, S. H., Kim, S. Z., Park, W. H. (2008) Apoptosis in arsenic trioxide-treated Calu-6 lung cells is correlated with the depletion of GSH levels rather than the changes of ROS levels. *J. Cell. Biochem.* **104**, 862–878.
 73. Jacobson, M. D., Raff, M. C. (1995) Programmed cell death and Bcl-2 protection in very low oxygen. *Nature* **374**, 814–816.
 74. Han, Y. H., Kim, S. Z., Kim, S. H., Park, W. H. (2008) Apoptosis in pyrogallol-treated Calu-6 cells is correlated with the changes of intracellular GSH levels rather than ROS levels. *Lung Cancer* **59**, 301–314.
 75. Sedlak, T. W., Snyder, S. H. (2004) Bilirubin benefits: cellular protection by a biliverdin reductase antioxidant cycle. *Pediatrics* **113**, 1776–1782.

KEY WORDS:

unconjugated bilirubin · p38MAPK · CD95 · Bax · oxidative stress



Original Contribution

Bilirubin augments radiation injury and leads to increased infection and mortality in mice: Molecular mechanisms

Q1 Nazir M. Khan, T.B. Poduval*

Immunology and Hyperthermia Section, Radiation Biology and Health Sciences Division, Bhabha Atomic Research Centre, Trombay, Mumbai 400 085, India

ARTICLE INFO

Article history:

Received 1 June 2012

Accepted 8 July 2012

Keywords:

p38MAPK

Infection

Hyperbilirubinemia

Immunosuppression

ABSTRACT

Our earlier results demonstrated that clinically relevant concentrations of unconjugated bilirubin (UCB) possessed immunotoxic effects. Whole-body irradiation (WBI) with 1 to 6 Gy leads to acute radiation syndrome, immunosuppression, and makes the host susceptible to infection. Since hyperbilirubinemia has been shown to be associated with several types of cancer, the present studies were undertaken to evaluate the radiomodifying effects of UCB in radiation-exposed mice having elevated levels of UCB. Pretreatment of splenic lymphocytes with UCB (1–50 μ M at UCB/BSA ratio < 1) augmented radiation-induced DNA strand breaks, MMP loss, calcium release, and apoptosis. Combination treatment of mice with UCB (50 mg/kg bw) followed by WBI (2 Gy) 0.5 h later, resulted in significantly increased splenic atrophy, bone marrow aplasia, decreased counts of peritoneal exudate cells, and different splenocyte subsets such as CD3+ T, CD4+ T, CD8+ T, CD19+ B, and CD14+ macrophages as compared to either UCB or WBI treatment. Hematological studies showed that WBI-induced lymphopenia, thrombocytopenia, and neutropenia were further aggravated in the combination treatment group. UCB pretreatment of mice potentiated WBI-induced apoptosis and decreased WBI-induced loss of functional response of various immune cells leading to augmentation of immunosuppression and infection susceptibility caused by WBI. In an acute bacterial peritonitis model, UCB pretreatment of mice significantly increased WBI-induced proinflammatory cytokines, nitric oxide, and peritoneal bacterial load resulting in increased infection and death. Studies using the pharmacological inhibitor of p38MAPK demonstrated the involvement of p38MAPK activation in the inflammatory cascade of peritonitis. These findings should prove useful in understanding the potential risk to hyperbilirubinemic patients during radiotherapy and victims of acute radiation exposure in the course of radiation accidents.

© 2012 Elsevier Inc. All rights reserved.

Introduction

Unconjugated bilirubin (UCB) has been demonstrated as a major physiologic immunosuppressant [1,2]. UCB decreases immune responses [3–6] and increased rates of infection have been documented in hyperbilirubinemic patients [7,8]. Our earlier work had demonstrated that clinically relevant concentrations of UCB induced both apoptosis and necrosis in immune cells via induction of oxidative stress [2]. Hyperbilirubinemia is common in intensive care unit patients, occurring in as many as 40% of

patients [7]. Studies have demonstrated the increased levels of UCB in various forms of cancer such as pancreatic ductal carcinoma, ampullary carcinoma, and pancreatic adenocarcinoma [9–13]. Recently, Park et al. reported that jaundice occurs in 19 to 40% of patients with hepatocellular carcinoma [14]. Radiation therapy is a widely recognized and most common treatment for these carcinomas [14–16]. Although hyperbilirubinemic cancer patients were exposed to ionizing radiation for cancer therapy, the data concerning the effects of hyperbilirubinemia on exposure of ionizing radiation were completely lacking. Characterizing the radiomodifying effects of clinically relevant concentrations of UCB is critical for understanding the potential risk to hyperbilirubinemic patients during radiotherapy and exposure to acute radiation in the course of radiation accidents.

Individuals may be exposed to doses of radiation of 1–10 Gy during the course of radiation therapy or as the result of radiation accidents or nuclear/radiological terrorism alone or in conjunction with bioterrorism [17]. Whole-body exposure to radiation greater than 1 Gy induces acute radiation syndrome (ARS) [18]. The earliest presentation of ARS is the hematopoietic syndrome or

Abbreviations: BSA, bovine serum albumin; Con A, concanavalin A; IL-1, 4, 6, interleukin 1, 4, 6; IFN- γ , interferon-gamma; JC-1, 5,5',6,6'-tetrachloro-1,1',3,3'-tetraethylbenzimidazolyl carbocyanine iodide; LPS, lipopolysaccharide; MMP ($\Delta\psi_m$), mitochondrial membrane potential; p38MAPK, p38 mitogen-activated protein kinase; PBMNCs, peripheral blood mononuclear cells; PEGs, peritoneal exudates cells; PI, propidium iodide; UCB, unconjugated bilirubin.

* Corresponding author. Fax: +91 22 2559515.

E-mail addresses: nazirbiotech@rediffmail.com (N.M. Khan), tbpodu@barc.gov.in (T.B. Poduval).

bone marrow syndrome (BMS) that occurs in patients who have received 2–6 Gy [19]. The seriously affected patients with bone marrow aplasia experience reduced defense against exogenous and endogenous factors, such as infection and inflammation, and consequently suffer from invasive infection and organ dysfunction [20–23]. Infection is the primary cause of death during radiation exposure that induces BMS.

Morbidity and mortality associated with radiation injuries are highly aggravated by secondary complications of stress, inflammation, infection, and trauma along with ARS [24–26]. Based on these findings, we hypothesize that hyperbilirubinemia during radiation exposure may worsen the radiation effects and increase the susceptibility of mice to develop infection. Hyperbilirubinemia is an abnormally high bilirubin concentration in the blood. Since, in normal circumstances, 96% of total plasma bilirubin is unconjugated [27–29], our study focused on the effects of UCB on exacerbation of radiation injury. We chose a dose of 2 Gy because at this dose BMS is a prominent component of ARS and further this dose is being used during radiation therapy of cancer. In the present report, we used a mouse model of ARS to study the effects of clinically relevant concentrations of UCB administration on suppression of immune responses in the irradiated host. Combination treatment protocol consisting of pretreatment of the mice with UCB followed by WBI was used to simulate hyperbilirubinemic conditions of patients exposed to radiation. We have also used an infection model of bacterial peritonitis to study the effects of clinically relevant concentrations of UCB on inflammatory cascade, infection susceptibility, and death in mice exposed to radiation.

Materials and methods

Reagents

UCB, bovine serum albumin (BSA, fraction V), propidium iodide (PI), lipopolysaccharide (LPS: *Escherichia coli* (O26:B6)), JC-1, Fura-2AM, RPMI 1640, sodium chloride, sodium hydrogen phosphate, disodium-hydrophosphate, Histopaque 1077, trypan blue, Trizma base, sodium azide, Triton X-100, Tween 20, 5-sulfosalicylic acid, dithiobis 2-nitrobenzoic acid (DTNB), NADPH, glutathione reductase (GR), glutathione (GSH), oxidized GSH (GSSG), triethanolamine, 2-vinylpyridine, 2,7-dichlorodihydrofluorescein-diacetate (H₂DCF-DA), dihydrorhodamine-123 (DHR-123), dihydroethidium (DHE), FITC-labeled *E. coli* and Griess reagent were purchased from Sigma Chemical Co. (St. Louis, MO, USA). Fetal calf serum (FCS) was obtained from GIBCO BRL (Grand Island, NY, USA). ELISA sets for detection of cytokines (IL-1 β , IL-6, TNF- α , IL-2, and IFN- γ), in situ cell death detection kit, and fluorescein were purchased from Roche Applied Science (Germany). Live/Dead assay kits were purchased from Molecular Probes, Invitrogen (Eugene, OR, USA). Concanavalin A (con A) and SB 203580 were purchased from Calbiochem (San Diego, CA, USA). Mouse CD 4 and CD 19-positive selection kits were purchased from Stem Cell Technologies (Vancouver, BC, Canada). Fluorescein diacetate (FDA) was purchased from MP Biomedicals (Irvine, CA, USA). Eosine methylene blue (EMB) agar media were procured from Himedia Labs Pvt. Ltd (Mumbai, India). Monoclonal antibodies against CD 3, CD 4, and CD 14 labeled with phycoerythrin (PE) and monoclonal antibodies against CD 19 and CD 8 labeled with FITC were obtained from BD Biosciences (San Jose, CA, USA).

Animal maintenance

Six- to 8-week-old inbred Balb/c male mice, weighing approximately 20–25 g, reared in the animal house of Bhabha Atomic Research Centre (BARC) were used. They were housed at constant

temperature (23 °C) with a 12/12 h light/dark cycle and were given mouse chow and water ad libitum. The guidelines issued by the Institutional Animal Ethics Committee of BARC, Government of India, regarding the maintenance and dissections of small animals were strictly followed. In our experiment, four to five mice per group were used, unless otherwise specified.

Preparation and treatment schedule of UCB

All preparations of UCB and experiments involving in vitro as well as in vivo were performed with minimal light to prevent its photodegradation. To ensure its chemical integrity, UCB stock solution was prepared just before experiment as described previously [2]. Briefly, stock solution of 900 μ M UCB was prepared by dissolving 1.05 mg of UCB in 2 ml of 0.1 N NaOH. After complete dissolution, 4 ml of BSA (450 μ M) was added to UCB stock to obtain a final concentration of 300 μ M UCB and BSA. The culture medium contained 10% FCS, which corresponds to a BSA concentration of approximately 45 μ M which was considered in calculating the molar ratio of UCB to BSA [2].

Experiments involving purified UCB were performed after further purifying the commercial preparation according to the method reported earlier [30]. In all in vitro experiments, cells were treated with UCB for 4 h in RPMI 1640 medium without FCS and were irradiated 2 Gy without washing the cells. Appropriate vehicle was for the control or radiation group in vitro. Cells were then supplemented with 10% FCS and cultured at 37 °C in a 95% air/5% CO₂ atmosphere.

For in vivo studies, UCB was dissolved in 0.1 N NaOH solution and the final concentration was adjusted to 5 mg/ml with 5% BSA. Mice were divided into four groups: The mice in the first group (UCB group) were injected with UCB 50 mg per kg body weight (50 mg/kg bw) intraperitoneally (ip). The second group received 2 Gy whole-body irradiation (WBI group) 0.5 h after vehicle administration. The third group received 2 Gy WBI, 0.5 h after UCB (50 mg/kg bw) administration (combination treatment group). Mice in the fourth group were treated with an equal volume of vehicle (vehicle group).

Measurement of bilirubin levels

Mice (5 animals per group) were administered with UCB (50 mg/kg bw). Blood was drawn from mice at various time points after ip administration of UCB. Serum bilirubin (total and direct) concentrations were measured using an autoanalyzer. Indirect bilirubin (unconjugated) levels were estimated by subtracting direct bilirubin levels from respective total bilirubin levels.

Irradiation schedule

Whole-body irradiation (WBI) and in vitro irradiation were carried out using a Gamma Cell 220 irradiator (AECL, Canada). BALB/c mice were placed in ventilated perspex boxes and exposed to 2 Gy WBI at a dose rate of 2.93 Gy/min. For in vitro experiments lymphocytes were resuspended in RPMI 1640 medium without FCS in 24-well plate and exposed to 2 Gy radiation.

Bone marrow and spleen cell suspensions

Bone marrow and spleen cell suspensions were prepared as reported earlier [31]. Briefly, bone marrow cell suspensions were prepared by injecting RPMI 1640 tissue culture medium through the marrow of the femur. Cells from both femurs of each mouse were centrifuged and suspended in a known volume of medium. Spleen was aseptically removed and placed in sterile dishes containing RPMI 1640 medium. Splenocytes were obtained by

squeezing the spleen through a nylon mesh of 70 μm pore size in a petri plate containing medium. The RBCs were lysed by brief hypotonic shock. Viable cells were counted using trypan blue dye exclusion methods.

Specific lymphocyte subsets were purified from splenocytes by using the positive selection magnetic separation method as reported earlier [32]. CD4+ T cells or CD19+ B cells were purified from splenic lymphocytes using anti CD4-PE or anti CD19-PE-labeled antibody in the presence of PE selection cocktail. Dextran-coated magnetic nanoparticles were used to select CD4+ T cells or CD19+ B cells in an EasySep magnet. Two rounds of separation were employed to yield high purity with good recovery of labeled cells. Since the positively selected cells have already been PE-labeled, purity was assessed directly by flow cytometry and it was found that >95% of the population were CD4+ or CD19+.

Human lymphocyte isolation

Informed, signed consent was taken from all the registered healthy volunteers before undertaking these studies. The guidelines issued by the Medical Ethics Committee of BARC, Government of India, were strictly followed during these studies. Peripheral venous blood (10 ml) was collected from the cubital vein of healthy volunteers and transferred immediately into heparinized vacutainer tubes (BD Pharmingen) and PBMCs were isolated as described earlier [33]. Briefly, blood was diluted 1:1 with sterile RPMI medium and gently layered on to 10 ml Histopaque 1077 in a 50-ml centrifuge tube. The tubes were centrifuged at 2500 rpm for 20 min and peripheral blood mononuclear cells (PBMCs) were collected from buffy coat. The PBMCs were washed three times with RPMI medium and viable cells were counted using trypan blue dye exclusion.

Estimation of apoptosis by PI staining

Lymphocytes (1×10^6) were incubated with or without UCB (1–50 μM) for 4 h before irradiation (2 Gy) and cultured for 24 h at 37 °C in RPMI 1640 medium supplemented with 10% FCS in a 95% air/5% CO₂ atmosphere. These cells were washed with 10 mM PBS and incubated with 1 ml of staining solution containing 0.5 $\mu\text{g}/\text{ml}$ PI, 0.1% sodium citrate, and 0.1% Triton X-100 overnight at 4 °C. A total of 20,000 cells were acquired in Partec PAS III flow cytometer and percentage apoptotic cells were determined by analyzing sub-G1 population (less than 2n DNA content) using FloMax software [34,35].

Estimation of apoptosis using DNA ladder assay

DNA fragmentation is the hallmark of apoptosis and was performed as reported earlier [35]. In brief, lymphocytes (1×10^6 cells) pretreated with or without UCB (50 μM) for 4 h were exposed to radiation 2 Gy and cultured for 24 h at 37 °C. The cells were washed with PBS and the pellet was suspended in 25 μl lysis buffer (50 mM Tris HCl, pH 8.0, 10 mM EDTA, 0.5% N-lauroyl sarcosine, 0.5 mg/ml proteinase K) and incubated at 50 °C for 1 h. RNase (5 μl) was added to the lysate and further incubated for 1 h at 50 °C. The DNA sample (10 μl) was mixed with 2 μl gel loading buffer, and electrophoresed in 1.8% agarose gel in TBE buffer (pH 8.0) containing ethidium bromide. The bands were visualized and photographed under UV light using Geldoc (Syngene, UK).

Estimation of apoptosis using TUNEL assay

To measure UCB (50 μM)-induced apoptosis in lymphocytes in the presence or absence of radiation, TUNEL assay was performed according to the manufacturer's protocols. The assays use an

optimized terminal transferase (TdT) to label free 3'OH ends in genomic DNA with fluorescein-dUTP. Apoptotic death was estimated using a flow cytometer by measuring the fluorescence of fluorescein-dUTP-labeled DNA nicks.

Live and Dead assay

To measure UCB (50 μM)-induced death in lymphocytes in the presence or absence of radiation, Live and Dead assay (Molecular Probes, Eugene, OR) was performed according to the manufacturer's protocol. The cell death was measured by increase in the fluorescence of dye bound to polyamine groups present in the inner surface of membrane using a flow cytometer.

Measurement of change in mitochondrial membrane potential (MMP) and intracellular calcium levels

Changes in MMP ($\Delta\psi\text{m}$) and intracellular calcium levels are considered as early events associated with apoptosis and were monitored 6 h after irradiation. Lymphocytes (1×10^6) pretreated with or without UCB (50 μM , 4 h) were exposed to radiation (2 Gy) and cultured for 6 h. Change in MMP was assessed using the mitochondrial-specific fluorescent probe JC-1 by spectrofluorimetric methods [2]. JC-1 (5 μM) was incubated with the cells for 0.5 h at 37 °C, prior to analysis. JC-1 has dual emission depending on the state of the mitochondrial membrane potential. JC-1 forms aggregates in cells with a high red fluorescence indicating a normal mitochondrial membrane potential. Loss of the mitochondrial membrane potential results in a reduction in the red fluorescence with a concurrent gain in green fluorescence as the dye shifts from an aggregate to monomeric state. Ratio of red to green fluorescence was used as an indicator of loss of MMP.

Fura 2-AM was used to measure the intracellular Ca²⁺ levels as described previously [35]. Fura 2-AM fluorescence changes when it is bound to Ca²⁺. Lymphocytes (1×10^6) were incubated with or without UCB (50 μM , 4 h), exposed to radiation (2 Gy) and 6 h irradiation, stained with Fura 2-AM (2 μM) for 0.5 h, and analyzed in a spectrofluorimeter (BMG Labtech Optima) at 335 nm excitation and 500 nm emission.

Estimation of DNA strand breaks by alkaline single-cell gel electrophoresis (Comet assay)

Lymphocytes (0.1×10^6 cells) pretreated with or without UCB (50 μM) for 4 h were exposed to radiation 2 Gy and immediately kept on ice to prevent repair. Two microscopy slides from each group were prepared and processed for comet assay as described previously [2]. The slides were immersed in lysis buffer for 1 h at 4 °C and equilibrated in alkaline solution for 20 min, followed by electrophoresis for 0.5 h at 25 V, 300 mA. After electrophoresis, the slides were neutralized and stained by 5X SYBR Green-II dyes. The images were captured using a Carl Zeiss Axioplan fluorescence microscope (Germany). Fifty images per slide were analyzed for percentage DNA content in the tail, tail length, tail moment, and olive tail moment using CASP software.

Measurements of ROS level

To monitor intracellular and radiation-induced ROS level, H₂DCF-DA, DHE, and DHR123 were used. To detect ROS level, splenocytes were preincubated with H₂DCF-DA (20 μM) or DHE (20 μM) or DHR123 (5 μM) for 20 min at 37 °C before treating with various concentrations of UCB. After 1 h of incubation, the change in fluorescence intensity of DCF, DHE, and Rhodamine123 was recorded at excitation wavelengths of 488, 480, and 488 nm and emission wavelengths of 535, 580, and 543 nm, respectively,

using a spectrofluorimeter [2]. The oxidized form of the dye acts as a control for changes in uptake, ester cleavage, and efflux. Further, Amplex Red assay was used to measure radiation-induced hydrogen peroxide as per the manufacturer's protocol.

Intracellular GSH assay

Cellular GSH (reduced and oxidized) levels were determined by the Tietze method as reported earlier [2]. Briefly, lymphocytes (1×10^6 cells) pretreated with or without UCB (50 μ M) were exposed to radiation 2 Gy and levels of GSH and GSSG were measured by the enzymatic recycling method. The sulfhydryl group of the molecule reacts with DTNB producing a yellow colored 5-thio-2-nitrobenzoic acid (TNB), and the disulfide is reduced by NADPH in the presence of glutathione reductase. GSSG was determined by derivatization of GSH by reaction with 2-vinylpyridine for 1 h at 4 °C. Supernatants were assayed in 100 mM sodium phosphate buffer, containing 0.62 mM EDTA, 1.7 mM NADPH, and 20.2 mM DTNB. The rate of TNB formation was monitored following addition of 1.2 U of glutathione reductase, at 420 nm. Glutathione concentrations were calculated using appropriate standards, treated as samples.

Administration of UCB to mice

Mice (four animals per group) were administered with UCB (50 mg/kg bw) or vehicle intraperitoneally (ip), 0.5 h before WBI (2 Gy), and sacrificed 24 h after irradiation. Viability of spleen cells, bone marrow cells, and PECs was enumerated by the trypan blue dye exclusion method. Spleen index was calculated [spleen index = (spleen weight/body weight) \times 100] as described previously [2]. Hematological parameters were assessed 24 h after WBI using an autoanalyzer. To study the p38MAPK activation in PECs, mice were sacrificed 3 h after WBI.

For apoptotic studies, mice were sacrificed immediately after WBI and cells (lymphocyte, bone marrow cells and PECs) were isolated and further cultured for 24 h at 37 °C and death was estimated by PI staining. The studies involving use of the p38MAPK inhibitor SB203580 (5 mg/kg bw) was injected ip, 2 h prior to UCB administration. The cell death in PECs isolated from these mice was estimated by esterase activity assay using FDA as fluorescent probe as described previously [2]. Briefly, PECs (1×10^6) isolated from mice sacrificed immediately after WBI were cultured for 24 h at 37 °C in complete medium. The cells were washed once with PBS and stained with FDA (20 μ M) for 0.5 h at 37 °C. Fluorescence intensity of FDA-stained cells was measured at an excitation wavelength of 485 nm and emission wavelength of 533 nm. Decrease in fluorescence intensity was taken as decrease in the viability of cell.

Antibody staining

Phenotype of the lymphocytes isolated from vehicle or UCB (50 mg/kg bw)-administered mice 0.5 h prior to WBI (2 Gy) were determined by flow cytometry using labeled antibodies specific for T cells (anti-CD3), helper T cells (anti-CD4), cytotoxic T cells (anti-CD8), B cells (anti-CD19), and macrophages (anti-CD14) as reported previously [35]. Lymphocytes (1×10^6) obtained 24 h after WBI were resuspended in 50 μ l buffer (PBS containing 10% fetal calf serum, 0.1% sodium azide) and were incubated on ice for 10 min for blocking Fc receptors. The cells were further incubated with 1 μ g of specific fluorescent-labeled antibody in 50 μ l buffer for 30 min on ice in the dark, and washed three times with the buffer. The number of CD3+ T cells, CD4+ T helper cells, CD8+ T cytotoxic cells, CD19+ B cells, and CD14+ macrophages in spleen-treated mice was determined by flow cytometry. The total cell yield was calculated

by multiplying the proportion of each cell subset by the total number of live cells obtained per spleen.

To study p38MAPK activation, PECs were isolated from treated mice 3 h after WBI and antibody staining was performed as illustrated earlier [2]. Briefly, PECs (1×10^6) were fixed with 4% paraformaldehyde for 10 min at room temperature and excess of paraformaldehyde was removed by washing once with wash buffer (PBS containing 1% BSA). Cells were permeabilized with PBST (PBS containing 0.02% Tween 20) thrice for 5 min each at room temperature followed by 2 washes with wash buffer and then incubated with PE-labeled anti-p38MAPK monoclonal antibody for 0.5 h at room temperature. Further cells were washed twice and analyzed on a FACS Calibur.

[³H]Thymidine incorporation assay

The assay was done as reported earlier [31]. Lymphocytes (2×10^6 /ml) isolated 24 h after WBI (2 Gy) exposures to vehicle or UCB-treated mice (50 mg/kg bw) were stimulated with LPS or Con A for 48 h or 72 h, respectively, in a 96-well plate. Cells were pulsed with [³H]thymidine (0.5 μ Ci/well, specific activity 6500 mCi/mM, Board of Radiation & Isotope Technology, Department of Atomic Energy, Mumbai, India) and further cultured for another 16 h. Cells were harvested on glass fiber filters using a Multimash-2000 harvester (Dynatech Laboratories Inc.). The incorporated radioactivity was counted in a liquid scintillation counter (LKB) and was expressed as counts per minute (CPM).

Measurement of cytokines

Lymphocytes isolated 24 h after WBI (2 Gy) exposure to vehicle or UCB-treated mice (50 mg/kg bw) were seeded in a 24-well plate at cell density of 2×10^6 /2 ml and were stimulated with Con A for 24 h at 37 °C. The concentration of IL-2, IL-6, and IFN- γ in the culture supernatant was estimated using cytokine ELISA sets as described earlier [35].

Phagocytic activity of peritoneal exudate cells

Phagocytic activity of peritoneal exudate cells (PECs) from WBI (2 Gy)-exposed mice injected with vehicle or UCB (50 mg/kg bw) was estimated using FITC-labeled *E. coli* as described earlier [36]. PECs were obtained 24 h after WBI by injection of 4 ml ice-cold RPMI 1640 medium into the peritoneal cavity and viable cells were counted using trypan blue dye exclusion. Cells (1×10^6) were mixed with FITC-labeled bacteria (1×10^7) in 1:10 effector to target ratio and centrifuged for 15 s to increase their interaction. The mixtures were incubated at 37 °C for 30 min. Ice-cold PBS was added to stop phagocytosis. Cells were acquired in a flow cytometer immediately with or without crystal violet to distinguish the fluorescence of surface-bound *E. coli* from phagocytosed *E. coli* [36]. A total of 20,000 PECs were acquired for each sample. The fraction of cells that had phagocytosed bacteria was calculated using Flowmax software.

The uptake of labeled bacteria by PECs was also studied by confocal laser microscopy. Cells were centrifuged on coverslips and mounted on glass slides with DABCO. Phagocytosed bacteria were observed using a LSM510 confocal microscope (Carl Zeiss, Jena GmbH, Germany) with a krypton-argon laser, coupled to an Orthoplan Zeiss photomicroscope using a 488 nm laser line and a 530 nm band pass filter.

Studies on mouse model of bacterial infection

To study the susceptibility of mice to develop infection in treated group, we have established an intraperitoneal bacterial

infection mouse model which is medically termed as bacterial peritonitis. Mice were exposed to WBI (2 Gy) 0.5 h after administration of UCB (50 mg/kg bw) or vehicle. To develop infection, these mice were injected ip with nonpathogenic *E. coli* K-12 strain (MG1655) 24 h after WBI exposure as described earlier [37].

MG1655 is an *E. coli* strain having fimbriae (pili), which are required for successful attachment and adhesion to the host tissues [38,39]; therefore, despite being nonpathogenic, it is an excellent model system for simulating the bacterial infection in animal models [40]. For infection purposes, cells of log-phase cultures ($OD_{600} \sim 0.5$) were collected by centrifugation, and resuspended in sterile normal saline at 4 °C. About 4×10^8 CFU (determined by plating) were injected ip into mice in 400- μ l aliquots. For survival studies acute doses (1×10^9 CFU) were injected in treated mice to record mortality. These mice were monitored for the presence of diarrhea and weight loss. Survival of mice was recorded for next 30 days and mean survival time was calculated.

Quantification of bacterial load in peritoneal cavity

Bacterial suspensions (4×10^8 CFU of MG1655) were injected 24 h after WBI (2 Gy) exposure to vehicle or UCB-treated mice (50 mg/kg bw). The animals were anesthetized 24 h after bacterial injection and their intraperitoneal cavity was flushed using 5 ml of chilled saline. The recovered peritoneal flush was 10-fold serially diluted and plated in duplicate on EMB agar, followed by overnight incubation at 37 °C for enumeration of the bacterial counts in the intraperitoneal cavity. The grown *E. coli* colonies give a distinctive metallic green sheen because of the ability of *E. coli* to ferment lactose and acidify the medium, and under acidic conditions the dyes produce a dark purple complex which is usually associated with a green metallic sheen. The EMB agar plates with grown *E. coli* were photographed using a Sony digital camera. The bacterial counts thus obtained were compared across different treatments to assess the effect of UCB administration in the presence of radiation on bacterial clearance from the given host.

Measurement of serum nitric oxide and cytokine

Mice (4 animals per group) were exposed to WBI (2 Gy) 0.5 h after administration of UCB (50 mg/kg bw) or vehicle and were injected with *E. coli* (4×10^8 CFU) 24 h after WBI. The mice were sacrificed at 6 h after bacterial injection and concentration of nitric oxide (NO) was measured in the serum by using Griess reagent as described earlier [35]. The levels of proinflammatory cytokines (IL-1 β , IL-6, and TNF- α) in the serum were estimated using cytokine ELISA sets as per manufacturer's instructions.

Statistical analysis

Data were presented as mean \pm SEM. Data from all the experiments were analyzed using one-way ANOVA followed by post hoc analyses using the Scheffe test. Significance was set at $P < 0.05$.

Results

UCB augmented radiation-induced apoptosis and DNA strand breaks in lymphocytes

Since cellular constituents of the immune system are highly sensitive to radiation, we examined the effects of UCB pretreatment on radiation-induced apoptosis in murine splenic lymphocytes, the

key players of adaptive immune response. Fig. 1A shows flow cytometric histograms of PI-stained cells exposed to radiation in the presence or absence of UCB. It was found that UCB at $\geq 25 \mu$ M was toxic to lymphocytes, which is in agreement with our earlier findings [2]. The pretreatment of lymphocytes with UCB before radiation exposure significantly increased apoptosis, when compared to either UCB or radiation group (Fig. 1B). The observed radiomodifying effects of UCB were further confirmed by Live and Dead assay (Supplementary Fig. 1A and B) TUNEL assay (Fig. 1C and D), changes in cell size (Fig. 1E), and DNA-fragmentation assay (Fig. 1F).

Since DNA is the primary target of radiation, we studied the effects of UCB on radiation-induced DNA strand breaks in lymphocytes. Results of the comet assay showed that UCB (50 μ M) treatment to lymphocytes induced DNA strand breaks and further augmented radiation-induced DNA strand break (Fig. 1G and H).

To eliminate the possible effect of surface active contaminants usually present in the commercial UCB preparations [30], experiments were conducted using purified UCB. The results showed that purified UCB also exhibited similar toxicity to splenic lymphocytes and further augmented radiation-induced death (Fig. 1I).

UCB augmented radiation-induced loss of MMP and calcium release in lymphocytes

Since UCB showed radiomodifying effects in lymphocytes by augmenting radiation-induced apoptosis, experiments were carried out to see the effects of UCB pretreatment on early events of radiation-induced apoptosis. Alterations in intracellular Ca^{2+} homeostasis and mitochondrial membrane integrity leading to loss of MMP are considered as early events of apoptosis. Results showed that treatment of lymphocytes with UCB (50 μ M) induced loss of MMP and release of calcium into cytoplasm (Fig. 2A and B). Our results also revealed that radiation-induced loss of MMP and calcium release were further augmented by pretreatment of lymphocytes with UCB (Fig. 2A and B). Taken together these results suggested that UCB increased the effects of radiation in lymphocytes by augmenting radiation-induced early events of intrinsic apoptotic pathways.

UCB augmented radiation-induced apoptosis of various immune cells

To ascertain whether the radiomodifying effects of UCB were of general importance for multiple cell types, similar experiments were performed in CD4+ T cells, CD19+ B cells, PECs, and human PBMCs. Results showed that UCB induced significant apoptosis in all cell types and further augmented radiation-induced apoptosis (Fig. 3A and B).

UCB augmented radiation-induced oxidative stress in lymphocytes

Oxidative stress results from an imbalance between ROS production and ROS elimination by GSH, a major cellular antioxidant [41]. The role of oxidative stress in UCB-mediated augmentation of radiation-induced apoptosis was investigated by measuring the GSH and ROS levels in UCB-treated lymphocytes exposed to radiation.

Cellular GSH exists predominantly in a reduced form, but small amounts of the oxidized disulfide form are also present; therefore, the GSH/GSSG ratio is taken as a more appropriate indicator of the cellular redox status. Results showed that either UCB or radiation treatment alone decreased the GSH/GSSG ratio. The combination treatment of lymphocytes further decreased the GSH/GSSG ratio (Fig. 4). To further investigate the role of UCB on the redox status of lymphocytes, we also measured its effect on intracellular and radiation-induced ROS levels by using

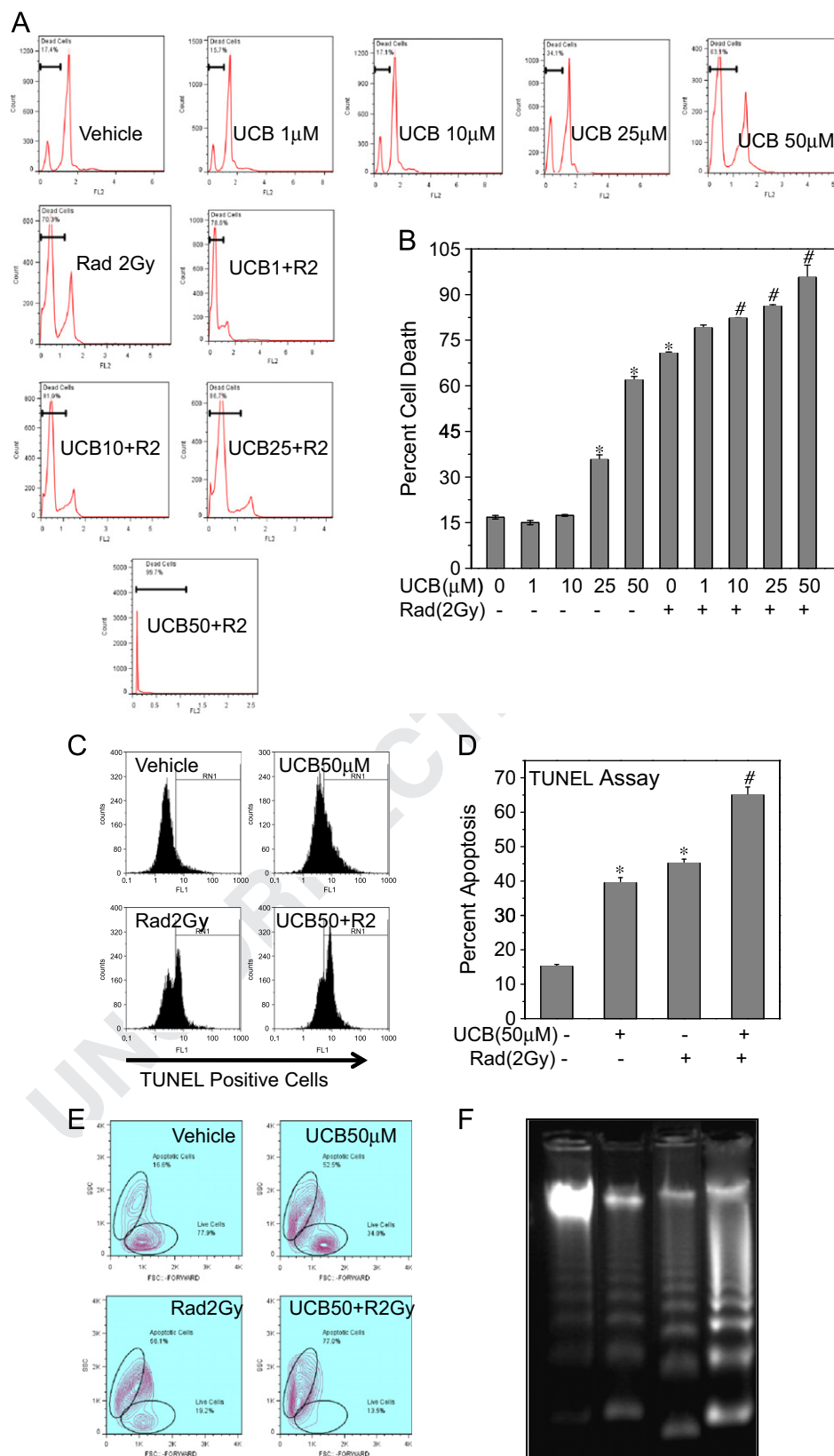


Fig. 1. UCB augmented radiation-induced cell death and DNA strand breaks in lymphocytes: Splenic lymphocytes (1×10^6) were incubated with UCB (1–50 μ M) for 4 h at 37 °C, exposed to 2 Gy gamma irradiation, and further cultured for 24 h and processed for (A, B) PI staining, (C, D) TUNEL assay, (E) changes in cell size, (F) DNA fragmentation assay, and (G, H) comet assay as described under Materials and methods. (I) Lymphocytes (1×10^6) preincubated with or without purified UCB (50 μ M, 4 h) were exposed to 2 Gy gamma irradiation and further cultured for 24 h and cell death was estimated by PI staining. The data are representative of two such independent experiments having similar results. Each bar represents mean \pm SEM. * $P < 0.05$, as compared to vehicle group, # $P < 0.05$, as compared to either UCB group or irradiated group.

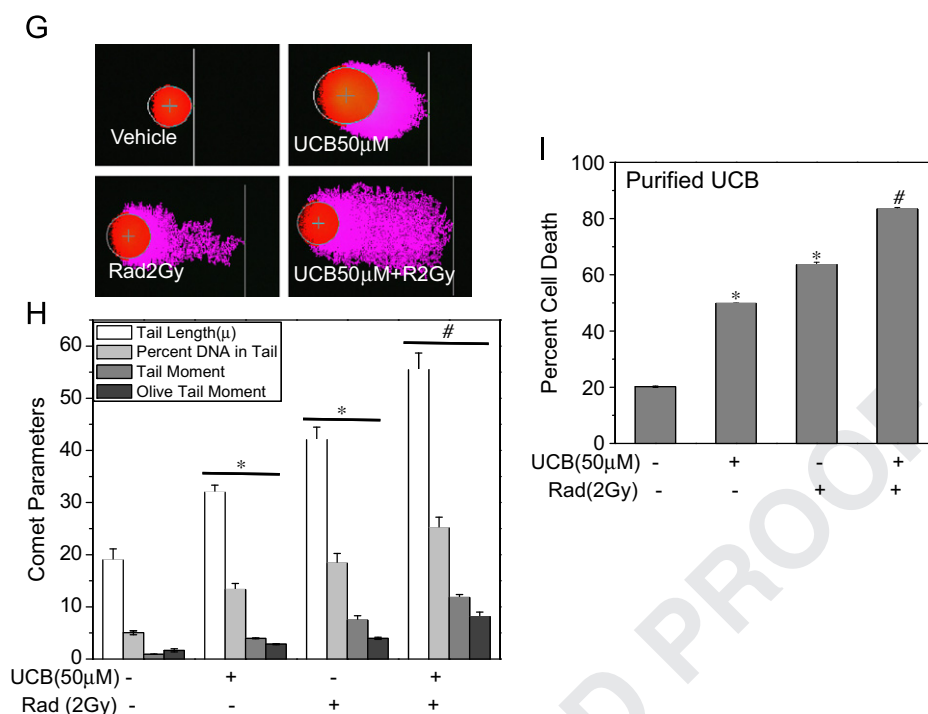


Fig. 1. (continued)

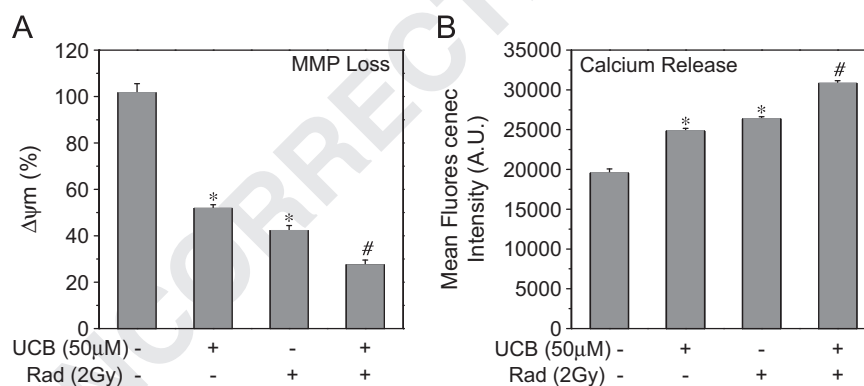


Fig. 2. UCB augmented radiation-induced loss of MMP and calcium release in lymphocytes: Splenic lymphocytes (1×10^6) incubated with UCB (50 μ M, 4 h) were exposed to radiation (2 Gy) and further culture for 6 h and cells were stained with (A) JC-1 (5 μ M) for measurement of MMP or (B) Fura 2-AM (2 μ M) for measurement of calcium as described under Materials and methods. The data are representative of two such independent experiments having similar results. Each bar represents mean \pm SEM from four replicates. * $P < 0.05$, as compared to vehicle group. # $P < 0.05$, as compared to either UCB group or irradiated group.

Amplex Red assay and the redox-sensitive fluorescent dye H_2DCF -DA, DHE, and DHR-123. The results showed that UCB treatment of lymphocytes decreased the basal as well as radiation-induced ROS levels (Supplementary Fig. 2A–D).

UCB pretreatment of mice augmented WBI-induced immunosuppression

To evaluate the relevance of in vitro radiomodifying effects of UCB under in vivo condition, we administered the mice with an immunotoxic dose of UCB (50 mg/kg bw) prior to WBI (2 Gy) and examined the ability of UCB to augment WBI-induced immunotoxicity in terms of loss of viability of splenocytes, bone marrow, PECs, and various hematological parameters. A WBI dose of 2 Gy was selected since this dose of radiation causes immunosuppression in mice [31]. The dose of 50 mg/kg bw was selected because our previous study demonstrated that this dose of UCB possessed immunosuppressive and immunotoxic activities in mice [2]. Our results showed that on

administration of UCB (50 mg/kg bw), serum bilirubin levels (total, unconjugated, conjugated) peaked to approximately 10-fold above the baseline at 0.5 h and then gradually decreased nearly to basal levels after 6 h (Fig. 5A). Hence mice were exposed to WBI, 0.5 h after UCB administration.

Results showed that UCB administration to mice reduced spleen weight, spleen index, and viability of splenocytes, suggesting its immunotoxic potential under in vivo condition (Fig. 5B–D). The combination treatment of mice with UCB and WBI significantly decreased the above immune parameters, when compared to either UCB or WBI group (Fig. 5B–D). Since UCB augmented WBI-induced splenic atrophy, we specifically monitored the effect of combination treatment of mice on various phenotypes of spleen cells. The results showed that combination treatment of mice significantly decreased the counts of different splenocyte subsets such as CD3+ T cells, CD4+ T helper cells, CD8+ T cytotoxic cells, CD19+ B cells, and also CD14+ macrophages when compared to either UCB or WBI group (Table 1). Additionally, UCB administration to mice further

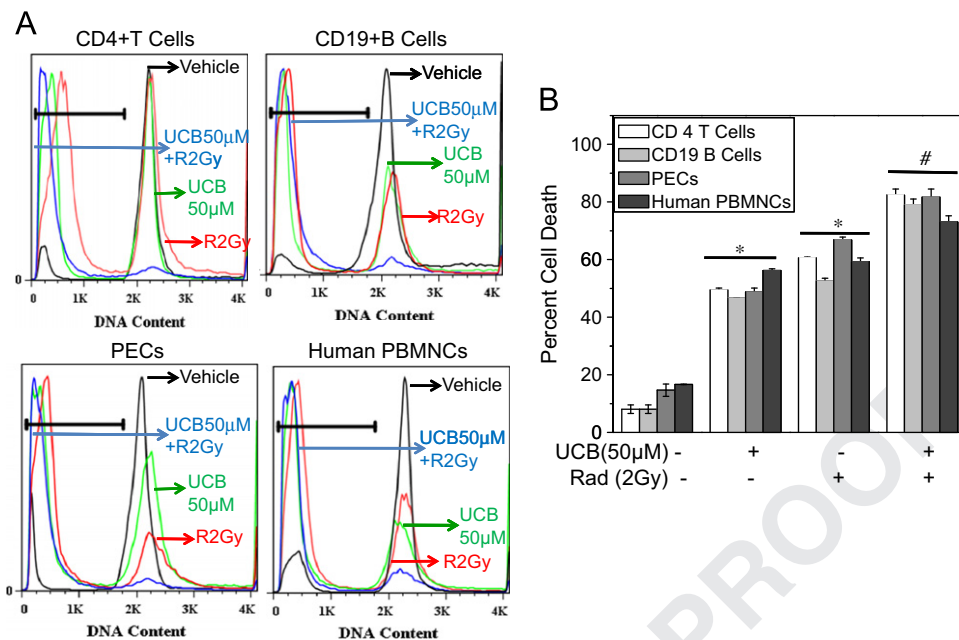


Fig. 3. UCB augmented radiation-induced apoptosis of various immune cells: Purified mouse splenic CD4+ T cells or CD19+ B cells or PECs or human PBMNCs (1×10^6 each) were treated with UCB (50 μ M) for 4 h before exposure to radiation (2 Gy) and further cultured for 24 h at 37 °C and cell death was estimated by PI staining. The data are representative of two such independent experiments having similar results. Each bar represents mean \pm SEM from three replicates. * $P < 0.05$, as compared to vehicle group. # $P < 0.05$, as compared to either UCB group or irradiated group.

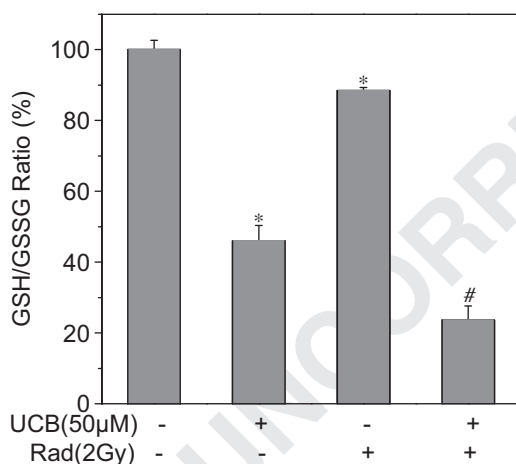


Fig. 4. UCB augmented radiation-induced oxidative stress in lymphocytes: UCB depleted cellular GSH levels and augmented radiation-induced GSH depletion. Lymphocytes (1×10^6) pretreated with or without UCB (50 μ M) were exposed to radiation (2 Gy) and cellular levels of GSH and GSSG were evaluated by an enzymatic recycling assay. The data are representative of two such independent experiments having similar results. Each bar represents mean \pm SEM from three replicates. * $P < 0.05$, as compared to vehicle group. # $P < 0.05$, as compared to either UCB group or irradiated group.

UCB pretreatment of mice augmented WBI-induced apoptosis in various immune cells

Since WBI-induced decrease in viable cell counts of various immune cells is mediated by induction of apoptosis in these cells, an experiment was set up to see the effects of UCB administration on induction of WBI-induced apoptosis. It was found that UCB administration alone to mice induced apoptosis in lymphocytes, bone marrow, and PECs (Fig. 6A). Results also showed that mice from the combination treatment group exhibited significantly increased apoptosis when compared to either UCB or WBI group (Fig. 6A).

UCB pretreatment of mice decreased WBI-induced loss of functional response of various immune cells

Since UCB administration to mice in the presence or absence of WBI exposure led to a significant reduction in the viable cell numbers in spleen, the ability of residual splenocytes to mount a proliferative immune response to T and B cell mitogens was examined. Results showed that lymphocytes taken from UCB (50 mg/kg bw)-administered mice showed significantly depressed proliferative responses to both mitogens (LPS, Con A), as compared to that obtained from vehicle-administered mice (Fig. 6B). It was found that lymphocytes obtained from the combination treatment group were less responsive to both mitogens, when compared to either UCB or WBI group (Fig. 6B). Similar depressed responses of lymphocytes from the combination treatment group as compared to either UCB or WBI group were obtained in terms of cytokine production (IL-2, IL-6, and IFN- γ) on Con A stimulation (Fig. 6C).

The functional response of residual PECs was also monitored in terms of bacterial phagocytosis using both flow cytometric quantitation and confocal microscopic examination. Flow cytometric analysis showed that PECs isolated from UCB (50 mg/kg bw)-administered mice showed significantly decreased phagocytosis as compared to that obtained from vehicle-treated mice (Fig. 6D and E). Further, PECs obtained from the combination treatment group showed significantly decreased phagocytosis as

augmented WBI-induced loss in viable cell counts of bone marrow and PECs (Fig. 5E and F).

Hematological studies showed that WBI-induced leucopenia, erythropenia, lymphopenia, thrombocytopenia, and neutropenia were further augmented in mice from the combination treatment group (Table 2). Further, additional decreases in hemoglobin level, packed cell volume, and mean corpuscular volume were seen in mice from the combination treatment group when compared to either UCB or WBI group (Table 2). These results demonstrated that combination treatment of mice with UCB and WBI resulted in a significant loss of viability of various murine immune cells, suggesting that UCB possessed in vivo radiomodifying effects.

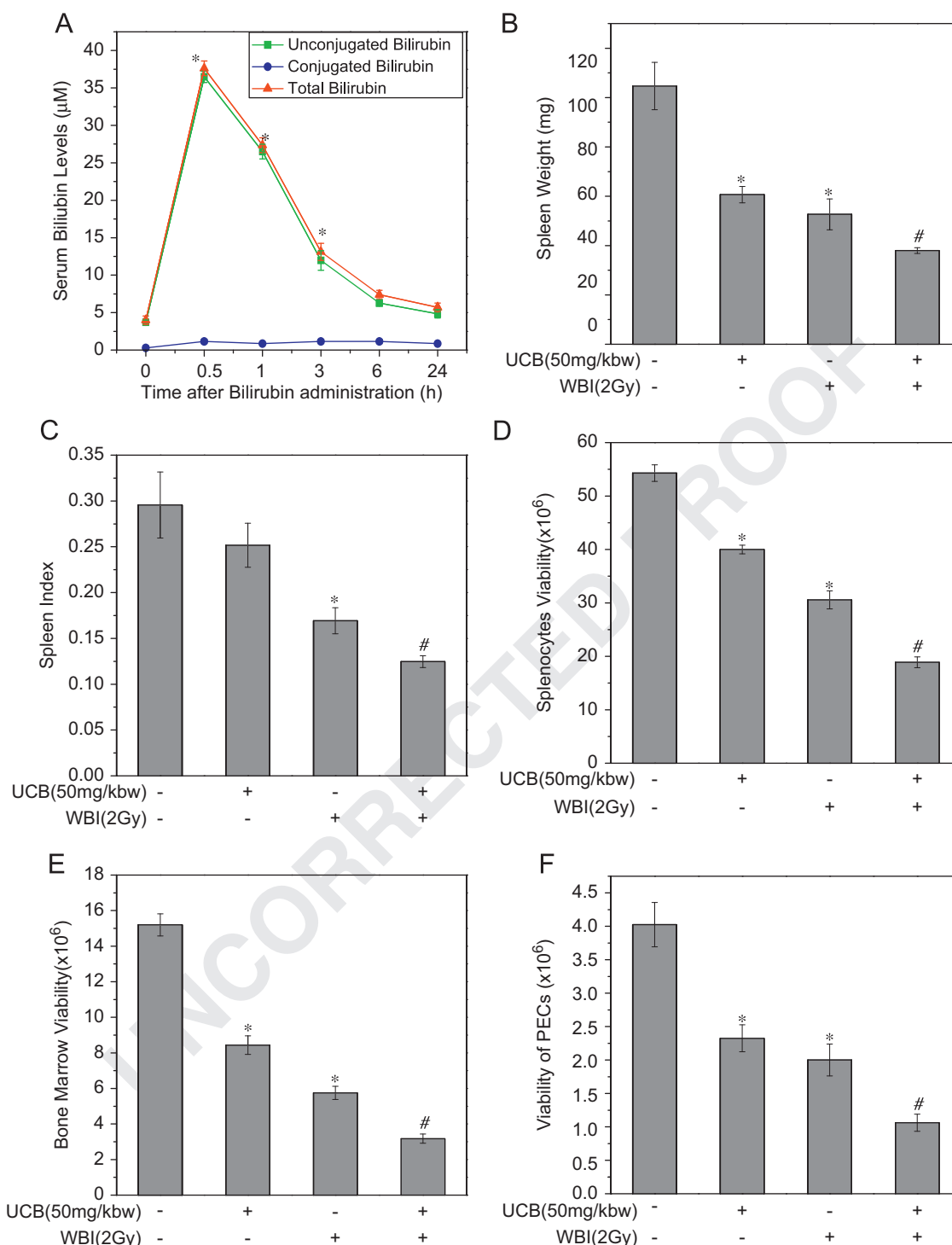


Fig. 5. UCB pretreatment of mice augmented WBI-induced immunosuppression: (A) Mice (5 animals per group) were administered ip with UCB (50 mg/kg bw), blood was drawn at indicated times, and serum bilirubin (total, conjugated) levels were measured using an autoanalyzer. (B–F) Mice were injected ip with UCB (50 mg/kg bw) 0.5 h prior to exposure of WBI (2 Gy). Control mice were injected with vehicle only. Mice were sacrificed 24 h after irradiation and spleen, femur bone marrow, and PECs were isolated. (B) Spleen weight and (C) spleen index were recorded and viable cell counts were enumerated by trypan blue dye exclusion method in (D) spleen, (E) bone marrow, (F) PECs. The data are derived from one of the three such independent experiments having similar results. In each experiment, data from four mice per group were assessed and each bar represents mean \pm SEM. * $P < 0.05$, as compared to vehicle group and # $P < 0.05$, as compared to either UCB group or WBI group.

compared to that obtained from either UCB or WBI group (Fig. 6D and E). Confocal studies also supported these findings (Fig. 6F). Altogether these results demonstrated that increased serum bilirubin levels during radiation exposure resulted in a decreased functional response of lymphocytes and PECs.

UCB pretreated mice were more susceptible to WBI-induced infection

Since UCB administration to mice during radiation exposure induced increased apoptosis and decreased functional responses of lymphocytes and PECs, the major responder against infection,

Table 1
UCB administration to mice augmented WBI-induced loss of splenocytes subsets

Splenocyte subsets	No. $\times 10^{-6}$ per spleen			
	Control	UCB 50 mg/kg bw ^a	WBI 2 Gy ^a	UCB 50 mg/kg bw + WBI 2 Gy ^b
Lymphocytes	47.03 \pm 3.7	26.57 \pm 1.7 ^a	19.49 \pm 0.7 ^a	12.21 \pm 1.1 ^b
CD3+T cells	18.90 \pm 1.4	10.68 \pm 0.6 ^a	7.83 \pm 0.3 ^a	4.91 \pm 0.4 ^b
CD4+T cells	13.07 \pm 1.0	7.38 \pm 0.4 ^a	5.41 \pm 0.21 ^a	3.39 \pm 0.3 ^b
CD8+T cells	1.88 \pm 0.1	1.06 \pm 0.06 ^a	0.78 \pm 0.03 ^a	0.49 \pm 0.04 ^b
CD19+B cells	14.67 \pm 1.1	8.29 \pm 0.5 ^a	6.08 \pm 0.24 ^a	3.81 \pm 0.35 ^b
CD14+ macrophages	2.16 \pm 0.17	1.22 \pm 0.07	0.89 \pm 0.03	0.56 \pm 0.05

Mice were administered with UCB (50 mg/kg bw) or vehicle 0.5 h prior to WBI (2 Gy) exposure and sacrificed 24 h after WBI. The number of CD3+T cells, CD4+ helper T cells, CD8+ cytotoxic T cells, CD19+ B cells, and CD14+ macrophages in spleen of treated mice was determined by flow cytometry. The total cell yield was calculated by multiplying the proportion of each cell subset by the total number of live cells obtained per spleen. Data from four mice per group were assessed and each bar represents mean \pm SEM.

^a $P < 0.05$, as compared to vehicle group.

^b $P < 0.05$, as compared to either UCB group or WBI group.

Table 2
UCB administration to mice augmented WBI-induced loss of hematological parameters.

Hematological parameters	Control	UCB 50 mg/kg bw ^a	WBI 2Gy ^a	UCB 50 mg/kg bw + WBI 2 Gy ^b
Platelet counts ($\times 10^5$ /ml)	3.86 \pm 0.20	2.46 \pm 0.12 ^a	2.39 \pm 0.11 ^a	1.53 \pm 0.17 ^b
WBCs ($\times 10^4$ /ml)	1.18 \pm 0.12	0.85 \pm 0.07 ^a	0.65 \pm .02 ^a	0.38 \pm 0.01 ^b
Lymphocytes (%)	44.0 \pm 1.18	32.4 \pm 1.44 ^a	25.2 \pm 1.24 ^a	20.0 \pm 1.18 ^b
Neutrophils (%)	54.6 \pm 2.52	63.5 \pm 1.53 ^a	66.2 \pm 0.58 ^a	74.2 \pm 0.66 ^b
RBCs ($\times 10^6$ /ml)	7.06 \pm 0.27	5.99 \pm 0.21 ^a	5.22 \pm 0.15 ^a	4.52 \pm 0.15 ^b
Hb (g/dl)	14.62 \pm 0.19	14.41 \pm 0.25	14.72 \pm 0.1 ^a	12.98 \pm 0.26 ^b
Packed cell volume (%)	40.76 \pm 0.49	31.18 \pm 0.22 ^a	28.04 \pm 0.9 ^a	22.62 \pm 1.25 ^b
Mean corpuscular volume (fl)	72.08 \pm 1.77	61.72 \pm 0.46	60.4 \pm 1.36	51.02 \pm 0.7

Mice were administered with UCB (50 mg/kg bw) or vehicle 0.5 h prior to WBI (2 Gy) exposure and blood from these treated mice was collected in heparinized tubes by retroorbital puncture and complete blood count was done by an autoanalyzer. Data from five mice per group were assessed and each bar represents mean \pm SEM.

^a $P < 0.05$, as compared to vehicle group

^b $P < 0.05$, as compared to either UCB group or WBI group.

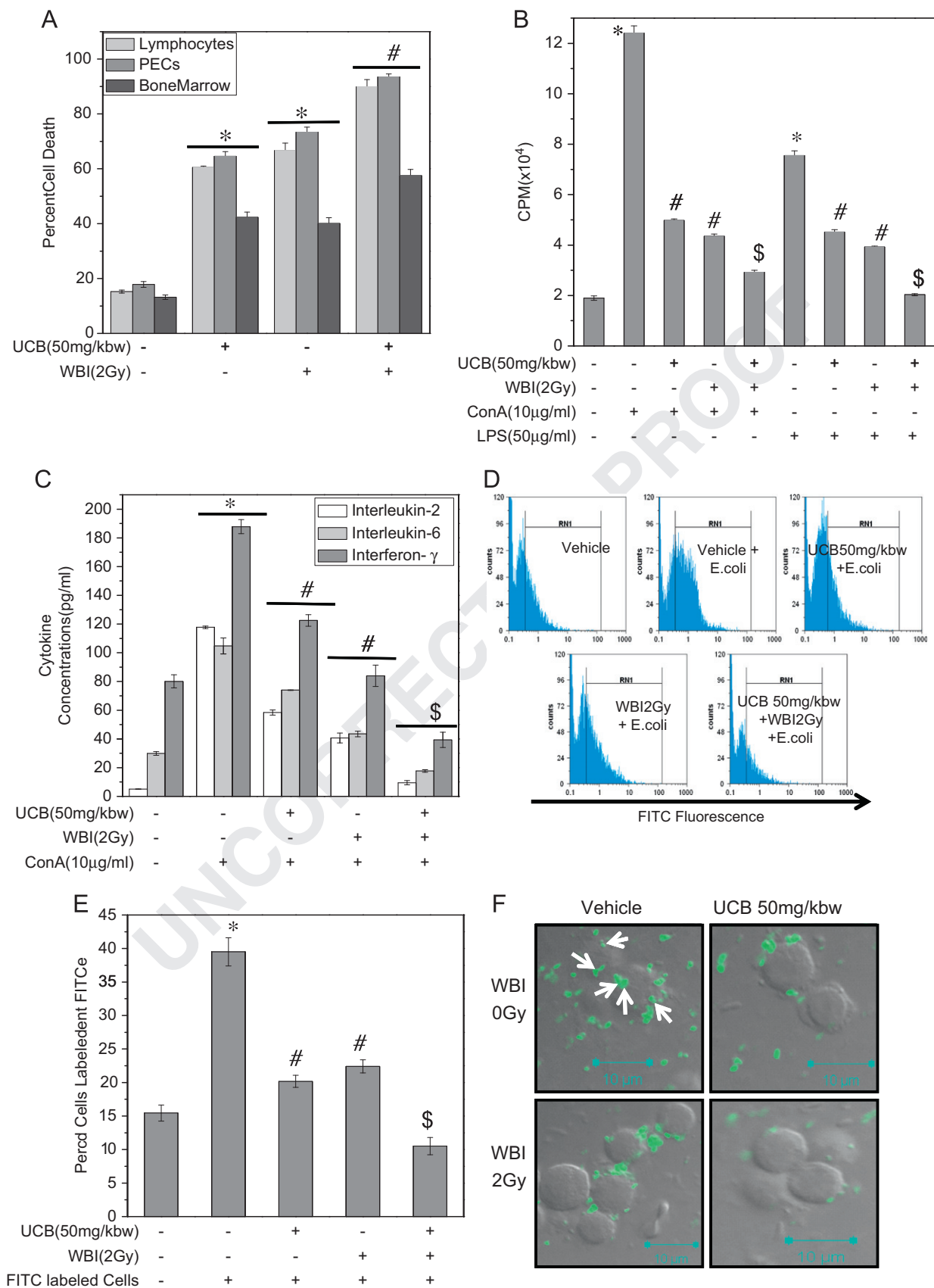
we hypothesized that these mice might be more prone to infection. To test the hypothesis, mice from various groups were injected with *E. coli* (K-12 strain) 24 h after WBI exposure. These mice were examined 24 h after bacterial injection for incidence of bacterial peritonitis by quantifying the bacterial overload in the peritoneum of treated mice. As shown in the Fig. 7A, the peritoneal cavity of mice from either UCB group or WBI group challenged with *E. coli* showed increased bacterial counts as compared to that of vehicle group, injected with *E. coli*. Further, combination treatment group injected with *E. coli* showed significantly increased bacterial counts as compared to that obtained from either UCB or WBI group injected with *E. coli* (Fig. 7A and B).

Further, experiments were designed to observe the loss of body weight and survival of mice from various groups injected with *E. coli*. Results showed that mice from either UCB group or WBI group challenged with *E. coli* showed increased weight loss, diarrhea, and mortality as compared to that of vehicle group, injected

with *E. coli* (Fig. 7C and D). Further, mice from the combination treatment group injected with *E. coli* showed significantly increased weight loss, diarrhea, and mortality as compared to that obtained from either UCB or WBI group injected with *E. coli* (Fig. 7C and D and Table 3). These results indicated that UCB administration before WBI exposure augmented the WBI-induced susceptibility of mice to develop infection and death.

Proinflammatory cytokines (TNF- α , IL-1 β , and IL-6) are important mediators for the establishment of bacterial peritonitis [42,43]. It is well documented that release of NO is one of the primary events of bacterial peritonitis, which lead to increased production of TNF- α . To study the effects of UCB administration on the release of proinflammatory cytokines and NO in mice challenged with bacteria, serum cytokines and NO were measured at +6 h after bacterial injection. Results demonstrated that mice from either UCB group or WBI group challenged with *E. coli* showed increased level proinflammatory cytokines (TNF- α , IL-1 β ,

Fig. 6. UCB pretreatment of mice augmented WBI-induced apoptosis and decreased WBI-induced loss of functional response of various immune cells: (A) Mice were administered with UCB (50 mg/kg bw) 0.5 h prior to WBI (2 Gy) exposure and sacrificed immediately after WBI and spleen, bone marrow, and PECs were removed from different groups and cultured for 24 h at 37 °C and cell death in each group was estimated by PI staining. Data from three mice per group were assessed and each bar represents mean \pm SEM. * $P < 0.05$, as compared to vehicle group and [#] $P < 0.05$, as compared to either UCB group or WBI group. (B–F) Mice administered with UCB (50 mg/kg bw) or vehicle, 0.5 h prior to WBI (2 Gy) exposure, and sacrificed 24 h after WBI and spleen and PECs were removed and their functional responses were evaluated. (B) Splenic lymphocytes (1×10^6 /ml) were stimulated with Con A (10 μ g/ml) or LPS (50 μ g/ml) for 72 or 48 h, respectively, and were pulsed with [³H]thymidine (0.5 μ Ci) and the cells were harvested after 16 h. The incorporated radioactivity was counted using a liquid scintillation counter. (C) Splenic lymphocytes (2×10^6 /2 ml) were stimulated with Con A (10 μ g/ml) for 24 h and cytokines (IL-2, IL-6, and IFN- γ) were estimated in culture supernatant using ELISA. In each experiment, data from three mice per group were assessed and each bar represents mean \pm SEM. * $P < 0.05$, as compared to vehicle group, [#] $P < 0.05$, as compared to either Con A or LPS group, and ^{\$} $P < 0.05$ as compared to either Con A+WBI group or Con A+UCB group or LPS+WBI group or LPS+UCB group. (D–F) PECs (1×10^6) from different groups were incubated with FITC-labeled *E. coli* at 37 °C for 0.5 h. Surface fluorescence on cells was quenched by the addition of crystal violet. FITC-positive cells were measured (D, E) using a flow cytometer and (F) confocal microscopy. RN1 population represents FITC-positive cells after quenching. (D) Representative flow cytometric histogram showing decreased phagocytosis in PECs isolated from treated group and (E) corresponding bars graph representing percentage phagocytic activity in each group are shown. In each experiment, data from three mice per group were assessed and each bar represents mean \pm SEM. * $P < 0.05$, as compared to untreated control group, [#] $P < 0.05$, as compared to FITC-labeled *E. coli*-treated control group and ^{\$} $P < 0.05$ as compared to either FITC-labeled *E. coli*-treated UCB group or FITC-labeled *E. coli*-treated WBI group.



and IL-6) and NO as compared to that of the vehicle group, injected with *E. coli* (Fig. 7E and F). Further, mice from the combination treatment group injected with *E. coli* showed a

significantly increased level of proinflammatory cytokines and NO as compared to that obtained from either UCB or WBI group injected with *E. coli* (Fig. 7E and F).

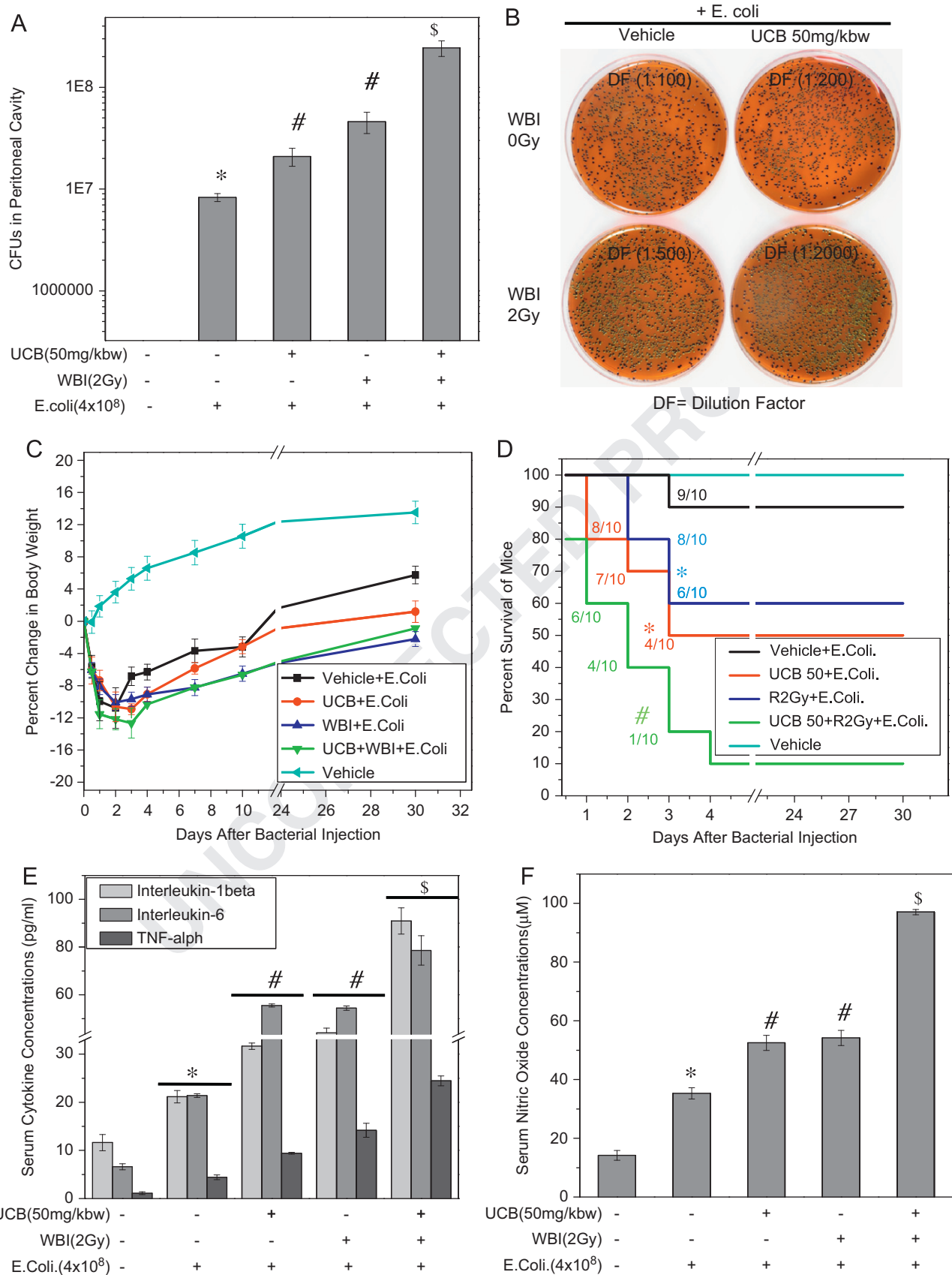


Fig. 7. UCB pretreated mice were more susceptible to WBI-induced infection: Mice were administered with UCB (50 mg/kg bw) or vehicle 0.5 h prior to WBI (2 Gy) exposure. Mice were challenged ip with bacterial inoculums (4×10^8 – 10^9 CFU/ml) 24 h after WBI exposure and different parameters were studied. (A, B) Mice were sacrificed 24 h after bacterial challenge and peritoneal flush isolated from different groups was serially diluted and plated on EMB agar in duplicate and incubated for 37 °C overnight and visible colonies were enumerated and photographed. Data from three mice per group were assessed and each bar represents mean \pm SEM. * $P < 0.05$, as compared to vehicle group, # $P < 0.05$, as compared to vehicle + *E. coli* group, and \$ $P < 0.05$ as compared to either UCB + *E. coli* group or WBI + *E. coli* group. (C, D) Weight loss and mortality of treated mice were monitored for period of 30 days. A total of 10 mice per group were used for assessment of mortality. * $P < 0.05$, as compared to vehicle + *E. coli* group, # $P < 0.05$, as compared to either UCB + *E. coli* group or WBI + *E. coli* group. (E, F) Blood was collected by retroorbital puncture at 6 h after bacterial challenge and serum was separated. (E) Levels of proinflammatory cytokines (TNF- α , IL-1 β , and IL-6) were estimated by ELISA. (F) NO level was estimated by Griess reagent. In each experiment, data from three mice per group were assessed and each bar represents mean \pm SEM. * $P < 0.05$, as compared to vehicle group, # $P < 0.05$, as compared to vehicle + *E. coli* group, and \$ $P < 0.05$ as compared to either UCB + *E. coli* group or WBI + *E. coli* group.

Table 3

UCB administration increases the mortality of WBI-exposed mice treated with bacterial **inoculums**.

Groups	Survival rate (%)	Mean survival time (days)
Vehicle + <i>E. coli</i>	90	27.2 ± 2.8
UCB 50 mg/kg bw + <i>E. coli</i>	50 ^a	12.8 ± 4.68 ^a
WBI 2 Gy + <i>E. coli</i>	60 ^a	18.6 ± 4.66 ^a
UCB 50 mg/kg bw + WBI 2 Gy + <i>E. coli</i>	10 ^b	4 ± 2.9 ^b

Mice were administered with UCB (50 mg/kg bw) or vehicle 0.5 h prior to WBI (2 Gy) exposure and injected with *E. coli* (1×10^9 CFU) 24 h after WBI exposure. Percentage mortality and mean survival time were recorded for 30 days. Data from 10 mice per group were assessed and each bar represents mean ± SEM.

^a $P < 0.05$, as compared to vehicle group.

^b $P < 0.05$, as compared to either UCB group or WBI group.

UCB pretreatment of mice augmented WBI-induced p38MAPK activation in PECs

p38MAPK has been implicated to play a critical role in the activation and function of immune cells, release of cytokines by immunocompetent cells, and also in the pathogenesis of peritonitis [44]. To elucidate the role of p38MAPK in radiomodifying effects of UCB, we have examined the ability of UCB administration in the presence or absence of WBI to activate p38MAPK in PECs. Results showed that either UCB or WBI treatment of mice activated p38MAPK in PECs and combination treatment of mice with UCB and WBI significantly augmented the phosphorylation of p38MAPK when compared to that obtained from either UCB or WBI group (Fig. 8A and B).

To confirm the involvement of p38MAPK in the observed radiomodifying effects of UCB, we administered mice with a pharmacological inhibitor of p38MAPK (SB203580) prior to combination treatment and analyzed whether a selective inhibitor could inhibit the responses observed during UCB challenge in the presence of WBI exposure. Results showed that SB203580 administration to mice significantly inhibited the combination treatment-induced loss of viable cell counts (Fig. 8C) and cell death in PECs (Fig. 8D). We also examined the effects of SB203580 administration on induction of peritonitis and various inflammatory mediators in mice from the combination treatment group injected with *E. coli*. Results showed that prior administration of SB203580 significantly decreased the peritoneal bacterial counts (Fig. 8E), serum TNF- α , and NO production (Fig. 8F) in mice from the combination treatment group injected with *E. coli*.

Discussion

There is a need to understand how increased UCB levels can modify the host response to WBI. In light of this background, we attempted to underscore radiomodifying effects of UCB using the mouse as an experimental model, because murine models are the best characterized animal model for initial assessment of radiation injury [31]. In the present study, we used molar ratios of UCB to BSA less than 0.5 to make the study clinically more relevant [45]. This molar ratio is very similar to the conditions prevailing in human and murine plasma [27]. It was found that after single administration of UCB, serum total bilirubin concentration peaked at levels approximately 10-fold ($37.62 \pm 0.98 \mu\text{M}$) above baseline ($3.9 \pm 0.57 \mu\text{M}$) by 0.5 h postinjection (Fig. 5A). Our results demonstrate that UCB is immunotoxic and has the ability to augment the toxic effects of radiation in various immune cells both in vitro and in vivo. Decreased functional responses of lymphocytes and PECs

observed in our studies revealed that UCB has radiomodifying effects in cells involved in both innate and adaptive immunity.

Acute radiation injury is associated with severe damage to immune cells by disrupting the cellular redox homeostasis via induction of oxidative stress [35]. Oxidative stress is the pathogenic outcome resulting from an imbalanced ratio between ROS production and ROS elimination by the cell's antioxidant capacity [41]. GSH is major cellular antioxidant which serves to eliminate the excess ROS production in the body. Our results demonstrate that radiation exposure to lymphocytes increased the basal ROS levels; however, pretreatment of lymphocyte with UCB decreased the basal as well as radiation-induced ROS level showing its antioxidant potentials (Figs. S2A–D). These results were in agreement with earlier published works [2,46]. Our results indicate the absence of augmentation of radiation-induced ROS production when lymphocytes were treated with UCB in vitro. Recent published studies, including ours, suggest a necessary and critical role of GSH depletion in the execution of apoptosis in lymphoid cells, independent of ROS formation [2,47]. Other studies have also shown that apoptosis seems to be actively regulated by GSH content and not by excessive ROS generation [48,49]. Therefore, we have studied the effects of UCB on GSH depletion in lymphocytes and the results showed that UCB treatment to lymphocytes depleted cellular GSH levels as evidenced by decreased GSH/GSSG ratios (Fig. 4). These results are in agreement with earlier published studies which demonstrate that reduced GSH levels in UCB-treated splenocytes/neuronal cells contribute to the altered redox state leading to apoptosis [2,50,51]. Further, our results also showed that UCB pretreatment of lymphocytes led to augmentation of radiation-induced GSH depletion (Fig. 4). These findings suggested that UCB-mediated augmentation of radiation-induced GSH depletion is a contributory factor for observed radiomodifying effects of UCB. These results imply a role of GSH beyond a simple antioxidant and suggest its role in the execution of programmed cell death.

Exposure of mice to radiation induces severe damage to the immune system because its cellular constituents are highly vulnerable to radiation-induced apoptosis [35]. Our results demonstrate that WBI exposure to mice induces myelosuppression by decreasing the viable bone marrow counts (Fig. 5E). UCB administration to mice prior to WBI exposure leads to augmented suppression of the viability of bone marrow cells. An earlier report by Wang et al. demonstrates that myelosuppression induced by ionizing radiation is the result of induction of apoptosis in hematopoietic progenitor and hematopoietic stem cells of bone marrow [52]. In agreement with this study, we also found that WBI-exposed mice showed increased apoptosis in bone marrow cells and combination treatment further augmented the apoptosis in these cells (Fig. 6A) and, thereby, exacerbated the WBI-induced myelosuppression. Acute myelosuppression is an immediate concern for radiation victims as it could cause high mortality and morbidity in exposed individual [52]. In accordance with our earlier published work [35], exposure of mice to WBI induces splenic atrophy and decreases spleen weight, spleen index, viable counts of total splenocytes, and its various subsets such as CD3+ T cells, CD4+ helper T cell, CD8+ cytotoxic T cells, CD19+ B cells, and CD14+ macrophages (Fig. 5B–D and Table 1). UCB administration to mice potentiated WBI-induced splenic atrophy by inducing increased apoptosis in splenocytes (Fig. 6A). The increased apoptosis in splenic lymphocytes obtained from UCB-administered mice exposed to radiation is well correlated with a decreased number of viable spleen cells. The earlier published studies from our laboratories had indicated that splenocytes from irradiated mice were suppressed in their ability to mount a proliferative immune response to T cell mitogen [31]. Further, decreased proliferative response and cytokine production on mitogenic stimulation were found in lymphocytes obtained from mice administered with UCB and exposed to radiation (Fig. 6B and

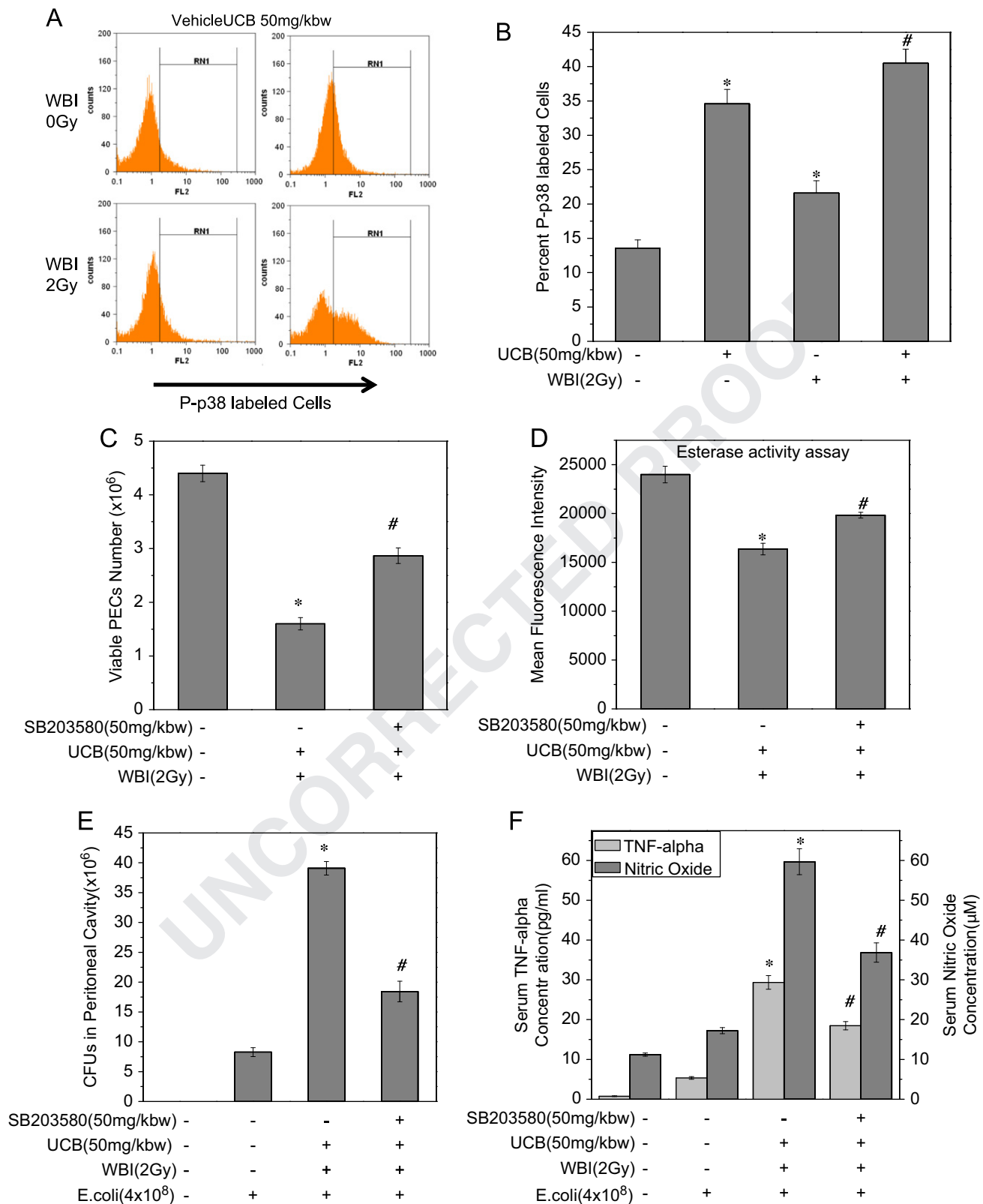


Fig. 8. UCB pretreatment of mice augmented WBI-induced p38MAPK activation in PECs: (A, B) Mice were administered with UCB (50 mg/kg bw) or vehicle 0.5 h prior to WBI (2 Gy) exposure and sacrificed 3 h after WBI exposure. PECs were isolated and processed for intracellular staining with anti-phospho-p38MAPK as described under Materials and methods. Data from three mice per group were assessed and each bar represents mean \pm SEM. * $P < 0.05$, as compared to vehicle group and # $P < 0.05$, as compared to either UCB group or WBI group. (C–F) Mice were injected ip with SB203580 (5 mg/kg bw) 2 h prior to UCB administration and were exposed to WBI 0.5 h later. (C) Mice were sacrificed 24 h after WBI and viable PECs were enumerated by the trypan blue dye exclusion method. (D) Mice were sacrificed immediately after WBI, PECs were isolated and further cultured for 24 h, and death was estimated by esterase activity assay. In each experiments (C, D) data from three mice per group were assessed and each bar represents mean \pm SEM. * $P < 0.05$, as compared to vehicle group, and # $P < 0.05$, as compared to the combination treatment group. (E,F) These mice were injected with *E. coli* (4×10^8 CFU) 24 h after WBI exposure. (E) Peritoneal flush isolated 24 h after bacterial challenge was plated on EMB agar in duplicate and incubated for 37 °C overnight and visible colonies were enumerated. (F) Blood was collected by retroorbital puncture at 6 h after bacterial challenge and serum was separated. Level of TNF- α was estimated by ELISA and NO level was estimated by Griess reagent. Data from three mice per group were assessed and each bar represents mean \pm SEM. * $P < 0.05$, as compared to vehicle+*E. coli* group, and # $P < 0.05$, as compared to combination treatment +*E. coli* group.

C). The observed increased immunosuppression in combination treatment group is the result of increased apoptosis, when compared to groups treated with either of the treatments. Lymphocyte apoptosis and monocyte dysfunction play a pivotal role in sepsis-induced immunosuppression [53,54]. Since lymphocytes are essential for both efficient immune function and the regulation of inflammation, the lymphocyte apoptosis induced by UCB may play a role in the observed immunosuppression and inflammation. The initial proinflammatory response observed in sepsis is often followed by complex immune suppression that may compromise the eradication of the primary infection and favor the emergence of secondary infections and can damage tissue and necrosis can provoke inflammation [55,56]. The earlier works by Fernandes [57] and Gordo [58] demonstrated that increased levels of UCB induced the secretion of inflammatory cytokines by astrocytes and microglial cells which can be detrimental to the central nervous system during neonatal life. The data also suggested that UCB-induced cytokine production, by mediating cell injury, can further contribute to exacerbate neurotoxicity. The increased immunosuppression is associated with increased risk of infection and death. Thus the presence of elevated levels of UCB during radiation exposure of patients should be considered in a clinical situation.

Since, obstructive jaundice has been shown to increase the expression of toll-like receptor (TLR) 4, we attempted whether increased UCB in our experimental condition mediates its immunotoxic effects via upregulation of TLR-4 [7]. Results showed that treatment of lymphocytes with UCB did not affect the expression of TLR-4; thus, it mediates its immunotoxic effects independent of TLR-4 (Fig. S3). Although TLR controls the magnitude of the inflammatory response, our results indicate that TLR signaling does not contribute to the development of UCB-induced inflammation and immune suppression and the subsequent susceptibility to secondary infections.

Our present study further probed the radiation sensitivity of PECs in UCB-treated mice. Corroborating recent reports by Du et al., we found that radiation exposure to mice reduces the viability of PECs [59]. UCB administration further depleted radiation-induced loss of the viability in these cells. Further, the decreased PECs obtained in mice from the combination treatment group are suggestive of active destruction of mature PECs, as evidenced by the increased apoptosis in these cells (Fig. 6A). Since PECs are highly rich in macrophages which are the most efficient phagocytes, and can phagocytose substantial numbers of bacteria or other cells or microbes, the functional response was studied by phagocytosis of FITC-labeled bacteria using flow cytometry. Earlier report by Sablonniere et al. demonstrated that whole-body gamma radiation exposure to rat decreased the phagocytic activity of alveolar macrophages on the first day postirradiation [60]. In agreement with this study, we found that WBI exposure to mice reduced the phagocytic activity of PECs at 24 h postirradiation and combination treatment further decreased bacterial phagocytosis (Fig. 6D–F). Therefore the combination treatment significantly decreases the innate immunity of the host, which may contribute to the increased susceptibility to infection in these mice.

Our studies pertaining to hematological parameters revealed that exposure of mice to WBI induced thrombocytopenia, leucopenia, neutropenia, lymphopenia, and erythropenia and further UCB administration exacerbated the effects of radiation exposure (Table 2). WBI exposure to mice did not have any effect on blood bilirubin levels till 24 h postirradiation (data not presented). These results were in agreement with earlier published work by Katanyutanon et al. who have demonstrated that WBI exposure to rats did not change the blood total bilirubin level on Day 1 postirradiation [61]. Radiation exposure to mice is known to induce hematopoietic suppression by dropping the peripheral blood counts. Additionally, Patchen et al. in his murine studies

demonstrated that radiation-induced neutropenia and thrombocytopenia led to hemorrhagic complications and life-threatening opportunistic infection and thus appeared as major factors contributing to morbidity and mortality after radiation exposure [62]. Importantly a recent study showed that there is a quantitative relationship between the degree of neutropenia and the increased risk of infectious complications. As the duration of neutropenia increases, the risk of secondary infections such as invasive mycoses also increases [63]. However, preclinical studies involving large animals have demonstrated that hemorrhage due to radiation-induced loss of platelets remains a life-threatening problem [64]. In addition, hemorrhage exacerbates anemia, which also occurs following radiation-induced hematopoietic injury [62]. Results obtained from our murine model of radiation injury clearly showed that combination treatment of mice augmented WBI-induced hematopoietic injury.

Suppressing the functionality of the important immune cells involved in both innate and adaptive immunity by combination treatment of mice may pose the organism at serious risk of opportunistic pathogens. To study the effects of combination treatment on host susceptibility to infection, we have experimentally induced acute bacterial peritonitis as an infection model by injecting *E. coli* cells through the ip route. Intraperitoneal infection is a prominent reason for morbidity and mortality in humans [65]. Among diverse known pathogens, *E. coli* emerge as the predominant causative agent for intraperitoneal infections [65,66]. As reported earlier by Billips et al., we found that ip injection of *E. coli* cells in vehicle-administered mice induced bacterial infection as evidenced by increased levels of NO and proinflammatory cytokines (IL-1 β , IL-6, and TNF- α) and incidence of bacterial overload (Fig. 7A, E, and F) [40]. Excessive production of TNF and IL-1 β causes shock and high plasma levels of TNF, IL-1 β , and IL-6 are associated with high mortality rates [67]. Increased mortality (20%) due to establishment of peritonitis in vehicle-administered mice may be due to increased production of these proinflammatory cytokines (Fig. 7D and E and Table 3). The studies further revealed that serum levels of proinflammatory cytokines, occurrence of bacterial peritonitis, and associated mortality were significantly higher in mice from the UCB group as compared to mice from the vehicle group (Fig. 7A, D, and E). The increased bacterial counts found in the peritoneum of UCB-administered mice could be the consequence of depressed phagocytosis by peritoneal macrophages (Fig. 6E). Our data may provide a molecular basis by which hyperbilirubinemia predisposes the patients to infection [7,68,69] and contributes to sepsis-related acute respiratory distress syndrome development and mortality [8].

Additionally our results demonstrate that mice from the combination treatment group injected with *E. coli* had increased occurrence of peritonitis characterized by increased peritoneal bacterial overload, increased proinflammatory cytokines (TNF- α , IL-6, and IL-1 β), increased NO, decreased body weight, and increased mortality (Fig. 7A–F and Table 3). Plum et al. had reported that in the case of acute peritonitis, inflammatory mediators (especially IL-1 and bacterial LPS) induced expression of iNOS in macrophages and increased levels of NO [70]. Moshayed et al. suggested that during acute inflammation, proinflammatory cytokines such as TNF- α may induce anorexia and weight loss in mice [71]. Martineau et al., in his randomized, controlled study using a rat model of peritonitis, reported that peritoneal proinflammatory cytokines (TNF- α , IL-1 β , and IL-6) were adversely correlated with survival outcome [72]. The decreased body weight and increased mortality found in our experiments were well correlated with increased cytokine profile (Fig. 7C–E).

The p38MAPK activation has been shown to play a key role in the immune dysfunction seen during murine peritonitis induced by cecal ligation and puncture [73]. The activation of p38MAPK has been implicated as an important regulator of the coordinated release

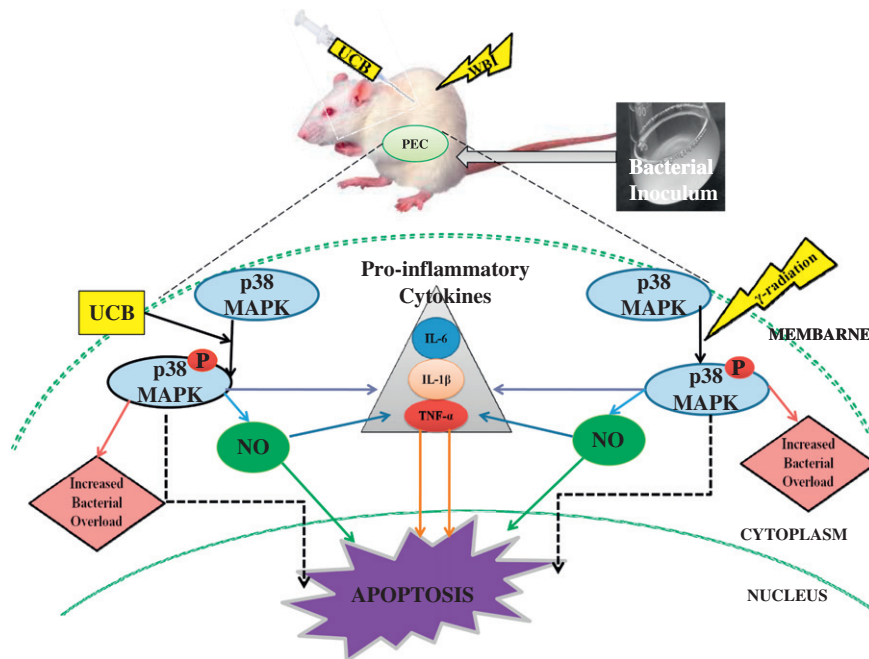


Fig. 9. Schematic representation of radiomodifying effects of UCB: UCB pretreatment of mice increased WBI-induced apoptosis by augmenting radiation-induced p38MAPK activation and NO and proinflammatory cytokine (TNF- α , IL-1 β , IL-6) production in response to bacterial challenge. Further, p38MAPK activation in mice from the combination treatment group increased bacterial overload leading to increased peritonitis.

of various inflammatory mediators (proinflammatory cytokines, nitric oxide) by host defense cells like macrophages [74]. Lu et al. showed the regulative effects of p38MAPK on release of TNF- α and NO from alveolar macrophages under endotoxin stimulation [75]. Our results demonstrated that UCB administration to mice induced phosphorylation of p38MAPK (Fig. 8A and B). These results are in agreement with earlier work by Lin et al. [76] and Fernandes et al. [77] who had demonstrated the role of p38MAPK in UCB-induced death in neuron and astrocytes [76,77]. The increased cytokine profile and NO seen in the serum of combination treatment mice injected with *E. coli* is well correlated with increased p38MAPK activation in these mice (Fig. 8A and B). Further, studies using a pharmacological inhibitor confirmed the involvement of p38MPAK in the inflammatory cascades of peritonitis (Fig. 8C–F). Recent studies using Mkp-1^{-/-} (MAPK phosphatase 1) mice having increased p38MAPK activation showed that knockout of Mkp-1 sensitized mice to sepsis caused by cecal ligation and puncture [78]. Further, Salojin et al. demonstrated that MKP-1^{-/-} mice showed enhanced constitutive activation of p38MAPK and were hyperresponsive to bacterial endotoxin (LPS)-induced toxicity and exhibit significantly increased serum TNF- α , IL-6, IL-12, IFN- γ , and IL-10 levels after systemic administration of LPS [79]. Additionally, Mkp-1 deficiency predisposed animals to accelerated mortality and was associated with greater bacterial burden [78]. The increased bacterial overload found in the combination treatment group injected with *E. coli* and further decreased bacterial counts due to prior administration of SB203580 in these mice showed that p38MAPK activation plays a key role in the pathogenesis of bacterial peritonitis in mice treated with UCB and WBI (Fig. 8E). The proposed model of UCB-induced radiomodifying effects in mice has been summarized in Fig. 9.

To the best of our knowledge, this is the first study demonstrating the role of increased UCB, in exacerbating the effects of radiation exposure and increasing the infection susceptibility by suppressing the host defense against microbial infection. In conclusion, our results collectively proved that administration of the physiologically and clinically relevant dose of UCB (50 mg/kg bw) prior to exposure of 2 Gy ionizing radiation (the dose typically used during radiotherapy) to mice deteriorates the host's innate and adaptive immune response

and in response to subsequent bacterial challenge, heightened the immediate inflammatory reaction by inducing increased production of NO and proinflammatory cytokines, thus making the host more susceptible to infection, sepsis, and mortality. These experimental data are very relevant to human health especially in understanding the potential risk to hyperbilirubinemic patients during radiotherapy and acute radiation exposure in the course of radiation accidents and also helping in understanding the radiomodifying effects of UCB in ARS patients.

Acknowledgments

The authors thank Ms. Shweta Suryavanshi for her help in confocal microscopy and Dr. Manish Goswami and C. Vijay Kumar for their help in bacterial experiments. The authors also acknowledge the technical assistance of Mr. Prayag Amin, Ms. Jisha Menon Mr. Manjoor Ali, Mr. Narendra Sidnalkar, Mr. Kashinath Munankar, and Mr. Deepak Kathole. Funding was provided by the Department of Atomic Energy, Government of India. N.M.K. designed and performed research and analyzed the data and T.B.P. interpreted the data and drafted the manuscript. The authors have no financial conflict of interest.

Appendix A. Supporting information

Supplementary data associated with this article can be found in the online version at <http://dx.doi.org/10.1016/j.freeradbiomed.2012.07.007>.

References

- [1] Liu, Y.; Li, P.; Lu, J.; Xiong, W.; Oger, J.; Tetzlaff, W.; Cynader, M. Bilirubin possesses powerful immunomodulatory activity and suppresses experimental autoimmune encephalomyelitis. *J. Immunol.* **181**:1887–1897; 2008.
- [2] Khan, N. M.; Poduval, T. B. Immunomodulatory and immunotoxic effects of bilirubin: molecular mechanisms. *J. Leukoc. Biol.* **90**:997–1015; 2011.

- [3] Sima, P.; Mala, J.; Miler, I.; Hodr, R.; Truxova, E. The suppressive effect of continuous infusion of bilirubin on the immune response in mice. *Folia Microbiol. (Praha)* **25**:483–490; 1980.
- [4] Rola-Plezczyński, M.; Hensen, S. A.; Vincent, M. M.; Bellanti, J. A. Inhibitory effects of bilirubin on cellular immune responses in man. *J. Pediatr.* **86**:690–696; 1975.
- [5] Vetricka, V.; Sima, P.; Miler, I.; Bilej, M. The immunosuppressive effects of bilirubin. *Folia Microbiol. (Praha)* **36**:112–119; 1991.
- [6] Miler, I.; Sima, P.; Vetricka, V.; Indrova, M.; Slavikova, M. The potential immunosuppressive effect of bilirubin. *Allerg. Immunol. (Leipz.)* **34**:177–184; 1988.
- [7] Field, E.; Horst, H. M.; Rubinfeld, I. S.; Copeland, C. F.; Waheed, U.; Jordan, J.; Barry, A.; Brandt, M. M. Hyperbilirubinemia: a risk factor for infection in the surgical intensive care unit. *Am. J. Surg.* **195**:304–306; 2008. discussion 306–307.
- [8] Zhai, R.; Sheu, C. C.; Su, L.; Gong, M. N.; Tejera, P.; Chen, F.; Wang, Z.; Convery, M. P.; Thompson, B. T.; Christiani, D. C. Serum bilirubin levels on ICU admission are associated with ARDS development and mortality in sepsis. *Thorax* **64**:784–790; 2009.
- [9] Monson, J. R.; Guillou, P. J. Immunological perspectives on pancreatic cancer and jaundice. *Hepatogastroenterology* **36**:437–441; 1989.
- [10] Uchida, H.; Shibata, K.; Iwaki, K.; Kai, S.; Ohta, M.; Kitano, S. Ampullary cancer and preoperative jaundice: possible indication of the minimal surgery. *Hepatogastroenterology* **56**:1194–1198; 2009.
- [11] Guglielmi, A.; De Manzoni, G.; Giralda, R.; Framaglia, M.; Cordiano, C. [Palliative treatment of pancreatic adenocarcinoma]. *Ann. Ital. Chir.* **68**: 635–641; 1997.
- [12] Mazza, E.; Carmignani, L.; Stecco, A.; Lucibello, P. [Interventional radiology in the palliative treatment of pancreatic cancer]. *Tumori* **85**:S54–S59; 1999.
- [13] Dumanski, Iu, V.; Khaletskii, I. V. [Palliative treatment of nonresectable pancreatic cancer complicated by obturator jaundice]. *Klin. Khir.* :24–29; 2010.
- [14] Park, C. K.; Bae, S. H.; Yang, H. J.; Chun, H. J.; Choi, I. B.; Choi, J. Y.; Yoon, S. K. Successful treatment of stereotactic body radiation therapy combined with transarterial chemolipiodolization for hepatocellular carcinoma with biliary obstruction. *Korean J. Intern. Med.* **26**:94–98; 2011.
- [15] Yamaguchi, K.; Kobayashi, K.; Ogura, Y.; Nakamura, K.; Nakano, K.; Mizumoto, K.; Tanaka, M. Radiation therapy, bypass operation and celiac plexus block in patients with unresectable locally advanced pancreatic cancer. *Hepatogastroenterology* **52**:1605–1612; 2005.
- [16] Nakayama, H.; Tsuji, K.; Matsui, R.; Shiotani, S.; Atake, S.; Isaka, N.; Wada, M.; Tokuyue, K.; Ishikawa, A.; Akine, Y. External radiotherapy for decompression of cholangiocellular carcinoma with obstructive jaundice: report of a case. *Radiat. Med.* **19**:297–301; 2001.
- [17] Coleman, C. N.; Blakely, W. F.; Fike, J. R.; MacVittie, T. J.; Metting, N. F.; Mitchell, J. B.; Moulder, J. E.; Preston, R. J.; Seed, T. M.; Stone, H. B.; Tofilon, P. J.; Wong, R. S. Molecular and cellular biology of moderate-dose (1–10 Gy) radiation and potential mechanisms of radiation protection: report of a workshop at Bethesda, Maryland. *Radiat. Res.* **159**:812–834; 2003.
- [18] Pellmar, T. C.; Rockwell, S. Priority list of research areas for radiological nuclear threat countermeasures. *Radiat. Res.* **163**:115–123; 2005.
- [19] Greenberger, J. S. Radioprotection. *In Vivo* **23**:323–336; 2009.
- [20] Fauci, A. S., editor. Harrison's principles of internal medicine; 2008.
- [21] EJ. H. *Radiobiology for the radiologist*. Lippincott Williams & Wilkins; 2000.
- [22] Cerveny, T. J.; Young, M. T. *RW Acute radiation syndrome in humans*. TMM Publications; 1989.
- [23] Anno, G. H.; Baum, S. J.; Withers, H. R.; Young, R. W. Symptomatology of acute radiation effects in humans after exposure to doses of 0.5–30 Gy. *Health Phys.* **56**:821–838; 1989.
- [24] DiCarlo, A. L.; Hatchett, R. J.; Kaminski, J. M.; Ledney, G. D.; Pellmar, T. C.; Okunieff, P.; Ramakrishnan, N. Medical countermeasures for radiation combined injury: radiation with burn, blast, trauma and/or sepsis. Report of an NIAID Workshop, March 26–27, 2007. *Radiat. Res.* **169**:712–721; 2008.
- [25] Palmer, J. L.; Deburghraeve, C. R.; Bird, M. D.; Hauer-Jensen, M.; Kovacs, E. J. Development of a combined radiation and burn injury model. *J. Burn Care Res.* **32**:317–323; 2011.
- [26] Shah, K. G.; Wu, R.; Jacob, A.; Blau, S. A.; Ji, Y.; Dong, W.; Marini, C. P.; Ravikumar, T. S.; Coppa, G. F.; Wang, P. Human ghrelin ameliorates organ injury and improves survival after radiation injury combined with severe sepsis. *Mol. Med.* **15**:407–414; 2009.
- [27] Wang, X. Bilirubin metabolism: applied physiology. *Curr. Paediatr.* **16**:70; 2006.
- [28] Shapiro, S. M. Bilirubin toxicity in the developing nervous system. *Pediatr. Neurol.* **29**:410–421; 2003.
- [29] Ostrow, J. D.; Pascolo, L.; Tiribelli, C. Mechanisms of bilirubin neurotoxicity. *Hepatogastroenterology* **35**:1277–1280; 2002.
- [30] McDonagh, A. F.; Assisi, F. The ready isomerization of bilirubin IX- in aqueous solution. *Biochem. J.* **129**:797–800; 1972.
- [31] Shukla, J.; Chatterjee, S.; Thakur, V. S.; Premachandran, S.; Checker, R.; Poduval, T. B. L-Arginine reverses radiation-induced immune dysfunction: the need for optimum treatment window. *Radiat. Res.* **171**:180–187; 2009.
- [32] Sharma, D.; Kumar, S. S.; Checker, R.; Raghu, R.; Khanam, S.; Krishnan, S.; Sainis, K. B. Spatial distribution, kinetics, signaling and cytokine production during homeostasis driven proliferation of CD4+ T cells. *Mol. Immunol.* **46**:2403–2412; 2009.
- [33] Checker, R.; Sharma, D.; Sandur, S. K.; Khan, N. M.; Patwardhan, R. S.; Kohli, V.; Sainis, K. B. Vitamin K3 suppressed inflammatory and immune responses in a redox-dependent manner. *Free Radic. Res.* **45**:975–985; 2011.
- [34] Sharma, D.; Sandur, S. K.; Rashmi, R.; Maurya, D. K.; Suryavanshi, S.; Checker, R.; Krishnan, S.; Sainis, K. B. Differential activation of NF-kappaB and nitric oxide in lymphocytes regulates in vitro and in vivo radiosensitivity. *Mutat. Res.* **703**:149–157; 2010.
- [35] Khan, N. M.; Sandur, S. K.; Checker, R.; Sharma, D.; Poduval, T. B.; Sainis, K. B. Pro-oxidants ameliorate radiation-induced apoptosis through activation of the calcium-ERK1/2-Nrf2 pathway. *Free Radic. Biol. Med.* **51**:115–128; 2011.
- [36] Sharma, D.; Kumar, S. S.; Sainis, K. B. Antiapoptotic and immunomodulatory effects of chlorophyllin. *Mol. Immunol.* **44**:347–359; 2007.
- [37] Tan, X. X.; Actor, J. K.; Chen, Y. Peptide nucleic acid antisense oligomer as a therapeutic strategy against bacterial infection: proof of principle using mouse intraperitoneal infection. *Antimicrob. Agents Chemother.* **49**:3203–3207; 2005.
- [38] Krogfelt, K. A.; Bergmans, H.; Klemm, P. Direct evidence that the FimH protein is the mannose-specific adhesin of *Escherichia coli* type 1 fimbriae. *Infect. Immun.* **58**:1995–1998; 1990.
- [39] Muller, C. M.; Aberg, A.; Straseviciene, J.; Emody, L.; Uhlin, B. E.; Balsalobre, C. Type 1 fimbriae, a colonization factor of uropathogenic *Escherichia coli*, are controlled by the metabolic sensor CRP-cAMP. *PLoS Pathog.* **5**:e1000303; 2009.
- [40] Billips, B. K.; Forrestal, S. G.; Rycyk, M. T.; Johnson, J. R.; Klumpp, D. J.; Schaeffer, A. J. Modulation of host innate immune response in the bladder by uropathogenic *Escherichia coli*. *Infect. Immun.* **75**:5353–5360; 2007.
- [41] Landriscina, M.; Maddalena, F.; Laudiero, G.; Esposito, F. Adaptation to oxidative stress, chemoresistance, and cell survival. *Antioxid. Redox Signal.* **11**:2701–2716; 2009.
- [42] Montravers, P.; Mohler, J.; Saint Julien, L.; Carbon, C. Evidence of the proinflammatory role of *Enterococcus faecalis* in polymicrobial peritonitis in rats. *Infect. Immun.* **65**:144–149; 1997.
- [43] Sterns, T.; Pollak, N.; Echtenacher, B.; Mannel, D. N. Divergence of protection induced by bacterial products and sepsis-induced immune suppression. *Infect. Immun.* **73**:4905–4912; 2005.
- [44] Branger, J.; van den Blink, B.; Weijer, S.; Madwed, J.; Bos, C. L.; Gupta, A.; Yong, C. L.; Polmar, S. H.; Olszyna, D. P.; Hack, C. E.; van Deventer, S. J.; Peppelenbosch, M. P.; van der Poll, T. Anti-inflammatory effects of a p38 mitogen-activated protein kinase inhibitor during human endotoxemia. *J. Immunol.* **168**:4070–4077; 2002.
- [45] Ostrow, J. D.; Tiribelli, C. New concepts in bilirubin neurotoxicity and the need for studies at clinically relevant bilirubin concentrations. *J. Hepatol.* **34**:467–470; 2001.
- [46] Stocker, R.; Yamamoto, Y.; McDonagh, A. F.; Glazer, A. N.; Ames, B. N. Bilirubin is an antioxidant of possible physiological importance. *Science* **235**:1043–1046; 1987.
- [47] Franco, R.; Panayiotidis, M. I.; Cidlowski, J. A. Glutathione depletion is necessary for apoptosis in lymphoid cells independent of reactive oxygen species formation. *J. Biol. Chem.* **282**:30452–30465; 2007.
- [48] Franco, R.; Cidlowski, J. A. Apoptosis and glutathione: beyond an antioxidant. *Cell Death Differ.* **16**:1303–1314; 2009.
- [49] Han, Y. H.; Kim, S. H.; Kim, S. Z.; Park, W. H. Apoptosis in arsenic trioxide-treated Calu-6 lung cells is correlated with the depletion of GSH levels rather than the changes of ROS levels. *J. Cell. Biochem.* **104**:862–878; 2008.
- [50] Brito, M. A.; Lima, S.; Fernandes, A.; Falcao, A. S.; Silva, R. F.; Butterfield, D. A.; Brites, D. Bilirubin injury to neurons: contribution of oxidative stress and rescue by glucosylated cholic acid. *Neurotoxicology* **29**:259–269; 2008.
- [51] Brito, M. A.; Rosa, A. I.; Falcao, A. S.; Fernandes, A.; Silva, R. F.; Butterfield, D. A.; Brites, D. Unconjugated bilirubin differentially affects the redox status of neuronal and astroglial cells. *Neurobiol. Dis.* **29**:30–40; 2008.
- [52] Wang, Y.; Schulte, B. A.; LaRue, A. C.; Ogawa, M.; Zhou, D. Total body irradiation selectively induces murine hematopoietic stem cell senescence. *Blood* **107**:358–366; 2006.
- [53] Zhang, Y.; Zhou, Y.; Lou, J.; Li, J.; Bo, L.; Zhu, K.; Wan, X.; Deng, X.; Cai, Z. PD-L1 blockade improves survival in experimental sepsis by inhibiting lymphocyte apoptosis and reversing monocyte dysfunction. *Crit. Care* **14**:R220; 2010.
- [54] Pinheiro da Silva, F.; Nizet, V. Cell death during sepsis: integration of disintegration in the inflammatory response to overwhelming infection. *Apoptosis* **14**:509–521; 2009.
- [55] Cohen, J. The immunopathogenesis of sepsis. *Nature* **420**:885–891; 2002.
- [56] Nathan, C.; Ding, A. Nonresolving inflammation. *Cell* **140**:871–882; 2010.
- [57] Fernandes, A.; Silva, R. F.; Falcao, A. S.; Brito, M. A.; Brites, D. Cytokine production, glutamate release and cell death in rat cultured astrocytes treated with unconjugated bilirubin and LPS. *J. Neuroimmunol.* **153**:64–75; 2004.
- [58] Gordo, A. C.; Falcao, A. S.; Fernandes, A.; Brito, M. A.; Silva, R. F.; Brites, D. Unconjugated bilirubin activates and damages microglia. *J. Neurosci. Res.* **84**:194–201; 2006.
- [59] Du, X.; Pan, H.; Zhang, C.; Zhang, H.; Liu, H.; Chen, Z.; Zeng, X. Zingiber officinale extract modulates g-rays-induced immunosuppression in mice. *J. Med. Plants Res.* **4**:1647–1655; 2010.
- [60] Sablonniere, B.; Nicolas, J.; Neveux, Y.; Drouet, J. Effect of whole-body irradiation on phagocytic activity of rat alveolar macrophages. *Int. J. Radiat. Biol. Relat. Stud. Phys. Chem. Med.* **44**:575–584; 1983.
- [61] Katanyutanon, S.; Wu, R.; Wang, P. The effect of whole-body radiation on blood levels of gastrointestinal peptides in the rat. *Int. J. Clin. Exp. Med.* **1**:332–337; 2008.
- [62] Patchen, M. L.; MacVittie, T. J.; Williams, J. L.; Schwartz, G. N.; Souza, L. M. Administration of interleukin-6 stimulates multilineage hematopoiesis and accelerates recovery from radiation-induced hematopoietic depression. *Blood* **77**:472–480; 1991.

- [63] Heslet, L.; Bay, C.; Nepper-Christensen, S. Acute radiation syndrome (ARS)—treatment of the reduced host defense. *Int. J. Gen. Med* **5**:105–115; 2012.
- [64] MacVittie, T. J.; Monroy, R. L.; Patchen, M. L.; Souza, L. M. Therapeutic use of recombinant human G-CSF (rhG-CSF) in a canine model of sublethal and lethal whole-body irradiation. *Int. J. Radiat. Biol.* **57**:723–736; 1990.
- [65] May, A. K.; Gleason, T. G.; Sawyer, R. G.; Pruett, T. L. Contribution of *Escherichia coli* alpha-hemolysin to bacterial virulence and to intraperitoneal alterations in peritonitis. *Infect. Immun.* **68**:176–183; 2000.
- [66] Hau, T. Bacteria, toxins, and the peritoneum. *World J. Surg.* **14**:167–175; 1990.
- [67] Rodriguez-Ramos, C.; Galan, F.; Diaz, F.; Elvira, J.; Martin-Herrera, L.; Giron-Gonzalez, J. A. Expression of proinflammatory cytokines and their inhibitors during the course of spontaneous bacterial peritonitis. *Dig. Dis. Sci.* **46**:1668–1676; 2001.
- [68] Chand, N.; Sanyal, A. J. Sepsis-induced cholestasis. *Hepatology* **45**:230–241; 2007.
- [69] Omar, C.; Hamza, S.; Bassem, A. M.; Mariam, R. Urinary tract infection and indirect hyperbilirubinemia in newborns. *N. Am. J. Med. Sci.* **3**:544–547; 2011.
- [70] Plum, J.; Tabatabaei, M. M.; Lordnejad, M. R.; Pipinika, O.; Razeghi, P.; Huang, C.; Meyer-Kirchraht, J.; Grabensee, B. Nitric oxide production in peritoneal macrophages from peritoneal dialysis patients with bacterial peritonitis. *Perit. Dial. Int.* **19**(Suppl. 2):S378–S383; 1999.
- [71] Moshlyedi, A. K.; Josephs, M. D.; Abdalla, E. K.; Mackay, S. L.; Edwards 3rd C. K.; Copeland 3rd E. M.; Moldawer, L. L. Increased leptin expression in mice with bacterial peritonitis is partially regulated by tumor necrosis factor alpha. *Infect. Immun.* **66**:1800–1802; 1998.
- [72] Martineau, L.; Shek, P. N. Peritoneal cytokine concentrations and survival outcome in an experimental bacterial infusion model of peritonitis. *Crit. Care Med* **28**:788–794; 2000.
- [73] Song, G. Y.; Chung, C. S.; Chaudry, I. H.; Ayala, A. MAPK p38 antagonism as a novel method of inhibiting lymphoid immune suppression in polymicrobial sepsis. *Am. J. Physiol. Cell Physiol* **281**:C662–C669; 2001.
- [74] Nick, J. A.; Young, S. K.; Brown, K. K.; Avdi, N. J.; Arndt, P. G.; Suratt, B. T.; Janes, M. S.; Henson, P. M.; Worthen, G. S. Role of p38 mitogen-activated protein kinase in a murine model of pulmonary inflammation. *J. Immunol.* **164**:2151–2159; 2000.
- [75] Lu, J.; Yang, Z.; Jiang, J.; Wang, Z.; Zhu, P. Regulative effect of P38MAPK on release of TNFalpha and NO from alveolar macrophages under endotoxin stimulation. *Chin. J. Traumatol* **4**:75–77; 2001.
- [76] Lin, S.; Yan, C.; Wei, X.; Paul, S. M.; Du, Y. p38 MAP kinase mediates bilirubin-induced neuronal death of cultured rat cerebellar granule neurons. *Neurosci. Lett.* **353**:209–212; 2003.
- [77] Fernandes, A.; Falcao, A. S.; Silva, R. F.; Brito, M. A.; Brites, D. MAPKs are key players in mediating cytokine release and cell death induced by unconjugated bilirubin in cultured rat cortical astrocytes. *Eur. J. Neurosci.* **25**:1058–1068; 2007.
- [78] Frazier, W. J.; Wang, X.; Wancket, L. M.; Li, X. A.; Meng, X.; Nelin, L. D.; Cato, A. C.; Liu, Y. Increased inflammation, impaired bacterial clearance, and metabolic disruption after gram-negative sepsis in Mkp-1-deficient mice. *J. Immunol.* **183**:7411–7419; 2009.
- [79] Salojin, K. V.; Owusu, I. B.; Millerchip, K. A.; Potter, M.; Platt, K. A.; Oravec, T. Essential role of MAPK phosphatase-1 in the negative control of innate immune responses. *J. Immunol.* **176**:1899–1907; 2006.